frontiers | Research Topics

Advances in non-invasive brain stimulation techniques

Edited by
Mark H. Myers and Gahangir Hossain

Published in
Frontiers in Neuroscience
Frontiers in Human Neuroscience

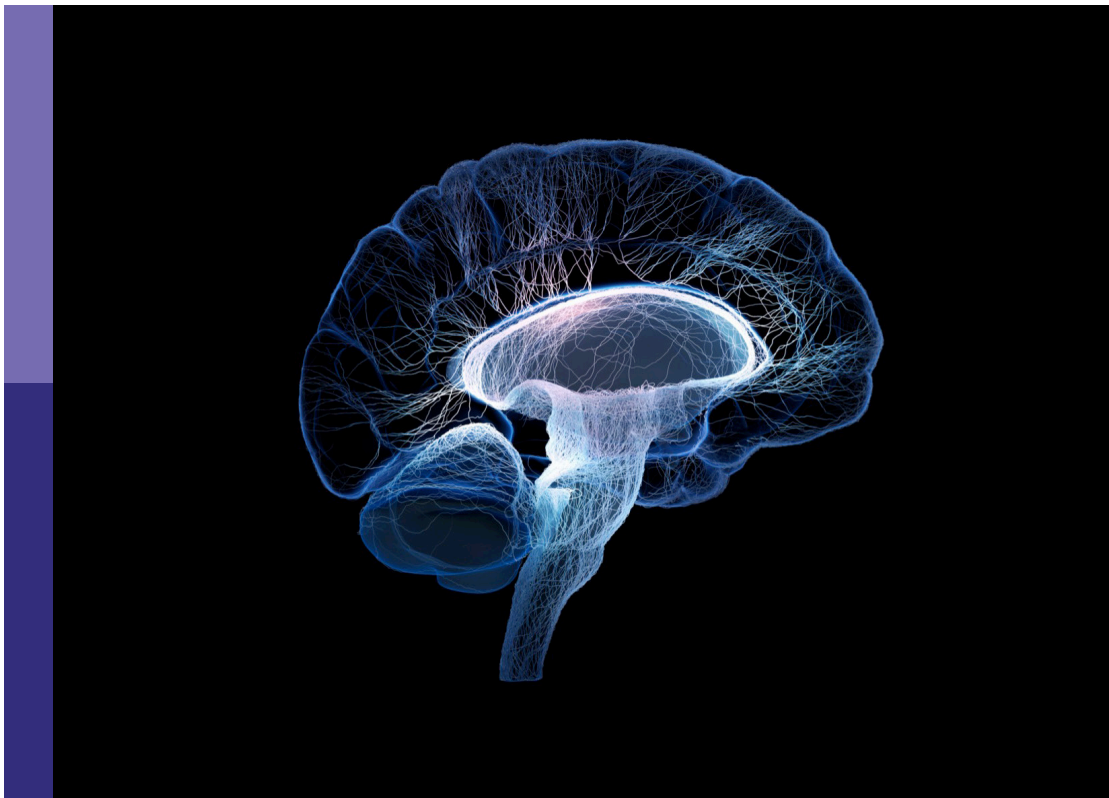

ISSN 1664-8714
ISBN 978-2-8325-5885-0
DOI 10.3389/978-2-8325-5885-0

About Frontiers

Frontiers is more than just an open access publisher of scholarly articles: it is a pioneering approach to the world of academia, radically improving the way scholarly research is managed. The grand vision of Frontiers is a world where all people have an equal opportunity to seek, share and generate knowledge. Frontiers provides immediate and permanent online open access to all its publications, but this alone is not enough to realize our grand goals.

Frontiers journal series

The Frontiers journal series is a multi-tier and interdisciplinary set of open-access, online journals, promising a paradigm shift from the current review, selection and dissemination processes in academic publishing. All Frontiers journals are driven by researchers for researchers; therefore, they constitute a service to the scholarly community. At the same time, the *Frontiers journal series* operates on a revolutionary invention, the tiered publishing system, initially addressing specific communities of scholars, and gradually climbing up to broader public understanding, thus serving the interests of the lay society, too.

Dedication to quality

Each Frontiers article is a landmark of the highest quality, thanks to genuinely collaborative interactions between authors and review editors, who include some of the world's best academicians. Research must be certified by peers before entering a stream of knowledge that may eventually reach the public - and shape society; therefore, Frontiers only applies the most rigorous and unbiased reviews. Frontiers revolutionizes research publishing by freely delivering the most outstanding research, evaluated with no bias from both the academic and social point of view. By applying the most advanced information technologies, Frontiers is catapulting scholarly publishing into a new generation.

What are Frontiers Research Topics?

Frontiers Research Topics are very popular trademarks of the *Frontiers journals series*: they are collections of at least ten articles, all centered on a particular subject. With their unique mix of varied contributions from Original Research to Review Articles, Frontiers Research Topics unify the most influential researchers, the latest key findings and historical advances in a hot research area.

Find out more on how to host your own Frontiers Research Topic or contribute to one as an author by contacting the Frontiers editorial office: frontiersin.org/about/contact

Advances in non-invasive brain stimulation techniques

Topic editors

Mark H. Myers — University of Tennessee Health Science Center (UTHSC), United States

Gahangir Hossain — University of North Texas, United States

Citation

Myers, M. H., Hossain, G., eds. (2025). *Advances in non-invasive brain stimulation techniques*. Lausanne: Frontiers Media SA. doi: 10.3389/978-2-8325-5885-0

Table of contents

frontiers | Frontiers in Neuroscience

TYPE Editorial
PUBLISHED 20 December 2024
DOI 10.3389/fnins.2024.1524097

OPEN ACCESS

EDITED AND REVIEWED BY
Michela Chiappalone,
University of Genoa, Italy

*CORRESPONDENCE
Mark H. Myers
mhmyers99@gmail.com

RECEIVED 07 November 2024
ACCEPTED 29 November 2024
PUBLISHED 20 December 2024

CITATION
Myers MH and Hossain G (2024) Editorial: Advances in non-invasive brain stimulation techniques. *Front. Neurosci.* 18:1524097. doi: 10.3389/fnins.2024.1524097

Editorial: Advances in non-invasive brain stimulation techniques

Mark H. Myers[1]* and Gahangir Hossain[2]

[1]Department of Anatomy and Neurobiology, University of Tennessee Health Sciences Center, Memphis, TN, United States, [2]Department of Information Science, University of North Texas, Denton, TX, United States

KEYWORDS

transcranial magnetic stimulation, transcranial direct current stimulation (tDCS), transcranial magneto-acoustic stimulation (TMAS), transcranial alternating current stimulation (tACS), photobiomodulation (PBM)

Editorial on the Research Topic
Advances in non-invasive brain stimulation techniques

Non-invasive brain stimulation offers a painless and safe approach to neurological rehabilitation, providing minimal side effects, and has been used by thousands of people worldwide. Non-invasive brain stimulation modulates the brain's excitability to aid in treating neurological disorders. The latest work has moved well beyond implementations of transcranial magnetic stimulation/transcranial direct current stimulation (TMS/tDCS) and deep brain stimulation (DBS) techniques, such as repetitive transcranial magnetic stimulation (rTMS), transcranial magneto-acoustic stimulation (TMAS), transcranial alternating current stimulation (tACS), transcutaneous auricular vagus nerve stimulation (taVNS), and peripheral electrical stimulation (PES). Previous intervention techniques, which were applied to alcohol addiction, have moved on to stroke intervention, Alzheimer's, epilepsy, depression, migraine, and tremor alleviation, such as in Parkinson's disease. Exciting research in eSports for performance improvement and remote non-invasive brain stimulation is now being considered. The Frontiers in Neuroscience Research Topic, "*Advances in non-invasive brain stimulation techniques*", has 19 articles covering the latest research in this exciting area.

Transcranial magnetic stimulation has been used in the treatment of Parkinson's disease (PD). In an analysis of 1,894 papers between 1991 and 2022, PD was used as a topic and analyzed. The ranking of publications was found in the following order: United States (293), Italy (184), China (151), England (119), and Canada (100). An analysis of institutions found that the most publications were from the University of Toronto (95), Harvard University (74), and the Sapienza University of Rome (63) (Wei et al.).

A magnetic pulsing approach has been applied to aid those with difficulty swallowing (dysphagia). A therapy involving motor-evoked potentials that applies a 5 ms session-monophasic quadripulse magnetic stimulation (QPS5) was studied. A stimulation that applies 5 ms session sets of four burst trains has been found to facilitate bilateral mylohyoid MEPs enormously. These studies provide insight into motor-evoked potential therapy and the central nervous system response to dysphagia (Fujiki et al.).

TMS has been found to modulate the excitability and plasticity of ascending corticospinal respiratory pathways. Both rTMS and tDCS can regulate respiratory functionality networks in healthy and diseased brains.

Phrenic motor neurons (PMN) and the supplementary motor area (SMA) may also be critical regulatory areas. Diaphragmatic motor-evoked potentials (DiMEPs) decreased on the non-injured side but not the injured side after an injury, indicating increased excitability of PMNs on the ipsilateral side. In the manuscript, the authors review two cases where one patient is administered peripheral electrical stimulation (PES) on the pectoral and abdominal muscles and anode tDCS on the SMA. The application of sensory PES stimulation is inhibitory in this instance. For the second patient, they received excitatory PES on the abdominal muscles. The application of PES on the abdominal muscles enables an excitatory motor response. Both patients had spinal cord injuries with long-term tracheotomy. The results from this study demonstrate that the SMA, under both TMS and tDCS, may be considered for respiratory regulation (Lv et al.).

Repetitive transcranial magnetic stimulation (rTMS) is a practical post-stroke cognitive impairment (PSCI) intervention. After a stroke, increased neural excitability of the unaffected hemisphere and heightened inhibition of the damaged hemisphere are likely to occur. Conversely, reduced inhibition appears in the damaged hemisphere of the skull. Cortical homeostasis is restored by applying high frequency (HF)-rTMS to the affected side to reduce cortical excitability and then using low frequency (LF)-rTMS on the healthy side of the bilateral dorsolateral prefrontal cortex DLPEF (Wang Y. et al.). Another study featuring stroke rehabilitation involves intermittent theta-burst stimulation on the upper limbs for motor recovery. Performance improvement has been found for stroke patients involving improved motor recovery from impairment and better quality of life to perform daily activities (Chen et al.).

Repetitive high-frequency transcranial magnetic stimulation applied over consecutive 2- and 25-s intervals increased cortical excitability. Increased alpha activity was seen in the central regions of the brain. Enhanced functionality was also exhibited in the same central areas toward other brain areas (Jin et al.).

Transcranial magneto-acoustic stimulation (TMAS) has been found to improve the spatial memory deficits of the APP/PS1 mouse model of Alzheimer's disease (AD). The technique involves ultrasound stimulation within a static magnetic field. TMAS was applied to mice for several weeks and then evaluated using *in-vivo* electrophysiology and the Morris water maze (MWM) task. Through analyzing brain oscillations, TMAS improved the performance of MWM-related spatial cognitive functions in the mouse model of Alzheimer's disease (Zhang S. et al.).

Transcranial-focused ultrasound (FUS) offers higher spatial resolution when positioning the radius to targeted brain tumors. This method also provides improvement over targeted depth therapies. Through this therapy, focused ultrasound treatment can be delivered with higher precision (Gao et al.).

Several approaches have been considered for the treatment of fibromyalgia. Transcranial alternating current stimulation (tACS) applies a sinusoidal alternating current to modulate an electric field within the brain. This approach parallels the induced changes of cortical activity in the brain and modulates long-term synaptic plasticity. Additionally, transcranial-focused ultrasound (FUS) provides both spatial precision and deep penetration of brain regions involving ultrasound pulses that have been proven effective in the treatment of fibromyalgia (Zhang J.-H. et al.).

Vagus nerve stimulation (VNS) has traditionally been utilized for the treatment of intractable instances of epilepsy. Transcutaneous auricular VNS (taVNS) has also been applied to patients who have stimulation delivered to the auricular branch of the vagus nerve (ABVN). taVNS could be used for epilepsy, depression, and migraine. taVNS has even been found to elevate cerebral blood flow through repetitive auditory stimuli (RtAS) in patients with consciousness disorders (Wang L. et al.).

Transcranial alternating current stimulation (tACS) is an emerging tool for improving cognitive response and reaction times in Electronic Sports (eSports) and Shooting Games. By modulating oscillatory cortical networks, tACS can alter regional and more extensive network connectivity, decreasing reaction time in visual spatial attention and improving quick classification tasks, such as exact aiming. High-definition HD-tACS has exhibited an improvement in cognitive responses through the reduction of distraction during task performance. Additionally, high coherence between frontal and parietal lobes was also demonstrated. This approach may be carried onto rehabilitation training in patients with cognitive deficits (Jiao et al.).

Transcranial alternating current stimulation may be considered for patients with cerebellar damage, affecting areas such as timing, attention, memory, and language, and those who suffer from tremor-type conditions. Transcranial alternating current stimulation can induce Purkinje cell spike synchrony, which may be helpful for patients with cerebellar damage. This approach may address deficits in language, memory, and attention (Kang et al.).

Other areas of experimental stimulation include cortico-cortical paired associative stimulation (ccPAS), low-intensity pulsed ultrasound (LIPUS), transcranial Photobiomodulation (tPBM), Transcranial Burst Electrical Stimulation (tBES), and Rapid X-ray based genetically targeted (X-genetic) manipulation. This work highlights remote intervention, low power systems to reduce patient risk, generalized pain reduction, merged interventions such as tBES, and genetic modulation. This work is still in its infancy but shows the next advancement in neurological intervention and cognition research.

Cortico-cortical paired associative stimulation (ccPAS) differs from paired associative stimulation (PAS), which uses a dual-coil TMS approach to apply repetitive paired-pulse stimulations over two cortical regions. ccPAS is believed to induce spike-timing dependent timing over a cortico-cortical connection, such as primary motor cortex to primary motor cortex (M1), ventral premotor cortex to primary motor cortex, supplementary motor area to primary motor cortex, and posterior parietal cortex (PPC)-M1. ccPAS over the ventral premotor cortex (PMv) and M1 tapped into motor tasks could increase the motor-evoked potential in healthy adults. ccPAS over the PMv and M1 could decrease the motor-evoked potential in healthy adults. These effects may be due to PMv-M1 glutamatergic projections, which activate the local inhibitory circuits more than the excitatory circuits within the M1. ccPAS may be a therapeutic solution for a host of various neurological issues such as stroke, Parkinson's disease, and major depressive disorders that involve brain connectivity and networks (Zhang).

Low-intensity pulsed ultrasound (LIPUS) has been used to promote nerve regeneration and repair. Rapamycin (mTOR) signaling pathways are known as neurological regulators. Applying LIPUS treatments has led to increased neurite length and mammalian target of rapamycin (mTOR) signaling pathways, where aberrant mTOR signaling equates to abnormal neuronal function. Additionally, LIPUS is considered an application to stimulate neuroblastoma cells to enable neurite outgrowth for neurological diseases such as Alzheimer's, Parkinson's, and many other areas (Ye et al.).

Transcranial Photobiomodulation (tPBM) is a method administered to the cerebral cortex that has been shown to enhance human cognition and attentional performance and treat Alzheimer's and Parkinson's disease. The treatment involves the application of a 1,064-nm continuous-wave laser onto the frontal region of the brain (Fp2) without any contact. The left parietal region has increased alpha activity during a tPBM session. This application may be a non-evasive method that can be applied to many neurological applications (Truong et al.).

Deep brain stimulation is a technique that involves implanting electrodes into subcortical areas of the brain to administer electrical currents. It is considered minimally invasive, considering other surgical methods. A study focusing on deep brain stimulation (DBS) for the treatment of chronic pain considers two significant areas: chronic pain treatment (DBS-P) and DBS for other indications (DBS-O), such as Parkinson's disease or dystonia. The analysis included 966 patients with chronic pain who underwent DBS (340 for DBS-P and 625 for DBS-O). An average pain reduction of ∼48% for the DBS-P group and ∼60% for both groups was found. Additional research is needed to optimize the outcomes of DBS's utility for chronic pain (Shaheen et al.).

A closed-loop neurostimulation simulator has been developed based on stimulation sets through observations. Through this simulator, researchers may find that tDCS therapy can be optimized for more extended periods at higher yields without yielding any adverse health risks. This work presents a brain stimulation simulator to provide several techniques applied to a range of clinical issues, such as Parkinson's disease (PD) or obsessive-compulsive disorders (Wahl et al.).

Transcranial Burst Electrical Stimulation (tBES) combines direct current (DC) and theta burst stimulation (TBS) for brain neuromodulation. In a study by Nguyen et al., tBES (–) stimulation caused an elevation in GAD-65 expression, which has been used as a marker for excitatory and inhibitory neuronal activity in rodent brains. Compared to the baseline and sham state, a decrease in MEPS from tBES (–) stimulation was found. tBES has shown promising results in modulating motor cortical excitability and treating neurological disorders (Nguyen et al.).

Rapid X-ray-based genetically targeted (X-genetic) manipulation of cellular electrical activity for intact-behaving animals has been demonstrated in *Caenorhabditis elegans*. Transgenic expression of LITE-1 in *C. elegans* muscle cells resulted in paralysis and egg ejection responses to stimulation. This experiment shows that LITE-1 could be an X-ray-sensitive receptor in *C. elegans*. This study identifies an X-ray receptor protein that can be trans-genetically expressed in cell types to acutely control the activity of those cells using X-rays and demonstrates X-genetic control of cellular electrical activity. These findings suggest a minimally invasive approach to neuromodulation using transcranial X-ray signals for the manipulation of neural activity in mammals (Cannon et al.).

Altogether, neurological pathologies and the approach to non-invasive intervention is a multi-pronged, multi-layered approach. Electrical intervention (direct/alternating), magnetic, acoustic, ultrasound, paired-pulsed, electrical bursts, photobiomodulation, rapid X-ray-based, and deep brain stimulation have their merits in solving various neurological diseases. Parkinson's and stroke intervention present the initial beachhead to provide early results through this intervention and prove its efficacy. There are specialized techniques that focus on a specific condition, such as respiratory rehabilitation for spinal injury patients, directed treatments for dysphagia, and further bolstering the cognitive capabilities of those who have Alzheimer's disease. Non-invasive techniques are now considered an approach to higher spatial precision and regulation depth to brain tumors. What was considered improbable regarding rapid memory and learning enhancement is now in practice for improving cognitive functions, such as in Electronic Sports. High-definition HD-tACS has been shown to reduce visual spatial attention distraction and enhance task performance during stimulation for eSports participants.

Furthermore, it is now being considered as a rehabilitation approach. Even remote intervention is possible while maintaining low power incidence to the patient. Various research articles highlight generalized pain reduction, merged interventions, and genetic modulation. This work represents research that may find itself very quickly in clinical environments. This field of neurological intervention and rehabilitation is advancing in many fascinating directions. The most interesting non-invasive measures are just around the corner!

Author contributions

MM: Writing – original draft, Writing – review & editing. GH: Investigation, Writing – review & editing.

Conflict of interest

The authors declare that the research was conducted in the absence of any commercial or financial relationships that could be construed as a potential conflict of interest.

Publisher's note

frontiers | Frontiers in Neuroscience

TYPE Original Research
PUBLISHED 25 May 2023
DOI 10.3389/fnins.2023.1163779

OPEN ACCESS

EDITED BY
Mark H. Myers,
The University of Tennessee Health Science Center (UTHSC), United States

REVIEWED BY
Yasuo Terao,
Kyorin University, Japan
Zicai Liu,
Shaoguan First People's Hospital, China

*CORRESPONDENCE
Minoru Fujiki
✉ fujiki@oita-u.ac.jp

†These authors have contributed equally to this work

RECEIVED 11 February 2023
ACCEPTED 28 April 2023
PUBLISHED 25 May 2023

CITATION
Fujiki M, Hata N, Anan M, Matsushita W, Kawasaki Y and Fudaba H (2023) Monophasic-quadri-burst stimulation robustly activates bilateral swallowing motor cortices. *Front. Neurosci.* 17:1163779. doi: 10.3389/fnins.2023.1163779

Monophasic-quadri-burst stimulation robustly activates bilateral swallowing motor cortices

Minoru Fujiki*†, Nobuhiro Hata†, Mitsuhiro Anan†, Wataru Matsushita†, Yukari Kawasaki† and Hirotaka Fudaba†

Department of Neurosurgery, School of Medicine, Oita University, Oita, Japan

A stable, reliable, non-invasive, quantitative assessment of swallowing function remains to be established. Transcranial magnetic stimulation (TMS) is commonly used to aid in the diagnosis of dysphagia. Most diagnostic applications involve single-pulse TMS and motor evoked potential (MEP) recordings, the use of which is not clinically suitable in patients with severe dysphagia given the large variability in MEPs measured from the muscles involved in swallowing. Previously, we developed a TMS device that can deliver quadripulse theta-burst stimulation in 16 monophasic magnetic pulses through a single coil, enabling the measurement of MEPs related to hand function. We applied a system for MEP conditioning that relies on a 5 ms interval-monophasic quadripulse magnetic stimulation (QPS5) paradigm to produce 5 ms interval-four sets of four burst trains; quadri-burst stimulation (QBS5), which is expected to induce long-term potentiation (LTP) in the stroke patient motor cortex. Our analysis indicated that QBS5 conditioned left motor cortex induced robust facilitation in the bilateral mylohyoid MEPs. Swallowing dysfunction scores after intracerebral hemorrhage were significantly correlated with QBS5 conditioned-MEP parameters, including resting motor threshold and amplitude. The degree of bilateral mylohyoid MEP facilitation after left side motor cortical QBS5 conditioning and the grade of severity of swallowing dysfunction exhibited a significant linear correlation ($r = -0.48/-0.46$ and 0.83/0.83; $R^2 = 0.23/0.21$ and 0.68/0.68, $P < 0.001$; Rt./Lt. side MEP-RMT and amplitudes, respectively). The present results indicate that RMT and amplitude of bilateral mylohyoid-MEPs after left motor cortical QBS5 conditioning as surrogate quantitative biomarkers for swallowing dysfunction after ICH. Thus, the safety and limitations of QBS5 conditioned-MEPs in this population should be further explored.

KEYWORDS

swallowing dysfunction, magnetic stimulation, quadripulse theta-burst stimulation, motor evoked potentials, quadripulse stimulation

1. Introduction

Swallowing is a complex physiological phenomenon consisting of voluntary movements and reflexes, which are accomplished by the perfectly coordinated action of 50 pairs of related muscle groups innervated by the bilateral hemispheres. In older adults, there is a loss of oral and pharyngeal mucosal sensation and a general weakening of the pharyngeal muscle groups, which delays laryngeal elevation in response to the entry of food mass into the pharynx, resulting in aspiration (Macrae et al., 2014). Most cases of pneumonia in older adults are aspiration pneumonia, which is a major cause of death among both older adults and patients with stroke. Despite the high risk of aspiration pneumonia after stroke, stable and reliable methods for the non-invasive quantification of swallowing function remain to be fully established. Although the popularity of non-invasive transcranial magnetic stimulation (TMS) for assessing swallowing function has grown; motor evoked potentials (MEPs) recorded from the swallowing muscles are problematic because of the large standard deviation in their values (Macrae et al., 2014). To address this issue, we developed a system for measuring MEPs that relies on monophasic quadripulse theta-burst magnetic stimulation (QTS). In this system, the outputs of 16 stimulators (**Magstim 200^2** is a product by the Magstim Co., Ltd.) are combined using a specially designed module, following which four sets of four-monophasic magnetic pulses are transmitted via a single coil (Fujiki et al., 2022; patent number 7189594). We applied a system for MEP conditioning that relies on a 5 ms interval-monophasic quadripulse magnetic stimulation (QPS5) paradigm (Hamada et al., 2008), which is known to induce long-term potentiation (LTP) in the human hand motor cortex. Furthermore, Tsutsumi et al. (2014) revealed that QPS5, well established method for motor cortical LTP induction using four monophasic pulses induces bilateral motor cortical facilitaion in transcallosal interhemispheric and intracortical facilitation mechanisms. Furthermore, a recent study showed that the swallowing motor cortex in normal subjects has a right hemispheric dominance of lateralization, and electro acupuncture instantly promotes excitability in the bilateral swallowing motor cortex (Tang et al., 2022). In the present study, we aimed to investigate whether 5 ms interval-four burst trains; quadri-burst stimulation (QBS5) can also strongly amplify swallowing-related MEPs and determine whether the quantifiable functional parameters obtained during TMS-based assessments exhibit correlations with neurogenic swallowing disorders.

2. Materials and methods

2.1. Participants

We analyzed data from the same 65 participants included in our previous study, which demonstrated the superiority of monophasic quadripulse theta-burst magnetic stimulation (QTS) in patients with hand motor paralysis following left hemisphere intracerebral hemorrhage (ICH) (Fujiki et al., 2022). The original study included a control group of 10 healthy, right-handed men (age range: 40–68 years; mean ± SD: 58.5 ± 10.8 years) without any contraindications to TMS, as well as 65 patients with hypertension who had experienced putaminal ICH (5 women, 60 men; age range: 55–80 years; mean ± SD: 68.9 ± 11.8 years). No individuals in the control group took regular medications, and none had a history of psychiatric or neurologic illness (Rossi et al., 2009). The original study was approved by the ethics committee of the School of Medicine at Oita University (protocol number: 265), and all individuals in the control and patient groups provided written informed consent to participate.

The participants, 65 consecutive patients, who underwent conservative treatment without surgery between January 2008 and December 2021, demonstrated impaired motor function, which was mostly caused by the compression or destruction of the corticospinal tract due to hemorrhage (>5 and <30 ml in volume, symptom onset <24 h before admission, clear consciousness, no neurological deficits apart from swallowing and motor dysfunction). The median time from onset to examination was 3.3 (range: 1–7) days. The severity of swallowing dysfunction was evaluated using a modified water swallowing test (MWST), in which 3-ml of cold water was placed on the floor of the mouth using a 5-ml syringe. The patient was instructed to swallow, and their swallowing was scored as follows: 1, inability to swallow accompanied by choking and/or changes in breathing; 2, ability to swallow but with changes in breathing; 3, ability to swallow without changes in breathing but with choking and/or wet hoarseness; 4, successfully swallowing without choking or wet hoarseness; 5, original score of 4 with additional deglutition (dry swallowing) more than twice within 30 s (Tohara et al., 2003). Patients who were unable to attempt the MWST were excluded (n = 10). The mean swallowing score (range: 1–5) was 2.55 ± 1.72 (score 1, n = 12; score 2, n = 11; score 3, n = 12; score 4, n = 10; score 5, n = 10). Patient characteristics are shown in **Table 1**.

2.2. System configuration and control study

Control studies for healthy participants [under electroencephalographic (EEGs) monitoring for detection of subclinical abnormalities] were performed as described in our previous study (**Figure 1B**; Fujiki et al., 2022) to test three different configurations of the posterior- anterior directed induced current flow (i.e., monophasic single pulse [SP], 500 Hz [i.e., 2-ms interstimulus interval (ISI)-quadripulse single train stimulation (QPS)] and QBS5) were validated in both hemisphere in each modality. A 70-mm figure-8 coil was used to deliver magnetic pulses at 1.2 times the resting motor threshold (RMT) for MEP recording. A QBS5 at the left hemisphere [four sets of four monophasic pulses at a frequency of 500 Hz, repeated at 200 Hz; i.e., 5-ms interburst interval, with an inter-train interval of 5-s] at 0.9 times active motor threshold (AMT) for left motor cortical conditioning was delivered for 30 min. A navigated brain stimulation system (NBS; Nexstim eXima; Nexstim Ltd., Helsinki, Finland) was used to target the primary motor cortex for the mylohyoid muscle using the first dorsal interosseous muscle (FDI) as a positive control. The NBS is an optical tracking system for precise TMS tracking in real time real-time (see **Figure 1C**).

Our preliminary study revealed that SP- mylohyoid MEPs were always constantly recordable only in healthy control. Stable

10.3389/fnins.2023.1163779

TABLE 1 Summary of patient characteristic.

Case	Age	Sex	MWST grade	Type of ICH	Location	Hematoma volume (mL)	Days after onset
1	65	M	5	Subcortical	Frontal	18	2
2	80	M	5	Subcortical	Frontal	7	3
3	80	M	5	Subcortical	Frontal	12	3
4	78	M	5	Subcortical	Frontal	19	3
5	67	M	5	Subcortical	Frontal	10.4	5
6	66	M	5	Subcortical	Frontal	5	1
7	73	M	5	Subcortical	Frontal	8	2
8	58	M	5	Subcortical	Frontal	28	7
9	68	M	5	Subcortical	Parietal	19	7
10	60	M	5	Subcortical	Frontal	5	1
11	62	M	4	Subcortical	Temporal	12	1
12	64	M	4	Subcortical	Frontal	18	5
13	71	M	4	Subcortical	Diffuse	11	5
14	63	F	4	Subcortical	Frontal	12	4
15	66	F	4	Basal ganglia	Putamen	5	3
16	69	F	4	Subcortical	Frontal	11.1	5
17	66	F	4	Basal ganglia	Putamen	6	5
18	65	F	4	Subcortical	Frontal	11	3
19	64	M	4	Subcortical	Temporal	15	3
20	60	M	4	Subcortical	Parietal	5.4	3
21	68	M	3	Basal ganglia	Putamen	12	8
22	59	M	3	Basal ganglia	Putamen	11	7
23	55	M	3	Basal ganglia	Putamen	8	2
24	63	M	3	Subcortical	Parietal	17	5
25	62	M	3	Subcortical	Temporal	15.5	5
26	79	M	3	Subcortical	Frontal	11	5
27	80	M	3	Subcortical	Frontal	10	5
28	81	M	3	Subcortical	Temporal	10	2
29	80	M	3	Subcortical	Parietal	11	2
30	63	M	3	Basal ganglia	Putamen	12	2
31	60	M	3	Basal ganglia	Putamen	17	2
32	78	M	3	Subcortical	Parietal	15	2
33	63	M	2	Subcortical	Parietal	8.8	1
34	63	M	2	Subcortical	Frontal	9.8	1
35	80	M	2	Subcortical	Frontal	10.2	1
36	78	M	2	Subcortical	Frontal	8.2	3
37	80	M	2	Subcortical	Frontal	19	3
38	66	M	2	Subcortical	Frontal	11	3
39	69	M	2	Subcortical	Temporal	12	2
40	79	M	2	Basal ganglia	Putamen	5.5	2
41	68	M	2	Subcortical	Parietal	15	2
42	80	M	2	Basal ganglia	Putamen	6.1	1

(Continued)

TABLE 1 (Continued)

Case	Age	Sex	MWST grade	Type of ICH	Location	Hematoma volume (mL)	Days after onset
43	65	M	2	Basal ganglia	Putamen	10	3
44	62	M	1	Basal ganglia	Putamen	5	3
45	61	M	1	Basal ganglia	Putamen	10	3
46	80	M	1	Subcortical	Parietal	8.7	3
47	71	M	1	Subcortical	Parietal	14.5	3
48	77	M	1	Basal ganglia	Putamen	6.5	3
49	68	M	1	Basal ganglia	Putamen	8.8	3
50	59	M	1	Subcortical	Frontal	19	3
51	80	M	1	Subcortical	Parietal	19	3
52	63	M	1	Basal ganglia	Putamen	5.2	3
53	68	M	1	Basal ganglia	Putamen	5.9	3
54	68	M	1	Basal ganglia	Putamen	8	3
55	64	M	1	Basal ganglia	Putamen	7	3

MEP, motor evoked potential; RMT, resting motor threshold; QBS5, quadr burst stimulation-5ms interburst interval; QPS, quadripulse stimulation; SP, single pulse; MWST, modified water swallowing test. Fifty five patients with swallowing dysfunction following left hemisphere intracerebral hemorrhage.

and reproducible 500Hz QPS-mylohyoid MEPs were employed, as these may reflect MWST scores. Before and after the QBS5 conditionings, MEPs were measured to determine the RMT, amplitude, and latency (dark blue dashed box, **Figures 1A**, **2**). After determining the hot spot of the FDI muscle using NBS, individual MRI-based anatomical maps placed orthogonally to the central sulcus on the NBS were used as candidate targets to guide further assessment of the cortical physiology of mylohyoid muscle activations in the left M1. The mylohyoid muscle "hotspot" was further identified as the location of the "strongest" mylohyoid MEP amplitude evoked with the lowest-intensity motor threshold that elicited discernible MEPs. After the motor cortical point was registered on the reconstructed 3D MRI images, Euclidian distances between the mylohyoid and FDI were calculated via the NBS (mm). When appropriate stimulation was delivered to the representative areas of M1, MEPs could be observed from the respective mylohyoid and FDI hot spots (Hannula et al., 2005; Macrae et al., 2014; Li et al., 2020). In accordance with previous report for FDI-MEPs (Hamada et al., 2008), AMT for conditioning of mylohyoid motor hotspot was defined as the lowest intensity to evoke mylohyoid MEPs (>100 μV) with weak (5–10% of maximal) jaw contraction maintenance.

2.3. Magnetic stimulation of the motor cortex and MEP recording in patients with ICH

To assess swallowing function in patients with ICH, we validated the affected and unaffected motor cortex under NBS assistance to determine appropriate stimulus intensities for the RMT before and after QBS5 conditioning at the left motor cortex. The MEPs were measured from the affected and contralateral mylohyoid muscles, respectively. Unstable recording sessions (under 50 μV MEPs, peak-to-peak) after 30 trials due to severe swallowing dysfunction were interrupted.

2.4. Data analysis

Motor evoked potential data were analyzed offline as previously described (Sykes et al., 2016; Fujiki et al., 2021, 2022). All data are presented as the mean ± standard deviation (SD), and the level of statistical significance was set at $P \leq 0.05$. For multiple comparisons among the different configurations used for stimulation, the latencies, RMT and MEP amplitudes were analyzed via two-way, repeated measures analysis of variance (ANOVAs). In these analyses, stimulus condition [SP, before and after QBS5 in both side mylohyoid MEP recordings] was used as a between-subject factor, while MWST scores [5–1] were used as a within-subject factor. *Post hoc* Bonferroni corrections was also employed in cases of multiple comparison. Correlations of post-ICH swallowing function with MEP parameters, RMTs, and amplitude were evaluated using correlation coefficients (r) and coefficients of determination (R^2). The analyses were performed using SPSS (Cary, NC, USA).

3. Results

3.1. Mylohyoid MEP amplification after QBS5 in healthy controls

All participants did not report any adverse effects during or after the recording. Additionally, EEG abnormalities were not noted during or ≥30 min post-recording. The distance between the mylohyoid and FDI cortical representation was 23.22 ± 7.34 mm, with a range of 14.28–33.01 (**Figure 2A**).

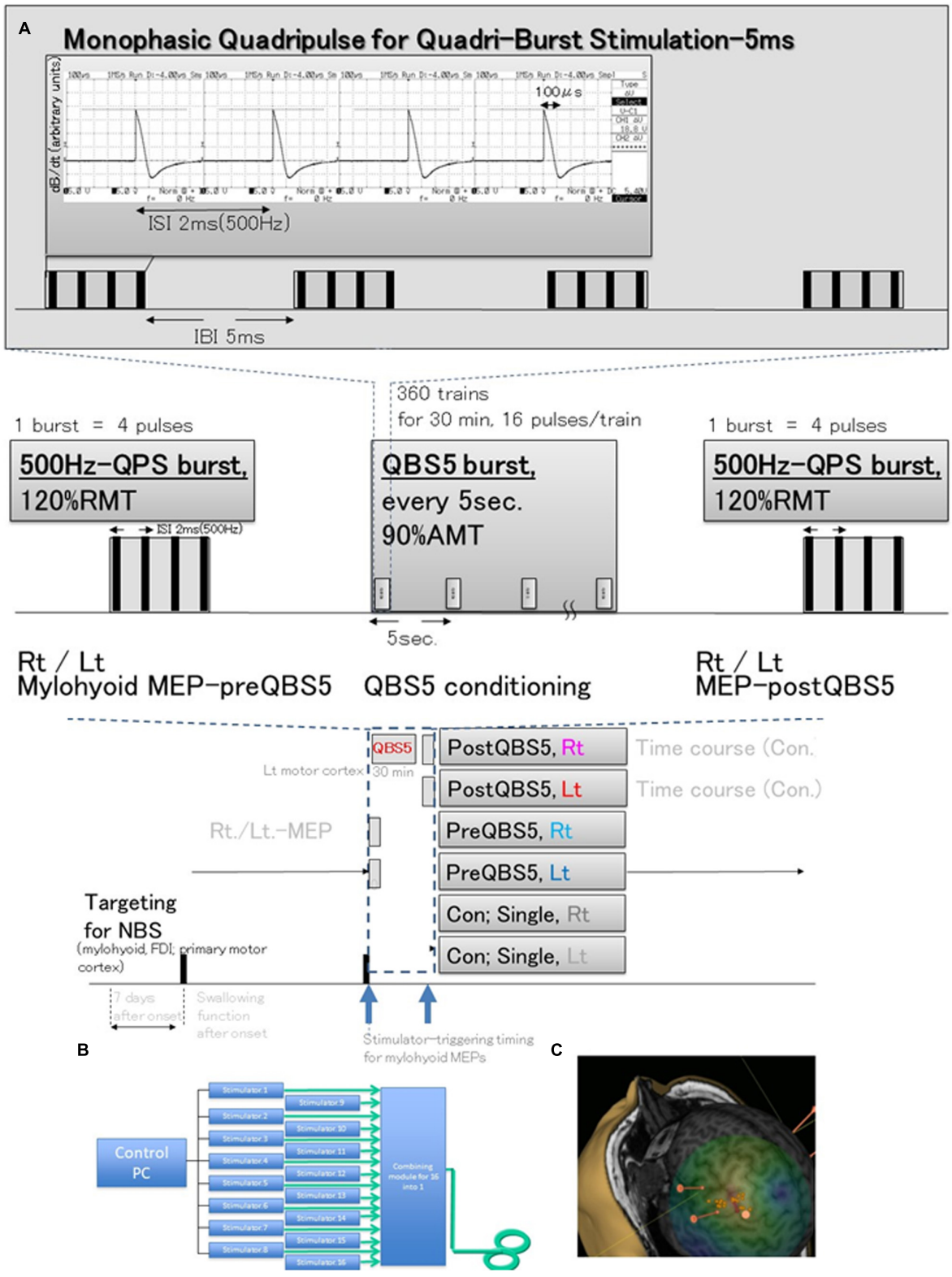

FIGURE 1
Schematic illustration of the experimental protocol and stimulus configurations. Comparison between standard single-pulse magnetic stimulation-induced-MEPs, QPS; single 500-Hz bursts, and before and after QBS-5; four 500-Hz bursts, repeated at 200-Hz (i.e., 5 ms interbust interval) stimulation MEPs. **(A)** Stimulus conditions: five-ms-quadri-burst stimulation [QBS5], 500-Hz quadripulse single train stimulation [QPS], and monophasic single-pulse stimulation. QBS5 consisted of four bursts, each consisting of four high-frequency monophasic pulses which were delivered at 500 Hz (i.e., 2 ms-ISI), repeated at 200 Hz (i.e., 5-ms interburst interval), and delivered every 5 s continuously for 30 min, resulting in a total of 360 trains, 16 pulses/train. QPS consisted of four high-frequency monophasic pulses delivered at 500 Hz (i.e., 2-ms interstimulus interval [ISI]). MEP acquisitions were performed from the final burst at stimulus intensity of 120% RMT. Mylohyoid motor cortices were conditioned with

(Continued)

FIGURE 1 (Continued)
QBS5 for 30 min at stimulus intensity of 90% AMT. Monophasic magnetic flux data recorded using ossiloscope and pickup coil was originated from our previous publication (Fujiki et al., 2022). **(B)** SP, QPS, or QBS5 was applied to the hand and mylohyoid muscle area of the left motor cortex with a PA directed monophasic magnetic QBS-induced MEPs device system, including a set of 16 separate magnetic stimulators (Magstim, 2002; The Magstim Co., Ltd., Wales, UK) connected with a specially designed combining module (Fujiki et al., 2022; patent number 7189594). This device combines the outputs from the 16 stimulators to deliver a train of 16 monophasic magnetic pulses through a single coil. QBS5, QPS, or SP were applied to the hand and mylohyoid area of the left motor cortex with a PA-directed monophasic pulse. **(C)** MEPs were recorded under the targeted primary motor cortex for mylohyoid muscle and first dorsal interosseous (FDI) muscle using a navigated brain stimulation system within 7 days after onset. The screenshot depicts a representative control case with the area mapped to identify the motor optimal location (hotspot) in the target muscle. Each dot on the scalp can be visualized as orange balls, and the red arrow shows the current direction in the brain. The colors show the relative strength of the E-field (red, high E-field strength; blue, low E-field strength). The position feedback indicator (small window on the right for repeated constant stimulation) provides real-time feedback for surface location-enabled manual holding and reliable targeting. QBS5, five-ms-quadri-burst stimulation; QPS, quadripulse stimulation; PA, posterior-anterior; ISI, inter-stimulus interval; IBI, inter-burst interval; RMT, resting motor threshold; TMS, transcranial magnetic stimulation; MEP, motor evoked potential; NBS, navigated brain stimulation.

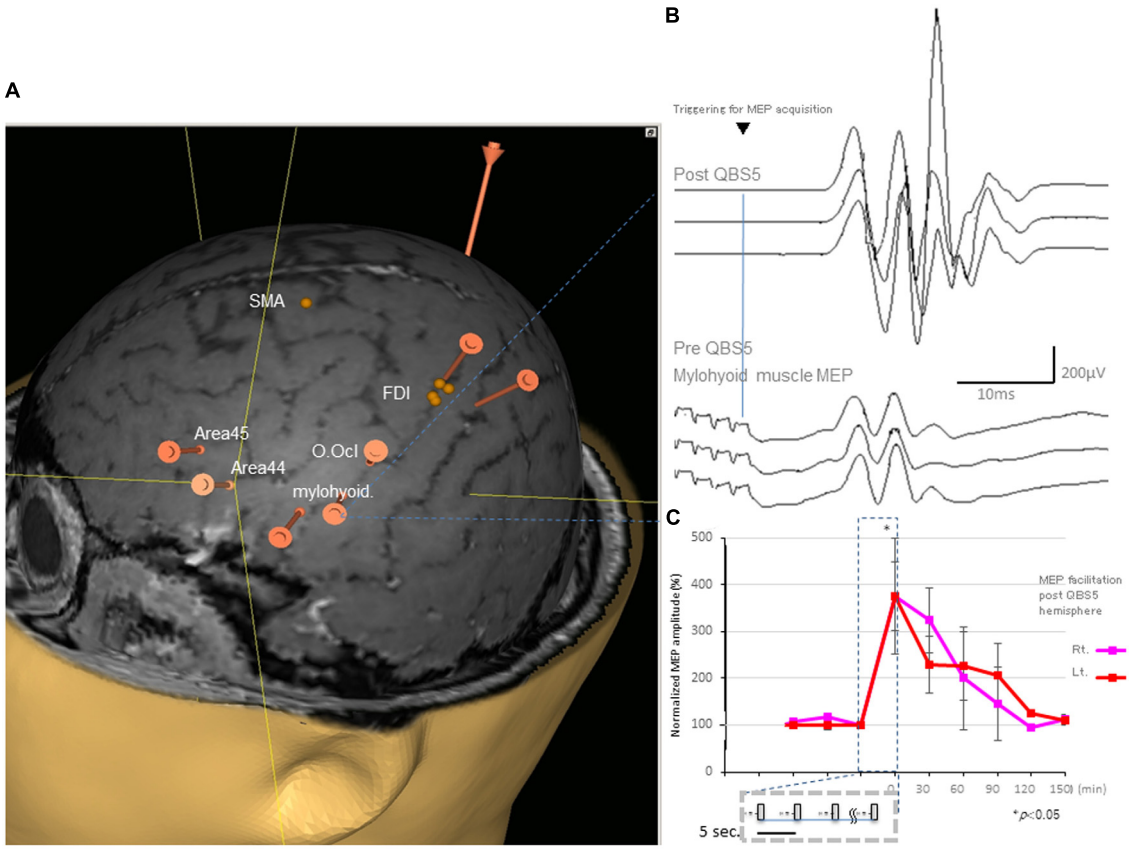

FIGURE 2
Representative MEPs following QPS recorded from the mylohyoid muscle and facilitation after QBS5 in a healthy control. **(A)** Target areas registered before mylohyoid and FDI mapping using the navigated brain stimulation (NBS) system [orange bars; mylohyoid, FDI muscle and orbicularis oculi (O. Ocl.)], supplementary motor area [SMA], Brodmann's area 44, 45 [Area 44, Area 45] for reference, respectively. QBS5, five-ms-quadri-burst stimulation; MEP, motor evoked potential; FDI, first dorsal interosseous. **(B)** Representative MEPs following QPS before (lower traces) and after (upper traces) recorded from the mylohyoid muscle in a healthy control. **(C)** MEP facilitation in after left motor cortical QBS5 conditioning in a healthy participant. Amplitudes increased by 350–370% when compared with those for pre conditioned-MEPs. Note that mylohyoid MEPs recorded from bilateral side was facilitated following QBS5-left hemisphere-conditioning.

Figure 2B illustrates representative right mylohyoid MEP traces after left hemisphere stimulation. The average traces for right and left mylohyoid muscle MEP amplification after left hemisphere QBS5 stimulation are shown in Figure 2C (Rt: pink, Lt: red). The gray boxes within the dashed represent each QBS5 burst. Time course analysis indicated that MEP amplification persisted for approx. 90-min after QBS5. The dark blue dashed box highlights the 30 min-left hemisphere-conditioning stimulus time window corresponding to Figure 1A). Immediately after QBS5 conditioning, mylohyoid muscle MEP amplitudes were higher than those at baseline, gradually decreasing to near-control levels by 90 min. Note that mylohyoid MEPs recorded from the bilateral side facilitated following QBS5-left hemisphere-conditioning. As shown in Figures 2A, B, the ANOVA revealed a significant main effect of MEP after QBS5, suggesting that the stimulation elicited different effects in the four-time points groups [main effect of GROUP,

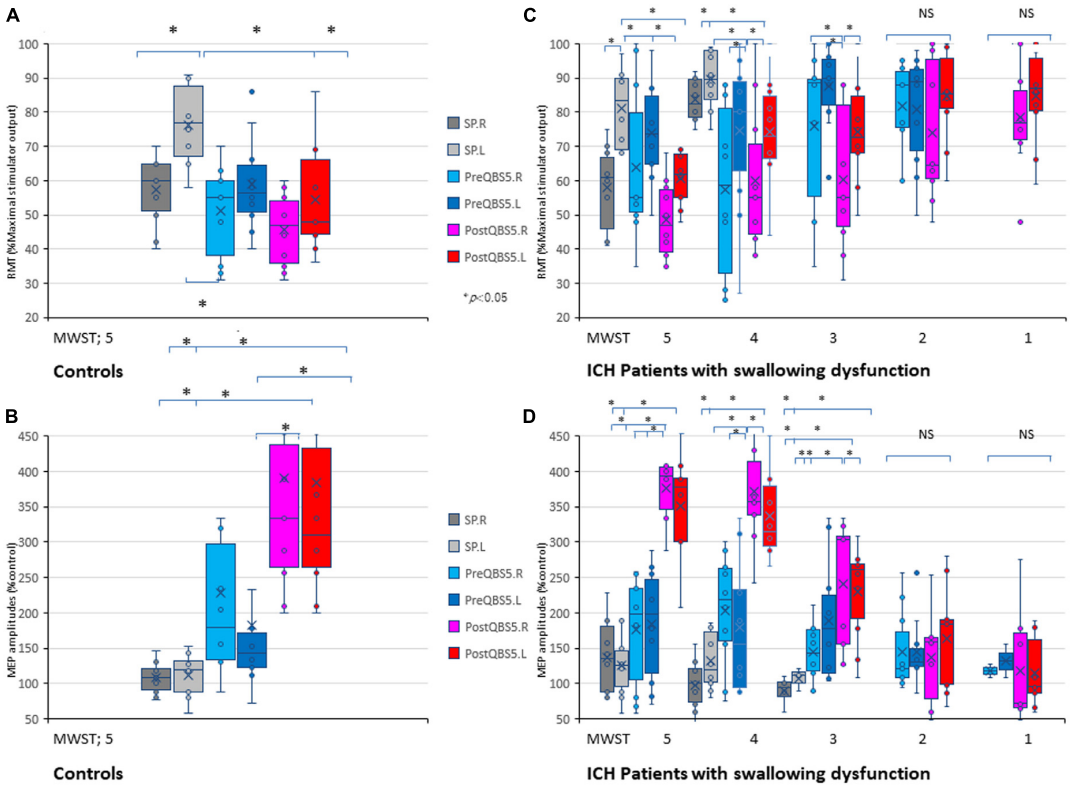

FIGURE 3
Validations of mylohyoid MEP parameters before and after QBS5 conditioning: comparison of characteristic RMT and amplitude profiles and the correlation with MWST scores in healthy controls and ICH patients. Quantitative differences in RMT **(A)** and amplitude **(B)** between the six-mylohyoid muscle conditions were statistically significant in healthy controls ($P < 0.05$). RMTs were significantly lower on the right side ($P < 0.05$). A multiple comparison test revealed significant differences in RMT and MEP amplitudes, and that the QBS5 induces higher amplitudes with lower stimulus intensities in healthy controls ($P < 0.05$). Quantitative differences in RMT **(C)** and amplitude **(D)** between the six-mylohyoid muscle conditions were compared in patients with ICH. Significant differences in RMT and amplitude (MWST scores 5 to 3) were observed in patients with ICH (**C,D**; $P < 0.001$). MWST scores were significantly correlated with RMTs and postQBS5-Rt./Lt.-MEP amplitudes ($P < 0.001$, respectively) but not those of preQBS5-Rt./Lt. or single-pulse-Rt./Lt. Colors in the graph represent each condition before and after TMS [red: postQBS5-Lt., pink: postQBS5-Rt.; dark blue: preQBS5-Lt.; light blue: preQBS5-Rt.; dark gray: single-pulse Rt.; right gray: single-pulse-Lt. in healthy controls **(A,B)** and MWST-parameter correlations in patients with ICH **(C,D)**, respectively]. QBS5, five-ms-quadri-burst stimulation; QPS, quadripulse stimulation; SP, single pulse; ICH, intracerebral hemorrhage; RMT, resting motor threshold; MEP, motor evoked potential; MWST, modified water swallowing test.

$F(3,28) = 18.16$, $P < 0.001$; main effect of TIME, $F(5,118) = 12.75$, $P < 0.001$; GROUP × TIME interaction, $F(15,336) = 2.91$, $P < 0.001$].

Post hoc analysis indicated that MEP amplitudes increased significantly relative to baseline and following SP-MEP after QBS5 left hemisphere stimulation in the Rt. and Lt. mylohyoid-MEPs ($P < 0.001$). Multiple comparisons between the QBS5 and baseline groups indicated that MEP amplitudes were increased for both Rt. and Lt. MEPs only immediately after QBS5 conditioning ($P < 0.001$, Figure 2C).

3.2. Characteristic RMT and amplitude profiles for mylohyoid MEPs in healthy controls

We compared SP-, 500Hz-QPS before and after left hemisphere QBS5 conditioned-MEPs in healthy controls to validate the methodological and physiological configurations used for each condition. Figures 3A, B and Table 1 show the comparison of RMTs, amplitudes before and after QBS5 and single-pulse MEPs. The ANOVA indicated that MEP parameters differed significantly among the bilateral six stimulation conditions (RMT: $F(5,54) = 6.65$ $P < 0.001$, amplitude: $F(5,54) = 8.07$, respectively, $P < 0.001$; Table 1). However, there were no significant differences in latency among the six conditions [$F(5,54) = 0.364$, $P = 0.871$]. In the *post hoc* analysis, both RMT and MEP amplitude differed among the conditions ($P < 0.05$; Figures 3A, B). Furthermore, we observed no significant differences in RMTs and latencies of SP-MEP parameters relative to baseline after QBS5 trials (RMT: 57.3 ± 10.34 vs. 57.4 ± 10.47%; latency: 12.4 ± 1.62 vs. 11.6 ± 3.78 ms; after SP-control and QBS, respectively). In addition, RMT [$t(18) = -0.02$; $P > 0.05$], latency [$t(18) = 0.62$; $P > 0.05$] were not significantly affected by QBS5.

When SP, before and after QBS5 conditioning MEP parameters for healthy controls were compared between hemisphere, only the right side mylohyoid MEP exhibited significantly lower RMTs for SP-MEP [RMT-Rt vs Lt, 57.3 ± 10.34 vs 76.4 ± 11.65; $P = 0.008$]. In addition, there were no significant differences in RMT or amplitude between right and left MEPs for other modalities [$t(9) = 0.06 – 0.79$ range; $P > 0.05$].

TABLE 2 Quantitative differences in the mylohyoid MEP parameters between six conditions.

		Single		PreQBS5 conditioning		PostQBS5 conditioning		*F*	*P*
MWST		SP-Rt.	SP-Lt.	PreQBS5-Rt.	PreQBS5-Lt.	PostQBS5-Rt.	PostQBS-Lt.		
Healthy controls									
5	RMT (%)	57.3 ± 10.34	76.4 ± 11.65	51.9 ± 13.69	59.1 ± 14.12	45.5 ± 10.76	54.4 ± 15.96	$F(5,54) = 6.65$	<**0.001**
($n = 10$)	Amplitude (μV)	108.1 ± 22.57	111.3 ± 30.68	228.8 ± 141.11	182.3 ± 133.7	390.6 ± 206.2	383.9 ± 208.21	$F(5,54) = 8.07$	<**0.001**
	MEP recordable	10	10	10	10	10	10		
ICH patients									
5	RMT (%)	57.9 ± 12.28	81.1 ± 11.45	63.7 ± 22.81	73.9 ± 14.48	48.5 ± 11.47	60.6 ± 7.86	$F(5,54) = 6.76$	<**0.001**
($n = 10$)	Amplitude (μV)	136.8 ± 52.94	125.7 ± 42.86	176.4 ± 78.82	183.6 ± 79.09	375.6 ± 42.25	350.9 ± 71.86	$F(5,54) = 30.07$	<**0.001**
	MEP recordable	10	10	10	10	10	10		
4	RMT (%)	83.6 ± 6.12	89. ± 8.26	57.4 ± 25.81	74.5 ± 22.84	60.4 ± 21.23	74.4 ± 16.52	$F(5,54) = 4.88$	<**0.001**
($n = 10$)	Amplitude (μV)	97.6 ± 37.01	132.2 ± 40.79	203.7 ± 79.25	179.3 ± 93.99	371.6 ± 77.52	336.1 ± 57.67	$F(5,54) = 26.59$	<**0.001**
	MEP recordable	10	10	10	10	10	10		
3	RMT (%)	100	100	75.9 ± 23.25	87.6 ± 12.06	60.4 ± 21.23	74.3 ± 14.78	$F(5,49) = 5.78$	<**0.001**
($n = 12$)	Amplitude (μV)	89.5 ± 21.63	107.3 ± 15.82	144.2 ± 41.12	188.8 ± 85.62	226.9 ± 94.58	229.9 ± 66.93	$F(5,49) = 4.37$	<**0.001**
	MEP recordable	4 (33.3%)	3 (25%)	12	12	12	12		
2	RMT (%)	>100	>100	81.9 ± 13.37	80.9 ± 16.54	74.4 ± 20.27	84.8 ± 13.28	$F(5,38) = 0.71$	0.623
($n = 11$)	Amplitude (μV)	Not recordable	Not recordable	108.4 ± 13.12	116.2 ± 25.44	137.1 ± 63.89	163.7 ± 73.49	$F(5,38) = 0.27$	0.924
	MEP recordable	0	0	11	11	11	11		
1	RMT (%)	>100	>100	100	100	78.4 ± 15.46	84.8 ± 13.81	$F(5,22) = 1.48$	0.23
($n = 12$)	Amplitude (μV)	Not recordable	Not recordable	118.5 ± 14.14	131.5 ± 33.23	117.7 ± 74.98	114.9 ± 49.38	$F(5,22) = 0.07$	0.98
	MEP recordable	0	0	2 (16.7%)	2 (16.7%)	12	12		

MEP, motor evoked potential; RMT, resting motor threshold; QBS5, quadr burst stimulation-5ms interburst interval; QPS, quadripulse stimulation; SP, single pulse. Bold indicates *P*-value less than 0.05.

3.3. Correlation between MWST scores and mylohyoid MEP parameters in patients with swallowing dysfunction after ICH

In the ICH group, age (68.8 ± 7.6 years) and hematoma volume (5–28 ml, with a mean of 11.2 ± 4.87) were not significantly correlated with MWST scores. SP-mylohyiod MEPs were recordable only in patients with ICH with MWST scores 5 to 3 [5; 100%, 4; 100% and 3; 25(left)–33.3(right)%, respectively, Table 2].

When the six mylohyoid MEP conditions (SP-Rt./Lt., PreQBS5-Rt./Lt., and PostQBS5-Rt./Lt.) were compared in each MWST score group, RMT and amplitude significantly differed for patients with MWST scores of 5–3 ($P < 0.001$; Table 1). A one-way ANOVA revealed that RMT and amplitude differed significantly among the six mylohyoid MEP conditions (RMT: $F_{(31,305)} = 6.78$ $P < 0.001$, amplitude: $F_{(31,305)} = 11.45$, respectively, $P < 0.001$). In the two-way repeated-measures ANOVA, the interaction between CONDITION (SP-Rt./Lt., PreQBS5-Rt./Lt., and PostQBS5-Rt./Lt.) and MWST (RMT: $F(21,305) = 2.37$, $P < 0.001$, amplitude: $F(21,305) = 2.41$, $P < 0.001$, respectively) was significant. The *post hoc* analysis also revealed significant differences in RMT (between PostQBS5-Rt. and PostQBS5-Lt.; PostQBS5-Lt. and PreQBS5-Rt., SP-Lt., respectively) and amplitude (between PostQBS5-Lt. and PreQBS5-Rt./Lt., SP-Rt./Lt., respectively, $P < 0.001$; Figures 3C, D).

We observed significant correlations among swallowing function (MWST scores), RMTs, and PostQBS5-MEP amplitude (RMT: $r = -0.48$, $R^2 = 0.23$, $P < 0.001/r = -0.46$, $R^2 = 0.21$, $P < 0.001$; amplitudes: $r = 0.83$, $R^2 = 0.68$, $P < 0.001/r = 0.83$, $R^2 = 0.68$, $P < 0.001$, PostQBS5-Rt./Lt. side, respectively; Figures 3C, D; pink [Rt.] and red [Lt.]). However, no such findings were observed for PreQBS5-Rt./Lt or single-pulse-Rt./Lt.-MEPs.

4. Discussion

The current findings indicate that mylohyoid-MEPs after left motor cortical QBS5 (four sets of four monophasic pulses at frequency of 500 Hz, repeated at 200 Hz; i.e., 5-ms interburst interval, with an inter-train interval of 5 s) conditioning, strongly facilitates bilateral mylohyoid MEPs. Previous studies have reported that changes in the excitability of cortical projections in various swallowing muscles can be observed using TMS-induced MEP (Doeltgen et al., 2011; Macrae et al., 2014). These studies provide valuable insight into the central nervous system response to dysphagia and, more importantly, to the adaptations associated with functional recovery. However, rigorous methodological controls and qualitative assessment measures are

needed to obtain robust and clinically applicable findings in neurophysiological studies of swallowing.

4.1. Mapping of swallowing-related regions for stable, non-invasive evaluations of swallowing function

One of the gold standards for functional brain mapping is functional MRI (fMRI), which has been used to assess swallowing function for some time (Hamdy et al., 1999; Mosier and Bereznaya, 2001). Since Amassian et al. (1987) first recorded laryngeal MEPs using TMS, various efforts have been made to evaluate the function of the pharyngeal and laryngeal regions (Ertekin et al., 2001; Gallas et al., 2007; Khedr et al., 2008). These findings indicate that impairments in the cortical projections to swallowing musculature directly affect the sensitivity of MEPs. Impaired corticobulbar projections in patients may result in the disappearance of MEPs. On the other hand, high variability has been observed when measuring MEPs from the swallowing muscles, with research indicating that 40–50% of MEPs from the submental muscles cannot be recorded during volitional and reflexive swallows (Doeltgen et al., 2011).

Recent studies have also attempted to achieve swallowing related target in a multimodal fashion by integrating fMRI and MEP recordings for the lip orbicularis oris muscle (Li et al., 2020). Cricothyroid muscle-targeting for Broca's area mapping (Rogiæ et al., 2014) is a highly sensitive and specific recording method that uses intramuscular wire electrodes. On the other hand, it is somewhat invasive, and there is room for improvement. The mylohyoid muscle sites for eliciting MEPs during swallowing assessments can be accurately determined by combining stable MEP and NBS mapping. Present result confirmed right side dominant laterization and bilateral facilitation after neuromodulations in the swallowing motor cortex mylohyoid muscle, only in RMT but not in latencies and amplitudes in comparison with previous research (Tang et al., 2022). Different stimulus configurations in the present study may affect the difference. In this regard, bilateral mylohyoid MEP facilitation after left side motor cortical QBS5 conditioning provides further important questions for swallowing neurophysiology and non-invasive neuromodulations. Original QPS5 induces LTP-like plasticity effects in the contralateral motor cortex in the healthy subjects (Tsutsumi et al., 2014). For further exploration, because the mylohyoid MEPs recorded in this study were less specific due to the compound muscle action potentials of the genio-mylo-dygastric-hyoideus muscles regions, and simultaneous bilateral-multi-muscle targeted recording is an issue for further investigation.

4.2. RMT and amplitude of bilateral mylohyoid-MEPs after left motor cortical QBS5 conditioning as surrogate quantitative biomarkers for swallowing dysfunction after ICH

Single-pulse TMS of the hand motor cortex induces 2-ms periodical descending volleys, resulting in temporal summation that generates cortico-muscular MEPs under healthy conditions (Amassian et al., 1990; Di Lazzaro et al., 2003). This is not always guaranteed in patients with motor paresis. In fact, MEP induction rates after single-pulse stimulation are considerably reduced in patients with severe motor paresis (Rogiæ et al., 2014). This is because configurations of corticospinal D and I wave descending volleys that generate cortico-muscular MEPs after a single TMS pulse are easily affected by various pathological conditions, resulting in failure of temporal summation at spinal motor neurons (Amassian et al., 1990; Di Lazzaro et al., 2003). In addition, it is unclear whether descending volleys occur at the same cycle from the cerebral cortex to the spinal nerve nuclei involved in human swallowing function. Moreover, swallowing movements are established by the integrated function of many neural regions. The primary motor cortex is involved in the induction of swallowing; the supplementary motor cortex is involved in the inhibition of swallowing movements; the cingulate gyrus is involved in the initiation of voluntary swallowing, and the sensory cortex is involved in the somatosensation of the pharyngeo-larynx in the swallowing reflex. Furthermore, the insula acts in coordination with the cortex and solitary bundle nucleus, the cerebellum contributes to regulation of areas in the primary motor cortex and other regions, and the basal ganglia play a role in the elicitation and regulation of swallowing via thalamocortical association areas (Hamdy et al., 1999; Mosier and Bereznaya, 2001). Therefore, the mylohyoid-MEP reflects only a portion of cortico-lingual muscle group function (i.e., the early voluntary motor phase of all swallowing), which may not be the most important factor to consider in assessments of swallowing function. Nevertheless, it is noteworthy that left side motor cortical QBS5 conditioning elicit 380–390% of the bilateral control MEP amplitude at significantly lower stimulus intensities. Furthermore, there were significant correlations between the mylohyoid-MEPs after left motor cortical QBS5 conditioning and MWST scores. These correlations were higher for amplitude than for RMTs, and linear correlations were observed for mylohyoid-MEPs after QBS5 alone. Although these correlations were relatively weak, they are clearly compatible with previous QTS results for FDI-MEPs (Fujiki et al., 2022). Mylohyoid MEP facilitations after QBS5 conditioning and QTS amplification for FDI MEP relies on fundamentally different neuromodulations, this supports the hypothesis that presynaptic projections to pyramidal cells in the swallowing-related hyoid muscle group are less frequent than in the hand muscles and therefore less accessible to transsynaptic stimulation (Guggisberg et al., 2001). In contrast, it is important to note that bilateral mylohyoid MEP facilitation after left side motor cortical QBS5 conditioning attenuates according to the severity grade of swallowing dysfunction. Exploration of corticospinal and corticobulbar tract excitability using QBS5 neuromodulation will contribute to our understanding of the mechanisms underlying stroke and subsequent pathophysiological changes.

4.3. Limitations and future work

The current findings suggest that QBS5 conditioned-mylohyoid MEP assessments represent a reliable, non-invasive method for quantifying swallowing dysfunction. However, this study

has several limitations. First, present study recruited only patients with ICH, which comprise a lower proportion of stroke patients compared to cerebral infarction. This is because for the purpose that all participants only exhibited targeted motor paresis and swallowing dysfunction with small volume so that morphologically cerebral cortical intact, which was therefore favorable for motor function-oriented MEP studies. Accordingly, comparison between ICH and ischemic stroke patients with same degree of swallowing dysfunction may provide useful information about neurophysiological and pathopysiological mechanisms and/or understanding of swallowing dysfunction. Second, the mylohyoid-MEP reflects only a portion of cortico-lingual muscle group function (i.e., the early voluntary motor phase of all swallowing), and this may not be representative of total swallowing function. Careful interpretation is required given that QBS5 conditioned-mylohyoid MEP parameters may differ from corticospinal FDI and MWST scores, which are both non-linear (Macrae et al., 2014). Furthermore, QBS5; fundamentally different paradigm from original QPS5, to address potential safety issues, additional studies are required to determine the precise relationships of neurobehavioral features with the results of electrophysiological, morphological, and molecular-level assessments. Language mapping (Rogiæ et al., 2014; Honda et al., 2021) or neuromodulation-oriented therapeutics (Carmel et al., 2010; Müller-Dahlhaus and Vlachos, 2013) using the QBS5 paradigm may also be possible.

5. Conclusion

The current results suggest that left motor cortical QBS5 conditioning strongly facilitates bilateral mylohyoid MEPs both in controls and patients with dysphagia. Our analysis also indicated that MWST scores were significantly correlated with RMTs and amplitudes for mylohyoid-MEPs after conditioning, suggesting that these two parameters can be used as surrogate quantitative biomarkers in the assessment of swallowing function.

Data availability statement

The original contributions presented in this study are included in the article/supplementary material, further inquiries can be directed to the corresponding author.

Ethics statement

The studies involving human participants were reviewed and approved by the Ethics Committee of the School of Medicine at Oita University. The patients/participants provided their written informed consent to participate in this study.

Author contributions

MF and NH designed the research paradigm. MF and HF analyzed the data. MF, NH, WM, and HF wrote the manuscript. All authors performed the research and contributed to the article and approved the submitted version.

Funding

This work was supported by a medical research grant on traffic accidents by the General Insurance Association of Japan (MF) and a grant from the Ministry of Education, Culture, Sports, Science and Technology (MF, YK, and HF).

Acknowledgments

We thank Dr. Kenji Sugita for his helpful technical support.

Conflict of interest

The authors declare that the research was conducted in the absence of any commercial or financial relationships that could be construed as a potential conflict of interest.

Publisher's note

All claims expressed in this article are solely those of the authors and do not necessarily represent those of their affiliated organizations, or those of the publisher, the editors and the reviewers. Any product that may be evaluated in this article, or claim that may be made by its manufacturer, is not guaranteed or endorsed by the publisher.

References

Amassian, V. E., Anziska, B. J., Cracco, J. B., Cracco, R. Q., and Maccabee, P. J. (1987). Focal magnetic excitation of the frontal cortex activates laryngeal muscles in man. *Proc. Physiol. Soc.* 41.

Amassian, V. E., Quirk, G. J., and Stewart, M. (1990). A comparison of corticospinal activation by the magnetic coil and electrical stimulation of monkey motor cortex. *Electroencephalogr. Clin. Neurophysiol.* 77, 390–401. doi: 10.1016/0168-5597(90)90061-H

Carmel, J. B., Berrol, L. J., Brus-Ramer, M., and Martin, J. H. (2010). Chronic electrical stimulation of the intact corticospinal system after unilateral injury restores skilled locomotor control and promotes spinal axon outgrowth. *J. Neurosci.* 30, 10918–10926. doi: 10.1523/JNEUROSCI.1435-10.2010

Di Lazzaro, V., Oliviero, A., Profice, P., Pennisi, M. A., Pilato, F., Zito, G., et al. (2003). Ketamine increases human motor cortex excitability to transcranial magnetic stimulation. *J. Physiol.* 547, 485–496. doi: 10.1113/jphysiol.2002.030486

Doeltgen, S. H., Ridding, M. C., Dalrymple-Alford, J., and Huckabee, M. L. (2011). Task-dependent differences in corticobulbar excitability of the submental motor projections: Implications for neural control of swallowing. *Brain Res. Bull.* 84, 88–93. doi: 10.1016/j.brainresbull.2010.11.006

Ertekin, C., Turman, B., Tarlaci, S., Celik, M., Aydogdu, I., Secil, Y., et al. (2001). Cricopharyngeal sphincter muscle responses to transcranial magnetic stimulation in normal subjects and in patients with dysphagia. *Clin. Neurophysiol.* 112, 86–94. doi: 10.1016/s1388-2457(00)00504-6

Fujiki, M., Kuga, K., Ozaki, H., Kawasaki, Y., and Fudaba, H. (2021). Blockade of motor cortical long-term potentiation induction by glutamatergic dysfunction causes abnormal neurobehavior in an experimental subarachnoid hemorrhage model. *Front. Neural Circuits* 15:670189. doi: 10.3389/fncir.2021.670189

Fujiki, M., Matsushita, W., Kawasaki, Y., and Fudaba, H. (2022). Monophasic-quadripulse theta burst magnetic stimulation for motor palsy functional evaluation after intracerebral hemorrhage. *Front. Integr. Neurosci.* 16:827518. doi: 10.3389/fnint.2022.827518

Gallas, S., Moirot, P., Debono, G., Navarre, I., Denis, P., Marie, J. P., et al. (2007). Mylohyoid motor-evoked potentials relate to swallowing function after chronic stroke dysphagia. *Neurogastroenterol. Motil.* 19, 453–458. doi: 10.1111/j.1365-2982.2006.00892.x

Guggisberg, A. G., Dubach, P., Hess, C. W., Wüthrich, C., and Mathis, J. (2001). Motor evoked potentials from masseter muscle induced by transcranial magnetic stimulation of the pyramidal tract: The importance of coil orientation. *Clin. Neurophysiol.* 112, 2312–2319. doi: 10.1016/s1388-2457(01)00677-0

Hamada, M., Terao, Y., Hanajima, R., Shirota, Y., Nakatani-Enomoto, S., Furubayashi, T., et al. (2008). Bidirectional long-term motor cortical plasticity and metaplasticity induced by quadripulse transcranial magnetic stimulation. *J. Physiol.* 586, 3927–3947. doi: 10.1113/jphysiol.2008.152793

Hamdy, S., Mikulis, D. J., Crawley, A., Xue, S., Lau, H., Henry, S., et al. (1999). Cortical activation during human volitional swallowing: An event-related fMRI study. *Am. J. Physiol.* 277, G219–G225. doi: 10.1152/ajpgi.1999.277.1.G219

Hannula, H., Ylioja, S., Pertovaara, A., Korvenoja, A., Ruohonen, J., Ilmoniemi, R. J., et al. (2005). Somatotopic blocking of sensation with navigated transcranial magnetic stimulation of the primary somatosensory cortex. *Hum. Brain Mapp.* 26, 100–109. doi: 10.1002/hbm.20142

Honda, Y., Nakamura, S., Ogawa, K., Yoshino, R., Tobler, P. N., Nishimura, Y., et al. (2021). Changes in beta and high-gamma power in resting-state electrocorticogram induced by repetitive transcranial magnetic stimulation of primary motor cortex in unanesthetized macaque monkeys. *Neurosci. Res.* 171, 41–48. doi: 10.1016/j.neures.2021.02.002

Khedr, E. M., Abo-Elfetoh, N., Ahmed, M. A., Kamel, N. F., Farook, M., and El Karn, M. F. (2008). Dysphagia and hemispheric stroke: A transcranial magnetic study. *Neurophysiol. Clin.* 38, 235–242. doi: 10.1016/j.neucli.2008.04.004

Li, S., Eshghi, M., Khan, S., Tian, Q., Joutsa, J., Ou, Y., et al. (2020). Localizing central swallowing functions by combining non-invasive brain stimulation with neuroimaging. *Brain Stimul.* 13, 1207–1210. doi: 10.1016/j.brs.2020.06.003

Macrae, P. R., Jones, R. D., and Huckabee, M. L. (2014). The effect of swallowing treatments on corticobulbar excitability: A review of transcranial magnetic stimulation induced motor evoked potentials. *J. Neurosci. Methods* 233, 89–98. doi: 10.1016/j.jneumeth.2014.06.010

Mosier, K., and Bereznaya, I. (2001). Parallel cortical networks for volitional control of swallowing in humans. *Exp. Brain Res.* 140, 280–289. doi: 10.1007/s002210100813

Müller-Dahlhaus, F., and Vlachos, A. (2013). Unraveling the cellular and molecular mechanisms of repetitive magnetic stimulation. *Front. Mol. Neurosci.* 6:50. doi: 10.3389/fnmol.2013.00050

Rogiæ, M., Deletis, V., and Fernández-Conejero, I. (2014). Inducing transient language disruptions by mapping of Broca's area with modified patterned repetitive transcranial magnetic stimulation protocol. *J. Neurosurg.* 120, 1033–1041. doi: 10.3171/2013.11.JNS13952

Rossi, S., Hallett, M., Rossini, P. M., Pascual-Leone, A., and Safety of TMS Consensus Group. (2009). Safety, ethical considerations, and application guidelines for the use of transcranial magnetic stimulation in clinical practice and research. *Clin. Neurophysiol.* 120, 2008–2039. doi: 10.1016/j.clinph.2009.08.016

Sykes, M., Matheson, N. A., Brownjohn, P. W., Tang, A. D., Rodger, J., Shemmell, J. B., et al. (2016). Differences in motor evoked potentials induced in rats by transcranial magnetic stimulation under two separate anesthetics: Implications for plasticity studies. *Front. Neural Circuits* 10:80. doi: 10.3389/fncir.2016.00080

Tang, X., Xu, M., Zhao, J., Shi, J., Zi, Y., Wu, J., et al. (2022). Effect of electro-acupuncture on lateralization of the human swallowing motor cortex excitability by navigation-transcranial magnetic stimulation-electromyography. *Front. Behav. Neurosci.* 16:808789. doi: 10.3389/fnbeh.2022.808789

Tohara, H., Saitoh, E., Mays, K. A., Kuhlemeier, K., and Palmer, J. B. (2003). Three tests for predicting aspiration without videofluorography. *Dysphagia* 18, 126–134. doi: 10.1007/s00455-002-0095-y

Tsutsumi, R., Hanajima, R., Terao, Y., Shirota, Y., Ohminami, S., Shimizu, T., et al. (2014). Effects of the motor cortical quadripulse transcranial magnetic stimulation (QPS) on the contralateral motor cortex and interhemispheric interactions. *J. Neurophysiol.* 111, 26–35. doi: 10.1152/jn.00515.2013

frontiers | Frontiers in Neuroscience

TYPE Original Research
PUBLISHED 05 July 2023
DOI 10.3389/fnins.2023.1183670

OPEN ACCESS

EDITED BY
Mark H. Myers,
University of Tennessee Health Science Center (UTHSC), United States

REVIEWED BY
Shuang Zhang,
University of Electronic Science and Technology of China, China
Vineet Tiruvadi,
Hume AI, United States

*CORRESPONDENCE
Thomas Wahl
✉ thomas.wahl@etu.unistra.fr

RECEIVED 10 March 2023
ACCEPTED 13 June 2023
PUBLISHED 05 July 2023

CITATION
Wahl T, Riedinger J, Duprez M and Hutt A (2023) Delayed closed-loop neurostimulation for the treatment of pathological brain rhythms in mental disorders: a computational study. *Front. Neurosci.* 17:1183670. doi: 10.3389/fnins.2023.1183670

Delayed closed-loop neurostimulation for the treatment of pathological brain rhythms in mental disorders: a computational study

Thomas Wahl[1]*, Joséphine Riedinger[1,2], Michel Duprez[1] and Axel Hutt[1]

[1]ICube, MLMS, MIMESIS Team, Inria Nancy - Grand Est, University of Strasbourg, Strasbourg, France, [2]INSERM U1114, Neuropsychologie Cognitive et Physiopathologie de la Schizophrénie, Strasbourg, France

Mental disorders are among the top most demanding challenges in world-wide health. A large number of mental disorders exhibit pathological rhythms, which serve as the disorders characteristic biomarkers. These rhythms are the targets for neurostimulation techniques. Open-loop neurostimulation employs stimulation protocols, which are rather independent of the patients health and brain state in the moment of treatment. Most alternative closed-loop stimulation protocols consider real-time brain activity observations but appear as adaptive open-loop protocols, where e.g., pre-defined stimulation sets in if observations fulfil pre-defined criteria. The present theoretical work proposes a fully-adaptive closed-loop neurostimulation setup, that tunes the brain activities power spectral density (PSD) according to a user-defined PSD. The utilized brain model is non-parametric and estimated from the observations via magnitude fitting in a pre-stimulus setup phase. Moreover, the algorithm takes into account possible conduction delays in the feedback connection between observation and stimulation electrode. All involved features are illustrated on pathological α- and γ-rhythms known from psychosis. To this end, we simulate numerically a linear neural population brain model and a non-linear cortico-thalamic feedback loop model recently derived to explain brain activity in psychosis.

KEYWORDS

neurostimulation, closed-loop, control, real-time, delay, EEG

1. Introduction

Electrical neurostimulation is an old human idea, and has been a well-established therapy for mental disorders for few decades. Caius Plinius during Antiquity and Scribonius Largus, who lived in the first century AD, proposed respectively contacts with the Electric ray (Torpedo Fish) for the treatment of post-partum pain and severe headaches. In the 19th century, electrical stimulation was commonly prescribed by neurologists for nervous disease (Edel and Caroli, 1987). Today, various electrical stimulation techniques exist to modulate neuronal systems and novel techniques for an optimal clinical treatment of a specific pathology gain more and more attention (Sun and Morrell, 2014; Chen et al., 2022). They could be used as an additional therapeutic lever or as an alternative to pharmacological medication, thus representing a hope for pharmaco-resistant forms of disease.

Brain oscillations result from coordinated electrical neuronal tissues activity within and between structures and networks. Implicated in various neural processes, such as perception, attention and cognition, their disruption yields pathological rhythms, which reflect abnormal activity of the implicated brain network, notably at the cellular and molecular level (Basar, 2013). These pathological rhythms serve as good biomarkers for neuropathologies. For instance, neurophysiological studies have revealed that a large number of mental disorders exhibit pathological rhythms, which do not occur in healthy patients (Schulman et al., 2011). Neurostimulation techniques have identified such pathological rhythms as good stimulation targets for the treatment of brain oscillatory disorders. Neurostimulation induces electric currents in neuronal tissue. Depending on the stimulation protocol, i.e. the temporal stimulation current shape, its duration and pause and the number of repetitions, neurostimulation can lead to neural plasticity effects or to pacemaker-like brain stimulation, respectively.

For example, Deep Brain Stimulation (DBS) is an invasive technique and proposed for patients suffering from severe pharmaco-resistant Parkinson's disease (PD) or obsessive-compulsive disorders. In PD patients aberrant hypersynchronicity and hyperactivity in the β-frequency band (12–30 Hz) of the basal ganglia-thalamocortical network can be addressed by the pharmacological medication (e.g. Levodopa) or DBS. The conventional DBS protocols focus on the subthalamic nucleus or globus pallidus stimulation continuously at a temporally constant frequency about 130 Hz. The suppression of the pathological beta oscillations was correlated with improving motor symptoms (Kühn et al., 2008). Recent techniques (Hosain et al., 2014; Fleming et al., 2020) propose to apply an adaptive closed-loop stimulation protocol based on observed intracranial brain activity. In addition to this intracranial neurostimulation technique, transcranial electrical stimulation (TES) and transcranial magnetic stimulation (TMS) are non-invasive neuromodulation approaches in which, respectively, a low electrical current and a magnetic field are applied to the cortical tissues. The TES current modalities include direct currents (tDCS), i.e. constant currents, alternating current (tACS), i.e. typically oscillatory currents, and random noise-shape currents (tRNS), which typically includes frequencies above the β-frequency band. It was shown that tDCS can improve cognitive performance in healthy subjects (Brunelin et al., 2012) and patients (Stagg et al., 2018) and it is applied as a therapeutic means to target brain network dysfunctions, such as Attention-Deficit/Hyperactivity Disorder (Nejati et al., 2020) and major depressive disorder (Bennabi and Haffen, 2018).

Although the neurostimulation techniques mentioned above may permit to alleviate mental disorder patients from symptoms, the success rate of these treatments is still limited (Nasr et al., 2022). This underperformance results from non-optimal choices of the stimulation protocol originating from the lack of understanding of the underlying neural response to stimulations and the non-patient specific stimulation protocol. In other words, typically the stimulation protocol (including size, duration, repetition cycle of the stimulation signal) is open-loop, i.e. pre-defined by the clinician based on heuristic criteria before the stimulation starts (Paulus, 2011). This non-optimal approach is inferior to so-called closed-loop techniques, which automatically adapt to the patients current brain/health state. Such an adaptive, or closed-loop, approach has been introduced for intracranial (Hartshorn and Jobst, 2018; Prosky et al., 2021; Stanslaski et al., 2022) and transcranial stimulation (Tervo et al., 2022) and has been shown to improve neurostimulation in major depression patients (Scangos et al., 2021), epilepsy (Haeusermann et al., 2023) and affective and anxiety disorders (Guerrero Moreno et al., 2021). These proposed closed-loop methods are adaptive in the sense that a pre-defined stimulation signal is applied when observed brain activity fulfills certain criteria, such as passing an amplitude or power threshold. While this adaptive approach improves existing open-loop methods, the pre-defined stimulation signal may still be non-optimally chosen. Recently proposed methods produce better results by using reference signal tracking control schemes such as proportional integral (PI) controller (Westover et al., 2015; Bolus et al., 2018; Su et al., 2019; Zhu et al., 2021), linear quadratic regulator (LQR) (Yang et al., 2018, 2019; Bolus et al., 2021) or model predictive control (MPC) (Fang and Yang, 2022, 2023) which uses an LQR in a MPC framework. However this form of control requires to pre-define a reference signal which is often non-trivial to provide in a patient specific manner. Furthermore, because of the stochastic nature of brain signals, forcing the resting state signal to follow a reference signal with its own independent noise creates an unnecessary constraint for the stimulation signal when we only want to regulate the power in given frequency bands.

We propose to estimate a stimulation signal on the basis of observed brain activity without the need to track a reference signal. The target stimulation signal is computed directly via a linear controller synthesized using a user-defined filter that encodes the desired frequency-domain modifications. We argue that it is the natural choice for a closed-loop optimization in the presence of pathological rhythms: typically the pathology is identified by an abnormal power in a certain frequency band and the closed-loop control aims to modify this power value in such a way that the final brain activity power spectral distribution resembles the distribution of a healthy subject. Examples are pathological too strong β-rhythm magnitudes in Parkinson's disease (Martin et al., 2018) and too weak α-rhythm (Howells et al., 2018) and too strong γ-rhythm in schizophrenia (Y et al., 2015). This approach implies the hypothesis that modifying the observed pathological brain rhythms of a patient to resemble brain rhythms of a healthy subject renders the patients brain state and improves the patients health situation. This assumption was motivated by the impressive improving impact of DBS in psychiatric disorders (Holtzheimer and Mayberg, 2011).

Technically, the proposed method aims to reshape the spectral distribution of observed data, such as electroencephalographic data (EEG). For illustration, we consider pathological brain rhythms observed in psychosis in the α- (Howells et al., 2018) and γ-band (Leicht et al., 2015). Our method relies on the extraction and the filtering in real-time of the brain resting state activity signal, using the EEG and an estimated brain response model. The underlying brain model is fully non-parametric and estimated from observed resting state EEG. Moreover, we consider the fact that the closed-loop feedback exhibits a certain conduction delay between measurement and stimulation. This conduction

delay results from the transmission delay in the hardware and the numerical computation time of the stimulation signal. Very first estimates of this delay time are in the range of few tens of milliseconds (Private communication, Isope, 2020), i.e. in the range of EEG signal time scales. Consequently, the present feedback delay in real-world systems may affect the methods performance. Fang and Yang (2022) presents a method to increase the robustness of an adaptive closed-loop controller against delay by reducing the sensitivity of the closed-loop to high frequency disturbances. However, while this decreases generally the error in the closed-loop output, this also prevents to apply the control signal specifically to high frequency ranges like the γ-range. To our best knowledge, the present study is the first providing a method to effectively compensate the frequency-domain errors created by the feedback delay in closed-loop neurostimulation systems without sacrificing the controllability of high frequency ranges.

The remaining article is organized as follows: Section 2 presents the neurostimulation setup and the closed-loop circuit studied in the rest of this paper. Then, we propose a model-based controller design to apply desired modifications to the observed activity signal. Subsequently, we propose a model estimation method to extract the brain input response model needed for the controller design. Later, we address the problem of the closed-loop delay by designing an additional system to approximate the future values of the observations. Finally, we present two brain models, which illustrate and validate the proposed method. Then, Section 3 presents the simulation results of our circuits, including the accuracy of the model estimation step and the delay compensation. Lastly, in Section 4, we discuss the results of the method presented in the paper compared to the state of the art, mention limitations and pinpoint some perspectives and possible experimental tests.

2. Materials and methods

2.1. Simulated neurostimulation

We build a theoretical plant as a circuit containing a stimulation element and an observation element, both connected to the model brain system under study. In real practice, the stimulation element corresponds to the neurostimulation device, such as a TES system or a TMS coil. In contrast, the observation element may represent electro-/magneto-encephalographic electrodes (in the following called EEG) or electrodes observing Local Field Potential. We define the time-dependent functions $u : \mathbb{R} \to \mathbb{R}$ and $y : \mathbb{R} \to \mathbb{R}$ as the input stimulation current and the output EEG signal, respectively.

If no input current is applied, the output is a non-zero stochastic signal y_0 corresponding to the measured resting state EEG activity and a non-zero neurostimulation current alters the output signal as a linear response. This alteration is caused by a change in the brain activity in response to the neurostimulation input and a direct measurement of the input current. The latter is undesirable as it is not correlated with brain dynamics but only with neurostimulation and measurement devices. In the following, we assume that observations include brain dynamics correlated output only while direct current measurements are filtered out. A method to remove the direct current measurement from the EEG signal is discussed in Section 4.

Then, we define the plant $\mathcal{P}$ as the system that takes u as its input and generates an output y which is equal to y_0 when no input is applied. By modeling the dynamics of $\mathcal{P}$, our goal is a neurostimulation signal u that causes predetermined changes in the spectral power amplitude of the output signal y. In our case, the goal is to increase the activity in the alpha band ($8-12$ Hz) and decrease the activity in the gamma band ($25-55$ Hz) motivated by aberrant power spectrum magnitudes in schizophrenia (Howells et al., 2018; Martin et al., 2018). A possible experimental setup involving our method is sketched in Figure 1A.

2.2. Linear time invariant model

We assume that the observed output response to a small neurostimulation input u is linear and time-invariant (LTI). This assumption is supported by multiple results across literature (Popivanov et al., 1996; Liu et al., 2010; Kim and Ching, 2016). Thus, there is an underlying LTI system $\mathcal{G}$ that produces an output y_u for any given input u. For this system, we can define a function $g : \mathbb{R} \to \mathbb{R}$, which is the output produced by the plant input response system $\mathcal{G}$ in response to a unit impulse signal $\delta(t)$ where $t \in \mathbb{R}$ is the time elapsed since the start of the signal. This function g is also called the unit impulse response of $\mathcal{G}$ and we have

$$y_u(t) = g(t) * u(t) := \int_{-\infty}^{+\infty} g(t')u(t-t')dt'.$$

with time t and $*$ denotes the convolution over time. It leads to the total plant output

$$y(t) = y_0(t) + y_u(t) = y_0(t) + g(t) * u(t). \quad (1)$$

With this choice of model, the contribution of the neurostimulation response to the total output is purely additive, allowing us to focus the analysis on $\mathcal{G}$, which represents the neurostimulation response part of the plant system. We also see that y_0, the resting state activity, contains the stochastic part of the output, while y_u can be predicted for any known input signal u if we have a model for the system $\mathcal{G}$. A method to estimate the plant input response model $\mathcal{G}$ is presented in Section 2.4.

2.3. Closed-loop control

In this section, we suppose that the function g is known. The estimation of g will be the aim of Section 2.4.

To close the loop, we generate the plant input signal u as the output of a linear controller $\mathcal{K}$ in response to the plant output y

$$u(t) = k(t) * y(t),$$

where $k : \mathbb{R} \to \mathbb{R}$ is the unit impulse response of the controller $\mathcal{K}$. We can now rewrite Eq. (1) as

$$y(t) = y_0(t) + g(t) * k(t) * y(t). \quad (2)$$

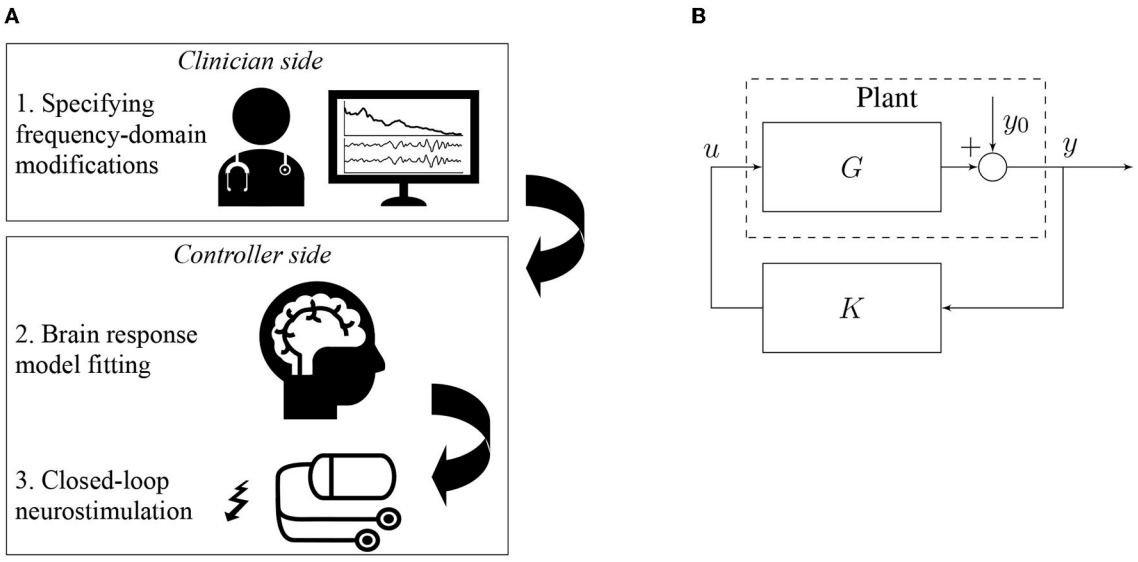

FIGURE 1
Closed-loop neurostimulation setup. **(A)** The different steps of our method in a possible experimental setup. First, the clinician specifies the desired frequency domain modifications to apply e.g. increase α-activity and decrease γ-activity. Second, the brain input response model is fitted to the measured EEG signal in order to match as closely as possible the current brain dynamics of the patient. Finally, the clinician's specifications and the fitted model are used to synthesize the closed-loop controller $\mathcal{K}$ that is directly used for closed-loop neurostimulation. **(B)** The controller directly produces the stimulation signal u in function of the measured total brain output y in real-time.

Here, we assume that no delay between observation and stimulation application is present. We will relax this condition in Section 2.5. To solve Eq. (2), we apply the Laplace transform defined for each time-dependent function $x : \mathbb{R} \to \mathbb{R}$ by

$$X(s) = \mathcal{L}\{x(t)\}(s) := \int_{0^-}^{+\infty} x(t)e^{-st}dt, \tag{3}$$

Thus, we define $Y : \mathbb{C} \to \mathbb{C}$, $Y_0 : \mathbb{C} \to \mathbb{C}$, $G : \mathbb{C} \to \mathbb{C}$ and $K : \mathbb{C} \to \mathbb{C}$ as the Laplace transforms of respectively y, y_0, g and k, allowing us to write Eq. (2) as

$$Y(s) = Y_0(s) + G(s)K(s)Y(s).$$

Hence

$$Y(s) = \frac{1}{1 - G(s)K(s)} Y_0(s). \tag{4}$$

We now have an equation for the closed-loop output in function of the resting state activity. A block diagram of the closed-loop circuit is shown in Figure 1B.

Hence to design the frequency distribution of y we tune the frequency distribution of the transfer function K of the controller $\mathcal{K}$.

2.3.1. Controller synthesis

Our closed-loop setup aims to tune the observation power spectrum, or equivalently, the choice of $Y(s)$ subjected to the resting state $Y_0(s)$. To this end, we define a linear filter $\mathcal{H}$ with transfer function $H : \mathbb{C} \to \mathbb{C}$ and

$$Y(s) = Y_0(s) + H(s)Y_0(s). \tag{5}$$

Specifically, we intend to restore the physiological state of the brain, e.g., of a schizophrenic patient as our motivation, with an observed EEG presenting low alpha activity and high gamma activity. The chosen filter $\mathcal{H}$ is a weighted double bandpass filter with positive weight in the α-frequency band to increase α-power and negative weights in the γ-band to decrease the systems γ-activity. The filter's transfer function is defined as

$$H(s) = c_1 \frac{2\pi B_1 s}{s^2 + 2\pi B_1 s + (2\pi f_1)^2} + c_2 \frac{2\pi B_2 s}{s^2 + 2\pi B_2 s + (2\pi f_2)^2}.$$

The exact parameters of $\mathcal{H}$ are shown in Table 1.

We can synthesize the closed-loop controller $\mathcal{K}$, by combining equations (4) and (5) and solving for K as

$$\begin{aligned} \frac{1}{1 - G(s)K(s)} Y_0(s) &= Y_0(s) + H(s)Y_0(s) \\ K(s) &= \frac{H(s)}{(1 + H(s))G(s)}. \end{aligned} \tag{6}$$

Therefore, if we know the plant input response transfer function G, we can find that desired controller transfer function K by Eq. (6). Once the transfer function is obtained, we can use it to find a corresponding state-space representation (Hespanha, 2018) for time domain simulations. The state-space system's ordinary differential equations can then be implemented by any device that can measure the brain activity and produce a custom neurostimulation signal in real-time.

TABLE 1 Parameter set of the filter $\mathcal{H}$.

Parameter	Description	Value
f_1	α-band natural frequency	10ms
B_1	α-band width	4Hz
c_1	α-band weight	1.0
f_2	γ-band natural frequency	40ms
B_2	γ-band width	30Hz
c_2	γ-band weight	-0.5

The frequency parameters are chosen based on the alpha frequency range (8–12Hz) and the gamma frequency range (25–55 Hz) in an EEG. The weighting parameters c_1 and c_2, respectively positive and negative, corresponding to the choice to increase the alpha activity and decrease the gamma activity.

2.4. Model estimation

The design of our closed-loop controller requires estimating the plant input response system $\mathcal{G}$, which in practice includes the brain dynamics, the neurostimulation device and the observation device. Our approach includes the estimation of $\mathcal{G}$ directly from observed brain activity, such as EEG of the patient. This ensure that the estimated plant model will be as close as possible to the real brain dynamics in the corresponding experimental conditions. To this end, we first need to find a way to measure the plant input response without also measuring the plant resting state activity. This is not trivial since the observed signal is the sum of the resting state activity and the stimulation response.

2.4.1. Signal extraction

Let us consider an open-loop setup with an arbitrary input u applied to the plant, which generates the output described by Eq. (1). In this equation, we only know u and y, and want to estimate the impulse response g. The problem is that we cannot observe y_0 only during the stimulation. Hence, based on previous data recordings, we need to find a way to predict the dynamics of y_0 during the stimulation.

First, we provide the following standard definitions that are important in the subsequent discussion. For any time domain signal $x : \mathbb{R} \to \mathbb{R}$, we denote the Fourier transform by

$$\hat{x}(f) = \mathcal{F}\{x(t)\}(f) := \int_{-\infty}^{\infty} x(t) e^{-2\pi i f t} dt. \tag{7}$$

We define $\alpha_0 : \mathbb{R} \to \mathbb{R}$ and $\alpha_u : \mathbb{R} \to \mathbb{R}$ such as $\alpha_0(t) = y_0(t) - \bar{y}_0$ and $\alpha_u(t) = y_u(t) - \bar{y}_u$ where $\bar{y}$, $\bar{y}_0$ and $\bar{y}_u$ are respectively the ensemble means of y, y_0 and y_u.

We assume that y_0 is a wide-sense-stationary (WSS) random process, i.e. its mean and variance do not depend on time. According to the Wiener-Khinchin theorem (Khintchine, 1934; Gardiner, 2004), the autocorrelation function of a wide-sense-stationary random process has a spectral decomposition given by the power spectrum of that process

$$S_{yy}(f) = |\hat{\alpha}(f)|^2,$$

where $\hat{\alpha} : \mathbb{R} \to \mathbb{C}$ is the Fourier transform of $\alpha(t) = y(t) - \bar{y} \in \mathbb{R}$ and $S_{yy} : \mathbb{R} \to \mathbb{R}^+$ is the spectral density of y.

Then, we can write Eq. (1) as

$$\bar{y} + \alpha(t) = \bar{y}_0 + \alpha_0(t) + \bar{y}_u + \alpha_u(t),$$

where $\bar{y} = \bar{y}_0 + \bar{y}_u$. The equation then simplifies to

$$\alpha(t) = \alpha_0(t) + \alpha_u(t).$$

By application of the Fourier transform, we obtain

$$\hat{\alpha}(f) = \hat{\alpha}_0(f) + \hat{\alpha}_u(f)$$

and

$$|\hat{\alpha}(f)|^2 = |\hat{\alpha}_0(f)|^2 + |\hat{\alpha}_u(f)|^2 + 2\mathrm{Re}[\hat{\alpha}_0(f)\hat{\alpha}_u(f)^*].$$

In the following, we compute the ensemble average of each term of this equation. Since α and α_u are two independent processes sampled at different times and $\langle\hat{\alpha}_0\rangle = \langle\hat{\alpha}_u\rangle = 0$.

Hence

$$\langle 2\mathrm{Re}(\hat{\alpha}_0(f)\hat{\alpha}_u(f)^*)\rangle = 2\mathrm{Re}[\langle\hat{\alpha}_0(f)\hat{\alpha}_u(f)^*\rangle] = 0.$$

Here and in the following, $\langle\cdot\rangle$ denotes the ensemble average. We point out that although Eq. (8) does hold when considering the ensemble average of the signals, fluctuations around 0 still remain in Eq. (8) for finite ensemble number of finite time signals.

We define the amplitude ratio (AR) as

$$\mathrm{AR} = \left\langle \frac{|\hat{a}(f)|^2}{|\hat{a}_0(f)|^2} \right\rangle, \tag{8}$$

which quantifies the gain of amplitude between the resting-state output and the stimulated output. The fluctuations mentioned above can also be reduced by increasing the input current which will lead to a higher AR and therefore, a higher contribution to the total signal of the $\hat{a}_u$ term (which is known) compared to the other terms.

Nevertheless, this yields

$$\langle|\hat{\alpha}_u(f)|^2\rangle = \langle|\hat{\alpha}(f)|^2\rangle - \langle|\hat{\alpha}_0(f)|^2\rangle. \tag{9}$$

Using Eq. (1), we can express $\hat{\alpha}_u$ in terms of the input impulse response g and the input u

$$\begin{aligned} \hat{\alpha}_u(f) &= \mathcal{F}\{y_u(t) - \bar{y}_u\}(f) \\ &= \mathcal{F}\{g(t) * [u(t) - \bar{u}]\}(f) \\ &= \hat{g}(f)\mathcal{F}\{u(t) - \bar{u}\}(f)\,. \end{aligned} \tag{10}$$

This equation permits to estimate the transfer function $\hat{g}$, see Section 3.

To express the transfer function $\hat{g}$ in Laplace space, we use the fact that a unit impulse response function is non-zero only for positive time values t. Hence, based on equations (3) and (7), for $s = 2\pi i f$, we can write the Laplace transform G as

$$G(2\pi i f) = \int_{0^-}^{+\infty} g(t) e^{-2\pi i f t} dt = \int_{-\infty}^{+\infty} g(t) e^{-2\pi i f t} dt = \hat{g}(f),$$

where the unit impulse response function g directly relates the output y to the resting-state output y_0 and the stimulation signal u, cf. Eq. (1).

We now need a method to generate a LTI system with a transfer function that matches the magnitude data computed with the formula. This is achieved by the magnitude vector fitting algorithm.

2.4.2. Magnitude vector fitting

Our goal is now to find a transfer function G corresponding the magnitude data $|\hat{g}(f)|^2$. For this purpose, we use a variant of the vector fitting algorithm design to work even with only the magnitude data. This method is called magnitude vector fitting (De Tommasi et al., 2010).

It allows to fit a passive LTI system to data by fitting the model transfer function. The system is synthesized such that the mean square error between the magnitude data sample and the transfer function evaluated at the same frequency points is minimized. De Tommasi et al. (2010) show that the transfer function of the fitted model reproduces both the magnitude and the phase shift of the original transfer function, although the fitting has been performed using sampled magnitude data only.

By minimizing the mean square error, the algorithm ensures that the transfer function of the fitted model accurately matches the original model as represented by the reconstructed gain data. Furthermore, to assess the accuracy of the reconstruction, we also compare the fitted model to the transfer function of the linearized brain model used for the simulation. This allows to double-check the validity of the reconstructed magnitude and also to verify if the reconstructed phase fits the phase of the original model as closely as possible (cf. Figures 3C, D).

We define the root-mean-square error (RMSE) as

$$\mathrm{RMSE} = \sqrt{\left\langle \left| \frac{\tilde{G}(2\pi if) - G(2\pi if)}{G(2\pi if)} \right|^2 \right\rangle}, \tag{11}$$

where $\tilde{G}$ is the fitted model's transfer function, G is the original model's transfer function and $f \in \mathbb{R}^+$ are the frequency points used for the fitting. This allows to quantify the accuracy of the fitting step.

2.5. Delay compensation

Realistic feedback loops exhibit conduction delays between the moment of observation and feedback stimulation. Reasons for such delays are finite conduction speeds in cables, electronic switches, interfaces and delays caused by the controller device to compute numerically adapted stimuli. In systems with large time scales, such as controlled mechanical devices on the centimeter or larger scale, such delays may be negligible. Conversely biological systems such as the brain evolve on a millisecond scale and conduction delays may play an important role. Preliminary estimation of input and output devices of desktop computers have revealed an approximate delay of $\sim$ 10ms. By virtue of such delays, it is important to take them into account in the closed-loop between the moment of observation and stimulation.

The different sources of delay can be represented as plant input and output delays. Since the controller $\mathcal{K}$ is LTI, the input and output delays can be concatenated into one single plant input delay. Hence, in our setup, we model the delay as an input delay τ in the system $\mathcal{G}$, modifying $y(t) = g(t) * u(t)$ in Eq. (1) to $y(t) = g(t) * u(t - \tau)$. The Smith predictor (Smith, 1959; Morari and Zafiriou, 1989) is a known method to compensate such delay times. However, in the present problem, this approach allows controlling a limited frequency band only (Figures 7A, B). Consequently, it was necessary to invent another method. Since the plant input u is generated by the controller $\mathcal{K}$, we modify the controller to compensate the delay. To this end, the new controller $\mathcal{K}$ is chosen to estimate the future value of u instead of the present value. The new proposed method to apply this controller modification is presented in the Results Section 3.2.

2.6. Comparison to the state of the art

Our method is tested against two main control schemes commonly used in adaptive closed-loop neurostimulation. These control schemes are closed-loop control with a PI controller (Westover et al., 2015; Bolus et al., 2018; Su et al., 2019; Zhu et al., 2021) and Linear Quadratic Gaussian (LQG) control (Yang et al., 2018, 2019; Bolus et al., 2021) which refers to the combination of a Linear Quadratic Estimator (LQE) (or Kalman filter) with a Linear Quadratic Regulator (LQR) (Åström, 2012). For both these methods, the tracked reference signal is generated from pre-recorded pathological resting state activities to which we apply a filter restoring the target α- and γ-activities. In order to prevent closed-loop destabilization and regulate high frequency disturbances, a Smith predictor (Smith, 1959) is used for the PI and LQG controller to compensate the delay, while we use our own delay compensation method for our controller.

2.7. Brain models

Our closed-loop control method works for any LTI brain model. Furthermore, we want to show that it also produces good results on non-linear brain models, for which the neurostimulation input response behaves closely to an LTI system, when the input is sufficiently small. To this end, we present two models used to test our method. The first one is a linear neural population model of cortical activity, and the second one is a non-linear cortico-thalamic neural population model with cortico-thalamic delay.

2.7.1. Linear brain model

We describe neural population activity with a noise-driven linear model (Hutt, 2013). The model is composed of two pairs of interacting excitatory and inhibitory populations. Here we have $V_{e,i}^{(1,2)} : \mathbb{R} \to \mathbb{R}$, representing the mean activity of the associated population, where $V_e^{(1,2)}$ and $V_i^{(1,2)}$ correspond respectively to excitatory and inhibitory populations. Each population is driven by

TABLE 2 Parameter set of model (12).

Parameter	Description	Value
$\tau_{e,1,2}$	exc. synaptic time constant	5ms
$\tau_{i,1,2}$	inhib. synaptic time constant	20ms
N_{11}	first exc. linear coefficient	1.15
N_{21}	first inhib. linear coefficient	0.63
N_{12}	second exc. linear coefficient	2.52
N_{22}	second inhib. linear coefficient	6.6
N	number of neurons	1000
$\kappa_{1,2}^2$	noises variances (pathological)	$10^{-4}/N$
$(\kappa_1')^2$	first noise variance (healthy)	$3.6 \cdot 10^{-4}/N$
$(\kappa_2')^2$	second noise variance (healthy)	$2.5 \cdot 10^{-5}/N$
$b_{1,2}$	input coupling constants	0.18
$b_{3,4}$	input coupling constants	0.14

The choice of parameter is partially based on the paper in which it was developed (see Hutt, 2013). The difference between the healthy and pathological state is modeled by changes in the amplitude of the finite size fluctuations of each population.

noise $\xi_{1,2} : \mathbb{R} \to \mathbb{R}$ and the external input $u : \mathbb{R} \to \mathbb{R}$, according to the following differential equations:

$$\begin{cases} \tau_{e,1} \frac{dV_e^{(1)}(t)}{dt} &= (-1 + N_{11}) V_e^{(1)}(t) - N_{11} V_i^{(1)}(t) + b_1 u(t) + \xi_1(t), \\ \tau_{i,1} \frac{dV_i^{(1)}(t)}{dt} &= N_{21} V_e^{(1)}(t) + (-1 - N_{21}) V_i^{(1)}(t) + b_2 u(t), \\ \tau_{e,2} \frac{dV_e^{(2)}(t)}{dt} &= (-1 + N_{12}) V_e^{(2)}(t) - N_{12} V_i^{(2)}(t) + b_3 u(t) + \xi_2(t), \\ \tau_{i,2} \frac{dV_i^{(2)}(t)}{dt} &= N_{22} V_e^{(2)}(t) + (-1 - N_{22}) V_i^{(2)}(t) + b_4 u(t), \end{cases} \tag{12}$$

where the noise $\xi_{1,2}$ is uncorrelated Gaussian distributed with zero mean and variance $\kappa_{1,2}^2 = 10^{-7}$, and the stimulation u is weighted by the coupling constants $b_i > 0$ of the corresponding population. In addition, $\tau_{(e,i),(1,2)}$ are the synaptic time constants of the populations, and constants $N_{ij} > 0$ are interaction gains of the respective population. Table 2 provides the parameters employed in subsequent simulations.

The observed output

$$y(t) = V_e^{(1)}(t) - V_i^{(1)}(t) + V_e^{(2)}(t) - V_i^{(2)}(t)$$

is a sum of the effective field potential $V_e^{(j)} - V_i^{(j)}$ of both populations $j = 1, 2$, (cf. Figure 2A).

The simulation of the linear brain model in time domain is done using the library control of python. The numerical integration is computed thanks to matrix exponential (Van Loan, 1978), with a simulation sampling time of 1ms. The resting state activity of the linear brain model in shown in Figure 2A.

2.7.2. Cortico-thalamic brain model

A different model considers the cortico-thalamic feedback circuit (Riedinger and Hutt, 2022). It describes the cortex layers I-III and the cortico-thalamic loop between cortical layers IV-VI, the thalamic relay cell population and the reticular structure. The cortical layer I-III exhibits mean activity of excitatory cells v and inhibitory cells w. Similarly, layer IV-VIs exhibits the mean activity V_e and V_i and thalamic relay cell populations the mean activity $V_{th,e}$ and $V_{th,i}$. Moreover, the reticular structure has the mean activity V_{ret}. The fibers between the cortex and thalamus and the cortex and reticular structure exhibit a finite conduction delay τ (Hashemi et al., 2015; Riedinger and Hutt, 2022). The 7-dimensional dynamical system of the brain state $\mathbf{x} = (v, w, V_e, V_i, V_{th,e}, V_{th,i}, V_{ret}) \in \mathbb{R}^7$ obeys

$$\begin{cases} \dot{\mathrm{x}}(t) &= \mathrm{F}(\mathrm{x}(t), \mathrm{x}(t-\tau)) + \boldsymbol{\xi}(t) + \mathrm{B}u(t), \\ y(t) &= \mathrm{C}\mathrm{x}(t), \end{cases} \tag{13}$$

where the superscript t denotes transposition, $\mathbf{F} \in \mathbb{R}^7$ is a nonlinear vector function, $\mathbf{B} \in \mathbb{R}^{7\times 1}$ is the input coupling matrix and $\mathrm{C} \in \mathbb{R}^{1\times 7}$ is the observation matrix. We mention that $\mathrm{B} = (b_1, b_2, b_3, b_4, 0, 0, 0)^t$, $b_i > 0$, i.e. only the cortical layers are stimulated with weights b_i. The observation y captures the activity of the cortical excitatory populations (Nunez and Srinivasan, 2006; Riedinger and Hutt, 2022) with $\mathrm{C} = (c_1, 0, c_3, 0, 0, 0, 0)$, $c_i > 0$. For more details, please see the Supplementary material.

The time domain simulations of the cortico-thalamic model is done by numerical integration using the fourth-order Runge-Kutta method implemented by the scipy library in python with a maximum simulation time step of 1 ms. The resting state activity of the cortico-thalamic brain model is shown in Figure 2B.

2.8. Measuring brain activity

The general activity in EEG measurement is measured by first estimating the power spectral density of the signal using frequency bins of 1 Hz and then summing all the frequency bins up to the Nyquist frequency. In practice, the sum will be mostly determined by the activity in low frequencies and more precisely, near the α- and γ-activity peaks. To measure the results of our method, we define the α- and γ-activities as the sum of 1Hz frequency bins only in their respective frequency bands, i.e., respectively 8–12 Hz and 25–55 Hz. Meanwhile, the total activity of the neurostimulation signal, that we call the mean amplitude of u is computed from 0 Hz to the Nyquist frequency.

3. Results

The present work addresses two major problems in closed-loop control: the correct model choice of the systems dynamics and the present conduction delay. The subsequent sections propose solutions for both problems and illustrate them in some detail by applying them to the linear brain activity model from Section 2.7.1. The final section demonstrates the closed feedback loop for the cortico-thalamic brain model from Section 2.7.2.

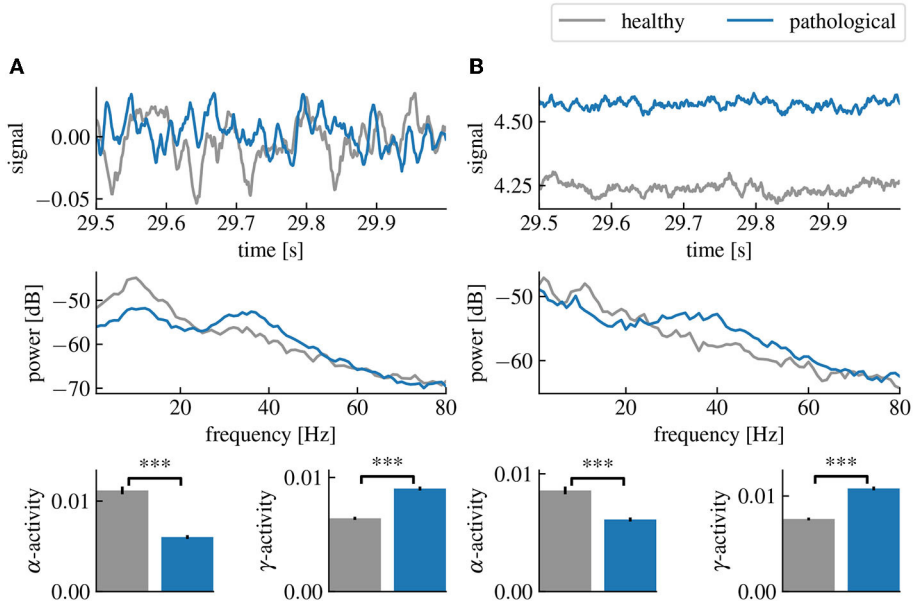

FIGURE 2
Healthy and pathological resting state activity of the linear and cortico-thalamic brain models. The pathological state is characterized by a decreased α-activity and an increased γ-activity. **(A)** Comparison of the healthy and pathological state of the linear brain model. The first row shows the last 500 ms of the simulated time series. The second row shows the power spectral densities estimated from the time series and the last row shows the estimated α- and γ-activities computed from the spectral densities and averaged over 50 simulations. **(B)** Same as **(A)** but using the cortico-thalamic brain model. "***" corresponds to a p-value less than 0.0005 using Welch's t-test.

3.1. Model estimation

Equations (9) and 10 permit to express the magnitude of $\hat{g}(f)$ in terms of the spectral densities of observable signals

$$\begin{aligned} |\hat{g}(f)|^2 |\mathcal{F}\{u(t) - \bar{u}\}(f)|^2 &= |\hat{\alpha}(f)|^2 - |\hat{\alpha}_0(f)|^2 \\ |\hat{g}(f)|^2 S_{uu}(f) &= S_{yy}(f) - S_{y_0y_0}(f) \\ |\hat{g}(f)|^2 &= \frac{S_{yy}(f) - S_{y_0y_0}(f)}{S_{uu}(f)}. \end{aligned} \tag{14}$$

The spectral density functions $S_{y_0y_0}$ and S_{yy} may be estimated numerically from output data before and during a stimulation with a known chosen stimulation function u. The estimation may be performed by applying conventional methods, such as the Welch method (Welch, 1967). These estimations provide the magnitude of the transfer function $|\hat{g}|$ by utilizing Eq. (14). In detail, at first, we considered the linear model (12) and injected a white noise current into the plant gaining the system's response signal together with the resting state activity, (cf. Figure 3A). The subsequent estimation of $S_{yy}(f)$, $S_{y_0y_0}(f)$ and $S_{uu}(f)$ (Figure 3B) from the data permitted to compute the brain input response model $\hat{g}(f)$ by Eq. (14). We observe a very good accordance of the original model response function and its estimation in magnitude (Figure 3C) and phase (Figure 3D).

3.1.1. Robustness

The remaining error in the estimated model compared to the original model depends on the amplitude ratio between the stimulated output y and the resting state output y_0, (cf. Figure 4). Low stimulation currents or high driving noise can also cause the magnitude vector fitting algorithm not to converge, leading to a non-minimal mean-square error between the fitted and the original models when evaluated at the frequency sample points used for the algorithm.

This problem can be solved by increasing the amplitude of the input current u that we inject in the plant, which decreases the contribution of the resting state driving noise ξ to the output signal relative to the input current. Although the remaining dominant input current is also noisy, its value at any time or frequency is known, meaning that it is canceled out in the ratio $\frac{S_{yy}}{S_{uu}}$ in Eq. (14). This effectively leads to lower noise in the transfer function magnitude data extracted with Eq. (14). The limitation is then set by the maximum amplitude of the current we are allowed to inject into the brain in a given neurostimulation setup. Indeed, the amplitude of the current is limited both for safety reasons that are beyond the scope of this paper and because of the assumption of linearity on which our method is based and which requires small currents. On the other hand, we can also decrease the noise in the spectral density data by increasing the stimulation time, and hence increasing the amount of data which decreases the contribution of the noise in the power spectral density estimation. Therefore, the accuracy of the model fitting step can be optimized by finding a trade-off between the maximum amplitude of the stimulation current, and the maximum duration of the stimulation.

The accuracy of the fitting is generally easily assessed by computing the root mean square error between the data and the fitted model's transfer function. In practise, this could be used as an indicator to evaluate if sufficient stimulation amplitude and time were chosen and then possibly reiterate this step with different

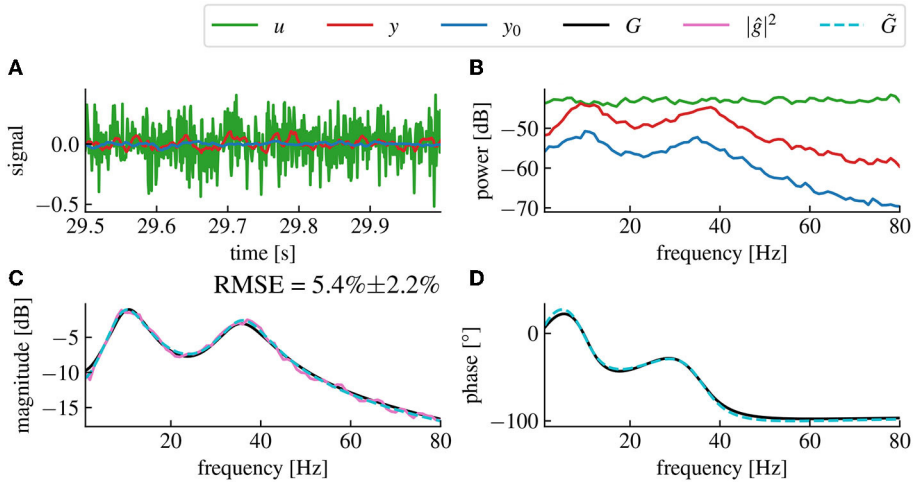

FIGURE 3
The magnitude vector fitting algorithm successfully reconstructs the transfer function G from magnitude-only data. **(A)** Time series of the resting state activity (blue), the input signal (green) and the stimulation response (red). **(B)** Spectral densities of the simulated input signal (green), the resting state activity (blue) and the stimulation response (red). The input signal is a white noise with chosen standard deviation 0.005. **(C)** Reconstructed gain $|\hat{g}|$ of the plant input response. The fitted model (dashed cyan) accurately matches the original model (black) with a root mean square error (RMSE) of 5.4% ± 2.2% (Confidence Interval (CI) 95%). The RMSE represents the error percentage between the fitted model's transfer function and the original model's transfer function averaged over 50 trials. The pink curve is the raw data used for fitting, computed from the spectral density data in **(A)** using Eq. (14). **(D)** Reconstructed phase of the plant input response $\hat{g}$.

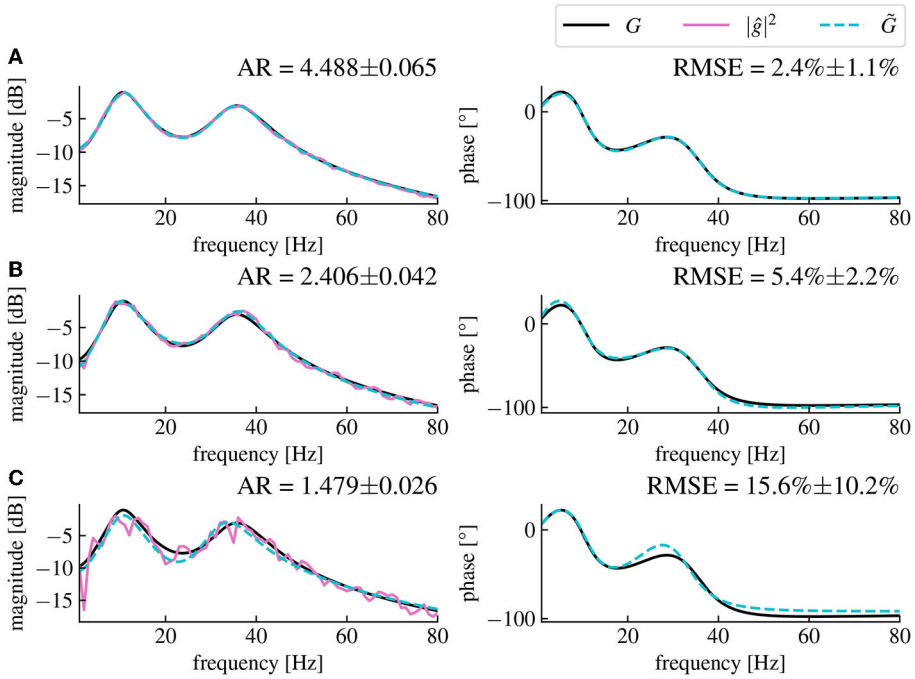

FIGURE 4
The magnitude vector fitting algorithm's performances depend on the amplitude ratio of the stimulation current and the driving noise. **(A)** Reconstructed magnitude and phase data for an amplitude ratio (AR) of 4.488 ± 0.065. The AR is computed as the ratio between the mean amplitude of y and the mean amplitude of y_0 averaged over 50 simulations (CI 95%). The fitted model has a corresponding RMSE of 2.4% ± 1.1% (CI 95%). **(B)** Same as **(A)**, but with an AR of 2.406 ± 0.042, the presented data are the same as in Figures 3C, D. **(C)** Same as **(A)**, but with an AR of 1.479 ± 0.026 resulting in a RMSE of 15.6% ± 10.2% for the fitted model. We see that the noise level in magnitude data is higher for smaller AR, which leads to higher RMSE (CI 95%) between the fitted model's transfer function and the original model's transfer function. The fitted model is coded in dashed cyan and deviates more from the original model for higher noise levels. All data have been computed from 30s long simulated time series.

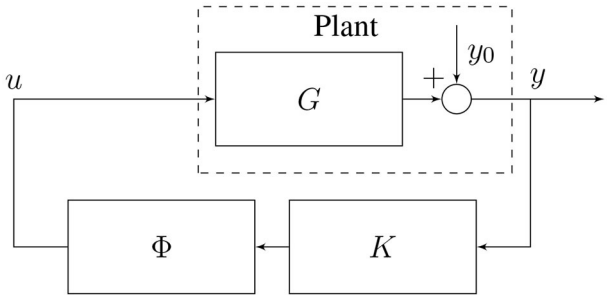

FIGURE 5
Closed-loop neurostimulation circuit with predictor.

parameters. The root mean square error could also be used to directly quantify the error between the transfer function of the estimated model and the original model, which can be an important parameter regarding the stability and the robustness of the closed-loop while performing delay compensation as discussed in the next section.

3.2. Delay compensation

Delay compensation is achieved by adding another LTI system at the output of the controller $\mathcal{K}$ (cf. Figure 5), whose purpose is to reproduce the transfer function of a negative delay. We call this system the predictor ϕ.

However, perfectly reproducing the transfer function of a negative delay would be impossible since the associated time-domain system would then be a perfect predictor, which is a non-causal, i.e. un-physical, system. Nonetheless, we can build a causal and stable system that behaves almost like a perfect predictor, however only in the frequency ranges of interest.

The numerical implementation of the controller necessitates discretization in time. Consequently, it is reasonable to choose the predictor design as a discrete-time system, meaning that for any input signal at $x_t : \mathbb{R} \to \mathbb{R}$ at an instant $t \in \mathbb{R}$, it approximately predicts the future signal $x_{t+\Delta t}$ where $\Delta t \in \mathbb{R}$ is the sampling time chosen when building the predictor. Since x is a discrete sequence, its transfer function is obtained using the Z-transform, defined as

$$X(z) = \mathcal{Z}\{x_{n\Delta t}\}(z) := \sum_{n=0}^{\infty} x_{n\Delta t} z^{-n},$$

with $z \in \mathbb{C}$ and $X : \mathbb{C} \to \mathbb{C}$. Then the transfer function $\Phi : \mathbb{C} \to \mathbb{C}$ of a negative delay of one step Δt applied to x would simply be $\Phi(z) = z$, the Z-transform of a one-step delay. However, this choice would be non-causal, which is not implementable numerically in time. Nevertheless, to obtain a stable and implementable system with a transfer function as close as possible to z, we chose the ansatz

$$\Phi(z_0) = \frac{b_0 z_0 + b_1}{z_0 - a} = z_0, \tag{15}$$

for a fixed value $z = z_0$ and where $a \in \mathbb{R}$ is the pole of the system and $b_0 \in \mathbb{R}$ and $b_1 \in \mathbb{R}$ are the polynomial coefficients of the numerator of Φ. This equation corresponds to the transfer function of a discrete LTI system with exactly one pole and one zero, which is the closest form of a proper rational function to the identity function of z in the sense that it has only one more pole. We add the additional constraints that $|a| < 1$, since this is the necessary and sufficient condition for the discrete predictor ϕ to be stable.

We choose to reformulate this problem by setting a as a free parameter. This way, we can select any a between -1 and 1, and the remaining parameters are found by solving the linear equation $b_0 z_0 + b_1 = z_0(z_0 - a)$, where $z \in \mathbb{C}$ is a chosen complex frequency point at which we want this equation to hold. Since there are two unknowns, we can write a second equation in which we want the derivative of each side of the equation also to be equal, yielding $b_0 = 2z_0 - a$. By replacing b_0 in the first equation, we obtain

$$\begin{aligned} z_0(2z_0 - a) + b_1 &= z_0(z_0 - a) \\ b_1 &= -z_0^2. \end{aligned}$$

In the z-domain, the zero frequency corresponds to $z_0 = 1$. We choose to solve this equation for this point, hence we can replace a, b_0 and b_1 in Eq. (15) which yields

$$\Phi(z) = \frac{(2 - a)z - 1}{z - a}. \tag{16}$$

This transfer function can then be converted to an associated state-space representation and used for time domain simulations with a sampling time Δt. The output of this system will then be $y_t \approx u_{t+\Delta t}$ for any input signal u_t. Simulating delays greater than the system sampling time is simply achieved by concatenating multiple times this predictor system. Here the delay has to be a multiple of the sampling time. This predictor can then be appended to the output of the digital controller $\mathcal{K}$.

To avoid closed-loop instability, we must limit the amplitude of the feedback signal computed from the controller input signal. This amplitude is determined by the three systems $\mathcal{G}$, $\mathcal{H}$ and $\mathcal{K}$. Since $\mathcal{G}$ is defined by the system under study and $\mathcal{H}$ is the chosen filter defining the desired modifications in the frequency distribution of the observed signal, ϕ (or equivalently parameter a) is the only degree of freedom. Figure 6 shows the region of closed-loop stability as a function of the predictor pole a and the delay.

Because the predictor has a gain that is still slightly greater than one in the frequency ranges of interest, we reduce the weights of the filter $\mathcal{H}$ to compensate for the excess gain at the α and γ-peaks. To do this, we simply divide the weight of each band by the magnitude of the predictor system evaluated at the band's natural frequency. This reduces the errors in the closed-loop transfer function in the α and γ-ranges.

Figure 7C shows results combining the model estimation by vector fitting and the delay compensation. The proposed closed-loop control yields an increase in α-power and a decrease in γ-power according to the employed target filter $\mathcal{H}$. The application of PI and LQG control with a Smith predictor for delay compensation (Figures 7A, B) has poor performances for higher γ-frequency activity.

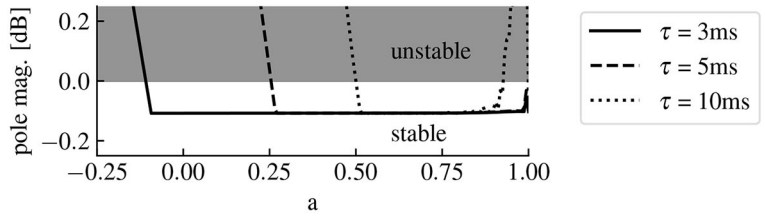

FIGURE 6
The predictor pole location affects the closed-loop stability. The magnitude of the pole with the highest magnitude in the closed-loop transfer function parameterizes the stability of the closed-loop. Indeed, if this value is less than 0 dB, then all the poles of the closed-loop transfer function have a magnitude less than 0 dB, meaning that the system is stable. The system is unstable otherwise. Here the full curve, the dashed curve and the dotted curve correspond to predictors for delays of 3 ms, 5 ms and 10 ms, respectively. The higher the delay is, the lower is the size of the region of closed-loop stability for *a*.

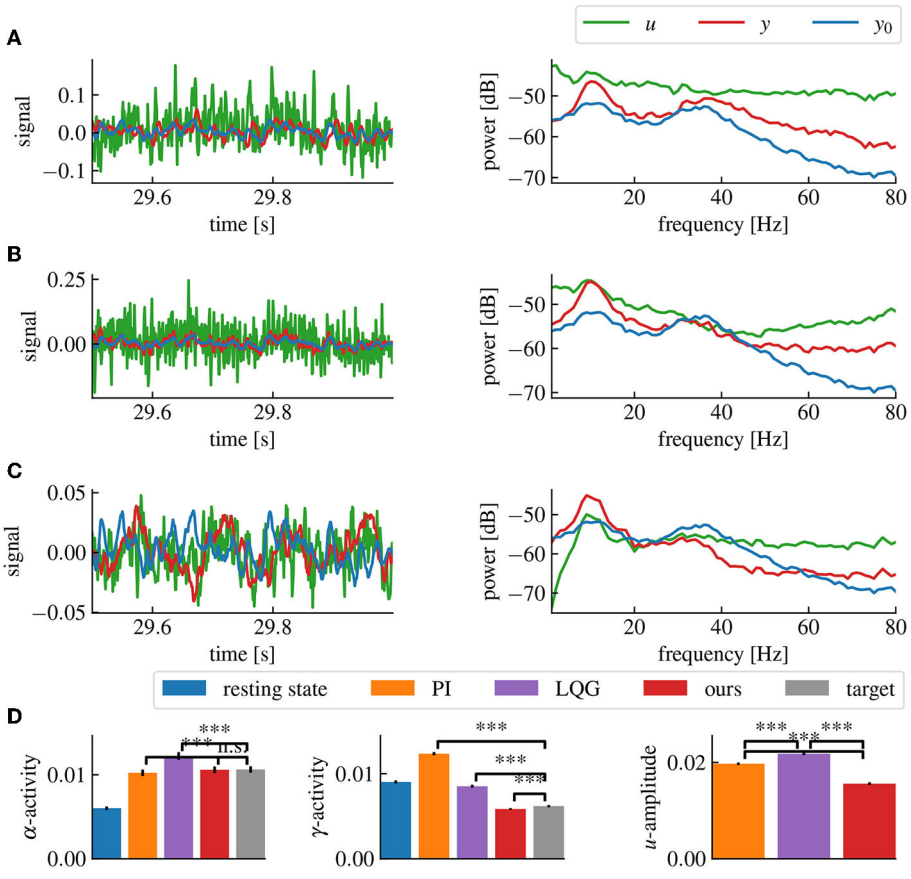

FIGURE 7
Our method successfully decreases α- and γ-activities in the presence of a 5ms delay, while maintaining a low stimulation current. **(A)** Simulation time series (left panel) and power spectral densities (right panel) of the PI control loop with Smith predictor. **(B)** Same as **(A)** for the LQG control loop with Smith predictor. **(C)** Same as **(A)** for our method, including delay compensation. **(D)** α-, γ-activities and mean amplitude of *u* for each method, averaged over 50 simulations. "***" corresponds to a *p*-value less than 0.05 with Welch's *t*-test, while "n.s." correspond to a *p*-value higher than 0.05. Our method provides both the closest match to the target α- and γ-activities and the lowest stimulation current (*u*) amplitude. The parameters for all controllers have been chosen to match the target activities as closely as possible without destabilizing the closed-loop. The activities are computed by averaging the spectral densities in their corresponding ranges while the *u*-amplitude correspond to the average spectral density of *u* from 0Hz to the Nyquist frequency.

3.2.1. Accuracy

The error between the achieved closed-loop output activity levels and the target activity levels is highly affected by the delay (cf. Figure 8). This is caused by the phase shift between the input and the output signal, which changes the effect of the control signal on the output in a frequency dependent manner. Our frequency range of interest is limited to frequencies below 55 Hz, which is the higher limit we use for the γ-range. In this case, the effect of delays of the order of milliseconds will be more visible for higher frequencies and higher delays (cf. Figure 8). However, using

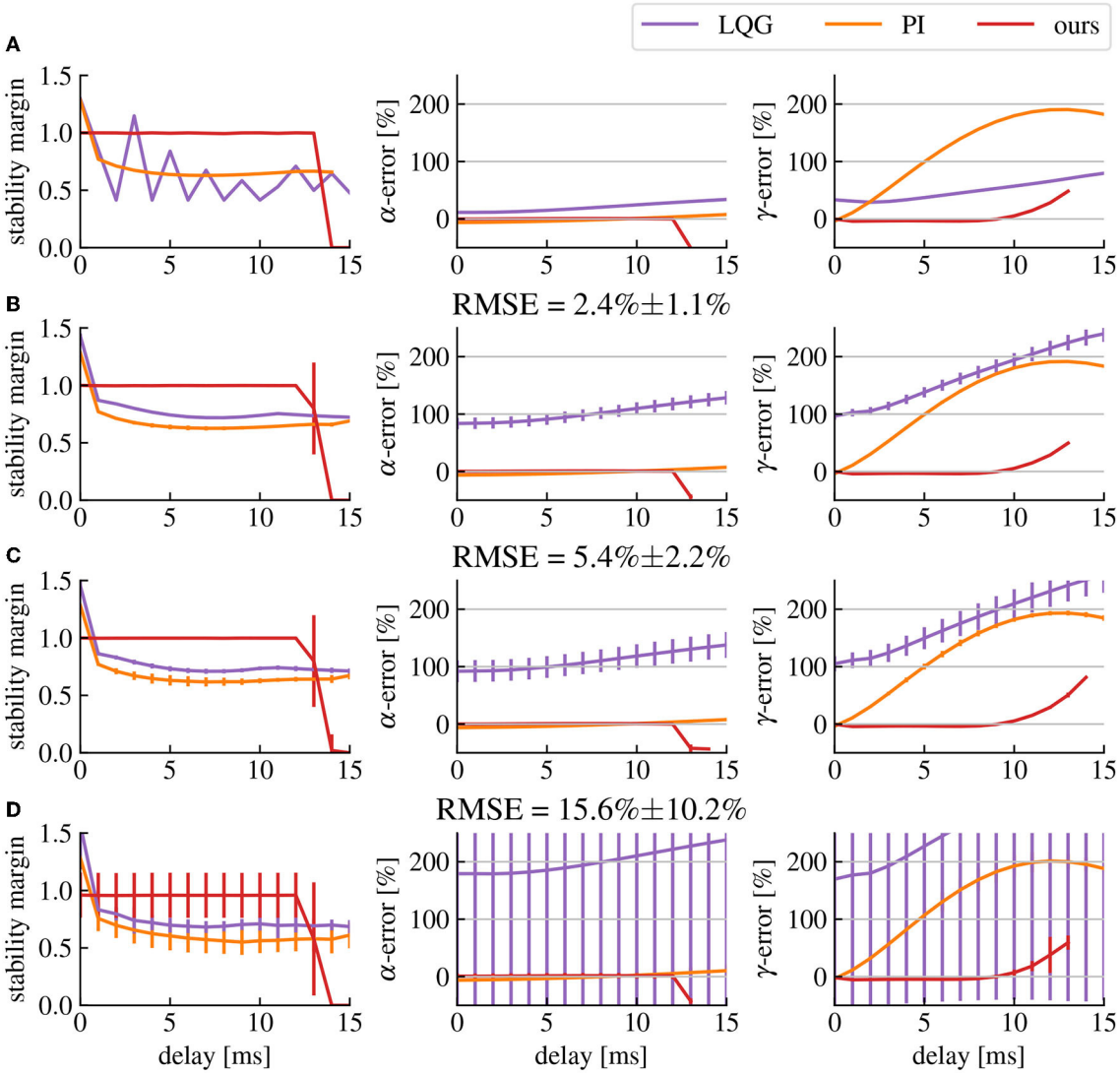

FIGURE 8
Delay affects the stability and robustness of the closed-loop transfer function. **(A)** Stability margin and α- and γ-activities errors in function of the delay with no model errors. The stability margin is computed as the shortest distance between the Nyquist plot and the point −1. The higher the stability margin, the more robust the closed-loop is to model uncertainties. The α- and γ-errors represent the error percentage between the measured activity and the target activity. **(B–D)** Same as row **(A)** but with model errors (quantified as the RMSE of the model fitting step) corresponding respectively to the model fits shown in Figures 4A–C. The vertical bars represent the standard deviation of their corresponding point.

our predictor design, we significantly mitigate the effects of the delay in the frequency ranges of interest (cf. Figure 8) red curve. Nonetheless, these effect are still present, creating a limit to the maximum delay our predictor is able to compensate, which in our case is situated around 10ms.

3.2.2. Stability and robustness

As discussed earlier, delay compensation can destabilize the closed-loop system depending on the parameters of its components. However, if the correct predictor pole is chosen based on Figure 6, the closed-loop will remain stable. These values are computed under the assumption that there are no model estimation errors. If we take into account the inaccuracies in the fitted brain model compared to the original brain model, extra gain can add up in the feedback signal, introducing again the risk of destabilizing the closed-loop (cf. Figure 8). The solution is either to simply reduce the amplitude of the spectral density modification that we want to apply by reducing the amplitude of the transfer function of filter $\mathcal{H}$, or to reduce the amplitude of the predictor Φ reducing its accuracy and possibly increasing delay errors. There is then a trade-off between how much we want to change the gain of the closed-loop transfer function while also compensating delay errors and how much we want to avoid closed-loop destabilization caused by model uncertainties. In any case, the inaccuracies in the estimated brain model create errors in the closed-loop transfer function regardless of the delay, which makes them the main determinant of the performance limits of our method in any given setup. Nevertheless, our method produces smaller α- γ-activities errors than LQG control and produces the smallest error for γ-activities

for delays of 1 to 12ms (cf. Figure 8). Comparisons lead to p-values less than 0.0005 using Welch's t-test, except for LQG control in row D where the variance of the data was to high to find any significant difference with this test.

3.3. Application to cortico-thalamic circuit model

To extend the analysis to a biologically more realistic model, we employed a nonlinear cortico-thalamic brain model (cf. Section 2.7.2). Fitting a linear transfer function to the brain model activity as described above, we found a good accordance of fitted and original model as can be seen in Figures 9A, B. Small deviations in the gain and the phase resulted from the internal delay in the brain model and its non-linearity. Indeed, the magnitude vector fitting algorithm does not reproduce this delay but instead synthesizes a linear system that has no delay but still approximates well the transfer function of the original model. Nonetheless, the non-linearity of this model can also decrease the accuracy of the fitting, as we are trying to represent a non-linear input response model by a linear one. However, this effect is only seen when the current is large enough for the non-linear part of the response to be significant.

In fact, the model-based control enhances α-activity and diminishes γ-activity in good accordance to the imposed filter $\mathcal{H}$ (Figure 9C). The closed-loop transfer function deviates from the target transfer function for large frequencies beyond the γ-frequency range. This results from the employed conduction delay.

To elucidate better the functions of the different elements of the proposed method, we applied a second closed-loop setup, where the neurostimulation input was applied to the first three layers of the cortex modeled by u and v and to the reticulum modeled by V_{ret} (Figure 10). In this setting, the response in the high-frequency ranges are mainly produced by the cortex, while the response in low-frequency ranges originates mainly from the reticulum and the thalamic relay structure, with a gap approximately between 10Hz and 20Hz. The weak response between 10 and 20 Hz observable (cf. Figure 10A) is compensated by the controller, which produces a high magnitude stimulation in the closed-loop for these frequencies (cf. Figure 10C). The second consequence is the inaccuracy of the closed-loop output in the low-frequency ranges, this is caused by the rather long cortico-thalamic internal delay. This delay yields a larger phase shift at low-frequencies and originates from the fact that we observe signals in the cortex, but stimulate in the reticulum.

4. Discussion

The goal of the proposed method was to design a delayed closed-loop control method to apply defined modifications to the spectral distribution of an observed signal, such as EEG or LFP. Under the assumption of linear brain stimulation response, the presented work explicitly describes all the steps needed to build a delayed closed-loop neurostimulation setup to restore the physiological brain state of a patient (Hebb et al., 2014). Since the controller is modeled as a linear time-invariant system, its implementation is lightweight, straightforward, and easily applicable in most embedded systems. Applications to a simple neural populations model (Figure 7) and to a biologically plausible cortico-thalamic feedback system (Figures 9, 10) demonstrate its elements and their impact on the control performance.

4.1. Main contributions

Our method allows to precisely specify the desired frequency-domain modifications we want to apply to the brain activity. The resulting closed-loop controller can then synthesize in real-time the required closed-loop neurostimulation signal necessary to reach the desired output, without the need to track a pre-defined reference signal. This make the method more flexible since it requires to specify relative rather that absolute signal modifications which is preferable considering the intra- and inter-patients variability of the EEG spectrum. Furthermore, specifying a reference signal which is a stochastic signal uncorrelated with the noise of the current plant output introduces additional noise in the feedback signal, since the controller needs to compensate for both the mean difference between the frequency distributions of the two signal and the difference between the driving noises of the two signals. Therefore, our method is able to track a target frequency distribution for the brain output with a lower current amplitude than classical methods (cf. Figure 7).

4.1.1. Model estimation

We assume resting state activity signal driven by noise, when no neurostimulation is applied. Injecting a stimulation creates an additional response that adds to the resting state. Consequently, both the resting state signal and response signal can be observed separately in experimental practice and they serve to estimate a linear state-space model as outlined in Section 3.1. This approach is successful for both simplified linear models (cf. Figures 3, 4) and neurophsysiological realistic nonlinear models (cf. Figure 9). This approximation is suitable for nonlinear systems whose dynamics evolve close to a stationary state. Several studies have already exposed evidence confirming that the measured brain dynamics behave mostly linearly at macroscopic scales (Popivanov et al., 1996; Liu et al., 2010). Moreover, in the case of the brain response to small neurostimulation input, our assumption of the linear brain response is supported by results of Kim and Ching (2016). The authors of this study measured the controllability Gramian of their brain model with nonlinear sigmoid transfer function, similar to the cortico-thalamic brain model (Riedinger and Hutt, 2022) used in this paper. If the system exhibits nonlinear dynamics far from any linear approximation, such as bistable dynamics and chaotic evolution, the proposed vector fitting technique may yield a too large model error and thus instability of the closed-loop feedback. The hypothesis of macroscopically linear dynamics has also recently been tested against various nonlinear models (Nozari et al., 2020). While that work included fitting methods for both linear and nonlinear brain models, our work chose the paradigm of purely frequency domain model fitting with the magnitude vector fitting algorithm (De Tommasi et al., 2010) and applied it to the brain input response system, which we could isolate thanks to a simple open-loop neurostimulation

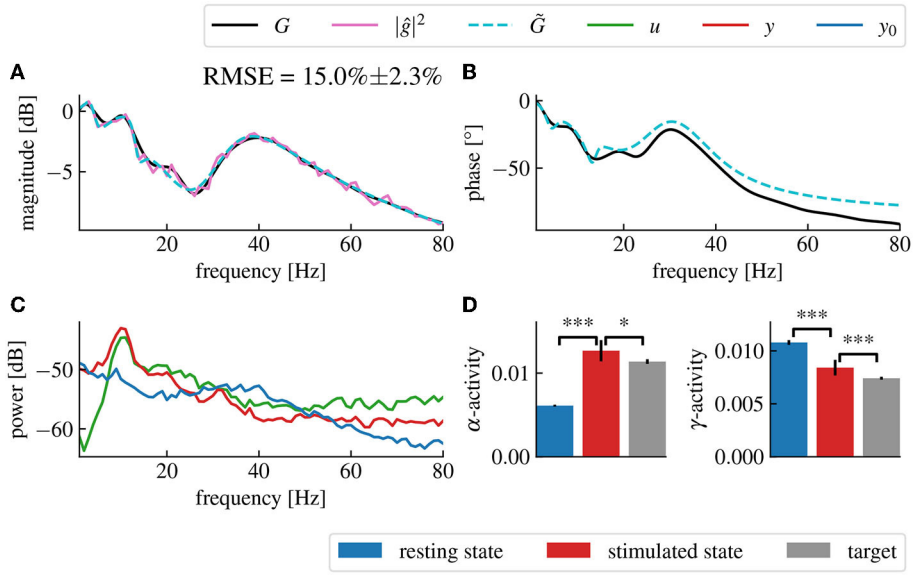

FIGURE 9
Fitted model-based control using the cortico-thalamic brain model successfully reproduces the target transfer function in the frequency domains of interest. **(A)** Magnitude of the fitted brain model transfer function (dashed cyan) obtained from the power spectral density data (pink) compared to the magnitude of the original cortico-thalamic brain model transfer function (black). **(B)** Phase shift of the fitted transfer function (dashed cyan) compared to the phase shift of the original transfer function (black). **(C)** Spectral densities of the resting state activity signal (blue), the stimulated brain output (red) and the stimulation signal (green). **(D)** α- and γ-activities of the closed-loop output averaged over 50 trials for which the fitting step was repeated each time. "***" corresponds to a p-value less than 0.0005 with Welch's t-test while "*" corresponds to a p-value less than 0.05. The α- and γ-activities are respectively increased and decreased after application of the closed-loop.

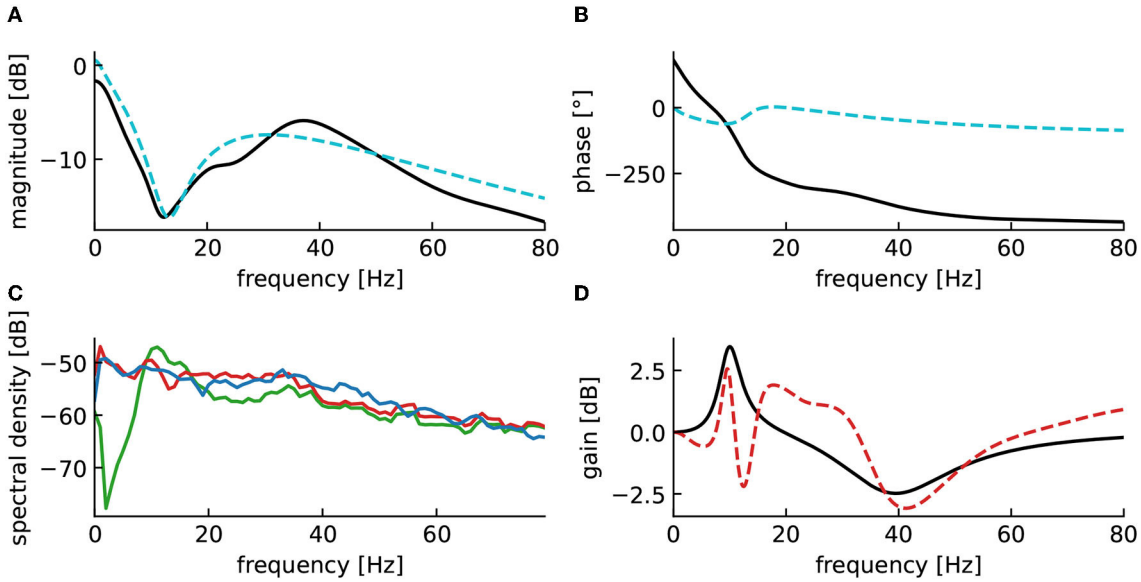

FIGURE 10
Reticulum stimulation yields incorrect closed-loop gain in low-frequency ranges. **(A)** Magnitude of the fitted brain model transfer function (dashed cyan) compared to the magnitude of the original cortico-thalamic brain model transfer function (black). **(B)** Phase shift of the fitted transfer function (dashed cyan) compared to the magnitude of the original transfer function (black). **(C)** Spectral densities of the resting state activity signal (blue), the stimulated brain output (red) and the stimulation signal (green). **(D)** Closed-loop transfer function (dashed red), compared to the target transfer function $1 + H(s)$ (black).

setup. While models have already been studied in application to neurostimulation (Modolo et al., 2011; Wagner et al., 2014), we propose a straightforward black box modeling approach that is directly usable for adaptive closed-loop neurostimulation, and is technically applicable easily for each individual patients before any closed-loop neurostimulation sessions.

4.1.2. Delay compensation

Conduction delays of a few milliseconds in the transmission between observation and stimulation may be negligible in systems evolving on time scales of seconds or longer, but may play an important role in neural systems. Our study demonstrates that such feedback delays may introduce control errors and we show how these errors can be avoided by a novel delay compensation method (Section 3.2). Application to the linear model (7) demonstrated its superior performance compared to conventional delay compensation methods. Delay compensating systems have already been described in other work (Guo et al., 2004; Hosseini et al., 2019). However, we used a design primarily focused on the correction of a gain error in the closed-loop transfer function, whereas the majority of the current research is based on time domain criterion and stability enforcement (Sönmez and Ayasun, 2015; Ledva et al., 2017). The methods performance, i.e. how well the total gain function fits to the pre-defined transfer function, is good for low-frequencies but weakens for frequencies exceeding a limit frequency. Note that frequency domain compensation has also already been achieved, notably via delay equalizers (Podilchak et al., 2009). However, this would restrict the frequency range in which the delay is compensated, and create additional errors in the surrounding frequencies. Other designs include filters with negative group delays, however their applications are limited to band limited input signals (Bukhman and Bukhman, 2004; Voss, 2017). The predictor design we presented also relies on negative group delay, enabling delay compensation in a large frequency band, while still being applicable to the brain EEG, which is inherently not band limited, because of the noise. Nonetheless, while our predictor design allows to significantly decreases the delay errors in the closed-loop transfer function, the delay still imposes a limit on the controllable frequency range. The larger the delay, the smaller is this limit frequency. Low performance may induce instability in the feedback loop (Mirkin and Palmor, 2005) and thus should be avoided. A corresponding stability criteria has been proposed, (cf. Figure 6). Better predictor designs could allow better performance of the closed-loop system for larger delays. The improvement of the accuracy of our closed-loop neurostimulation setup by building more efficient predictor designs is in progress and we refer the reader to future work.

4.2. Limits of our methodology

4.2.1. Experimental stimulation parameters and safety

Experimental stimulation protocols have to ensure the subjects safety (Ko, 2021) and thus avoide stimulus-induced health risks and complications. For instance, tDCS may be administered for a duration of 60 minutes and a maximum current of 4 mA without yielding health risks. However, parameters beyond these limits may yield adverse effects in subjects, such as skin lesions similar to burns and mania or hypomania in patients with depression (Matsumoto and Ugawa, 2017). The proposed method does not limit the stimulation duration *per se*, but of course the duration can be chosen accordingly without constrating the method. The method adapts the systems brain rhythms to the target rhythms very rapidly on a time scale of less than a second and hence permits rather short stimulation duration longer than a second.

Moreover, the proposed method does not specify absolute stimulation current magnitude applied. The impact of stimulation at certain magnitudes depends heavily on the stimulation type. In tDCS, anodal stimulation with positive currents have a different impact as cathodal stimulation with negative currents. In addition, currents are thought to have to pass a certain threshold to yield a measurable effect. In tACS (Moliadze et al., 2012), stimulating in the α-frequency range large and small magnitudes yield excitation and inhibition, respectively, while intermediate magnitudes yield weak effects. Stimulating with a range of frequencies, as in tRNS (Potok et al., 2022), a 1mA peak-to-peak amplitude for 10 minutes stimulation duration does not yield adverse effects. We conclude that it is not straight-forward to decide which stimulation magnitude applied in the presented method would be safe for human subjects, since the stimulation signal is neither constant, single frequency oscillation nor random noise. In sum, we argue that a maximum peak-to-peak amplitude of 1mA for few tens of minutes may not yield adverse effects, but still may evoke a measurable impact on observations and the brain state. Of course, future experimental studies will gain deeper insights.

4.2.2. Model internal delay

The internal delay in the brain is not reproducible by the magnitude vector fitting algorithm, which relies on the time invariance of the signals. Hence, this will cause errors in the transfer function of the fitted model (cf. Figure 9) that are larger for higher contribution of the delay in the output (cf. Figure 10). To limit this effect, we must minimize the delay between the application of the neurostimulation input and the measurement of the response to this input as much as possible by taking into account the delay between the different brain regions.

4.2.3. Estimating the closed-loop delay

For delay compensation, in this paper, we assumed that we know the conduction delay in the closed-loop. However, although it is a single constant parameter, we would need a method to measure it for a real closed-loop neurostimulation setup. A straightforward way to do this would be to inject any current into the plant and measure the time lag between the moment at which we inject the input current and the moment at which we measure the output signal. This estimated delay would then correspond to the total closed-loop delay except for the computation delay of the digital controller $\mathcal{K}$. This computation delay can be easily measured with the same software used for computation, as it corresponds to the delay needed to perform constant-size matrix multiplications. Moreover, several methods have already been developed to estimate the conduction delays in linear systems (Schier, 1997; Dudarenko et al., 2014).

4.2.4. Direct input current measurements

One of the main challenges to solve for closed-loop neurostimulation is the elimination of direct transmission

artifacts from the measured EEG signal (Iturrate et al., 2018). Indeed, when measuring the plant output signal, a portion of the measured signal might be a direct measurement of the input current without any influence from the brain dynamics. In the ideal case, one intends to minimize the contribution of the stimulation input to the observed signal since it would mean that the measured EEG signal does not fully correspond to the brain activity. Hence, reading the EEG of the patient would be more difficult for the user of our closed-loop setup, and the contribution of the brain dynamics to the closed-loop would be smaller. A simple solution to this problem is discussed further below.

4.3. Perspectives

The control proposed allows to perform accurate frequency shaping of the systems' activity spectral distribution. However, this approach is limited to linear models of the brain stimulation response. This may be disadvantageous if the systems dynamics exhibit nonlinear behavior (see e.g., Hutt and beim Graben, 2017) as we want to represent the brain dynamics realistically. Furthermore, in real-case scenarios, we would also have to take into account the noise in the acquisition of the signal by the sensor and in the application of the input signal by the actuator.

4.3.1. Filtering out direct input current measurements

Filtering out the direct input current measurements is achievable with our setup removing the strictly proper system requirement while using the magnitude vector fitting algorithm to measure the brain input response. In other words, while fitting the brain input response system, we want the fitted model to be able to contain a direct transmission term corresponding to the direct current measurement. Hence, if the real plant input response contains a significant direct transmission term, it will be identified by the magnitude vector fitting algorithm when synthesizing the estimated plant input response. The second step is them simply to substract the feedtrough term multiplied by the input current to the plant output signal. Thus, the remaining part of the signal would only correspond to the brain dynamics.

4.3.2. Application to multiple inputs multiple outputs plants

For now, we only focused on plant with a signal input signal and a single output signal. However, in a real setup, the EEG measurement is typically composed of multiple channels corresponding to different electrodes. This can also be true for the neurostimulation device. For example, with electric current stimulation, we can inject multiple signals using multiple electrodes. This can be simply solved by feeding a single input to each input channel and summing each output to a single output channel. However, when we separate the different channels, we can have more control over each individuals output channels. When we have multiple inputs and output, the plant is then a Multiple-Inputs Multiple-Outputs (MIMO) system. Everything developed in this paper is generalizable to MIMO systems, with one caveat: when solving E.q., (6), a unique solution only exists if the system has as more outputs than it has inputs. The user can always ensure this, by using as many neurostimulation input channels than there are EEG output channels. In this generalized setup, we can also define the filter $\mathcal{H}$ to apply different modifications to each output channel.

4.3.3. Neurostimulation effects on larger time scales

Our method relies only on the short term dynamics of the brain, using signal feedback and delay compensation to produce an adaptive stimulation current and obtain the desired EEG frequency distribution. However, more traditional neurostimulation techniques rely on the long term dynamics of neural plasticity, which is not modeled in the brain models we use in this paper. Long term brain adaptation to neurostimulation could cause the EEG frequency distribution to diverge from the desired frequency distribution after several minutes of stimulation. This effect could be compensated either by reiterating the model identification step and performing neurostimulation again, or by adjusting the weight of the filter $\mathcal{H}$ according to the observed changes in real-time. Incorporating the effect of neural plasticity in the brain models would allow our method to produce predictable and durable modification to the EEG frequency distribution, even after we stop the stimulation.

Data availability statement

The source code used for the simulation results can be freely accessed here: https://github.com/Thomas-Wahl/neuroclodec.

Author contributions

TW, AH, and MD contributed to the development of the methods presented in this study. TW produced the source code used for the simulations. JR and AH wrote the introduction section. TW and AH wrote the other sections of the manuscript. All authors read and approved the submitted version.

Funding

This research was funded by Inria in the Action Exploratoire project *A/D Drugs*.

Conflict of interest

The authors declare that the research was conducted in the absence of any commercial or financial relationships that could be construed as a potential conflict of interest.

Publisher's note

All claims expressed in this article are solely those of the authors and do not necessarily represent those of

their affiliated organizations, or those of the publisher, the editors and the reviewers. Any product that may be evaluated in this article, or claim that may be made by its manufacturer, is not guaranteed or endorsed by the publisher.

Supplementary material

The Supplementary Material for this article can be found online at: https://www.frontiersin.org/articles/10.3389/fnins.2023.1183670/full#supplementary-material

References

Åström, K. J. (2012). *Introduction to Stochastic Control Theory*. Chelmsford, MA: Courier Corporation.

Basar, E. (2013). Brain oscillations in neuropsychiatric disease. *Dialogues Clin. Neurosci*. 15, 291–300. doi: 10.31887/DCNS.2013.15.3/ebasar

Bennabi, D., and Haffen, E. (2018). Transcranial direct current stimulation (tdcs): a promising treatment for major depressive disorder? *Brain Sci.* 8, 81. doi: 10.3390/brainsci8050081

Bolus, M. F., Willats, A. A., Rozell, C. J., and Stanley, G. B. (2021). State-space optimal feedback control of optogenetically driven neural activity. *J. Neural Eng.* 18, 036006. doi: 10.1088/1741-2552/abb89c

Bolus, M. F., Willats, A. A., Whitmire, C. J., Rozell, C. J., and Stanley, G. B. (2018). Design strategies for dynamic closed-loop optogenetic neurocontrol *in vivo*. *J. Neural Eng.* 15, 026011. doi: 10.1088/1741-2552/aaa506

Brunelin, J., Mondino, M., Gassab, L., Haesebaert, F., Gaha, L., Suaud-Chagny, M., et al. (2012). Examining transcranial direct-current stimulation (tDCS) as a treatment for hallucinations in schizophrenia. *Am. J. Psychiatry*. 169, 719–724. doi: 10.1176/appi.ajp.2012.11071091

Bukhman, N., and Bukhman, S. (2004). On the negative delay time of a narrow-band signal as it passes through the resonant filter of absorption. *Radiophys. Quantum Electron*. 47, 68–76. doi: 10.1023/B:RAQE.0000031672.70934.3a

Chen, Z. S., Kulkarni, P. P., Galatzer-Levy, I. R., Bigio, B., Nasca, C., and Zhang, Y. (2022). Modern views of machine learning for precision psychiatry. *Patterns* 3,100602. doi: 10.1016/j.patter.2022.100602

De Tommasi, L., Gustavsen, B., and Dhaene, T. (2010). Robust transfer function identification via an enhanced magnitude vector fitting algorithm. *IET Control Theory & Applicat*. 4, 1169–1178. doi: 10.1049/iet-cta.2009.0025

Dudarenko, N., Polinova, N., and Ushakov, A. (2014). Fundamental matrix of linear continuous system in the problem of estimating its transport delay. *Nauchno-Tekhnicheskii Vestnik Informatsionnykh Tekhnologii, Mekhaniki i Optiki*. 14, 5.

Edel, Y., and Caroli, F. (1987). Histoire de l'électrochoc : des traitements électriques à la convulsivothérapie en psychiatrie. *Bulletin d'histoire de l'électricité*. 9, 87–114. doi: 10.3406/helec.1987.1012

Fang, H., and Yang, Y. (2022). Designing and validating a robust adaptive neuromodulation algorithm for closed-loop control of brain states. *J. Neural Eng.* 19, 036018. doi: 10.1088/1741-2552/ac7005

Fang, H., and Yang, Y. (2023). Predictive neuromodulation of cingulo-frontal neural dynamics in major depressive disorder using a brain-computer interface system: A simulation study. *Front. Comput. Neurosci.* 17, 1119685. doi: 10.3389/fncom.2023.1119685

Fleming, J., Dunn, E., and Lowery, M. (2020). Simulation of closed-loop deep brain stimulation control schemes for suppression of pathological beta oscillations in parkinson's disease. *Front. Neurosci.* 14, 166. doi: 10.3389/fnins.2020.00166

Gardiner, C. (2004). *Handbook of Stochastic Methods*. Berlin: Springer. doi: 10.1007/978-3-662-05389-8

Guerrero Moreno, J., Biazoli, J.r,., C., Fontes Baptista, A., and Remoaldo Trambaiolli, L. (2021). Closed-loop neurostimulation for affective symptoms and disorders: an overview. *Biol. Psychol*., 161:108081. doi: 10.1016/j.biopsycho.2021.108081

Guo, L., Cardullo, F., Houck, J., Kelley, L., and Wolters, T. (2004). "New predictive filters for compensating the transport delay on a flight simulator," in *AIAA Modeling and Simulation Technologies Conference and Exhibit* (American Institute of Aeronautics and Astronautics). p. 5441. doi: 10.2514/6.2004-5441

Haeusermann, T., Lechner, C., Fong, K., Sideman, A., Jaworska, A., Chiong, W., et al. (2023). Closed-loop neuromodulation and self-perception in clinical treatment of refractory epilepsy. *AJOB Neurosci.* 14, 32–44. doi: 10.1080/21507740.2021.1958100

Hartshorn, A., and Jobst, B. (2018). Responsive brain stimulation in epilepsy. *Ther. Adv. Chronic Dis*. 9, 135–142. doi: 10.1177/2040622318774173

Hashemi, M., Hutt, A., and Sleigh, J. (2015). How the cortico-thalamic feedback affects the EEG power spectrum over frontal and occipital regions during propofol-induced anaesthetic sedation. *J. Comput. Neurosci.* 39, 155. doi: 10.1007/s10827-015-0569-1

Hebb, A. O., Zhang, J. J., Mahoor, M. H., Tsiokos, C., Matlack, C., Chizeck, H. J., et al. (2014). Creating the feedback loop: closed-loop neurostimulation. *Neurosurg. Clini.* 25, 187–204. doi: 10.1016/j.nec.2013.08.006

Hespanha, J. P. (2018). *Linear Systems Theory*. Princeton: Princeton University Press. doi: 10.23943/9781400890088

Hirano, Y., Orbie, N., Kanba, S., Onitsuka, T., Nestor, P., and Spencer, K. (2015). Spontaneous gamma activity in schizophrenia. *JAMA Psychiat*. 72, 813–821. doi: 10.1001/jamapsychiatry.2014.2642

Holtzheimer, P., and Mayberg, H. (2011). Deep brain stimulation for psychiatric disorders. *Annu. Rev. Neurosci.* 34, 2890307. doi: 10.1146/annurev-neuro-061010-113638

Hosain, M., Kouzani, A., and Tye, S. (2014). Closed loop deep brain stimulation: an evolving technology. *Australas. Phys. Eng. Sci. Med.* 37, 619–634. doi: 10.1007/s13246-014-0297-2

Hosseini, S. A., Toulabi, M., Dobakhshari, A. S., Ashouri-Zadeh, A., and Ranjbar, A. M. (2019). Delay compensation of demand response and adaptive disturbance rejection applied to power system frequency control. *IEEE Transac. Power Syst.* 35, 2037–2046. doi: 10.1109/TPWRS.2019.2957125

Howells, F., Temmingh, H., Hsieh, J., van Dijen, A., Baldwin, D., and Stein, D. (2018). Electroencephalographic delta/alpha frequency activity differentiates psychotic disorders: a study of schizophrenia, bipolar disorder and methamphetamine-induced psychotic disorder. *Transl. Psychiatry*. 8:75. doi: 10.1038/s41398-018-0105-y

Hutt, A. (2013). The anesthetic propofol shifts the frequency of maximum spectral power in eeg during general anesthesia: analytical insights from a linear model. *Front. Comput. Neurosci.* 7, 2. doi: 10.3389/fncom.2013.00002

Hutt, A., and beim Graben, P. (2017). Sequences by metastable attractors: interweaving dynamical systems and experimental data. *Front. Appl. DYn. Syst. Stat.* 3, 11. doi: 10.3389/fams.2017.00011

Iturrate, I., Pereira, M., and Millán, J. R. (2018). Closed-loop electrical neurostimulation: challenges and opportunities. *Curr. Opini. Biomed. Eng.* 8, 28–37. doi: 10.1016/j.cobme.2018.09.007

Khintchine, A. (1934). Korrelationstheorie der stationären stochastischen prozesse. *Mathematische Annalen*. 109, 604–615. doi: 10.1007/BF01449156

Kim, S. A., and Ching, S. (2016). "Quasilinearization-based controllability analysis of neuronal rate networks," in *2016 American Control Conference (ACC)*. Boston, MA: IEEE. p. 7371–7376.

Ko, M. (2021). Safety of transcranial direct current stimulation in neurorehabilitation. *Brain Neurorehabil*. 14, e9. doi: 10.12786/bn.2021.14.e9

Kühn, A. A., Kempf, F., Brücke, C., Gaynor Doyle, L., Martinez-Torres, I., Pogosyan, A., et al. (2008). High-frequency stimulation of the subthalamic nucleus suppresses oscillatory β activity in patients with parkinson's disease in parallel with improvement in motor performance. *J. Neurosci*. 28, 6165–6173. doi: 10.1523/JNEUROSCI.0282-08.2008

Ledva, G. S., Vrettos, E., Mastellone, S., Andersson, G., and Mathieu, J. L. (2017). Managing communication delays and model error in demand response for frequency regulation. *IEEE Transact. Power Syst*. 33, 1299–1308. doi: 10.1109/TPWRS.2017.2725834

Leicht, G., Vauth, S., Polomac, N., Andreou, C., Rauh, J., Mußmann, M., et al. (2015). EEG-Informed fMRI reveals a disturbed gamma-band–specific network in subjects at high risk for psychosis. *Schizophr. Bull.* 42, 239–249. doi: 10.1093/schbul/sbv092

Liu, Z., Rios, C., Zhang, N., Yang, L., Chen, W., and He, B. (2010). Linear and nonlinear relationships between visual stimuli, eeg and bold fmri signals. *Neuroimage*. 50, 1054–1066. doi: 10.1016/j.neuroimage.2010.01.017

Martin, S., Iturrate, I., Chavarriaga, R., Leeb, R., Sobolewski, A., Li, A., et al. (2018). Differential contributions of subthalamic beta rhythms and 1/f broadband

activity to motor symptoms in parkinson's disease. *NPJ Parkinson's Dis.* 4, 32. doi: 10.1038/s41531-018-0068-y

Matsumoto, H., and Ugawa, Y. (2017). Adverse events of tdcs and tacs: a review. *Clini. Neurophysiol. Pract.* 2, 19–25. doi: 10.1016/j.cnp.2016.12.003

Mirkin, L., and Palmor, Z. J. (2005). *Control Issues in Systems with Loop Delays, chapter 59*. Boston, MA: Birkhäuser Boston. p. 627–648.

Modolo, J., Legros, A., Thomas, A. W., and Beuter, A. (2011). Model-driven therapeutic treatment of neurological disorders: reshaping brain rhythms with neuromodulation. *Interface Focus*. 1, 61–74. doi: 10.1098/rsfs.2010.0509

Moliadze, V., Atalay, D., Antal, A., and Paulus, W. (2012). Close to threshold transcranial electrical stimulation preferentially activates inhibitory networks before switching to excitation with higher intensities. *Brain Stimul.* 5, 505–511. doi: 10.1016/j.brs.2011.11.004

Morari, M., and Zafiriou, E. (1989). *Robust Process Control*. Madison, WI: Morari.

Nasr, K., Haslacher, D., Dayan, E., Censor, N., Cohen, L. G., and Soekadar, S. R. (2022). Breaking the boundaries of interacting with the human brain using adaptive closed-loop stimulation. *Prog. Neurobiol.* 216, 102311. doi: 10.1016/j.pneurobio.2022.102311

Nejati, V., Salehinejad, M., Nitsche, M., Najian, A., and Javadi, A. (2020). Transcranial direct current stimulation improves executive dysfunctions in adhd: Implications for inhibitory control, interference control, working memory, and cognitive flexibility. *J. Atten. Disord.* 24, 1928–1943. doi: 10.1177/1087054717730611

Nozari, E., Bertolero, M. A., Stiso, J., Caciagli, L., Cornblath, E. J., He, X., et al. (2020). Is the brain macroscopically linear? a system identification of resting state dynamics. *arXiv*. [preprint]. doi: 10.1101/2020.12.21.423856

Nunez, P., and Srinivasan, R. (2006). *Electric Fields of the Brain: The Neurophysics of EEG*. New York – Oxford: Oxford University Press.

Paulus, W. (2011). Transcranial electrical stimulation (tes – tdcs; trns, tacs) methods. *Neuropsychol.Rehabilitat.* 21, 602–617. doi: 10.1080/09602011.2011.557292

Podilchak, S. K., Frank, B. M., Freundorfer, A. P., and Antar, Y. M. (2009). "High speed metamaterial-inspired negative group delay circuits in cmos for delay equalization," in *2009 2nd Microsystems and Nanoelectronics Research Conference*. Ottawa, ON: IEEE. p. 9–12.

Popivanov, D., Dushanova, J., Mineva, A., and Krekule, I. (1996). "Detection of successive changes in dynamics of eeg time series: linear and nonlinear approach," in *Proceedings of 18th Annual International Conference of the IEEE Engineering in Medicine and Biology Society*. Amsterdam: IEEE. p. 1590–1591.

Potok, W., van der Groen, O., Bächinger, M., Edwards, D., and Wenderoth, N. (2022). Transcranial random noise stimulation modulates neural processing of sensory and motor circuits, from potential cellular mechanisms to behavior: a scoping review. *eNeuro*. 9, ENEURO.0248-21.2021. doi: 10.1523/ENEURO.0248-21.2021

Prosky, J., Cagle, J., Sellers, K., Gilron, R., de Hemptinne, C., Schmitgen, A., et al. (2021). Practical closed-loop strategies for deep brain stimulation: lessons from chronic pain. *Front. Neurosci.* 15, 762097. doi: 10.3389/fnins.2021.762097

Riedinger, J., and Hutt, A. (2022). Mathematical model insights into eeg origin under transcranial direct current stimulation (tdcs) in the context of psychosis. *J. Clin. Med.* 11, 1845. doi: 10.3390/jcm11071845

Scangos, K., Khambhati, A., Daly, P., Makhoul, G., Sugrue, L., Zamanian, H., et al. (2021). Closed-loop neuromodulation in an individual with treatment-resistant depression. *Nat. Med.* 27, 1696–1700. doi: 10.1038/s41591-021-01480-w

Schier, J. (1997). Estimation of transport delay using parallel recursive modified gram-schmidt algorithm. *Int. J. Adapt. Control Signal Proc.* 11, 431–442. doi: 10.1002/(SICI)1099-1115(199708)11:5<431::AID-ACS417>3.0.CO;2-Q

Schulman, J. J., Cancro, R., Lowe, S., Lu, F., Walton, K. D., and Llinás, R. R. (2011). Imaging of thalamocortical dysrhythmia in neuropsychiatry. *Front. Hum. Neurosci.* 5, 69. doi: 10.3389/fnhum.2011.00069

Smith, O. J. (1959). A controller to overcome dead time. *ISA J.* 6, 28–33.

Sönmez, S., and Ayasun, S. (2015). Stability region in the parameter space of pi controller for a single-area load frequency control system with time delay. *IEEE Transact. Power Syst.* 31, 829–830. doi: 10.1109/TPWRS.2015.2412678

Stagg, C., Antal, A., and Nitsche, M. (2018). Physiology of transcranial direct current stimulation. *J. ECT.* 34, 144–152. doi: 10.1097/YCT.0000000000000510

Stanslaski, S., Farooqi, H., Sanabria, D., and Netoff, T. (2022). Fully closed loop test environment for adaptive implantable neural stimulators using computational models. *J. Med. Device*. 16, 034501. doi: 10.1115/1.4054083

Su, F., Kumaravelu, K., Wang, J., and Grill, W. M. (2019). Model-based evaluation of closed-loop deep brain stimulation controller to adapt to dynamic changes in reference signal. *Front. Neurosci.* 13, 956. doi: 10.3389/fnins.2019.00956

Sun, F., and Morrell, M. (2014). Closed-loop neurostimulation: the clinical experience. *Neurotherapeutics* 11, 553–563. doi: 10.1007/s13311-014-0280-3

Tervo, A. E., Nieminen, J. O., Lioumis, P., Metsomaa, J., Souza, V. H., Sinisalo, H., et al. (2022). Closed-loop optimization of transcranial magnetic stimulation with electroencephalography feedback. *Brain Stimul.* 15, 523–531. doi: 10.1016/j.brs.2022.01.016

Van Loan, C. (1978). Computing integrals involving the matrix exponential. *IEEE Trans. Automat. Contr.* 23, 395–404. doi: 10.1109/TAC.1978.1101743

Voss, H. U. (2017). A universal negative group delay filter for the prediction of band-limited signals. *arXiv*. [preprint].

Wagner, T., Eden, U., Rushmore, J., Russo, C. J., Dipietro, L., Fregni, F., et al. (2014). Impact of brain tissue filtering on neurostimulation fields: a modeling study. *Neuroimage.* 85, 1048–1057. doi: 10.1016/j.neuroimage.2013.06.079

Welch, P. (1967). The use of fast fourier transform for the estimation of power spectra: A method based on time averaging over short, modified periodogram. *Trans. Audio Electroacoustics.* AU-15, 70–73. doi: 10.1109/TAU.1967.1161901

Westover, M. B., Kim, S.-E., Ching, S., Purdon, P. L., and Brown, E. N. (2015). Robust control of burst suppression for medical coma. *J. Neural Eng.* 12, 046004. doi: 10.1088/1741-2560/12/4/046004

Yang, Y., Connolly, A. T., and Shanechi, M. M. (2018). A control-theoretic system identification framework and a real-time closed-loop clinical simulation testbed for electrical brain stimulation. *J. Neural Eng.* 15, 066007. doi: 10.1088/1741-2552/aad1a8

Yang, Y., Lee, J. T., Guidera, J. A., Vlasov, K. Y., Pei, J., Brown, E. N., et al. (2019). Developing a personalized closed-loop controller of medically-induced coma in a rodent model. *J. Neural Eng.* 16, 036022. doi: 10.1088/1741-2552/ab0ea4

Zhu, Y., Wang, J., Li, H., Liu, C., and Grill, W. M. (2021). Adaptive parameter modulation of deep brain stimulation based on improved supervisory algorithm. *Front. Neurosci.* 15, 750806. doi: 10.3389/fnins.2021.750806

frontiers | Frontiers in Neuroscience

TYPE Original Research
PUBLISHED 05 July 2023
DOI 10.3389/fnins.2023.1157080

OPEN ACCESS

EDITED BY
Mark H. Myers,
University of Tennessee Health Science Center (UTHSC), United States

REVIEWED BY
Ilya Bakulin,
Research Center of Neurology, Russia
Angel Nunez,
Autonomous University of Madrid, Spain
Ying Shen,
The First Affiliated Hospital of Nanjing Medical University, China

*CORRESPONDENCE
Zhipeng Liu
✉ lzpeng67@163.com
Tao Yin
✉ bme500@163.com

†These authors have contributed equally to this work and share first authorship

RECEIVED 02 February 2023
ACCEPTED 20 June 2023
PUBLISHED 05 July 2023

CITATION
Jin J, Wang X, Wang H, Li Y, Liu Z and Yin T (2023) Train duration and inter-train interval determine the direction and intensity of high-frequency rTMS after-effects. *Front. Neurosci.* 17:1157080. doi: 10.3389/fnins.2023.1157080

Train duration and inter-train interval determine the direction and intensity of high-frequency rTMS after-effects

Jingna Jin[1†], Xin Wang[1†], He Wang[1], Ying Li[1], Zhipeng Liu[1*] and Tao Yin[1,2*]

[1]Institute of Biomedical Engineering, Chinese Academy of Medical Sciences and Peking Union Medical College, Tianjin, China, [2]Neuroscience Center, Chinese Academy of Medical Sciences, Beijing, China

Background and objective: It has been proved that repetitive transcranial magnetic stimulation (rTMS) triggers the modulation of homeostatic metaplasticity, which causes the effect of rTMS to disappear or even reverse, and a certain length of interval between rTMS trains might break the modulation of homeostatic metaplasticity. However, it remains unknown whether the effects of high-frequency rTMS can be modulated by homeostatic metaplasticity by lengthening the train duration and whether homeostatic metaplasticity can be broken by prolonging the inter-train interval.

Methods: In this study, 15 subjects participated in two experiments including different rTMS protocols targeting the motor cortex. In the first experiment, high-frequency rTMS protocols with different train durations (2s and 5s) and an inter-train interval of 25s were adopted. In the second experiment, high-frequency rTMS protocols with a train duration of 5s and different inter-train intervals (50s and 100s) were adopted. A sham protocol was also included. Changes of motor evoked potential amplitude acquired from electromyography, power spectral density, and intra-region and inter-region functional connectivity acquired from electroencephalography in the resting state before and after each rTMS protocol were evaluated.

Results: High-frequency rTMS with 2s train duration and 25s inter-train interval increased cortex excitability and the power spectral density of bilateral central regions in the alpha frequency band and enhanced the functional connectivity between central regions and other brain regions. When the train duration was prolonged to 5s, the after-effects of high-frequency rTMS disappeared. The after-effects of rTMS with 5s train duration and 100s inter-train interval were the same as those of rTMS with 2s train duration and 25s inter-train interval.

Conclusion: Our results indicated that train duration and inter-train interval could induce the homeostatic metaplasticiy and determine the direction of intensity of rTMS after-effects, and should certainly be taken into account when performing rTMS in both research and clinical practice.

KEYWORDS

high-frequency repetitive transcranial magnetic stimulation, metaplasticity, train duration, inter-train interval, motor evoked potential, electroencephalography

1. Introduction

Repetitive transcranial magnetic stimulation (rTMS) is a non-invasive brain stimulation technology that can modulate cortical activity using time-varying magnetic fields, and the effects of rTMS can outlast the stimulation time (Hayashi et al., 2004; Thut and Pascual-Leone, 2010). Furthermore, rTMS can modulate not only the targeted cortex but also distal brain regions that have functional connections with the targeted cortex (Di Lazzaro et al., 2011; Jin et al., 2017). As an effective tool to improve motor function and cognitive learning, rTMS has been used in the treatment of neuropsychiatric disorders (Lewis, 2018; Li et al., 2018; Lefaucheur et al., 2020).

Many parameters of rTMS protocols can be adjusted, including stimulation intensity, stimulation frequency, stimulation duration, train duration, and inter-train interval. By adjusting these stimulation parameters, rTMS can modulate the neural activity in both directions and improve brain function (Arai et al., 2007; Taylor and Loo, 2007; Jung et al., 2008). Previously, it was thought that the excitatory or inhibitory properties of rTMS protocols are dependent on the stimulation frequency; specifically, low-frequency (≤1 Hz) rTMS decreases the excitability of the motor cortex, and high-frequency (≥5 Hz) rTMS induces facilitatory effects (Houdayer et al., 2008; Di Lazzaro et al., 2011). However, many recent studies have confirmed that the dichotomy of the rTMS effect based solely on stimulation frequency is not reasonable (Rothkegel et al., 2010; Wischnewski and Schutter, 2015). By adjusting stimulation parameters, such as inter-train interval and stimulation duration, high-frequency rTMS can reduce the excitability of the motor cortex, low-frequency rTMS can improve the excitability of the motor cortex, and the after-effects of rTMS on the motor cortex can be eliminated. These observations suggest that it is important to research the after-effects of rTMS stimulation parameters on the brain in order to apply rTMS reasonably.

The effects of rTMS modulating the brain is also affected by the instantaneous state of neural oscillation. It was reported that the instantaneous phase of mu-rhythm in motor area might be reflect the instantaneous state of brain neuron, and the amplitude of MEP induced by TMS at different phase of mu-rhythm was significantly different (Hussain et al., 2019). In 2018, Zrenner et al. (2018) developed a brain-state dependent TMS based on mu-rhythm phase, and demonstrated causally the brain-state-dependent effect of rTMS. On the other hand, The after-effect of rTMS stimulation parameters on brain activity is affected by homeostatic metaplasticity, an important mechanism for maintaining overall synaptic weight and firing rate in a neuronal network within the physiological range (Ziemann and Siebner, 2008; Karabanov et al., 2015; Müller-Dahlhaus and Ziemann, 2015). For example, high-frequency rTMS without inter-train interval does not increase cortical excitability (Rothkegel et al., 2010). Additionally, doubling the stimulation duration of intermittent theta burst stimulation (iTBS) and continuous theta burst stimulation (cTBS) respectively decreased and increased cortical excitability (Gamboa et al., 2010, 2011; Murakami et al., 2012). These findings in humans can be explained by the homeostatic metaplasticity mechanism, that is, if rTMS with a long stimulation duration is applied, the first epoch of the rTMS pulses modulate the brain activities to a specific state, and the effects of the second epoch of the rTMS pulses on brain activities are restricted or reversed because of homeostatic metaplasticity.

An animal study using rat hippocampal slices showed that doubling the stimulation duration of iTBS induced homeostatic plasticity, but additive long-term potentiation effects occurred if a delay of 1 h was set between iTBS sessions (Kramár et al., 2012). This phenomenon was also found in subsequent studies with human subjects, indicating that the stimulation interval of rTMS could make the rTMS after-effect break the homeostatic plasticity, and even produce a stronger effect (Opie et al., 2017; Tse et al., 2018). Hence, the stimulation interval and the stimulation duration during high-frequency rTMS might be the crucial factors determining the direction and intensity of neuroplastic changes.

The after-effect of high-frequency rTMS refers to the accumulated effects of each stimulation train. In theory, if the effect of a single stimulation train of the high-frequency rTMS is to increase the cortical excitability, then the after-effect of high-frequency rTMS would be the augmentation of cortical excitability. If the duration of a single stimulation train of the high-frequency rTMS is prolonged, homeostatic metaplasticity might be triggered, resulting in the disappearance or reversal of rTMS after-effects. Furthermore, by prolonging the inter-train intervals of a high-frequency rTMS protocol, the effect of rTMS on cortical excitability can be increased or reproduced. By understanding the homeostatic metaplasticity characteristics of the brain induced by train duration and inter-train interval, brain-state dependent TMS protocols based on homeostatic metaplasticity would be developed in the future, and the effect of rTMS on the brain would be further enhanced. However, the effects of train duration and inter-train interval in high-frequency rTMS have been largely overlooked. Therefore, we hypothesized that (1) prolonging the train duration of high-frequency rTMS might result in the disappearance or reversal of excitatory effects and (2) the excitatory effect can be maintained by extending the inter-train intervals.

In our study, we designed two experiments involving 10 Hz high-frequency rTMS. In the first experiment, the train durations were set to 2 s and 5 s, and the inter-train interval was 25 s. Several studies have proved that high-frequency rTMS with 2 s train duration increases the excitability of the motor cortex (Di Lorenzo et al., 2013; Cha and Hwang, 2022). In the second experiment, considering that too long train duration might lead to safety problems, and it was safe to not exceed 5 s for train duration according to TMS safety guidelines when stimulation frequency is 10 Hz (Rossi et al., 2009, 2020). And there were study showing that rTMS with 5 s train duration could not enhance the cortical excitability (Jung et al., 2008; Huang et al., 2017). So, in our study, the train duration was set to 5 s, and the inter-train interval was prolonged to 50 s and 100 s. The motor evoked potential (MEP) and electroencephalography (EEG) in the resting closed-eye state were measured before and after rTMS. The changes of cortical excitability, power spectral density, and intra-region and inter-region functional connectivity were observed.

2. Methods

2.1. Subjects

Fifteen healthy subjects participated in the study (mean age 25.07 ± 1.79 years; 8 women). All subjects were screened for any contraindications to TMS (Nyffeler and Müri, 2010). None had been diagnosed with any significant neurological disorder, had any implanted metallic electrical device, or had taken any medication in the 7 days before their participation in the experiment. All subjects

were right-handed according to the Edinburgh Handedness Inventory (Oldfield, 1971) and naïve to rTMS, and all of them provided written informed consent in accordance with the Declaration of Helsinki. The Ethics Committee of the Institute of Biomedical Engineering, Chinese Academy of Medical Sciences and Peking Union Medical College, approved the study.

2.2. Procedure

A frequency of 10 Hz was chosen for rTMS, as this has been shown to be effective and has been widely used in the research on human brain function and the treatment of disease. Based on the rTMS safety guidelines (Chen et al., 1997; Wassermann, 1998; Rossi et al., 2009, 2020), 10 Hz rTMS at 80% resting motor threshold (RMT) was performed, and 1,200 pulses were delivered for each rTMS protocol. All experiments were performed at the same time of day (from 9 a.m. to 11 a.m.) to avoid variability due to diurnal effects (Sale et al., 2007; Ridding and Ziemann, 2010). All experiments were performed by an experienced experimenter to ensure consistency.

The experimental paradigm was shown in Figure 1A. At the beginning of each rTMS session, the RMT was measured to prevent RMT fluctuations over time. Before and after each rTMS protocol, EEG was recorded for at least 3 min in the resting state with eyes closed, and MEP was measured through single pulse TMS targeting the motor cortex. After recording the resting state EEG signals after rTMS, we needed switch on the rTMS instrument and set the stimulus parameters required for MEP measurement, so MEP was measured at an interval of 5 min after rTMS. All subjects participated in both experiment 1 and experiment 2. Throughout the experiments, the subjects were not told which rTMS protocol was being used.

Experiment 1

We studied the effects of train duration of high-frequency rTMS on brain activities (Figure 1B). All subjects received three rTMS protocols, administered at least 5 days apart. For each protocol, the inter-train interval was 25 s. One protocol was rTMS with 2 s train duration (total duration: ~30 min), and another protocol was rTMS with 5 s train duration (total duration: ~12 min). A sham rTMS protocol was also adopted, and the pattern of the sham protocol was identical to the rTMS protocol with 2 s train duration. For the sake of convenience, we used intuitive abbreviations for protocols: the abbreviation for rTMS with 2 s train duration and 25 s inter-train interval was rTMS2s/25 s, rTMS with 5 s train duration and 25 s inter-train interval was rTMS5s/25 s. The order in which the protocols were administered was pseudo-randomized and counterbalanced.

Experiment 2

We studied the effects of inter-train interval of high-frequency rTMS on brain activities (Figure 1C). All subjects received two rTMS protocols, administered at least 5 days apart. One protocol had an inter-train interval of 50 s (total duration: ~18 min), and the other had an inter-train interval of 100 s (total duration: ~30 min). Both protocols had a train duration of 5 s. For the sake of convenience, we used

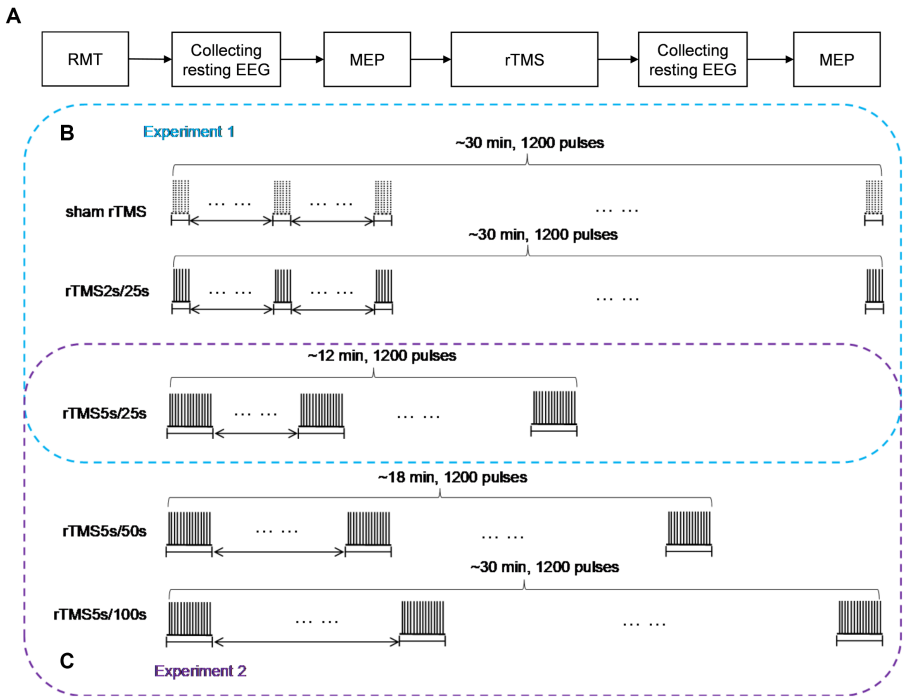

FIGURE 1
Study design schematic. **(A)** Baseline RMT was assessed before each rTMS protocol, resting EEG in closed eye state, and MEP measurements were obtained before and after 10Hz rTMS. **(B)** In experiment 1, rTMS protocols with a train duration of either 2s or 5s and an inter-train interval of 25s, a sham protocol were also administered, the order of which was pseudo-randomized and counterbalanced. **(C)** In experiment 2, rTMS protocols with an inter-train interval of either 50s or 100s and a train duration of 5s were administered, the order of which was pseudo-randomized and counterbalanced. The 25s inter-train interval was adopted in experiment 1. So, we could obtain the effects of rTMS with three different inter-train intervals in experiment 2. rTMS2s/25s, 2s train duration and 25s inter-train interval; rTMS5s/25s, 5s train duration and 25s inter-train interval; rTMS5s/50s, 5s train duration and 50s inter-train interval; rTMS5s/100s, 5s train duration and 100s inter-train interval.

intuitive abbreviations for protocols: the abbreviation for rTMS with 5 s train duration and 50 s inter-train interval was rTMS5s/50s, rTMS with 5 s train duration and 100 s inter-train interval was rTMS5s/100 s. The order in which the protocols were administered was pseudo-randomized and counterbalanced. It should be noted that the 25 s inter-train interval was adopted in experiment 1. So, we could obtain the effects of rTMS with three different inter-train intervals.

2.3. TMS

TMS was generated through a figure-eight shaped coil (70 mm standard coil, Mastic, Whitland, United Kingdom) connected to a Magnetic Rapid^2 stimulator (The Magstim Company, Whitland, United Kingdom). For all TMS in our study, the stimulation was guided by a neuronavigation system (Brainsight, Rogue Inc., United Kingdom) to precisely define the neuroanatomical target of TMS from a T1-weighted magnetic resonance image of the subject's brain. The coil was held tangentially to the skull with the handle pointing backward, at an angle of 45° to the sagittal plane, such that an anterior–posterior current flow, followed by a posterior–anterior current flow (AP-PA), was induced in the underlying cortex. The coil was held over the hand area of the left motor cortex. The scalp position resulting in the most consistent and largest MEP in the first dorsal interosseous muscle (i.e., the motor "hotspot") was determined and used throughout the session. The RMT was then determined as the minimum intensity necessary to elicit at least 5 out of 10 continuous MEPs with a peak-to-peak amplitude greater than 50 μV while the target muscle was relaxed.

2.4. Electromyography

The surface EMG was recorded from the first dorsal interosseous muscle via Ag/AgCl electrodes in a belly-tendon montage (Myoquick Matrix Line-Micromed Srl, Mogliano Veneto, Italy). The ground electrode was placed over the pisiform bone. The sampling rate of the signal was 32,768 Hz. The stimulus intensity was then set to 120% RMT to test the MEP, according to previous literatures (Di Lazzaro et al., 2011; Casula et al., 2014; Pellegrini et al., 2018; Hussain et al., 2019; Thomson et al., 2019). This stimulus intensity was used throughout the experiment to index changes in cortical excitability. A total of 20 stimulus pulses were delivered, with an interval of 5 s. The EMG signals were filtered and stored in a laboratory computer for offline analysis. To index changes in cortical excitability following rTMS, peak-to-peak MEP amplitudes were averaged across trials before and after each rTMS protocol.

2.5. EEG acquisition

Subjects were seated in a reclining armchair with the neck and back supported with a pillow, arms relaxed, and eyes closed. They were asked to avoid eye movements and blinks during recordings. We chose to test subjects with eyes closed to reduce the interference of eye movements and muscle artifacts. Electrode montage and placement were set up according to the international 10/20 system. EEG signals were acquired through a 64-channel BrainAmp EEG system (Brain, Brain Products GmbH, Munich, Germany). A 64-channel EEG cap was positioned on each subject's head. The reference electrode was at the FCz site, and the ground electrode was at the FPz site. The impedance for all electrodes was kept below 5 kΩ. EEG was recorded for at least 3 min before and after rTMS in the resting state with the eyes closed. The EEG data were sampled at a frequency of 1,000 Hz and filtered through a 0–200 Hz band-pass filter. Data were subsequently processed offline.

2.6. EEG processing

EEG data were processed offline using MATLAB (version 17.0) and EEGLAB toolbox (version 14.1.1). All channels were re-referenced to the common average. Unnecessary electrodes (TP9, TP10, FT9, FT10) were removed. Signal periods that contained large muscular and other nonstereotyped artifacts were then carefully pruned from the signals. Continuous recordings were band-pass filtered between 0.5 and 45 Hz and then notched to remove power-line interference (50 Hz). This data selection was followed by independent component analysis. The components, amplitude topography, frequency spectra, and component time series were inspected to identify eye blinks, eye movements, and heart rhythms (Delorme and Makeig, 2004; Delorme et al., 2007), which were removed. 150 s EEG signals without artifacts were selected manually from each subject's EEG recording. The band-pass filters were used to extract the alpha (8–13 Hz) frequency bands. Finally, a total of 75 segments, each lasting 2 s, were chosen for data analysis. Subsequent power spectral density and functional connectivity analyses were conducted on these 5 s data segments. Fast Fourier transform was applied to estimate the spectral power density for each electrode.

2.7. Phase lag index

The functional connectivity between different brain regions was computed using the phase lag index (PLI; Stam et al., 2007). PLI is an indicator of the asymmetry in the distribution of phase differences between two signals, and it reflects the consistency with which one signal is phase leading or lagging in comparison with another. If the phase difference between two time series is $\Delta\Phi(t_k)(k=1\ldots N)$, then the PLI can be computed as follows:

$$\mathrm{PLI} = \left| sign\left[\Delta\Phi(t_k)\right]\right|$$

where $\langle\cdot\rangle$ is the mean value operator. The value of PLI ranges between 0 and 1. A PLI of 0 indicates either no coupling or coupling with a phase difference centered at approximately 0 mod π, whereas a PLI of 1 indicates perfect phase locking at a value of $\Delta\Phi$ from 0 mod π. The stronger the nonzero phase locking, the larger the value of PLI. A 59×59 channel matrix consisting of the PLI values for each electrode pair was obtained for each subject before and after rTMS.

To evaluate changes of functional connectivity induced by each rTMS protocol, EEG electrodes were grouped into eight regions—left frontal region (FP1, AF3, AF7, F1, F3, F5) and right frontal region (Fp2, AF4, AF8, F2, F4, F6), left temporal region (F7, FT7, FC5, C5, T7, CP5, TP7, P7) and right temporal region (F8, FC6, FT8, C6, T8,

CP6, TP8, P8), left central region (FC3, FC1, C1, C3, CP1, CP3) and right central region (FC2, FC4, C2, C4, CP2, CP4), left occipital region (P5, P3, P1, PO3, PO7, O1) and right occipital region (P2, P4, P6, PO4, PO8, O2), as shown in Figure 2. In this study, inter-region connections were defined as the mean PLI of the electrode pairs between one region and the other region. The intra-region connections were defined as the mean PLI of the electrode pairs within one region. Midline channels were not used.

2.8. Statistical analyses

All data were expressed as mean ± standard deviation. All analyses were performed using SPSS (version 21.0) and MATLAB (version 17.0). Responders and non-responders were classified according to the changes of MEP amplitude, below and above 100% of the baseline, induced by each rTMS protocol. The data normality was tested by the Shapiro–Wilk test for each group. In this study, if changes of each rTMS protocol were normally distributed data, the paired sample *t*-test was used to obtain the changes induced by each rTMS protocol. If the changes of each rTMS protocol were non-Gaussian distributions, the Wilcoxon test was used. For group comparisons of normally distributed data, one-way analysis of variance (ANOVA) was used to obtain the difference between rTMS protocols. *Post hoc* statistics were obtained using Tukey's method for multiple comparisons. The Kruskal–Wallis test was used for non-Gaussian distributions. The Friedman test with factor "5 rTMS protocols" was applied for MEP amplitude, and Dunn's method was used for multiple comparisons. The significance level was set at 0.05, unless otherwise indicated.

3. Results

All subjects completed the experiments. No subjects reported serious adverse effects during or after the experiments.

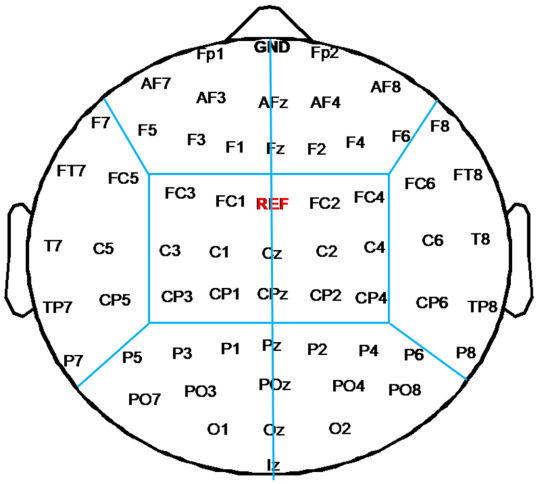

FIGURE 2
Electrode partition diagram. EEG channels were grouped into eight regions: left and right frontal region, left and right temporal region, left and right central region, left and right occipital region. They are denoted by the letters F, T, C, and T, respectively.

3.1. Baseline RMT and rTMS intensity

The RMT and rTMS intensity (wearing EEG cap) values at baseline for each rTMS protocol are presented in Table 1. The RMT was about 75% machine output. The rTMS intensity in this study was 80% RMT, which was about 60% machine output. One-way ANOVA confirmed that there were no differences in baseline RMT or rTMS intensity among the five groups ($F = 0.022$, $p = 0.999$).

3.2. MEP amplitude

The MEP amplitudes were tested before and after each rTMS protocol, and the results are shown in Figure 3. The MEP amplitude did not change after sham rTMS ($t = -0.6808$, $p = 0.507$). The MEP amplitude increased significantly after rTMS2s/25 s ($t = -2.734$, $p = 0.016$). However, when the train duration was prolonged to 5 s, the MEP amplitude did not change ($t = -0.319$, $p = 0.755$). No change was found when the inter-train interval was prolonged to 50 s ($t = -1.438$, $p = 0.172$), but the MEP amplitude increased compared to the baseline when the inter-train interval was prolonged to 100 s ($t = -3.222$, $p = 0.006$). The results showed that 10 Hz rTMS2s/25 s increased the excitability of the corticospinal tract. The effects of 10 Hz rTMS on the excitability of the corticospinal tract disappeared when the train duration was prolonged to 5 s from 2 s but appeared when the inter-train interval was 100 s.

Furthermore, we calculated the changes of MEP amplitude induced by each rTMS protocol through after rTMS minus before rTMS. The changes of MEP amplitude for different rTMS protocols were analyzed using one-way ANOVA. As shown in Figure 3B, different rTMS protocols had significant main effects ($F = 6.876$, $p = 0.0001$). After *post hoc* statistical analysis, the results showed that the changes of MEP amplitude induced by the rTMS2s/25 s and the rTMS5s/100 s were significantly different from those induced by sham rTMS, rTMS5s/25 s and rTMS5s/50s. The changes of MEP amplitude induced by the rTMS5s/25 s and the rTMS5s/50s were not different compared to those induced by sham rTMS. The rTMS2s/25 s was not different compared to the rTMS5s/100 s. The results confirmed that the rTMS2s/25 s and rTMS5s/100 s had a significant influence on the MEP amplitude, whereas the rTMS5s/25 s and rTMS5s/50s did not.

To quantify the percentage of individuals in which MEPs were facilitated or inhibited following each rTMS protocol, the MEP amplitudes were normalized to the baseline. Greater than 110% baseline MEP amplitude was counted was as a facilitated response, less than 90% was counted as an inhibited response, and between 90 and 110% was counted as no responders (Nettekoven et al., 2015; Thomson et al., 2019; Tiksnadi et al., 2020; Bakulin et al., 2022). As shown in Figure 3C, facilitated MEPs were observed in 13.33, 46.67, 13.33, 26.67, and 53.33% of individuals following sham rTMS, rTMS2s/25 s, rTMS5s/25 s, rTMS5s/50s, and rTMS5s/100 s, respectively.

3.3. Power spectral density

Changes of power spectral density in the alpha frequency band (8–12 Hz) were calculated following each rTMS protocol, the results are shown in Figure 4. Electrodes showing significant differences are marked with blue stars ($p < 0.01$). The power spectral density in the

TABLE 1 RMT and rTMS intensity at baseline.

	Sham	TD: 2s, ITI: 25s	TD: 5s, ITI: 25s	TD: 5s, ITI: 50s	TD: 5s, ITI: 100s
RMT	75.00% ± 6.89%	75.33% ± 6.84%	75.67% ± 6.03%	75.53% ± 6.61%	75.47% ± 6.51%
rTMS intensity	60.00% ± 5.51%	60.27% ± 5.47%	60.53% ± 4.83%	60.43% ± 5.29%	60.37% ± 5.21%

RMT, resting motor threshold; rTMS, repetitive transcranial magnetic stimulation; TD, train duration; ITI, inter-train interval.

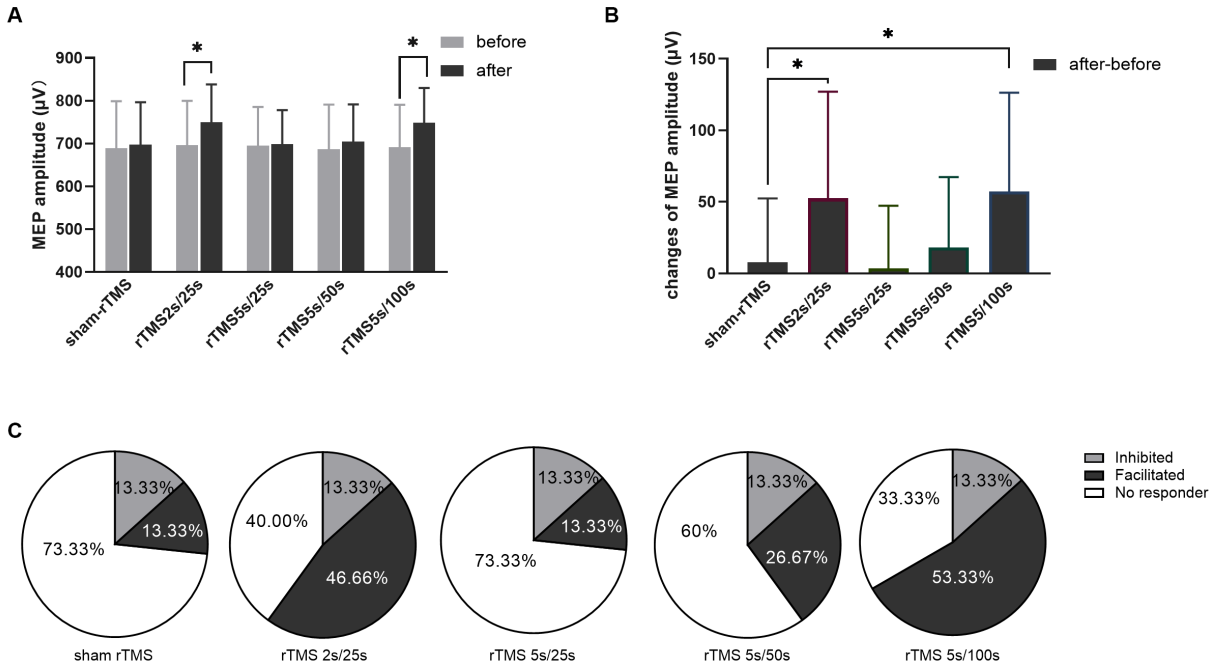

FIGURE 3
Effects of each rTMS protocol on the MEP amplitude. **(A)** MEP amplitude before and after each rTMS protocol. **(B)** Changes of MEP amplitudes induced by five rTMS protocols. **(C)** Percentage of individuals showing facilitated or inhibited MEPs following each rTMS protocol. Greater than 110% baseline MEP amplitude was counted was as a facilitated response, less than 90% was counted as an inhibited response, and between 90 and 110% was counted as no responders. rTMS2s/25s, 2s train duration and 25s inter-train interval; rTMS5s/25s, 5s train duration and 25s inter-train interval; rTMS5s/50s, 5s train duration and 50s inter-train interval; rTMS5s/100s, 5s train duration and 100s inter-train interval. The changes of MEP amplitudes with significant differences are marked with stars (*p<0.05).

alpha frequency band increased after all active (i.e., not sham) rTMS protocols in most brain regions. The power spectral density in the central and temporal regions of both hemispheres increased significantly after the rTMS2s/25 s. Also, the power spectral density in the central and temporal regions of both hemispheres and in the frontal and parietal-occipital junctions of the stimulated hemisphere increased significantly after the. Compared to the rTMS2s/25 s, the changes of power spectral density induced by rTMS5s/100 s were wider in the stimulated hemisphere. The power spectral density increased after the rTMS5s/25 s and after the rTMS5s/50s, but no statistically significant differences were found in any regions. No change was found to be significant following the sham rTMS protocol.

The difference of power spectral density in the alpha frequency band among five rTMS protocol were analyzed to assess the different effects of rTMS protocols. The results were shown in Figure 5. Significant effects were observed in the frontal, central, and temporal regions of the stimulated hemisphere for the alpha frequency band (p < 0.05). After *post hoc* statistical analysis, the results showed that the power spectral density induced by the rTMS2s/25 s and rTMS5s/100 s was significantly different from that induced by the sham rTMS, which was distributed in the frontal and central regions of the stimulated hemisphere. The power spectral density induced by the rTMS5s/100 s inter-train interval was distributed in a broader brain region, compare to the rTMS2s/25 s, which was distributed in the central and frontal regions of the stimulated hemisphere. There were no significant differences between other active rTMS protocols and the sham rTMS protocol or among active rTMS protocols. The results confirmed that the rTMS2s/25 s and the rTMS5s/100 s had a significant influence on the power spectral density in the alpha frequency band, whereas the rTMS5s/25 s and the rTMS5s/50s did not.

3.4. Functional connectivity

First, the intra-region PLI values of each region and the inter-region PLI values between all regions in the alpha frequency band were calculated, then significant changes of inter-region and intra-region PLI in the alpha frequency band induced by each rTMS protocol were assessed. The results were shown in Figure 6. The sham-rTMS (Figure 6A) and rTMS5s/25 s (Figure 6C) did not change the PLI in the alpha frequency band. When the inter-train interval was prolonged from 25 s to 50 s, the PLI increased in the

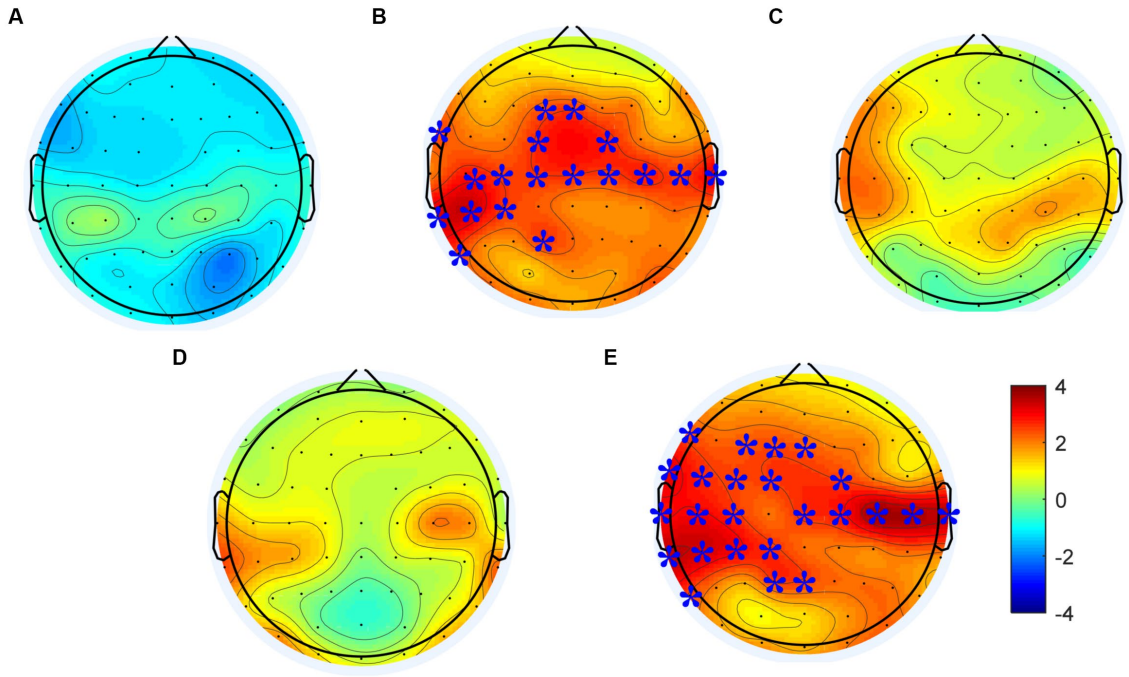

FIGURE 4
Changes in power spectral density in the alpha frequency band induced by each rTMS protocol. **(A)** sham-rTMS; **(B)** rTMS2s/25s; **(C)** rTMS5s/25s; **(D)** rTMS5s/50s; **(E)** rTMS5s/100s. rTMS2s/25s, 2s train duration and 25s inter-train interval; rTMS5s/25s, 5s train duration and 25s inter-train interval; rTMS5s/50s, 5s train duration and 50s inter-train interval; rTMS5s/100s, 5s train duration and 100s inter-train interval. Electrodes showing significant differences are marked with blue stars (*p<0.01).

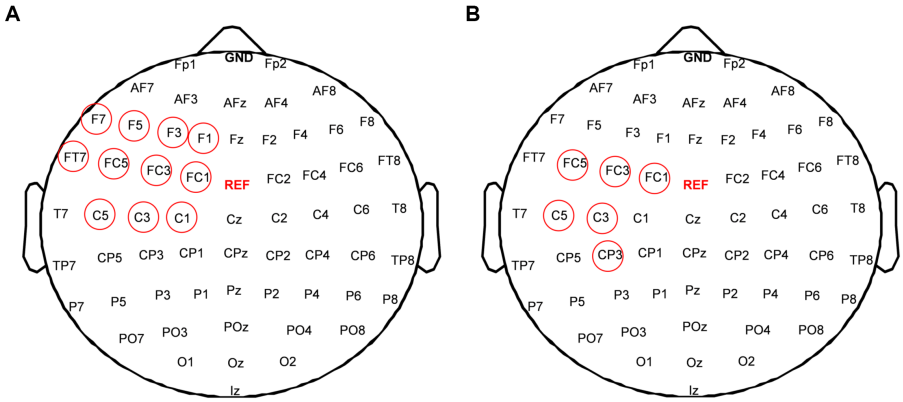

FIGURE 5
Difference of power spectral density in alpha frequency band among five rTMS protocols; **(A)** between the rTMS2s/25s and sham-rTMS; **(B)** between the rTMS5s/100s and sham-rTMS. rTMS2s/25s, 2s train duration and 25s inter-train interval; rTMS5s/25s, 5s train duration and 25s inter-train interval. Red circles show the electrodes which showed the significant difference of power spectral density between two rTMS protocols (*p<0.01).

central region of the stimulated hemisphere, the inter-regions between the central region and frontal region, and the temporal region of the stimulated hemisphere (Figure 6D). For the rTMS2s/25 s (Figure 6B) and rTMS5s/100 s (Figure 6E), the functional connectivity increased in lots of intra-regions and inter-regions. For the rTMS2s/25 s, the PLI of the inter-regions in the alpha frequency band increased in the central region of the stimulated hemisphere, the inter-regions between the central region of the stimulated hemisphere and the frontal and occipital regions of the stimulated hemisphere, and between the central regions of both hemispheres. The rTMS5s/100 s affected not only the long functional connectivity of inter-regions but also the short functional connectivity of intra-regions in the alpha frequency band, mainly between the central region of the stimulated hemisphere and other regions. More specifically, the rTMS5s/100 s changed the functional connectivity in the central region of the stimulated hemisphere, the connectivity between the central region of the stimulated hemisphere and the frontal and temporal regions of the stimulated

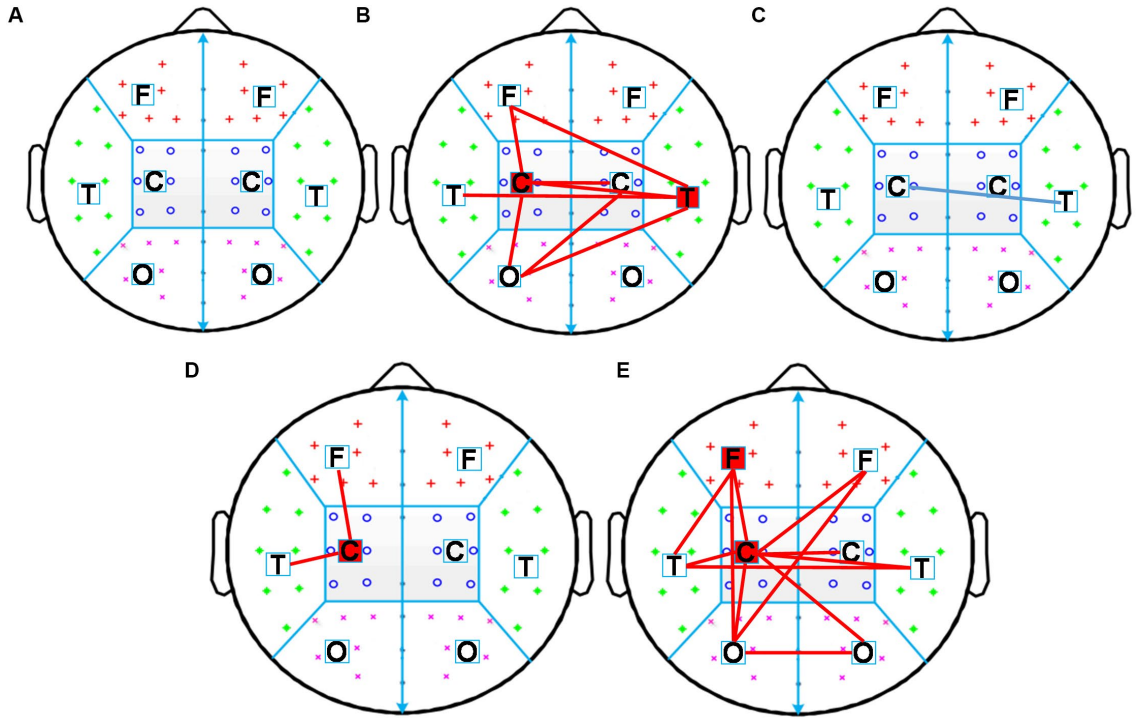

FIGURE 6
Changes in inter-region and intra-region functional connectivity induced by five rTMS protocols. Inter-region connections is defined as the mean PLI of the electrode pairs between one region and the other region. The intra-region connections is defined as the mean PLI of the electrode pairs within one region. Midline channels were not used. **(A)** sham-rTMS; **(B)** rTMS2s/25s; **(C)** rTMS5s/25s; **(D)** rTMS5s/50s; **(E)** rTMS5s/100s. rTMS2s/25s, 2s train duration and 25s inter-train interval; rTMS5s/25s, 5s train duration and 25s inter-train interval; rTMS5s/50s, 5s train duration and 50s inter-train interval; rTMS5s/100s, 5s train duration and 100s inter-train interval. A significant increase in inter-and intra-regions is indicated by red lines and red blocks, respectively. A significant decrease in inter-and intra-regions is indicated by blue lines and blue blocks, respectively.

hemisphere, and the connectivity between the occipital regions of both hemispheres.

4. Discussion

Our study found that 10 Hz rTMS2s/25 s could increase cortex excitability and the power spectral density of bilateral central regions in the alpha band and enhance the functional connectivity between the central regions and other brain regions. When the train duration was prolonged to 5 s, the after-effects of high-frequency rTMS disappeared, and there was no change in any brain region or intra-regions or inter-regions. Furthermore, when the train duration was 5 s and the inter-train interval was extended to 100 s from 25 s, high-frequency rTMS had the same effect as the rTMS2s/25 s. Our results suggested that a single train might be modulated by homeostatic metaplasticity, while a certain length of inter-train interval might make the stimulation train break through the modulation of homeostatic metaplasticity. The train duration and inter-train interval significantly affected the after-effect of high-frequency rTMS.

4.1. The effect of train duration on brain activities

It was reported that high-frequency rTMS could produce different effects with different stimulation durations, which was consistent with our findings. Rothkegel et al. found that continuous rTMS could not improve the cortical excitability, and thought the intervals during rTMS were essential for facilitatory after-effects (Rothkegel et al., 2010). Jung et al. investigated the changes in cortical excitability of the human motor cortex induced by high-frequency TMS of different stimulation durations, and found high-frequency rTMS with 5 s train duration could not improve the cortical excitability. The results of those study were inconsistent with the traditional viewpoint that high frequency rTMS can improve cortical excitability (Houdayer et al., 2008; Di Lazzaro et al., 2011). To date, few studies have focused on the after-effect of train duration in high-frequency rTMS.

In recent years, several studies had investigated the modulation of homeostatic metaplasticity induced by rTMS, using priming stimulation combined with testing stimulation methods (Gamboa et al., 2011; Kramár et al., 2012; Opie et al., 2017). These studies used priming stimulation to change the excitability of the cerebral cortex and the testing stimulation to evaluate the effect of rTMS on cortical excitability. The results demonstrated that the after-effect of rTMS was related to the state of brain activity before rTMS stimulation.

In our study, we speculated that, the single long stimulation train, might be understood as two consecutive short stimulation trains, where the first short stimulation train is a priming stimulation to modulate brain activities to a certain state, and the second short stimulation train is a testing stimulation, the after-effects of which are modulated by homeostatic metaplasticity and, thus, prolonging the train duration might not induce changes in brain activity.

We selected 10 Hz rTMS with 2 s or 5 s train duration. We found that high frequency rTMS with 2 s train duration can increase the amplitude of MEP, the power spectral density of alpha band and functional connectivity. This is consistent with the traditional viewpoint that high frequency rTMS can improve cortical excitability (Houdayer et al., 2008; Di Lazzaro et al., 2011). However, when the train duration was extended to 5 s, high-frequency rTMS not only did not change the amplitude of MEP, but also did not significantly change the EEG power spectrum and brain interval connections. This confirms our hypothesis (1) prolonging the train duration of high-frequency rTMS might result in the disappearance. The results of this study were consistent with the modultaion characteristics of the homeostatic metaplasticity.

4.2. The effect of inter-train interval on brain activities

In high frequency rTMS, after a certain number of pulse stimulation, often set a period of time interval, in order to prevent coil heating and safety consideration. Later, it was found that the inter-train intervals were incorporated into high-frequency rTMS protocols not only to avoid overheating and for safety purposes but also to impact the characteristics of the central nervous system. Rothkegel et al. (2010) found that intervals during 5 Hz rTMS were essential for facilitatory after-effects, and cortical excitability could not be improved by continuous high-frequency rTMS without inter-train interval (Rothkegel et al., 2010). Cash et al. (2017) studied the excitatory and disinhibitory effect of 20 Hz rTMS modulated by different inter-train interval, and found the changes in MEPs did not depend on the inter-train interval, but shorter inter-train interval resulted in greater disinhibitory effects. In our study, we selected 10 Hz rTMS with train duration of 25 s, 50s and 100 s, and found that brain activities, including MEP, power spectral density and functional connectivity, did not change significantly with inter-train intervals of 25 s and 50s. When the inter-train interval was extended to 100 s, not only the MEP amplitude increased, but also the power spectral density and functional connection were significantly changed, compared with the sham group. Our study again demonstrated the importance of inter-train interval in high frequency rTMS.

There might be two possible reasons about the improvement by prolonging the inter-train interval to 100 s. First, neurons firing produces the action potential, which is followed by hyperpolarized postpotential. A series of action potentials have a cumulative effect on the amplitude of hyperpolarized postpotentials, and the duration of the hyperpolarized postpotentials lengthens with the increase of the number of action potentials (Yarom et al., 1985). TMS causes the neuron to depolarize, which is followed by hyperpolarization. With the increase of the number of TMS pulses, the number of action potentials increased, and the amplitude and duration of hyperpolarization increased. Second, a long enough time must pass for high-threshold synapses to be activated and have an effect. That is, because no interval or a short interval is not enough to reduce the threshold of high-threshold synapses, resulting in the enhancement of high-threshold synaptic plasticity. On the other hand, in synapses with different plasticity thresholds, the activation of synaptic mechanisms and protein synthesis required for hard-to-induce LTP effects takes a sufficiently long time (Kramár et al., 2012). In the study of TMS, the tradeoff between train duration and inter-train interval needs to be further studied.

4.3. rTMS changed the activities of alpha rhythm

The alpha rhythm in the sensorimotor cortex is the most specific rhythm of this cortex in the resting state (Hari, 2006). In our study, the power spectral density in the alpha frequency band increased when induced by high-frequency rTMS, a finding consistent with existing views: alpha generation may represent an intrinsic induced response and a basic signature response to TMS targeting the human resting motor cortex (Veniero et al., 2011; Jin et al., 2019). Alpha frequency oscillation (8–13 Hz) in the resting state is an important neural substrate for cognition and motor function. Brain activity in the alpha frequency band can predict the efficiency of cognitive, motor, and other neural processes (Klimesch, 1997; Klimesch et al., 2003; Babiloni et al., 2010). It might be possible to predict the changes of brain efficiency with the changes of train duration and inter-train interval, according to the alpha frequency band. In our study, the results suggested that the changes in the power spectral density and functional connectivity of resting alpha band might reflect whether the brain was in homeostatic metaplasticity moduation.

A number of studies had demonstrated that rTMS over primary motor cortex could alter the activity and function of targeted brain region as well as its related remote regions (Jing and Takigawa, 2000; Plewnia et al., 2008; Grefkes et al., 2010). In our study, we found that there was no significant difference in the amplitude of MEP induced by rTMS2s/25 s and rTMS5s/100 s (Figure 3). However, we found that compared to sham rTMS, rTMS2s/25 s and rTMS5s/100 s increased the power spectral density and functional connectivity in alpha frequency band, and rTMS5s/100 s caused the increase in a wider range of brain regions (Figures 4, 5). This suggested that rTMS5s/100 s might modulate the brain better, in the form of affecting multiple brain regions and brain networks. The activity of many cortices related to motor function, such as premotor, primary motor, and posterior parietal cortex (Youssofzadeh et al., 2016; De Vico Fallani et al., 2017), and the functional connectivity between multi-regions reflects the functional interactions between the underlying brain regions (Ward and Cohen, 2004; Grefkes et al., 2010). Maybe, rTMS5s/100 s might be a more effective protocol to improve the motor function, which is worthy of further study in the future.

4.4. The contribution of this study and future directions

It was found in our study that the excitatory effect of high-frequency rTMS disappeared when the train duration was prolonged, but it reappeared when the inter-train interval was prolonged to a specific value, that is, when the excitatory effect of high-frequency rTMS was increased, if a longer train duration was used, a longer inter-train interval was required. If only the train duration was increased without a corresponding increase in inter-train interval, the modulation effect on the brain activities may reach the threshold of no response, or even exceed the threshold of long-term potentiation, and make the effect of rTMS reverse. Therefore, there is a trade-off between train duration and inter-train interval, which influences the effects of high-frequency rTMS.

First, our study suggested that the train duration and inter-train interval should be taken into account when discussing stimulation

protocols in both research and clinical practice. More importantly, since the effect of high-frequency rTMS on the brain activities is the superposition of multiple trains, and each train is composed of multiple magnetic pulses. We speculated that for the train duration of rTMS, the neuron excitation state gradually increased with the increase of the number of rTMS stimulation pulses, and the neuron excitation state reached the highest value when the pulses number increased to a certain number. At this time, if the pulse output continued, the neuron excitation began to decrease or even reverse under the influence of homeostatic metaplasticity mechanism. Our study suggested that the brain-state stimulation rTMS methods based on homeostatic metaplasticity would be the future directions, in order to improve the effects of rTMS.

In our study, the power spectral density and functional connectivity induced by rTMS with different train duration and inter-train interval were different, which suggested that in the future, we might be able to use power spectral density or functional connectivity as a sign of homeostatic metaplasticity. That is, we might judge the brain-state through the changes of power spectral density or functional connectivity, and decide whether to continue rTMS pulse output.

Our results suggested that the effects of rTMS with different the train duration and inter-train interval were different, which might be influenced by the mechanism of homeostatic metaplasticity. Similarly, we belive that when rTMS was performed over other brain regions, that the homeostatic metaplasticity also existed. However, it is worth mentioning that the train duration inducing the homeostatic metaplasticity might be different for other brain regions, which needs to be verified by detailed experiments in the future. Furthermore, the results in our study might be used to other stimulation protocols. For example, different TBS and tES protocols might induce the homeostatic metaplasticity, the power spectral density and functional connectivity might be used to optimize the parameters to improve the effects of brain-stimulation.

4.5. Limitations

This is the first study describing neural activity changes as a response to prolonged duration of stimulation train in high-frequency rTMS in the same subjects. We ensured that, except for the inter-train interval parameter in experiments 1 and 2, the experimental conditions and TMS parameters were the same for all rTMS protocols to eliminate the impact of all other factors. However, our study has some limitations. First, the number of subjects was small (15 subjects were included in the final analysis), although we performed the experiment 90 times. Studies with a larger sample could help provide more reliable results on the homeostasis mechanism, which was reduced by prolonging the duration of stimulation trains. Despite these limitations, the results confirm that rTMS with different inter-train intervals can induce different oscillatory brain activity. Second, in our study, the persistent post-rTMS effects were not measured, but we measured neural oscillations across the brain using EEG and still found no changes in activity induced by prolonged duration of stimulation train of high-frequency rTMS. Third, in our study, MEPs were collected when the hand muscles were relaxed, which was the most commonly used method to detect motor cortical excitability. MEPs collected during muscle contraction is another method that can be used to assess the motor cortical excitability and will be considered in the future.

5. Conclusion

Our study showed that the high-frequency rTMS with a longer train duration could trigger the modulation of homeostatic metaplasticity, which was reflected by the MEP amplitude, power spectral density, and functional connectivity before and after rTMS. Furthermore, a longer interval in rTMS might break the modulation of homeostatic metaplasticity. Our results indicated that train duration and inter-train interval significantly affected the after-effect of high-frequency rTMS. Clinicians and researchers should not only use stimulation frequency but also train duration and inter-train interval when performing rTMS stimulation treatments and experiments to classify the after-effect of rTMS.

Data availability statement

The raw data supporting the conclusions of this article will be made available by the authors, without undue reservation.

Ethics statement

The studies involving human participants were reviewed and approved by the Ethics Committee of the Institute of Biomedical Engineering, Chinese Academy of Medical Sciences and Peking Union Medical College. The patients/participants provided their written informed consent to participate in this study.

Author contributions

JJ, XW, HW, ZL, and TY designed the study. JJ and XW conducted the study. HW and XW recruited subjects. JJ conducted the statistical analyses and drafted the manuscript, which all authors critically revised. All authors contributed to the article and approved the submitted version.

Funding

This study was supported by the National Natural Science Foundation of China (grant number: 52007199, 81927806), the China Key Research and Development Program (grant number: 2022YFC2402202), and the CAMS Initiative for Innovative Medicine (grant number: 2021-I2M-1-058).

Acknowledgments

The authors thank LetPub (www.letpub.com) for its linguistic assistance during the preparation of this manuscript.

Conflict of interest

The authors declare that the research was conducted in the absence of any commercial or financial relationships that could be construed as a potential conflict of interest.

Publisher's note

All claims expressed in this article are solely those of the authors and do not necessarily represent those of their affiliated organizations, or those of the publisher, the editors and the reviewers. Any product that may be evaluated in this article, or claim that may be made by its manufacturer, is not guaranteed or endorsed by the publisher.

Supplementary material

The Supplementary material for this article can be found online at: https://www.frontiersin.org/articles/10.3389/fnins.2023.1157080/full#supplementary-material

References

Arai, N., Okabe, S., Furubayashi, T., Mochizuki, H., Iwata, N. K., Hanajima, R., et al. (2007). Differences in after-effect between monophasic and biphasic high-frequency rTMS of the human motor cortex. *Clin. Neurophysiol.* 118, 2227–2233. doi: 10.1016/j.clinph.2007.07.006

Babiloni, C., Marzano, N., Iacoboni, M., Infarinato, F., Aschieri, P., Buffo, P., et al. (2010). Resting state cortical rhythms in athletes: a high-resolution EEG study. *Brain Res. Bull.* 81, 149–156. doi: 10.1016/j.brainresbull.2009.10.014

Bakulin, I., Zabirova, A., Sinitsyn, D., Poydasheva, A., Lagoda, D., Suponeva, N., et al. (2022). Adding a second iTBS block in 15 or 60 min time interval does not increase iTBS effects on motor cortex excitability and the responder rates. *Brain Sci.* 12:1064. doi: 10.3390/brainsci12081064

Cash, R. F. H., Dar, A., Hui, J., De Ruiter, L., Baarbé, J., Fettes, P., et al. (2017). Influence of inter-train interval on the plastic effects of rTMS. *Brain Stimul.* 10, 630–636. doi: 10.1016/j.brs.2017.02.012

Casula, E. P., Tarantino, V., Basso, D., Arcara, G., Marino, G., Toffolo, G. M., et al. (2014). Low-frequency rtms inhibitory effects in the primary motor cortex: insights from TMS-evoked potentials. *NeuroImage* 98, 225–232. doi: 10.1016/j.neuroimage.2014.04.065

Cha, T. H., and Hwang, H. S. (2022). Rehabilitation interventions combined with noninvasive brain stimulation on upper limb motor function in stroke patients. *Brain Sci.* 12:994. doi: 10.3390/brainsci12080994

Chen, R., Gerloff, C., Classen, J., Wassermann, E. M., Hallett, M., and Cohen, L. G. (1997). Safety of different inter-train intervals for repetitive transcranial magnetic stimulation and recommendations for safe ranges of stimulation parameters. *Electroencephalogr. Clin. Neurophysiol.* 105, 415–421. doi: 10.1016/s0924-980x(97)00036-2

De Vico Fallani, F., Clausi, S., Leggio, M., Chavez, M., Valencia, M., Maglione, A. G., et al. (2017). Interhemispheric connectivity characterizes cortical reorganization in motor-related networks after cerebellar lesions. *Cerebellum* 16, 358–375. doi: 10.1007/s12311-016-0811-z

Delorme, A., and Makeig, S. (2004). EEGLAB: an open source toolbox for analysis of single-trial EEG dynamics including independent component analysis. *J. Neurosci. Methods* 134, 9–21. doi: 10.1016/j.jneumeth.2003.10.009

Delorme, A., Sejnowski, T., and Makeig, S. (2007). Enhanced detection of artifacts in EEG data using higher-order statistics and independent component analysis. *NeuroImage* 34, 1443–1449. doi: 10.1016/j.neuroimage.2006.11.004

Di Lazzaro, V., Dileone, M., Pilato, F., Capone, F., Musumeci, G., Ranieri, F., et al. (2011). Modulation of motor cortex neuronal networks by rTMS: comparison of local and remote effects of six different protocols of stimulation. *J. Neurophysiol.* 105, 2150–2156. doi: 10.1152/jn.00781.2010

Di Lorenzo, C., Tavernese, E., Lepre, C., Mangone, M., Currà, A., Pierelli, F., et al. (2013). Influence of rTMS over the left primary motor cortex on initiation and performance of a simple movement executed with the contralateral arm in healthy volunteers. *Exp. Brain Res.* 224, 383–392. doi: 10.1007/s00221-012-3318-y

Gamboa, O. L., Antal, A., Laczo, B., Moliadze, V., Nitsche, M. A., and Paulus, W. (2011). Impact of repetitive theta burst stimulation on motor cortex excitability. *Brain Stimul.* 4, 145–151. doi: 10.1016/j.brs.2010.09.008

Gamboa, O. L., Antal, A., Moliadze, V., and Paulus, W. (2010). Simply longer is not better: reversal of theta burst after-effect with prolonged stimulation. *Exp. Brain Res.* 204, 181–187. doi: 10.1007/s00221-010-2293-4

Grefkes, C., Nowak, D. A., Wang, L. E., Dafotakis, M., Eickhoff, S. B., and Fink, G. R. (2010). Modulating cortical connectivity in stroke patients by rTMS assessed with fMRI and dynamic causal modeling. *NeuroImage* 50, 233–242. doi: 10.1016/j.neuroimage.2009.12.029

Hari, R. (2006). Action-perception connection and the cortical mu rhythm. *Prog. Brain Res.* 159, 253–260. doi: 10.1016/S0079-6123(06)59017-X

Hayashi, T., Ohnishi, T., Okabe, S., Teramoto, N., Nonaka, Y., Watabe, H., et al. (2004). Long-term effect of motor cortical repetitive transcranial magnetic stimulation induces. *Ann. Neurol.* 56, 77–85. doi: 10.1002/ana.20151

Houdayer, E., Degardin, A., Cassim, F., Bocquillon, P., Derambure, P., and Devanne, H. (2008). The effects of low-and high-frequency repetitive TMS on the input/output properties of the human corticospinal pathway. *Exp. Brain Res.* 187, 207–217. doi: 10.1007/s00221-008-1294-z

Huang, H., Liu, W. C., and Song, Y. H. (2017). Effects of repetitive transcranial magnetic stimulation on masseter motor-neuron pool excitability. *Arch. Oral Biol.* 73, 289–294. doi: 10.1016/j.archoralbio.2016.10.015

Hussain, S. J., Claudino, L., Bönstrup, M., Norato, G., Cruciani, G., Thompson, R., et al. (2019). Sensorimotor oscillatory phase-power interaction gates resting human corticospinal output. *Cereb. Cortex* 29, 3766–3777. doi: 10.1093/cercor/bhy255

Jin, J. N., Wang, X., Li, Y., Jin, F., Liu, Z. P., and Yin, T. (2017). The effects of rTMS combined with motor training on functional connectivity in alpha frequency band. *Front. Behav. Neurosci.* 11:234. doi: 10.3389/fnbeh.2017.00234

Jin, J. N., Wang, X., Li, Y., Wang, H., Liu, Z. P., and Yin, T. (2019). rTMS combined with motor training changed the inter-hemispheric lateralization. *Exp. Brain Res.* 237, 2735–2746. doi: 10.1007/s00221-019-05621-z

Jing, H., and Takigawa, M. (2000). Observation of EEG coherence after repetitive transcranial magnetic stimulation. *Clin. Neurophysiol.* 111, 1620–1631. doi: 10.1016/s1388-2457(00)00357-6

Jung, S. H., Shin, J. E., Jeong, Y. S., and Shin, H. I. (2008). Changes in motor cortical excitability induced by high-frequency repetitive transcranial magnetic stimulation of different stimulation durations. *Clin. Neurophysiol.* 119, 71–79. doi: 10.1016/j.clinph.2007.09.124

Karabanov, A., Ziemann, U., Hamada, M., George, M. S., Quartarone, A., Classen, J., et al. (2015). Consensus paper: probing homeostatic plasticity of human cortex with non-invasive transcranial brain stimulation. *Brain Stimul.* 8, 442–454. doi: 10.1016/j.brs.2015.01.404

Klimesch, W. (1997). EEG-alpha rhythms and memory processes. *Int. J. Psychophysiol.* 26, 319–340. doi: 10.1016/s0167-8760(97)00773-3

Klimesch, W., Sauseng, P., and Gerloff, C. (2003). Enhancing cognitive performance with repetitive transcranial magnetic stimulation at human individual alpha frequency. *Eur. J. Neurosci.* 17, 1129–1133. doi: 10.1046/j.1460-9568.2003.02517.x

Kramár, E. A., Babayan, A. H., Gavin, C. F., Cox, C. D., Jafari, M., Gall, C. M., et al. (2012). Synaptic evidence for the efficacy of spaced learning. *Proc. Natl. Acad. Sci. U S A.* 109, 5121–5126. doi: 10.1073/pnas.1120700109

Lefaucheur, J. P., Aleman, A., Baeken, C., Benninger, D. H., Brunelin, J., Di Lazzaro, V., et al. (2020). Evidence-based guidelines on the therapeutic use of repetitive transcranial magnetic stimulation (rTMS): an update (2014–2018). *Clin. Neurophysiol.* 131, 474–528. doi: 10.1016/j.clinph.2019.11.002

Lewis, G. (2018). Transcranial magnetic stimulation for depression. *Lancet* 391, 1639–1640. doi: 10.1016/S0140-6736(18)30863-8

Li, Y., Fan, J., Yang, J., He, C., and Li, S. (2018). Effects of repetitive transcranial magnetic stimulation on walking and balance function after stroke: a systematic review and meta-analysis. *Am. J. Phys. Med. Rehabil.* 97, 773–781. doi: 10.1097/PHM.0000000000000948

Müller-Dahlhaus, F., and Ziemann, U. (2015). Metaplasticity in human cortex. *Neuroscientist* 21, 185–202. doi: 10.1177/1073858414526645

Murakami, T., Müller-Dahlhaus, F., Lu, M. K., and Ziemann, U. (2012). Homeostatic metaplasticity of corticospinal excitatory and intracortical inhibitory neural circuits in human motor cortex. *J. Physiol.* 590, 5765–5781. doi: 10.1113/jphysiol.2012.238519

Nettekoven, C., Volz, L. J., Leimbach, M., Pool, E. M., Rehme, A. K., Eickhoff, S. B., et al. (2015). Inter-individual variability in cortical excitability and motor network connectivity following multiple blocks of rTMS. *NeuroImage* 118, 209–218. doi: 10.1016/j.neuroimage.2015.06.004

Nyffeler, T., and Müri, R. (2010). Comment on: safety, ethical considerations, and application guidelines for the use of transcranial magnetic stimulation in clinical

practice and research, by Rossi et al. (2009). *Clin. Neurophysiol.* 121, 6:980. doi: 10.1016/j.clinph.2010.04.001

Oldfield, R. C. (1971). The assessment and analysis of handedness: the Edinburgh inventory. *Neuropsychologia* 9, 97–113. doi: 10.1016/0028-3932(71)90067-4

Opie, G. M., Vosnakis, E., Ridding, M. C., Ziemann, U., and Semmler, J. G. (2017). Priming theta burst stimulation enhances motor cortex plasticity in young but not old adults. *Brain Stimul.* 10, 298–304. doi: 10.1016/j.brs.2017.01.003

Pellegrini, M., Zoghi, M., and Jaberzadeh, S. (2018). The effect of transcranial magnetic stimulation test intensity on the amplitude, variability and reliability of motor evoked potentials. *Brain Res.* 1700, 190–198. doi: 10.1016/j.brainres.2018.09.002

Plewnia, C., Rilk, A. J., Soekadar, S. R., Arfeller, C., Huber, H. S., Sauseng, P., et al. (2008). Enhancement of long-range EEG coherence by synchronous bifocal transcranial magnetic stimulation. *Eur. J. Neurosci.* 27, 1577–1583. doi: 10.1111/j.1460-9568.2008.06124.x

Ridding, M. C., and Ziemann, U. (2010). Determinants of the induction of cortical plasticity by non-invasive brain stimulation in healthy subjects. *J. Physiol.* 588, 2291–2304. doi: 10.1113/jphysiol.2010.190314

Rossi, S., Antal, A., Bestmann, S., Bikson, M., Brewer, C., Brockmller, J., et al. (2020). Safety and recommendations for tms use in healthy subjects and patient populations, with updates on training, ethical and regulatory issues: expert guidelines. *Clin. Neurophysiol.* 132, 269–306. doi: 10.1016/j.clinph.2020.10.003

Rossi, S., Hallett, M., Rossini, P. M., and Pascual-Leone, A. (2009). Safety, ethical considerations, and application guidelines for the use of transcranial magnetic stimulation in clinical practice and research. *Clin. Neurophysiol.* 120, 2008–2039. doi: 10.1016/j.clinph.2009.08.016

Rothkegel, H., Sommer, M., and Paulus, W. (2010). Breaks during 5Hz rTMS are essential for facilitatory after effects. *Clin. Neurophysiol.* 121, 426–430. doi: 10.1016/j.clinph.2009.11.016

Sale, M. V., Ridding, M. C., and Nordstrom, M. A. (2007). Factors influencing the magnitude and reproducibility of corticomotor excitability changes induced by paired associative stimulation. *Exp. Brain Res.* 181, 615–626. doi: 10.1007/s00221-007-0960-x

Stam, C. J., Nolte, G., and Daffertshofer, A. (2007). Phase lag index: assessment of functional connectivity from multi channel EEG and MEG with diminished bias from common sources. *Hum. Brain Mapp.* 28, 1178–1193. doi: 10.1002/hbm.20346

Taylor, J. L., and Loo, C. K. (2007). Stimulus waveform influences the efficacy of repetitive transcranial magnetic stimulation. *J. Affect. Disord.* 97, 271–276. doi: 10.1016/j.jad.2006.06.027

Thomson, A. C., de Graaf, T. A., Kenis, G., Rutten, B. P. F., Schuhmann, T., and Sack, A. T. (2019). No additive meta plasticity effects of accelerated iTBS with short inter-session intervals. *Brain Stimul.* 12, 1301–1303. doi: 10.1016/j.brs.2019.05.012

Thut, G., and Pascual-Leone, A. (2010). A review of combined TMS-EEG studies to characterize lasting effects of repetitive TMS and assess their usefulness in cognitive and clinical neuroscience. *Brain Topogr.* 22, 219–232. doi: 10.1007/s10548-009-0115-4

Tiksnadi, A., Murakami, T., Wiratman, W., Matsumoto, H., and Ugawa, Y. (2020). Direct comparison of efficacy of the motor cortical plasticity induction and the interindividual variability between TBS and QPS. *Brain Stimul.* 13, 1824–1833. doi: 10.1016/j.brs.2020.10.014

Tse, N. Y., Goldsworthy, M. R., Ridding, M. C., Coxon, J. P., Fitzgerald, P. B., Fornito, A., et al. (2018). The effect of stimulation interval on plasticity following repeated blocks of intermittent theta burst stimulation. *Sci. Rep.* 8:8526. doi: 10.1038/s41598-018-26791-w

Veniero, D., Brignani, D., Thut, G., and Miniussi, C. (2011). Alpha-generation as basic response-signature to transcranial magnetic stimulation (TMS) targeting the human resting motor cortex: a TMS/EEG co-registration study. *Psychophysiology* 48, 1381–1389. doi: 10.1111/j.1469-8986.2011.01218.x

Ward, N. S., and Cohen, L. G. (2004). Mechanisms underlying recovery of motor function after stroke. *Arch. Neurol.* 61, 1844–1848. doi: 10.1001/archneur.61.12.1844

Wassermann, E. M. (1998). Risk and safety of repetitive transcranial magnetic stimulation: report and suggested guidelines from the international workshop on the safety of repetitive transcranial magnetic stimulation, June 5–7, 1996. *Electroencephalogr. Clin. Neurophysiol.* 108, 1–16. doi: 10.1016/s0168-5597(97)00096-8

Wischnewski, M., and Schutter, D. J. (2015). Efficacy and time course of Theta burst stimulation in healthy humans. *Brain Stimul.* 8, 685–692. doi: 10.1016/j.brs.2015.03.004

Yarom, Y., Sugimori, M., and Llinás, R. (1985). Ionic currents and firing patterns of mammalian vagal motoneurons in vitro. *Neurosci*, 16, 719–737. doi: 10.1016/0306-4522(85)90090-9

Youssofzadeh, V., Zanotto, D., Wong-Lin, K., Agrawal, S. K., and Prasad, G. (2016). Directed functional connectivity in fronto-centroparietal circuit correlates with motor adaptation in gait training. *IEEE Trans. Neural Syst. Rehabil. Eng.* 24, 1265–1275. doi: 10.1109/TNSRE.2016.2551642

Ziemann, U., and Siebner, H. R. (2008). Modifying motor learning through gating and homeostatic metaplasticity. *Brain Stimul.* 1, 60–66. doi: 10.1016/j.brs.2007.08.003

Zrenner, C., Desideri, D., Belardinelli, P., and Ziemann, U. (2018). Real-time EEG-defined excitability states determine efficacy of TMS-induced plasticity in human motor cortex. *Brain Stimul.* 11, 374–389. doi: 10.1016/j.brs.2017.11.016

frontiers | Frontiers in Neuroscience

TYPE Original Research
PUBLISHED 10 August 2023
DOI 10.3389/fnins.2023.1210138

OPEN ACCESS

EDITED BY
Mark H. Myers,
University of Tennessee Health Science Center, United States

REVIEWED BY
Vassiliy Tsytsarev,
University of Maryland, United States
Guillem Pratx,
Stanford University, United States
Takayuki Yamashita,
Fujita Health University, Japan

*CORRESPONDENCE
Kelli E. Cannon
✉ kecannon@uab.edu
Mark Bolding
✉ mbolding@uab.edu

RECEIVED 21 April 2023
ACCEPTED 26 June 2023
PUBLISHED 10 August 2023

CITATION
Cannon KE, Ranasinghe M, Millhouse PW, Roychowdhury A, Dobrunz LE, Foulger SH, Gauntt DM, Anker JN and Bolding M (2023) LITE-1 mediates behavioral responses to X-rays in *Caenorhabditis elegans*. *Front. Neurosci.* 17:1210138. doi: 10.3389/fnins.2023.1210138

LITE-1 mediates behavioral responses to X-rays in *Caenorhabditis elegans*

Kelli E. Cannon[1,2,3]*, Meenakshi Ranasinghe[4], Paul W. Millhouse[4], Ayona Roychowdhury[3], Lynn E. Dobrunz[2], Stephen H. Foulger[5], David M. Gauntt[3], Jeffrey N. Anker[4] and Mark Bolding[3]*

[1]Department of Vision Sciences, School of Optometry, University of Alabama at Birmingham, Birmingham, AL, United States, [2]Department of Neurobiology, Heersink School of Medicine, University of Alabama at Birmingham, Birmingham, AL, United States, [3]Department of Radiology, Heersink School of Medicine, University of Alabama at Birmingham, Birmingham, AL, United States, [4]Department of Chemistry, Clemson University, Clemson, SC, United States, [5]Department of Materials Science and Engineering, College of Engineering, Computing and Applied Sciences, Clemson University, Clemson, SC, United States

Rapid sensory detection of X-ray stimulation has been documented across a wide variety of species, but few studies have explored the underlying molecular mechanisms. Here we report the discovery of an acute behavioral avoidance response in wild type *Caenorhabditis elegans* to X-ray stimulation. The endogenous *C. elegans* UV-photoreceptor protein LITE-1 was found to mediate the locomotory avoidance response. Transgenic expression of LITE-1 in *C. elegans* muscle cells resulted in paralysis and egg ejection responses to X-ray stimulation, demonstrating that ectopic expression of LITE-1 can confer X-ray sensitivity to otherwise X-ray insensitive cells. This work represents the first demonstration of rapid X-ray based genetically targeted (X-genetic) manipulation of cellular electrical activity in intact behaving animals. Our findings suggest that LITE-1 has strong potential for use in this minimally invasive form of neuromodulation to transduce transcranial X-ray signals for precise manipulation of neural activity in mammals, bypassing the need for invasive surgical implants to deliver stimulation.

KEYWORDS

noninvasive neuromodulation, X-rays, X-genetics, optogenetics, lite-1, X-ray optogenetics

1. Significance statement

Here we report the discovery of LITE-1 dependent behavioral responses to X-radiation. Importantly, we show that LITE-1 can confer X-ray sensitivity when transgenically expressed in otherwise X-ray insensitive cells. This is the first demonstration of acute X-ray mediated modulation of cellular electrical activity that has similar functionality to optogenetics, but avoids the need for surgical implantation of optic fibers and improves targeting capabilities.

2. Introduction

Neuroscientists today can manipulate neural activity with unprecedented precision. Spatially restricted genetically targeted cell-type-specific expression of proteins gives researchers the ability to test very specific hypotheses about nervous system function. Optogenetic techniques employ light to modulate neuronal activity using light-sensitive photoreceptor proteins (Boyden

et al., 2005). Since its debut in 2005, optogenetics has led to many new discoveries, been extensively developed and adapted, and become an indispensable tool in the neuroscientist's armamentarium (Josselyn, 2018). Applying optogenetics *in vivo*, however, is hindered by optical absorption and scattering in thick tissue. To guide light through the skull to specific brain regions in mammalian models, invasive cranial windows or optical fiber implants are required (Aravanis et al., 2007). Moreover, these light guides have limited fields of view and cannot be easily moved to new regions. To avoid these limitations, researchers have been investigating the use of alternative wavelengths, such as near-infrared (NIR) and X-rays, which are capable of efficiently transmitting externally generated control signals through the skull and brain tissue, allowing for cleaner experiments with results that are less confounded by technical shortcomings.

Researchers have been studying how X-rays affect cells and organisms since X-rays were discovered in 1895 and have reported X-ray responses in retinal photoreceptors (Baily and Noell, 1958; Bachofer and Wittry, 1961; Hunt and Kimeldorf, 1962; Garcia and Buchwald, 1963; Doly et al., 1980), cellular processes (especially related to cell replication and death, Barron and Seki, 1952; Puck and Marcus, 1956; Harmon and Allan, 1988; Boothman et al., 1994; Maier et al., 2015), and animal behavior (Smith et al., 1963; Dedrick and Kimeldorf, 1974; Kernek and Kimeldorf, 1975). Recently several groups have begun investigating a technique known as X-ray optogenetics for minimally invasive manipulation of neural activity in deep brain areas (Berry et al., 2015; Bartley et al., 2019; Chen et al., 2021; Matsubara et al., 2021). The approach uses X-rays to excite radioluminescent particles (RLPs) delivered to the extracellular space surrounding neurons; these RLPs convert the incident X-ray energy into visible light, which in turn activates transgenically expressed photoreceptors. The main difficulty with X-ray optogenetics is producing enough light to generate a meaningful change in neural activity using reasonable X-ray doses and RLP concentrations. Use of a highly sensitive receptor protein that is capable of generating a larger current from fewer photons would facilitate the approach. We therefore searched the literature for more sensitive photoreceptor proteins, including G-protein coupled receptors (GPCRs), which benefit from multiple amplification steps such that a single photon absorbed by the GPCR results in the opening of many channels.

We came across LITE-1, an unusual UV-sensitive photoreceptor protein found in *C. elegans* that has been found to absorb photons orders of magnitude more efficiently than several common opsins (Gong et al., 2016). Unrelated to other known photoreceptor families, LITE-1 belongs to a family of 7-transmembrane-domain invertebrate gustatory receptors and the exact nature of LITE-1's photosensitivity is still an area of active research. G-proteins have been found to act downstream of LITE-1 activation in ASJ neurons (Liu et al., 2010), but the receptor's inverted membrane topology and lack of homology with other GPCRs (Gong et al., 2016) suggest that it may not be considered a true GPCR. LITE-1 mediates locomotory avoidance behavior in wild type *C. elegans* in response to UV (Edwards et al., 2008). We were surprised to discover that X-rays alone elicit a behavioral avoidance response in wild type *C. elegans* in the absence of RLPs. The response was absent in LITE-1 deficient worms, suggesting that LITE-1 plays a critical role in mediating X-ray avoidance behavior. Importantly, we show that LITE-1 can confer X-ray sensitivity when transgenically expressed in otherwise X-ray insensitive cells. This is the first demonstration of X-ray mediated modulation of cellular electrical activity that has similar functionality to optogenetics, while avoiding the disadvantages associated with the use of visible light stimulation.

3. Methods

3.1. X-ray avoidance experiments

3.1.1. Experimental model

C. elegans roundworms were maintained at 20°C on nematode growth medium (NGM) agar plates seeded with OP50 *E. coli* lawns (Brenner, 1974). A wild type strain (N2, Bristol) was assayed, along with three mutant strains with severely defective responses to UV light due to mutations *lite-1*(*ce314*) and/or *gur-3*(*ok2245*). These strains of *C. elegans* were obtained from the Caenorhabditis Genetics Center, which is funded by the NIH Office of Research Infrastructure Programs (P40 OD010440).

3.1.2. X-ray stimulation

X-rays were generated by a iMOXS-MFR W-target X-ray unit with polycapillary optics (XOS) to focus the X-ray beam to a FWHM diameter of 0.85 mm at the level of the agar surface, located approximately 5 cm from the tip of the capillary attachment. The unit was operated at 50 kV and the current was varied from 0 to 600 μA to achieve different stimulation intensities. At the highest intensity, a radiation dose of 1 Gy/s was approximated using RADSticker dosimeter stickers (JP Laboratories, Inc.). The dose decreased to approximately 0.2 Gy/s when the X-ray unit was operated at 25% of the maximum current, i.e., 150 μA. Although the exact X-ray doses may vary somewhat from these values, we expect these dose estimates to be accurate within a factor of two. An internal X-ray shutter was used to control the timing of the X-ray stimulation.

3.1.3. Imaging setup

Worm behavioral responses to X-ray stimulation were recorded on a custom imaging setup, as shown in Figure 1. Video data was recorded using an Amscope MU1003 10MP CMOS camera with a 0.7X-180X magnification lens. Back lighting was provided by a white LED source with a diffuser. The X-ray unit was mounted above the stage. The stage was positioned using a motorized x-y translator controlled by the joystick of an Xbox controller (Microsoft, Redmond WA). The entire imaging setup was enclosed in a steel box with no detectable external X-ray leakage during use.

The irradiation zone—a sharply defined, 0.85 mm diameter spot on the agar surface—was visualized using a small piece of radiochromic film (Gafchromic, XR-QA2) placed on the agar surface (see Figure 1 inset). The camera recording software (Amscope 3.7) was used to annotate the video monitor with a circle outlining the irradiation zone as visualized with the radiochromic film for targeting purposes.

X-ray shutter timing was synced to video timing *post hoc* using a second video recording device outside of the steel enclosure that acquired audio data. The camcorder collected video of the live recording feed with a timestamp displayed as well as audio data capturing the click of the X-ray shutter opening and closing. The timestamp on the video recording updated at a rate of 1 Hz, limiting the precision of the timing data to ±1 s.

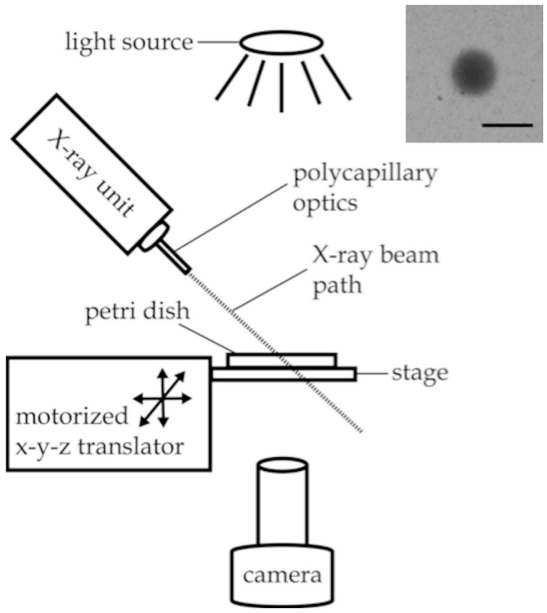

FIGURE 1
Experimental setup for X-ray avoidance and egg ejection experiments. Inset image: X-ray beam visualized with a piece of radiochromic film placed on the agar surface. Scale bar indicates 1 mm.

3.1.4. Experimental design

All experiments were conducted on OP50-lawned 100 mm NGM plates inoculated with approximately 20–50 worms 24–48 h prior. Looking at one worm per trial, a total of 130 trials were conducted on worms from 11 different plates, targeting 3 to 20 individual worms from each plate. A small piece of radiochromic film was placed on the agar surface of each plate before the plate was placed, uncovered, on the imaging stage in the irradiation chamber. After calibrating the location of the X-ray spot with the radiochromic film as described above, an adult hermaphrodite was selected and the stage was moved to position the worm in the center of the calibrated X-ray spot. Each trial began with 30 s during which baseline behavior was recorded with the X-ray shutter closed. After 30 s, if the worm moved out of the center of the calibrated spot, the stage was moved to reposition the worm in the irradiation zone. Once the worm was in position, the shutter was opened to deliver a 10 s X-ray pulse. The pulse was terminated by closing the shutter, and worm behavior was recorded for another 10 s after stimulation offset.

For the dose-rate response experiments, behavioral responses of wild type worms to increasing intensities of X-ray stimulation were recorded. Five X-ray intensities between zero and the maximum intensity deliverable by our iMOX X-ray unit were tested. Intensities of approximately 0, 0.2, 0.5, 0.7, and 1.0 Gy/s were achieved by setting the current applied to the X-ray tube to 0, 150, 300, 450, and 600 μA, respectively. Twenty trials of each the null and highest intensities, and 10 trials at each of the three intermediate intensities were collected, for a total of 70 trials. The five intensities were delivered in an interspersed and randomized order.

For the strain comparison experiments, the responses of three mutant strains of *C. elegans* were tested at the null and maximum X-ray intensities, as described above. Ten trials at each of the two intensities were conducted for each strain for a total of 60 trials.

3.1.5. Data analysis

Video recordings were stabilized in Matlab (due to plate movement from recentering the target worm in the irradiation zone) and analyzed using WormLab software (MBF Bioscience, version 2019.1.1) to track and measure the activity levels of worm subjects. Prior analysis of an independent preliminary dataset (unpublished data) found the behavioral metric most sensitive to the X-ray avoidance response was *activity*, in units of body area per minute, as defined by CeleST tracking software (Restif et al., 2014). Activity time courses were calculated in WormLab and combined with stimulation timing info in Matlab (R2019a) to calculate the peak change in activity—the maximum activity reached during the 10 s X-ray pulse minus the average activity during 30 s baseline period—normalized to the baseline activity for each trial. We defined a positive avoidance response as an increase in activity greater than 45%, using the largest increase observed in the negative control condition to guide threshold selection. Three trials were excluded due to tracking problems. The three images in Figures 3D–F were created by calculating the difference between the maximum and minimum intensities of each pixel across all frames during the 10 s X-ray pulse and subtracting the difference image from the green component of the RGB image of the last frame. For statistical analysis of the X-ray intensity response plot in Figure 3J, a Kruskal-Wallace test was performed, followed by a series of one-sided unpaired Mann Whitney U tests to compare each of the four non-sham stimulation conditions to the sham condition. For statistical analysis of the X-ray avoidance strain comparison data in Figure 4E, a Scheirer-Ray-Hare test was performed, followed by a series of one-tailed unpaired Mann Whitney *U* tests to compare the responses to sham versus X-ray stimulation for each strain. Bonferroni correction was used to adjust Mann Whitney *p*-values for multiple comparisons.

3.2. X-ray paralysis experiments

3.2.1. Experimental model

C. elegans roundworms were maintained at 20°C on nematode growth medium (NGM) agar plates seeded with OP50 *E. coli* lawns (Brenner, 1974). The wild type N2 strain was used as a negative control. N2 nematodes were obtained from the Caenorhabditis Genetics Center, which is funded by the NIH Office of Research Infrastructure Programs (P40 OD010440). *Xuls98 [pmyo-3::lite-1::1D4::SL2::YFP]* worms (henceforth referred to as *pmyo-3::lite-1* worms) were generously provided by the lab of Dr. Shawn Xu. This transgenic strain that expresses *lite-1* in muscle cells using a *myo-3* promoter has been shown to respond to UV with muscle contraction leading to paralysis and sometimes egg ejection (Gong et al., 2016).

3.2.2. X-ray stimulation

X-rays were generated by a portable Amptek Mini-X X-ray unit (Ag target, nozzle and filters removed). In contrast to the focused X-ray beam produced by the iMOXS unit for the X-ray avoidance experiments, the Mini-X unit produced a 120° cone of X-rays,

resulting in relatively uniform diffuse irradiation over the entire field of view. The unit was operated at 20 kV and the current was varied from 0 to 198 μA to achieve different stimulation intensities. RadCal 9010 X-ray dosimeter with a RadCal10x6 ionization chamber was used to measure tube output. At the worms' location approximately 1 cm from the X-ray focal spot, dose rates of 0, 0.19, 0.38, 0.56, and 0.74 Gy/s were calculated for the five X-ray intensity settings employed—i.e., when 0, 50, 100, 150, and 198 μA currents, respectively, were applied to the X-ray tube. The worms were in a 5 μL drop of M9 buffer that had a maximum height of approximately 0.5 mm. Assuming an average photon energy of 10 keV, 0.5 mm of water would attenuate about 1 out of every 100 photons administered. A custom-built X-ray shutter was used to control the timing of the X-ray stimulation.

3.2.3. Imaging Setup

Worm behavioral responses to X-ray stimulation were recorded on a custom imaging setup, as shown in Figure 2. Video data was recorded using an Amscope MU1003 10MP CMOS camera with a 0.7X-180X magnification lens. Back lighting was provided by a white LED source with a diffuser. The X-ray unit was mounted above the stage, and the stage was positioned using manual x-y-z translators. A custom-built triggering device controlled the video recording software and the X-ray shutter, automating the recording and stimulation processes.

3.2.4. Experimental design

For each trial a fresh adult hermaphrodite was placed in a 5 μL drop of M9 buffer on a glass slide with no coverslip, and the slide was positioned on the stage touching the nozzle of the X-ray unit as shown in Figure 2. Video recording of the animals' swimming behavior began after a 60 s recovery period. Twenty seconds of baseline behavioral data was collected prior to a 20 s pulse of X-ray stimulation. Behavior was recorded for another 20 s after the termination of the X-ray stimulation. Importantly, the unfocused X-ray stimulation provided by the Mini-X unit made it such that the worm was not able to move out of the irradiation zone to escape the stimulation, as was the case for the avoidance experiments.

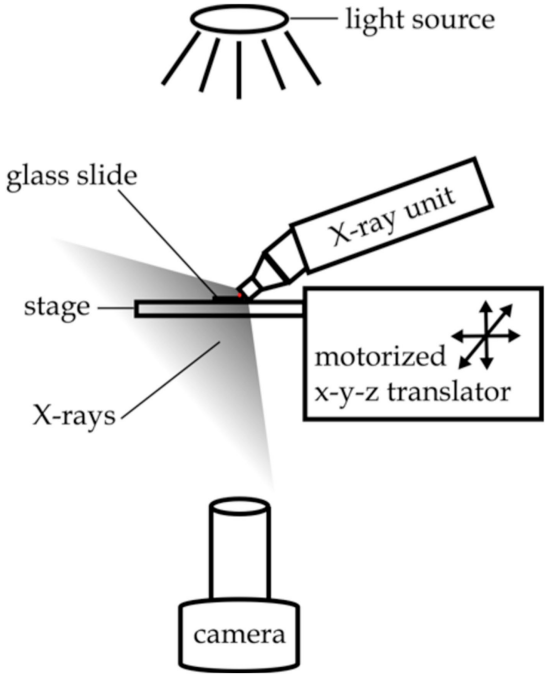

FIGURE 2
Experimental setup for X-ray paralysis experiments. The red dot indicates the location of the nematode.

For the dose–response experiments, behavioral responses of *pmyo-3::lite-1* worms to increasing intensities of X-ray stimulation were recorded. Five X-ray intensities between zero and the maximum intensity deliverable by our Mini-X X-ray unit were tested. Intensities of 0, 0.19, 0.37, 0.56, and 0.74 Gy/s were achieved by setting the current applied to the X-ray tube to 0, 50, 100, 150, and 198 μA, respectively. Since the worms were not able to escape the diffuse, unfocused X-ray stimulation as was the case with the X-ray avoidance experiments, all worms were exposed to X-radiation for the entire duration of the 20 s pulse. As a result, a given X-ray intensity deposited approximately the same X-ray dose in each worm across trials. Ten trials were collected for each dose condition, resulting in a total of 50 trials. The five X-ray doses were delivered in an interspersed and randomized order.

For the strain comparison experiments, the behavioral responses of wild type and *pmyo-3::lite-1* nematodes to the null and maximum X-ray doses were recorded. Twelve trials at each of the two intensities were conducted for each strain for a total of 48 trials.

3.2.5. Data analysis

C. elegans activity was quantified by manually counting the number of body bends in each 5 s video segment. The change in body bend frequency was calculated as the average bend frequency during the 20 s after X-ray stimulation minus the average bend frequency during the 20 s baseline period. This value was divided by the worm's baseline bend frequency in order to normalize the metric with respect to the worm's baseline activity level. A Scheirer-Ray-Hare test followed by post-hoc unpaired one-sided Mann Whitney U tests were used to determine the significance of the changes in body bend frequency observed in response to 0.74 Gy/s X-ray stimulation compared to those observed for the sham stimulation condition for each of the strains in Figure 5E. For statistical analysis of the X-ray dose rate response plot in Figure 5F, a Kruskal-Wallace test was performed, followed by a series of unpaired one-tailed Mann Whitney U tests to compare each of the four non-sham stimulation conditions to the sham condition. Bonferroni correction was used to adjust Mann Whitney *p*-values for multiple comparisons.

3.3. Egg ejection experiments

3.3.1. Experimental model

C. elegans roundworms were maintained at 22°C on nematode growth medium (NGM) agar plates seeded with OP50 *E. coli* lawns (Brenner, 1974). The wild type N2 strain was used as a negative control. N2 nematodes were obtained from the Caehabditiris Genetics Center, which is funded by the NIH Office of Research Infrastructure Programs (P40 OD010440). *Pmyo-3::lite-1* worms were generously provided by the lab of Dr. Shawn Xu.

3.3.2. X-ray stimulation

X-ray stimulation for the egg ejection experiments was delivered using the iMOXS-MFR focused X-ray unit and setup described above for the avoidance experiments. Two dose rates, 0 and 1 Gy/s, were

tested by applying 0 and 600 μA currents, respectively, to the X-ray tube at a voltage of 50 kV.

3.3.3. Imaging setup

The imaging setup was as described above for the avoidance experiments.

3.3.4. Experimental design

All experiments were conducted on OP50-lawned 100 mm NGM plates inoculated with approximately 20–50 worms 72 h prior. Looking at one worm per trial, a total of 40 trials were conducted on worms from 8 different plates, targeting 3 to 7 individual worms from each plate. As described above for the avoidance experiments, a small piece of radiochromic film was used to calibrate the location of the X-ray beam on the agar surface. An adult hermaphrodite was selected and the stage was moved to position the worm in the center of the calibrated X-ray spot. Each trial began with 10 s during which baseline behavior was recorded with the X-ray shutter closed. Then the shutter was opened to deliver a 15 s X-ray pulse.

The responses of wild type and *pmyo-3::lite-1* transgenic nematodes were tested at the null and maximum X-ray intensities, as described above. Ten trials at each of the two intensities were conducted for each strain for a total of 40 trials.

3.3.5. Data analysis

Egg ejections during the X-ray pulse were manually tallied for each worm. A one-sided unpaired Mann Whitney U test was used to compare the mean number of eggs ejected by wild type versus *pmyo-3::lite-1* nematodes in response to 1 Gy/s X-ray stimulation.

4. Results

4.1. Wild type *C. elegans* exhibit locomotory avoidance behavior in response to focused X-ray stimulation

To demonstrate the sensitivity of wild type *C. elegans* to X-rays, individual worms were positioned in the path of a focused X-ray beam that produced an irradiation area with a 0.85 mm full-width half maximum diameter at the level of the agar surface (Figure 1, inset). Wild type worms exhibited a robust increase in activity in response to 1 Gy/s X-ray stimulation (Figure 3; Supplementary Video 1). Figures 3A–C show example traces of the activity of wild type worms before, during, and after a 10 s pulse of focused X-ray stimulation at dose rates of 0 Gy/s (sham, 3A), 0.5 Gy/s (3B), and 1 Gy/s (3C). Figures 3D–F show images indicating nematode movement during the

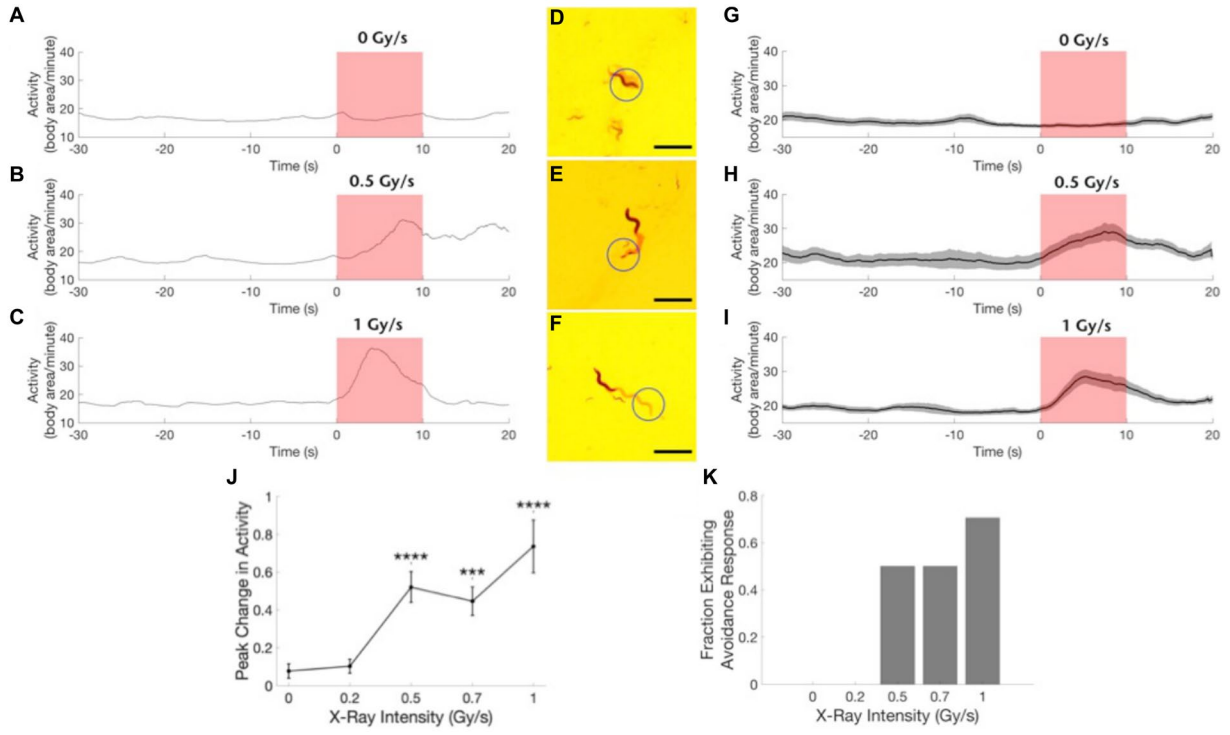

FIGURE 3
Wild type worms exhibit an avoidance response to focused X-ray stimulation. **(A–C)** Example traces of worm activity before, during, and after X-ray stimulation at dose rates of 0 Gy/s **(A)**, 0.5 Gy/s **(B)**, and 1 Gy/s **(C)**. Red shading indicates the timing of the X-ray pulse. **(D–F)** Images showing worm locomotion over the course of the 10-s X-ray pulse. Circle indicates the location of the X-ray beam. The light red paths show the area covered by the worm during the pulse. Worm is shown in its position at the end of the pulse. Scale bars indicate 1 mm. **(G–I)** Activity time courses averaged across worms before, during, and after X-ray stimulation at dose rates of 0 Gy/s **(G)**, 0.5 Gy/s **(H)** and 1 Gy/s **(I)**. Gray shading indicates the standard error of the mean time series. Red shading indicates the timing of the X-ray pulse. $N = 20$ for 0 Gy/s condition. $N = 10$ for 0.5 Gy/s condition. $N = 17$ for 1 Gy/s condition. **(J)** The peak change in activity during the X-ray pulse as a fraction of mean baseline activity is shown as a function of stimulation intensity. ***Bonferroni corrected $p < 0.001$, ****Bonferroni corrected $p < 0.0001$. **(K)** The fraction of worms exhibiting an avoidance response, defined as $a > 45\%$ increase in activity, is shown for each stimulation intensity.

10 s X-ray pulse. The nematodes are shown at their location at the termination of the pulse, and the red shading indicates the nematode's trail, or the area covered by the nematode during the pulse. Figures 3C,F illustrate typical positive avoidance responses, wherein the worm increases forward locomotion to escape the irradiation zone, which is indicated by the blue circle. In contrast, there was no avoidance response to application of a sham stimulation (0 Gy/s, Figures 3A,D), and the worm remained within the circle for the duration of the sham stimulation. Additionally, when more than one worm was in view, only the worm exposed to the focused X-ray beam responded consistently. Figures 3G–I show activity traces averaged across worms for the three dose rates. Similar to the locomotory avoidance response seen in wild type worms exposed to UV stimulation (Edwards et al., 2008), the increase in activity manifested primarily as an increase in forward locomotion and sometimes involved reversals and omega bends. Nematode velocity increased during the first 5 s, with a significant response often observed within the first 2 s (example trace in Figure 3C, group average data in Figure 3I). After 5 s, the response dwindled as the nematode escaped the beam of radiation. At lower X-ray intensities, (i.e., 0.5 and 0.7 Gy/s), only 50% of worms exhibited a significant response (Figure 3K, defined as a > 45% increase in activity), response amplitudes were smaller (Figure 3J), and escape latencies were longer (not quantified, but seen as a later peak in activity in the time courses shown in Figures 3B,H compared to Figures 3C,I). Worm activity appeared unaltered by X-ray stimulation at either 0.2 Gy/s or the null intensity condition (Figures 3A,D,G,J,K). X-ray intensity, or dose rate, was found to significantly modulate the observed change in activity (Figures 3J,H(5) = 32.5, $p = 1.5\times10^{-6}$). Post-hoc pairwise comparisons revealed significant differences between the sham condition (0 Gy/s) and the 0.5 Gy/s ($U = 11$, Bonferroni corrected $p = 2.6\times10^{-5}$), 0.7 Gy/s ($U = 20$, Bonferroni corrected $p = 8.1\times10^{-5}$), and 1 Gy/s ($U = 42$, Bonferroni corrected $p = 1.7\times10^{-5}$) conditions.

4.2. Worms lacking functional LITE-1 have a dysfunctional X-ray avoidance response

We next tested whether either of 2 *C. elegans* photoreceptor proteins, LITE-1 or GUR-3, plays a role in the avoidance response to X-rays. Three mutant strains of *C. elegans* with mutated, dysfunctional *lite-1* [*lite-1* (*ce314*) *X*], *gur-3* [*gur-3* (*ok2245*) *X*] or both *lite-1* and *gur-3* [*lite-1* (*ce314*) *X gur-3* (*ok2245*) *X*] were subjected to sham and 1 Gy/s X-ray stimulation. Activity levels of the *gur-3* (*ok2245*) *X* mutant showed a significant increase in response to X-ray stimulation (Figure 4B; Supplementary Video 2), similarly to the wild type strain (Figure 4A). On average, the magnitudes of the increases were 74 ± 14% and 101 ± 17% of baseline activity for wild type and *gur-3* (*ok2245*) *X* strains, respectively, compared in negligible increases of 8 ± 4% and 6 ± 2% observed for the respective strains in response to sham stimulation [wild type $U = 42$, Bonferroni corrected $p = 2.6\times10^{-5}$; *gur-3* (*ok2245*) *X* $U = 0$, Bonferroni corrected $p = 2.2\times10^{-5}$; Figure 4E]. In contrast, the activities of the two strains with dysfunctional LITE-1—i.e., the *lite-1* (*ce314*) *X* mutant and the *gur-3* (*ok2245*) *X lite-1* (*ce314*) *X* double mutant—appeared largely unaltered by stimulation (Figures 4C–E, Supplementary Video 3, 4), suggesting that functional LITE-1 is required for the X-ray avoidance response.

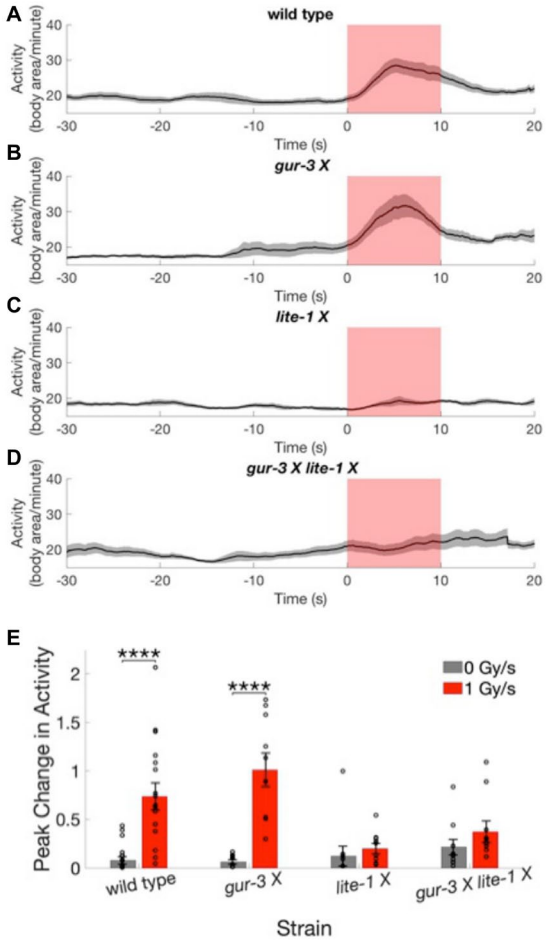

FIGURE 4
Worms lacking functional LITE-1 have severely defective X-ray avoidance responses. **(A–D)** Activity time courses averaged across worms of the wild type strain **(A)** and 3 mutant strains **(B–D)** before, during, and after X-ray stimulation at a dose rate of 1 Gy/s. Gray shading indicates the standard error of the mean time series. Red shading indicates the timing of the X-ray pulse. $N = 20$ for wild type strain. $N = 10$ for mutant strains. **(E)** The peak change in activity during the X-ray pulse as a fraction of mean baseline activity is shown for the four strains at 0 and 1 Gy/s stimulation intensities. Error bars indicate standard error. ****$p < 0.0001$.

4.3. LITE-1 confers X-ray sensitivity to muscle cells resulting in a paralysis response to X-ray stimulation

To determine whether transgenic expression of LITE-1 is capable of conferring X-ray sensitivity to otherwise X-ray insensitive cells, we looked at X-ray induced behavioral responses in *pmyo-3::lite-1* nematodes, which transgenically express LITE-1 in muscle cells. UV stimulation has been shown to result in LITE-1 mediated muscle contraction in this strain, leading to paralysis and egg ejection (Edwards et al., 2008; Bhatla et al., 2015; Gong et al., 2016). Using a swimming assay, we found that the *pmyo-3::lite-1* worms exhibited a robust paralysis response to diffuse, unfocused X-ray stimulation (Figures 5D,E; Supplementary Video 5) that was not observed in wild

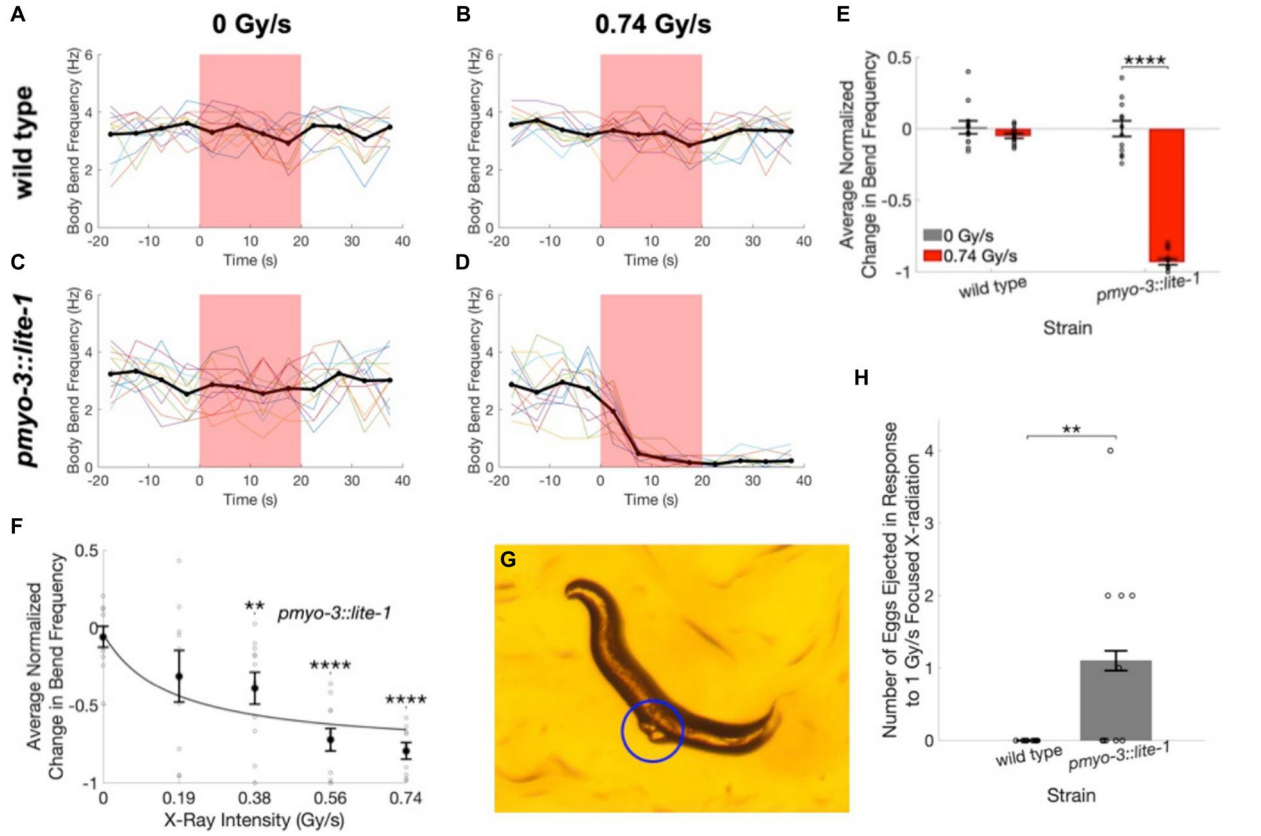

FIGURE 5
Worms expressing LITE-1 in muscle cells exhibit a paralysis response to X-ray stimulation. **(A–D)** Time courses of wild type **(A,B)** and *pmyo-3::lite-1* **(C,D)** *C. elegans* activity quantified as the number of body bends per 5-s interval before, during, and after unfocused X-ray stimulation at dose rates of 0 Gy/s **(A,C)** and 0.74 Gy/s **(B,D)**. Thin colored traces represent individual worms, and the mean across worms is indicated by the thick black line. Red shading indicates the timing of the X-ray pulse. N = 12 for each strain and stimulation condition. **(E)** The average change in body bend frequency after the X-ray pulse as a fraction of mean baseline bend frequency is shown for wild type and *pmyo-3::lite-1* worms at 0 and 0.74 Gy/s stimulation intensities. Error bars indicate standard error. ****$p < 0.0001$. **(F)** The average change in body bend frequency of *pmyo-3::lite-1* worms is shown as a function of stimulation intensity. Values for individual worms are indicated by circles. $N = 10$ at 0 Gy/s. $N = 9$ at 0.19 and 0.74 Gy/s. N = 11 at 0.38 and 0.56 Gy/s. Error bars indicate standard error. **Bonferroni corrected $p < 0.01$, ****Bonferroni corrected $p < 0.0001$. **(G)** Image of a *pmyo-3::lite-1* worm that ejected two eggs, indicated by blue circle, when exposed to 1 Gy/s focused X-ray stimulation. **(H)** The number of eggs ejected by wild type and *pmyo-3::lite-1* nematodes in response to a 15 s pulse of 1 Gy/s focused X-ray stimulation. Error bars indicate standard error. Values for individual worms are indicated by circles. **$p < 0.01$.

type nematodes (Figures 5B,E Supplementary Video 6). The average body bend frequency was found to decrease by 72 ± 5% in response to 0.74 Gy/s X-ray stimulation in the *pmyo-3::lite-1* strain (Figures 5D,E, $U = 144$, $p = 1.8\times10^{-5}$). Only negligible changes in bend frequency were observed at the same dose in the wild type strain (3 ± 2%, Figures 5B,E) and at the null X-ray dose in the *pmyo-3::lite-1* (2 ± 18%, Figures 5C,E) and wild type (0 ± 3%, Figures 5A,E) strains.

To determine whether the X-ray paralysis response in the *pmyo-3::lite-1* strain exhibits a typical dose–response relationship, we varied the current applied to the X-ray tube to achieve five levels of stimulation intensity—0, 0.19, 0.38, 0.56, and 0.74 Gy/s. The magnitude of the average decrease in bend frequency was found to increase with increasing X-ray dose rate [Figures 5F,H$(5) = 38.2$, $p = 1.0\times10^{-7}$]. *Post-hoc* tests found significant differences between the sham condition (0 Gy/s) and the 0.38 Gy/s ($U = 333$, Bonferroni corrected $p = 0.008$), 0.56 Gy/s ($U = 376$, Bonferroni corrected $p = 3.7\times10^{-6}$), and 0.74 Gy/s conditions ($U = 340$, Bonferroni corrected $p = 6.9\times10^{-6}$).

The paralysis assay was also repeated on the focused X-ray setup used for the avoidance experiments. For these experiments, crawling wild type and *pmyo-3::lite-1* nematodes were exposed to a 15 s pulse of 1 Gy/s focused X-ray stimulation. These experiments confirmed the finding that X-ray induced paralysis is observed in *pmyo-3::lite-1*, but not wild type worms. Additionally, the focused X-ray stimulation evoked egg ejection in five out of 10 *pmyo-3::lite-1* worms (Supplementary Video 7) and zero out of 10 wild type worms (Figures 5G,H).

5. Discussion

Here we have shown that wild type and LITE-1 intact *C. elegans* display a short-latency avoidance response to X-radiation that is absent in strains deficient for LITE-1. Additionally, transgenic expression of LITE-1 in *C. elegans* muscle cells was found to elicit a paralysis response to X-rays, demonstrating that transgenic expression of LITE-1 can confer X-ray sensitivity to otherwise X-ray insensitive cells. Together, these results suggest that LITE-1 can function as an X-ray sensitive receptor protein, playing a critical role in the transduction of X-ray signals into ionic currents and neural activity to produce behavioral responses.

We show using two different behavioral assays that X-rays produce behavioral responses in *C. elegans* that are dependent upon LITE-1. First, X-ray stimulation causes a dose-rate dependent increase in activity of wild type worms that is consistent with a locomotory avoidance response. The X-ray avoidance response was absent in worms with loss of function mutations in either LITE-1 alone or in both LITE-1 and GUR-3, but intact in worms with a loss of function mutation in GUR-3 alone. This indicates that the X-ray avoidance response depends upon LITE-1, but not GUR-3. Both LITE-1 and GUR-3 have previously been shown to be involved in the inhibition of pharyngeal pumping in wild type nematodes in response to UV (Bhatla and Horvitz, 2015), demonstrating that both are UV-sensitive photoreceptor proteins. However, only LITE-1 appears to be involved in the locomotory avoidance response to UV stimulation (Edwards et al., 2008; Bhatla and Horvitz, 2015), consistent with our observations in response to X-ray stimulation. Our next experiments show that the paralysis and egg ejection responses that have been reported in *pmyo-3::lite-1* worms in response to UV stimulation (Edwards et al., 2008; Bhatla and Horvitz, 2015; Gong et al., 2016) are similarly evoked by X-ray stimulation. This implies that X-rays, like UV, are capable of activating transgenically expressed LITE-1, leading to a calcium influx into muscle cells and muscle contraction (Gong et al., 2016). Together, our results demonstrate that LITE-1 can act as an X-ray sensitive receptor protein to mediate X-ray avoidance behavior in wild type nematodes and paralysis in *pmyo-3::lite-1* transgenic nematodes.

Our results with LITE-1 are the first demonstration of a protein being able to confer X-ray sensitivity in the form of a rapid behavioral response when trangenically expressed. Human intermediate-conductance Ca^{2+}-activated K^+ channels (hIK channels) have been found to confer X-ray sensitivity to otherwise X-ray insensitive HEK293 cells in the form of delayed (several minutes latency) and sustained voltage-dependent outward K^+ currents after a 1 Gy dose of X-radiation (Roth et al., 2015). Thousands of studies have investigated the delayed biological effects of ionizing radiation, but only a few dozen have looked at immediate sensory detection of ionizing radiation. X-ray detection by ocular photoreceptor proteins such as rhodopsin has been suggested by reports of X-ray phosphenes (i.e., sensations of light produced by X-rays) experienced by astronauts and radiation-therapy patients (Lipetz, 1955; Fuglesang et al., 2006; Thariat et al., 2016). Additionally, there have been numerous reports of behavioral and electroretinogram (ERG) responses to X-rays and other types of ionizing radiation in diverse animal models (Baily and Noell, 1958; Bachofer and Wittry, 1961; Baldwin and Sutherland, 1965; Martinsen and Kimeldorf, 1972). The nearly ubiquitous finding that the retina must be in the scotopic, or dark-adapted state, in order to produce a response to X-radiation suggests that rhodopsin in rod cells, rather than cone opsins in cone cells, is involved in the response. Despite this, multiple researchers have reported that X-ray stimulation of the dark-adapted retina can increase its sensitivity to subsequent stimulation with visible light (Gaffey and Kelley, 1963; Dawson and Wiederwohl, 1965), suggesting that X-rays do not bleach the rhodopsin pigment, as does visible light. Additionally, it has not been investigated whether transgenic expression of rhodopsin outside of the specialized structure of the retina is capable of conferring X-ray sensitivity to different cell types. Although our experiments did not probe the X-ray sensitivity of GUR-3, other behaviors that are more dependent upon GUR-3 activation, such as the inhibition of feeding (Bhatla and Horvitz, 2015), might still demonstrate a behavioral effect of X-rays via GUR-3. Future studies could investigate whether other photoreceptors like GUR-3 become activated by X-radiation and confer X-ray sensitivity when transgenically expressed.

While sensory responses to X-rays have been documented in a variety of species, the cellular and molecular mechanisms by which X-radiation impinges on sensory system components have not been well explored. Similarly, the mechanisms by which X-ray activation of LITE-1 causes behavioral responses are not yet known. Given the similarity between UV and X-ray evoked behaviors, it is reasonable to assume that the cellular and molecular pathways downstream of LITE-1 activation are the same, regardless of which type of radiation is used to activate the receptor proteins. Because UV and X-ray photons exhibit major differences in their interactions with matter, however, the mechanisms by which the two types of radiation activate the photoreceptor protein may differ.

LITE-1 is unique among photoreceptor proteins, and its sequence does not contain any of the known chromophore binding sites found in nearly all other photoreceptor proteins that have been identified (Edwards et al., 2008). Despite lacking a small-molecule chromophore binding partner needed to capture photons for any other type of photoreceptor, isolated LITE-1 has been shown to absorb UV photons with astonishingly high efficiency, with measured extinction coefficients averaging two orders of magnitude larger than those of opsins (Gong et al., 2016). Interestingly, LITE-1's high UV absorbance cross section is drastically diminished when particular residues of the protein, including two tryptophan moieties, are mutated (Gong et al., 2016). These mutations that inhibit photon absorption by LITE-1 also render the protein dysfunctional at mediating the UV paralysis response in *pmyo-3::lite-1* worms (Gong et al., 2016). Together, these data suggest that LITE-1, although unrelated to known photoreceptor families, may be a legitimate photoreceptor that can be activated by the direct absorption of UV photons *via* an intrinsic chromophore domain consisting of a particular arrangement of tryptophan residues.

In contrast, the chemical bonds and electron configuration that promote absorption of UV radiation by tryptophan have negligible effects on the absorption of X-radiation, which is primarily determined by atomic number (Bushberg et al., 2012). As a ~ 50 kDa protein, only about 1 out of 50 million molecules of LITE-1 can be expected to absorb an X-ray photon per Gy of irradiation (see Supplemental Information for calculations). In the present study, behavioral responses were observed in wild type nematodes within two seconds of the onset of X-ray stimulation at 1 Gy/s—i.e., at a total dose of <~2 Gy. Endogenous LITE-1 expression is low (Gong et al., 2016) and would not be expected to exceed 50 million functional LITE-1 proteins expressed at a given time in a single worm. It is improbable that activation of merely two LITE-1 receptors within a worm expressing 50 million LITE-1 receptors in total would be sufficient to drive a behavioral response. Considering further that this is a generous over-estimate, which is based on the highly improbable assumption that X-ray absorption by any atom within LITE-1 will yield the same result (i.e., LITE-1 activation), we reason that it is highly unlikely that the mechanism underlying LITE-1's X-ray sensitivity involves direct X-ray photon absorption by the receptor, as has been demonstrated to be the case for UV photons. It is much more likely that secondary electrons and reactive oxygen species (ROS), which are generated in the hundreds to thousands for each X-ray absorption (Bushberg et al., 2012), are involved in the activation of LITE-1 by X-rays.

It has been shown that the predominant immediate effect of X-radiation on biological systems is the generation of ROS, primarily from the radiolysis of water (Zaider et al., 1988, see Supplemental Information). Interestingly, electron-rich tryptophan residues readily participate in redox reactions (Ehrenshaft et al., 2015). Tryptophan can become oxidized by UV radiation (Davies and Truscott, 2001; Pattison et al., 2012) and act as a photosensitizer to generate ROS upon UV photoabsorption (Davies, 2003; Chin et al., 2008). Furthermore, it has been shown that radiogenic hydroxyl radicals, hydrated electrons, and hydrogen atoms all react rapidly with tryptophan in aqueous solutions (Jayson et al., 1954; Armstrong and Swallow, 1969; Shen et al., 1987). As such, it could be that radiogenic ROS or their reaction products are interacting with the chromophoric tryptophan residues of LITE-1 in order to activate the receptor.

The precise mechanisms underlying the activation of LITE-1 are at present unknown, but ROS are heavily implicated in the process (Bhatla and Horvitz, 2015; Zhang et al., 2020; Ghosh et al., 2021; Quintin et al., 2022). When absorbed by endogenous photosensitizing molecules and moieties such as riboflavin and tryptophan, UV radiation generates ROS in biological specimens. Evidence suggests that these UV-generated ROS can mediate photoresponses in both *C. elegans* and yeast (Bhatla and Horvitz, 2015; Bodvard et al., 2017). GUR-3, which shares 40% homology with LITE-1, appears to function not as a true UV photoreceptor, but more like a chemoreceptor that detects hydrogen peroxide generated by UV (Bhatla and Horvitz, 2015). While LITE-1 does appear to be capable of functioning as a legitimate photoreceptor that absorbs UV photons (Gong et al., 2016), LITE-1 dependent behavioral and calcium responses to ROS have also been reported (Bhatla et al., 2015; Ghosh et al., 2021; Quintin et al., 2022). LITE-1 and GUR-3 mediated H_2O_2 detection in PHA and I2 neurons, respectively, has been found to rely on H_2O_2-reducing peroxiredoxin-2 (PRDX-2, Quintin et al., 2022), suggesting that the receptors may interact with an oxidized intermediate rather than directly with ROS. Interestingly, PRDX-2 deficiency had no effect on LITE-1 mediated photoresponses in PHA neurons (Quintin et al., 2022), possibly indicating divergent mechanisms for photon and ROS detection. Others have reported diminished phototaxis and ASH neuron photocurrents in the presence of H_2O_2, claiming that the ROS acts to inhibit, rather than activate, LITE-1 (Zhang et al., 2020). Still another study found that both light and ROS were required for LITE-1 dependent avoidance responses (Ghosh et al., 2021). While the activation of LITE-1 appears to be complex and uncertainty remains regarding the mechanism underlying LITE-1's X-ray sensitivity, the present study has clearly demonstrated that X-rays effectively activate LITE-1.

For any neuromodulation technique, thermal effects of the deposited energy should be considered. *C. elegans* display robust thermotaxic behavior and are capable of detecting changes in temperature as small as 0.05°C (Clark et al., 2006). Despite the nematodes' high thermal sensitivity and the relatively high X-ray dose rates employed in this study, X-ray stimulation did not lead to changes in worm activity in the *lite-1*(*ce314*) *X* and *gur-3*(*ok2245*) *X lite-1*(*ce314*) *X* mutant strains. These mutant strains are expected to have intact thermosensory capacities, as there is no evidence that LITE-1 plays any role in thermosensation. Moreover, even ignoring the rapid thermal diffusion and local heat dissipation, the largest cumulative X-ray dose delivered here (14.8 Gy or J/kg) would cause a temperature increase of only about 0.004°C (based on the heat capacity of water, 4.2 kJ/kg/K). As such, thermal effects of the X-ray stimulation protocol employed here can be considered negligible and dismissed as a potential concern.

Another potential limitation of the present study is the use of a single mutated allele of LITE-1—i.e., *lite-1*(*ce314*) *X*. It is possible that a background mutation in the *lite-1*(*ce314*) *X* strain could be responsible for the X-ray unresponsive behavioral phenotype; however, if this were the case it would not be expected that transgenically expressing LITE-1 in muscle cells would confer them with X-ray sensitivity. Our discovery that LITE-1 can confer X-ray sensitivity when transgenically expressed provides strong support for the hypothesis that the behavioral phenotype observed in the *lite-1*(*ce314*) *X* strain is in fact due to the *ce314* mutation in *lite-1*, rather than some unknown background mutation in the strain.

The baseline period of each experiment was collected with the X-ray unit on, but with a lead shutter blocking the X-ray beam. Given that the avoidance and paralysis responses are not seen until shortly after stimulation onset, when the shutter is opened, we can be confident that it is the X-rays, rather than some artifact of the X-ray unit, that is triggering the responses. Additionally, given that no responses are seen in the sham X-ray stimulation condition—in which the shutter opens and closes, but the X-ray tube current is set to 0 μA—we can be certain that the worms are not responding to the auditory signal of the X-ray shutter opening and closing.

It should be noted that this study employs relatively high X-ray dose rates, with significant responses seen above about 0.38 Gy/s. As a species, *C. elegans* have been found to exhibit a high resistance to ionizing radiation. For example, acute γ irradiation of young adult wild type worms has been found to only modestly decrease lifespan at doses over 1,000 Gy (Johnson and Hartman, 1988; Ishii and Suzuki, 1990). Nematode locomotion has been found to decrease after irradiation in a dose-dependent manner, with body bend frequency decreasing about 40% after a 541 Gy dose of γ rays (Sakashita et al., 2008). Even at the highest X-ray dose delivered in the present study (14.8 Gy), wild type worms displayed no significant decrease in locomotion, so the dramatic paralysis effect seen in the *pmyo-3*::*lite-1* strain is clearly in excess to any radiogenic dampening of locomotion observed at the doses employed here. Lower doses of ionizing radiation can, however, affect more radiosensitive processes such as ROS signaling, gene expression, and cellular replication. A 3 Gy dose was sufficient to induce changes in gene expression in stage L4 larva, which are generally more radiosensitive than adult nematodes (Nelson et al., 2002). Mammals are typically much more radiosensitive than nematodes, and routine human clinical radioscopy typically involves dose rates below 1 Gy/min. Future physiological investigations will reveal the appropriate X-ray pulse duration for LITE-1 activation, which likely occurs on a millisecond timescale not investigated by these initial behavioral studies. This and other important future experiments will be needed to optimize the efficacy of LITE-1 mediated neural modulation in order to minimize total exposure and off-target radiogenic effects.

In conclusion, we discovered that LITE-1 mediates an avoidance response to X-rays in wild type nematodes and paralysis and egg ejection responses to X-rays in *pmyo-3*::*lite-1* transgenic nematodes, providing strong evidence that LITE-1 can function as an X-ray sensitive receptor in *C. elegans*. The findings were robust and produced in two different labs with different X-ray units and experimental

setups. This is the first study to identify an X-ray receptor protein that can be transgenically expressed in different cell types to acutely control the activity of those cells using X-rays. As such, it is the first demonstration of X-genetic control of cellular electrical activity in intact, behaving animals. Future studies will reveal whether LITE-1 also has the potential to enable minimally invasive X-genetic neural control in mammalian animal models.

Data availability statement

The original contributions presented in the study are publicly available. This data can be found here: https://figshare.com/projects/WormX_Data/171786.

Author contributions

KC, MR, PM, SF, JA, and MB contributed to conception and design of the study. KC, MR, and DG performed experiments. KC, MR, and AR analyzed data. KC wrote the first draft of the manuscript. KC, MR, and JA wrote sections of the manuscript. All authors contributed to manuscript revision, read, and approved the submitted version.

Funding

This research was supported in part by an NSF EPSCoR Research Infrastructure grant to Clemson University [NSF 1632881] and by AlaEPSCoR GRSP15. The funders had no role in study design, data collection and analysis, decision to publish, or preparation of the manuscript.

Acknowledgments

The advice of Melissa LaBonty and the lab of Brad Yoder was very helpful, and we would like to express gratitude for their support.

Conflict of interest

The authors declare that the research was conducted in the absence of any commercial or financial relationships that could be construed as a potential conflict of interest.

Publisher's note

All claims expressed in this article are solely those of the authors and do not necessarily represent those of their affiliated organizations, or those of the publisher, the editors and the reviewers. Any product that may be evaluated in this article, or claim that may be made by its manufacturer, is not guaranteed or endorsed by the publisher.

Supplementary material

The Supplementary material for this article can be found online at: https://www.frontiersin.org/articles/10.3389/fnins.2023.1210138/full#supplementary-material

References

Aravanis, A. M., Wang, L.-P., Zhang, F., Meltzer, L. A., Mogri, M. Z., Bret Schneider, M., et al. (2007). An optical neural interface: *in vivo* control of rodent motor cortex with integrated fiberoptic and optogenetic technology. *J. Neural Eng.* 4, S143–S156. doi: 10.1088/1741-2560/4/3/S02

Armstrong, R. C., and Swallow, A. J. (1969). Pulse- and gamma-radiolysis of aqueous solutions of tryptophan. *Radiat. Res.* 40, 563–579. doi: 10.2307/3573010

Bachofer, C. S., and Wittry, S. E. (1961). Electroretinogram in response to X-ray stimulation. *Science* 133, 642–644. doi: 10.1126/science.133.3453.642

Baily, N. A., and Noell, W. K. (1958). Relative biological effectiveness of various qualities of radiation as determined by the electroretinogram. *Radiat. Res.* 9, 459–468. doi: 10.2307/3570772

Baldwin, W. F., and Sutherland, J. B. (1965). Extreme sensitivity to low-level X-rays in the eye of the cockroach Blaberus. *Radiat. Res.* 24:513. doi: 10.2307/3571642

Barron, E. S. G., and Seki, S. L. (1952). Studies on the mechanism of action of ionizing radiations. VII. Cellular respiration, cell division, and ionizing radiations. *J. Gen. Physiol.* 35, 865–871. doi: 10.1085/jgp.35.6.865

Bartley, A. F., Abiraman, K., Stewart, L. T., Hossain, M. I., Gahan, D. M., Kamath, A. V., et al. (2019). Lso:Ce Inorganic scintillators are biocompatible with neuronal and circuit function. *Front. Synaptic Neurosci.* 11:24. doi: 10.3389/fnsyn.2019.00024

Berry, R., Getzin, M., Gjesteby, L., and Wang, G. (2015). X-Optogenetics and U-Optogenetics: feasibility and possibilities. *Photo-Dermatology* 2, 23–39. doi: 10.3390/photonics2010023

Bhatla, N., Droste, R., Sando, S. R., Huang, A., and Horvitz, H. R. (2015). Distinct neural circuits control rhythm inhibition and spitting by the myogenic pharynx of c. Elegans. *Curr. Biol.* 25, 2075–2089. doi: 10.1016/j.cub.2015.06.052

Bhatla, N., and Horvitz, H. R. (2015). Light and hydrogen peroxide Inhibit *C. elegans* feeding through gustatory receptor Orthologs and pharyngeal neurons. *Neuron* 85, 804–818. doi: 10.1016/j.neuron.2014.12.061

Bodvard, K., Peeters, K., Roger, F., Romanov, N., Igbaria, A., Welkenhuysen, N., et al. (2017). Light-sensing via hydrogen peroxide and a Peroxiredoxin. *Nat. Commun.* 8:14791. doi: 10.1038/ncomms14791

Boothman, D. A., Majmudar, G., and Johnson, T. (1994). Immediate X-ray-inducible responses from mammalian cells. *Radiat. Res.* 138, S44–S46. doi: 10.2307/3578759

Boyden, E. S., Zhang, F., Bamberg, E., Nagel, G., and Deisseroth, K. (2005). Millisecond-timescale, genetically targeted optical control of neural activity. *Nat. Neurosci.* 8, 1263–1268. doi: 10.1038/nn1525

Brenner, S. (1974). The genetics of *Caenorhabditis Elegans*. *Genetics* 77, 71–94. doi: 10.1093/genetics/77.1.71

Bushberg, J. T., Seibert, A., Leidholdt, E. M., and Boone, J. M. (2012). *The essential physics of medical imaging*. 3rd Edn.

Chen, Z., Vassiliy Tsytsarev, Y., Finfrock, Z., Antipova, O. A., Cai, Z., Arakawa, H., et al. (2021). Wireless Optogenetic modulation of cortical neurons enabled by Radioluminescent nanoparticles. *ACS Nano* 15, 5201–5208. doi: 10.1021/acsnano.0c10436

Chin, K. K., Trevithick-Sutton, C. C., McCallum, J., Jockusch, S., Turro, N. J., Scaiano, J. C., et al. (2008). Quantitative determination of singlet oxygen generated by excited state aromatic amino acids, proteins, and immunoglobulins. *J. Am. Chem. Soc.* 130, 6912–6913. doi: 10.1021/ja800926v

Clark, D. A., Biron, D., Sengupta, P., and Samuel, A. D. T. (2006). The AFD sensory neurons encode multiple functions underlying thermotactic behavior in *Caenorhabditis Elegans*. *J. Neurosci.* 26, 7444–7451. doi: 10.1523/JNEUROSCI.1137-06.2006

Davies, M. J. (2003). Singlet oxygen-mediated damage to proteins and its consequences. *Biochem. Biophys. Res. Commun.* 305, 761–770. doi: 10.1016/s0006-291x(03)00817-9

Davies, M. J., and Truscott, R. J. (2001). Photo-oxidation of proteins and its role in Cataractogenesis. *J. Photochem. Photobiol. B* 63, 114–125. doi: 10.1016/s1011-1344(01)00208-1

Dawson, W. W., and Wiederwohl, H. (1965). Functional alteration of visual receptor units and retinal pigments by X-irradiation. *Radiat. Res.* 24, 292–304. doi: 10.2307/3571575

Dedrick, M. C., and Kimeldorf, D. J. (1974). Immediate behavioral responses of an echinoderm to ionizing radiations. *Physiol. Behav.* 12, 393–398. doi: 10.1016/0031-9384(74)90114-0

Doly, M., Isabelle, D. B., Vincent, P., Gaillard, G., and Meyniel, G. (1980). Mechanism of the formation of X-ray-induced Phosphenes. I. Electrophysiological investigations. *Radiat. Res.* 82, 93–105. doi: 10.2307/3575240

Edwards, S. L., Charlie, N. K., Milfort, M. C., Brown, B. S., Gravlin, C. N., Knecht, J. E., et al. (2008). A novel molecular solution for ultraviolet light detection in *Caenorhabditis Elegans*. *PLoS Biol.* 6:e198. doi: 10.1371/journal.pbio.0060198

Ehrenshaft, M., Deterding, L. J., and Mason, R. P. (2015). Tripping up Trp: modification of protein tryptophan residues by reactive oxygen species, modes of detection, and biological consequences. *Free Radic. Biol. Med.* 89, 220–228. doi: 10.1016/j.freeradbiomed.2015.08.003

Fuglesang, C., Narici, L., Picozza, P., and Sannita, W. G. (2006). Phosphenes in low earth orbit: survey responses from 59 astronauts. *Aviat. Space Environ. Med.* 77, 449–452.

Gaffey, C. T., and Kelley, A. K. (1963). Bioelectric sensitivity to irradiation of the retina and visual pathways. *UCRL-11005. UCRL [Reports]. U.S. Atomic Energy Commission* 86, 1–35.

Garcia, J., and Buchwald, N. A. (1963). Perception of ionizing radiation. A study of behavioral and electrical responses to very low doses of x-ray. *Boletin Del Instituto de Estudios Medicos y Biologicos, Universidad Nacional Autonoma de Mexico* 21, 391–405.

Ghosh, D. D., Lee, D., Xin Jin, H., Horvitz, R., and Nitabach, M. N. (2021). *C. elegans* discriminates colors to guide foraging. *Science* 371, 1059–1063. doi: 10.1126/science.abd3010

Gong, J., Yuan, Y., Ward, A., Kang, L., Zhang, B., Zhiping, W., et al. (2016). The *C. elegans* taste receptor homolog LITE-1 is a photoreceptor. *Cells* 167, 1252–1263.e10. doi: 10.1016/j.cell.2016.10.053

Harmon, B. V., and Allan, D. J. (1988). X-ray-induced cell death by apoptosis in the immature rat cerebellum. *Scanning Microsc.* 2, 561–568.

Hunt, E. L., and Kimeldorf, D. J. (1962). Evidence for direct stimulation of the mammalian nervous system with ionizing radiation. *Science* 137, 857–859. doi: 10.1126/science.137.3533.857

Ishii, N., and Suzuki, K. (1990). X-ray inactivation of *Caenorhabditis Elegans* embryos or larvae. *Int. J. Radiat. Biol.* 58, 827–833. doi: 10.1080/09553009014552201

Jayson, G. G., Scholes, G., and Weiss, J. (1954). Formation of Formylkynurenine by the action of X-rays on tryptophan in aqueous solution. *Biochem. J.* 57, 386–390. doi: 10.1042/bj0570386

Johnson, T. E., and Hartman, P. S. (1988). Radiation effects on life span in *Caenorhabditis Elegans*. *J. Gerontol.* 43, B137–B141. doi: 10.1093/geronj/43.5.b137

Josselyn, S. A. (2018). The past, present and future of light-gated ion channels and optogenetics. *elife* 7. doi: 10.7554/eLife.42367

Kernek, S. P., and Kimeldorf, J. (1975). X-ray induced behavioral reactions and detection mechanisms in the shrimp. *Physiol. Behav.* 15, 1–5. doi: 10.1016/0031-9384(75)90269-3

Lipetz, L. E. (1955). The X-ray and radium phosphenes. *Br. J. Ophthalmol.* 39, 577–598. doi: 10.1136/bjo.39.10.577

Liu, J., Ward, A., Gao, J., Dong, Y., Nishio, N., Inada, H., et al. (2010). *C. elegans* Phototransduction requires a G protein-dependent CGMP pathway and a taste receptor homolog. *Nat. Neurosci.* 13, 715–722. doi: 10.1038/nn.2540

Maier, P., Hartmann, L., Wenz, F., and Herskind, C. (2015). Cellular pathways in response to ionizing radiation and their targetability for tumor radiosensitization. *Int. J. Mol. Sci.* 17:102. doi: 10.3390/ijms17010102

Martinsen, D. L., and Kimeldorf, D. J. (1972). The prompt detection of ionizing radiations by carpenter ants. *Biol. Bull.* 143, 403–419. doi: 10.2307/1540062

Matsubara, T., Yanagida, T., Kawaguchi, N., Nakano, T., Yoshimoto, J., Sezaki, M., et al. (2021). Remote control of neural function by X-ray-induced scintillation. *Nat. Commun.* 12:4478. doi: 10.1038/s41467-021-24717-1

Nelson, G. A., Jones, T. A., Chesnut, A., and Smith, A. L. (2002). Radiation-induced gene expression in the nematode *Caenorhabditis Elegans*. *J. Radiat. Res.* 43 Suppl, S199–S203. doi: 10.1269/jrr.43.s199

Pattison, D. I., Rahmanto, A. S., and Davies, M. J. (2012). Photo-oxidation of proteins. *Photochem. Photobiol. Sci.* 11, 38–53. doi: 10.1039/c1pp05164d

Puck, T. T., and Marcus, P. I. (1956). Action of X-rays on mammalian cells. *J. Exp. Med.* 103, 653–666. doi: 10.1084/jem.103.5.653

Quintin, S., Aspert, T., Ye, T., and Charvin, G. (2022). Distinct mechanisms underlie H2O2 sensing in *C. elegans* head and tail. *PLoS One* 17:e0274226. doi: 10.1371/journal.pone.0274226

Restif, C., Ibáñez-Ventoso, C., Vora, M. M., Guo, S., Metaxas, D., and Driscoll, M. (2014). CeleST: computer vision software for quantitative analysis of *C. elegans* swim behavior reveals novel features of locomotion. *PLoS Comput. Biol.* 10:e1003702. doi: 10.1371/journal.pcbi.1003702

Roth, B., Gibhardt, C. S., Becker, P., Gebhardt, M., Knoop, J., Fournier, C., et al. (2015). Low-dose photon irradiation alters cell differentiation via activation of HIK channels. *Pflugers Arch.* 467, 1835–1849. doi: 10.1007/s00424-014-1601-4

Sakashita, T., Hamada, N., Ikeda, D. D., Suzuki, M., Yanase, S., Ishii, N., et al. (2008). Locomotion-learning behavior relationship in *Caenorhabditis Elegans* following γ-ray irradiation. *J. Radiat. Res.* 49, 285–291. doi: 10.1269/jrr.07102

Shen, X., Lind, J., and Merenyi, G. (1987). One-Electron oxidation of indoles and Acid-Base properties of the Indolyl radicals. *J. Phys. Chem.* 91, 4403–4406. doi: 10.1021/j100300a039

Smith, J. C., Kimeldorf, D. J., and Hunt, E. L. (1963). Motor responses in moths to low-intensity X-ray exposure. *Res Dev Tech Rep* February, 1–12. doi: 10.21236/ad0401027

Thariat, J., Leal, C., d'Ascoli, A., Jardel, P., Caujolle, J. P., Herault, J., et al. (2016). Phosphenes in patients receiving radiotherapy. *Lancet Oncol.* 17, 869–871. doi: 10.1016/S1470-2045(16)30034-1

Zaider, M., Brenner, D. J., Hall, E. J., and Kliauga, P. J. (1988). The link between physics and biology. *Am. J. Clin. Oncol.* 11, 212–219. doi: 10.1097/00000421-198806000-00002

Zhang, W., He, F., Ronan, E. A., Liu, H., Gong, J., Liu, J., et al. (2020). Regulation of photosensation by hydrogen peroxide and antioxidants in *C. elegans*. *PLoS Genet.* 16:e1009257. doi: 10.1371/journal.pgen.1009257

frontiers | Frontiers in Neuroscience

TYPE Review
PUBLISHED 23 August 2023
DOI 10.3389/fnins.2023.1226660

OPEN ACCESS

EDITED BY
Gahangir Hossain,
University of North Texas, United States

REVIEWED BY
Axel Hutt,
Inria Nancy – Grand-Est Research Centre, France
Jie Jia,
Fudan University, China

*CORRESPONDENCE
Xinyuan Chen
✉ fychenxinyuan@fjmu.edu.cn
Jun Ni
✉ nijun3527@fjmu.edu.cn

†These authors have contributed equally to this work and share first authorship

RECEIVED 22 May 2023
ACCEPTED 09 August 2023
PUBLISHED 23 August 2023

CITATION
Lv L, Cheng X, Yang J, Chen X and Ni J (2023) Novel role for non-invasive neuromodulation techniques in central respiratory dysfunction. *Front. Neurosci.* 17:1226660. doi: 10.3389/fnins.2023.1226660

Novel role for non-invasive neuromodulation techniques in central respiratory dysfunction

Lan Lv[1,2†], Xiaoping Cheng[1†], Jiaying Yang[1], Xinyuan Chen[1*] and Jun Ni[1*]

[1]Department of Rehabilitation Medicine, The First Affiliated Hospital of Fujian Medical University, Fuzhou, China, [2]Department of Rehabilitation Medicine, National Regional Medical Center, Binhai Campus of the First Affiliated Hospital, Fujian Medical University, Fuzhou, China

Respiration is a crucial steady-state function of human life. Central nervous system injury can damage the central respiratory pattern generator (CRPG) or interrupt its outflow, leading to central respiratory paralysis and dysfunction, which can endanger the patient's life. At present, there is no effective means to reverse this process. Commonly used non-invasive neuromodulation techniques include repetitive transcranial magnetic stimulation (rTMS), transcranial direct current stimulation (tDCS) and so forth, which have been widely applied in nervous system diseases and their various secondary symptoms, but rarely in respiratory function. Clinical and animal studies have confirmed that TMS is also suitable for investigating the excitability and plasticity of ascending corticospinal respiratory pathways. In addition, although rTMS and tDCS differ in their respective mechanisms, both can regulate respiratory networks in healthy individuals and in diseased states. In this review, we provide an overview of the physiology of respiration, the use of TMS to assess the excitability of corticophrenic pathways in healthy individuals and in central respiratory disorders, followed by an overview of the animal and clinical studies of rTMS, tDCS and so forth in regulating respiratory circuits and the possible mechanisms behind them. It was found that the supplementary motor area (SMA) and the phrenic motor neuron (PMN) may be key regulatory areas. Finally, the challenges and future research directions of neuroregulation in respiratory function are proposed. Through understanding how neuromodulation affects the respiratory neural circuit non-invasively, we can further explore the therapeutic potential of this neuromodulation strategy, so as to promote the recovery of respiratory function after central nervous system diseases or injury.

KEYWORDS

non-invasive neuromodulation techniques, respiratory dysfunction, TMS, tDCS, central

Introduction

Respiration is a crucial steady-state function of human life. Central nervous system injury can damage the central respiratory pattern generator (CRPG) or interrupt its outflow, such as in stroke, high cervical spinal cord injury and so forth, thus leading to central respiratory paralysis and dysfunction, which can endanger the patient's life. At present, there is no effective means to reverse this process, and the commonly used methods are alternative, such as mechanical ventilation support, oxygen therapy and so forth. Neuromodulation techniques are defined as "the alteration of nerve activity through targeted delivery of a stimulus, such as electrical stimulation or chemical agents, to specific neurological sites in the body" (Knotkova et al., 2021). Commonly used non-invasive neuromodulation techniques include repetitive transcranial magnetic stimulation (rTMS) and transcranial direct current stimulation (tDCS),

which have been widely applied in nervous system diseases and their various secondary symptoms, but rarely in respiratory function.

Clinical and animal studies have confirmed that TMS is also suitable for investigating the excitability and plasticity of ascending corticospinal respiratory pathways (Urban et al., 2002; Miscio et al., 2006; Harraf et al., 2008; Vinit et al., 2014; Lee et al., 2021). Generally, TMS relies on the generation of a strong magnetic field through an electromagnetic coil, which creates an electric current that travels approximately 3 cm through the cerebral cortex and depolarizes the cortical neurons (Lefaucheur et al., 2014; Kubis, 2016). Repetitive TMS (rTMS) involves a series of continuous or periodic pulses that are thought to induce long-term changes in cortical excitability. The mechanism of cortical excitability changes is not fully understood, but some researchers believe that it is similar to long-term potentiation (LTP) and long-term depression (LTD) (Bates and Rodger, 2015; Kubis, 2016). However, there are arguments that rTMS mediated effects are usually the result of a mixture of synaptic events (Kemps et al., 2022). The mechanism underlying tDCS is also not fully understood. Unlike the direct induction of neuronal activity by TMS, tDCS is thought to have a main mechanism involving the subliminal regulation of neuronal membrane potential, which biases cortical excitability (Nitsche and Paulus, 2000). The direct effect of tDCS on corticospinal excitability is mainly determined by changes in subliminal resting membrane potential (Nitsche et al., 2005). In addition to acute effects on brain function, specific protocols are suitable for inducing long-lasting alterations in cortical excitability and activity, which share features with long-term potentiation and depression (Stagg et al., 2018). However, a cadaver study doubts the mechanism and effectiveness of tDCS, and Underwood (2016) suggests that 1–2 mA currents are unlikely to have dramatic effects on neurons. Although the mechanisms of rTMS and tDCS are different, both can alter respiratory excitability by stimulating relevant regions (Raux et al., 2010; Azabou et al., 2013; Laviolette et al., 2013; Niérat et al., 2014; Nierat et al., 2015; Carvalho et al., 2021). Through understanding how neuromodulation affects the respiratory neural circuit non-invasively, we can further explore the therapeutic potential of this neuromodulation strategy, to promote the recovery of respiratory function after central nervous system diseases or injury. In the following section, we provide an overview of TMS in evaluating the excitability of the cortico-diaphragmatic pathway (Supplementary Table 1), animal and clinical studies on rTMS and tDCS regulating respiratory function (Supplementary Tables 2, 3), as well as the difficulties encountered and future directions for development.

Physiology of respiration

The central control of respiration is dual, automatic at the brainstem level and voluntary at the cortical level. The preBötzinger complex (preBötC) of the medulla oblongata underlies automatic inspiratory rhythm generation, while the retrotrapezoidnucleus/parafacial respiratory group (RTN/pFRG) generates active expiration (Feldman et al., 2013). Autonomous respiratory command originates in the cerebral cortex, and is transmitted to respiratory motor neurons in the spinal cord through the medullary reticulospinal tract and corticospinal tract, among which phrenic motor neurons (PMNs) are the main respiratory motor neurons located in the cervical spine (C3–C5) (Verin et al., 2011). The contraction of the diaphragm depends on the PMN discharge. Functional magnetic resonance imaging (fMRI) studies have shown that the sensory-motor cortex, cerebellum, supplementary motor area (SMA) and premotor area are mostly activated in neuroimaging for respiratory motor control, while additional respiratory motor activities are detected in the basal ganglia, thalamus and prefrontal cortex by high-sensitivity neuroimaging (Evans, 2010).

Preclinical studies on examination and neuromodulation of respiration

Respiratory dysfunction associated with neural control is life-threatening. To date, there is no effective treatment method for improving damaged function. Therefore, it is important to establish a preclinical model for further respiratory research to develop a non-invasive therapeutic tool suitable for animal phrenic neural circuits. Vinit et al. (2014) firstly established an animal model of TMS-induced diaphragmatic motor evoked potentials (DiMEPs) in Sprague–Dawley (SD) rats for trans-synaptic neuroanatomical tracing with pseudorabies virus (applied to the diaphragm), which revealed that supraspinal stimulation could (directly or indirectly) transmit anatomical substrates of descending action potentials to spinal motor neurons. The authors further applied it to the study on respiratory plasticity in rats with respiratory dysfunction following C2 hemisection, and observed profound reorganization in the TMS-induced diaphragm. DiMEPs decreased on the non-injured side, but not the injured side, indicating increased excitability of PMNs on the ipsilateral side. In addition, there was a correlation between the DiMEP amplitude and spontaneous contralateral diaphragmatic activity. The higher the degree of diaphragmatic activity, the higher the DiMEPs on the injured side, and the lower the DiMEPs on the non-injured side. This suggests, for the first time, the occurrence of a functional neuroplasticity process involving changes in motoneuron excitability balance between the injured and the non-injured sides in a short time after injury (Vinit et al., 2016). On this basis, Michel-Flutot et al. (2021) conducted two interventional studies. One study compared different rTMS protocols and found that the 10-Hz rTMS protocol induced a sustained and stable increase in the excitability of PMNs compared with 3 Hz and 30 Hz. Another study investigated the effect of chronic high-frequency (10 Hz) rTMS on the cortical regions of rats with C2 hemisection. One month after treatment with 7-d, 1-month or 2-month rTMS, an increase in activity and excitability (DiMEPs) was observed on the non-injured side in diaphragmatic electromyography (EMG). Interestingly, although rTMS treatment did not have an actual functional impact on damaged diaphragmatic activity during respiratory stimulation, a 2-month rTMS treatment strengthened the existing crossed phrenic pathway, increasing the activity of the damaged diaphragm during respiratory stimulation. These findings demonstrate that chronic high-frequency rTMS can improve respiratory dysfunction after cervical spinal cord injury, and that this therapeutic tool can be used and/or combined with other interventional measures to further improve beneficial clinical outcomes (Michel-Flutot et al., 2022). In addition to inducing DiMEPs through TMS, some scholars have conducted animal studies on trans-spinal magnetic stimulation. When Lee et al. (2021) placed the rat head 30 mm right or left to the coil center, and a single magnetic

stimulation could induce significant DiMEPs in non-injured animals. In the acute stage of left cervical spinal cord injury, cervical magnetic stimulation reduced the DiMEP threshold and enhanced its amplitude. In addition, during the subchronic and chronic stages, the bilateral DiMEPs of the contused animals increased when the coil was placed in the left cervical spinal cord, suggesting that cervical magnetic stimulation can be used to detect the excitability of diaphragmatic motor output after injury, and the more lateral the magnetic stimulation direction, the better the effect of triggering DiMEPs. In another study, Lee et al. (2022) explored the rostral-caudal effect of spinal cord magnetic stimulation on DiMEPs following cervical spinal cord injury, and the effects of coils at the rostral, middle and caudal levels of rats. The results showed that cervical magnetic stimulation could induce intensity-dependent MEP in the bilateral diaphragm of both normal rats and rats with left cervical spinal cord contusion, but the amplitude of the left diaphragm was higher and its occurrence was earlier than that of the right. Moreover, the intensity-response curve of magnetic stimulation shifted upwards in the rostral-caudal direction, indicating that caudal cervical magnetic stimulation generated higher DiMEPs than rostral cervical magnetic stimulation. After cervical magnetic stimulation, the DiMEPs of contused rats were similar to that of normal rats, but the diaphragmatic inspiratory activity of contused rats was weaker. Additionally, in rats with contusion, the amplitude of DiMEPs in the chronic stage was higher than that in the early stage.

However, the respiratory physiology of humans and animals is not entirely consistent. Rats have specific respiratory medullary spinal axons with C3-C6 spinal cord segments crossing the midline, known as the crossed phrenic pathway (Goshgarian, 2003), which has not been observed in humans. Further research is required to determine whether the results of animal models are applicable to humans.

Evaluation of cortico-diaphragmatic spinal pathway and respiration-related cortical excitability using TMS

TMS has been used to characterize the motor cortex of the diaphragm and evaluate the cortico-diaphragmatic pathways in both hemispheres. Murphy et al. (1990) first used non-focal TMS to determine the optimal location for eliciting DiMEPs, centered on a circular coil with an average of 2 cm posterior to the vertex in the median sagittal line, where bilateral diaphragmatic responses could be induced. Subsequently, it was recorded that under TMS, a focal 8-shaped coil mainly caused contraction of the contralateral diaphragm with its center approximately 3 cm right to the midline and 2 ± 3 cm in front of the auricular plane, however, small EMG responses were also observed on the ipsilateral side. The bilateral corticospinal cord and the diaphragm have crossed and uncrossed connections, mainly crossed tracts (Maskill et al., 1991; Khedr and Trakhan, 2001). All the above stimuli corresponded to the primary motor cortex of the diaphragm. Sharshar et al. (2003) found that TMS of the supplementary motor area (SMA)in front of the primary motor cortex of the diaphragmcan also elicit DiMEPs. During spontaneous inspiration, the two cortical regions that can lead to diaphragmatic responses showed significant differences in inhibitory/excitatory balance and output facilitation in the cortex, suggesting another SMA-diaphragm conduction pathway. The authors concluded that SMA might play a major excitatory role on PMNs.

Clinically, TMS has been used to record respiratory muscle involvement in patients with nervous system diseases. It has been shown that the excitability threshold of the diaphragmatic cortex decreases and the conduction time of the diaphragm and intercostal muscle involvement pathways are prolonged in patients with stroke (Khedr et al., 2000; Urban et al., 2002). In addition to the inspiratory muscles, a TMS study on expiratory muscle weakness in acute ischemic stroke was conducted using TMS at the vertex (a representative area of the diaphragmatic cortex) and bilateral hemispheric expiratory muscular cortex, as well as magnetic stimulation over the T 10–11 spinal roots (Tw T10) and phrenic nerves bilaterally (BAMPS), with surface electrodes recording MEPs of the rectus abdominis (RA) and external oblique (EO). The results revealed that the latency and amplitude of MEPs induced by TMS in the abdominal muscles in the uninjured hemisphere of patients with stroke were comparable to those in the control group, but no MEPs were recorded in the abdominal muscles after TMS of the injured hemisphere. TMS at the cortical area of the expiratory muscles in the injured hemisphere resulted in lower intragastric pressure compared to the uninjured side, suggesting that ischemic cortical injury is correlated with expiratory muscle weakness and may cause cough in stroke patients with acute respiratory failure (Harraf et al., 2008). TMS has also been used to explore cortico-diaphragmatic pathways in patients with amyotrophic lateral sclerosis (ALS), with no changes in vital capacity or blood gas levels in all 14 patients. Seven patients had a decrease in maximal transdiaphragmatic pressure (Pdimx), and eight patients showed a decrease in MEPs. Four patientshad delayed spinal motor-evoked potentials (Sp-MEPs). Cortical motor-evoked potentials (Cx-MEPs) were not elicited in one patient. The correlations between Cx-MEPs and central motor conduction time (CMCT) with any respiratory measurement were not significant, indicating that cortico-diaphragmatic research is a sensitive method to reveal subclinical diaphragmatic injury, although it is not correlated with respiratory measurements (Miscio et al., 2006). Similar studies have also been carried out in multiple sclerosis (MS), and the results showed prolonged Cx-MEP latency and CMCT in the diaphragm (Dia) of 31 and 23% respectively, as well as in the abductor digiti minimi (Abd) of 76 and 79% patients. Phrenic nerve-compound motor action potentials (PN-CMAPs) were normal. This suggests that the cortico-diaphragmatic pathways are damaged only in a few MS patients (Miscio et al., 2003). Furthermore, DiMEPs have also been used to predict whether patients with respiratory failure can be weaned from the ventilator. Once study followed up the DiMEPs of ventilator-dependent patients due to central respiratory failure, and found that the MEPs were all restored in patients who were able to wean from the ventilator, while those who could not wean did not. This suggests that TMS can play a role in predicting recovery of respiratory function in central respiratory paralysis (Duguet et al., 2006).

Non-invasive neuromodulation techniques as interventions in respiration

The cortical motor center of the diaphragm is considered to be located at the vertex (circular coil) or approximately 3 cm right to the midline and 2 ± 3 cm in front of the auricular plane (8-shaped coil), and the SMA is considered to have another conduction pathway

between the diaphragm. Interestingly, several stimulus locations for TMS-based neuromodulation of respiration in healthy individuals are all located in the SMA. A TMS study revealed that 5-Hz rTMS acting on the SMA simultaneously increased MEP amplitude in the diaphragm and the first dorsal interosseous (FDI) muscle, suggesting that changing SMA excitability can cause excitability changes in the diaphragmatic motor cortex.However, 1-Hz rTMS could not reduce the MEP amplitude of the diaphragm or FDI muscle (Raux et al., 2010). However, in another clinical study, magnetic stimulation of the SMA bi-directionally regulated the corticospinal pathway of the diaphragm, and continuous theta burst stimulation (cTBS, inhibitory) of the SMA during quiet and natural respiration suppressed the excitability of the corticospinal pathway to the diaphragm. The excitatory repetitive magnetic stimulation (5 Hz, excitatory) paradigm applied to the SMA enhanced the excitability of the corticospinal pathway to the diaphragm (Laviolette et al., 2013). In addition to changing the excitability of the diaphragmatic motor cortex, magnetic stimulation of the SMA can also alter respiratory pattern.One study confirmed that controlling SMA excitability through rTMS could alter the respiratory response mode to experimental inspiratory load and may improve respiratory discomfort. The 5-Hz pre-treatment scheme could reduce the excessive ventilation caused by the inspiratory threshold load. Inhibitory pre-treatment did not affect ventilation, but prolonged expiratory time. After sham stimulation, there were no significant changes in the respiratory pattern to inspiratory load (Nierat et al., 2015). Currently, TMS in regulating patients with respiratory dysfunction has rarely been reported. A newly reported clinical study on the application of TMS in stroke patients with respiratory dysfunction found that rTMS acting on the diaphragmatic cortical center five times a week for 8 weeks could improve pulmonary function after acute ischemic stroke. However, this study did not measure DiMEPs;therefore it cannot confirm the direct effect of TMS on the diaphragm (Cao et al., 2022).

tDCS has also been used to regulate the respiratory centers. In a study about the effect of tDCS on the diaphragmatic corticospinal pathway in healthy individuals, anode, cathode and sham tDCS were randomly applied to the left diaphragmatic motor cortex of 12 healthy right-handed males. The excitability of the corticospinal pathway was evaluated using TMS-induced MEPs. The results showed that the excitability of the diaphragmatic corticospinal pathway decreased regardless of polarity (Azabou et al., 2013). In a recent clinical case report(Carvalho et al., 2021), the authors selected tDCS on SMA combined with peripheral electrical stimulation (PES) based on the results of high-frequency TMS research. Corticospinal excitability may also be affected by PES, depending on the parameters used. Sensory PES is often inhibitory, while motor PES is usually excitatory (Chipchase et al., 2011a,b). The authors reported two cases of SCI (P1 and P2) with long-term tracheotomy (>40 days) and hospitalization (>50 days). P1 received the combined application of sensory PES on the pectoral and abdominal muscles and anode tDCS on the SMA, while P2 received isolated excitatory PES on the abdominal muscles. Both patients were extubated 15 times after stimulation, and presented clinical effects such as cough effectiveness. This suggests that the SMA, under both TMS and tDCS, may be a key area for respiratory regulation, but this still needs to be confirmed in clinical trials with a large sample size.

The spinal motor center of the diaphragm is considered another regulatory target. Data from a randomized clinical trial showed that both anode and cathode transcutaneous spinal direct current stimulation (tsDCS) at the C3–C5 levels induced a progressive increase in DiMEP amplitude during stimulation, lasting at least 15 min after the end of stimulation. Interestingly, tsDCS induced a sustained increase in tidal volume at the cathode rather than at the anode. However, the long-term increase in tidal volume after cathode tsDCS is particularly noteworthy, as this finding paves the way for therapeutic research to evaluate tsDCS as a tool for increasing ventilation in patients with various neurorespiratory diseases (Niérat et al., 2014).

Underlying mechanisms

Plasticity of the respiratory network

In recent years, increasing evidence has shown that respiratory rhythm generation networks exhibit high plasticity. Although spontaneous functional recovery after cervical hemisection is limited, inducing additional plasticity (such as repeated exposure to intermittent hypoxia) can significantly enhance the respiratory motor outputin experimental models of cervical spine injury (cervical hemisection). The longer the duration after injury, the stronger the ability to induce functional recovery (Vinit et al., 2009; Dale-Nagle et al., 2010a; Lovett-Barr et al., 2012). Training can also alter respiratory plasticity. Diaphragm training leads to a decrease in the threshold intensity of stimulation, an increase in the number of responding sites mapped to the diaphragm under focal stimulation, and shortened latency of MEPs in response to non-focal stimulation (Demoule et al., 2008). The increased respiratory motor output induced by various factors is called phrenic motor facilitation (PMF). The most widely studied form of PMF is phrenic long-term facilitation (pLTF) after acute intermittent hypoxia (AIH). At least five different cellular mechanisms generate long-lasting phrenic motor facilitation (pMF) with similar intensity and time domains, including the Gq pathway. The Gq pathway is the "classic" mechanism of diaphragmatic LTF in anesthetized rats, initiated by the intermittent activation of 5-hydroxytryptaminergic neurons in the median raphe, which activates 5-hydroxytryptamine (Gq-coupled) type 2 metabotropic receptors located at or near PMNs. The downstream intracellular cascade of 5-hydroxytryptamine 2 receptor activation includes the new synthesis of brain-derived neurotrophic factor (BDNF) and the activation of its high-affinity receptor tyrosine kinase B (TrkB), followed by the activation of extracellular regulated protein kinases /mitogen-activated protein(ERK/MAP)kinase. The Gs pathway, which triggers similar pMF through a unique mechanism, requires the synthesis of new TrkB (rather than BDNF) and the activation of agammaglobulinaemia tyrosine kinase(Akt) (rather than ERK MAP kinase). In addition, other mechanisms include activation of the spinal vascular endothelial growth factor (VEGF) receptor, erythropoietin and persistent diaphragm inactivity (Dale-Nagle et al., 2010a,b, 2012; Mahamed et al., 2011). Inflammation induced by low-dose lipopolysaccharide may undermine mAIH-induced pLTF (Marciante and Mitchell, 2023).

Transcranial direct current induces respiratory excitability

tDCS can induce sustained changes in excitability in the human motor cortex. Transcranial magnetic stimulation showed an approximately 150% increase in motor cortical excitability from

baseline up to 90 min after stimulation ended (Nitsche and Paulus, 2001). Anode stimulation selectively increases cortical excitability, whereas cathode stimulation selectively reduces cortical excitability. A study found that the post-stimulation effects of anode and cathode tDCS can be inhibited by dextromethorphan (DMO), an N-methyl-D-aspartic acid (NMDA) receptor antagonist, which strongly suggests that NMDA receptors are involved in the two types of tDCS-induced neuroplasticity. On the contrary, the sodium (+) channel blocker carbamazepine (CBZ) selectively eliminated the anode effect. CBZ stabilizes the membrane potential based on the voltage, and the aftereffect of anode tDCS requires depolarization of the membrane potential. Consequently, it is believed that the polar drive changes in resting membrane potential are the key mechanism of the aftereffect of transcranial direct current induction, leading to changes in the spontaneous discharge rate and NMDA receptor activation (Liebetanz et al., 2002). The after effects of tDCS are also considered to involve non-synaptic mechanisms based on changes in neural membrane function. These changes not only reflect the local changes in ion concentrations, but also may be attributed to the changes in transmembrane proteins and relevant to [H(+)] electrolysis induced by a constant electric field (Ardolino et al., 2005).

Trans-spinal direct current stimulation (tsDCS) enhance respiratory excitability

The mechanism underlying DiMEP enhancement after tsDCS may also involve changes in neurotransmission. During inspiration, glutamate drives the PMN pathway. NMDA and non-NMDA ionic glutamate receptors located in PMNs play an important role in the neurotransmission of inspiratory drive in adult rats (Chitravanshi and Sapru, 1996). However, activating NMDA rather than NMDA receptors is necessary for the formation and maintenance of ventilatory long-term facilitation (vLTF) in conscious rats (McGuire et al., 2008). A study found that both anode and cathode tsDCS can increase the *in vitro* release of glutamic acid analogue D-2,3-3H aspartic acid (Ahmed and Wieraszko, 2012).In contrast,expiratory neurons of the medulla oblongata-Rötzinger complex have a long-term descending inhibitory connection with PMNs (Merrill and Merrill and Fedorko, 1984). The γ-aminobutyric acid (GABA)-ergic system is closely related to respiratory motor control, and cathode tsDCS may act by directly inhibiting the spinal GABA-ergic system or by overexciting postsynaptic neurons (Ahmed, 2013). A study (Niérat et al., 2014) used paired-pulse technique to induce short interval intra-cortical inhibition (sICI) after tsDCS at C3-C5 levels, and found that sICI was not affected by tsDCS, suggesting that reducing GABA-mediated intra-cortical inhibition is not the cause for DiMEP enhancement after tsDCS. The residual effects induced by tsDCS do not occur at the brainstem or cortical level, but may mainly occur at the spinal cord level.

Transcranial magnetic stimulation (TMS) enhance respiratory excitability

Some signaling pathways are believed to be related to respiratory plasticity. It is known that high-frequency rTMS (hfrTMS) strongly activates molecular pathways crucial for plasticity. A recent study demonstrated that acute hfrTMS can induce increased phosphorylation of the synaptic plasticity-related ribosomal protein S6 (rpS6). S6 phosphorylation is a downstream marker for the activation of multiple signaling pathways in neurons, including mitogen-activated protein kinase (MAPK)/extracellular signal-regulated kinase (ERK), ERK, kinase phosphatidylinositol 3-kinase (PI3K) and AKT/mammalian target of rapamycin (mTOR) signaling pathways, the combined action of which make synaptic and cellular changes the basis of plasticity (Gobert et al., 2008; Fujiki et al., 2020). Human and animal experiments have also confirmed that hfrTMS can induce increased expression of BDNF (Yukimasa et al., 2006; Gersner et al., 2011; Wang et al., 2011; Dall'Agnol et al., 2014). BDNF is believed to be involved in respiratory plasticity of PMNs (Baker-Herman et al., 2004). This factor also plays a crucial role in respiratory control during the injury after SCI (Lovett-Barr et al., 2012). In an animal experiment(Wang et al., 2011), 5-Hz rTMS was used daily for 5 days to improve rat BDNF–TrkB signaling by increasing the affinity of BDNF for tyrosine receptor kinase B (TrkB), resulting in an increase in TrkB phosphorylation. The increase in BDNF–TrkB signaling was accompanied by an increased correlation between activated TrkB and NMDA receptors (NMAR). In normal human subjects, 5-d rTMS of the motor cortex reduced the resting motor threshold, which is related to the enhancement of the BDNF–TrkB signaling pathway in lymphocytes and TrkB-NMDAR correlation. These results indicate that rTMS promotes the function of BDNF–TrkB-NMDARs in the cortex and lymphocytes. TMS can also alter respiratory excitability by reducing the intensity of inhibitory synapses. Studies (Michel-Flutot et al., 2021) have found that a single 10-Hz rTMS in anesthetized rats can induce an increase in the excitability of the phrenic neural network. Intravenous injection of $GABA_A$ and $GABA_B$ receptor agonists before treatment with 10-Hz rTMS can eliminate the enhanced PMN excitability, indicating that a single high-frequency rTMS protocol at 10 Hz can alleviate the increased PMN excitability through local GABA-ergic-mediated inhibition. In *in vitro* experiments, it was also observed that 10-Hz magnetic stimulation could induce a decrease in the postsynaptic GABA-ergic synaptic strength of neurons (2–4 h after stimulation), which was Ca (2+)-dependent and accompanied by remodeling of the postsynaptic gephyrin scaffold (Lenz et al., 2016). Additionally, TMS may induce respiratory plasticity by reducing inflammatory responses. A recent study found that 10-Hz rTMS treatment could reduce inflammation of the spinal cord (C1-C3) in rats with C2 hemisection (reduced CD68 and Iba1 labeling) and accelerate the intracellular plasticity of PMNs, thereby enhancing the respiratory descending fibers in the ventrolateral funiculus (increased GAP-43-positive fibers), indicating that chronic high-frequency rTMS can improve respiratory dysfunction after cervical spinal cord injury and induce neuronal plasticity by reducing harmful post-traumatic inflammatory processes (Michel-Flutot et al., 2022).

Safety and tolerability of TMS/tDCS

The most commonly reported adverse events of TMS are transient or mild headaches and local discomfort at the site of irritation (Hao et al., 2013). The only potentially serious side effect is seizures. It is now certain that the risk is very low (Rossi et al., 2009, 2021). The most commonly reported effects of tDCS are tingling and itching

under electrodes, headache, and fatigue (Poreisz et al., 2007; Fertonani et al., 2015). Unlike rTMS, no cases of induced seizures have been reported to date. Skin damage has occasionally been reported (Palm et al., 2008), in most cases,it is associated with program defects, such as dryness of the contact medium under the electrode. In summary, the commonly used tDCS/TMS protocol is safe and well tolerated.

Challenges and open issues faced

The application of rTMS/tdc in respiratory function is still investigational. The study of the effect of TMS on respiratory muscle function is challenging. The effectiveness of TMS-MEP mainly depends on the appropriate positioning of electromyographic electrodes and the control of background muscle activity and noise. Through this technique, the signals recorded during non-specific muscle contractions (such as contraction generated by cortical magnetic stimulation) are the sum of the electrical activities generated by all muscles below the electrodes. Therefore, we may question whether these signals indeed originate from the diaphragm and there are several factors that support diaphragmatic origin, including the latency from the cortex to the diaphragm, changes in intrathoracic and abdominal pressure or abdominal circumference and electrode positioning (Similowski et al., 1996). Compared to the diaphragm, the cortical center of the expiratory muscle (abdominal muscle) is more difficult to locate, resulting in a smaller MEPs amplitude. Other challenges include ensuring that the TMS coil is correctly positioned and maintained in the cortical area of interest throughout the entire TMS process. However, TMS neuronavigation devices have been proven to effectively reduce this potential confoundingly (Caulfield et al., 2022; Nieminen et al., 2022). Moreover, respiration-related indicators of TMS still have significant individual differences and lack standard values forhealthy individuals. Clinical trials with a large sample size are needed to establish standard values. When applying tDCS in the clinical population, it should be considered that tDCS has a brain-state-dependent effect as a neuroregulatory intervention (Thirugnanasambandam et al., 2011; Antal et al., 2014). Concurrent drug therapy can further alter the effect of tDCS, which is an important consideration in all tDCS studies (Stagg and Nitsche, 2011). Another problem with tDCS is that the spatial resolution is too low to accurately stimulate functional subdivisions of the cortical regions. Improving tDCS focus is an important direction in the future (Woods et al., 2016). For rTMS/tDCS mode, in addition to identifying ideal cortical regions to maximize the therapeutic response (which may require a combination of clinical, neuroimaging and neurophysiological information), it is important to optimize the stimulation mode, so as to best regulate the activity of these regions and move them toward the expected direction. Future work and exploration will focus on the combination of neuroregulation with other therapeutic interventions (including respiration training and exercise therapy), simultaneous central and peripheral interventions, as well as the application of closed-loop theory. The closed-loop theory, which was first proposed in 2016 and refers to combining central intervention measures with peripheral intervention measures to form a positive feedback loop to promote motor function rehabilitation in stroke patients (Jia, 2016, 2022).

Conclusion and future directions

Although TMS/tDCS is not currently approved as adjuvant treatments for respiratory dysfunction, considering the clinical importance of respiratory dysfunction and the lack of treatment means, it is of great significance to further explore the therapeutic potential of this neuromodulation strategy in respiratory dysfunction. We suggest four fields for future research on TMS in central respiratory dysfunction. These studies will ultimately help to develop better neuromodulation-based interventions for patients: (1) Optimizing animal models. At present, most preclinical studies mainly involve rodents, whose respiratory physiology is very different from that of humans, but in the future, preclinical models can be considered in mammals that are more similar to human respiratory physiology, such as cats, rabbits and so forth. (2) TMS-MEP was used to determine respiratory corticospinal tract conduction and cortical excitability abnormalities and to further clarify the disorders of respiratory neural circuits in different physiological and pathological states in combination with techniques such as EEG, providing more accurate neural targets for non-invasive regulation of respiratory dysfunction. (3) rTMS/tDCS was used to regulate respiratory neural circuits to determine the impact of this neuromodulation on respiration-related biological and clinical parameters. Before and after acute rTMS/tDCS, neuroimaging and/or neurophysiological evaluation, as well as clinical evaluation can elucidate the causal role of respiratory neural circuits in specific symptoms or behavioral development to better guide subsequent therapeutic intervention based on neuromodulation. Functional neuroimaging, especially functional imaging including functional connectivity measurement, has been used to prospectively determine non-invasive neuroregulatory targets for future therapeutic interventions. (4) Combining neuroimaging, neurophysiology and clinical measures relevant to respiration-targeted neural circuits to better predict and track outcomes in clinical trial studies.

Author contributions

LL and XiaC conceived and organized the manuscript. LL, XiaC, and JY researched literature. JN and XinC proofread the manuscript. All authors contributed to the manuscript and approved the submitted version.

Funding

This work was supported by the Fujian Provincial Health Technology Project (grant number: 2020TG016), the Startup Fund for Scientific Research of Fujian Medical University (grant number: 2020QH1017), and the Fujian Provincial Health Youth Research Project (grant number: 2021QNA024).

Acknowledgments

We thank the reviewers for their valuable and constructive comments.

Conflict of interest

The authors declare that the research was conducted in the absence of any commercial or financial relationships that could be construed as potential conflicts of interest.

Publisher's note

All claims expressed in this article are solely those of the authors and do not necessarily represent those of their affiliated organizations, or those of the publisher, the editors and the reviewers. Any product that may be evaluated in this article, or claim that may be made by its manufacturer, is not guaranteed or endorsed by the publisher.

Supplementary material

The Supplementary material for this article can be found online at: https://www.frontiersin.org/articles/10.3389/fnins.2023.1226660/full#supplementary-material

References

Ahmed, Z. (2013). Effects of cathodal trans-spinal direct current stimulation on mouse spinal network and complex multijoint movements. *J. Neurosci.* 33, 14949–14957. doi: 10.1523/JNEUROSCI.2793-13.2013

Ahmed, Z., and Wieraszko, A. (2012). Trans-spinal direct current enhances corticospinal output and stimulation-evoked release of glutamate analog, D-2, 3-H-3-aspartic acid. *J. Appl. Physiol.* 112, 1576–1592. doi: 10.1152/japplphysiol.00967.2011

Antal, A., Ambrus, G. G., and Chaieb, L. (2014). Toward unraveling reading-related modulations of tdcs-induced neuroplasticity in the human visual cortex. *Front. Psychol.* 5:642. doi: 10.3389/fpsyg.2014.00 642

Ardolino, G., Bossi, B., Barbieri, S., and Priori, A. (2005). Non-synaptic mechanisms underlie the after-effects of cathodal transcutaneous direct current stimulation of the human brain. *J. Physiol.* 568, 653–663. doi: 10.1113/jphysiol.2005.088310

Azabou, E., Roche, N., Sharshar, T., Bussel, B., Lofaso, F., and Petitjean, M. (2013). Transcranial direct-current stimulation reduced the excitability of diaphragmatic corticospinal pathways whatever the polarity used. *Respir. Physiol. Neurobiol.* 189, 183–187. doi: 10.1016/j.resp.2013.07.024

Baker-Herman, T. L., Fuller, D. D., Bavis, R. W., Zabka, A. G., Golder, F. J., Doperalski, N. J., et al. (2004). BDNF is necessary and sufficient for spinal respiratory plasticity following intermittent hypoxia. *Nat. Neurosci.* 7, 48–55. doi: 10.1038/nn1166

Bates, K. A., and Rodger, J. (2015). Repetitive transcranial magnetic stimulation for stroke rehabilitation-potential therapy or misplaced hope? *Restor. Neurol. Neurosci.* 33, 557–569. doi: 10.3233/RNN-130359

Cao, H., Chen, X., Ren, X., Chen, Z., Liu, C., Ni, J., et al. (2022). Repetitive transcranial magnetic stimulation combined with respiratory muscle training for pulmonary rehabilitation after ischemic stroke-a randomized, case-control study. *Front. Aging Neurosci.* 14:1006696. doi: 10.3389/fnagi.2022.1006696

Carvalho, P. D., Goulardins, J. B., Nakamura de Sousa, D. M., da Silva Barbosa, C. M., Candido Caetano, T. C., Macedo Dos Santos, L., et al. (2021). Noninvasive neuromodulation techniques in difficult tracheostomy weaning of patients with spinal cord injury: report of two cases. *Chest* 159, e299–e302. doi: 10.1016/j.chest.2020.11.065

Caulfield, K. A., Fleischmann, H. H., Cox, C. E., Wolf, J. P., George, M. S., and McTeague, L. M. (2022). Neuronavigation maximizes accuracy and precision in TMS positioning: evidence from 11,230 distance, angle, and electric field modeling measurements. *Brain Stimul.* 15, 1192–1205. doi: 10.1016/j.brs.2022.08.013

Chipchase, L. S., Schabrun, S. M., and Hodges, P. W. (2011a). Peripheral electrical stimulation to induce cortical plasticity: a systematic review of stimulus parameters. *Clin. Neurophysiol.* 122, 456–463. doi: 10.1016/j.clinph.2010.07.025

Chipchase, L. S., Schabrun, S. M., and Hodges, P. W. (2011b). Corticospinal excitability is dependent on the parameters of peripheral electric stimulation: a preliminary study [Internet]. *Arch. Phys. Med. Rehabil.* 92, 1423–1430. doi: 10.1016/j.apmr.2011.01.011

Chitravanshi, V. C., and Sapru, H. N. (1996). NMDA as well as non-NMDA receptors mediate the neurotransmission of inspiratory drive to phrenic motoneurons in the adult rat. *Brain Res.* 715, 104–112. doi: 10.1016/0006-8993(95)01565-5

Dale-Nagle, E. A., Hoffman, M. S., Mac Farlane, P. M., and Mitchell, G. S. (2010a). Multiple pathways to long-lasting phrenic motor facilitation. *Adv. Exp. Med. Biol.* 669, 225–230. doi: 10.1007/978-1-4419-5692-7_45

Dale-Nagle, E. A., Hoffman, M. S., Mac Farlane, P. M., Satriotomo, I., Lovett-Barr, M. R., Vinit, S., et al. (2010b). Spinal plasticity following intermittent hypoxia: implications for spinal injury. *Ann. N. Y. Acad. Sci.* 1198, 252–259. doi: 10.1111/j.1749-6632.2010.05499.x

Dale-Nagle, E. A., Satriotomo, I., and Mitchell, G. S. (2012). Cervical spinal erythropoietin induces phrenic motor facilitation via extracellular signal-regulated protein kinase and Akt signaling. *J. Neurosci.* 32, 5973–5983. doi: 10.1523/JNEUROSCI.3873-11.2012

Dall'Agnol, L., Medeiros, L. F., Torres, I. L., Deitos, A., Brietzke, A., Laste, G., et al. (2014). Repetitive transcranial magnetic stimulation increases the corticospinal inhibition and the brain-derived neurotrophic factor in chronic myofascial pain syndrome: an explanatory double-blinded, randomized, sham-controlled trial. *J. Pain* 15, 845–855. doi: 10.1016/j.jpain.2014.05.001

Demoule, A., Verin, E., Montcel, S. T., and Similowski, T. (2008). Short-term training-dependent plasticity of the corticospinal diaphragm control in normal humans. *Respir. Physiol. Neurobiol.* 160, 172–180. doi: 10.1016/j.resp.2007.09.007

Duguet, A., Demoule, A., Gonzalez, J., Remy-Neris, O., Derenne, J. P., and Similowski, T. (2006). Predicting the recovery of ventilatory activity in central respiratory paralysis. *Neurology* 67, 288–292. doi: 10.1212/01.wnl.0000224881.88971.6c

Evans, K. C. (2010). Cortico-limbic circuitry and the airways: insights from functional neuroimaging of respiratory afferents and efferents. *Biol. Psychol.* 84, 13–25. doi: 10.1016/j.biopsycho.2010.02.005

Feldman, J. L., Del Negro, C. A., and Gray, P. A. (2013). Understanding the rhythm of breathing: so near yet so far. *Annu. Rev. Physiol.* 75, 423–452. doi: 10.1146/annurev-physiol-040510-130049

Fertonani, A., Ferrari, C., and Miniussi, C. (2015). What do you feel if I apply transcranial electricstimulation? Safety, sensations and secondary induced effects. *Clin. Neurophysiol.* 126, 2181–2188. doi: 10.1016/j.clinph.2015.03.015

Fujiki, M., Yee, K. M., and Steward, O. (2020). Non-invasive high frequency repetitive Transcranial Magnetic Stimulation (hfr TMS) robustly activates molecular pathways implicated in neuronal growth and synaptic plasticity in select populations of neurons. *Front. Neurosci.* 14:558. doi: 10.3389/fnins. 2020.00558

Gersner, R., Kravetz, E., Feil, J., Pell, G., and Zangen, A. (2011). Long-term effects of repetitive transcranial magnetic stimulation on markers for neuroplasticity: differential outcomes in anesthetized and awake animals. *J. Neurosci.* 31, 7521–7526. doi: 10.1523/JNEUROSCI.6751-10.2011

Gobert, D., Topolnik, L., Azzi, M., Huang, L., Badeaux, F., Desgroseillers, L., et al. (2008). Forskolin induction of late-LTP and up-regulation of 5' TOP mRNAs translation via mTOR, ERK, and PI3K in hippocampal pyramidal cells. *J. Neurochem.* 106, 1160–1174. doi: 10.1111/j.14714159.2008.05470.x

Goshgarian, H. G. (2003). The crossed phrenic phenomenon: a model for plasticity in the respiratory pathways following spinal cord injury. *J. Appl. Physiol.* 94, 795–810. doi: 10.1152/japplphysiol.00847.2002

Hao, Z., Wang, D., Zeng, Y., and Liu, M. (2013). Repetitive transcranial magnetic stimulation for improving function after stroke. *Cochrane Database Syst. Rev.* 5:CD008862. doi: 10.1002/14651858.cd008862

Harraf, F., Ward, K., Man, W., Rafferty, G., Mills, K., Polkey, M., et al. (2008). Transcranial magnetic stimulation study of expiratory muscle weakness in acute ischemic stroke. *Neurology* 71, 2000–2007. doi: 10.1212/01.wnl.0000336927.30977.56

Jia, J. (2016). "Central–Periphery–Center" closed loop rehabilitation: a new concept of hand function rehabilitation after stroke. *Chin. J. Rehabil. Med.* 31, 1180–1182. doi: 10.3969/j.issn.1001-1242.2016.11.001

Jia, J. (2022). Exploration on neurobiological mechanisms of the central-peripheral-central closed-loop rehabilitation. *Front. Cell. Neurosci.* 16:982881. doi: 10.3389/fncel.2022.982881

Kemps, H., Gervois, P., Brône, B., Lemmens, R., and Bronckaers, A. (2022). Non-invasive brain stimulation as therapeutic approach for ischemic stroke: insights into the (sub) cellular mechanisms. *Pharmacol. Ther.* 35:108160. doi: 10.1016/j.pharmthera.2022.108160

Khedr, E. M., el Shinawy, O., Khedr, T., Abdel aziz ali, Y., and Awad, E. M. (2000). Assessment of corticodiaphragmatic pathway and pulmonary function in acute ischaemic stroke patients. *Eur. J. Neurol.* 7, 509–516. doi: 10.1046/j.1468-1331.2000.00104.x

Khedr, E. M., and Trakhan, M. N. (2001). Localization of diaphragm motor cortical representation and determination of corticodiaphragmatic latencies by using magnetic stimulation in normal adult human subjects. *Eur. J. Appl. Physiol.* 85, 560–566. doi: 10.1046/j.1468-1331.2000.00104.x

Knotkova, H., Hamani, C., Sivanesan, E., Le Beuffe, M. F. E., Moon, J. Y., Cohen, S. P., et al. (2021). Neuromodulation for chronic pain. *Lancet* 397, 2111–2124. doi: 10.1016/S0140-6736(21)00794-7

Kubis, N. (2016). Non-invasive brain stimulation to enhance post-stroke recovery. *Front. Neural Circuits* 10:56. doi: 10.3389/fncir.2016.00056

Laviolette, L., Niérat, M. C., Hudson, A. L., Raux, M., Allard, E., and Similowski, T. (2013). The supplementary motor area exerts a tonic excitatory influence on corticospinal projections to phrenic motoneurons in awake humans. *PLoS One* 8:e62258. doi: 10.1371/journal.pone.0062258

Lee, K. Z., Liou, L. M., and Vinit, S. (2021). Diaphragm motor-evoked potential induced by cervical magnetic stimulation following cervical spinal cord contusion in the rat. *J. Neurotrauma* 38, 2122–2140. doi: 10.1089/neu.2021.0080

Lee, K. Z., Liou, L. M., Vinit, S., and Ren, M. Y. (2022). Rostral-caudal effect of cervical magnetic stimulation on the diaphragm motor evoked potential after cervical spinal cord contusion in the rat. *J. Neurotrauma* 39, 683–700. doi: 10.1089/neu.2021.0403

Lefaucheur, J. P., André-Obadia, N., Antal, A., Ayache, S. S., Baeken, C., Benninger, D. H., et al. (2014). Evidence-based guidelines on the therapeutic use of repetitive transcranial magnetic stimulation (rTMS). *Clin. Neurophysiol.* 125, 2150–2206. doi: 10.1016/j.clinph.2014.05.021

Lenz, M., Galanis, C., Muller-Dahlhaus, F., Opitz, A., Wierenga, C. J., Szabo, G., et al. (2016). Repetitive magnetic stimulation induces plasticity of inhibitory synapses. *Nat. Commun.* 7:10020. doi: 10.1038/ncomms10020

Liebetanz, D., Nitsche, M. A., Tergau, F., and Paulus, W. (2002). Pharmacological approach to the mechanisms of transcranial DC-stimulation-induced after effects of human motor cortex excitability. *Brain* 125, 2238–2247. doi: 10.1093/brain/awf238

Lovett-Barr, M. R., Satriotomo, I., Muir, G. D., Wilkerson, J. E., Hoffman, M. S., Vinit, S., et al. (2012). Repetitive intermittent hypoxia induces respiratory and somatic motor recovery after chronic cervical spinal injury. *J. Neurosci.* 32, 3591–3600. doi: 10.1523/JNEUROSCI.2908-11.2012

Mahamed, S., Strey, K. A., Mitchell, G. S., and Baker-Herman, T. L. (2011). Reduced respiratory neural activity elicits phrenic motor facilitation. *Respir. Physiol. Neurobiol.* 175, 303–309. doi: 10.1016/j.resp.2010.12.005

Marciante, A. B., and Mitchell, G. S. (2023). Mild inflammation impairs acute intermittent hypoxia-induced phrenic long-term facilitation by a spinal adenosine-dependent mechanism. *J. Neurophysiol.* 129, 799–806. doi: 10.1152/jn.00035.2023

Maskill, D., Murphy, K., Mier, A., Owen, M., and Guz, A. (1991). Motor cortical representation of the diaphragm in man. *J. Physiol. Lond.* 443, 105–121. doi: 10.1113/jphysiol.1991.sp018825

McGuire, M., Liu, C., Cao, Y., and Ling, L. (2008). Formation and maintenance of ventilatory long-term facilitation require NMDA but not non-NMDA receptors in awake rats. *J. Appl. Physiol.* 105, 942–950. doi: 10.1152/japplphysiol.01274.2006

Merrill, E. G., and Fedorko, L. (1984). Mono-synaptic inhibition of phrenic motoneurons-along descending projection from Botzinger neurons. *J. Neurosci.* 4, 2350–2353. doi: 10.1523/JNEUROSCI.04-09-02350.1984

Michel-Flutot, P., Jesus, I., Vanhee, V., Bourcier, C. H., Laila Emam, L., Ouguerroudj, A., et al. (2022). Effects of chronic high-frequency rTMS protocol on respiratory neuroplasticity following C2 spinal cord Hemisection in rats. *Biology* 11:473. doi: 10.3390/biology1103 0473

Michel-Flutot, P., Zholudeva, L. V., Randelman, M. L., Deramaudt, T. B., Mansart, A., Alvarez, J. C., et al. (2021). High frequency repetitive transcranial magnetic stimulation promotes long lasting phrenic motoneuron excitability via GABAergic networks. *Respir. Physiol. Neurobiol.* 292:103704. doi: 10.1016/j.resp.2021.103704

Miscio, G., Guastamacchia, G., Priano, L., Baudo, S., and Mauro, A. (2003). (2003). Are the neurophysiological techniques useful for the diagnosis of diaphragmatic impairment in multiple sclerosis (MS)? *Clin. Neurophysiol.* 114, 147–153. doi: 10.1016/s1388-2457(02)00339-5

Miscio, G., Gukov, B., Pisano, F., Mazzini, L., Baudo, S., Salvadori, A., et al. (2006). The corticodiaph-ragmatic pathway involvement in amyotrophic lateral sclerosis: neurophysiological, respiratory and clinical considerations. *J. Neurol. Sci.* 251, 10–16. doi: 10.1016/j.jns.2006.05.059

Murphy, K., Mier, A., Adams, L., and Guz, A. (1990). Putative cerebral cortical involvement in the ventilatory response to inhaled CO, inconscious man. *J. Physiol. Lond.* 420, 1–18. doi: 10.1113/jphysiol.1990.sp017898

Nieminen, A. E., Nieminen, J. O., Stenroos, M., Novikov, P., Nazarova, M., Vaalto, S., et al. (2022). Accuracy and precision of navigated transcranial magnetic stimulation. *J. Neural Eng.* 19:66037. doi: 10.1088/1741-2552/aca71a

Nierat, M. C., Hudson, A. L., Chaskalovic, J., Similowski, T., and Laviolette, L. (2015). Repetitive transcranial magnetic stimulation over the supplementary motor area modifies breathing pattern in response to inspiratory loading in normal humans. *Front. Physiol.* 6:273. doi: 10.3389/fphys.2015.00273

Niérat, M. C., Similowski, T., and Jean-Charles Lamy, J. C. (2014). Does trans-spinal direct current stimulation alter phrenic motoneurons and respiratory neuromechanical outputs in humans? A double-blind, sham-controlled, randomized, crossover study. *J. Neurosci.* 34, 14420–14429. doi: 10.1523/JNEUROSCI.1288-14.2014

Nitsche, M. A., and Paulus, W. (2000). Excitability changes induced in the human motor cortex by weak transcranial direct current stimulation. *J. Physiol. Lond.* 527, 633–639. doi: 10.1111/j.1469-7793.2000.t01-1-00633.x

Nitsche, M. A., and Paulus, W. (2001). Sustained excitability elevations induced by transcranial DC motor cortex stimulation in humans. *Neurology* 57, 1899–1901. doi: 10.1212/WNL.57.10.1899

Nitsche, M. A., Seeber, A., Frommann, K., Klein, C. C., Rochford, C., Nitsche, M. S., et al. (2005). Modulating parameters of excitability during and after transcranial direct current stimulation of the human motor cortex. *J. Physiol.* 568, 291–303. doi: 10.1113/jphysiol.2005.092429

Palm, U., Keeser, D., Schiller, C., Fintescu, Z., Reisinger, E., Padberg, F., et al. (2008). Skin lesions after treatment with transcranial direct current stimulation (tDCS). *Brain Stimul.* 1, 386–387. doi: 10.1016/j.brs.2008.04.003

Poreisz, C., Boros, K., Antal, A., and Paulus, W. (2007). Safety aspects of transcranial direct current stimulation concerning healthy subjects and patients. *Brain Res. Bull.* 72, 208–214. doi: 10.1016/j.brainresbull.2007.01.004

Raux, M., Xie, H., Similowski, T., and Koski, L. (2010). Facilitatory conditioning of the supplementary motor area in humans enhances the corticophrenic responsiveness to transcranial magnetic stimulation. *J. Appl. Physiol.* 108, 39–46. doi: 10.1152/japplphysiol.91454.2008

Rossi, S., Antal, A., Bestmann, S., Bikson, M., Brewer, C., Brockmöller, J., et al. (2021). Safety and recommendations for TMS use in healthy subjects and patient populations, with updates on training, ethical and regulatory issues: expert guidelines. *Clin. Neurophysiol.* 132, 269–306. doi: 10.1016/j.clinph.2020.10.003

Rossi, S., Hallett, M., Rossini, P. M., and Pascual-Leone, A.Safety of TMS Consensus Group (2009). Safety, ethical considerations, and application guidelines for the use of transcranial magnetic stimulation in clinical practice and research. *Clin. Neurophysiol.* 120, 2008–2039. doi: 10.1016/j.clinph.2009.08.016

Sharshar, T., Ross, E., Hopkinson, N. S., Dayer, M., Nickol, A., Lofaso, F., et al. (2003). Effect of voluntary facilitation on the diaphragmatic response to transcranial magnetic stimulation. *J. Appl. Physiol.* 95, 26–34. doi: 10.1152/japplphysiol.00918.2002

Similowski, T., Catala, M., Rancurel, G., and Derenne, J. P. (1996). Impairment of central motor condu-ction to the diaphragm in stroke. *Am. J. Respir. Crit. Care Med.* 154, 436–441. doi: 10.1164/ajrccm.154.2.8756819

Stagg, C. J., Antal, A., and Nitsche, M. A. (2018). Physiology of transcranial direct current stimulation. *J. ECT* 34, 144–152. doi: 10.1097/YCT.0000000000000510

Stagg, C. J., and Nitsche, M. A. (2011). Physiological basis of transcranial direct current stimulation. *Neuroscientist* 17, 37–53. doi: 10.1177/1073858410386614

Thirugnanasambandam, N., Sparing, R., Dafotakis, M., Meister, I. G., Paulus, W., Nitsche, M. A., et al. (2011). Isometric contraction interferes with transcranial direct current stimulation (tDCS) induced plasticity – evidence of state-dependent neuromodulation in human motor cortex. *Restor. Neurol. Neurosci.* 29, 311–320. doi: 10.3233/RNN-2011-0601

Underwood, E. (2016). Cadaver study challenges brain stimulation methods. *Science* 352:397. doi: 10.1126/science.352.6284.397

Urban, P. P., Morgenstern, M., Brause, K., Wicht, S., Vukurevic, G., Kessler, S., et al. (2002). Distribution and course of cortico-respiratory projections for voluntary activation in man: a transcranial magnetic stimulation study in healthy subjects and patients with cerebral ischaemia. *J. Neurol.* 249, 735–744. doi: 10.1007/s00415-002-0702-8

Verin, E., Marie, J. P., and Similowski, T. (2011). Cartography of human diaphragmatic innervation: preliminary data. *Respir. Physiol. Neurobiol.* 176, 68–71. doi: 10.1016/j.resp.2010.11.003

Vinit, S., Keomani, E., Deramaudt, T. B., Bonay, M., and Petitjean, M. (2016). Reorganization of respiratory descending pathways following cervical spinal partial section investigated by transcranial magnetic stimulation in the rat. *PLoS One* 11:e0148180. doi: 10.1371/journal.pone.0148180

Vinit, S., Keomani, E., Deramaudt, T. B., Spruance, V. M., Bezdudnaya, T., Lane, M. A., et al. (2014). Interdisciplinary approaches of transcranial magnetic stimulation applied to a respiratory neuronal circuitry model. *PLoS One* 9:e113251. doi: 10.1371/journal.pone.0113251

Vinit, S., Lovett-Barr, M. R., and Mitchell, G. S. (2009). Intermittent hypoxia induces functional recovery following cervical spinal injury. *Respir. Physiol. Neurobiol.* 169, 210–217. doi: 10.1016/j.resp.2009.07.023

Wang, H. Y., Crupi, D., Liu, J., Stucky, A., Cruciata, G., Di Rocco, A., et al. (2011). Repetitive transcranial magnetic stimulation enhances BDNF-Trk B signaling in both brain and lymphocyte. *J. Neurosci.* 31, 11044–11054. doi: 10.1523/JNEUROSCI.2125-11.2011

Woods, A. J., Antal, A., Bikson, A. M., Boggio, P. S., Brunoni, A. R., Celnik, P., et al. (2016). A technical guide to tDCS, and related non-invasive brain stimulation tools. *Clin. Neurophysiol.* 127, 1031–1048. doi: 10.1016/j.clinph.2015.11.012

Yukimasa, T., Yoshimura, R., Tamagawa, A., Uozumi, T., Shinkai, K., Ueda, N., et al. (2006). High-frequency repetitive transcranial magnetic stimulation improves refractory depression by influencing catecholamine and brain-derived neurotrophic factors. *Pharmacopsychiatry* 39, 52–59. doi: 10.1055/s-2006-931542

frontiers | Frontiers in Neuroscience

TYPE Original Research
PUBLISHED 11 October 2023
DOI 10.3389/fnins.2023.1277906

OPEN ACCESS

EDITED BY
Gahangir Hossain,
University of North Texas, United States

REVIEWED BY
Goutam Ghoshal,
Philips Healthcare (United States),
United States
Kevin Pierre,
University of Florida, United States

*CORRESPONDENCE
Linlin Wang
✉ wanglinlinatjn@163.com

RECEIVED 15 August 2023
ACCEPTED 28 September 2023
PUBLISHED 11 October 2023

CITATION
Gao P, Sun Y, Zhang G, Li C and Wang L (2023) A transducer positioning method for transcranial focused ultrasound treatment of brain tumors.
Front. Neurosci. 17:1277906.
doi: 10.3389/fnins.2023.1277906

A transducer positioning method for transcranial focused ultrasound treatment of brain tumors

Penghao Gao[1], Yue Sun[3], Gongsen Zhang[1], Chunsheng Li[3] and Linlin Wang[1,2]*

[1]Artificial Intelligence Laboratory, Shandong Cancer Hospital and Institute, Shandong First Medical University and Shandong Academy of Medical Sciences, Jinan, Shandong, China, [2]Department of Radiation Oncology, Shandong Cancer Hospital and Institute, Shandong First Medical University and Shandong Academy of Medical Sciences, Jinan, Shandong, China, [3]Department of Biomedical Engineering, Shenyang University of Technology, Shenyang, Liaoning, China

Purpose: As a non-invasive method for brain diseases, transcranial focused ultrasound (tFUS) offers higher spatial precision and regulation depth. Due to the altered path and intensity of sonication penetrating the skull, the focus and intensity in the skull are difficult to determine, making the use of ultrasound therapy for cancer treatment experimental and not widely available. The deficiency can be effectively addressed by numerical simulation methods, which enable the optimization of sonication modulation parameters and the determination of precise transducer positioning.

Methods: A 3D skull model was established using binarized brain CT images. The selection of the transducer matrix was performed using the radius positioning (RP) method after identifying the intracranial target region. Simulations were performed, encompassing acoustic pressure (AP), acoustic field, and temperature field, in order to provide compelling evidence of the safety of tFUS in sonication-induced thermal effects.

Results: It was found that the angle of sonication path to the coronal plane obtained at all precision and frequency models did not exceed 10° and 15° to the transverse plane. The results of thermal effects illustrated that the peak temperatures of tFUS were 43.73°C, which did not reach the point of tissue degeneration. Once positioned, tFUS effectively delivers a Full Width at Half Maximum (FWHM) stimulation that targets tumors with diameters of up to 3.72 mm in a one-off. The original precision model showed an attenuation of 24.47 ± 6.13 mm in length and 2.40 ± 1.42 mm in width for the FWHM of sonication after penetrating the skull.

Conclusion: The vector angles of the sonication path in each direction were determined based on the transducer positioning results. It has been suggested that when time is limited for precise transducer positioning, fixing the transducer on the horizontal surface of the target region can also yield positive results for stimulation. This framework used a new transducer localization method to offer a reliable basis for further research and offered new methods for the use of tFUS in brain tumor-related research.

KEYWORDS

transcranial focused ultrasound, transducer positioning, acoustic field, FWHM, sonication-induced, thermal effects

1. Introduction

Brain tumors have been represented as the second most frequent etiology in patients with focal seizures, mostly in the temporal lobe (Slegers and Blumcke, 2020). In the early stage of temporal lobe tumors, there are no obvious clinical symptoms, but as the disease progresses, the tumor increases in size and is often accompanied by temporal lobe seizures. Due to the complexity of the functional areas of the temporal lobe, surgery was the choice in the past, but the considerable risks were carried by surgical resection and a high risk of long-term side effects owing to the specificity of the tumor itself and effects including surgical complications, radioactive neurotoxic effects and chemotherapy-induced debility (Vargo, 2011). Related studies by Monje have revealed that tumor cells have the ability to manipulate and respond to signals produced by neurons, which aid their growth. Additionally, these cells have been observed to grow faster in the vicinity of highly active neurons, suggesting a link between tumor cells and neurons (Svider et al., 2017; Venkatesh and Monje, 2017). Despite the considerable advancements in therapeutic approaches to other malignancies, the treatment of brain tumors has not improved significantly in recent decades (Venkatesh et al., 2015).

Transcranial focused ultrasound (tFUS) is a non-invasive neuromodulation tool that focuses and delivers ultrasound energy to localized areas of the brain to modulate neuronal activity (Min et al., 2011; Lescrauwaet et al., 2022; Armstrong et al., 2023). The subsequent biological models (Konofagou et al., 2012; Zou, 2020; Yan et al., 2021; Cain et al., 2022) have found a significant reduction in the number and duration of seizures after low-intensity tFUS stimulation, providing important experimental evidence for clinical translation. Preliminary evidence that tFUS has a role in modulating the therapeutic and tumor suppressor activity of abnormal neural networks. Compared to other neuromodulation techniques of tFUS, transcranial magnetic stimulation (TMS) and transcranial direct-current stimulation (tDCS) have garnered approval for the treatment of select neurological disorders, based on their demonstrated effectiveness (Klomjai et al., 2015; Iglesias, 2020; Cappon et al., 2022; Marder et al., 2022). Compared to magnetic fields, acoustic fields are controllable and acoustic waves can be focused on a point in the deep brain like light (Bystritsky et al., 2011; Kubanek, 2018). Therefore, tFUS has a broader research prospect with its higher spatial precision and regulation depth.

In previous studies of single-element transducers, the transducer had to be manually repositioned to achieve a nearly perpendicular angle of orientation toward the target area along the skull surface, a process which often resulted in unintentional errors and variations that compromised the intended focus of the acoustic beam (Yoon et al., 2018). The numerical modeling of tFUS treatments remains complex, mainly owing to the non-linearity arising along ultrasound propagation, the anatomical complexity, the heterogeneity of the medium, the inter-individual variability of the properties of the medium, *in vivo* tissue movements and the correlation between temperature and biological damage (Grisey et al., 2016). Heger et al. have simulated sonication acoustic fields by modifying transducer components to evaluate the potential application of targeted FUS systems in animals sensitive to cerebral hemorrhage (Grudzenski et al., 2022). Park's numerical approach based on subject-specific sonication beamline simulations to find the optimal configuration of ultrasound probes for sonication stimulation has demonstrated that the specific tFUS framework he developed can be effectively used for human neuromodulation studies (Park et al., 2022). Shen's study on the effect of low-frequency sonication (21 kHz, 26 mW/cm^2, 40% duty cycle, 3 min) combined with microbubbles on nude mice with subcutaneous prostate adenoma showed a loss of blood flow signal at the tumor and a decrease in tumor volume (Shen et al., 2014).

Sonication of 200 kHz to 1.5 MHz are mostly used in clinical practice, among which low and medium frequency sonication of 100 kHz to 1 MHz can be effectively applied in tissue destruction and neuromodulation, with the intensity of 30 to 500 mW/cm^2 can penetrate the skull to stimulate the functional brain region and regulate neuronal functions through mechanical effects (Krishna et al., 2018; Maresca et al., 2018). Low-intensity tFUS destroys tumor blood vessels by increasing tissue permeability to promote apoptosis and inhibit tumor growth and proliferation for the purpose of anti-tumor. However, the acoustic parameters of the skull are strongly inhomogeneous, which have been demonstrated that sonication penetration through thick and dense skull and focusing on a predetermined point is very tricky. Owing to the presence of the skull in sonication stimulation, the offset between the focal point and the preset intracranial target region caused by the acoustic properties between different media (i.e., speed of sound, density, and attenuation coefficient). Accurate prediction of the sonication path of stimulation has also become an international conundrum (Servick, 2020).

The absorption of acoustic energy by biological tissues leads to an increase in temperature, resulting in increased excitability of neurons. Sonication of a certain intensity causes transient high temperature in the target region of the brain through other effects, leading to protein denaturation and tissue coagulation necrosis, permanently damaging the lesion and modulating the neural network. Denaturation of tissue temperature occurs at 42°C (Dickson and Calderwood, 1980). At 43 to 60°C, tissue damaged at an exponential rate, reaching 47°C leads to cancellous bone necrosis (Augustin et al., 2012), and reaching 50°C causes necrosis of cardiac muscle cells, producing irreversible tissue damage (Darrow, 2019).

In this study, we performed numerical simulation of sonication stimulation penetration through the skull with different parameters based on the effective cavitation effect stimulation parameters obtained from the research and located the optimal position of the transducer. The new RP (Radius Positioning) method performed the selection of the effective range of stimulation based on the parameters of the transducer, which was not available in other studies. Acoustic field simulation and calculation of sonication stimulation paths were performed based on transducer positioning results, with the effective error of FWHM (Full Width at Half Maximum) obtained, which provided a numerical theoretical reference for achieving accurate and effective neuromodulation (Schwenke et al., 2017). We also verified the effectiveness of transducer positioning by simulating each directional angle of the control group. The transducer after positioned was non-serendipitous compared to the given position in other studies, while the temperature field simulation with added thermal effects was able to verify the safety feasibility of this study, showing that only small temperature changes are produced by sonication at low intensities, providing a new simple and effective numerical method for the application of the tFUS in clinical neuromodulation.

2. Materials and methods

Firstly, a 3D skull model was reconstructed from the binarized CT images in this study. Secondly, the transducer matrix and transducer positioning of matrix were performed by acoustic pressure (AP) simulations based on the settings of target region and the parameters of the transducer. Successively, the distribution of the sonication beam in the skull was simulated and the distance of the stimulation and directional angles were calculated based on the transducer positioning results. The correctness of transducer positioning was proven according to the simulation results by adding sonication stimulus with different directional angles at the target region. Finally, we demonstrated the safety of whole process by predicting the acoustic temperature field of the thermal effects.

2.1. Data acquisition

The data of this research were the CT images of the brain collected in Shandong Cancer Hospital and Institute with the size of $512 \times 512 \times 245$, including the CT data and contour information of the patient, which was used to obtain the 3D skull anatomical structure. The study was conducted in accordance with the Declaration of Helsinki, and the protocol was approved by the Ethics Committee of Shandong First Medical University Affiliated Cancer Hospital (Approval ID: SDTHEC2023002013). Written informed consent for participation was not required for this study in accordance with the national legislation and institutional requirements.

2.2. Skull model

The 3D CT images were all resampled to a spatial size of $1\,mm \times 1\,mm \times 1\,mm$ assuring that the same physical size information contained within the voxel. The resampled CT data (Hounsfield Unit) were extracted using 3D Slicer at a threshold intensity of $H = 100\,HU$ to filter other tissues, which was reconstructed into a 3D skull model after binarization by MATLAB (R2019b, MathWorks Inc., Natick, MA, USA). The skull model was established for the subsequent application of temporal lobe hippocampal acoustic field simulation, therefore the model removed the parietal bone for better observation of the 3D sonication beam distribution. A simple simulation schematic under the transverse plane was depicted in Figure 1, where the target region was located.

2.3. Sonication setup

2.3.1. Ultrasound

In this study, the sonication parameters were selected according to the function of the Olympus Scientific Solutions (Olympus America Inc., PA, US) V301-SU ultrasound probe. The optimal parameters for the simulation of low-frequency sonication were conducted at a frequency of 500 kHz and with a pressure level of 1 MPa, while it has been shown that soft tissue does not play a significant role at this frequency and has relatively deep penetration and fine spatial resolution (Mueller et al., 2017). At the time of this study, no prior literature existed on the applications of radius filtering in the positioning of neuromodulations in focused ultrasound. Considering that most focused ultrasound systems were used for cellular ablation, the optimization of parameters was warrantable. We have carefully selected the parameters in this study, ensuring that they remained well below the U.S. Food and Drug Administration (FDA) guidelines for diagnostic sonication (mechanical index $(MI) \leq 1.9$, spatial-peak pulse-average intensity $(I_{SPPA}) \leq 190 W/cm^2$) after transcranial transmission. The classical frequency of focused ultrasound, 250 kHz, 690 kHz, and 1.1 MHz were also chosen in sonication simulation by considering previous studies regarding FUS-induced BBB disruption (Kinoshita et al., 2006; Cho et al., 2016; Ilovitsh et al., 2018; Huh et al., 2020; Park et al., 2021). The F-number of the transducer was calculated as the ratio of the radius of curvature to the diameter of the transducer. Specifically, a focused radius of curvature of 30 mm and a diameter of 25 mm (which was the nominal wafer size) were selected. Additionally, the diameter of the transducer (which was 31 mm) was considered a control parameter in this study. The numerical parameters were chosen a fundamental frequency of 500 kHz, an excitation AP of 1 MPa, a stimulation duration of 500 ms, a single tone burst duration (TBD) of 200 μs, a PRF of 300 Hz (150 cycles) and a duty cycle (DC) of 6% for the simulation of the AP and sonication-induced thermal effects. We posited that low-intensity sonication, when employed with lower duty cycles, does not induce substantial thermal effects, thus effectively suppressing the excitability of tumor cells. A typical schematic and parameters of sonication pulse sequences used for neuromodulation were shown in Figure 2. The sonication sequences in this schematic were generated by programming the MATLAB toolbox.

2.3.2. Acoustic property

The soft tissues mainly supported the propagation of compressional waves and hardly support shear waves, while the skull

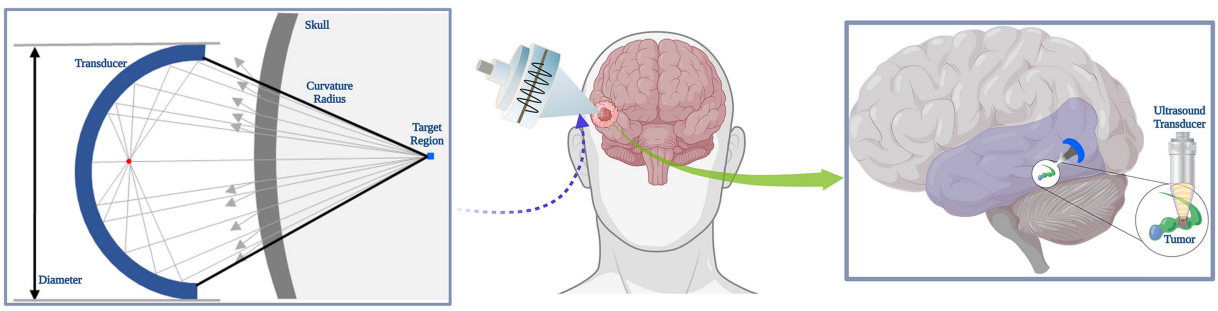

FIGURE 1
Schematic of sonication simulation. A simple schematic diagram of tFUS stimulation effects in brain tumor.

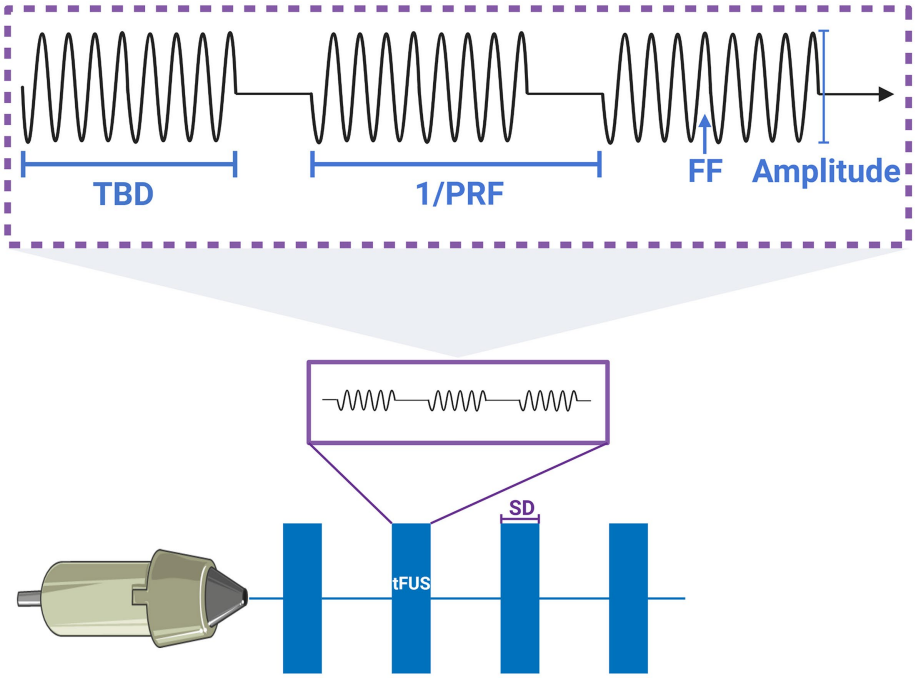

FIGURE 2
Typical schematic and parameters of pulsed sonication sequences for neuromodulation. The explanation of parameters that SD was sonication duration; PRF was pulse repetition frequency, the 1/PRF was the one cycle; TBD was tone burst duration; FF was fundamental frequency.

TABLE 1 Acoustic parameters.

Speed (m/s)	Density (kg/m^3)	Attenuation coefficient (Np/MHz·m)
c_{water}=1,482	ρ_{water}=1,000	α_{water}=3.48 × 10^{-4}
c_{bone}=3,100	ρ_{bone}=2,200	$\alpha_{\min,skull}$=21.5,$\alpha_{\max,skull}$ =208.9 (Connor, 2005)

was capable of transmitting both waves, but the shear waves were very weak when low-frequency sonication penetrating the skull, therefore the effect of shear waves was not considered in this study. The results of relevant acoustic characterization studies demonstrate that the nonlinear parameters BonA were between 5 and 11 in most soft tissues, while solids have a negligible ability to generate nonlinearities (Slezak et al., 2022; Armstrong et al., 2023). Given the highly similar properties of tissue fluid and water, the skull model was considered to be immersed in water to couple it to the ultrasound source. Furthermore, the brain tissues were approximated as being water to lessen the model complexity and computational time. The nonlinear parameter BonA was set to a value of 5.2 (Bjørnø, 2010). Meanwhile, owing to the homogenization of the model grid, the effect of pulsation of cerebrospinal fluid flow was avoided. The Courant Friedrichs Lewy (CFL) in this study was a constant 0.3 and the power law absorption exponent was set to a constant 1.51 (Duck, 1990).

Owing to differences in the acoustic properties of the skull, the feasibility of numerical calculation of tFUS attenuation varies among individuals (Jing and Lindsey, 2021). The acoustic properties of the skull model were calculated from the porosity (ψ) of the CT images at a given ultrasound frequency by eq. (1). Based on the results of high-resolution CT images simulation studies showed that the attenuation of tFUS was highly dependent on the porosity of the individual skull (Mueller et al., 2017). The porosity was used to calculate the absorption of sonication, which lead to an increase with high porosity in simulated absorption values. The compressive sound velocity c, density ρ, and attenuation coefficient α of the skull were calculated by eqs. (2)–(4) as shown in Table 1, where the maximum and minimum skull compression attenuation were referred to in the literature (Mueller et al., 2017).

$$\psi = 1 - \frac{H}{1000} \quad (1)$$

$$c_{skull,c} = c_{water}\psi + c_{bone,c}\left(1-\psi\right) \quad (2)$$

$$\rho_{skull} = \rho_{water}\psi + \rho_{bone}\left(1-\psi\right) \quad (3)$$

$$\alpha_{skull,c} = \alpha_{\min,skull,c} + \left(\alpha_{\max,skull,c} - \alpha_{\min,skull,c}\right)\psi^{0.5} \quad (4)$$

2.4. Acoustic pressure simulation

The acoustic simulation was performed based on the k-space pseudospectral method of MATLAB k-Wave toolbox. The linear wave equation resolved by numerical simulation had been proven to be a reliable method for calculating sonication beams in complex structures (Legon et al., 2018). The k-wave toolbox, an open-source

software package highly regarded in the field of acoustic wave simulations, has been developed to effectively model and analyze the intricate behavior of acoustic waves within complex media. Its versatile functionality encompasses a broad range of applications, including ultrasound imaging, ultrasound therapy, and bioacoustics (Treeby and Cox, 2010). The domain of the acoustic simulation performed in this study was $256 \times 256 \times 256$ in the 3D model represented the skull model with $256\ mm \times 256\ mm \times 256\ mm$. In view of the high computational time cost of this precision model, this study introduced a twofold-precision model with a size of $128 \times 128 \times 128$ to expedite the computation process. Successively, the 31 mm transducer was selected in the domain of $210 \times 210 \times 210$. For simplicity, the target regions in this study were assumed to be a point instead of a 3D target region volume. The volume stimulated in the target region was observed through the 3D acoustic field.

2.5. Radius positioning method

The approach taken by some researchers in defining a target region solely within the region under the skull vault and assessing the acoustic field effect at several extracranial points perpendicular to the skull vault is inherently restrictive. Such an approach fails to adequately identify an optimal location for the practical implementation of target region definition in tFUS investigations. To ascertain the effective range of transducer centroid arrays, we developed a RP algorithm to refine the options and enhance computational efficiency. This algorithm narrowed down the transducer matrix to a specific range by excluding areas inside the skull and outside the circle formed by the radius of curvature, as determined by the established transducer curvature. Additionally, to prevent contact with the skull, another component of the RP algorithm identified points that were too close to the skull layer, thus ensuring safe transducer placement. The underlying concept of the RP algorithm is outlined as follows.

In the skull model with inhomogeneity, the center of the tumor in the hippocampal region of the medial temporal lobe was selected as the target region. With the target region selected as the center, a ball was outlined and the point matrix in the intersection of the ball and the skull layer was screened. The center of the model was established by identifying the midpoint of the skull profile at the extremes on the coordinate axis. The average distance from the model center to the intersecting skull layer was meticulously calculated. The points, outside the model but within the ball having a distance greater than the calculated average from the center point, were selectively assembled into the transducer matrix. Simultaneously, the algorithm effectively removed the center points that may correspond to the contact area between the transducer and the skull layer, accounting for the size of the transducer. The calculated transducer matrix will be utilized in the subsequent stage of transducer positioning.

2.6. Transducer positioning

The transducer matrix was subjected to acoustic pressure simulation to screen the center of the transducer, as the transducer positioning flow chart shown in Figure 3. With the uniform attenuation medium in an inhomogeneous skull, the precise location of the transducer point was determined as the region with the lowest level of attenuation after penetrating the skull. Based on the conditions of transducer positioning, the fraction of the control group cases greater than the directional angle of 45 degrees neglected the effect of weak shear waves. Acoustic field simulation of the target region was performed after transducer positioning, with the path from the center to the target region screened as the best stimulation path, the vector angles in each direction were calculated as well as the stimulation distance. Related studies have confirmed that sonication-induced neuromodulatory effects appear within the FWHM (Lee et al., 2015, 2016; Legon et al., 2018). The contours of FWHM at different frequencies were depicted after the normalization of the acoustic field.

Sonication stimulations from various directional angles (i.e., 0°, 30°, 45°, 60°) were administered to the target region as a simulated control group, with the transducer positioned extracranially along the directional path and the curvature radius as stimulation distance. Directional angles in the transverse plane and coronal plane were explored in the control group.

2.7. Thermal simulation

The open-source k-Wave toolbox was also used to solve the Pennens' bioheat equation (Treeby and Cox, 2010; Legon et al., 2018), as the peak temperature of thermal effects generated in the tissue during sonication stimulation was simulated by k-Wave (Xu et al., 2020). The spatial conditions (i.e., simulation domain and grid size) of the thermal simulation were the same as acoustic simulation. Uniform segmentation of inhomogeneous brain tissue through a spatial grid of the simulation domain. The thermal effect simulation not only added the medium properties related to thermal diffusion, as the value of the skull [specific heat= $1300\ J/kg/K$, thermal conductivity= $1.16 \times 10^{-2}\ W/cm/°C$ (Nelson and Nunneley, 1998)] and water [specific heat= $4178\ J/kg/K$, thermal conductivity= $0.54 W/cm/°C$ (Duck, 1990)] were assigned, but also explored the temperature change under sonication stimulus through the parameters of ultrasound source (i.e., opening time, closing time and time step),while the temperature field of thermal effects was also monitored in real-time. The stimulation parameters were a duration of 500 ms and a duty cycle of 6% for the sonication interval. The initial tissue temperature in the simulated cranium was set at 38.5°C, which was the experimentally derived average value of the relevant studies (Rzechorzek et al., 2022).

3. Results

3.1. Acoustic pressure On target region

Different frequencies of sonication were performed for positioning under different precision models. Figure 4 illustrated the normalized AP distribution results of the transducer matrix in the transverse plane of the target region. The highest AP values were predominantly concentrated at the lower end of the matrix. Figure 5B illustrated the distribution of simulated AP at various frequencies, along with the corresponding distance from the transducer to the target region, in different precision models. The transducer matrix, chosen using the RP algorithm, exhibited comparable AP distributions following

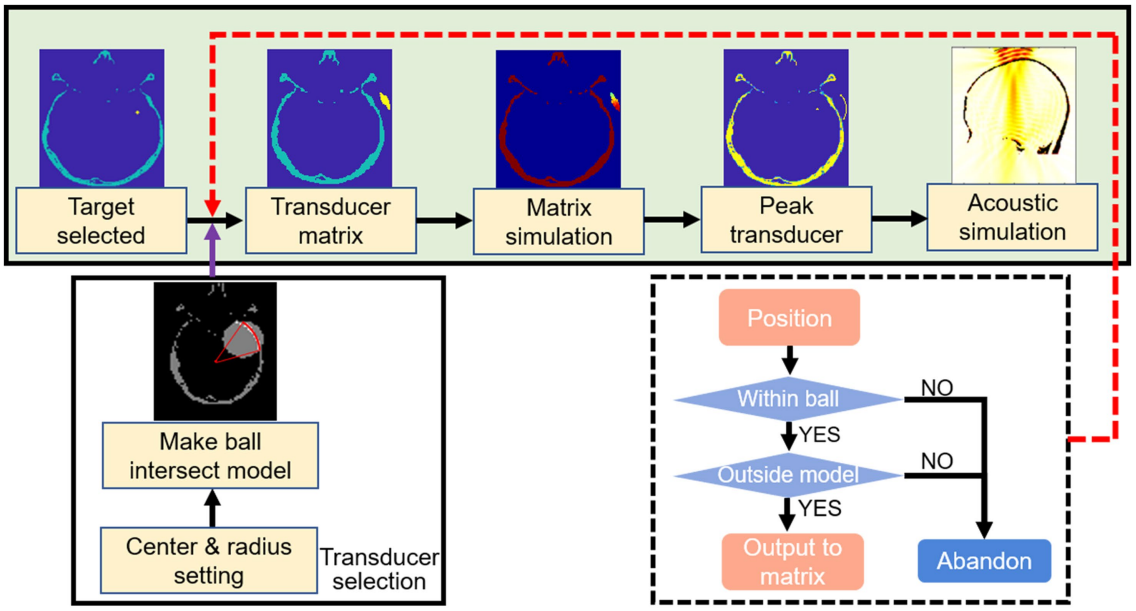

FIGURE 3
Flow chart of transducer positioning. Selected the center of tumor as the target region. A ball was outlined according to the parameters of ultrasound probe. The transducer matrix was selected after the outlined ball intersected with the skull layer. The transducer was positioned by simulated the transducer matrix and selected the point with peak pressure. The acoustic field of sonication penetrated the skull was simulated.

sonication stimulation at various frequencies, with a notable concentration of points approximately 30 mm away from the target region. It can be proved that the AP stimulated on the target region was less influenced by the distance between the transducer and the target region. This was supported by Figure 4, which demonstrated a relationship between the direction angle applied to the target area and the resulting AP. As the precision of the model improved, the effectiveness of the RP algorithm was more obviously explored. The accuracy of the algorithm exceeded 99.50% for models with a precision of 1 mm/grid. It was noteworthy that the AP distribution at 690 kHz differed from the other three frequencies examined, as the peak AP point from the transducer remained approximately constant at a distance of approximately 30 mm from the target region, despite increased in modeling precision.

3.2. Transducer positioning

The simulation results of the transducer matrix were shown in Tables 2, 3, where the points with the peak AP in the transducer matrix were selected as the center of the transducer. The calculation of the transducer matrix AP at a single frequency with a 256-grid model required approximately 490.5 h. Figure 5A presented the results of the AP comparison between the positioned transducer and the transducer at different angles corresponding to the plane directions where the target region was located. The AP of transducer center on the coronal axis ($XY, YZ = 0°$) was closest to the positioned transducer in each model, with ratios at each frequency was 250 kHz: 84.57% ± 9.67%, 500 kHz: 80.80% ± 18.42%, 690 kHz: 94.55% ± 3.94%, 1,100 kHz: 89.24% ± 4.96%. The vector angles in each direction of the sonication path were determined based on the transducer positioning results in each precision model, indicating that the incidence angle of sonication changed while the thickness of the skull layer affected by model precision. The variation in the angle between the positioned sonication path and the coronal and transverse planes was found to be insignificant with low-frequency. Notably, as the frequency increases, the angle variation with different precisions becomes more pronounced. It was found that the angle to the coronal plane obtained at all precision and frequency models did not exceed 10° and 15° to the transverse plane. The stimulus distances between the positioned center and the target region were observed to have a range of 27 to 31 mm. Additionally, our findings, as shown in Table 3, indicated that this distance remained stable and did not significantly vary with increasing model precision.

3.3. Effects of FWHM

The results in the 256 × 256 × 256 domain were 250 kHz: MI 0.19 and spatial-peak temporal-average intensity (I_{SPTA}) 630.24 mW/cm^2, 500 kHz: MI 0.13 and I_{SPTA} 487.26 mW/cm^2, 690 kHz: MI 0.11 and I_{SPTA} 487.26 mW/cm^2, 1,100 kHz: MI 0.02 and I_{SPTA} 175.49 mW/cm^2. The acoustic field results of sonication penetrating the skull in the 256 × 256 × 256 domain were shown in Figure 6. Figure 6A illustrated the spatial acoustic field under sonication at 500 kHz, while Figure 6B provided a comparison of the acoustic field under sonication at each frequency after penetrating through water and experiencing attenuation in the skull. In this study, the range of FWHM contours was analyzed as an indicator of the most effective region of sonication stimulation. Tables 2, 3 presented the length-width measurements of the FWHM at each frequency and precision model, as well as the attenuation observed after penetrating the skull. The results indicated that as the skull layer was refined, the attenuation of the FWHM diminished accordingly. Notably, the 128-grid model in twofold

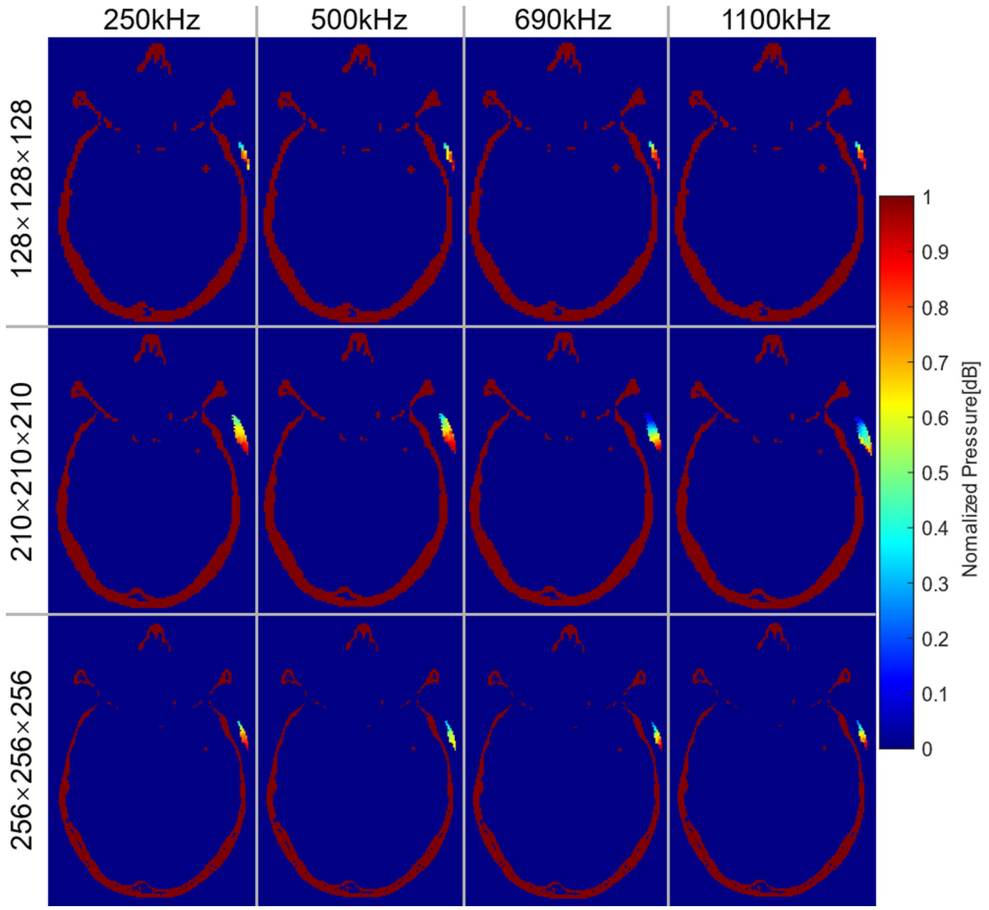

FIGURE 4
Normalized AP distribution of transducer matrix at the transverse plane of the target region. Each row represented the results under different precision models. Each column represented the results at different frequencies.

precision yielded highly comparable results to the FWHM deviation observed in the 256-grid model while also improving computational time efficiency. However, no significant changes were observed in FWHM deviation and AP attenuation across different frequencies. The generated FWHM in the transverse plane of the target region under sonication stimulation at each frequency can effectively cover the treatment range for tumors with a diameter approximately within the 30 mm range.

3.4. Effects of thermal effect

The peak temperatures generated through sonication stimulation at various frequencies were depicted in Tables 2, 3, corresponding to distinct precision models. Notably, in the original precision model, the peak temperature produced by sonication stimulation at 690 kHz was measured at 43.73°C. The temperature field of sonication-induced thermal effects at the target region was shown in Figures 7A,B, indicating that most of the heat generated in the skull layer and did not achieve the denaturation value of 47°C that lead to cancellous osteonecrosis. As previously mentioned (Dickson and Calderwood, 1980; Augustin et al., 2012; Darrow, 2019), low-intensity tFUS has been observed to have no detrimental effects on brain tissue and its effects on brain tumors are not attributed to thermal effects.

4. Discussion

In this study, we presented a novel framework for tFUS simulation aimed at treating temporal lobe tumors by using the cavitation effect based on the latest advances in neuromodulation research. In this paper, a new RP method was proposed to position the sonication transducer. To our knowledge, we were the first to build a framework for sonication treatment based on numerical simulation of the RP method for transducer positioning to ensure safety under sonication stimulation through the thermal effects and matrix selection of transducer positioning among all known tFUS studies. The results of the sonication-induced temperature field analysis suggested that the influence of tFUS on tumors was independent of thermal effects. Obtaining the optimal range of ultrasonic stimulation pathways based on the selected transducer parameters. Significantly, we incorporate the conventional algorithm in simulating the transducer peak pressure, setting our study apart from earlier studies that rely on arbitrary transducer positioning. The results demonstrated the superior effectiveness of our positioned transducer in tFUS applications.

So many researchers were attracted by tFUS due to its noninvasiveness, high resolution, and ability to focus deeply. However, different stimulation parameters had been used in sonication neuromodulation studies leading to diverse results,

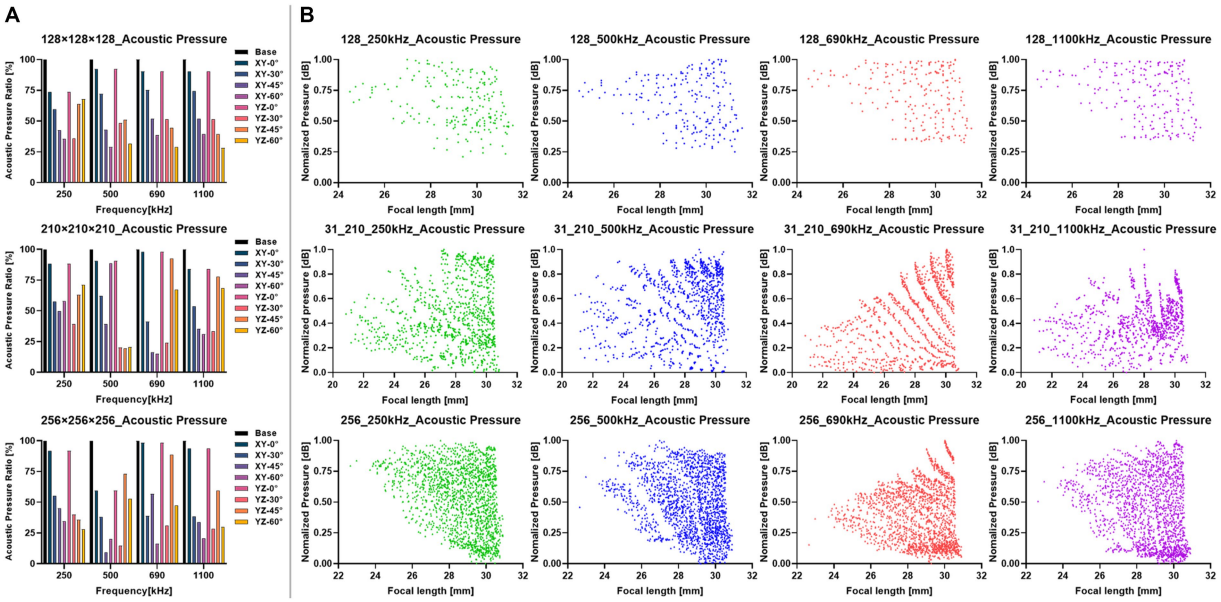

FIGURE 5
Results of the sonication stimulations at different transducer positions. **(A)** Comparison of acoustic pressure in the target region at each directional angle with different precision models (i.e., $128\times128\times128$, $210\times210\times210$, $256\times256\times256$). The directional angle of XY was at the transverse plane, the YZ was at the coronal plane. The Base was the AP of the positioned transducer. **(B)** Distribution of AP at the distance from the transducer to the target region. Each row represented the results under different precision models. Each column represented the results at different frequencies.

TABLE 2 Simulation results at different frequencies.

Parameters		Group 1	Group 2	Group 3	Group 4
Frequency (kHz)		250 kHz	500 kHz	690 kHz	1,100 kHz
Angles with transverse plane; sagittal plane; coronal plane		9.88° ± 3.03° 78.44° ± 3.95° 5.64° ± 2.51°	11.46° ± 3.45° 76.42° ± 2.56° 6.67° ± 2.40°	5.01° ± 5.37° 83.44° ± 6.14° 3.75° ± 3.73°	6.19° ± 6.44° 82.93° ± 7.84° 2.84° ± 4.92°
Stimulus distance (mm)		27.25 ± 0.28	28.81 ± 1.78	30.31 ± 0.47	28.38 ± 1.62
Deviation*	Length (mm)	23.66 ± 4.70(43.87% ± 11.19%)	22.60 ± 10.75(52.41% ± 21.91%)	28.80 ± 2.71(55.76% ± 7.00%)	21.96 ± 8.59(43.30% ± 10.34%)
	Width (mm)	4.62 ± 3.04(37.05% ± 19.72%)	2.49 ± 1.97(28.00% ± 21.95%)	1.61 ± 0.96(18.65% ± 13.02%)	1.72 ± 1.59(15.76% ± 13.72%)
	Offset (°)	3.20 ± 0.93	2.28 ± 5.51	2.11 ± 6.10	1.72 ± 2.97
	AP (%)	47.97 ± 23.41	48.51 ± 23.16	47.52 ± 16.41	47.73 ± 7.54
Peak temperature (°C)		39.10 ± 0.35	39.95 ± 1.43	41.44 ± 2.67	38.64 ± 0.11

*The deviation captured the error associated with the FWHM measurements in both the water medium and the sonication that penetrated the skull.

where the focus was hard to determine after penetrating the skull. In this study, a model was constructed based on the CT images of the brain after binarization. Next, a simulation framework was built using the k-Wave toolbox for AP simulation based on the actual transducer probe properties. And the accuracy of positioning was verified by the control group simulation of each directional angle. Finally, the acoustic field and temperature fields of sonication-induced thermal effects were performed. The results demonstrated that the positioned sonication transducer provided a safe and effective maximum effect. Furthermore, this framework presented a new approach to positioning error control for practical tFUS neuromodulation, which will advance the application of tFUS in ultrasound neuromodulation. It has been suggested that when time is limited for precise positioning, using a twofold precision model to calculate the optimal stimulus path can also yield positive results for stimulation.

In porous media, the propagation of ultrasonic waves becomes more intricate due to the non-uniformity inherent in the medium. Consequently, strictly relying on linear assumptions for simulation may not be entirely valid. To address this concern, we constructed a grid domain to discretize the inhomogeneous skull, aiming to achieve the most accurate simulation of the complex acoustic field possible. To ensure precision, we calculated the porosity by utilizing CT image data, enabling us to describe the speed of sound and attenuation within the medium. While indirect assumptions were made regarding pore structure, pore spacing, and pore shape, our approach aimed to approximate these characteristics to the best of our ability. In an attempt to conduct more precise calculations, we tried to perform a

TABLE 3 Simulation results with different precision models.

Parameters		Group 1	Group 2	Group 3
Simulation domain (grid)		128 × 128 × 128	210 × 210 × 210	256 × 256 × 256
Angles with transverse plane; sagittal plane; coronal plane (°)		11.11° ± 2.51° 76.20° ± 2.28° 8.01° ± 0.60°	5.56° ± 6.22° 83.39° ± 6.15° 3.00° ± 2.01°	7.73° ± 4.89° 81.33° ± 6.04° 3.18° ± 4.08°
Stimulus distance (mm)		28.56 ± 1.22	28.84 ± 2.15	28.67 ± 1.65
FWHM at transverse plane	Length (mm) Width (mm) Offset (°)	25.62 ± 1.89 9.41 ± 3.56 12.50 ± 2.72	28.17 ± 6.84 6.79 ± 2.25 −1.55 ± 6.95	22.90 ± 11.2 5.12 ± 1.40 6.56 ± 5.12
Deviation*	Length (mm) Width (mm) Offset (°) AP (%)	29.93 ± 2.33(53.87% ± 2.02%) 4.32 ± 2.64(33.07% ± 24.97%) 4.20 ± 1.04 52.29 ± 13.27	20.64 ± 7.44(41.73% ± 12.30%) 1.21 ± 1.24(13.76% ± 14.89%) −1.22 ± 3.75 31.62 ± 10.46	24.47 ± 6.13(54.54% ± 17.96%) 2.40 ± 1.42(31.14% ± 16.76%) 4.00 ± 3.51 59.89 ± 9.21
Peak temperature (°C)		38.62 ± 0.18	40.83 ± 2.25	38.90 ± 1.54
Matrix points		213	977 (2 points intracranial)	1811 (9 points intracranial)
Distance between matrix and target region (mm)		Average: 29.21; Min: 24.49; Max: 31.56	Average: 27.83; Min: 20.86; Max: 30.82	Average: 28.64; Min: 22.65; Max: 30.90
Computational time (per frequency)		4.8 h	143 h	490.5 h

*The deviation captured the error associated with the FWHM measurements in both the water medium and the sonication that penetrated the skull.

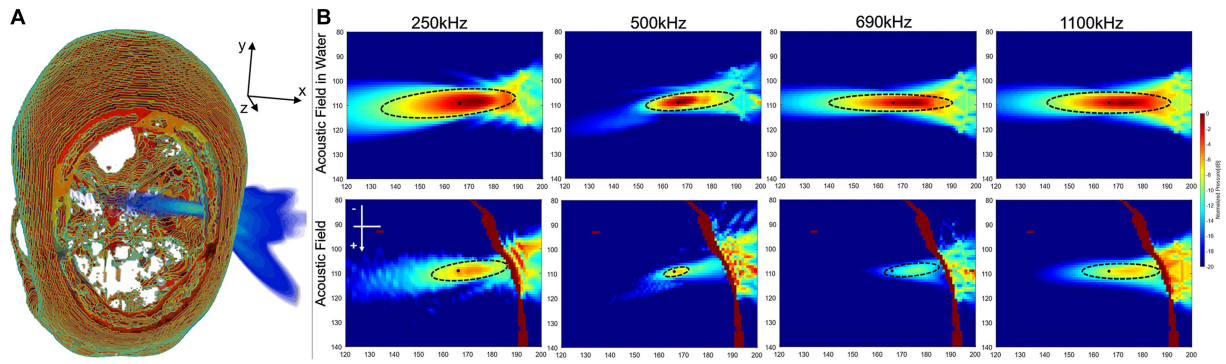

FIGURE 6
Results of sonication penetrating the skull. **(A)** Spatial field of sonication penetrating the skull. **(B)** The acoustic field in the transverse plane was analyzed both in the water medium surrounding the target region and within the skull medium in the high-precision model of the 256 × 256 × 256 domain.

higher resolution model. However, due to a substantial increase in computational time from 4.8 h to 490.5 h when transitioning from the twofold precision model to the original precision model, this computational cost dictated the upper limit of resolution within the scope of this study.

In similar tFUS studies, Park et al. compared duty cycle and sonication duration by used a single exploration of ultrasound parameters, focusing on assessing the feasibility of ultrasound framework (Park et al., 2022). Furthermore, we focused on numerical simulation results of the effect of sonication beam parameters on the intracranial target region. Due to the time-consuming nature of the transducer positioning accurately (taking more than 490.5 h for high-precision models), most studies (Beisteiner et al., 2019; Grudzenski et al., 2022; Koh et al., 2022) explored the effect of tFUS by arbitrary choosing a region as the transducer center, which may result in the peak pressure region of stimulation being off-target. The arbitrary transducer positions also explored the attenuation of ultrasound with a high degree of contingency for non-uniform skull layer. The results (Figure 4) illustrated that the contingency for the simulation results in skull not only pertained to the position of the transducer but also to the chosen target region for different precision models.

Previous studies by Nelson and Nunneley (1998) and Park et al. (2022) had investigated the safety of sonication stimulation based on thermal variation, using duration of stimulation versus depth. In this study, we took a different approach by performing real-time detection of the intracranial temperature of each precision model, using assigned thermal diffusion coefficients (i.e., specific heat capacity and

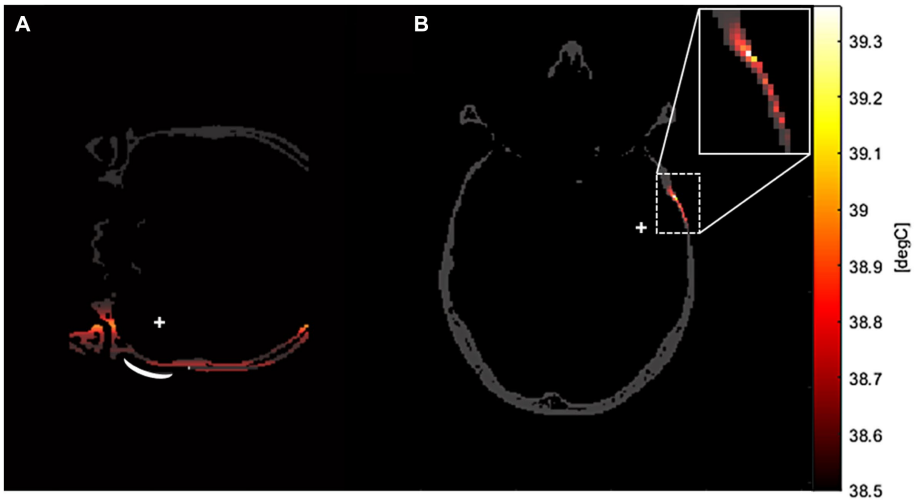

FIGURE 7
The temperature field of sonication-induced thermal effects in the transverse plane of the target region in the high-precision model. This thermal simulation was conducted in a $256 \times 256 \times 256$ domain, with a stimulation frequency of 500 kHz. As depicted in the example graphs, the majority of the heat generation in tFUS occurred in the skull layer across all frequency models. **(A)** Was the coronal plane of the temperature field. **(B)** Was the transverse plane of the temperature field.

thermal conductivity) to the cerebrospinal fluid and skull layer, indicated that most of the heat generated within short-term sonication stimulation was absorbed by the skull layer. This was in line with the study by Augustin et al. (2012) and Dickson and Calderwood (1980), where the peak temperature generated by sonication did not exceed the threshold for damage to the skull layer, further supporting the overall safety of tFUS.

One limitation of our study was the time-consuming nature of the computation, which restricted the number of frequency controls we could perform. The transducer positioning procedure at a frequency of 1 mm/grid precision model took an average of 490.5 h accelerated by NVIDIA GeForce RTX 2070 GPU. Additionally, ethical considerations hindered the application of tFUS in clinical, making it impossible for us to prove its effectiveness in a practical setting. Nonetheless, we took into account all evaluable results as much as possible under the simulated conditions at all current hotspot sets of frequencies in our study.

Based on our findings, the ability to modulate the directional angle of the sonication stimulus within ±15° in the coronal plane resulted in an average computation time of 24.62% when employing the high-precision model, which required 120.76 h of computation. Additionally, compromising the model precision led to a calculation time of 63.9% of the original duration, allowing completion of the calculations in 184 min using a model with reduced granularity. These results demonstrate the potential for approximating the clinical environment and pave the way for future investigations into the feasibility of utilizing lower granularity models for calculations.

In the future, this research will be further enriched with the following methods. Firstly, this study will be further enriched by collecting additional data to validate the potential effects of inter-individual differences on transducer positioning. Secondly, the method will be used in animal models (i.e., rats, rabbits) for simulation to demonstrate the feasibility of this ultrasound framework, with the expectation of achieving positive results for any size of skull. Successively, the parameters in this study will be pinned down for application to animal experiments through actual sonication output. Finally, based on the combination of existing research (Kim et al., 2018; Mohammadjavadi et al., 2019; Bobola et al., 2020; Wang et al., 2021), including error analysis of measurement results under actual sonication stimulation and simulation results. The method will be evolved into a practical tFUS framework system, ultimately serving clinicians.

5. Conclusion

We have proposed a framework for predicting tFUS treatment using the k-Wave toolbox, which determines the optimal treatment position through a specialized transducer positioning method (RP method) and explores the distribution of the sonication beam at different frequencies using brain CT images. Notably, we have demonstrated the feasibility of this tFUS framework by predicting the acoustic temperature field of sonication-induced thermal effects. The angle of sonication stimulation path in both the coronal and transverse planes plays a critical role in determining the appropriate program for transducer positioning during the preliminary stages. Successively, we verify the effectiveness of the transducer positioning by the results of the control group at each directional angle. This framework proposed offers an accurate and effective method for numerical prediction of brain tumors treatment using sonication. In the future, as we continue to refine our method, this framework may eventually play a pivotal role in clinical settings for precise treatment of brain tumors.

Data availability statement

The raw data supporting the conclusions of this article will be made available by the authors, without undue reservation.

Ethics statement

The study involving human participants was approved by the Ethics Committee of Shandong First Medical University Affiliated Cancer Hospital (Approval ID: SDTHEC2023002013) and the written informed consent was waived in accordance with the national legislation and the institutional requirements.

Author contributions

PG: Conceptualization, Investigation, Methodology, Software, Validation, Visualization, Writing – original draft. YS: Investigation, Writing – review & editing. GZ: Formal analysis, Writing – review & editing. CL: Conceptualization, Methodology, Writing – review & editing. LW: Data curation, Funding acquisition, Writing – review & editing.

Funding

The author(s) declare financial support was received for the research, authorship, and/or publication of this article. This research was funded by the National Natural Science Foundation of China (No. 82172865), the Key Research and Development Program of Shandong (No. 2021SFGC0501), and the National Key Research and Development Program of China (No. 2022YFC2404605).

Acknowledgments

The authors gratefully acknowledge all the members of the Artificial Intelligence Laboratory of Shandong Cancer Hospital and Institute for their support and assistance.

Conflict of interest

The authors declare that the research was conducted in the absence of any commercial or financial relationships that could be construed as a potential conflict of interest.

Publisher's note

All claims expressed in this article are solely those of the authors and do not necessarily represent those of their affiliated organizations, or those of the publisher, the editors and the reviewers. Any product that may be evaluated in this article, or claim that may be made by its manufacturer, is not guaranteed or endorsed by the publisher.

References

Armstrong, S. A., Jafary, R., Forsythe, J. S., and Gregory, S. D. (2023). Tissue-mimicking materials for ultrasound-guided needle intervention phantoms: a comprehensive review. *Ultrasound Med. Biol.* 49, 18–30. doi: 10.1016/j.ultrasmedbio.2022.07.016

Augustin, G., Zigman, T., Davila, S., Udilljak, T., Staroveski, T., Brezak, D., et al. (2012). Cortical bone drilling and thermal osteonecrosis. *Clin. Biomech.* 27, 313–325. doi: 10.1016/j.clinbiomech.2011.10.010

Beisteiner, R., Matt, E., Fan, C., Baldysiak, H., Schönfeld, M., Philippi Novak, T., et al. (2019). Transcranial pulse stimulation with ultrasound in Alzheimer's disease-a new navigated focal brain therapy. *Adv. Sci. (Weinh).* 7:1902583.

Bjørnø, L. (2010). Introduction to nonlinear acoustics. *Phys. Procedia* 3, 5–16. doi: 10.1016/j.phpro.2010.01.003

Bobola, M. S., Chen, L., Ezeokeke, C. K., Olmstead, T. A., Nguyen, C., Sahota, A., et al. (2020). Transcranial focused ultrasound, pulsed at 40 Hz, activates microglia acutely and reduces Aβ load chronically, as demonstrated *in vivo*. *Brain Stimul.* 13, 1014–1023. doi: 10.1016/j.brs.2020.03.016

Bystritsky, A., Korb, A. S., Douglas, P. K., Cohen, M. S., Melega, W. P., Mulgaonkar, A. P., et al. (2011). A review of low-intensity focused ultrasound pulsation. *Brain Stimul.* 4, 125–136. doi: 10.1016/j.brs.2011.03.007

Cain, J. A., Spivak, N. M., Coetzee, J. P., Crone, J. S., Johnson, M. A., Lutkenhoff, E. S., et al. (2022). Ultrasonic deep brain neuromodulation in acute disorders of consciousness: a proof-of-concept. *Brain Sci.* 12:428. doi: 10.3390/brainsci12040428

Cappon, D., den Boer, T., Jordan, C., Yu, W., Metzger, E., and Pascual-Leone, A. (2022). Transcranial magnetic stimulation (TMS) for geriatric depression. *Ageing Res. Rev.* 74:101531. doi: 10.1016/j.arr.2021.101531

Cho, H., Lee, H.-Y., Han, M., Choi, J.-R., Ahn, S., Lee, T., et al. (2016). Localized Down-regulation of P-glycoprotein by focused ultrasound and microbubbles induced blood-brain barrier disruption in rat brain. *Sci. Rep.* 6:31201. doi: 10.1038/srep31201

Connor, C.W. Simulation methods and tissue property models for non-invasive transcranial focused ultrasound surgery. Doctor's Thesis, Massachusetts Institute of Technology, Massachusetts (2005).

Darrow, D. P. (2019). Focused ultrasound for neuromodulation. *Neurotherapeutics* 16, 88–99. doi: 10.1007/s13311-018-00691-3

Dickson, J. A., and Calderwood, S. K. (1980). Temperature range and selective sensitivity of tumors to hyperthermia: a critical review. *Ann. N. Y. Acad. Sci.* 335, 180–205. doi: 10.1111/j.1749-6632.1980.tb50749.x

Duck, F.A. *Physical properties of tissue. A comprehensive reference book*, London, England: Academic Press (1990).

Grisey, A., Heidmann, M., Letort, V., Lafitte, P., and Yon, S. (2016). Influence of skin and subcutaneous tissue on high-intensity focused ultrasound beam: experimental quantification and numerical modeling. *Ultrasound Med. Biol.* 42, 2457–2465. doi: 10.1016/j.ultrasmedbio.2016.06.013

Grudzenski, S., Heger, S., de Jonge, A., Schipp, J., Dumont, E., Larrat, B., et al. (2022). Simulation, implementation and measurement of defined sound fields for blood-brain barrier opening in rats. *Ultrasound Med. Biol.* 48, 422–436. doi: 10.1016/j.ultrasmedbio.2021.10.003

Huh, H., Park, T. Y., Seo, H., Han, M., Jung, B., Choi, H. J., et al. (2020). A local difference in blood–brain barrier permeability in the caudate putamen and thalamus of a rat brain induced by focused ultrasound. *Sci. Rep.* 10:19286. doi: 10.1038/s41598-020-76259-z

Iglesias, A. H. (2020). Transcranial magnetic stimulation as treatment in multiple neurologic conditions. *Curr. Neurol. Neurosci. Rep.* 20:1. doi: 10.1007/s11910-020-1021-0

Ilovitsh, T., Ilovitsh, A., Foiret, J., Caskey, C. F., Kusunose, J., Fite, B. Z., et al. (2018). Enhanced microbubble contrast agent oscillation following 250 kHz insonation. *Sci. Rep.* 8:16347. doi: 10.1038/s41598-018-34494-5

Jing, B., and Lindsey, B. D. (2021). Effect of skull porous trabecular structure on transcranial ultrasound imaging in the presence of elastic wave mode conversion at varying incidence angle. *Ultrasound Med. Biol.* 47, 2734–2748. doi: 10.1016/j.ultrasmedbio.2021.05.010

Kim, S., Kim, H., Shim, C., and Lee, H. J. (2018). Improved target specificity of transcranial focused ultrasound stimulation (TFUS) using double-crossed ultrasound transducers. *Annu. Int. Conf. IEEE Eng. Med. Biol. Soc.* 2679–2682. doi: 10.1109/ EMBC.2018.8512812

Kinoshita, M., McDannold, N., Jolesz, F. A., and Hynynen, K. (2006). Noninvasive localized delivery of Herceptin to the mouse brain by MRI-guided focused ultrasound-induced blood–brain barrier disruption. *Proc. Natl. Acad. Sci. U. S. A.* 103, 11719–11723. doi: 10.1073/pnas.0604318103

Klomjai, W., Katz, R., and Lackmy-Vallée, A. (2015). Basic principles of transcranial magnetic stimulation (TMS) and repetitive TMS (rTMS). *Ann. Phys. Rehabil. Med.* 58, 208–213. doi: 10.1016/j.rehab.2015.05.005

Koh, H., Park, T. Y., Chung, Y. A., Lee, J. H., and Kim, H. (2022). Acoustic simulation for transcranial focused ultrasound using GAN-based synthetic CT. *IEEE J. Biomed. Health Inform.* 26, 161–171. doi: 10.1109/JBHI.2021.3103387

Konofagou, E. E., Tung, Y. S., Choi, J., Deffieux, T., Baseri, B., and Vlachos, F. (2012). Ultrasound-induced blood-brain barrier opening. *Curr. Pharm. Biotechnol.* 13, 1332–1345. doi: 10.2174/138920112800624364

Krishna, V., Sammartino, F., and Rezai, A. (2018). A review of the current therapies, challenges, and future directions of transcranial focused ultrasound technology: advances in diagnosis and treatment. *JAMA Neurol.* 75, 246–254. doi: 10.1001/jamaneurol.2017.3129

Kubanek, J. (2018). Neuromodulation with transcranial focused ultrasound. *Neurosurg. Focus.* 44:E14. doi: 10.3171/2017.11.FOCUS17621

Lee, W., Chung, Y. A., Jung, Y., Song, I. U., and Yoo, S. S. (2016). Simultaneous acoustic stimulation of human primary and secondary somatosensory cortices using transcranial focused ultrasound. *BMC Neurosci.* 17:68. doi: 10.1186/s12868-016-0303-6

Lee, W., Kim, H., Jung, Y., Song, I. U., Chung, Y. A., and Yoo, S. S. (2015). Image-guided transcranial focused ultrasound stimulates human primary somatosensory cortex. *Sci. Rep.* 5:8743. doi: 10.1038/srep08743

Legon, W., Ai, L., Bansal, P., and Mueller, J. K. (2018). Neuromodulation with single-element transcranial focused ultrasound in human thalamus. *Hum. Brain Mapp.* 39, 1995–2006. doi: 10.1002/hbm.23981

Lescrauwaet, E., Vonck, K., Sprengers, M., Raedt, R., Klooster, D., Carrette, E., et al. (2022). Recent advances in the use of focused ultrasound as a treatment for epilepsy. *Front. Neurosci.* 16:886584. doi: 10.3389/fnins.2022.886584

Marder, K. G., Barbour, T., Ferber, S., Idowu, O., and Itzkoff, A. (2022). Psychiatric applications of repetitive transcranial magnetic stimulation. *Focus (Am. Psychiatr. Publ).* 20, 8–18. doi: 10.1176/appi.focus.20210021

Maresca, D., Lakshmanan, A., Abedi, M., Bar-Zion, A., Farhadi, A., Lu, G. J., et al. (2018). Biomolecular ultrasound and Sonogenetics. *Annu. Rev. Chem. Biomol. Eng.* 9, 229–252. doi: 10.1146/annurev-chembioeng-060817-084034

Min, B. K., Bystritsky, A., Jung, K. I., Fischer, K., Zhang, Y., Maeng, L. S., et al. (2011). Focused ultrasound-mediated suppression of chemically-induced acute epileptic EEG activity. *BMC Neurosci.* 12:23. doi: 10.1186/1471-2202-12-23

Mohammadjavadi, M., Ye, P. P., Xia, A., Brown, J., Popelka, G., and Pauly, K. B. (2019). Elimination of peripheral auditory pathway activation does not affect motor responses from ultrasound neuromodulation. *Brain Stimul.* 12, 901–910. doi: 10.1016/j.brs.2019.03.005

Mueller, J. K., Ai, L., Bansal, P., and Legon, W. (2017). Numerical evaluation of the skull for human neuromodulation with transcranial focused ultrasound. *J. Neural Eng.* 14:066012. doi: 10.1088/1741-2552/aa843e

Nelson, D. A., and Nunneley, S. A. (1998). Brain temperature and limits on transcranial cooling in humans: quantitative modeling results. *Eur. J. Appl. Physiol. Occup. Physiol.* 78, 353–359. doi: 10.1007/s004210050431

Park, T. Y., Jeong, J. H., Chung, Y. A., Yeo, S. H., and Kim, H. (2022). Application of subject-specific helmets for the study of human visuomotor behavior using transcranial focused ultrasound: a pilot study. *Comput. Methods Prog. Biomed.* 226:107127. doi: 10.1016/j.cmpb.2022.107127

Park, C. Y., Seo, H., Lee, E.-H., Han, M., Choi, H., Park, K.-S., et al. (2021). Verification of blood-brain barrier disruption based on the clinical validation platform using a rat model with human skull. *Brain Sci.* 11:1429. doi: 10.3390/brainsci11111429

Rzechorzek, N. M., Thrippleton, M. J., Chappell, F. M., Mair, G., Ercole, A., Cabeleira, M., et al. (2022). A daily temperature rhythm in the human brain predicts survival after brain injury. *Brain* 145, 2031–2048. doi: 10.1093/brain/awab466

Schwenke, M., Georgii, J., and Preusser, T. (2017). Fast numerical simulation of focused ultrasound treatments during respiratory motion with discontinuous motion boundaries. *IEEE Trans. Biomed. Eng.* 64, 1455–1468. doi: 10.1109/TBME.2016.2619741

Servick, K. (2020). Hope grows for targeting the brain with ultrasound. *Science* 368, 1408–1409. doi: 10.1126/science.368.6498.1408

Shen, Z. Y., Shen, E., Diao, X. H., Bai, W. K., Zeng, M. X., Luan, Y. Y., et al. (2014). Inhibitory effects of subcutaneous tumors in nude mice mediated by low-frequency ultrasound and microbubbles. *Oncol. Lett.* 7, 1385–1390. doi: 10.3892/ol.2014.1934

Slegers, R. J., and Blumcke, I. (2020). Low-grade developmental and epilepsy associated brain tumors: a critical update 2020. *Acta Neuropathol. Commun.* 8:27. doi: 10.1186/s40478-020-00904-x

Slezak, C., Flatscher, J., and Slezak, P. (2022). A comparative feasibility study for transcranial extracorporeal shock wave therapy. *Biomedicine* 10:1457. doi: 10.3390/biomedicines10061457

Svider, P. F., Blasco, M. A., Raza, S. N., Shkoukani, M., Sukari, A., Yoo, G. H., et al. (2017). Head and neck Cancer. *Otolaryngol. Head Neck Surg.* 156, 10–13. doi: 10.1177/0194599816674672

Treeby, B. E., and Cox, B. T. (2010). K-wave: MATLAB toolbox for the simulation and re-construction of photoacoustic wave fields. *J. Biomed. Opt.* 15:021314. doi: 10.1117/1.3360308

Vargo, M. (2011). Brain tumor rehabilitation. *Am. J. Phys. Med. Rehabil.* 90, 50–62.

Venkatesh, H. S., Johung, T. B., Caretti, V., Noll, A., Tang, Y., Nagaraja, S., et al. (2015). Neuronal activity promotes glioma growth through Neuroligin-3 secretion. *Cells* 161, 803–816. doi: 10.1016/j.cell.2015.04.012

Venkatesh, H., and Monje, M. (2017). Neuronal activity in ontogeny and oncology. *Trends Cancer.* 3, 89–112. doi: 10.1016/j.trecan.2016.12.008

Wang, J., Li, G., Deng, L., Mamtilahun, M., Jiang, L., Qiu, W., et al. (2021). Transcranial focused ultrasound stimulation improves neurorehabilitation after middle cerebral artery occlusion in mice. *Aging Dis.* 12, 50–60. doi: 10.14336/AD.2020.0623

Xu, L., Lee, W., Rotenberg, A., Böhlke, M., Yoon, K., and Yoo, S. S. (2020). Localized disruption of blood albumin–phenytoin binding using transcranial focused ultrasound. *Ultrasound Med. Biol.* 46, 1986–1997. doi: 10.1016/j.ultrasmedbio.2020.04.011

Yan, Y., Chen, Y., Liu, Z., Cai, F., Niu, W., Song, L., et al. (2021). Brain delivery of curcumin through low-intensity ultrasound-induced blood-brain barrier opening via lipid-PLGA Nanobubbles. *Int. J. Nanomedicine* 16, 7433–7447. doi: 10.2147/IJN.S327737

Yoon, K., Lee, W., Croce, P., Cammalleri, A., and Yoo, S. S. (2018). Multi-resolution simulation of focused ultrasound propagation through ovine skull from a single-element transducer. *Phys. Med. Biol.* 63:105001. doi: 10.1088/1361-6560/aabe37

Zou, J.J. Therapeutic effect of low-intensity focused ultrasound on non-human primate epilepsy model. Master's Thesis, Southern Medical University, Guangzhou (2020).

frontiers | Frontiers in Neuroscience

TYPE Systematic Review
PUBLISHED 12 October 2023
DOI 10.3389/fnins.2023.1272003

OPEN ACCESS

EDITED BY
Mark H. Myers,
University of Tennessee Health Science Center (UTHSC), United States

REVIEWED BY
Jack Jiaqi Zhang,
Hong Kong Polytechnic University, Hong Kong SAR, China
Peiyang Li,
Chongqing University of Posts and Telecommunications, China

*CORRESPONDENCE
Hai Li
lihai2018@smu.edu.cn
Yue Lan
bluemooning@163.com

†These authors have contributed equally to this work

RECEIVED 03 August 2023
ACCEPTED 21 September 2023
PUBLISHED 12 October 2023

CITATION
Chen S, Zhang S, Yang W, Chen Y, Wang B, Chen J, Li X, Xie L, Huang H, Zeng Y, Tian L, Ji W, Wei X, Lan Y and Li H (2023) The effectiveness of intermittent theta burst stimulation for upper limb motor recovery after stroke: a systematic review and meta-analysis of randomized controlled trials. *Front. Neurosci.* 17:1272003. doi: 10.3389/fnins.2023.1272003

The effectiveness of intermittent theta burst stimulation for upper limb motor recovery after stroke: a systematic review and meta-analysis of randomized controlled trials

Songbin Chen[1,2†], Shunxi Zhang[2†], Wenqing Yang[2], Yujie Chen[2], Bingshui Wang[1], Jixiang Chen[2], Xiaotong Li[2], Lanfang Xie[1], Huangjie Huang[3], Yangkang Zeng[4], Lingling Tian[1], Wenxue Ji[1], Xijun Wei[1], Yue Lan[2]* and Hai Li[1]*

[1]Department of Rehabilitation Medicine, Shenzhen Hospital, Southern Medical University, Shenzhen, China, [2]Department of Rehabilitation Medicine, Guangzhou First People's Hospital, School of Medicine, South China University of Technology, Guangzhou, China, [3]Department of Rehabilitation Medicine, The First Affiliated Hospital, Sun Yat-sen University, Guangzhou, China, [4]Department of Rehabilitation Medicine, Shenzhen University General Hospital, Shenzhen, China

Background: Intermittent theta burst stimulation (iTBS) is a promising noninvasive therapy to restore the excitability of the cortex, and subsequently improve the function of the upper extremities. Several studies have demonstrated the effectiveness of iTBS in restoring upper limb function and modulating cortical excitability. We aimed to evaluate the effects of iTBS on upper limb motor recovery after stroke.

Objective: The purpose of this article is to evaluate the influence of intermittent theta-burst stimulation on upper limb motor recovery and improve the quality of life.

Method: A literature search was conducted using PubMed, EMBASE, MEDLINE, The Cochrane Library, Web of Science, and CBM, including only English studies, to identify studies that investigated the effects of iTBS on upper limb recovery, compared with sham iTBS used in control groups. Effect size was reported as standardized mean difference (SMD) or weighted mean difference (WMD).

Results: Ten studies were included in the meta-analysis. The results of the meta-analysis indicated that when compared to the control group, the iTBS group had a significant difference in the Fugl-Meyer Assessment (FMA) and Action Research Arm Test (ARAT) (WMD: 3.20, 95% CI: 1.42 to 4.97; WMD: 3.72, 95% CI: 2.13 to 5.30, respectively). In addition, there was also a significant improvement in the modified Ashworth scale (MAS) compared to the sham group (WMD: −0.56; 95% CI: −0.85 to −0.28). More evidence is still needed to confirm the effect of Barthel Index (BI) scores after interventions. However, no significant effect was found for the assessment of Motor Evoked Potential (MEP) amplitude and MEP latency (SMD: 0.35; 95% CI: −0.21 to 0.90; SMD: 0.35, 95% CI: −0.18 to 0.87; SMD: 0.03, 95% CI: −0.49 to 0.55; respectively).

Conclusion: Our results showed that iTBS significantly improved motor impairment, functional activities, and reduced muscle tone of upper limbs, thereby increasing the ability to perform Activities of Daily Living (ADL) in stroke

patients, while there were no significant differences in MEPs. In conclusion, iTBS is a promising non-invasive brain stimulation as an adjunct to therapy and enhances the therapeutic effect of conventional physical therapy. In the future, more randomized controlled trials with large sample sizes, high quality, and follow-up are necessary to explore the neurophysiological effects.

Systematic review registration: https://www.crd.york.ac.uk/PROSPERO/, identifier CRD42023392739.

KEYWORDS

stroke, intermittent theta burst stimulation, upper limb function, meta-analysis, rehabilitation

1. Introduction

Stroke is one of the leading causes of long-term upper limb disability worldwide (Feigin et al., 2014). It is reported that up to 75% of post-stroke patients live with upper limb functional impairment, which results in restrictions in functional tasks and daily activities, even after traditional rehabilitation programs (Feigin et al., 2017). Impaired motor function is associated with a decrease in corticospinal excitability of the affected hemisphere after stroke (McDonnell and Stinear, 2017). Also, according to neuroimaging studies, the unaffected primary motor cortex (M1) appears to be overactivated during movement control of the affected hand in stroke patients (Grefkes and Ward, 2014). Repetitive transcranial magnetic stimulation (rTMS) is a promising non-invasive technique to modulate the excitability of specific brain areas that have been reported to be robust in the recovery of motor function after stroke (Li et al., 2020). Intermittent theta burst stimulation (iTBS) is a specific type of rTMS that effectively improves cortex excitability by generating facilitatory or inhibitory effects on synaptic transmission (Huang et al., 2005). As an excitatory rTMS, the underlying mechanism of iTBS can be attributed in part to the removal of magnesium ion blockages in the N-methyl-D-aspartate glutamate receptors during depolarization, resulting in intracellular calcium entry and enhancing the postsynaptic response to behavioral learning (Zhang et al., 2022). This repetitive stimulation pattern has been shown to induce long-term potentiation (LTP) in the neural circuits associated with motor function (Koch et al., 2008). The persistent motor deficits poststroke may be due to abnormal cortical excitability and brain network connection (Desowska and Turner, 2019). Therefore, better clinical outcomes for the affected limb result from the reduction of asymmetry of corticomotor excitability (Cabral et al., 2022). With shorter stimulation and lower stimulation intensity, iTBS has been suggested to be a promising rTMS option compared to traditional rTMS in clinical treatment (Talelli et al., 2007). iTBS become more frequently applied with conventional rehabilitation to enhance the improvement in motor function after stroke. However, individual studies have yielded inconsistent or conflicting findings, possibly due to the limitations associated with an individual study and the small sample size. Although cortical excitability of the M1 was significantly increased after multiple sessions of iTBS in one study (Sung et al., 2013), Watanabe et al. (2018) found that the motor performance did not reach statistical significance, and Zhang et al. (2022) found that motor outcomes showed a significantly greater improvement than the sham group. To clarify these conflicting results and to better evaluate the relationship between iTBS and upper limb motor recovery in stroke patients, we performed a meta-analysis of published studies. The aim of this article is to evaluate the influence of intermittent theta-burst stimulation on upper limb motor recovery and quality of life.

2. Methods and analysis

2.1. Study registration

This trial has been registered in PROSPERO (registration number: CRD42023392739). This protocol is reported in accordance with the Preferred Reporting Items for Systematic Reviews and Meta-Analyzes Protocols (PRISMA-P) statement guidelines (Moher et al., 2015).

2.2. Inclusion criteria

We included studies involving adult patients with a CT or MRI diagnosis of stroke and upper limb dysfunction. iTBS with a 2-s burst train of three 50 Hz pulses repeated every 200 ms (5 Hz) must be included in the intervention. The comparison intervention could be sham iTBS or no intervention. We only included randomized controlled trials (RCTs) published in English that use iTBS as an intervention for upper limb motor dysfunction in post-stroke patients.

2.3. Outcome measures

The primary outcomes were motor function, the Upper Limb Fugl-Meyer Scale, and the neurophysiological indicator, Motor Evoked Potential (MEP). Secondary outcomes included the Action Research Arm Test (ARAT), Modified Barthel Index (MBI), and Modified Ashworth Scale (MAS). Adverse events included dizziness, epilepsy, headache, paresthesia, and others.

2.4. Exclusion criteria

The following types of studies were excluded: animal studies, published repeatedly, opinion articles, dissertations, and full text not available through various approaches.

TABLE 1 The detail of search strategy in each database.

Database	Search strategy	Results
PubMed	((("Stroke"[Mesh]) OR ((((((cerebrovascular accident[Title/Abstract]) OR (CVA[Title/Abstract])) OR (Brain Vascular Accident[Title/Abstract])) OR (hemiplegia[Title/Abstract])) OR (apoplexy[Title/Abstract])) OR (hemiparesis[Title/Abstract]))) AND (((theta-burst stimulation[Title/Abstract]) OR (TBS[Title/Abstract])) OR (intermittent theta burst stimulation[Title/Abstract]))) AND (randomized controlled trial[Publication Type] OR randomized[Title/Abstract] OR placebo[Title/Abstract])	46
EMBASE	('Stroke':ab,tI OR 'cerebrovascular accident':ab,tI OR 'CVA':ab,tI OR 'Brain Vascular Accident':ab,tI OR 'hemiplegia':ab,tI OR 'apoplexy':ab,tI OR 'hemiparesis':ab,tI) AND ('theta-burst stimulation':ab,tI OR 'TBS':ab,tI OR 'intermittent theta burst stimulation':ab,tI) AND ('randomized controlled trial':ab,tI OR 'randomized':ab,tI OR 'placebo':ab,tI OR 'RCT':ab,tI)	98
MEDLINE	1: TS = (Stroke OR cerebrovascular accident OR CVA OR Brain Vascular Accident OR hemiplegia OR apoplexy OR hemiparesis) 2: TS = (theta-burst stimulation OR TBS OR intermittent theta burst stimulation) 3: TS = (randomized controlled trial OR randomized OR placebo OR RCT) 4: #3 AND #2 AND #1	67
The Cochrane Library	#1 MeSH descriptor: [Stroke] explode all trees #2 (cerebrovascular accident):ab,ti,kw OR (CVA):ab,ti,kw OR (Brain Vascular Accident):ab,ti,kw OR (hemiplegia):ab,ti,kw OR (apoplexy):ab,ti,kw OR (hemiparesis):ab,ti,kw #3 #1 OR #2 #4 (theta-burst stimulation):ab,ti,kw OR (TBS):ab,ti,kw OR (intermittent theta burst stimulation):ab,ti,kw #5 (randomized controlled trial):ab,ti,kw OR (randomized):ab,ti,kw OR (placebo):ab,ti,kw OR (RCT):ab,ti,kw #6 #3 AND #4 AND #5	124
Web of Science	1: TS = (Stroke OR cerebrovascular accident OR CVA OR Brain Vascular Accident OR hemiplegia OR apoplexy OR hemiparesis) 2: TS = (theta-burst stimulation OR TBS OR intermittent theta burst stimulation) 3: TS = (randomized controlled trial OR randomized OR placebo OR RCT) 4: #1 AND #2 AND #3	130
CBM	"stroke"[Common field: Intelligence] OR "cerebrovascular accident"[Common field: Intelligence] OR "CVA"[Common field: Intelligence] OR "Brain Vascular Accident"[Common field: Intelligence] OR "hemiplegia"[Common field: Intelligence] OR "apoplexy"[Common field: Intelligence] OR "hemiparesis"[Common field: Intelligence] "theta-burst stimulation"[Common field: Intelligence] OR "TBS"[Common field: Intelligence] OR "intermittent theta burst stimulation"[Common field: Intelligence] "randomized controlled trial"[Common field: Intelligence] OR "randomized"[Common field: Intelligence] OR "placebo"[Common field: Intelligence] OR "RCT"[Common field: Intelligence] (#5) AND (#3) AND (#2)	30

2.5. Search and database

A comprehensive literature search was conducted using PubMed, EMBASE, MEDLINE, The Cochrane Library, Web of Science, and CBM. The bibliographies of identified studies and relevant journals were searched manually. Unpublished data were searched for by contacting experts in the field of physiotherapy research and through conference listings identified in the search. The detailed search strategy in each database is shown in Table 1. The search was conducted in February 2023.

According to the inclusion and exclusion criteria, two reviewers (CSB and ZSX) independently performed the screening method. Disagreements were resolved by discussion or consultation with the third reviewer (YWQ).

Two reviewers (CSB and ZSX) extracted the literature data independently, with any disagreements discussed or reviewed by the third researcher (YWQ) until a consensus was reached. The extracted data included first author, year of publication, disease course, sample size, age, type of intervention, duration of intervention, stimulation site and outcome measures, and mean differences (MD) and standard deviations (SD) of change scores or mean and SD of post-intervention scores. For the motor function, the results of the Upper Limb Fugl-Meyer Scale, ARAT, WOLF, and MAS were extracted. For the quality of life, the results of BI were used to assess poststroke ADLs. The incidence of adverse events was also extracted. Inclusion data were collected in Excel and cross-checked by the two reviewers. For studies without numerical data, Engauge Digitizer 4.1 was employed for data extraction from the graphs. For missing data, the author was contacted to obtain complete information.

2.6. Quality assessment

The quality of the included studies was independently evaluated by two assessors using the Cochrane Collaboration risk of bias tool, which includes the following items: random sequence generation, allocation concealment, blind subjects and therapists, blind assessors, incomplete outcome data, selective outcome reporting, and other biases. According to the Cochrane Handbook for Systematic Reviews of Interventions, low, unclear, and high risk of bias are used to assess

the risk of bias in each included study. Two reviewers (CSB and ZSX) independently assessed the risk of bias and discussed disagreements. A third reviewer was involved if necessary.

2.7. Data analysis

Meta-analysis was performed using Review Manager software (Revman, version 5.3). Uncertainty was expressed as 95% confidence intervals (95% CI). The I^2 statistic and Cochrane's Q test were used to assess heterogeneity among the included studies. The appropriate effect model was selected according to the heterogeneity result. A fixed-effects model was used if acceptable heterogeneity was found ($I^2 < 50\%$). Alternatively, a random-effects model was used, it was necessary to describe the source of the heterogeneity as much as possible. Sensitivity analysis was used to assess the stability of the system trial and a value of $p \leq 0.05$ was considered to be statistically significant.

3. Results

3.1. Characteristics of the studies

A total of 495 studies were retrieved from the database search (Figure 1). After removing duplicates, the remaining 281 studies were screened using the titles and abstracts, resulting in the exclusion of 248 articles. Using the full text of the remaining 33 articles, their eligibility was also assessed based on the inclusion criteria described above. Of these, 23 articles did not meet the eligibility criteria for the following reasons: the intervention was cTBS (5 studies); crossover design (4 studies); no outcomes of interest (9 studies); iTBS for lower limb (1 study); missing data (4 studies).

A total of 10 high-quality randomized controlled trials with 236 stroke patients were included in this meta-analysis. The characteristics of the included studies are shown in Table 2. The distribution of participants was 126 experiments and 110 controls. The ages of the participants ranged from 18 to 85 years old. The sex distribution of the studies was 79 females and 157 males. As mentioned in the included studies, most studies included patients with both ischemic and hemorrhagic stroke, except for 2 studies (Ackerley et al., 2016; El Nahas et al., 2022) which did not report stroke type and 3 studies (Talelli et al., 2012; Hsu et al., 2013; Watanabe et al., 2018) which only included patients with ischemic stroke. All of the articles included in this study had an iTBS protocol, consisting of the delivery of a 2-s train of theta-burst stimulation (bursts of 3 stimuli at 50 Hz with an inter-burst interval of 200 ms) repeated every 10 s. The highest intensity in the studies (Talelli et al., 2012; Hsu et al., 2013; Chen, 2018; Chen Y. H. et al., 2021) was set at 80% of the active motor threshold (AMT) of nonparetic hand, while two (Sung et al., 2013; Chen Y. et al., 2021) set it at 80% AMT of paretic FDI. The intensity in three further articles was reported to be 70% (Zhang et al., 2022), 80% (Watanabe et al., 2018), and 90% (Ackerley et al., 2016) RMT of nonparetic FDI, respectively. The stimulation intensity in only one article (El Nahas et al., 2022) was set above the threshold of the targeted muscles with 8 sessions. As for the sham stimulation, some (Sung et al., 2013; Ackerley et al., 2014; Watanabe et al., 2018; El Nahas et al., 2022) used a sham coil, some (Talelli et al., 2012; Hsu et al., 2013; Chen Y. et al., 2021) rotated the coil by 90°, and the rest (Chen, 2018; Chen Y. H. et al., 2021; Zhang et al., 2022) used a lower intensity of AMT. With the exception of two studies that delivered stimulation to the cerebellum (Chen Y. et al., 2021) and targeted muscle (El Nahas et al., 2022), the majority of the articles in the study applied the intervention to the ipsilesional M1 (see Table 3).

3.2. Risk of bias of included studies

With the exception of one study, Chen (2018) in which the risk was unclear, random sequence generation scored a low risk in the included studies. Allocation concealment showed a high risk in one study (Talelli et al., 2012) and an unclear risk in two studies (Hsu et al., 2013; Chen, 2018) in all included articles. Blinding of participants and personnel resulted in an unclear risk in some of the included studies, which may have led to performance bias (Watanabe et al., 2018; El Nahas et al., 2022; Zhang et al., 2022). According to the studies, the assessors were blinded to group allocation and not involved in treating patients. Blinding of outcome assessment scored low risk in all studies. As for attrition bias, some studies were scored high risk or unclear risk because of incomplete outcome data (Hsu et al., 2013; Sung et al., 2013; Ackerley et al., 2016; Chen Y. et al., 2021; Zhang et al., 2022). Additionally, three studies had unclear selective reporting bias (Sung et al., 2013; Chen Y. et al., 2021; El Nahas et al., 2022) and four studies reported other bias (Hsu et al., 2013; Sung et al., 2013; Chen, 2018; Chen Y. H. et al., 2021) (Figures 2, 3).

3.3. Effects of iTBS on upper limb impairment after stroke

The FMA is a clinical assessment of upper limb motor impairment after stroke (Fugl-Meyer et al., 1975). Pooled data from six studies (Hsu et al., 2013; Sung et al., 2013; Chen, 2018; Watanabe et al., 2018; Chen Y. H. et al., 2021; Zhang et al., 2022) were used to determine the effects of iTBS on upper limb impairment after stroke (Figure 4). The results from the meta-analysis indicated that when compared to the control group, the iTBS group had a significant difference in the assessment of FMA (WMD: 3.20, 95%CI:1.42 to 4.97, $p = 0.0004$), with relatively low heterogeneity ($I^2 = 28\%$, $p = 0.23$). In order to explore the sources of heterogeneity, subgroup analyzes were performed to examine the influence of stroke duration on the outcomes. The mean difference for the <6 months subgroup was 6.68 (95% CI: 3.46 to 9.89; $p < 0.00001$), without heterogeneity ($I^2 = 0\%$, $p = 0.89$). The mean difference for the ≥6 months subgroup was 1.68 (95% CI: −0.45 to 3.81; $p = 0.12$), without heterogeneity ($I^2 = 0\%$, $p = 0.92$). From the results of the meta-analysis, it can be concluded that it is effective in improving upper limb motor function in the early (<6 months) but not significant in chronic (≥6 months) stages, and the improvement in the early stage is better than the chronic stage.

3.4. Effects of iTBS on upper limb function after stroke

The ARAT is used to assess upper limb functional activities (Rossini et al., 1994). The effect of iTBS on upper extremity motor function was assessed by pooling data from five studies (Talelli et al.,

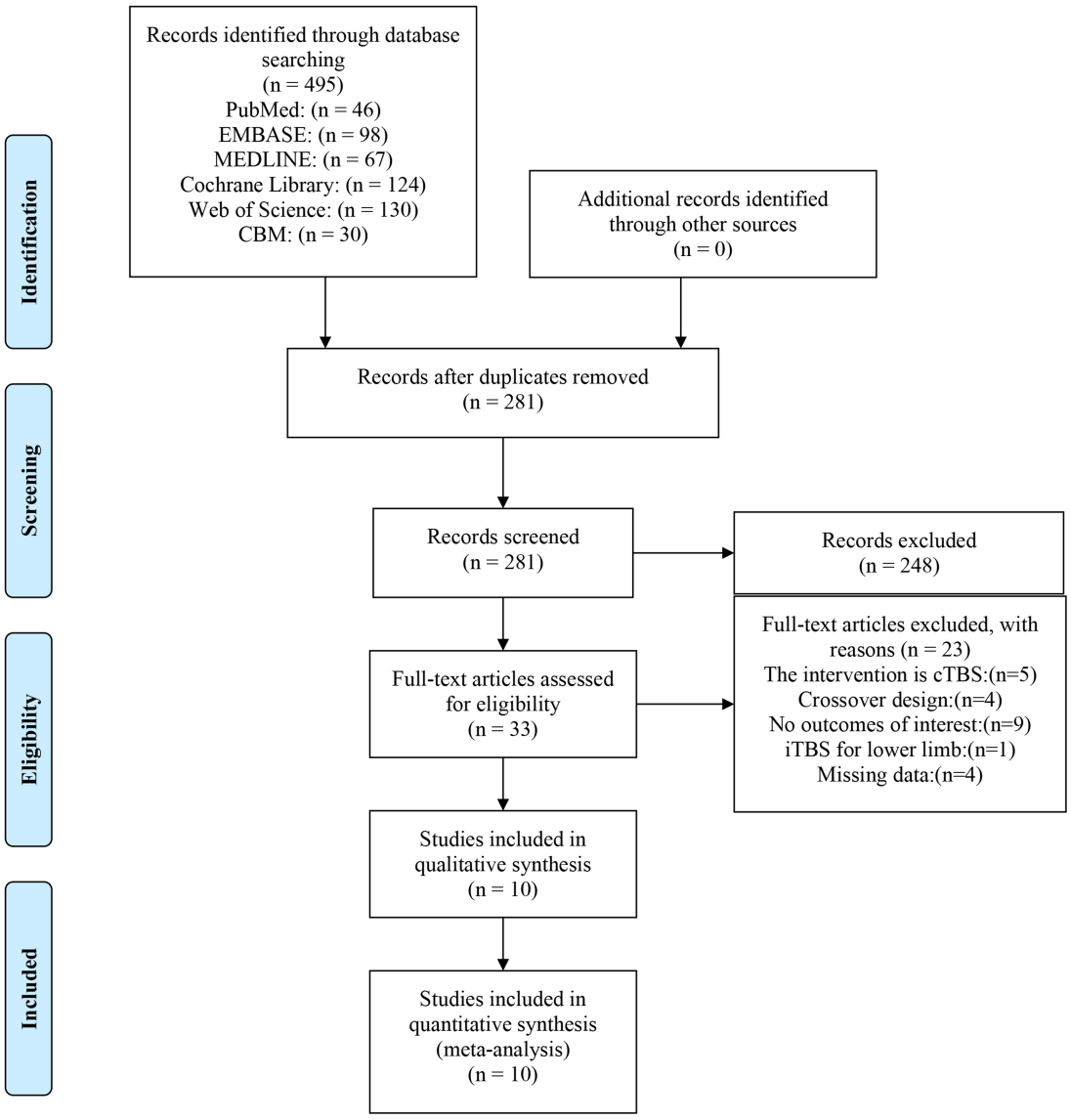

FIGURE 1
PRISMA flow chart on the selection and inclusion of studies.

2012; Ackerley et al., 2016; Chen, 2018; Chen Y. H. et al., 2021; Zhang et al., 2022) with significant improvement in the iTBS group (WMD: 3.72, 95%CI:2.13 to 5.30, $p < 0.00001$), without heterogeneity ($I^2 = 0\%$, $p = 0.99$) (Figure 5).

3.5. Effects of iTBS on muscle tone of upper limb after stroke

The MAS is a reliable scale for evaluating muscle tone in individuals with stroke which has shown satisfactory inter- and intra-rater reliability and agreement (Meseguer-Henarejos et al., 2018). The effect of improvement on muscle tone in stroke patients after iTBS intervention was assessed by pooling data from five studies (Chen, 2018; Watanabe et al., 2018; Chen Y. et al., 2021; Chen Y. H. et al., 2021; El Nahas et al., 2022) (Figure 6). There was a significant improvement in MAS compared with the sham group (WMD: -0.56; 95% CI: −0.85 to −0.28; $p = 0.0001$), with low heterogeneity ($I^2 = 31\%$, $p = 0.22$).

3.6. Effects of iTBS on electrophysiological measures after stroke

The latency and peak-to-peak amplitude of MEPs from the abductor pollicis brevis muscle is used evaluate corticomotor excitability (Volz et al., 2016). Pooling data from three studies (Hsu et al., 2013; Sung et al., 2013; Watanabe et al., 2018), the results of our meta-analysis indicated that when compared to the sham group, a significant effect for the assessment of MEP amplitude from the ipsilesional hemisphere was not found (SMD: 0.35; 95% CI: −0.21 to 0.90; $p = 0.22$) with 0% heterogeneity (Figure 7). The MEP amplitude from the contralesional hemisphere was assessed by pooling data from two studies (Sung et al., 2013; Chen Y. et al., 2021). Compared to the

TABLE 2 Characteristic of patients included in the studies.

Study	Participants		Age (years)		Gender (Female/Male)		Side of effect (L/R)		Type of stroke (H/I)	
	E	C	E	C	E	C	E	C	E	C
Ackerley et al. (2016)	9	9	61 (21–80)	71 (38–79)	3/6	3/6	3/6	3/6	–	–
Chen (2018)	11	11	52.9 (11.1)	52.6 (8.3)	7/4	7/4	6/5	9/2	9/2	8/3
Chen Y. et al. (2021)	16	16	57.38 (8.04)	51.44 (9.19)	3/13	4/12	12/4	7/9	6/10	8/8
Chen Y. H. et al. (2021)	12	11	54.36 (10.56)	48.95 (9.63)	4/8	1/10	7/5	7/4	6/6	9/2
Hsu et al. (2013)	6	6	56.8 (6.85)	62.3 (8.45)	1/5	3/3	3/3	5/1	0/6	0/6
El Nahas et al. (2022)	25	11	47.88 (14.8)	41.6 (14.9)	5/20	4/7	–	–	–	–
Sung et al. (2013)	12	14	64.2 (11.9)	63.1 (12.8)	3/9	3/11	–	–	4/8	5/9
Talelli et al. (2012)	13	12	54.4 (15.8)	58.5 (12.0)	6/7	3/9	6/7	9/3	0/13	0/12
Watanabe et al. (2018)	8	6	72.5 (6.5)	75.2 (5.5)	3/5	3/3	4/4	5/3	0/8	0/6
Zhang et al. (2022)	14	14	59.50 (8.56)	64 (5.39)	7/7	6/8	8/6	7/7	6/8	4/10

control group, the iTBS group did not show a significant improvement (SMD: 0.35; 95% CI: −0.18 to 0.87; $p = 0.19$) with 0% heterogeneity (Figure 8). Furthermore, the latency of MEP in stroke patients after iTBS was assessed by pooling data from two studies (Sung et al., 2013; Chen Y. H. et al., 2021). There was no statistical difference in the latency of MEP between the two groups (SMD: 0.03; 95% CI: −0.49 to 0.55; $p = 0.90$), with moderate heterogeneity ($I^2 = 45\%$, $p = 0.18$) (Figure 9).

3.7. Effects of iTBS on the ability to perform activities of daily living after stroke

The Barthel Index is used to quantify functional change by assessing the ability to perform activities of daily living after rehabilitation intervention (Silveira et al., 2018). A study conducted by Chen Y. H. et al. (2021) showed a significant improvement in BI scores compared to baseline after interventions both in the iTBS and sham groups. However, there were no differences between the groups.

3.8. Adverse events

All of the included studies reported patients could well tolerate the intervention without significant adverse effects. No adverse events were reported except for one article, which included transient local pain/mild ipsilateral headache and discomfort/mild tingling (Hsu et al., 2013). Therefore, larger randomized controlled trials are needed to further confirm the safety of iTBS for stroke in the future.

4. Discussion

The aim of this article is to systematically review the influence of iTBS on the function of upper limb motor recovery and improving the quality of life in stroke patients. According to the included studies, iTBS, consisting of the delivery of a 2 s train of theta-burst stimulation (bursts of 3 stimuli at 50 Hz with an interburst interval of 200 ms) repeated every 10 s, was commonly delivered at 70–90% AMT of nonparetic FDI to ipsilesional M1 with 600 pulses or 1,200 pulses. After delivery five times/week for 2 consecutive weeks, the majority of studies yielded positive results in motor function of the upper limbs, while some demonstrated no positive effect on the excitability of the cortex, which may need more robust evidence due to inadequate data. According to the results of the meta-analysis, the iTBS group had significant improvement in FMA, ARAT, MAS, and BI compared to the control group. However, no significant differences were found in MEP amplitude and MEP latency between the iTBS group and the control group. Considering that the sample size we used was limited, this result is not very convincing, which warrants further evidence and a larger sample size.

Regarding iTBS for upper limb motor impairment after stroke, patients' FMA scores improved significantly after iTBS intervention treatment. Based on subgroup analysis of stroke duration， patients benefit more in the early phase than in the chronic stage in FMA. These results are consistent with those of previous studies. Facilitatory iTBS combined with upper limb training was found to enhance fine upper limb movement and the recovery of gross manual dexterity in acute, subacute, and chronic stroke (Hsu et al., 2013; Chen, 2018; Watanabe et al., 2018). This can be explained by the vicariation theory that the brain areas induced by iTBS are reorganized to substitute the functions of nearby injured areas (Murphy and Corbett, 2009). It is accepted that gross and fine motor function can be controlled by M1 and corticospinal tract (Lang and Schieber, 2004). As the stimulation point, the regulation of M1 and the corticospinal tract can account for the improvement in FMA. Several studies have shown increased neuroplasticity and greater behavioral recovery in the early post-stroke period (Maulden et al., 2005; Murphy and Corbett, 2009). As far as we know, the first 6 months after stroke are the ideal time for recovering motor function. From the results of the meta-analysis, iTBS is a promising adjuvant to therapy delivered at the early stage of stroke.

Regarding iTBS for upper limb functional activities after stroke, patients' ARAT scores improved significantly after iTBS intervention treatment. The mean difference in improvement in the ARAT score was modest, which may be explained by the fact that the improvement of the majority of stroke patients included in the analysis lasted more than 6 months (Talelli et al., 2012; Ackerley

TABLE 3 Characteristic of protocol.

Study	Stroke duration		Protocol		Sessions	Stimulated site	Outcome measures
	E	C	E	C			
Ackerley et al. (2016)	20 (6–72)	18 (7–56)	600 stimuli, 90% AMT of nonparetic FDI	delivered with a sham coil	daily,10 days	ipsilesional M1	ARAT, FMA, corticomotor excitability
Chen (2018)	≥6 months	≥6 months	600 pulses,80% AMT of paretic FDI	60% AMT, conventional rehabilitation therapy	five times/ for 2 consecutive weeks	ipsilesional M1	MAS, FMA, ARAT, BBT, MAL
Chen Y. et al. (2021)	80.13 (35.19) days	101.50 (54.15) days	600 pulses,80% AMT of nonparetic	rotated 90°	10 sessions, 2 weeks	cerebellar	MAS, MTS, SWV, Hmax/Mmax ratio, MEP latency and amplitude, CMCT, BI
Chen Y. H. et al. (2021)	5.01 (4.39)	7.99 (5.41)	two iTBS with 600 pulses, 80% AMT of paretic， VCT	60% AMT, VCT	15 consecutive work days	ipsilesional M1	MAS, FMA, ARAT, NHPT, BBT, MAL, SIS
Hsu et al. (2013)	22.0 (5.3) days	20.8 (3.6) days	iTBS1200, 80% AMT of paretic	perpendicularly to the scalp	every day for 10 consecutive days	ipsilesional M1	NIHSS, mRS, FMT, ARAT, and affected aMT and MEPs from ECR
El Nahas et al. (2022)	42.74 (52.74)	64.09 (67.07)	600 pulses, supra threshold of paretic	a sham coil	8 sessions	targeted muscles	mAS and eBTD
Sung et al. (2013)	8.1 (1.5)	8.2 (1.6)	600 pulses,80% AMT of nonparetic	a placebo coil	10 sessions, 2 weeks	ipsilesional M1	WOLF, FMA, MRC, Electrophysiological measures probing rMT, maximal amplitude, latency of MEP, and motor map area
Talelli et al. (2012)	17.5 (5.1)	38.5 (57.2)	600 pulses,80% AMT of paretic FDI	rotated 90°, 50% of maximum output	10 working days	ipsilesional M1	9HPT, JTT, grip and pinch-grip dynamometry, VAS
Watanabe et al. (2018)	<7 days	<7 days	600 pulses,80% RMT of nonparetic FDI	10-cm-thick plastic board, conventional rehabilitation therapy	10 days	ipsilesional M1	FMA, SIA, MAS, MEP
Zhang et al. (2022)	63.93 (46.85)	50.86 (29.50)	600 pulse, 70% RMT of nonparetic FDI	same coil with 20% RMT, Robot-Assisted Training	10 sessions	ipsilesional M1	FMA-UE, ARAT, mean velocity of movement, sensorimotor ERD

AMT, Active motor threshold; FDI, First dorsal interosseous; ARAT, the action research arm test; FMA, Fugl-Meyer Assessment; MAS, modified Ashworth scale; BBT, Box and Block test; MTS, Modified Tardieu Scale; SWV, Shear Wave Ultrasound Elastography; CMCT, Central motor conduction time; BI, Barthel Index; VCT, virtual reality-based cycling training; NHPT, the nine hole peg test; MAL, the motor activity log; SIS, Stroke Impact Scale; NIHSS, National Institutes of Health Stroke Scale; mRS, modified Rankin Scale; eBTD, estimated Botulinum toxin dose; WOLF, Wolf Motor Function test; MRC, Medical Research Council; JTT, Jebsen–Taylor Hand Function Test; VAS, visual analog scale; ERD, Event related desynchronization.

et al., 2016; Chen, 2018; Zhang et al., 2022). The likelihood of motor recovery was lower in the chronic phase. Talelli et al. (2012) and Zhang et al. (2022) reported that iTBS did not significantly augment the gains from a retraining protocol for the upper limbs in those with chronic stroke in small sample sizes. However, Ackerley et al. (2016), Chen (2018), and Chen Y. H. et al. (2021) demonstrated that iTBS induced a greater increase in ARAT in the iTBS group than in the control group. A reason for this controversial finding might be that the spontaneous reorganization of chronic stroke is nearing completion, which may limit the induction of neural plasticity and the enhancement of training effects (Volz et al., 2016). Further studies on a larger scale are warranted to confirm this controversial finding.

Regarding iTBS for upper limb muscle tone after stroke, patients' MAS scores improved significantly after iTBS intervention treatment. The results indicated that iTBS significantly reduced spasticity in stroke patients. Our results were partially compatible with those of previous iTBS studies (Chen, 2018; Watanabe et al., 2018; Chen Y. et al., 2021; Chen Y. H. et al., 2021; El Nahas et al., 2022). The postulated pathophysiology of spasticity is that upper motor neuron lesions impair supraspinal inhibitory inputs, leading to increased excitability of alpha and gamma motor neurons and spinal interneurons (Gharooni et al., 2018). iTBS has been found to induce a phenomenon called long-term potentiation (LTP), a process of strengthening synapses between neurons (Huang et al., 2017) and functional connectivity of brain that leads to a reorganization of

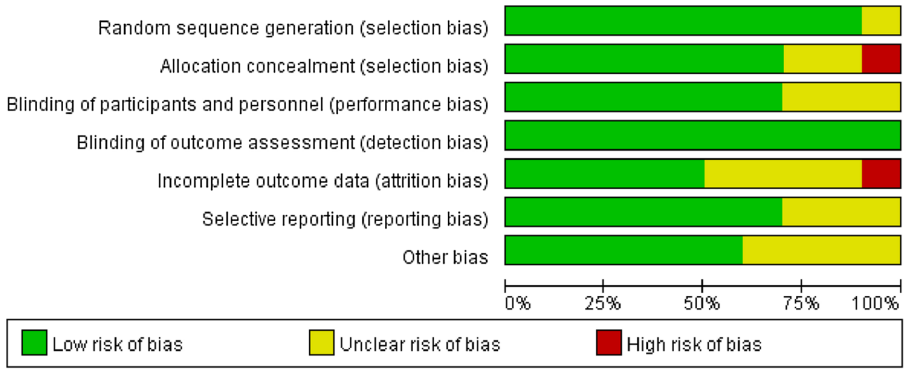

FIGURE 2
Risk of bias graph.

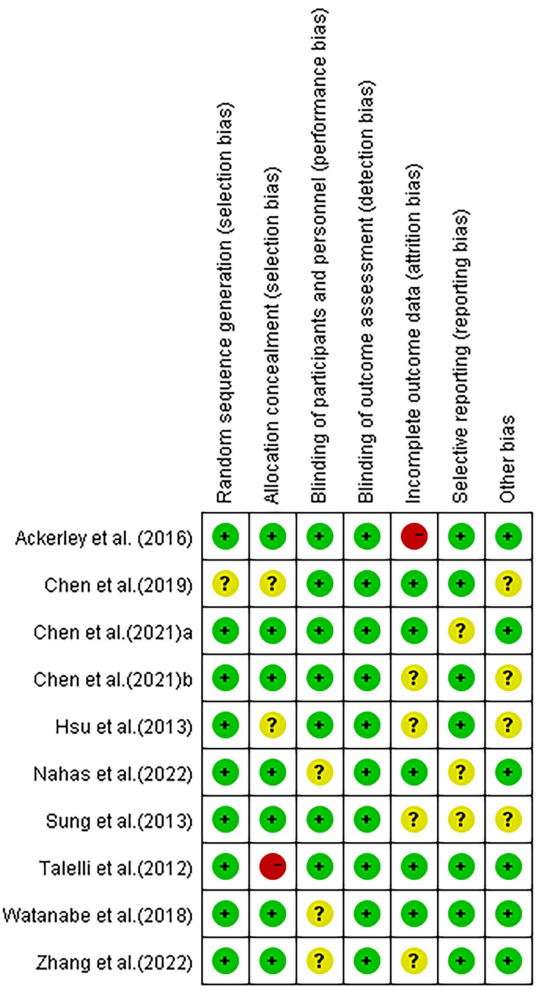

FIGURE 3
Risk of bias summary.

neural pathways (Mori et al., 2010). However, Chen (2018) found no significant difference in corticospinal excitability assessment between the iTBS and sham groups. Further neurophysiological studies are therefore warranted to identify the underlying mechanism.

Regarding iTBS for corticomotor excitability after stroke, no significant differences were found after iTBS intervention treatment. First, the sample size included in the studies was limited. Second, of note, not all the MEPs of stroke patients in the ipsilesional hemisphere could be elicited, especially in severely impaired patients (Ding et al., 2022). The corticomotor excitability among participants could influence the response to iTBS. Using various electrophysiological indicators, Ding et al. (2021) found an increase in interhemispheric functional connectivity and global efficiency using EEG after iTBS intervention. Volz et al. (2016) demonstrated that M1 connectivity with motor areas of the contralesional hemisphere and ipsilesional areas significantly increased using fMRI in the iTBS group (Volz et al., 2016). Third, the heterogeneity in the sample characteristics could contribute to the lack of consistent effects on corticomotor excitability. To acknowledge the limitations and potential sources of heterogeneity, the results must be interpreted with caution.

Regarding iTBS for the ability to perform activities of daily living after stroke, patients' BI scores improved significantly after iTBS intervention treatment, but there were no differences between the groups. Preliminary evidence was not sufficient to support that iTBS could augment the effect of conventional therapy in activities of daily living after 10 administration sessions.

Last but not least, iTBS was well tolerated and no significant adverse events were found in any included studies.

Our review has several limitations that need to be recognized. First, due to the multiple outcomes included in the studies, only a small amount of evidence was available, which caused the limited sample size. Further research and well-designed randomized controlled trials are needed to clarify the effects of iTBS. Second, it is not yet possible to determine the optimal stimulation parameters, location, and patient characteristics for different functional improvements in iTBS intervention. Parameters such as burst frequency, intensity, and duration are being optimized to induce more robust neuroplastic changes. Some studies are experimenting with priming iTBS (Zhang and Fong, 2020) or paired-pulse TMS (Rawji et al., 2021) to explore their potential advantages over traditional iTBS. To date, M1 stimulation has primarily been investigated, and the cerebellum is also considered to be involved in motor adaptation and learning processes (Liao et al., 2021). Finally, the MEP results are usually not recordable in patients with severe motor impairments and

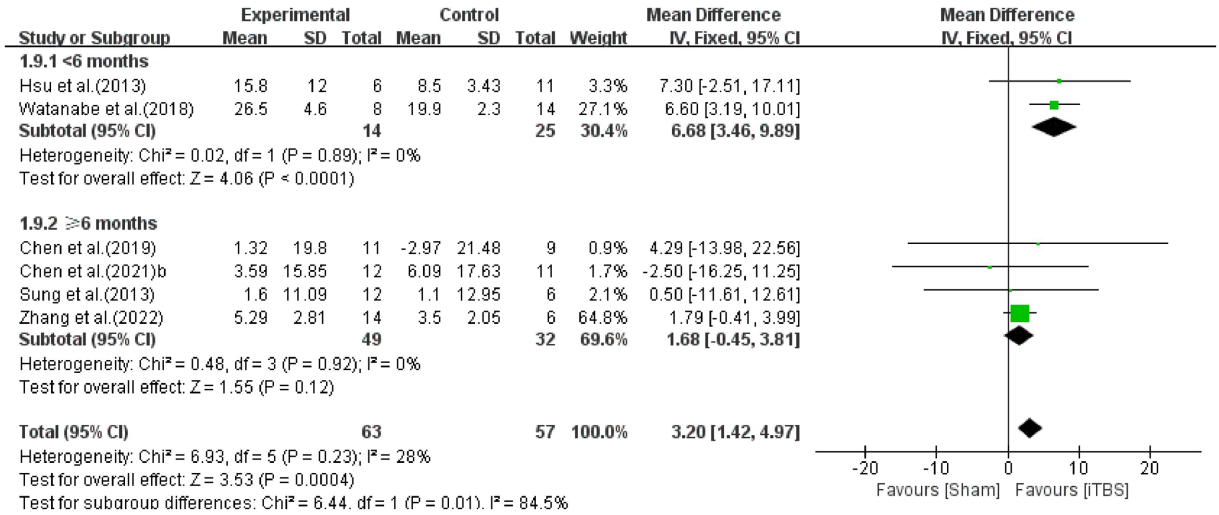

FIGURE 4
Forest plot of the effect of iTBS treatment on FMA.

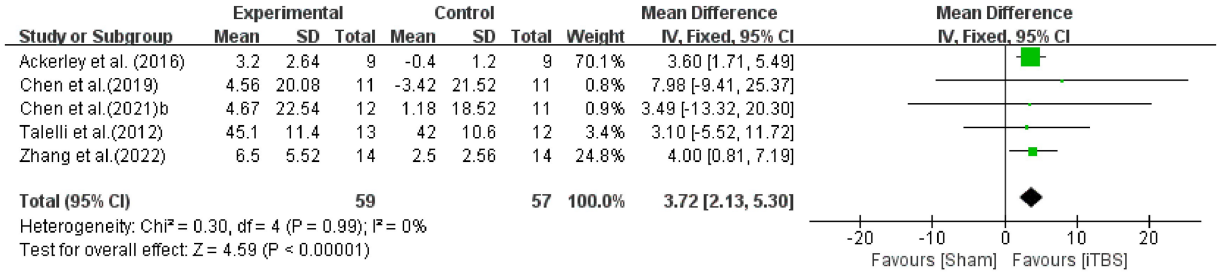

FIGURE 5
Forest plot of the effect of iTBS treatment on ARAT.

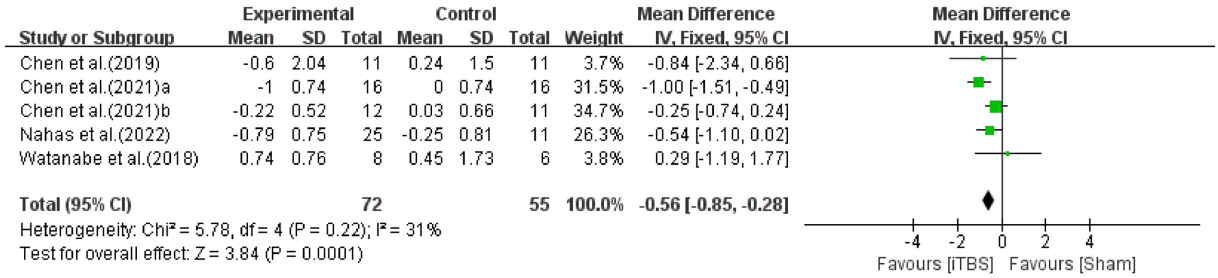

FIGURE 6
Forest plot of the effect of iTBS treatment on MAS.

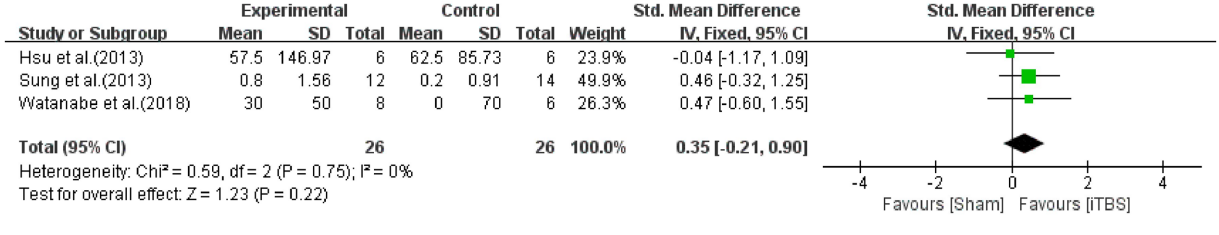

FIGURE 7
Forest plot of the effect of iTBS treatment on MEP of ipsilesional hemisphere.

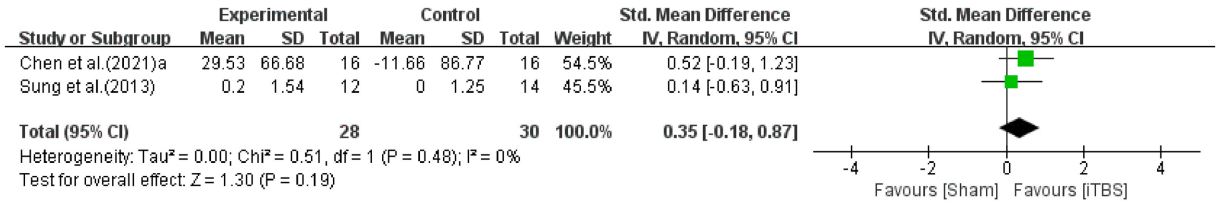

FIGURE 8
Forest plot of the effect of iTBS treatment on MEP of contralesional hemisphere.

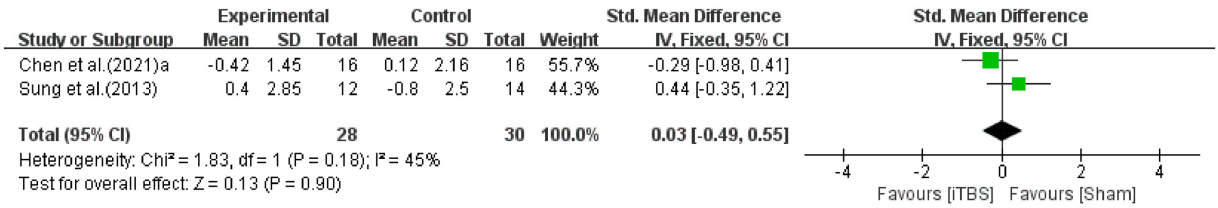

FIGURE 9
Forest plot of the effect of iTBS treatment on the latency of MEP.

in the early stage of stroke. More sensitive and direct methods, such as EEG, fMRI, or fNIRs, could be used to reflect electrophysiological measures and corticomotor excitability. It is crucial to identify patients who are more likely to benefit from iTBS. Advanced neuroimaging and neurophysiological markers are being investigated to predict responders. This will allow more targeted use of iTBS, optimizing resources and enhancing the motor recovery prospects for stroke survivors.

5. Conclusion

The current study systematically reviewed existing research investigating the effects of iTBS on upper limb motor recovery after stroke. Our results showed that iTBS significantly improved motor impairment, functional activities, and muscle tone of the upper limbs, thereby increasing the ability to perform ADL in stroke patients, while no significant differences were found in MEPs. In conclusion, while iTBS is a promising non-invasive brain stimulation as an adjunct to therapy and enhances the therapeutic effect of conventional physical therapy, further studies are needed to investigate the neurophysiological effects.

Data availability statement

The original contributions presented in the study are included in the article/supplementary material, further inquiries can be directed to the corresponding authors.

Author contributions

SC: Writing – original draft, Writing – review & editing. SZ: Writing – review & editing. WY: Writing – review & editing. YC: Writing – review & editing. BW: Writing – review & editing. JC: Writing – review & editing. XL: Writing – review & editing. LX: Writing – review & editing. HH: Writing – review & editing. YZ: Writing – review & editing. LT: Writing – review & editing. WJ: Data curation, Methodology, Supervision, Writing – original draft. XW: Writing – original draft, Data curation, Formal analysis, Methodology. YL: Writing – review & editing. HL: Writing – original draft, Writing – review & editing.

Funding

The author(s) declare financial support was received for the research, authorship, and/or publication of this article. This work was supported by Shenzhen Science and Technology Program (No. GJHZ20190823115412789, JCYJ20210324134401004, JCYJ20190814114207451, and JCYJ20190814112607443); Medical Scientific Research Foundation of Guangdong Province of China (A2023367).

Conflict of interest

The authors declare that the research was conducted in the absence of any commercial or financial relationships that could be construed as a potential conflict of interest.

Publisher's note

All claims expressed in this article are solely those of the authors and do not necessarily represent those of their affiliated organizations, or those of the publisher, the editors and the reviewers. Any product that may be evaluated in this article, or claim that may be made by its manufacturer, is not guaranteed or endorsed by the publisher.

References

Ackerley, S. J., Byblow, W. D., Barber, P. A., MacDonald, H., McIntyre-Robinson, A., and Stinear, C. M. (2016). Primed physical therapy enhances recovery of upper limb function in chronic stroke patients. *Neurorehabil. Neural Repair* 30, 339–348. doi: 10.1177/1545968315595285

Ackerley, S. J., Stinear, C. M., Barber, P. A., and Byblow, W. D. (2014). Priming sensorimotor cortex to enhance task-specific training after subcortical stroke. *Clin. Neurophysiol.* 125, 1451–1458. doi: 10.1016/j.clinph.2013.11.020

Cabral, D. F., Fried, P., Koch, S., Rice, J., Rundek, T., Pascual-Leone, A., et al. (2022). Efficacy of mechanisms of neuroplasticity after a stroke. *Restor. Neurol. Neurosci.* 40, 73–84. doi: 10.3233/RNN-211227

Chen, Y. (2018). Intermittent theta burst stimulation enhances upper limb motor function in patients with chronic stroke: a randomized controlled trial. *Ann. Phys. Rehabil. Med.* 61:e26. doi: 10.1016/j.rehab.2018.05.056

Chen, Y. H., Chen, C. L., Huang, Y. Z., Chen, H. C., Chen, C. Y., Wu, C. Y., et al. (2021). Augmented efficacy of intermittent theta burst stimulation on the virtual reality-based cycling training for upper limb function in patients with stroke: a double-blinded, randomized controlled trial. *J. Neuroeng. Rehabil.* 18:91. doi: 10.1186/s12984-021-00885-5

Chen, Y., Wei, Q. C., Zhang, M. Z., Xie, Y. J., Liao, L. Y., Tan, H. X., et al. (2021). Cerebellar intermittent Theta-burst stimulation reduces upper limb spasticity after subacute stroke: a randomized controlled trial. *Front. Neural Circuits* 15:15. doi: 10.3389/fncir.2021.655502

Desowska, A., and Turner, D. L. (2019). Dynamics of brain connectivity after stroke. *Rev. Neurosci.* 30, 605–623. doi: 10.1515/revneuro-2018-0082

Ding, Q., Chen, S., Chen, J., Zhang, S., Peng, Y., Chen, Y., et al. (2022). Intermittent Theta burst stimulation increases natural oscillatory frequency in Ipsilesional motor cortex post-stroke: a transcranial magnetic stimulation and electroencephalography study. *Front. Aging Neurosci.* 14:818340. doi: 10.3389/fnagi.2022.818340

Ding, Q., Zhang, S., Chen, S., Chen, J., Li, X., Chen, J., et al. (2021). The effects of intermittent Theta burst stimulation on functional brain network following stroke: an electroencephalography study. *Front. Neurosci.* 15:755709. doi: 10.3389/fnins.2021.755709

El Nahas, N., Kenawy, F. F., Abd Eldayem, E. H., Roushdy, T. M., Helmy, S. M., Akl, A. Z., et al. (2022). Peripheral magnetic theta burst stimulation to muscles can effectively reduce spasticity: a randomized controlled trial. *J. Neuroeng. Rehabil.* 19:5. doi: 10.1186/s12984-022-00985-w

Feigin, V. L., Forouzanfar, M. H., Krishnamurthi, R., Mensah, G. A., Connor, M., Bennett, D. A., et al. (2014). Global and regional burden of stroke during 1990-2010: findings from the global burden of disease study 2010. *Lancet* 383, 245–255. doi: 10.1016/s0140-6736(13)61953-4

Feigin, V. L., Norrving, B., and Mensah, G. A. (2017). Global burden of stroke. *Circ. Res.* 120, 439–448. doi: 10.1161/CIRCRESAHA.116.308413

Fugl-Meyer, A. R., Jaasko, L., Leyman, I., Olsson, S., and Steglind, S. (1975). The post-stroke hemiplegic patient. 1. A method for evaluation of physical performance. *Scand. J. Rehabil. Med.* 7, 13–31. doi: 10.2340/1650197771331

Gharooni, A. A., Nair, K. P. S., Hawkins, D., Scivill, I., Hind, D., and Hariharan, R. (2018). Intermittent theta-burst stimulation for upper-limb dysfunction and spasticity in spinal cord injury: a single-blind randomized feasibility study. *Spinal Cord* 56, 762–768. doi: 10.1038/s41393-018-0152-5

Grefkes, C., and Ward, N. S. (2014). Cortical reorganization after stroke: how much and how functional? *Neuroscientist* 20, 56–70. doi: 10.1177/1073858413491147

Hsu, Y.-F., Huang, Y.-Z., Lin, Y.-Y., Tang, C.-W., Liao, K.-K., Lee, P.-L., et al. (2013). Intermittent theta burst stimulation over ipsilesional primary motor cortex of subacute ischemic stroke patients: a pilot study. *Brain Stimul.* 6, 166–174. doi: 10.1016/j.brs.2012.04.007

Huang, Y. Z., Edwards, M. J., Rounis, E., Bhatia, K. P., and Rothwell, J. C. (2005). Theta burst stimulation of the human motor cortex. *Neuron* 45, 201–206. doi: 10.1016/j.neuron.2004.12.033

Huang, Y. Z., Lu, M. K., Antal, A., Classen, J., Nitsche, M., Ziemann, U., et al. (2017). Plasticity induced by non-invasive transcranial brain stimulation: a position paper. *Clin. Neurophysiol.* 128, 2318–2329. doi: 10.1016/j.clinph.2017.09.007

Koch, G., Mori, F., Marconi, B., Codecà, C., Pecchioli, C., Salerno, S., et al. (2008). Changes in intracortical circuits of the human motor cortex following theta burst stimulation of the lateral cerebellum. *Clin. Neurophysiol.* 119, 2559–2569. doi: 10.1016/j.clinph.2008.08.008

Lang, C. E., and Schieber, M. H. (2004). Reduced muscle selectivity during individuated finger movements in humans after damage to the motor cortex or corticospinal tract. *J. Neurophysiol.* 91, 1722–1733. doi: 10.1152/jn.00805.2003

Li, T., Zeng, X., Lin, L., Xian, T., and Chen, Z. (2020). Effects of repetitive transcranial magnetic stimulation with different frequencies on post-stroke aphasia: a PRISMA-compliant meta-analysis. *Medicine (Baltimore)* 99:e20439. doi: 10.1097/MD.0000000000020439

Liao, L. Y., Xie, Y. J., Chen, Y., and Gao, Q. (2021). Cerebellar Theta-burst stimulation combined with physiotherapy in subacute and chronic stroke patients: a pilot randomized controlled trial. *Neurorehabil. Neural Repair* 35, 23–32. doi: 10.1177/1545968320971735

Maulden, S. A., Gassaway, J., Horn, S. D., Smout, R. J., and DeJong, G. (2005). Timing of initiation of rehabilitation after stroke. *Arch. Phys. Med. Rehabil.* 86, 34–S40. doi: 10.1016/j.apmr.2005.08.119

McDonnell, M. N., and Stinear, C. M. (2017). TMS measures of motor cortex function after stroke: a meta-analysis. *Brain Stimul.* 10, 721–734. doi: 10.1016/j.brs.2017.03.008

Meseguer-Henarejos, A. B., Sanchez-Meca, J., Lopez-Pina, J. A., and Carles-Hernandez, R. (2018). Inter- and intra-rater reliability of the modified Ashworth scale: a systematic review and meta-analysis. *Eur. J. Phys. Rehabil. Med.* 54, 576–590. doi: 10.23736/S1973-9087.17.04796-7

Moher, D., Shamseer, L., Clarke, M., Ghersi, D., Liberati, A., Petticrew, M., et al. (2015). Preferred reporting items for systematic review and meta-analysis protocols (PRISMA-P) 2015 statement. *Syst. Rev.* 4:1. doi: 10.1186/2046-4053-4-1

Mori, F., Codeca, C., Kusayanagi, H., Monteleone, F., Boffa, L., Rimano, A., et al. (2010). Effects of intermittent theta burst stimulation on spasticity in patients with multiple sclerosis. *Eur. J. Neurol.* 17, 295–300. doi: 10.1111/j.1468-1331.2009.02806.x

Murphy, T. H., and Corbett, D. (2009). Plasticity during stroke recovery: from synapse to behaviour. *Nat. Rev. Neurosci.* 10, 861–872. doi: 10.1038/nrn2735

Rawji, V., Kaczmarczyk, I., Rocchi, L., Fong, P. Y., Rothwell, J. C., and Sharma, N. (2021). Preconditioning stimulus intensity alters paired-pulse TMS evoked potentials. *Brain Sci.* 11:326. doi: 10.3390/brainsci11030326

Rossini, P. M., Barker, A. T., Berardelli, A., Caramia, M. D., Caruso, G., Cracco, R. Q., et al. (1994). Non-invasive electrical and magnetic stimulation of the brain, spinal cord and roots: basic principles and procedures for routine clinical application. Report of an IFCN committee. *Electroencephalogr. Clin. Neurophysiol.* 91, 79–92. doi: 10.1016/0013-4694(94)90029-9

Silveira, L., Silva, J. M. D., Soler, J. M. P., Sun, C. Y. L., Tanaka, C., and Fu, C. (2018). Assessing functional status after intensive care unit stay: the Barthel index and the Katz index. *Int. J. Qual. Health Care* 30, 265–270. doi: 10.1093/intqhc/mzx203

Sung, W. H., Wang, C.-P., Chou, C.-L., Chen, Y.-C., Chang, Y.-C., and Tsai, P.-Y. (2013). Efficacy of coupling inhibitory and facilitatory repetitive transcranial magnetic stimulation to enhance motor recovery in hemiplegic stroke patients. *Stroke* 44, 1375–1382. doi: 10.1161/strokeaha.111.000522

Talelli, P., Greenwood, R. J., and Rothwell, J. C. (2007). Exploring Theta burst stimulation as an intervention to improve motor recovery in chronic stroke. *Clin. Neurophysiol.* 118, 333–342. doi: 10.1016/j.clinph.2006.10.014

Talelli, P., Wallace, A., Dileone, M., Hoad, D., Cheeran, B., Oliver, R., et al. (2012). Theta burst stimulation in the rehabilitation of the upper limb: A semirandomized, placebo-controlled trial in chronic stroke patients. *Neurorehabil. Neural Repair* 26, 976–987. doi: 10.1177/1545968312437940

Volz, L. J., Rehme, A. K., Michely, J., Nettekoven, C., Eickhoff, S. B., and Fink, G. R. (2016). Shaping early reorganization of neural networks promotes motor function after stroke. *Cereb. Cortex.* 26, 2882–2894. doi: 10.1093/cercor/bhw034

Watanabe, K., Kudo, Y., Sugawara, E., Nakamizo, T., Amari, K., Takahashi, K., et al. (2018). Comparative study of ipsilesional and contralesional repetitive transcranial magnetic stimulations for acute infarction. *J. Neurol. Sci.* 384, 10–14. doi: 10.1016/j.jns.2017.11.001

Zhang, J. J., Bai, Z., and Fong, K. N. K. (2022). Priming intermittent Theta burst stimulation for Hemiparetic upper limb after stroke: a randomized controlled trial. *Stroke* 53, 2171–2181. doi: 10.1161/STROKEAHA.121.037870

Zhang, J. J., and Fong, K. N. K. (2020). Effects of priming intermittent theta burst stimulation on upper limb motor recovery after stroke: study protocol for a proof-of-concept randomised controlled trial. *BMJ Open* 10:e035348. doi: 10.1136/bmjopen-2019-035348

frontiers | Frontiers in Neuroscience

TYPE Original Research
PUBLISHED 17 October 2023
DOI 10.3389/fnins.2023.1247290

OPEN ACCESS

EDITED BY
Gahangir Hossain,
University of North Texas, United States

REVIEWED BY
Ali Jahan,
Tabriz University of Medical Sciences, Iran
Luke Tait,
Cardiff University, United Kingdom

*CORRESPONDENCE
Hanli Liu
✉ hanli@uta.edu

RECEIVED 25 June 2023
ACCEPTED 25 September 2023
PUBLISHED 17 October 2023

CITATION
Truong NCD, Wang X and Liu H (2023) Temporal and spectral analyses of EEG microstate reveals neural effects of transcranial photobiomodulation on the resting brain. *Front. Neurosci.* 17:1247290. doi: 10.3389/fnins.2023.1247290

Temporal and spectral analyses of EEG microstate reveals neural effects of transcranial photobiomodulation on the resting brain

Nghi Cong Dung Truong, Xinlong Wang and Hanli Liu*

Department of Bioengineering, University of Texas at Arlington, Arlington, TX, United States

Introduction: The quantification of electroencephalography (EEG) microstates is an effective method for analyzing synchronous neural firing and assessing the temporal dynamics of the resting state of the human brain. Transcranial photobiomodulation (tPBM) is a safe and effective modality to improve human cognition. However, it is unclear how prefrontal tPBM neuromodulates EEG microstates both temporally and spectrally.

Methods: 64-channel EEG was recorded from 45 healthy subjects in both 8-min active and sham tPBM sessions, using a 1064-nm laser applied to the right forehead of the subjects. After EEG data preprocessing, time-domain EEG microstate analysis was performed to obtain four microstate classes for both tPBM and sham sessions throughout the pre-, during-, and post-stimulation periods, followed by extraction of the respective microstate parameters. Moreover, frequency-domain analysis was performed by combining multivariate empirical mode decomposition with the Hilbert-Huang transform.

Results: Statistical analyses revealed that tPBM resulted in (1) a significant increase in the occurrence of microstates A and D and a significant decrease in the contribution of microstate C, (2) a substantial increase in the transition probabilities between microstates A and D, and (3) a substantial increase in the alpha power of microstate D.

Discussion: These findings confirm the neurophysiological effects of tPBM on EEG microstates of the resting brain, particularly in class D, which represents brain activation across the frontal and parietal regions. This study helps to better understand tPBM-induced dynamic alterations in EEG microstates that may be linked to the tPBM mechanism of action for the enhancement of human cognition.

KEYWORDS

transcranial photobiomodulation (tPBM), electroencephalogram (EEG), EEG microstate, empirical mode decomposition, Hilbert-Huang transform

1. Introduction

Over the past decade, photobiomodulation (PBM) has attracted substantial interest as a practical method for treating a variety of pain and/or infections using low-dose red to near-infrared (630–1,100 nm) light. Examples of PBM applications include pain alleviation (Fulop et al., 2010) and wound healing (Mester et al., 1971; Conlan et al., 1996; Yasukawa et al., 2007; Peplow et al., 2010). Transcranial PBM (tPBM), which refers to PBM administered to the cerebral cortex, has also been proven to boost human cognition (Eells et al., 2004; Barrett and

Gonzalez-Lima, 2013; Holmes et al., 2019; Truong et al., 2022) including attentional performance (Jahan et al., 2019) and to be a treatment for traumatic brain injury (Choi et al., 2012; Figueiro Longo et al., 2020), Alzheimer's disease (Grillo et al., 2013; Nizamutdinov et al., 2021), and Parkinson's disease (Quirk et al., 2012; Liebert et al., 2021). A recent, comprehensive study by Zhao et al. reported significant enhancements in visual working memory capacity in healthy humans through four experiments using two separate laser wavelengths (850 and 1,064 nm) and two stimulation sites (left and right forehead; Zhao et al., 2022).

The mechanism underlying tPBM has been proposed to involve cytochrome c oxidase (CCO), a crucial component in mitochondria responsible for energy generation. The photochemical reactions of CCO initiate a cascade of biochemical events, which were believed to enhance cellular energy production, promote neuronal metabolism, and modulate neurovascular coupling (Rojas et al., 2012; Lee et al., 2017). To better understand the neurophysiological effects of tPBM on the human brain, different imaging modalities have been simultaneously employed, including electroencephalography (EEG; Wang et al., 2019; Ghaderi et al., 2021; Shahdadian et al., 2022), functional magnetic resonance imaging (fMRI; Vargas et al., 2017; Dmochowski et al., 2020), broadband near-infrared spectroscopy (bbNIRS; Tian et al., 2016; Wang et al., 2017; Pruitt et al., 2020; Wang et al., 2022a), and functional near-infrared spectroscopy (fNIRS; Holmes et al., 2019; Truong et al., 2022).

EEG is a widely used and effective measurement tool for noninvasive monitoring of human neurophysiological activity in neuroscience research and clinical applications. In a subset of EEG research, EEG microstate analysis is an established method for investigating brain dynamics in the resting state (Lehmann et al., 1987). EEG microstates are defined as global patterns of scalp potential topographies that dynamically alter over time in an ordered manner. Specifically, spontaneous EEG activity during the resting state can be described by a limited number of EEG topographical maps that remain stable for a short period (60–120 ms). These specific global scalp maps were obtained by spatial clustering of whole scalp topographies without considering the polarity inversion (Pascual-Marqui et al., 1995; Koenig et al., 1999; Koenig and Brandeis, 2016). Briefly, scalp topographies with high spatial correlation independent of polarity were first clustered into one representative topographical map, forming a class of microstates (Michel and Koenig, 2018). A dynamic train or alteration of the microstates is then found by fitting the template maps (or classes) back to the temporal data.

Recent publications have demonstrated that tPBM enables significant alterations in EEG spectral power across the human cortex (Zomorrodi et al., 2019; Wang et al., 2021) and in functional connectivity across several resting-state brain networks (Zomorrodi et al., 2019; Ghaderi et al., 2021; Shahdadian et al., 2022). However, previous EEG-based studies have not investigated the influence of tPBM on the temporal dynamics of the human brain. To the best of our knowledge, only a short conference abstract by Zomorrodi et al. (2021) has reported the effects of tPBM on the temporal dynamics of the human brain. Therefore, it remains unclear how tPBM dynamically modulates the human brain. Accordingly, this study addressed two key questions: can tPBM modulate EEG microstates and their topographical spectral parameters? If so, which temporal and spectral parameters of microstates would tPBM modulate significantly? We hypothesized that tPBM significantly affects the parameters of certain microstate classes.

This study shared the 64-channel EEG data reported earlier (Wang et al., 2021; Shahdadian et al., 2022; Wang et al., 2022b), comprising 45 healthy subjects undergoing both active and sham 8-min tPBM using a 1,064-nm laser applied to the right forehead. The novelty of this study differs from our prior work on several key analysis methodologies and findings. For the first time, EEG microstate analysis (Michel and Koenig, 2018) has been applied to investigate brain dynamics under tPBM. Different temporal microstate parameters were extracted and compared to assess the effects of tPBM on temporal dynamics in the human brain. In addition, EEG microstate spectral analysis was performed using multivariate empirical mode decomposition (MEMD; Lang et al., 2018) and the Hilbert-Huang transform (HHT; Huang et al., 1998; Huang and Wu, 2008). This newly developed frequency-domain analysis enabled us to quantify the alteration in the EEG power of microstate classes over different experimental periods for both tPBM and sham sessions. By the end of this study, our statistical results revealed significant changes in the occurrence, contribution, and transition probabilities of different microstate classes as well as alterations in frequency-band-specific microstate power, which affirmed our hypothesis.

2. Materials and methods

2.1. Participants

We recruited 49 healthy human subjects (29 males, 19 females, 26 ± 8.8 years of age) from the University of Texas at Arlington local community to participate in this study. Participants had to be satisfied the following criteria: (1) no psychiatric disorder or neurological condition, (2) no severe brain injury, (3) no history of violence or imprisonment, (4) no current intake of any psychotropic medicine, (5) no smoking or excessive alcohol consumption, (6) had not been diagnosed with diabetes, as required by the laser's manufacturer (Cell Gen Therapeutics LLC, Dallas, Texas). Due to observed fatigue or drowsiness during EEG measurements, four subjects were excluded from the dataset, leaving 45 remaining participants in the subsequent data analysis. The experimental protocol was approved by the Institutional Review Board of the University of Texas at Arlington. Prior to all measures, each participant's informed consent was obtained.

2.2. Experimental procedures

We employed a 1,064-nm continuous-wave (CW) laser with FDA clearance (Model CG-5000 Laser, Cell Gen Therapeutics LLC, Dallas, Texas) for our noninvasive tPBM experiment (Figure 1A). The laser had a 13.6 cm^2 irradiation area, and its power was set at 3.4 W. Using this laser's output, a total energy dose of 1,632 J was delivered throughout an 8-min tPBM session (3.4 W × 60 s/min × 8 min = 1,632 J), resulting in a laser power density of 0.25 W/cm^2. The light was delivered over the right frontopolar region close to the Fp2 site without physical contact (Figure 1B). For the sham condition, the laser device was also on to ensure subjects heard the device operation sound and were unaware of being in the sham

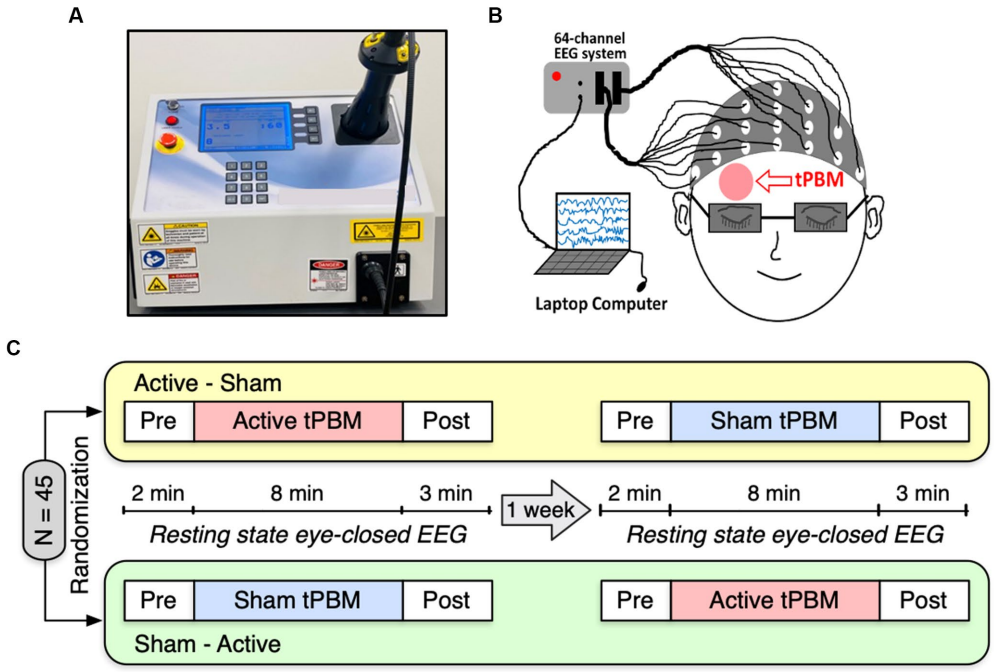

FIGURE 1
(A) A photograph of our 1,064-nm laser used for the study. **(B)** A cartoon showing the EEG setup and the tPBM site on the participant's right forehead. **(C)** Schematic diagram of the experimental protocol. A total of 45 subjects were randomly divided into two groups: active-sham or sham-active stimulation. Each experiment included EEG recordings of a 2-min baseline, an 8-min active or sham tPBM, and a 3-min recovery period. A minimum 1-week waiting period between two visits was required to avoid potential effects from active tPBM.

condition. However, the laser strength was reduced to 0.1 W for sham stimulation, and a black cap was placed in front of the laser aperture to obstruct the light further. Participants would not be aware of the cap as it was placed after they closed their eyes. Throughout the experiment, participants were required to wear a pair of laser protection goggles.

Figure 1C depicts the experimental protocol. Each subject was assigned a random order for the two study sessions: active tPBM and sham tPBM. In order to prevent any carry-over effects, two visits had to be separated by at least 1 week. Subjects were instructed to sit comfortably with their eyes closed during EEG acquisition. The resting state EEG data were recorded for 2 min of pre-stimulation, 8 min of active/sham stimulation, and 3 min of post-stimulation. We used a Biosemi (64-channel) 10–10 EEG equipment to acquire the EEG data (Figure 1B). The electrical gel was applied to each electrode prior to each EEG measurement in order to boost conductivity and the signal-to-noise ratio of the collected data.

2.3. EEG data analysis

2.3.1. EEG data preprocessing

We employed the EEGLAB toolbox (Delorme and Makeig, 2004) to preprocess 64-channel EEG data. Since either 256 or 512 Hz was used to acquire the EEG data, the 512 Hz data were first down-sampled to 256 Hz to ensure consistency. The EEG signals underwent bandpass filtering between 1 and 70 Hz using the EEGLAB "filtfilt" function. Additionally, a notch filter at 60 Hz was employed to remove line noise. Re-referencing was performed by subtracting the average voltage signals across all 64 electrodes from each of the EEG time series. The Independent Component Analysis (ICA) technique (Campos Viola et al., 2009) was applied to eliminate artifacts caused by eye blinks, eye movements, or jaw clenches. ICA components were manually inspected, and the noisy components corresponding to the noise and artifacts were excluded. Subsequently, the artifact-free EEG time series were split into four temporal segments to better characterize the EEG microstates in response to tPBM/sham stimulation: (1) a 2-min pre-stimulation (Pre) period, (2) the first 4-min temporal segment during active/sham tPBM (Stim1), (3) the last 4-min segment of active/sham tPBM (Stim2), and (4) a 3-min post-stimulation (Post) period.

2.3.2. EEG microstate analysis in the time domain

The EEG microstate analysis in the time domain was performed following the procedure presented in Koenig et al. (1999) and Michel and Koenig (2018). We employed a Matlab-based microstate toolbox (Koenig, 2017) compatible with EEGLAB (Delorme and Makeig, 2004) to compute EEG microstates. The main steps of the time-domain EEG microstate analysis are depicted by the gray-shaded left column in Figure 2 (i.e., Figures 2A–D) with 4 steps.

The principle of microstate analysis consists of finding a set of the most dominant topographical maps representing different crucial brain states and then fitting these maps back to the EEG data. The global field power (GFP) was calculated for each sample time as follows:

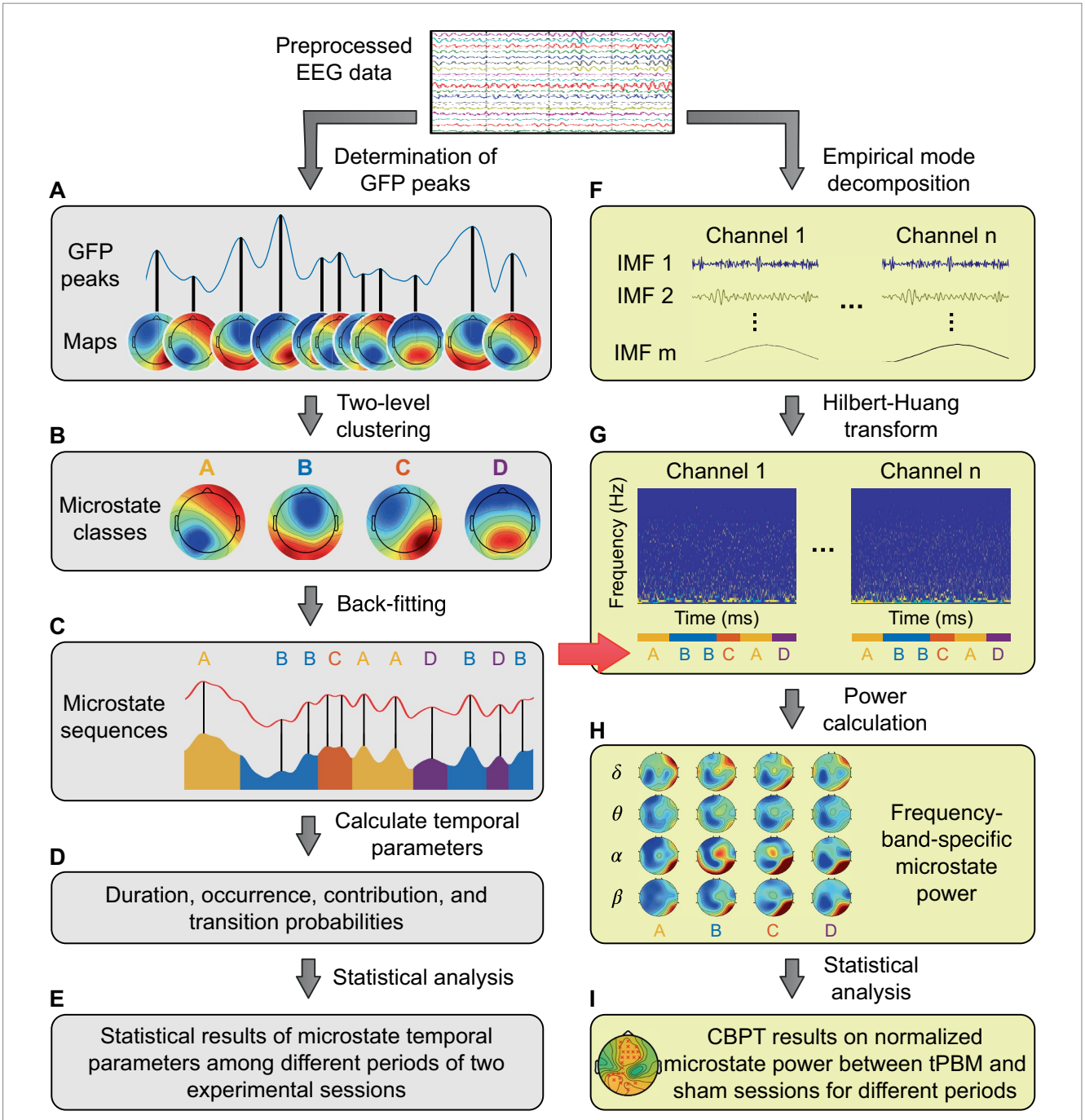

FIGURE 2
A flowchart for EEG microstate analysis. Panels **(A–D)** show steps of the time-domain EEG microstate analysis; Panels **(F–H)** show steps of the frequency-domain EEG microstate analysis. δ: delta band (0.5–4 Hz); θ: theta band (4–8 Hz); α: alpha band (8–13 Hz); β: beta band (13–30 Hz). Panels **(E,I)** represent the process for statistical analysis in the time and frequency domain, respectively.

$$\mathrm{GFP}(t) = \sqrt{\frac{\sum_{i=1}^{N} v_i(t)^2}{N}} \quad (1)$$

where N is the number of EEG electrodes (N = 64 in this study), and $v_i(t)$ is the voltage of electrode i at time t. The time-resolved GFP(t) reflects the global power alteration of the EEG signal at time t; the GFP peaks correspond to the moments of high global neuronal synchronization (Skrandies, 2007). It is known that the scalp topographies around the peaks remain quasi-stable (Lehmann and Skrandies, 1980; Skrandies, 1989; Koenig et al., 2002; Koenig and Brandeis, 2016; Michel and Koenig, 2018).

In step 1 (Figure 2A), we determined the scalp topographical maps at the GFP peaks for each participant within each experimental temporal period for both tPBM and sham sessions separately.

In step 2 (Figure 2B), we performed two-level clustering to identify global microstates. The first level of clustering was performed to identify the individual-level EEG microstates for each experimental segment (Pre, Stim1, Stim2, and Post), separately for tPBM and sham sessions. All topographical maps acquired per subject per each

temporal segment were clustered into 4 maps using the k-means clustering algorithm (Koenig et al., 2002; Murray et al., 2008). These 4 clustered maps present dominant microstate classes, which have been commonly used and reported in numerous EEG microstates studies. Since the individual microstate classes obtained by the k-means clustering had no particular order and thus were potentially mismatched between participants (Koenig et al., 2002; Koenig, 2017), the second level of clustering was performed on EEG microstates of all subjects for each experimental period (Koenig et al., 1999), separately for the tPBM or sham session. The outcome of this clustering was the group-level microstate classes for each experimental period (Pre, Stim1, Stim2, and Post), separately for the tPBM or sham session. Finally, a permutation-based clustering step was employed to identify the "global" microstate classes based on the two groups of 4 microstate classes from the tPBM and sham sessions, serving as representative microstates for all experimental periods of both tPBM and sham sessions.

In step 3 (Figure 2C), the global microstate classes were fitted back to each subject's temporal EEG data to assign a label of one microstate class to every EEG data instant. The assigned microstate class was chosen as the one that had the highest spatial correlation with the scalp topography of the corresponding EEG data instant (Brodbeck et al., 2012; Michel and Koenig, 2018). The spatial correlation was computed using Pearson's correlation coefficient (Brandeis et al., 1992) defined as follows:

$$C = \frac{\sum_{i=1}^{N}(u_i \cdot v_i)}{\sqrt{\sum_{i=1}^{N} u_i^2} \cdot \sqrt{\sum_{i=1}^{N} v_i^2}} \quad (2)$$

where N is the number of electrodes, u_i and v_i are the voltage of electrode i of the two topographical maps. At the end of Step 3, the labeled microstate time series for all subjects were obtained in both tPBM and sham sessions (Figure 2C).

In Step 4 (Figure 2D), the resulting microstate time series were used to compute four temporal microstate parameters as follows:

- Duration: the average duration that the microstate class is continuously presented (in ms). The microstate duration reflects the average time that the brain sustains synchronized activities.
- Occurrence: the number of occurrences of a microstate class divided by the total duration (in s) of the analyzed EEG data. The occurrence parameter reveals how frequently a microstate class occurs over time (Khanna et al., 2014; Michel and Koenig, 2018).
- Contribution: the proportion of the total occurrence duration of one microstate over the whole analysis time. The contribution parameter indicates the time coverage of each microstate class relative to other classes (Lehmann et al., 2005).
- Transition probability: proportion of the number of transitions from one microstate class to another over the number of all transitions occurring during the analysis period (Lehmann et al., 2005; Khanna et al., 2015).

2.3.3. EEG microstate analysis in the frequency domain

In parallel, we performed EEG microstate analysis in the frequency domain, following the framework proposed in Li et al. (2021). Because conventional time-frequency spectral analysis that employs Fourier or wavelet transform usually fails to analyze EEG signals with a short temporal length [60–120 ms for the case of EEG microstates (Pascual-Marqui et al., 1995; Mandic et al., 2013)], many studies have employed the Hilbert transform in microstate analysis because of its feasibility in analyzing short-length signals (Mandic et al., 2013; Milz et al., 2017; Comsa et al., 2019). Thus, following the methodology proposed in Shi et al. (2020) and Li et al. (2021), we performed a spectral analysis of EEG microstates (Shi et al., 2020) by employing a multivariate empirical mode decomposition (MEMD) algorithm incorporated with the Hilbert-Huang transform (HHT; Huang et al., 1998; Huang and Wu, 2008). The procedure of EEG microstate analysis in the frequency domain is depicted by the yellow-shaded right column in Figure 2 (i.e., Figures 2F–H) in 3 steps, as briefly described below. Detailed mathematical expressions are provided in Supplementary material.

First, MEMD was performed to decompose N-channel EEG signals into a set of intrinsic mode functions (IMFs) that represent different oscillatory levels embedded in the original signals. MEMD is an extended method of EMD, the latter of which is a data decomposition method for non-linear and non-stationary signals (Huang et al., 1998). EMD enables any complicated dataset to be expressed in a finite number of IMFs. MEMD was developed by taking signal projections along different directions in N-dimensional spaces, a generalization of EMD (Rehman and Mandic, 2010). This step is illustrated in Figure 2F.

Next, HHT was performed on each of IMFs to estimate the time-frequency Hilbert spectra of all EEG channels and to facilitate the sharp identification of imbedded structures. In addition, the EEG microstate sequences obtained by time-domain analysis (Figure 2C) were imported to generate the segmented Hilbert spectra for each EEG microstate (Figure 2G). Given that the Hilbert spectrum is written as $H^n(\omega, t)$ for the EEG data from the nth channel in the frequency ω at time t, the power for microstate m at the nth channel in the frequency band (<fb>) would be equal to:

$$P_{\langle fb \rangle}^{mn} = \frac{1}{\Delta\omega}\frac{1}{L_m}\iint_{\Delta\omega L_m} H^n(\omega,t)^2\, dtd\omega \quad (3)$$

where L_m is the total temporal length of the microstate m, and $\Delta\omega$ is the range of the frequency band <fb>. Specifically, <fb> covers delta band (δ: 0.5–4 Hz), theta band (θ: 4–8 Hz), alpha band (α: 8–13 Hz), and beta band (β: 13–30 Hz). This step is depictured and marked in Figure 2H.

Finally, the percentage changes of the power for microstate m during tPBM/sham and post-tPBM/sham periods with respect to the pre-stimulation (baseline) power were defined as follows:

$$\Delta P_{\langle seg \rangle,\langle fb \rangle}^{mn} = \frac{P_{\langle seg \rangle,\langle fb \rangle}^{mn} - P_{pre,\langle fb \rangle}^{mn}}{P_{pre,\langle fb \rangle}^{mn}} \times 100\% \quad (4)$$

where <seg> covers three temporal segments (Stim1, Stim2, and Post). These percentage changes were calculated for both tPBM and sham sessions.

2.3.4. Statistical analysis

For the time-domain microstate analysis (Figure 2E), we performed a one-way repeated-measures ANOVA on the microstate temporal results of the two experimental sessions (tPBM and sham) to test the period effects (Pre, Stim1, Stim2, Post). We verified the normality and homoscedasticity characteristics of the data to ensure that ANOVA usage was appropriate. Post-hoc pairwise comparisons were further carried out using Tukey's adjustment for multiple variable comparisons to assess significant differences across 4 experimental periods (Pre, Stim1, Stim2, Post).

For the frequency-domain microstate analysis (Figure 2I), we employed the cluster-based permutation test (CBPT; Maris and Oostenveld, 2007; Oostenveld et al., 2011; Pellegrino et al., 2016; Benavides-Varela and Gervain, 2017) to compare the normalized frequency-specific power of four microstate classes between tPBM and sham sessions. This analysis enabled us to assess the significant differences in microstate power between tPBM and sham sessions across these four microstate classes.

3. Results

3.1. Alterations of EEG microstate topographies induced by tPBM

The four most dominant EEG microstate classes (A, B, C, and D) were identified under different conditions, and the respective microstate topographies are presented in Figure 3. Specifically, Figure 3A shows four microstate topographies derived from all the temporal segments and two tPBM/sham sessions. Figures 3B,C illustrate the time-dependent topographies under sham and tPBM interventions across all four microstate classes. These figures clearly display that microstate A exhibited a left occipital to right frontal polarity orientation, while microstate B presented a right occipital to left frontal orientation. Microstates C and D revealed roughly symmetric occipital to frontal and central to frontal polarity patterns, respectively.

3.2. Alterations of EEG microstate parameters induced by tPBM

As mentioned in Section 2, the labeled microstate time series were obtained by fitting the global microstate classes to each subject's EEG data (Figure 2C). By using the microstate sequences, we computed several key temporal microstate parameters of the four experimental periods (Pre, Stim1, Stim2, and Post) for the tPBM and sham sessions. One-way repeated-measures ANOVA (rmANOVA) enabled us to reveal significant tPBM-induced changes in two key microstate temporal parameters throughout different experimental periods or segments for both tPBM and sham sessions.

Figures 4A,B depict the occurrence (per sec) and contribution (in %) of the four microstate classes throughout the different experimental periods (Pre, Stim1, Stim2, and Post) of the tPBM and sham sessions. The post-hoc rmANOVA tests along with Tukey's method revealed a significant increase in the occurrence of microstates A and D and a significant decrease in the contribution of microstate C during the tPBM session. Specifically, the occurrence of microstate A gradually increased during the tPBM stimulation, leading to a significant difference between the Pre and Stim2 periods ($p_{Tukey} = 0.022$). During the Post period, the occurrence of microstate A decreased significantly compared with that during Stim2 ($p_{Tukey} = 0.049$). The occurrence of microstate D also increased notably during Stim1 of the tPBM session ($p_{Tukey} = 0.038$ compared to Pre).

For the contribution parameter, the *post hoc* rmANOVA results showed that the contribution of microstate C of the tPBM session was significantly decreased during Stim2 compared to the baseline (Pre; $p_{Tukey} = 0.045$). Regarding the sham condition, the rmANOVA analysis revealed significant differences in the contribution parameter of microstate B across four periods ($p_{rmANOVA} = 0.038$). However, the *post hoc* test did not identify any significant differences for six pairs of

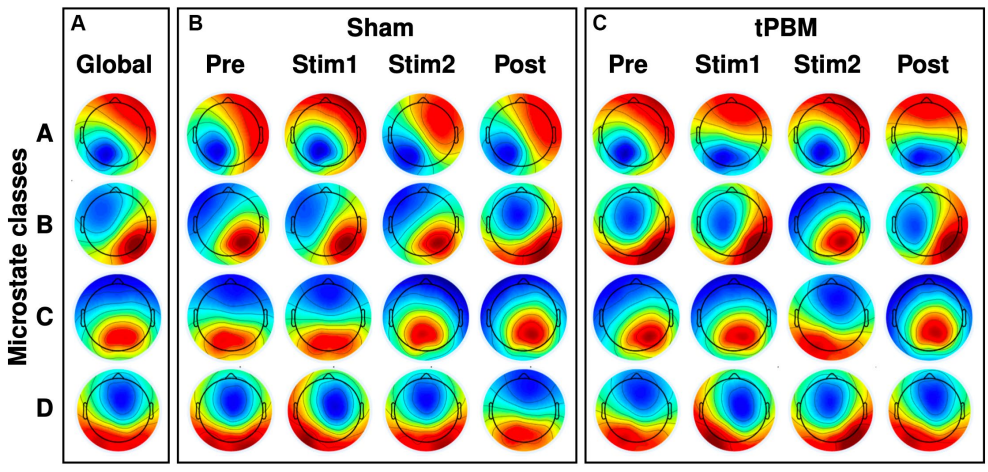

FIGURE 3
EEG microstate topographies of 4 microstate classes. **(A)** Global microstate topographies obtained from both tPBM and sham sessions during four experimental periods (Pre, Stim1, Stim2, and Post). **(B)** Microstate topographies during the four temporal segments under Sham session. **(C)** Microstate topographies during the four temporal segments under active tPBM session.

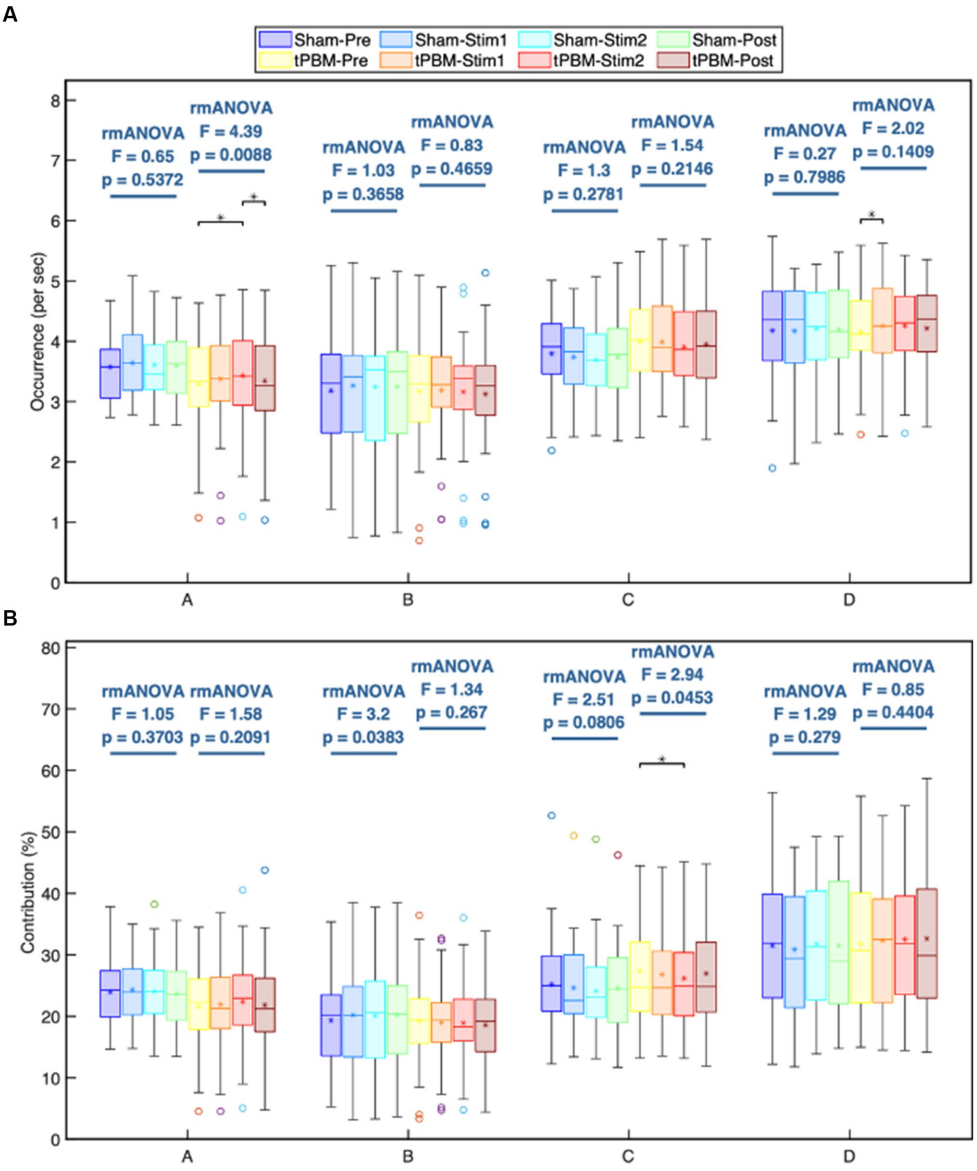

FIGURE 4
Statistical comparisons of the microstate **(A)** occurrence (1/s) and **(B)** contribution (%) parameters among four temporal segments (Pre, Stim1, Stim2, and Post) for each of the four microstate classes, A, B, C, and D. These comparisons are made independently for the active and sham sessions. Statistical results were obtained by one-way repeated measures ANOVA and the *post hoc* pairwise comparisons with Tukey correction. Significant differences between a period pair are marked as "∗" for $p < 0.05$ after Tukey correction.

periods. The smallest p_{Tukey} value for this case was 0.125 between the Pre and Stim1 periods. For other microstates, the statistical analysis did not reveal any significant differences across the four periods of both experimental sessions.

3.3. Alterations in transition probabilities among microstate classes induced by tPBM

Further analysis of the transition probabilities between different microstate classes revealed several significant differences induced by tPBM. Figure 5 shows the transition probabilities among the four microstate classes. Statistical results showed that the transition between microstates A and D increased significantly during the active stimulation period, whereas the transition between microstates B and C declined significantly. Specifically, the *post hoc* Tukey's test revealed significant increases in the transition probabilities from microstate A to D between the Pre and Stim 2 periods ($p_{Tukey} = 0.01$) and Stim1 and Stim2 periods ($p_{Tukey} = 0.013$). The transition from microstate D to A also significantly increased between Stim1 and Stim2 ($p_{Tukey} = 0.041$). In contrast, the transition probabilities from microstate B to C significantly decreased ($p_{Tukey} < 0.05$, when comparing the Pre and Stim2 periods). Similarly, a significant drop in the transition probabilities from microstate C to B was also observed ($p_{Tukey} = 0.01$ for Pre and Stim2 periods and $p_{Tukey} = 0.04$ for Stim1 and Stim2 periods). For the sham session, the statistical analysis did not reveal any significant differences in the transition probabilities across the four temporal periods.

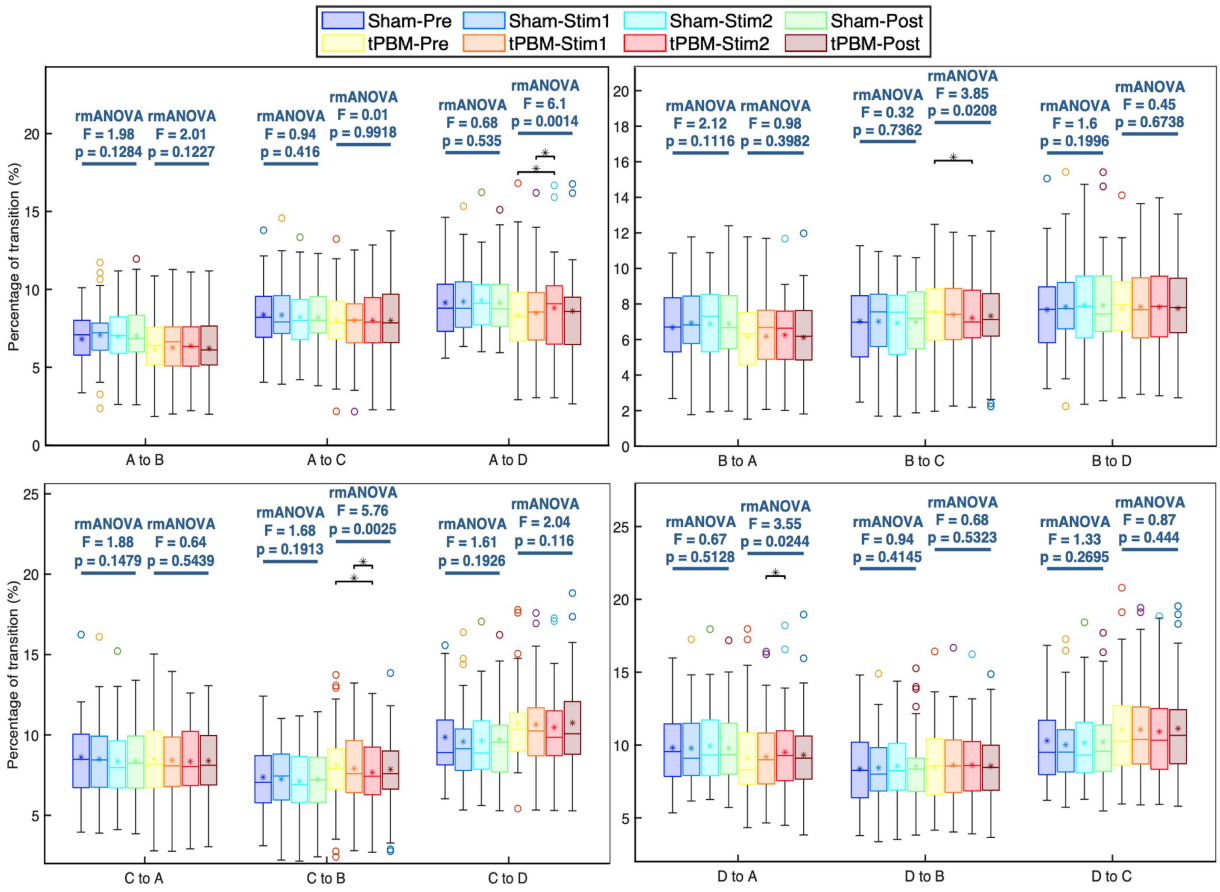

FIGURE 5
Transition probabilities between each pair of the four microstate classes and respective statistical comparisons under separate active and sham conditions. Statistical results were obtained by one-way repeated measures ANOVA and *post hoc* pairwise comparisons with Tukey's correction. Significant differences between respective pairs are marked as "*" for $p < 0.05$, after Tukey's correction.

3.4. Influences of tPBM on EEG microstate topographical power

As mentioned in section 2, we performed EEG microstate analysis in the frequency domain and calculated the percentage changes in power for each microstate across the delta (0.5–4 Hz), theta (4–8 Hz), alpha (8–13 Hz), and beta (13–30 Hz) frequency bands using Eq. (4). Accordingly, Figures 6A,B show the baseline-normalized changes in microstate power across the delta band (Figure 6A) and alpha band (Figure 6B) for the four microstate classes during the tPBM and post-tPBM periods. The topographical maps also highlight channels whose cluster-associated *p*-values were below 0.05.

CBPT revealed significant differences in normalized power between the tPBM and sham sessions across multiple microstates. Specifically, within the delta band, the results revealed significantly lower normalized powers during and after tPBM compared to the sham session across all four microstate classes. In contrast, in the alpha band, the microstate powers of class D exhibited significant augmentation during the active tPBM session (Stim 1 and Stim 2) compared to the sham session. This augmentation, prominently observed in the central to the left-parietal region during Stim1 and in the mid-frontal to the left-parietal region during Stim2, underscores the distinctive impact of tPBM on microstate D in the alpha band.

4. Discussion

4.1. Effects of tPBM on EEG microstate classes and respective brain networks

Regarding EEG microstate classes, several simultaneous EEG-fMRI studies have investigated correlations between EEG microstates and fMRI resting states (Smith et al., 2009; Britz et al., 2010; Musso et al., 2010). Accordingly, microstate A is related to the activation of the bilateral superior and middle temporal lobes; microstate B is associated with the activation of the bilateral occipital cortex (Smith et al., 2009; Britz et al., 2010; Michel and Koenig, 2018). In addition, microstate C is linked to the dorsal anterior cingulate cortex, bilateral inferior frontal cortices, and right insular area, while microstate D is correlated with activation in the right-lateralized dorsal and ventral areas of the frontal and parietal cortices (Smith et al., 2009; Britz et al., 2010). Compared with prior publications in the literature, the four EEG microstate classes identified in this study are in good agreement with previous findings (Koenig et al., 2002; Michel and Koenig, 2018).

As shown in section 3, the statistical analysis of the temporal and spectral characteristics of these four microstates revealed that tPBM mainly modulated microstates A and D. This set of modulations

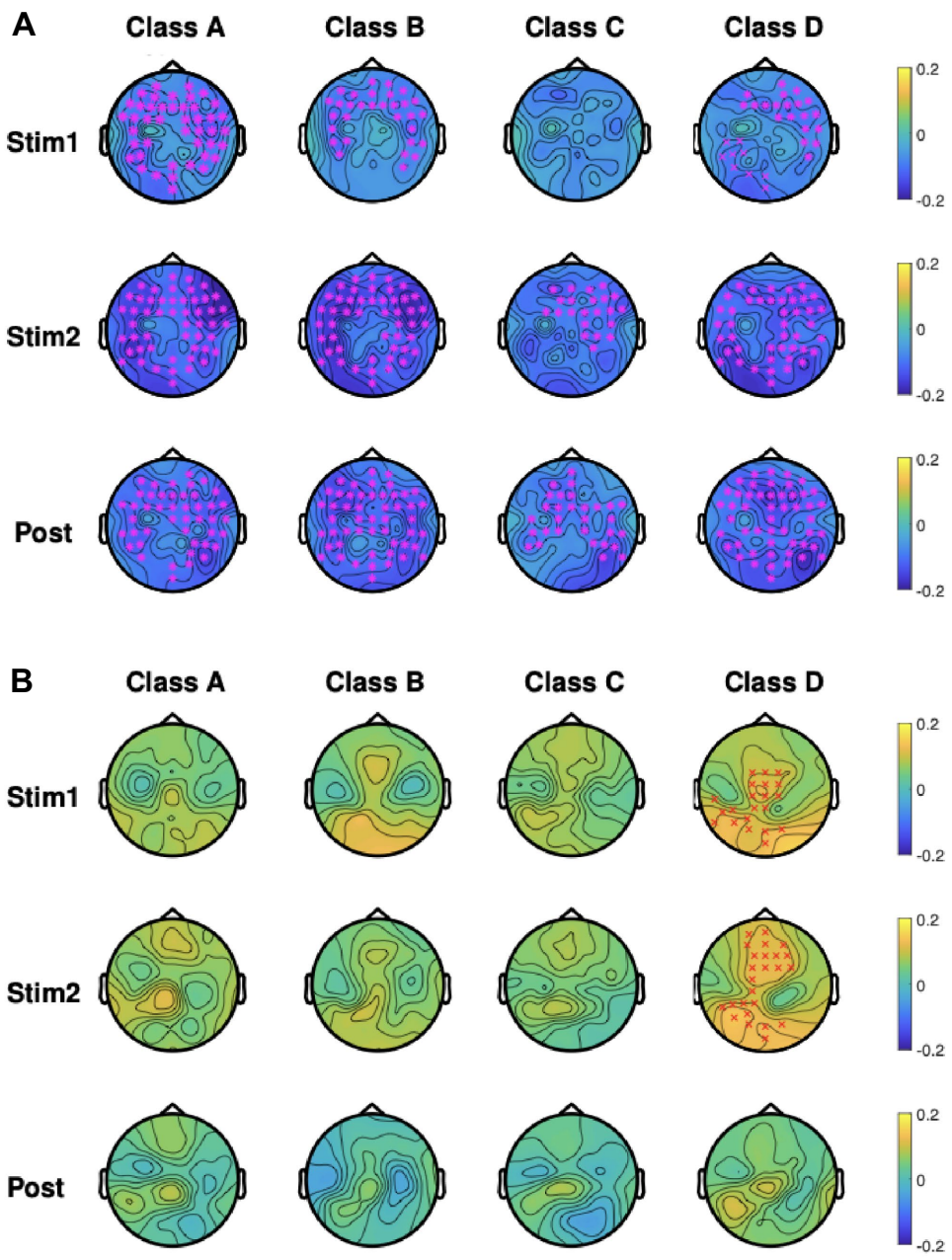

FIGURE 6
Topographic maps of group-averaged (n = 45), baseline-normalized changes in microstate power in four microstate classes during tPBM/sham and post-tPBM/sham periods in the **(A)** delta band and **(B)** alpha band. Stars/crosses indicate clusters of electrodes with significant differences between the conditions ("*" for $p_{cluster} < 0.01$ and "x" for $p_{cluster} < 0.05$). The purple color of the stars/crosses in **(A)** indicates that the normalized delta powers in the tPBM session were significantly lower than those in the sham session. The red color of the crosses in **(B)** indicates that the normalized alpha powers of the tPBM session were significantly higher than those in the sham session.

implies that tPBM has the ability to alter or stimulate the resting human brain in the frontal, temporal, and parietal cortices. A recent human study (Dmochowski et al., 2020) that employed BOLD-fMRI to assess tPBM-induced hemodynamic activity found increases in resting-state functional connectivity in seed regions in the frontal, temporal, and parietal cortices. Another report from our own group developed a combined analysis of Singular Value Decomposition and eLORETA (Wang et al., 2022b), which revealed a tPBM-induced enhancement in alpha power in the frontal–parietal network. Thus, our findings derived from the EEG microstate analysis supplemented prior findings in brain regions stimulated by tPBM.

4.2. Effects of tPBM on EEG microstate classes and respective brain networks

As presented in sections 3.2 and 3.3, the results showed significant increases in (i) the occurrence of microstates A and D and (ii) the

transition between microstates A and D during the stimulation period of the active tPBM session. These findings imply that tPBM promotes brain activity in microstates A and D, as well as more frequent transitions between them, all of which can also be considered potential indicators of active neuromodulation effects of tPBM. Previous studies on the functional significance of EEG microstates (Britz et al., 2010; Milz et al., 2016; Seitzman et al., 2017) have suggested that microstate A is associated with the auditory network, while microstate D is related to the dorsal attention network (DAN). A recent study using resting-state fMRI (Argilés et al., 2022) also reported an alteration in the functional connectivity of the DAN after red light exposure. Moreover, several papers have reported significant enhancement of attention and memory induced by tPBM (Barrett and Gonzalez-Lima, 2013; Hwang et al., 2016; Vargas et al., 2017; Jahan et al., 2019). In particular, Zhao et al. recently demonstrated that right-forehead tPBM with a 1,064-nm laser significantly enhances visual working memory capacity based on neuropsychological measurements of occipitoparietal contralateral delay activity (CDA; Zhao et al., 2022), which is well accepted as a robust neural correlate of visual working memory. Thus, we speculate that the tPBM-promoted increase in activity in microstates A and D may be a potential mechanism for brain function enhancement.

4.3. Alterations by tPBM in EEG microstate topographical delta and alpha powers

In addition to the time-domain EEG microstate analysis, we assessed the spectral information of microstate classes throughout the different experimental periods of both tPBM and sham sessions. To the best of our knowledge, only a few studies have focused on frequency-domain analysis of EEG microstates (Li et al., 2021). By combining the MEMD and HHT methods (Cho et al., 2017; Yang and Ren, 2019), we could overcome the tribulation due to the short-length signals of EEG microstates and estimate the frequency-specific power of different microstate classes. Accordingly, microstate spectral analysis revealed significant differences in the normalized power between the tPBM and sham sessions. Specifically, we observed that active tPBM induced significant reductions in normalized delta power in three microstates (A, B, and D). This aligns with prior findings (Jahan et al., 2019; Wang et al., 2021; Shahdadian et al., 2022) that have also reported a decrease in delta power during and after tPBM. For instance, a previous study demonstrated a significant decline in delta power in the tPBM group, as opposed to a notable increase in delta power in the sham group (Jahan et al., 2019). These observations resonate with previous EEG studies that have inferred a connection between the increase of slow wave oscillations and an individual's proclivity for rest and sleep. Thus, tPBM emerges as a potential mitigator of neuronal fatigue through its capacity to augment cellular energy production and promote neuronal metabolism.

Microstate spectral analysis also unveiled that tPBM significantly enhanced normalized alpha power topographies in microstate D during the active tPBM period. In particular, enhanced powers occurred in the central to left-parietal region during Stim1 and in the mid-frontal to left-parietal region during Stim2. This latter finding underscores the importance of both alpha power and microstate D. Because microstate D is closely associated with brain activity in the dorsal and ventral areas of the frontal and parietal cortices (Smith et al., 2009; Britz et al., 2010), our results imply that right-prefrontal tPBM facilitates significant promotion of EEG activity in microstate D across the frontal and parietal regions in alpha rhythm. Overall, both time-domain and frequency-domain EEG microstate analyses presented us with the same key microstate class, namely, class D, which was most significantly modulated by the right-forehead tPBM with a 1,064-nm laser compared to other EEG microstate classes.

It is worth noting that although the local stimulation site experienced a slight increase in skin temperature due to light absorption, the changes in microstate parameters observed in this study were not a result of the thermal effect caused by light. Studies on the effects of tPBM on brain temperature, conducted through a computational model (Bhattacharya and Dutta, 2019) and magnetic resonance thermometry (Dmochowski et al., 2020), revealed no significant difference in temperature between tPBM and sham conditions. Additionally, a recent EEG study comparing tPBM and thermal stimulation found notable differences in the alterations of EEG power topography between the two types of stimulation (Wang et al., 2021).

4.4. Limitations and future work

While this study has enabled us to obtain several new findings, several limitations exist. First, in Session 4.2, we attempted to elucidate the impact of tPBM on microstate parameters by considering the roles of microstates suggested by previous studies in the literature. However, the specific function of microstates may vary depending on the circumstances in which the EEG data was collected. Second, we took the ICA-based artifact correction approach, which could create an author-made artifact and thus affect the validity of the study. Third, we chose to adopt four microstate classes, as mostly employed in prior EEG microstate studies. Nevertheless, we acknowledge that integrating formal criteria to determine the optimal number of microstates holds the potential to bolster the robustness of the analysis. Last, it is possible that tPBM may affect the occurrence of artifacts since some of them are related to brain behaviors.

To overcome the limitations, further work includes (1) to conducting source localization analysis that can provide a more comprehensive explanation of the changes in microstate parameters throughout the tPBM session and further insights into its effects; (2) to perform artifact rejections to minimize potential confounds introduced by artifact correction methods; (3) to introduce a more systematic procedure for microstate selection to characterize more comprehensively/accurately the microstate patterns present in the EEG data; and (4) to investigate tPBM-induced artifacts on EEG microstates.

5. Conclusion

In this study, 64-channel EEG data were recorded from 45 healthy subjects under both active and sham 8-min tPBM with a 1,064-nm laser delivered on the right forehead of the subjects. Both time- and frequency-domain analyses were employed to identify and investigate tPBM-induced alterations in the dynamic EEG microstates in the human brain. Four global microstate classes for both the tPBM and sham sessions throughout the different experimental periods (i.e.,

pre-, during, and post-stimulation) were first identified using conventional EEG microstate analysis. Various temporal microstate parameters were then extracted and statistically analyzed to assess the effects of tPBM on temporal brain dynamics. Moreover, spectral analysis was also performed to investigate the variation in EEG power of microstate classes over the respective periods of tPBM and sham sessions. Statistical analyses revealed that tPBM resulted in (1) a significant increase in the occurrence of microstates A and D and a significant decrease in the contribution of microstate C; (2) a substantial increase in the transition probabilities between microstates A and D; and (3) a substantial increase in the alpha power of microstate D. These findings not only were consistent with our previous reports on tPBM-induced alterations in EEG power, but also confirmed the neurophysiological effects of tPBM on EEG microstates, particularly in class D, which reflects brain activation across the frontal and parietal regions. Future efforts should include investigations of the relationships between cognition-evoked functional improvement and alterations of EEG microstates in response to tPBM for a better understanding of the underlying mechanism between them.

Data availability statement

The raw data supporting the conclusions of this article will be made available by the authors, without undue reservation.

Ethics statement

The studies involving humans were approved by the Institutional Review Board of the University of Texas at Arlington, Arlington, TX, USA. The studies were conducted in accordance with the local legislation and institutional requirements. The participants provided their written informed consent to participate in this study.

Author contributions

NT analyzed the data, interpreted the results, and prepared the manuscript. XW assisted with data collection, discussed the results, and reviewed the manuscript. HL initiated and supervised the study, discussed and interpreted the results, as well as reviewed and revised the manuscript. All authors contributed to the article and approved the submitted version.

Funding

This work was supported in part by the National Institute of Mental Health of the National Institutes of Health under the BRAIN Initiative (RF1MH114285).

Acknowledgments

The authors acknowledge Hashini Wanniarachchi for her assistance with data acquisition.

Conflict of interest

The authors declare that the research was conducted in the absence of any commercial or financial relationships that could be construed as a potential conflict of interest.

Publisher's note

Supplementary material

The Supplementary material for this article can be found online at: https://www.frontiersin.org/articles/10.3389/fnins.2023.1247290/full#supplementary-material

References

Argilés, M., Sunyer-Grau, B., Arteche-Fernandez, S., and Peña-Gómez, C. (2022). Functional connectivity of brain networks with three monochromatic wavelengths: a pilot study using resting-state functional magnetic resonance imaging. *Sci. Rep.* 12:16197. doi: 10.1038/s41598-022-20668-9

Barrett, D. W., and Gonzalez-Lima, F. (2013). Transcranial infrared laser stimulation produces beneficial cognitive and emotional effects in humans. *Neuroscience* 230, 13–23. doi: 10.1016/j.neuroscience.2012.11.016

Benavides-Varela, S., and Gervain, J. (2017). Learning word order at birth: a NIRS study. *Dev. Cogn. Neurosci.* 25, 198–208. doi: 10.1016/j.dcn.2017.03.003

Bhattacharya, M., and Dutta, A. (2019). Computational modeling of the photon transport, tissue heating, and cytochrome C oxidase absorption during transcranial near-infrared stimulation. *Brain Sci.* 9:179. doi: 10.3390/brainsci9080179

Brandeis, D., Naylor, H., Halliday, R., Callaway, E., and Yano, L. (1992). Scopolamine effects on visual information processing, attention, and event-related potential map latencies. *Psychophysiology* 29, 315–335. doi: 10.1111/j.1469-8986.1992.tb01706.x

Britz, J., Van De Ville, D., and Michel, C. M. (2010). BOLD correlates of EEG topography reveal rapid resting-state network dynamics. *Neuroimage* 52, 1162–1170. doi: 10.1016/j.neuroimage.2010.02.052

Brodbeck, V., Kuhn, A., Von Wegner, F., Morzelewski, A., Tagliazucchi, E., Borisov, S., et al. (2012). EEG microstates of wakefulness and NREM sleep. *Neuroimage* 62, 2129–2139. doi: 10.1016/j.neuroimage.2012.05.060

Campos Viola, F., Thorne, J., Edmonds, B., Schneider, T., Eichele, T., and Debener, S. (2009). Semi-automatic identification of independent components representing EEG artifact. *Clin. Neurophysiol.* 120, 868–877. doi: 10.1016/j.clinph.2009.01.015

Cho, D., Min, B., Kim, J., and Lee, B. (2017). EEG-based prediction of epileptic seizures using phase synchronization elicited from noise-assisted multivariate empirical mode decomposition. *IEEE Trans. Neural Syst. Rehabil. Eng.* 25, 1309–1318. doi: 10.1109/TNSRE.2016.2618937

Choi, D.-H., Lee, K.-H., Kim, J.-H., Kim, M. Y., Lim, J. H., and Lee, J. (2012). Effect of 710nm visible light irradiation on neurite outgrowth in primary rat cortical neurons following ischemic insult. *Biochem. Biophys. Res. Commun.* 422, 274–279. doi: 10.1016/j.bbrc.2012.04.147

Comsa, I. M., Bekinschtein, T. A., and Chennu, S. (2019). Transient topographical dynamics of the electroencephalogram predict brain connectivity and Behavioural responsiveness during drowsiness. *Brain Topogr.* 32, 315–331. doi: 10.1007/s10548-018-0689-9

Conlan, M. J., Rapley, J. W., and Cobb, C. M. (1996). Biostimulation of wound healing by low-energy laser irradiation a review. *J. Clin. Periodontol.* 23, 492–496. doi: 10.1111/j.1600-051X.1996.tb00580.x

Delorme, A., and Makeig, S. (2004). EEGLAB: an open source toolbox for analysis of single-trial EEG dynamics including independent component analysis. *J. Neurosci. Methods* 134, 9–21. doi: 10.1016/j.jneumeth.2003.10.009

Dmochowski, G. M., Shereen, A. D., Berisha, D., and Dmochowski, J. P. (2020). Near-infrared light increases functional connectivity with a non-thermal mechanism. *Cerebr Cortex Commun* 1:tgaa004. doi: 10.1093/texcom/tgaa004

Eells, J. T., Wong-Riley, M. T. T., Verhoeve, J., Henry, M., Buchman, E. V., Kane, M. P., et al. (2004). Mitochondrial signal transduction in accelerated wound and retinal healing by near-infrared light therapy. *Mitochondrion* 4, 559–567. doi: 10.1016/j.mito.2004.07.033

Figueiro Longo, M. G., Tan, C. O., Chan, S. T., Welt, J., Avesta, A., Ratai, E., et al. (2020). Effect of transcranial low-level light therapy vs sham therapy among patients with moderate traumatic brain injury: a randomized clinical trial. *JAMA Netw. Open* 3:e2017337. doi: 10.1001/jamanetworkopen.2020.17337

Fulop, A. M., Dhimmer, S., Deluca, J. R., Johanson, D. D., Lenz, R. V., Patel, K. B., et al. (2010). A Meta-analysis of the efficacy of laser phototherapy on pain relief. *Clin. J. Pain* 26, 729–736. doi: 10.1097/AJP.0b013e3181f09713

Ghaderi, A. H., Jahan, A., Akrami, F., and Salimi, M. M. (2021). Transcranial Photobiomodulation changes topology, Synchronizability, and complexity of resting state brain networks. *J. Neural Eng.* 18, –046048. doi: 10.1088/1741-2552/abf97c

Grillo, S. L., Duggett, N. A., Ennaceur, A., and Chazot, P. L. (2013). Non-invasive infra-red therapy (1072 nm) reduces β-amyloid protein levels in the brain of an Alzheimer's disease mouse model, TASTPM. *J. Photochem. Photobiol. B* 123, 13–22. doi: 10.1016/j.jphotobiol.2013.02.015

Holmes, E., Barrett, D. W., Saucedo, C. L., O'connor, P., Liu, H., and Gonzalez-Lima, F. (2019). Cognitive enhancement by transcranial Photobiomodulation is associated with cerebrovascular oxygenation of the prefrontal cortex. *Front. Neurosci.* 13:1129. doi: 10.3389/fnins.2019.01129

Huang, N. E., Shen, Z., Long, S. R., Wu, M. C., Shih, H. H., Zheng, Q., et al. (1998). The empirical mode decomposition and the Hilbert Spectrum for nonlinear and non-stationary time series analysis. *Proc R Soc London Series A Maths Physic Engineer Sci* 454, 903–995.

Huang, N. E., and Wu, Z. (2008). A review on Hilbert-Huang transform: method and its applications to geophysical studies. *Rev. Geophys.* 46:228. doi: 10.1029/2007RG000228

Hwang, J., Castelli, D. M., and Gonzalez-Lima, F. (2016). Cognitive enhancement by transcranial laser stimulation and acute aerobic exercise. *Lasers Med. Sci.* 31, 1151–1160. doi: 10.1007/s10103-016-1962-3

Jahan, A., Nazari, M. A., Mahmoudi, J., Salehpour, F., and Salimi, M. M. (2019). Transcranial near-infrared Photobiomodulation could modulate brain electrophysiological features and attentional performance in healthy young adults. *Lasers Med. Sci.* 34, 1193–1200. doi: 10.1007/s10103-018-02710-3

Khanna, A., Pascual-Leone, A., and Farzan, F. (2014). Reliability of resting-state microstate features in electroencephalography. *PloS One* 9:e114163. doi: 10.1371/journal.pone.0114163

Khanna, A., Pascual-Leone, A., Michel, C. M., and Farzan, F. (2015). Microstates in resting-state EEG: current status and future directions. *Neurosci. Biobehav. Rev.* 49, 105–113. doi: 10.1016/j.neubiorev.2014.12.010

Koenig, T. (2017). *Microstates in EEGLAB*. Available at: https://www.thomaskoenig.ch/index.php/ work/software/microstates-in-eeglab

Koenig, T., and Brandeis, D. (2016). Inappropriate assumptions about EEG state changes and their impact on the quantification of EEG state dynamics. *Neuroimage* 125, 1104–1106. doi: 10.1016/j.neuroimage.2015.06.035

Koenig, T., Lehmann, D., Merlo, M. C. G., Kochi, K., Hell, D., and Koukkou, M. (1999). A deviant EEG brain microstate in acute, neuroleptic-naive schizophrenics at rest. European archives of. *Psychiatry Clin. Neurosci.* 249, 205–211. doi: 10.1007/s004060050088

Koenig, T., Prichep, L., Lehmann, D., Sosa, P. V., Braeker, E., Kleinlogel, H., et al. (2002). Millisecond by millisecond, year by year: normative EEG microstates and developmental stages. *Neuroimage* 16, 41–48. doi: 10.1006/nimg.2002.1070

Lang, X., Zheng, Q., Zhang, Z., Lu, S., Xie, L., Horch, A., et al. (2018). Fast Multivariate Empirical Mode Decomposition. *IEEE Access* 6, 65521–65538. doi: 10.1109/ACCESS.2018.2877150

Lee, H. I., Lee, S. W., Kim, S. Y., Kim, N. G., Park, K. J., Choi, B. T., et al. (2017). Pretreatment with light-emitting diode therapy reduces ischemic brain injury in mice through endothelial nitric oxide synthase-dependent mechanisms. *Biochem. Biophys. Res. Commun.* 486, 945–950. doi: 10.1016/j.bbrc.2017.03.131

Lehmann, D., Faber, P. L., Galderisi, S., Herrmann, W. M., Kinoshita, T., Koukkou, M., et al. (2005). EEG microstate duration and syntax in acute, medication-Naïve, first-episode schizophrenia: a multi-center study. *Psychiatry Res. Neuroimaging* 138, 141–156. doi: 10.1016/j.pscychresns.2004.05.007

Lehmann, D., Ozaki, H., and Pal, I. (1987). EEG alpha map series: brain Micro-states by space-oriented adaptive segmentation. *Electroencephalogr. Clin. Neurophysiol.* 67, 271–288. doi: 10.1016/0013-4694(87)90025-3

Lehmann, D., and Skrandies, W. (1980). Reference-free identification of components of checkerboard-evoked multichannel potential fields. *Electroencephalogr. Clin. Neurophysiol.* 48, 609–621. doi: 10.1016/0013-4694(80)90419-8

Li, Y., Shi, W., Liu, Z., Li, J., Wang, Q., Yan, X., et al. (2021). Effective brain state estimation during Propofol-induced sedation using advanced EEG microstate spectral analysis. *IEEE J. Biomed. Health Inform.* 25, 978–987. doi: 10.1109/JBHI.2020.3008052

Liebert, A., Bicknell, B., Laakso, E. L., Heller, G., Jalilitabaei, P., Tilley, S., et al. (2021). Improvements in clinical signs of Parkinson's disease using photobiomodulation: a prospective proof-of-concept study. *BMC Neurol.* 21:256. doi: 10.1186/s12883-021-02248-y

Mandic, D. P., Ur Rehman, N., Wu, Z., and Huang, N. E. (2013). Empirical mode decomposition-based time-frequency analysis of multivariate signals: the power of adaptive data analysis. *IEEE Signal Process. Mag.* 30, 74–86. doi: 10.1109/MSP.2013.2267931

Maris, E., and Oostenveld, R. (2007). Nonparametric statistical testing of EEG-and MEG-data. *J. Neurosci. Methods* 164, 177–190. doi: 10.1016/j.jneumeth.2007.03.024

Mester, E., Spiry, T., Szende, B., and Tota, J. G. (1971). Effect of laser rays on wound healing. *Am. J. Surg.* 122, 532–535. doi: 10.1016/0002-9610(71)90482-X

Michel, C. M., and Koenig, T. (2018). EEG microstates as a tool for studying the temporal dynamics of whole-brain neuronal networks: a review. *Neuroimage* 180, 577–593. doi: 10.1016/j.neuroimage.2017.11.062

Milz, P., Faber, P. L., Lehmann, D., Koenig, T., Kochi, K., and Pascual-Marqui, R. D. (2016). The functional significance of EEG microstates—associations with modalities of thinking. *Neuroimage* 125, 643–656. doi: 10.1016/j.neuroimage.2015.08.023

Milz, P., Pascual-Marqui, R. D., Achermann, P., Kochi, K., and Faber, P. L. (2017). The EEG microstate topography is predominantly determined by Intracortical sources in the alpha band. *Neuroimage* 162, 353–361. doi: 10.1016/j.neuroimage.2017.08.058

Murray, M. M., Brunet, D., and Michel, C. M. (2008). Topographic ERP analyses: a step-by-step tutorial review. *Brain Topogr.* 20, 249–264. doi: 10.1007/s10548-008-0054-5

Musso, F., Brinkmeyer, J., Mobascher, A., Warbrick, T., and Winterer, G. (2010). Spontaneous brain activity and EEG microstates. A novel EEG/fMRI analysis approach to explore resting-state networks. *Neuroimage* 52, 1149–1161. doi: 10.1016/j.neuroimage.2010.01.093

Nizamutdinov, D., Qi, X., Berman, M. H., Dougal, G., Dayawansa, S., Wu, E., et al. (2021). Transcranial near infrared light stimulations improve cognition in patients with dementia. *Aging Dis.* 12, 954–963. doi: 10.14336/AD.2021.0229

Oostenveld, R., Fries, P., Maris, E., and Schoffelen, J.-M. (2011). FieldTrip: open source software for advanced analysis of MEG, EEG, and invasive electrophysiological data. *Comput. Intell. Neurosci.* 2011, 1–9. doi: 10.1155/2011/156869

Pascual-Marqui, R. D., Michel, C. M., and Lehmann, D. (1995). Segmentation of brain electrical activity into microstates: model estimation and validation. *I.E.E.E. Trans. Biomed. Eng.* 42, 658–665. doi: 10.1109/10.391164

Pellegrino, G., Machado, A., Von Ellenrieder, N., Watanabe, S., Hall, J. A., Lina, J.-M., et al. (2016). Hemodynamic response to Interictal epileptiform discharges addressed by personalized EEG-fNIRS recordings. *Front. Neurosci.* 10:102. doi: 10.3389/fnins.2016.00102

Peplow, P. V., Chung, T.-Y., and Baxter, G. D. (2010). Laser Photobiomodulation of wound healing: a review of experimental studies in mouse and rat animal models. *Photomed. Laser Surg.* 28, 291–325. doi: 10.1089/pho.2008.2446

Pruitt, T., Wang, X., Wu, A., Kallioniemi, E., Husain, M. M., and Liu, H. (2020). Transcranial Photobiomodulation (tPBM) with 1,064-nm laser to improve cerebral metabolism of the human brain in vivo. *Lasers Surg. Med.* 52, 807–813. doi: 10.1002/lsm.23232

Quirk, B. J., Desmet, K. D., Henry, M., Buchmann, E., Wong-Riley, M., Eells, J. T., et al. (2012). Therapeutic effect of near infrared (NIR) light on Parkinson's disease models. *Front. Biosci. (Elite Ed.)* 4, 818–823. doi: 10.2741/E421

Rehman, N., and Mandic, D. P. (2010). Multivariate Empirical Mode Decomposition. *Proc R Soc A Maths Physic Engineer Sci* 466, 1291–1302. doi: 10.1098/rspa.2009.0502

Rojas, J. C., Bruchey, A. K., and Gonzalez-Lima, F. (2012). Low-level light therapy improves cortical metabolic capacity and memory retention. *J. Alzheimers Dis.* 32, 741–752. doi: 10.3233/JAD-2012-120817

Seitzman, B. A., Abell, M., Bartley, S. C., Erickson, M. A., Bolbecker, A. R., and Hetrick, W. P. (2017). Cognitive manipulation of brain electric microstates. *Neuroimage* 146, 533–543. doi: 10.1016/j.neuroimage.2016.10.002

Shahdadian, S., Wang, X., Wanniarachchi, H., Chaudhari, A., Truong, N. C. D., and Liu, H. (2022). Neuromodulation of brain power topography and network topology by prefrontal transcranial Photobiomodulation. *J. Neural Eng.* 19:066013. doi: 10.1088/1741-2552/ac9ede

Shi, W., Li, Y., Liu, Z., Li, J., Wang, Q., Yan, X., et al. (2020). Non-canonical microstate becomes salient in high density EEG during Propofol-induced altered states of consciousness. *Int. J. Neural Syst.* 30:2050005. doi: 10.1142/S0129065720500057

Skrandies, W. (1989). Data reduction of multichannel fields: global field power and principal component analysis. *Brain Topogr.* 2, 73–80. doi: 10.1007/BF01128845

Skrandies, W. (2007). The effect of stimulation frequency and retinal stimulus location on visual evoked potential topography. *Brain Topogr.* 20, 15–20. doi: 10.1007/s10548-007-0026-1

Smith, S. M., Fox, P. T., Miller, K. L., Glahn, D. C., Fox, P. M., Mackay, C. E., et al. (2009). Correspondence of the Brain's functional architecture during activation and rest. *Proc. Natl. Acad. Sci.* 106, 13040–13045. doi: 10.1073/pnas.0905267106

Tian, F., Hase, S. N., Gonzalez-Lima, F., and Liu, H. (2016). Transcranial laser stimulation improves human cerebral oxygenation. *Lasers Surg. Med.* 48, 343–349. doi: 10.1002/lsm.22471

Truong, N. C. D., Wang, X., Wanniarachchi, H., and Liu, H. (2022). Enhancement of frequency-specific hemodynamic power and functional connectivity by transcranial Photobiomodulation in healthy humans. *Front. Neurosci.* 16:896502. doi: 10.3389/fnins.2022.896502

Vargas, E., Barrett, D. W., Saucedo, C. L., Huang, L.-D., Abraham, J. A., Tanaka, H., et al. (2017). Beneficial neurocognitive effects of transcranial laser in older adults. *Lasers Med. Sci.* 32, 1153–1162. doi: 10.1007/s10103-017-2221-y

Wang, X., Dmochowski, J. P., Zeng, L., Kallioniemi, E., Husain, M., Gonzalez-Lima, F., et al. (2019). Transcranial Photobiomodulation with 1064-nm laser modulates brain electroencephalogram rhythms. *Neurophotonics* 6:025013. doi: 10.1117/1.NPh.6.2.025013

Wang, X., Ma, L.-C., Shahdadian, S., Wu, A., Truong, N. C. D., and Liu, H. (2022a). Metabolic connectivity and hemodynamic-metabolic coherence of human prefrontal cortex at rest and post Photobiomodulation assessed by Dual-Channel broadband NIRS. *Metabolites* 12:42. doi: 10.3390/metabo12010042

Wang, X., Tian, F., Reddy, D. D., Nalawade, S. S., Barrett, D. W., Gonzalez-Lima, F., et al. (2017). Up-regulation of cerebral cytochrome-c-oxidase and hemodynamics by transcranial infrared laser stimulation: a broadband near-infrared spectroscopy study. *J. Cereb. Blood Flow Metab.* 37, 3789–3802. doi: 10.1177/0271678X17691783

Wang, X., Wanniarachchi, H., Wu, A., Gonzalez-Lima, F., and Liu, H. (2021). Transcranial Photobiomodulation and thermal stimulation induce distinct topographies of EEG alpha and Beta power changes in healthy humans. *Sci. Rep.* 11:18917. doi: 10.1038/s41598-021-97987-w

Wang, X., Wanniarachchi, H., Wu, A., and Liu, H. (2022b). Combination of group singular value decomposition and eLORETA identifies human EEG networks and responses to transcranial Photobiomodulation. *Front. Hum. Neurosci.* 16:853909. doi: 10.3389/fnhum.2022.853909

Yang, Z., and Ren, H. (2019). Feature extraction and simulation of EEG signals during exercise-induced fatigue. *IEEE Access* 7, 46389–46398. doi: 10.1109/ACCESS.2019.2909035

Yasukawa, A., Hrui, H., Koyama, Y., Nagai, M., and Takakuda, K. (2007). The effect of low reactive-level laser therapy (LLLT) with helium-Neon laser on operative wound healing in a rat model. *J. Vet. Med. Sci.* 69, 799–806. doi: 10.1292/jvms.69.799

Zhao, C., Li, D., Kong, Y., Liu, H., Hu, Y., Niu, H., et al. (2022). Transcranial photobiomodulation enhances visual working memory capacity in humans. *Sci. Adv.* 8:eabq3211. doi: 10.1126/sciadv.abq3211

Zomorrodi, R., Loheswaran, G., Pushparaj, A., and Lim, L. (2019). Pulsed near infrared transcranial and intranasal Photobiomodulation significantly modulates neural oscillations: a pilot exploratory study. *Sci. Rep.* 9:6309. doi: 10.1038/s41598-019-42693-x

Zomorrodi, R., Rashidi-Ranjbar, N., Loheswaran, G., and Lim, L. (2021). Modifying resting-state EEG microstates with pulsed near-infrared transcranial Photobiomodulation: a randomized sham-controlled crossover study. *Brain Stimul.* 14:1697. doi: 10.1016/j.brs.2021.10.349

frontiers | Frontiers in Neuroscience

TYPE Review
PUBLISHED 18 October 2023
DOI 10.3389/fnins.2023.1286267

OPEN ACCESS

EDITED BY
Mark H. Myers,
University of Tennessee Health Science Center (UTHSC), United States

REVIEWED BY
Giorgio Bonmassar,
Massachusetts General Hospital, Harvard Medical School, United States
Mehmet Pektezel,
Ministry of Health, Türkiye

*CORRESPONDENCE
Litong Wang
litongwanglv@163.com

RECEIVED 31 August 2023
ACCEPTED 05 October 2023
PUBLISHED 18 October 2023

CITATION
Wang L, Gao F, Wang Z, Liang F, Dai Y, Wang M, Wu J, Chen Y, Yan Q and Wang L (2023) Transcutaneous auricular vagus nerve stimulation in the treatment of disorders of consciousness: mechanisms and applications. *Front. Neurosci.* 17:1286267. doi: 10.3389/fnins.2023.1286267

Transcutaneous auricular vagus nerve stimulation in the treatment of disorders of consciousness: mechanisms and applications

Likai Wang[1], Fei Gao[1], Zhan Wang[1], Feng Liang[2], Yongli Dai[1], Mengchun Wang[1], Jingyi Wu[1], Yaning Chen[1], Qinjie Yan[1] and Litong Wang[1]*

[1]Department of Rehabilitation Medicine, The Second Hospital of Dalian Medical University, Dalian, China, [2]First Clinical Medical College, Shanxi Medical University, Taiyuan, China

This review provides an in-depth exploration of the mechanisms and applications of transcutaneous auricular vagus nerve stimulation (taVNS) in treating disorders of consciousness (DOC). Beginning with an exploration of the vagus nerve's role in modulating brain function and consciousness, we then delve into the neuroprotective potential of taVNS demonstrated in animal models. The subsequent sections assess the therapeutic impact of taVNS on human DOC, discussing the safety, tolerability, and various factors influencing the treatment response. Finally, the review identifies the current challenges in taVNS research and outlines future directions, emphasizing the need for large-scale trials, optimization of treatment parameters, and comprehensive investigation of taVNS's long-term effects and underlying mechanisms. This comprehensive overview positions taVNS as a promising and safe modality for DOC treatment, with a focus on understanding its intricate neurophysiological influence and optimizing its application in clinical settings.

KEYWORDS

transcutaneous auricular vagus nerve stimulation, disorders of consciousness, neuroprotection, safety and tolerability, stimulation parameters, mechanisms of action

1. Introduction

Disorders of consciousness (DOC) are a group of conditions characterized by impaired awareness and arousal, characterized by impaired awareness and arousal, which typically result from severe brain injury, such as traumatic brain injury (TBI), stroke, and hypoxic–ischemic encephalopathy (Kang et al., 2022). Prolonged disorders of consciousness (pDOC) refer to pathological states of consciousness loss lasting more than 28 days, are classified by the patient's altered state of consciousness as minimally conscious state (MCS) or unresponsive wakefulness syndrome (UWS), previously known as a vegetative state (*VS*) (Laureys et al., 2010; Scolding et al., 2021). UWS patients exhibit spontaneous eye opening but lack any signs of self or environmental awareness (Machado, 2002), while MCS patients display inconsistent but discernible signs of consciousness (Thibaut et al., 2021; Guo et al., 2022). Currently, the available opportunities for intervention for DOC include providing supportive care, managing complications, and optimizing the patient's overall physical and neurological status (Edlow et al., 2021). Although pharmacological interventions (including dopaminergic and other

neurotransmitter-modulating drugs), have been extensively used and achieved clinical success, these interventions tend to be inefficient and associated with side effects, when faced with coexistence of multiple medical conditions in DOC patients (Kondziella et al., 2020). Invasive brain stimulation techniques are implemented in deep brain to improve the accuracy, but also increase the risks of infection, as well as the risk of device malfunction (Raguž et al., 2021). Taking into account the limitations of interventions, non-invasive techniques [including transcranial magnetic stimulation (TMS) and transcranial direct current stimulation (tDCS)], as the safer ways and more focused approach to modulating key brain networks are applied (Formica et al., 2021; Guo et al., 2022; Han et al., 2022).

Invasive cervical vagus nerve stimulation (VNS) is a technique that involves implanting a device under the skin of the chest that delivers electrical impulses to the vagus nerve (VN) in the neck (Giordano et al., 2017). It has received approval by the US Food and Drug Administration (FDA) for the treatment of conditions such as epilepsy, depression, obesity, and as a modality for stroke rehabilitation (Milby et al., 2008; Giordano et al., 2017; Austelle et al., 2022; Hilz, 2022). However, the procedure necessitates surgery and can present a range of side effects, including voice changes, coughing, headaches, infections, and bleeding. Furthermore, it is costly and not universally accessible, making it an unsuitable option for some patients (Giordano et al., 2017). Recognizing these challenges, transcutaneous auricular vagus nerve stimulation (taVNS) was introduced as a non-invasive, more affordable, and easily implemented alternative. TaVNS is a non-invasive brain stimulation technique that involves the delivery of electrical stimulation to the auricular branch of the vagus nerve (ABVN) (Badran et al., 2018), accessible through the skin of the outer ear. Considerable evidence has suggested that taVNS is a therapeutic intervention for various neurological and psychiatric conditions, such as epilepsy (Thompson et al., 2021), depression (Liu et al., 2020), and migraine (Zhang et al., 2021). Regarding DOC, taVNS has the potential to modulate thalamo-cortical connectivity and neurotransmitter systems (Vitello et al., 2023), which are critical for promoting awareness and arousal. As a non-invasive method, taVNS avoids the risks associated with invasive procedures and offers a more focused approach to modulating key brain networks involved in consciousness, characterized by its bottom-up neural transmission pathway, when compared to other non-invasive stimulation techniques like TMS and tDCS (Wu et al., 2021).

As taVNS continues to gain rapid traction in both popularity and application for DOC, a consensus remains elusive in the field regarding the optimal timing for initial intervention, preferred stimulation sites, and the most effective stimulation parameters. The inquiry into whether taVNS can yield comparable restorative outcomes in DOC recovery, along with an exploration of the underlying mechanisms and prospects for future research directions, requires further exploration. Hence, the primary objective of this comprehensive review is to delve into the existing body of research on taVNS in the context of DOC, offering narrative insights into its potential therapeutic efficacy and the mechanisms through which it might engender its positive effects. The abbreviations in this review are listed in Table 1.

2. TaVNS principles and mechanisms

TaVNS apples application of electrical microcurrents to specific points on the auricle to stimulate the ABVN (Ben-Menachem et al., 2015). This approach offers a more accessible and minimally invasive alternative to traditional VNS methods (Marin et al., 2018). However, non-invasive VNS also has some limitations, such as lower stimulation intensity, lower specificity, lower reliability, and higher variability (Ahmed et al., 2022). And it's worth noting that traditional VNS is still widely used because it has been shown to have greater efficacy for certain FDA-labeled conditions, including headache, epilepsy, and depression (Milby et al., 2008; Austelle et al., 2022; Hilz, 2022).

2.1. Auricular branch of the VN and stimulation techniques

The VN is a mixed nerve with approximately 80% afferent and 20% efferent axonal projections. The VN is mainly composed of sensory fibers, which can be classified by their conduction velocity

TABLE 1 List of abbreviations.

Abbreviation	Definition	Abbreviation	Definition
ABVN	The auricular branch of the vagus nerve	NE	Norepinephrine
ACh	Acetylcholine	Non-RtAS	Non-responded to auditory stimuli
BBB	Blood–brain barrier	NTS	Nucleus tractus solitarius
BDNF	Brain-derived neurotrophic factor	RtAS	Responded to auditory stimuli
CNS	Central nervous system	SN	Salience Network
CRS-R	Coma Recovery Scale-Revised	taVNS	Transcutaneous auricular vagus nerve stimulation
DMN	Default Mode Network	TBI	Traumatic brain injury
DOC	Disorders of consciousness	tVNS	Transcutaneous vagus nerve stimulation
EEG	Electroencephalography	UWS	Unresponsive wakefulness syndrome
EXN	External Network	VNS	Vagus nerve stimulation
HRV	Heart Rate Variability	VN	Vagus nerve
LC	Locus coeruleus	*VS*	Vegetative state
MCS	Minimally conscious state		

and diameter of A-fibers (fastest), B-fibers (slower), and C-fibers (slowest) (Yuan and Silberstein, 2016). Aα fibers are notably the largest and have the fastest conduction, while unmyelinated C fibers are the smallest and demonstrate the slowest velocity. Aβ, Aγ, Aδ, and B fibers occupy an intermediate position in terms of both size and conduction speed. Crucially, during VNS in pigs—whose vagus nerve structure and size closely resemble that of humans—the recruitment of neuronal fibers is governed by their closeness to the stimulation electrode and the intensity of the local electric field. There is an inverse relation between fiber size and its recruitment sequence, leading to A-type fibers being recruited before C-type fibers (Settell et al., 2020).

The cervical branch vagus nerve is made up of about 20% myelinated A and B fibers and 80% unmyelinated C fibers (Vonck et al., 2009). However, research to elucidate the mechanism of action of VNS has shown that effective stimulation in humans is primarily mediated by afferent vagal A- and B-fibers (Evans et al., 2004; Howland, 2014). According to several studies, the destruction of peripheral C-fibers does not alter subsequent VNS-induced seizure suppression in rats. Based on a particular study (Mourdoukoutas et al., 2018), with stimulation intensities aligned to clinical nVNS protocols and a current of 10 mA, there was a preferential activation of A-fibers and large B-fibers, while C-fibers remained unaffected. These results indicate that activation of vagal C fibers is not necessary for VNS-induced seizure suppression. However, effective therapeutic stimulation parameters appear to be subthreshold for these fibers in humans, and there are no clinical reports of the autonomic side effects that would be expected if these fibers were maximally activated (Krahl, 2012). The anatomic basis for non-invasive VNS relies on the fact that some branches of the VN have cutaneous distribution, meaning that they can be accessed through the skin. The external ear receives its complex sensory innervation from multiple nerves, including the auricular branch of the vagus, auriculotemporal nerve, greater auricular nerve, and lesser occipital nerve. Research on ear anatomy reveals that the tragus, concha, and cymba concha are sites on the human physique where there's a presence of cutaneous afferent vagal nerve pathways (Peuker and Filler, 2002). The cymba conchae region of the external ear known as the auricle is the unique area for stimulating vagus nerve (VN). The distribution of the auricular branch throughout the auricle is nearly 100%. It is the only surface area of the body where the ABVN is distributed, making it an ideal target for taVNS (Yakunina et al., 2017).

The ABVN primarily consists of myelinated Aβ fibers, myelinated Aδ fibers, and unmyelinated C fibers (Bermejo et al., 2017). The number of Aβ fibers is comparable between the left and right ABVN (Safi et al., 2016). Notably, the ABVN has approximately five to six times fewer Aβ class nerve fibers compared to the cervical branch of the VN (Safi et al., 2016). There's considerable individual variation in fiber count, complicating the determination of optimal stimulation sites and parameters for effective tVNS using the ABVN. Detailed examination of nerve fiber types within the ABVN, suitable for computational modeling, is lacking. As such, the understanding of the unique nerve fiber types remains somewhat speculative. Evaluations of therapeutic effectiveness largely rely on observed therapeutic benefits, further correlated with primary and secondary outcomes. In general, the VN is pivotal in brain–body interactions, sparking interest in its artificial stimulation for therapeutic applications.

2.2. Modulation of vagal activity and its therapeutic implications

The VN's afferent fibers terminate in multiple regions of the brainstem, including the nucleus ambiguus, nucleus dorsalis of the vagus, nucleus tractus solitarius (NTS), and spinal trigeminal nucleus (Wang et al., 2014). The NTS mainly receives and integrates these fiber signals and projects to other areas, which leads to changes in the release of significant neurotransmitters such as norepinephrine (NE), acetylcholine (ACh), serotonin, and dopamine (Hulsey et al., 2017; Zhang et al., 2019). The VN serves as a pivotal conduit between the brain and numerous bodily organs, transmitting both sensory and motor signals. It plays a fundamental role in the autonomic regulation of vital functions, including heart rate, blood pressure, respiration, and digestion (Mazzone and Undem, 2016; Waise et al., 2018). Furthermore, the VN also forms a link between the gut and the brain, known as which may influence conditions like obesity, epilepsy, and depression (Breit et al., 2018; Zhang et al., 2020). These demonstrate that taVNS impacts vagal activity through complex mechanisms and could be a potential treatment strategy for a variety of medical conditions involving the modulation of neuroplasticity, inflammatory responses, and the balance of sympathetic and parasympathetic activity.

NTS is the primary relay between the VN and the central nervous system (CNS), with projections extending to the cortex. Through direct or indirect anatomic connections via the NTS, VNS alters the activity of many cortical and subcortical regions (Breit et al., 2018). The consciousness and awareness networks such as the Default Mode Network (DMN) and the Salience Network (SN) are closely related. Recent studies have suggested that taVNS modulates or activates the cerebral cortices and subcortical areas that are related to the control of consciousness. The central projection of the ABVN is consistent with the classic central vagal projection, which includes the NTS, the locus coeruleus (LC), and the nucleus ambiguous (Knowles and Aziz, 2009; Butt et al., 2020). Then stimulation of the ABVN can activate these nuclei and influence their downstream targets, such as the amygdala, hippocampus, thalamus, and prefrontal cortex.

The DMN plays a foundational role in introspective and self-referential activities, with key areas including the medial prefrontal cortex (mPFC) and the posterior cingulate cortex/precuneus. And the SN is crucial for detecting and directing attention to salient stimuli, primarily involves the anterior cingulate cortex (ACC) and the insula. A study illustrated that the connectivity between the DMN and Central Executive Network (CEN) oscillates in response to taVNS frequencies (Rong et al., 2016): 1 Hz taVNS led to diminished DMN-CEN connectivity, while 25 Hz enhanced it. Moreover, both frequencies conspicuously bolstered the DMN-SN connectivity, elucidating the intricate interplay between introspection and attention processing (Li et al., 2016; Yakunina et al., 2017). NE exerts a range of functional effects in the CNS, especially in regulating alertness, attention, stress responses, and the sleep–wake cycle. Stimulation of the VN has been shown in some studies to activate the LC, leading to an increase in NE release (Hulsey et al., 2017; Jacobs et al., 2020; Farrand et al., 2023). Besides, ACh is fundamental to the brain's arousal systems, with its release being intrinsically linked to heightened arousal and alertness. VNS has been shown to induce the release of ACh in the brain (Meyers et al., 2019). The release of neurotransmitters ACh and NE widely activate the brain's neuromodulatory network, enhancing neural plasticit (Hays et al., 2013). Those are the neurological basis for exploring the therapeutic

potential of taVNS to modulate levels of consciousness. However, more research is needed to fully understand the complex pathways involved in the projections of the VN to the cortex.

3. Mechanisms of VNS in animal experiments for consciousness disorders

VNS in animal experiments has shown potential in consciousness disorders through its effects on reducing cell apoptosis, modulating neurotransmitters, decreasing inflammatory responses, and preserving the integrity of the blood–brain barrier (BBB).

3.1. Reducing cell apoptosis

Research has shown that VNS can have positive effects on the brain's health to reduce cell apoptosis in animal models through various mechanisms, which include the regulation of miR-210, appetite-regulating hormones, the PI3K/AKT signaling pathway, and brain-derived neurotrophic factor (BDNF) (Follesa et al., 2007; Dong and Feng, 2018; Lai et al., 2019).

Jiang et al. identified miR-210, caused by VNS, as a regulator of neuronal apoptosis in a mouse model of hypoxic–ischemic brain injury (Jiang et al., 2015). Zhao et al. also found that neuronal apoptosis significant decrease after VNS in a rat model of cerebral ischemia–reperfusion injury (Zhao et al., 2019). Considerable evidence has suggested that VNS affect cell apoptosis through the pathways mentioned above, which are associated with reducing the size of an infarct and promoting the survival of neurons.

3.2. Modulating neurotransmitters

VNS can regulate the expression of both excitatory (upregulate) and inhibitory (downregulate). This dual modulation may be the underlying mechanism for its arousal-promoting effects.

Several studies have indicated that the upregulate of excitatory neurotransmitters are particularly noticeable in brain regions associated with wakefulness (including the prefrontal cortex and hypothalamus which involved in sleep regulation) (Dong and Feng, 2018; Li et al., 2018) by boosting neuronal activity and promoting wakefulness. The reduction of inhibitory neurotransmitters resulting from VNS, such as gamma-aminobutyric acid (GABA) and serotonin, which are involved in sleep regulation, could promote arousal and wakefulness (Manta et al., 2013; Schwartz and Kilduff, 2015; Sanders et al., 2019).

3.3. Decreasing inflammatory response

VNS has a significant impact on regulating immune response and controlling inflammation through the cholinergic anti-inflammatory pathway.

This process consists of the CNS receiving inflammatory signals (Zachs et al., 2019), transmitted through efferent fibers from the dorsal motor nucleus of the VN sending anti-inflammatory signals to the spleen (Huston and Tracey, 2011; Stavrakis et al., 2015). At this point, peripheral nerve terminals in the spleen release NE (Hilderman et al., 2015), which activates adrenergic receptors on specific T lymphocytes. This activation triggers the expression of acetyltransferase and leads to the synthesis of ACh. After the synthesis of ACh, it acts on macrophages that express the nicotinic ACh receptor (α7nAChR) (Johnston and Webster, 2009; Calvillo et al., 2011; Wang et al., 2012; Wang J. Y. et al., 2021; Caravaca et al., 2022), suppressing the production and release of pro-inflammatory cytokines and promoting the release of anti-inflammatory cytokines (Lei and Duan, 2021; Chen et al., 2022). VNS is a highly effective way to regulate the activity of immune cells, leading to a significant reduction in inflammation. This makes it an invaluable tool in improving outcomes for individuals with consciousness disorders.

3.4. Lowering blood–brain barrier permeability

The integrity of the BBB plays crucial role in maintaining brain homeostasis and shielding the brain from harmful substances (Hugon et al., 2021). Disruption of the BBB following brain injury can lead to increased permeability, allowing the infiltration of inflammatory cells and molecules into the brain parenchyma, exacerbating neuroinflammation and neuronal damage (Åslund et al., 2017). VNS holds promise for reducing the permeability of the BBB following brain injuries, potentially mitigating neuroinflammation, preserving neuronal function, and thereby improving outcomes in consciousness disorders.

VNS's impact on BBB permeability is believed to stem from several mechanisms (Lopez et al., 2012; Chen et al., 2018). One of the mechanism involves the regulation of tight junction proteins, such as occludin and claudin (Chen et al., 2020). Research indicates that VNS can increase the expression of these tight junction proteins, thereby enhancing the barrier function of the BBB and reducing its permeability to inflammatory factors (Lopez et al., 2012; Chen et al., 2018). Furthermore, studies have demonstrated that VNS can inhibit the activity and expression of MMPs, thereby attenuating BBB disruption and reducing the entry of inflammatory cells and molecules into the brain (Yang et al., 2018; Li et al., 2020).

4. Application and evaluation of taVNS in disorders of consciousness

Through the analysis of behavioral and neurophysiological outcomes, a deeper understanding of the effects of taVNS on brain activity and behavioral response in DOC patients is achieved. By contrasting the efficacy of taVNS across various patient categories, including *VS*/UWS and MCS, differences in outcomes are revealed for diverse types and etiologies of consciousness disorders. This analysis assists in identifying the most effective application schemes for taVNS therapy.

4.1. Assessment methods and neurophysiological outcomes of taVNS treatment

In order to investigate the impact of behind taVNS on consciousness recovery, a combination of behavioral and

neurophysiological evaluations are employed, including the Coma Recovery Scale-Revised (CRS-R), electroencephalography (EEG), and functional magnetic resonance imaging (fMRI). These methodologies shed light on the influence of taVNS on brain activity, connectivity, and behavioral responsiveness in patients with DOC.

4.1.1. Behavioral assessment: CRS-R

The CRS-R, a behavioral scale that assesses responsiveness across auditory, visual, motor, communication, and arousal domains, is frequently used to investigate taVNS's efficacy in promoting consciousness recovery (Di et al., 2017). Despite the observed improvements in CRS-R scores for both UWS and MCS patients, additional research is necessary to pinpoint the specific factors driving these enhancements and understand the relationship between CRS-R scores and neurophysiological changes.

4.1.2. Electroencephalography

Electroencephalography provides insights into changes in brain activity following taVNS treatment. However, its usage in DOC patients is sometimes limited by artifacts and the necessity for a more standardized approach to data interpretation. Future enhancements might include high-density EEG for higher spatial resolution and improved signal quality, as well as improved algorithms for artifact reduction and data processing (Kondziella et al., 2020).

EEG-derived biomarkers, including EEG background activity, reactivity, event-related potentials (ERPs), and spectral power, are essential for diagnosing and predicting recovery in patients with DOC (Edlow et al., 2021). Among these biomarkers, reactive alpha rhythms in DOC patients indicate intact neural processing and the operational efficacy of crucial brain networks, especially the thalamocortical circuits (Porcaro et al., 2021). Reactive alpha rhythms can also help distinguish between levels of consciousness in DOC, with MCS patients typically showing more preserved alpha activity than those in *VS* or UWS (Bai et al., 2021). ERPs from EEG offer insights into the brain's particular responses to external stimuli, with components like the P300 serving as windows into the cognitive functioning of DOC patients (Rollnik, 2019). Studies suggest that the combination of EEG-based connectivity analysis and ERP analysis can significantly improve the detection of consciousness recovery after taVNS treatment.

4.1.3. Functional magnetic resonance imaging

In patients with DOC, fMRI can investigate altered brain network connectivity, highlighting changes in the DMN and other primary networks both before and after taVNS treatment, signifying the potential restoration of functional networks. Although studies have demonstrated the fMRI tend to expensive and inaccessibility, more efforts can be taken to explore different types of fMRI (resting-state and task-based) and offer more comprehensive understanding of the neural mechanisms involved in taVNS treatment (Kondziella et al., 2020; Snider and Edlow, 2020).

4.1.4. Integration of imaging techniques

Combining fMRI with other neuroimaging techniques like diffusion tensor imaging (DTI) or magnetoencephalography (MEG) could provide a broader perspective on the structural and functional changes following taVNS treatment (Pourmotabbed et al., 2022).

4.1.5. Emerging neuroimaging techniques: near-infrared spectroscopy

Near-Infrared Spectroscopy (NIRS), an upcoming neuroimaging technique, has potential to offer insights into the neural mechanisms underlying taVNS treatment and its effects on consciousness recovery. Although NIRS has advantages, further research is required to validate its reliability in evaluating the effect of taVNS on brain function in DOC patient (Si et al., 2018; Zhang et al., 2018).

4.2. Comparative analysis of taVNS effects in DOC patients

4.2.1. Effects of taVNS in *VS*/UWS and MCS patients

Several studies have investigated the effectiveness of taVNS in promoting consciousness recovery in patients with *VS*/UWS. Generally, these studies have utilized the CRS-R as the primary outcome measure to assess changes in patients' consciousness levels. For example, Yu 's case report demonstrated significant improvement in CRS-R scores for a 73-year-old female patient in a *VS* for 50 days following cardiopulmonary resuscitation after receiving taVNS treatment (Yu et al., 2017). In the case study by Osińska et al., (2022), a 28-year-old female with persistent UWS due to TBI for 6 years was examined. Behavioral indices of consciousness improved during taVNS but ceased post-stimulation. Additionally, EEG analysis demonstrated increasing alpha power over months of taVNS, suggesting possible neural reintegration.

Studies suggested that taVNS is a promising therapy for MCS patient. For instance, Noé et al. study observed significant improvements in CRS-R scores, particularly among MCS patients (Noé et al., 2020). Zhou conducted a randomized controlled trial and discovered that there were noticeable variations in CRS-R scores between the active taVNS and sham groups for patients in a state of minimal consciousness, but there were no significant differences in scores for patients in a *VS* (Zhou et al., 2023). Wang's RCT in China enrolled 12 participants (6 with MCS and 6 with *VS*). The study unveiled distinct modulatory effects of taVNS on consciousness states. Particularly, taVNS exhibited selective influence on delta wave energy and brain connectivity. Importantly, MCS patients displayed a notable taVNS response, showcasing heightened brain connection activity that could potentially facilitate awakening.

4.2.2. Effects of taVNS in TBI-related and non-TBI-related DOC

It is necessary to explore the therapeutic effect of taVNS on disturbance of consciousness caused by TBI and not-TBI, respectively. There may be different responses to taVNS depending on the etiology of the brain injury, such as TBI and not-TBI. For example, tbi may cause more diffuse axonal injury and damage to the white matter tracts, while non-TBI may cause more focal lesions and ischemia (Briand et al., 2020). These differences may affect the neural pathways and networks that are modulated by taVNS.

Studies on TBI-related DOC patients have shown promising results regarding the effectiveness of taVNS in promoting consciousness recovery. Hakon's feasibility study on patients with severe TBI reported progress in the consciousness state of three

patients (Hakon et al., 2020). Wang's RCT found that taVNS might improve brain connectivity, particularly in MCS patients with TBI (Yifei et al., 2022).

For non-TBI-related DOC patients, taVNS were found as potential strategy for promoting consciousness recovery. It has been discovered that patients who still have normal hearing abilities, particularly those who are not suffering from traumatic brain injuries, tend to have a more positive response to taVNS therapy. Additionally, taVNS has been observed to increase blood flow in various regions of the brain for these patients (Yu et al., 2021).

4.2.3. Effects of taVNS in RtAS and non-RtAS DOC

In the exploration of taVNS effects within the realm of DOC, Yu's study from China focused on patients categorized under responded to auditory stimuli (RtAS) and non-responded to auditory stimuli (non-RtAS) subtypes. The study encompassed 10 participants, comprising 7 in *VS* and 3 in MCS. Notably, the study revealed favorable outcomes following 4 weeks of taVNS treatment in RtAS DOC patients, while non-RtAS cases exhibited dissimilar responses. The influence of taVNS was further elucidated by elevated cerebral blood flow in diverse brain regions among RtAS DOC patients, with a notably restricted impact in non-RtAS individuals. Remarkably, the presence of preserved auditory function emerged as a pivotal determinant of taVNS responsiveness in DOC patients. These findings suggest the potential of taVNS to ameliorate RtAS DOC conditions through engagement with pivotal neural networks, including the salience network, limbic system, and interoceptive system. The study's insights illuminate the contrasting taVNS effects observed within disorders of consciousness, effectively distinguishing between RtAS and non-RtAS instances.

5. The impact of taVNS on consciousness in DOC

5.1. Brain networks involved in consciousness control

Understanding the neural mechanisms controlling consciousness is crucial for developing therapeutic strategies for DOC. While the complete understanding of the mechanisms involved is still unclear, several key brain networks and their interactions are involved in the regulation of consciousness.

These networks include: Ascending Reticular Activating System (ARAS): The ARAS originates in the upper brainstem and plays a key role in arousal, wakefulness, and alertness (Duclos et al., 2020). It connects with the central thalamus and cerebral cortex, providing neuronal input to other networks involved in consciousness; Forebrain Circuit: This cortico-striato-thalamo-cortical loop interacts with the ARAS, frontal lobe, and central thalamus, contributing to the regulation of forebrain arousal (Li et al., 2012); Frontoparietal Network: Comprising two subnetworks, DMN and the External Network (EXN), the frontoparietal network is responsible for internal consciousness, attention, and action selection (Amgalan et al., 2022); SN: The SN connects various regions of the brain and plays a switching role between the DMN and EXN, facilitating the regulation of consciousness (Li et al., 2017).

Understanding the roles of these networks in consciousness control is crucial for developing effective treatment methods for DOC, including taVNS. In the context of taVNS therapy, these networks serve as potential targets for inducing recovery of impaired consciousness in DOC patients.

5.2. Pathophysiology of UWS and MCS

The pathophysiological mechanisms of different consciousness disorders may vary, and understanding these differences may aid in developing more targeted and effective treatment methods. Research indicates that patients with UWS and MCS exhibit significant changes in the frontoparietal and DMNs, leading to differences in their levels of consciousness (Escrichs et al., 2022).

UWS patients display severe disruption of connectivity within the frontoparietal network and between the frontoparietal network and the DMN (Zhou et al., 2019). This disruption is associated with a lack of conscious awareness and response to external stimuli. Moreover, UWS patients exhibit reduced activity and connectivity in the DMN, which is related to a lack of self-referential processing and internal consciousness (Dong et al., 2018).

Compared to UWS patients, MCS patients showed partially preserved connections in the frontoparietal network and DMN (Farahani et al., 2019). Although these connections may be weaker than in healthy individuals, they are sufficient to support minimal levels of consciousness and responses to external stimuli (Fernández-Espejo et al., 2012; Crone et al., 2014). MCS patients exhibit higher activity in the DMN compared to UWS patients, indicating a degree of preserved self-referential processing and internal consciousness.

Understanding these differences in neural network connectivity and activity in UWS and MCS patients may inform the development of tailored treatment methods, including taVNS. By targeting specific disruptions in connectivity and activity within these networks, it may be possible to enhance the effectiveness of taVNS in promoting consciousness recovery in patients with different consciousness disorders.

5.3. Mechanisms of taVNS on consciousness recovery in DOC

The mechanisms of action of taVNS involve complex interactions between neural networks and functions. It has a comprehensive impact on brain network connectivity, neurotransmitters, neuronal excitability, neural plasticity, and inflammation, which may collectively contribute to the recovery of impaired consciousness in patients with DOC.

5.3.1. Brain network connectivity and neurotransmitters

Activation of the spinal trigeminal nucleus and NTS (Zhao et al., 2017): taVNS stimulates the ABVN, leading to the activation of the spinal trigeminal nucleus and NTS in the lower brainstem. This activation plays a crucial role in the arousal process and regulates various functional aspects of consciousness networks.

Activation of the reticular activating system (RAS) in the LC and raphe nuclei (Sumi-Akamaru et al., 2016): The activated NTS

influences the LC and raphe nuclei in the upper brainstem, part of the RAS. This activation contributes to arousal and alertness and is involved in neurotransmitter pathways, including the noradrenaline and serotonin pathways.

Regulation of the thalamus, striatum, and central loop model: The LC (noradrenaline pathway) and raphe nuclei (serotonin pathway) directly activate the thalamus, which in turn activates the striatum (Osińska et al., 2022). This activation helps reconstruct the central loop model, promoting consciousness recovery through the support of forebrain arousal regulation.

Activation of the SN, EXN, and DMN (Feng et al., 2022): Activation of the LC (noradrenaline pathway) influences consciousness by promoting SN and EXN activation, involved in attention and action selection. SN activation helps switch from DMN to EXN, improving negative connectivity between DMN and EXN, which is essential for internal awareness and self-referential processes.

Activation of the raphe nuclei and DMN connectivity (Rong et al., 2016): Activation of the raphe nuclei (serotonin pathway) can increase DMN activity and connectivity, which may help improve consciousness in DOC patients.

5.3.2. Effects on neural plasticity

TaVNS has been found to promote neural plasticity, the brain's ability to reorganize and form new neural connections. Studies have shown that taVNS can enhance long-term potentiation and increase the expression of neurotrophic factors, such as BDNF (Wang Y. M. et al., 2021). This is particularly important for DOC patients, as it can promote the recovery of damaged neural pathways and the reconstruction of more functional neural circuits. Significantly, taVNS is believed to influence neural activity through the global release of neuromodulators in the brain.

The cholinergic system is primarily characterized by the neurotransmitter ACh and has diverse effects throughout the body, especially in the CNS. The fundamental principle behind VNS-evoked cortical neuromodulation is to amplify the positive effects of VNS by coupling its activation with particular sensory or motor events. By temporally associating this neuromodulatory effect with distinct sensory or motor events, synaptic connections linked to those events are fortified, thus encouraging long-term potentiation and increased neural plasticity (Hays et al., 2013). Research indicates a significant contribution of VNS-evoked basal forebrain ACh release in the neocortex (Mridha et al., 2021). From a motor perspective, VNS paired with forelimb movements instigates reorganization within the motor cortex, but notably, this plasticity does not arise if lesions develop in the cortical cholinergic projections originating from the basal forebrain (Hulsey et al., 2016). On the sensory front, coordinating sound exposure with VNS induces a reshaping of the auditory cortical map, mirroring the alterations observed when sounds are synchronized with basal ganglia stimuli (Borland et al., 2019).

The maintenance of auditory function might play a crucial role in the responsiveness of patients with DOC to taVNS. This is supported by findings indicating that in patients who did not exhibit a response to auditory stimulation, the surge in cerebral blood flow during taVNS treatment was notably subdued (Yu et al., 2021). On another front, the effect of VNS on cortical excitatory synchrony diminishes when muscarinic receptors in the auditory cortex are inhibited, suggesting a significant role for ACh released from the basal forebrain (Engineer et al., 2011; Nichols et al., 2011). Further research (Mridha et al., 2021) has determined that the response of auditory cortical neurons to VNS is dependent on stimulation parameters, with varying degrees of activation in cholinergic neurons based on different stimulation settings. Moreover, this research also discovered that the pupil dilation is induced by cholinergic fibers triggered by VNS, and its behavior varies based on the immediate state of the brain. This suggests pupil dilation as a potential non-invasive biosensor for VNS-induced alterations in neuromodulatory brain states.

5.3.3. Neuronal excitability regulation

TaVNS can directly or indirectly influence neuronal excitability by stimulating the VN (Zheng et al., 2021). It may modulate the activity of ion channels and neurotransmitter systems, leading to changes in the excitability of neural circuits. By modulating neuronal excitability, taVNS may help restore the normal function of affected neural circuits, thereby improving cognitive and behavioral outcomes for DOC patients.

5.3.4. Anti-inflammatory effects

Inflammation is often associated with various neurological disorders, including brain injury and neurodegenerative diseases. TaVNS has been shown to have anti-inflammatory effects by modulating the release of cytokines and other inflammatory mediators (Rawat et al., 2019). By reducing inflammation, taVNS can promote a more favorable environment for neural recovery in DOC patients, which may ultimately contribute to improvements in consciousness and cognitive function.

5.3.5. Autonomic nervous system regulation

TaVNS has been shown to regulate the activity of the autonomic nervous system, particularly the balance between the sympathetic and parasympathetic branches (Clancy et al., 2014; Colzato et al., 2018). Stimulating the VN can increase parasympathetic activity, which can indirectly impact consciousness recovery by promoting overall brain health and function. Additionally, activation of the VN can regulate the release of neurotrophic factors, such as BDNF, which can promote neural plasticity and aid in the recovery of consciousness.

In conclusion, the mechanisms of action of taVNS on consciousness recovery involve the activation of vagal nerve cortical pathways, neurotransmitter regulation, and autonomic nervous system regulation. These mechanisms can collectively promote the restoration of functional networks that support consciousness, ultimately leading to improvements in behavioral and neurophysiological outcomes. Further research is needed to better understand the specific interactions and contributions of these mechanisms in the context of taVNS treatment for DOC.

6. Factors influencing treatment response

In administering taVNS treatment, it becomes clear that a one-size-fits-all approach is insufficient. The unique conditions and recovery goals of each patient demand that we adjust the stimulation parameters accordingly. Especially in the case of consciousness disorders, precision therapy is the crux of effective treatment. The delicate balance among stimulation parameters hinges on the complex interplay of the patient's condition, recovery goals, and the biophysical

characteristics of the nerve fibers. This intricate dance holds immense potential for unlocking new pathways to restore consciousness in patients with consciousness disorders. In Table 2, a summarized overview is provided, detailing the stimulation sites, device characteristics, parameter settings, stimulation duration, main findings, and side effects from relevant studies.

6.1. Stimulation parameters

In taVNS therapy, the choice of stimulation parameters is critical as it directly impacts the treatment outcomes. The primary stimulation parameters include the waveform, pulse width, intensity, frequency and duration of the stimulus.

6.1.1. Frequency

Four studies adopted a frequency of 20 Hz (Yu et al., 2017, 2021; Yifei et al., 2022; Zhou et al., 2023). On the other hand, four other studies each utilized a slightly higher frequency of 25 Hz (Hakon et al., 2020; Noé et al., 2020; Osińska et al., 2022; Vitello et al., 2023). The convergence around the 20 Hz to 25 Hz range indicates a potential sweet spot in frequency parameters for taVNS, yet the nuances of these choices underscore the continued efforts to fine-tune the therapy for optimal results.

While the FDA has approved 20–30 Hz frequencies for VNS (Groves and Brown, 2005), frequencies of 50 Hz and above may cause considerable and irreversible harm to the VN (Agnew and McCreery, 1990). Given the anatomical distinctions between the ABVN and neck VN, the safe frequency range for taVNS remains undefined. Thus, it's incorrect to assume that the 20–30 Hz range is optimal for taVNS. Comprehensive controlled studies are essential to determine the impacts of different stimulation frequencies. Some researchers have already unveiled their study protocols in which patients undergo taVNS at five distinct frequencies (1, 10, 25, 50, and 100 Hz) to pinpoint the most effective stimulation frequency for treating DOC patients (Zhai et al., 2023).

6.1.2. Pulse width

When considering taVNS parameter settings for the treatment of DOC, different studies have chosen varied pulse widths. One study used a pulse width of 200us (Zhou et al., 2023), aligning with the lower range of another that ranged from 200 to 300us (Vitello et al., 2023). Three other studies standardized their pulse width at 250us (Hakon et al., 2020; Noé et al., 2020; Osińska et al., 2022). Another RCT reported a pulse width of 500us (Yu et al., 2021), which is consistent with a broader parameter of less than 1000us observed in two other studies (Yu et al., 2017; Yifei et al., 2022). These varied choices reflect the diverse approaches researchers are taking in their quest to optimize therapeutic efficacy in DOC patients.

The choice of pulse width plays a pivotal role in determining the types of nerve fibers being activated (Rawat et al., 2019; Sclocco et al., 2020). For instance, short pulse width stimulations (such as 10 microseconds) are more likely to activate Aβ fibers, primarily associated with tactile transmission. On the other hand, longer pulse widths (e.g., 1,000 microseconds) are more inclined to stimulate various types of nerve fibers, including Aδ and C fibers related to pain perception (Salchow-Hömmen et al., 2018). Therefore, when selecting the pulse width, one must consider the target of stimulation and the anticipated sensory effects.

6.1.3. Waveform

In taVNS studies for DOC treatment, one used a single-phase square wave (Osińska et al., 2022), while another adopted a sinusoidal waveform (Noé et al., 2020). Notably, several other studies did not specify their choice of waveform, suggesting that device-specific waveforms may have been used in these instances (Yu et al., 2017, 2021; Hakon et al., 2020; Yifei et al., 2022; Vitello et al., 2023; Zhou et al., 2023). The variations and omissions in waveform descriptions underscore the need for more standardized reporting in future research to fully understand the potential nuances and effects of different waveforms in taVNS treatment.

The choice of waveform can also influence the stimulation effects. For example, peak waveform stimulations could be more precise as some types of nerve fibers (like Aβ fibers) show heightened sensitivity to such waveforms (Song et al., 2020). In this scenario, a shorter pulse width can activate Aβ fibers more effectively, leading to a more accurate stimulation effect.

6.1.4. Intensity

In the realm of taVNS treatments for DOC, various stimulation intensities are observed across studies. One study employed an intensity range from 0.2 mA to 1.5 mA (Osińska et al., 2022), another maintained a steady 1.5 mA (Noé et al., 2020), while a different research set the intensity at 3 mA (Vitello et al., 2023). Both an RCT and another study settled on an intensity span of 4–6 mA (Yu et al., 2021; Yifei et al., 2022), with a similar range seen in a separate case report (Yu et al., 2017). A distinct study adopted a more incremental strategy (Hakon et al., 2020), starting with an intensity of up to 0.5 mA for the initial 3 days and then elevating it to 1 mA for the subsequent eight-week duration. This variation in intensities across studies underscores the ongoing exploration to determine the optimal parameters for therapeutic efficacy in DOC patients.

The selection of stimulation intensity and frequency should be adjusted according to the patient's pain threshold, aiming to achieve effective nerve stimulation without causing excessive pain. For patients with consciousness disorders, their perception of pain induced by electrical stimulation may be reduced due to sensory and cognitive limitations (Wang J. Y. et al., 2021). Therefore, in certain cases, it may be necessary to employ longer stimulation pulse widths and greater stimulation intensity to activate a variety of nerve fiber types. In the practice of neuroelectric stimulation, the choice of stimulated nerve fiber type (such as C fibers or Aβ fibers) is indeed crucial to the stimulation effect and therapeutic goals (Huang et al., 2018). This decision depends on the specific therapeutic objectives and the patient's condition. Utilizing a larger pulse width may stimulate a variety of nerve fiber types concurrently, including motor and sensory nerves (Li et al., 2014).

6.1.5. Duration of treatment

In taVNS treatments for DOC, the duration and regularity of sessions might influence therapeutic outcomes. One study opted for a 4-week protocol with 30-min sessions (Zhou et al., 2023), while another pursued a rigorous 6-month regimen with daily 4-h sessions (Osińska et al., 2022). An approach spanning 14 days involved two daily treatments for four consecutive weeks, dedicating 30 min to each ear (Yifei et al., 2022). Another protocol was structured over 90 days with sessions lasting 45 min each (Vitello et al., 2023). Several studies adopted a regimen of twice-daily sessions, each lasting 30 min (Yu et al., 2017; Noé et al., 2020; Yu et al., 2021). Of these, one lasted

TABLE 2 Stimulation location, parameters, therapeutic effects, and side effects for all studies assessing the efficacy of taVNS in patient with DOC.

First author	Study groups	No. of disorders	Stimulation sites and device	Parameter settings	Stimulation Period	Assessment	Clinical outcomes	Side effects
Zhou, 2023	taVNS/sham group; RCT	*VS*:29; MCS:28	Left outer ear; tVNS 501 Changzhou Rishena Medical Device Co., Ltd., Jiangsu, China	20 Hz, 200us	4 weeks, 30 min/session	CRSR	Effective for MCS, not *VS*/UWS	Common side effects, unrelated to taVNS.
Osińska, 2022	Case Report	UWS for 6 years, TBI, 28-year-old female	tVNS Technologies, Erlangen, Germany	25 Hz, 250us, single-phase square wave, 30s-30s, 0.2 mA-1.5 mA	6 months; every day; 4 h/day	CRSR; EEG	Behavioral consciousness indices rose with tVNS, halted post-stimulation. EEG alpha power increased over months of tVNS, suggesting neural reintegration.	None reported
Wang, 2022	taVNS/sham group; RCT	*VS*/UWS:7; MCS:5	Bilateral auricular concha; Huatuo brand electronic acupuncture instrument (SDZ-II B type, Suzhou Medical Products Factory Co.)	20 Hz, <1000us, 4-6 mA	14 days, twice per day for four consecutive weeks, 30 min in each ear	CRSR; EEG	Differentially modulates consciousness states; Effective for MCS; Alters delta wave energy and brain connectivity selectively.	None reported
Vitello, 2022	taVNS/sham group; RCT	TBI 7–90 days	Bilateral over the cymba conchae; Cerbomed GmbH, Germany, NEMOS/tVNS®	25 Hz, 200-300us, 30s-30s, 3 mA	90 days, 45 min/day	CRSR, hd-EEG	None reported	None reported
Yu, 2021	RtAS/nRtAS; RCT	MCS:3; *VS*: 7	Over the concha	20 Hz, 500 ms, 4-6 mA	30 min; twice a day (8:00 and 16:00) for 4 weeks	CRSR; 3.0 T ASL-FMRI	Boosted CBF in RtAS, not in nRtAS.	None reported
Noé, 2020	RCT	*VS*/UW: 6; MCS: 8	Left tragus; Parasym® CE	20 Hz, 250us, 1.5 mA, Sinusoidal waveform	30-min sessions, twice a day (5 days per week), 40 sessions	CRSR	MCS patients respond better than *VS*/UWS patients; VNS benefits emerge with time and repeated treatment.	None reported
Hakon, 2020	Single-Armed Open-Label Feasibility Study	TBI: *VS*/UWS:3; MCS:2	Left cymba conchae; tVNS Nemos® (Cerbomed, Germany; CE-marked 2011)	25 Hz, 250us, 30 s on/30 s off, with up to 0.5 mA for the first 3 days, and subsequently 1 mA for the remaining eight-week period	8 weeks	CRSR	tVNS for 8 weeks, 4 h daily, is feasible and safe in *VS*/UWS and MCS patients	None reported
Yu, 2017	Case Report	*VS* for 50 days after cardiopulmonary resuscitation, 73-year-old female	Bilateral ear concha	20 Hz, <1000us, 4-6 mA	Twice daily for 30 min each, for four consecutive weeks	CRSR; 3.0 T fMRI	Shift from *VS*-MCS associated with altered brain FC patterns taVNS promotes enhanced functional connectivity of DMN.	None reported

10.3389/fnins.2023.1286267

4 weeks (Yu et al., 2021), while another covered 40 sessions over 5 days a week (Noé et al., 2020). A different study had an 8-week duration (Hakon et al., 2020). These variations underscore the diverse strategies in play, as researchers navigate the most effective treatment duration and frequency for taVNS in DOC patients.

6.2. Stimulation site

In taVNS treatments for DOC, studies have explored various ear locations for stimulation. One study targeted the left outer ear (Zhou et al., 2023), while others emphasized the bilateral auricular concha (Yu et al., 2017, 2021; Yifei et al., 2022). A different research chose a bilateral approach, specifically on the cymba conchae (Vitello et al., 2023). Another study selected the left tragus (Noé et al., 2020), and yet another preferred the left cymba conchae (Hakon et al., 2020). These variations in stimulation sites highlight the diverse approaches researchers are employing, potentially aiming to maximize the therapeutic efficacy of taVNS.

Among taVNS stimulation in DOC, several studies stimulate the concha bilaterally, whereas quite a few studies usually stimulate the left concha to avoid causing cardiac discomfort. The predominant concern with right-sided or bilateral cervical VNS is its potential to influence cardiac function since the right vagus nerve provides more substantial innervation to the heart (Capilupi et al., 2020). Thus, the traditional approach, especially in implantable VNS devices for epilepsy, is to stimulate the left cervical vagus nerve to mitigate this risk. However, when it comes to the auricular branches, the anatomical and physiological connections might be different (Elamin et al., 2023), which could account for differing side-effect profiles. While some studies have advocated for unilateral left-sided taVNS due to the perceived safety profile, others suggest that bilateral concha stimulation might not present the same cardiac risks as cervical VNS (Ardell et al., 2017; Elamin et al., 2023). However, it's crucial to approach this notion cautiously, as the evidence is still emerging. Clinical assessments and cardiac monitoring during taVNS can provide essential data regarding this.

6.3. Individual variability

6.3.1. Etiology of injury

The etiology of the brain injury may influence the response to taVNS treatment. For example, patients with traumatic brain injuries may have more focal lesions, which could disrupt the structural integrity of the thalamus and brainstem nuclei (Osińska et al., 2022; Yifei et al., 2022). In these cases, taVNS may be more effective in reinstating thalamo-cortical connectivity and promoting consciousness recovery (Yu et al., 2021). On the other hand, anoxic brain injuries often result in diffuse damage to subcortical regions and white matter, which might reduce the effectiveness of taVNS in some patients (Yifei et al., 2022).

6.3.2. Baseline patient characteristics

Baseline patient characteristics, such as the severity of the disorder of consciousness (e.g., UWS vs. MCS), age, and duration since injury, can also influence treatment response (Noé et al., 2020; Zhou et al., 2023). Patients in a MCS may display higher levels of neuroplasticity and reorganization within awareness networks, making them potentially more responsive to brain stimulation interventions like taVNS (Hakon et al., 2020). Additionally, younger patients and those in the early stages of injury may show better treatment responses due to higher neuroplasticity and recovery potential (Yu et al., 2017).

6.4. Safety and tolerability

6.4.1. Safety and tolerability of taVNS

TaVNS has generally been reported as a safe and well-tolerated treatment option for various conditions, including DOC, depression, epilepsy, and migraine. The low risk of severe complications associated with taVNS makes it an attractive treatment option for patients with DOC, who may have limited therapeutic options and be more susceptible to complications from invasive treatments (Dong and Feng, 2018). The non-invasive of the intervention, which involves delivering electrical stimulation through the skin overlying the VN, minimizes the risks associated with more invasive procedures such as implanted VNS devices (Yu et al., 2017, 2021; Hakon et al., 2020; Noé et al., 2020; Osińska et al., 2022; Yifei et al., 2022; Zhou et al., 2023). In clinical trials, taVNS has demonstrated good tolerability and compliance, with most patients with DOC able to complete the treatment without significant adverse events (Yu et al., 2017, 2021; Zhou et al., 2023). The side effects of taVNS are generally mild and transient, including skin irritation, itching, or redness at the site of electrode placement, as well as transient dizziness, headache, or nausea (Zhou et al., 2023).

To ensure safety and tolerability, researchers have carefully chosen stimulation parameters for taVNS (Yu et al., 2017, 2021; Hakon et al., 2020; Noé et al., 2020; Osińska et al., 2022; Yifei et al., 2022; Zhou et al., 2023). Current research suggests that typical parameters involve a frequency of 20–25 Hz and a pulse width range of 0.25–1 ms. Studies have shown that the probability of adverse events is extremely low when the stimulation frequency is within the range of 0.5–120 Hz and the pulse width is within 0.02–1 ms. The stimulation intensity generally ranges from 0.2 to 6 mA, but it is usually adjusted according to individual participants. In taVNS studies involving conscious patients, the stimulation current intensity is often set based on the patient's pain threshold. However, for DOC patients who cannot provide timely feedback, researchers have developed alternative methods, such as setting the stimulation current at 200% of the patient's perception threshold and calibrating the current to each participant's minimum perceptual level. Most studies have set the treatment duration to 30 min per session, twice a day.

6.4.2. Individualized treatment considerations

When DOC patients turn into chronic disorders of consciousness, patients may either be in a post-traumatic state or possess severe chronic underlying ailments. However, The relationship between taVNS and varying states of DOC patients remains an emerging area of research. It's important to note that the modulation of taVNS on Heart Rate Variability (HRV) metrics can differ based on the employed stimulation parameters (De Couck et al., 2017; Geng et al., 2022a). Although some research offers divergent perspectives on taVNS's influence on HRV metrics, a consensus is emerging that taVNS exhibits considerable potential in ameliorating HRV and augmenting cardiac autonomic regulation in healthy subjects (Geng et al., 2022b).

Furthermore, there's emerging evidence that taVNS could serve as a prophylactic intervention for conditions like pre-diabetes or impaired glucose tolerance (Huang et al., 2014; Li et al., 2018). However, it's pertinent to mention a significant contraindication: VNS is not recommended for individuals post-splenectomy. Several studies indicate that the spleen plays a critical role in the anti-inflammatory action of the VN (Huston et al., 2006, 2009; Gigliotti et al., 2013; Ji et al., 2014). Once the spleen is removed through splenectomy, the efficacy of VNS in curbing inflammation is notably compromised.

Despite the generally favorable safety profile of taVNS, some prevention strategies should be taken when administering this treatment. Patients with certain medical conditions, such as cardiac arrhythmias or uncontrolled epilepsy, may be at increased risk for complications and should be carefully evaluated before initiating taVNS treatment (Vaseghi et al., 2017; Yuan et al., 2017). Furthermore, individualized treatment protocols should be developed, taking into consideration the patient's clinical history, the severity of the DOC or other conditions being treated, and any potential contraindications.

7. Potential challenges and future research directions

7.1. Small sample sizes and lack of control groups

Many existing studies on taVNS in DOC patients have small sample sizes, which may limit the generalizability of the results (Osińska et al., 2022; Yifei et al., 2022). Additionally, some studies lack appropriate control groups, making it difficult to conclusively attribute observed improvements to taVNS treatment (Yu et al., 2017; Noé et al., 2020). Future research should aim to conduct large-scale, randomized controlled trials to provide more robust evidence on the efficacy of taVNS in DOC patients.

7.2. Diversity in treatment parameters

There is considerable variability in the treatment parameters used in taVNS research, such as stimulation frequency, intensity, duration, and electrode placement. This variability can make it challenging to compare and synthesize results across studies. Future research should focus on identifying optimal treatment parameters for specific patient populations, as well as investigating potential dose–response relationships and individual factors that may influence treatment outcomes.

7.3. Evaluating long-term treatment effects

Many studies have focused on the short-term effects of taVNS treatment, with limited data available on long-term outcomes. It is crucial to assess whether the observed improvements in consciousness and cognitive function persist over time, and whether repeated or prolonged taVNS treatment may yield cumulative benefits. Future studies should include long-term follow-up assessments to better understand the durability and potential lasting effects of taVNS therapy in DOC patients.

7.4. Investigating mechanisms of action

While several hypotheses have been proposed to explain the therapeutic effects of taVNS, the precise mechanisms of action remain incompletely understood. Some studies have suggested the involvement of specific brain regions or networks, such as the DMN (Yu et al., 2017), and others have reported changes in CBF (Yu et al., 2021). Future research should aim to elucidate the neural pathways and molecular mechanisms underlying the effects of taVNS, which may ultimately inform the development of more targeted and effective treatment strategies.

In conclusion, within the realm of brain regulation technology for DOC, taVNS technology emerges as a promising avenue for future exploration. Presently, research regarding the clinical outcomes of taVNS and its role in mediating brain–body interplay is nascent. The utilization of taVNS in addressing consciousness impairments is yet to be substantiated by comprehensive evidence-based medical studies, necessitating further scrutiny into its therapeutic modalities and stimulation parameters. As neuroscience research technologies evolve, there will undoubtedly be an enhanced and refined understanding of cerebral structure and functionality.

Author contributions

LikW: Writing – original draft, Writing – review & editing. FG: Writing – original draft, Writing – review & editing. ZW: Writing – original draft, Writing – review & editing. FL: Conceptualization, Methodology, Writing – original draft. YD: Investigation, Writing – review & editing. MW: Investigation, Writing – review & editing. JW: Conceptualization, Writing – review & editing. YC: Investigation, Writing – review & editing. QY: Investigation, Writing – original draft. LitW: Conceptualization, Investigation, Writing – original draft, Writing – review & editing.

Funding

The author(s) declare financial support was received for the research, authorship, and/or publication of this article. This project was partly supported by the Basic scientific research project of Liaoning Provincial Department of Education (LJKMZ20221292) and the Dalian Chinese Medicine Scientific Research Project (22Z12018).

Acknowledgments

We would like to thank Editage (www.editage.cn) for English language editing.

Conflict of interest

The authors declare that the research was conducted in the absence of any commercial or financial relationships that could be construed as a potential conflict of interest.

Publisher's note

References

Agnew, W. F., and McCreery, D. B. (1990). Considerations for safety with chronically implanted nerve electrodes. *Epilepsia* 31, S27–S32. doi: 10.1111/j.1528-1157.1990.tb05845.x

Ahmed, U., Chang, Y. C., Zafeiropoulos, S., Nassrallah, Z., Miller, L., and Zanos, S. (2022). Strategies for precision vagus neuromodulation. *Bioelectron. Med.* 8:9. doi: 10.1186/s42234-022-00091-1

Amgalan, A., Maher, A. S., Imms, P., Ha, M. Y., Fanelle, T. A., and Irimia, A. (2022). Functional connectome dynamics after mild traumatic brain injury according to age and sex. *Front. Aging Neurosci.* 14:852990. doi: 10.3389/fnagi.2022.852990

Ardell, J. L., Nier, H., Hammer, M., Southerland, E. M., Ardell, C. L., Beaumont, E., et al. (2017). Defining the neural fulcrum for chronic vagus nerve stimulation: implications for integrated cardiac control. *J. Physiol.* 595, 6887–6903. doi: 10.1113/jp274678

Åslund, A. K., Snipstad, S., Healey, A., Kvåle, S., Torp, S. H., Sontum, P. C., et al. (2017). Efficient enhancement of blood-brain barrier permeability using acoustic cluster therapy (ACT). *Theranostics* 7, 23–30. doi: 10.7150/thno.16577

Austelle, C. W., O'Leary, G. H., Thompson, S., Gruber, E., Kahn, A., Manett, A. J., et al. (2022). A comprehensive review of vagus nerve stimulation for depression. *Neuromodulation* 25, 309–315. doi: 10.1111/ner.13528

Badran, B. W., Dowdle, L. T., Mithoefer, O. J., LaBate, N. T., Coatsworth, J., Brown, J. C., et al. (2018). Neurophysiologic effects of transcutaneous auricular vagus nerve stimulation (taVNS) via electrical stimulation of the tragus: a concurrent taVNS/fMRI study and review. *Brain Stimul.* 11, 492–500. doi: 10.1016/j.brs.2017.12.009

Bai, Y., Lin, Y., and Ziemann, U. (2021). Managing disorders of consciousness: the role of electroencephalography. *J. Neurol.* 268, 4033–4065. doi: 10.1007/s00415-020-10095-z

Ben-Menachem, E., Revesz, D., Simon, B. J., and Silberstein, S. (2015). Surgically implanted and non-invasive vagus nerve stimulation: a review of efficacy, safety and tolerability. *Eur. J. Neurol.* 22, 1260–1268. doi: 10.1111/ene.12629

Bermejo, P., López, M., Larraya, I., Chamorro, J., Cobo, J. L., Ordóñez, S., et al. (2017). Innervation of the human cavum conchae and auditory canal: anatomical basis for transcutaneous auricular nerve stimulation. *Biomed. Res. Int.* 2017, 7830919–7830910. doi: 10.1155/2017/7830919

Borland, M. S., Vrana, W. A., Moreno, N. A., Fogarty, E. A., Buell, E. P., Vanneste, S., et al. (2019). Pairing vagus nerve stimulation with tones drives plasticity across the auditory pathway. *J. Neurophysiol.* 122, 659–671. doi: 10.1152/jn.00832.2018

Breit, S., Kupferberg, A., Rogler, G., and Hasler, G. (2018). Vagus nerve as modulator of the brain-gut Axis in psychiatric and inflammatory disorders. *Front. Psych.* 9:44. doi: 10.3389/fpsyt.2018.00044

Briand, M. M., Gosseries, O., Staumont, B., Laureys, S., and Thibaut, A. (2020). Transcutaneous auricular vagal nerve stimulation and disorders of consciousness: a hypothesis for mechanisms of action. *Front. Neurol.* 11:933. doi: 10.3389/fneur.2020.00933

Butt, M. F., Albusoda, A., Farmer, A. D., and Aziz, Q. (2020). The anatomical basis for transcutaneous auricular vagus nerve stimulation. *J. Anat.* 236, 588–611. doi: 10.1111/joa.13122

Calvillo, L., Vanoli, E., Andreoli, E., Besana, A., Omodeo, E., Gnecchi, M., et al. (2011). Vagal stimulation, through its nicotinic action, limits infarct size and the inflammatory response to myocardial ischemia and reperfusion. *J. Cardiovasc. Pharmacol.* 58, 500–507. doi: 10.1097/FJC.0b013e31822b7204

Capilupi, M. J., Kerath, S. M., and Becker, L. B. (2020). Vagus nerve stimulation and the cardiovascular system. *Cold Spring Harb. Perspect. Med.* 10:a034173. doi: 10.1101/cshperspect.a034173

Caravaca, A. S., Gallina, A. L., Tarnawski, L., Shavva, V. S., Colas, R. A., Dalli, J., et al. (2022). Vagus nerve stimulation promotes resolution of inflammation by a mechanism that involves Alox15 and requires the α7nAChR subunit. *Proc. Natl. Acad. Sci. U. S. A.* 119:e2023285119. doi: 10.1073/pnas.2023285119

Chen, H., Feng, Z., Min, L., Deng, W., Tan, M., Hong, J., et al. (2022). Vagus nerve stimulation reduces neuroinflammation through microglia polarization regulation to improve functional recovery after spinal cord injury. *Front. Neurosci.* 16:813472. doi: 10.3389/fnins.2022.813472

Chen, X., He, X., Luo, S., Feng, Y., Liang, F., Shi, T., et al. (2018). Vagus nerve stimulation attenuates cerebral microinfarct and colitis-induced cerebral microinfarct aggravation in mice. *Front. Neurol.* 9:798. doi: 10.3389/fneur.2018.00798

Chen, S., Tang, C., Ding, H., Wang, Z., Liu, X., Chai, Y., et al. (2020). Maf1 ameliorates Sepsis-associated encephalopathy by suppressing the NF-kB/NLRP3 inflammasome signaling pathway. *Front. Immunol.* 11:594071. doi: 10.3389/fimmu.2020.594071

Clancy, J. A., Mary, D. A., Witte, K. K., Greenwood, J. P., Deuchars, S. A., and Deuchars, J. (2014). Non-invasive vagus nerve stimulation in healthy humans reduces sympathetic nerve activity. *Brain Stimul.* 7, 871–877. doi: 10.1016/j.brs.2014.07.031

Colzato, L. S., Jongkees, B. J., de Wit, M., van der Molen, M. J. W., and Steenbergen, L. (2018). Variable heart rate and a flexible mind: higher resting-state heart rate variability predicts better task-switching. *Cogn. Affect. Behav. Neurosci.* 18, 730–738. doi: 10.3758/s13415-018-0600-x

Crone, J. S., Soddu, A., Höller, Y., Vanhaudenhuyse, A., Schurz, M., Bergmann, J., et al. (2014). Altered network properties of the fronto-parietal network and the thalamus in impaired consciousness. *Neuroimage Clin.* 4, 240–248. doi: 10.1016/j.nicl.2013.12.005

De Couck, M., Cserjesi, R., Caers, R., Zijlstra, W. P., Widjaja, D., Wolf, N., et al. (2017). Effects of short and prolonged transcutaneous vagus nerve stimulation on heart rate variability in healthy subjects. *Auton. Neurosci.* 203, 88–96. doi: 10.1016/j.autneu.2016.11.003

Di, H., He, M., Zhang, Y., Cheng, L., Wang, F., Nie, Y., et al. (2017). Chinese translation of the coma recovery scale-revised. *Brain Inj.* 31, 363–365. doi: 10.1080/02699052.2016.1255780

Dong, X. Y., and Feng, Z. (2018). Wake-promoting effects of vagus nerve stimulation after traumatic brain injury: upregulation of orexin-A and orexin receptor type 1 expression in the prefrontal cortex. *Neural Regen. Res.* 13, 244–251. doi: 10.4103/1673-5374.226395

Dong, D., Wang, Y., Chang, X., Luo, C., and Yao, D. (2018). Dysfunction of large-scale brain networks in schizophrenia: a meta-analysis of resting-state functional connectivity. *Schizophr. Bull.* 44, 168–181. doi: 10.1093/schbul/sbx034

Duclos, C., Dumont, M., Paquet, J., Blais, H., Van der Maren, S., Menon, D. K., et al. (2020). Sleep-wake disturbances in hospitalized patients with traumatic brain injury: association with brain trauma but not with an abnormal melatonin circadian rhythm. *Sleep* 43:zsz191. doi: 10.1093/sleep/zsz191

Edlow, B. L., Claassen, J., Schiff, N. D., and Greer, D. M. (2021). Recovery from disorders of consciousness: mechanisms, prognosis and emerging therapies. *Nat. Rev. Neurol.* 17, 135–156. doi: 10.1038/s41582-020-00428-x

Elamin, A. B. A., Forsat, K., Senok, S. S., and Goswami, N. (2023). Vagus nerve stimulation and its cardioprotective abilities: a systematic review. *J. Clin. Med.* 12:1717. doi: 10.3390/jcm12051717

Engineer, N. D., Riley, J. R., Seale, J. D., Vrana, W. A., Shetake, J. A., Sudanagunta, S. P., et al. (2011). Reversing pathological neural activity using targeted plasticity. *Nature* 470, 101–104. doi: 10.1038/nature09656

Escrichs, A., Perl, Y. S., Uribe, C., Camara, E., Türker, B., Pyatigorskaya, N., et al. (2022). Unifying turbulent dynamics framework distinguishes different brain states. *Commun. Biol.* 5:638. doi: 10.1038/s42003-022-03576-6

Evans, M. S., Verma-Ahuja, S., Naritoku, D. K., and Espinosa, J. A. (2004). Intraoperative human vagus nerve compound action potentials. *Acta Neurol. Scand.* 110, 232–238. doi: 10.1111/j.1600-0404.2004.00309.x

Farahani, F. V., Fafrowicz, M., Karwowski, W., Douglas, P. K., Domagalik, A., Beldzik, E., et al. (2019). Effects of chronic sleep restriction on the brain functional network, as revealed by graph theory. *Front. Neurosci.* 13:1087. doi: 10.3389/fnins.2019.01087

Farrand, A., Jacquemet, V., Verner, R., Owens, M., and Beaumont, E. (2023). Vagus nerve stimulation parameters evoke differential neuronal responses in the locus coeruleus. *Physiol. Rep.* 11:e15633. doi: 10.14814/phy2.15633

Feng, M., Zhang, Y., Wen, Z., Hou, X., Ye, Y., Fu, C., et al. (2022). Early fractional amplitude of low frequency fluctuation can predict the efficacy of transcutaneous auricular Vagus nerve stimulation treatment for migraine without Aura. *Front. Mol. Neurosci.* 15:778139. doi: 10.3389/fnmol.2022.778139

Fernández-Espejo, D., Soddu, A., Cruse, D., Palacios, E. M., Junque, C., Vanhaudenhuyse, A., et al. (2012). A role for the default mode network in the bases of disorders of consciousness. *Ann. Neurol.* 72, 335–343. doi: 10.1002/ana.23635

Follesa, P., Biggio, F., Gorini, G., Caria, S., Talani, G., Dazzi, L., et al. (2007). Vagus nerve stimulation increases norepinephrine concentration and the gene expression of BDNF and bFGF in the rat brain. *Brain Res.* 1179, 28–34. doi: 10.1016/j.brainres.2007.08.045

Formica, C., De Salvo, S., Corallo, F., Alagna, A., Logiudice, A. L., Todaro, A., et al. (2021). Role of neurorehabilitative treatment using transcranial magnetic stimulation in disorders of consciousness. *J. Int. Med. Res.* 49:300060520976472. doi: 10.1177/0300060520976472

Geng, D., Liu, X., Wang, Y., and Wang, J. (2022a). The effect of transcutaneous auricular vagus nerve stimulation on HRV in healthy young people. *PLoS One* 17:e0263833. doi: 10.1371/journal.pone.0263833

Geng, D., Yang, K., Fu, Z., Zhang, Y., Wang, C., and An, H. (2022b). Circadian stage-dependent and stimulation duration effects of transcutaneous auricular vagus nerve stimulation on heart rate variability. *PLoS One* 17:e0277090. doi: 10.1371/journal.pone.0277090

Gigliotti, J. C., Huang, L., Ye, H., Bajwa, A., Chattrabhuti, K., Lee, S., et al. (2013). Ultrasound prevents renal ischemia-reperfusion injury by stimulating the splenic cholinergic anti-inflammatory pathway. *J. Am. Soc. Nephrol.* 24, 1451–1460. doi: 10.1681/asn.2013010084

Giordano, F., Zicca, A., Barba, C., Guerrini, R., and Genitori, L. (2017). Vagus nerve stimulation: surgical technique of implantation and revision and related morbidity. *Epilepsia* 58, 85–90. doi: 10.1111/epi.13678

Groves, D. A., and Brown, V. J. (2005). Vagal nerve stimulation: a review of its applications and potential mechanisms that mediate its clinical effects. *Neurosci. Biobehav. Rev.* 29, 493–500. doi: 10.1016/j.neubiorev.2005.01.004

Guo, Y., Li, R., Zhang, R., Liu, C., Zhang, L., Zhao, D., et al. (2022). Dynamic changes of brain activity in patients with disorders of consciousness during recovery of consciousness. *Front. Neurosci.* 16:878203. doi: 10.3389/fnins.2022.878203

Hakon, J., Moghiseh, M., Poulsen, I., Øland, C. M. L., Hansen, C. P., and Sabers, A. (2020). Transcutaneous Vagus nerve stimulation in patients with severe traumatic brain injury: a feasibility trial. *Neuromodulation* 23, 859–864. doi: 10.1111/ner.13148

Han, J., Chen, C., Zheng, S., Yan, X., Wang, C., Wang, K., et al. (2022). High-definition transcranial direct current stimulation of the dorsolateral prefrontal cortex modulates the electroencephalography rhythmic activity of parietal occipital lobe in patients with chronic disorders of consciousness. *Front. Hum. Neurosci.* 16:889023. doi: 10.3389/fnhum.2022.889023

Hays, S. A., Rennaker, R. L., and Kilgard, M. P. (2013). Targeting plasticity with vagus nerve stimulation to treat neurological disease. *Prog. Brain Res.* 207, 275–299. doi: 10.1016/b978-0-444-63327-9.00010-2

Hilderman, M., Qureshi, A. R., Al-Abed, Y., Abtahi, F., Lindecrantz, K., Anderstam, B., et al. (2015). Cholinergic anti-inflammatory pathway activity in dialysis patients: a role for neuroimmunomodulation? *Clin. Kidney J.* 8, 599–605. doi: 10.1093/ckj/sfv074

Hilz, M. J. (2022). Transcutaneous vagus nerve stimulation - a brief introduction and overview. *Auton. Neurosci.* 243:103038. doi: 10.1016/j.autneu.2022.103038

Howland, R. H. (2014). Vagus nerve stimulation. *Curr. Behav. Neurosci. Rep.* 1, 64–73. doi: 10.1007/s40473-014-0010-5

Huang, F., Dong, J., Kong, J., Wang, H., Meng, H., Spaeth, R. B., et al. (2014). Effect of transcutaneous auricular vagus nerve stimulation on impaired glucose tolerance: a pilot randomized study. *BMC Complement. Altern. Med.* 14:203. doi: 10.1186/1472-6882-14-203

Huang, A. C., Yeh, K. Y., Cheng, Y. Y., Dubey, N. K., Chiu, A. W., and Tsai, T. H. (2018). Investigation of interactive activity of electro-acupuncture on pharmacokinetics of sildenafil and their synergistic effect on penile blood flow in rats. *Int. J. Mol. Sci.* 19:2153. doi: 10.3390/ijms19082153

Hugon, G., Goutal, S., Dauba, A., Breuil, L., Larrat, B., Winkeler, A., et al. (2021). [(18) F]2-Fluoro-2-deoxy-sorbitol PET imaging for quantitative monitoring of enhanced blood-brain barrier permeability induced by focused ultrasound. *Pharmaceutics* 13:1752. doi: 10.3390/pharmaceutics13111752

Hulsey, D. R., Hays, S. A., Khodaparast, N., Ruiz, A., Das, P., Rennaker, R. L. 2nd, et al. (2016). Reorganization of motor cortex by vagus nerve stimulation requires cholinergic innervation. *Brain Stimul.* 9, 174–181. doi: 10.1016/j.brs.2015.12.007

Hulsey, D. R., Riley, J. R., Loerwald, K. W., Rennaker, R. L. 2nd, Kilgard, M. P., and Hays, S. A. (2017). Parametric characterization of neural activity in the locus coeruleus in response to vagus nerve stimulation. *Exp. Neurol.* 289, 21–30. doi: 10.1016/j.expneurol.2016.12.005

Huston, J. M., Ochani, M., Rosas-Ballina, M., Liao, H., Ochani, K., Pavlov, V. A., et al. (2006). Splenectomy inactivates the cholinergic antiinflammatory pathway during lethal endotoxemia and polymicrobial sepsis. *J. Exp. Med.* 203, 1623–1628. doi: 10.1084/jem.20052362

Huston, J. M., Rosas-Ballina, M., Xue, X., Dowling, O., Ochani, K., Ochani, M., et al. (2009). Cholinergic neural signals to the spleen down-regulate leukocyte trafficking via CD11b. *J. Immunol.* 183, 552–559. doi: 10.4049/jimmunol.0802684

Huston, J. M., and Tracey, K. J. (2011). The pulse of inflammation: heart rate variability, the cholinergic anti-inflammatory pathway and implications for therapy. *J. Intern. Med.* 269, 45–53. doi: 10.1111/j.1365-2796.2010.02321.x

Jacobs, H. I. L., Priovoulos, N., Riphagen, J. M., Poser, B. A., Napadow, V., Uludag, K., et al. (2020). Transcutaneous vagus nerve stimulation increases locus coeruleus function and memory performance in older individuals. *Alzheimers Dement.* 16:e044766. doi: 10.1002/alz.044766

Ji, H., Rabbi, M. F., Labis, B., Pavlov, V. A., Tracey, K. J., and Ghia, J. E. (2014). Central cholinergic activation of a vagus nerve-to-spleen circuit alleviates experimental colitis. *Mucosal Immunol.* 7, 335–347. doi: 10.1038/mi.2013.52

Jiang, Y., Li, L., Tan, X., Liu, B., Zhang, Y., and Li, C. (2015). miR-210 mediates vagus nerve stimulation-induced antioxidant stress and anti-apoptosis reactions following cerebral ischemia/reperfusion injury in rats. *J. Neurochem.* 134, 173–181. doi: 10.1111/jnc.13097

Johnston, G. R., and Webster, N. R. (2009). Cytokines and the immunomodulatory function of the vagus nerve. *Br. J. Anaesth.* 102, 453–462. doi: 10.1093/bja/aep037

Kang, J., Huang, L., Tang, Y., Chen, G., Ye, W., Wang, J., et al. (2022). A dynamic model to predict long-term outcomes in patients with prolonged disorders of consciousness. *Aging (Albany NY)* 14, 789–799. doi: 10.18632/aging.203840

Knowles, C. H., and Aziz, Q. (2009). Basic and clinical aspects of gastrointestinal pain. *Pain* 141, 191–209. doi: 10.1016/j.pain.2008.12.011

Kondziella, D., Bender, A., Diserens, K., van Erp, W., Estraneo, A., Formisano, R., et al. (2020). European academy of neurology guideline on the diagnosis of coma and other disorders of consciousness. *Eur. J. Neurol.* 27, 741–756. doi: 10.1111/ene.14151

Krahl, S. E. (2012). Vagus nerve stimulation for epilepsy: a review of the peripheral mechanisms. *Surg. Neurol. Int.* 3, S47–S52. doi: 10.4103/2152-7806.91610

Lai, Y., Deng, J., Wang, M., Wang, M., Zhou, L., Meng, G., et al. (2019). Vagus nerve stimulation protects against acute liver injury induced by renal ischemia reperfusion via antioxidant stress and anti-inflammation. *Biomed. Pharmacother.* 117:109062. doi: 10.1016/j.biopha.2019.109062

Laureys, S., Celesia, G. G., Cohadon, F., Lavrijsen, J., León-Carrión, J., Sannita, W. G., et al. (2010). Unresponsive wakefulness syndrome: a new name for the vegetative state or apallic syndrome. *BMC Med.* 8:68. doi: 10.1186/1741-7015-8-68

Lei, W., and Duan, Z. (2021). Advances in the treatment of cholinergic anti-inflammatory pathways in gastrointestinal diseases by electrical stimulation of Vagus nerve. *Digestion* 102, 128–138. doi: 10.1159/000504474

Li, M., Chen, Z., Deng, W., He, Z., Wang, Q., Jiang, L., et al. (2012). Volume increases in putamen associated with positive symptom reduction in previously drug-naive schizophrenia after 6 weeks antipsychotic treatment. *Psychol. Med.* 42, 1475–1483. doi: 10.1017/s0033291711002157

Li, S., Demenescu, L. R., Sweeney-Reed, C. M., Krause, A. L., Metzger, C. D., and Walter, M. (2017). Novelty seeking and reward dependence-related large-scale brain networks functional connectivity variation during salience expectancy. *Hum. Brain Mapp.* 38, 4064–4077. doi: 10.1002/hbm.23648

Li, Y., Lao, J., Zhao, X., Tian, D., Zhu, Y., and Wei, X. (2014). The optimal distance between two electrode tips during recording of compound nerve action potentials in the rat median nerve. *Neural Regen. Res.* 9, 171–178. doi: 10.4103/1673-5374.125346

Li, Z., Liu, M., Lan, L., Zeng, F., Makris, N., Liang, Y., et al. (2016). Altered periaqueductal gray resting state functional connectivity in migraine and the modulation effect of treatment. *Sci. Rep.* 6:20298. doi: 10.1038/srep20298

Li, S., Sun, C., Rong, P., Zhai, X., Zhang, J., Baker, M., et al. (2018). Auricular vagus nerve stimulation enhances central serotonergic function and inhibits diabetic neuropathy development in Zucker fatty rats. *Mol. Pain* 14:1744806918787368. doi: 10.1177/1744806918787368

Li, J., Zhang, Q., Li, S., Niu, L., Ma, J., Wen, L., et al. (2020). α7nAchR mediates transcutaneous auricular vagus nerve stimulation-induced neuroprotection in a rat model of ischemic stroke by enhancing axonal plasticity. *Neurosci. Lett.* 730:135031. doi: 10.1016/j.neulet.2020.135031

Liu, C. H., Yang, M. H., Zhang, G. Z., Wang, X. X., Li, B., Li, M., et al. (2020). Neural networks and the anti-inflammatory effect of transcutaneous auricular vagus nerve stimulation in depression. *J. Neuroinflammation* 17:54. doi: 10.1186/s12974-020-01732-5

Lopez, N. E., Krzyzaniak, M. J., Costantini, T. W., Putnam, J., Hageny, A. M., Eliceiri, B., et al. (2012). Vagal nerve stimulation decreases blood-brain barrier disruption after traumatic brain injury. *J. Trauma Acute Care Surg.* 72, 1562–1566. doi: 10.1097/TA.0b013e3182569875

Machado, C. (2002). The minimally conscious state: definition and diagnostic criteria. *Neurology* 59:1473.

Manta, S., El Mansari, M., Debonnel, G., and Blier, P. (2013). Electrophysiological and neurochemical effects of long-term vagus nerve stimulation on the rat monoaminergic systems. *Int. J. Neuropsychopharmacol.* 16, 459–470. doi: 10.1017/s1461145712000387

Marin, J., Giffin, N., Consiglio, E., McClure, C., Liebler, E., and Davies, B. (2018). Non-invasive vagus nerve stimulation for treatment of cluster headache: early UK clinical experience. *J. Headache Pain* 19:114. doi: 10.1186/s10194-018-0936-1

Mazzone, S. B., and Undem, B. J. (2016). Vagal afferent innervation of the Airways in Health and Disease. *Physiol. Rev.* 96, 975–1024. doi: 10.1152/physrev.00039.2015

Meyers, E. C., Kasliwal, N., Solorzano, B. R., Lai, E., Bendale, G., Berry, A., et al. (2019). Enhancing plasticity in central networks improves motor and sensory recovery after nerve damage. *Nat. Commun.* 10:5782. doi: 10.1038/s41467-019-13695-0

Milby, A. H., Halpern, C. H., and Baltuch, G. H. (2008). Vagus nerve stimulation for epilepsy and depression. *Neurotherapeutics* 5, 75–85. doi: 10.1016/j.nurt.2007.10.071

Mourdoukoutas, A. P., Truong, D. Q., Adair, D. K., Simon, B. J., and Bikson, M. (2018). High-resolution multi-scale computational model for non-invasive cervical Vagus nerve stimulation. *Neuromodulation* 21, 261–268. doi: 10.1111/ner.12706

Mridha, Z., de Gee, J. W., Shi, Y., Alkashgari, R., Williams, J., Suminski, A., et al. (2021). Graded recruitment of pupil-linked neuromodulation by parametric stimulation of the vagus nerve. *Nat. Commun.* 12:1539. doi: 10.1038/s41467-021-21730-2

Nichols, J. A., Nichols, A. R., Smirnakis, S. M., Engineer, N. D., Kilgard, M. P., and Atzori, M. (2011). Vagus nerve stimulation modulates cortical synchrony and excitability through the activation of muscarinic receptors. *Neuroscience* 189, 207–214. doi: 10.1016/j.neuroscience.2011.05.024

Noé, E., Ferri, J., Colomer, C., Moliner, B., O'Valle, M., Ugart, P., et al. (2020). Feasibility, safety and efficacy of transauricular vagus nerve stimulation in a cohort of patients with disorders of consciousness. *Brain Stimul.* 13, 427–429. doi: 10.1016/j.brs.2019.12.005

Osińska, A., Rynkiewicz, A., Binder, M., Komendziński, T., Borowicz, A., and Leszczyński, A. (2022). Non-invasive Vagus nerve stimulation in treatment of disorders of consciousness - longitudinal case study. *Front. Neurosci.* 16:834507. doi: 10.3389/fnins.2022.834507

Peuker, E. T., and Filler, T. J. (2002). The nerve supply of the human auricle. *Clin. Anat.* 15, 35–37. doi: 10.1002/ca.1089

Porcaro, C., Nemirovsky, I. E., Riganello, F., Mansour, Z., Cerasa, A., Tonin, P., et al. (2021). Diagnostic developments in differentiating unresponsive wakefulness syndrome and the minimally conscious state. *Front. Neurol.* 12:778951. doi: 10.3389/fneur.2021.778951

Pourmotabbed, H., de Jongh Curry, A. L., Clarke, D. F., Tyler-Kabara, E. C., and Babajani-Feremi, A. (2022). Reproducibility of graph measures derived from resting-state MEG functional connectivity metrics in sensor and source spaces. *Hum. Brain Mapp.* 43, 1342–1357. doi: 10.1002/hbm.25726

Raguž, M., Predrijevac, N., Dlaka, D., Orešković, D., Rotim, A., Romić, D., et al. (2021). Structural changes in brains of patients with disorders of consciousness treated with deep brain stimulation. *Sci. Rep.* 11:4401. doi: 10.1038/s41598-021-83873-y

Rawat, J. K., Roy, S., Singh, M., Guatam, S., Yadav, R. K., Ansari, M. N., et al. (2019). Transcutaneous Vagus nerve stimulation regulates the cholinergic anti-inflammatory pathway to counteract 1, 2-Dimethylhydrazine induced Colon carcinogenesis in albino wistar rats. *Front. Pharmacol.* 10:353. doi: 10.3389/fphar.2019.00353

Rollnik, J. D. (2019). Clinical neurophysiology of neurologic rehabilitation. *Handb. Clin. Neurol.* 161, 187–194. doi: 10.1016/b978-0-444-64142-7.00048-5

Rong, P., Liu, J., Wang, L., Liu, R., Fang, J., Zhao, J., et al. (2016). Effect of transcutaneous auricular vagus nerve stimulation on major depressive disorder: a nonrandomized controlled pilot study. *J. Affect. Disord.* 195, 172–179. doi: 10.1016/j.jad.2016.02.031

Safi, S., Ellrich, J., and Neuhuber, W. (2016). Myelinated axons in the auricular branch of the human vagus nerve. *Anat. Rec. (Hoboken)* 299, 1184–1191. doi: 10.1002/ar.23391

Salchow-Hömmen, C., Jankowski, N., Valtin, M., Schönijahn, L., Böttcher, S., Dähne, F., et al. (2018). User-centered practicability analysis of two identification strategies in electrode arrays for FES induced hand motion in early stroke rehabilitation. *J. Neuroeng. Rehabil.* 15:123. doi: 10.1186/s12984-018-0460-1

Sanders, T. H., Weiss, J., Hogewood, L., Chen, L., Paton, C., McMahan, R. L., et al. (2019). Cognition-enhancing Vagus nerve stimulation alters the epigenetic landscape. *J. Neurosci.* 39, 3454–3469. doi: 10.1523/jneurosci.2407-18.2019

Schwartz, M. D., and Kilduff, T. S. (2015). The neurobiology of sleep and wakefulness. *Psychiatr. Clin. North Am.* 38, 615–644. doi: 10.1016/j.psc.2015.07.002

Sclocco, R., Garcia, R. G., Kettner, N. W., Fisher, H. P., Isenburg, K., Makarovsky, M., et al. (2020). Stimulus frequency modulates brainstem response to respiratory-gated transcutaneous auricular vagus nerve stimulation. *Brain Stimul.* 13, 970–978. doi: 10.1016/j.brs.2020.03.011

Scolding, N., Owen, A. M., and Keown, J. (2021). Prolonged disorders of consciousness: a critical evaluation of the new UK guidelines. *Brain* 144, 1655–1660. doi: 10.1093/brain/awab063

Settell, M. L., Pelot, N. A., Knudsen, B. E., Dingle, A. M., McConico, A. L., Nicolai, E. N., et al. (2020). Functional vagotopy in the cervical vagus nerve of the domestic pig: implications for the study of vagus nerve stimulation. *J. Neural Eng.* 17:026022. doi: 10.1088/1741-2552/ab7ad4

Si, J., Dang, Y., Zhang, Y., Li, Y., Zhang, W., Yang, Y., et al. (2018). Spinal cord stimulation frequency influences the hemodynamic response in patients with disorders of consciousness. *Neurosci. Bull.* 34, 659–667. doi: 10.1007/s12264-018-0252-4

Snider, S. B., and Edlow, B. L. (2020). MRI in disorders of consciousness. *Curr. Opin. Neurol.* 33, 676–683. doi: 10.1097/wco.0000000000000873

Song, K. M., Chung, D. Y., Choi, M. J., Ghatak, K., Minh, N. N., Limanjaya, A., et al. (2020). Vactosertib, a novel, orally bioavailable activin receptor-like kinase 5 inhibitor, promotes regression of fibrotic plaques in a rat model of Peyronie's disease. *World J Mens Health* 38, 552–563. doi: 10.5534/wjmh.190071

Stavrakis, S., Humphrey, M. B., Scherlag, B. J., Hu, Y., Jackman, W. M., Nakagawa, H., et al. (2015). Low-level transcutaneous electrical vagus nerve stimulation suppresses atrial fibrillation. *J. Am. Coll. Cardiol.* 65, 867–875. doi: 10.1016/j.jacc.2014.12.026

Sumi-Akamaru, H., Beck, G., Shinzawa, K., Kato, S., Riku, Y., Yoshida, M., et al. (2016). High expression of α-synuclein in damaged mitochondria with PLA2G6 dysfunction. *Acta Neuropathol. Commun.* 4:27. doi: 10.1186/s40478-016-0298-3

Thibaut, A., Panda, R., Annen, J., Sanz, L. R. D., Naccache, L., Martial, C., et al. (2021). Preservation of brain activity in unresponsive patients identifies MCS star. *Ann. Neurol.* 90, 89–100. doi: 10.1002/ana.26095

Thompson, S. L., O'Leary, G. H., Austelle, C. W., Gruber, E., Kahn, A. T., Manett, A. J., et al. (2021). A review of parameter settings for invasive and non-invasive vagus nerve stimulation (VNS) applied in neurological and psychiatric disorders. *Front. Neurosci.* 15:709436. doi: 10.3389/fnins.2021.709436

Vaseghi, M., Salavatian, S., Rajendran, P. S., Yagishita, D., Woodward, W. R., Hamon, D., et al. (2017). Parasympathetic dysfunction and antiarrhythmic effect of vagal nerve stimulation following myocardial infarction. *JCI Insight* 2:e86715. doi: 10.1172/jci.insight.86715

Vitello, M. M., Briand, M. M., Ledoux, D., Annen, J., El Tahry, R., Laureys, S., et al. (2023). Transcutaneous vagal nerve stimulation to treat disorders of consciousness: protocol for a double-blind randomized controlled trial. *Int. J. Clin. Health Psychol.* 23:100360. doi: 10.1016/j.ijchp.2022.100360

Vonck, K., De Herdt, V., and Boon, P. (2009). Vagal nerve stimulation--a 15-year survey of an established treatment modality in epilepsy surgery. *Adv. Tech. Stand. Neurosurg.* 34, 111–146. doi: 10.1007/978-3-211-78741-0_5

Waise, T. M. Z., Dranse, H. J., and Lam, T. K. T. (2018). The metabolic role of vagal afferent innervation. *Nat. Rev. Gastroenterol. Hepatol.* 15, 625–636. doi: 10.1038/s41575-018-0062-1

Wang, Q., Cheng, Y., Xue, F. S., Yuan, Y. J., Xiong, J., Li, R. P., et al. (2012). Postconditioning with vagal stimulation attenuates local and systemic inflammatory responses to myocardial ischemia reperfusion injury in rats. *Inflamm. Res.* 61, 1273–1282. doi: 10.1007/s00011-012-0527-6

Wang, Y. M., Xu, Y. Y., Zhai, Y., Wu, Q. Q., Huang, W., Liang, Y., et al. (2021). Effect of transcutaneous auricular vagus nerve stimulation on protracted alcohol withdrawal symptoms in male alcohol-dependent patients. *Front. Psych.* 12:678594. doi: 10.3389/fpsyt.2021.678594

Wang, Z., Yu, L., Chen, M., Wang, S., and Jiang, H. (2014). Transcutaneous electrical stimulation of auricular branch of vagus nerve: a noninvasive therapeutic approach for post-ischemic heart failure. *Int. J. Cardiol.* 177, 676–677. doi: 10.1016/j.ijcard.2014.09.165

Wang, J. Y., Zhang, Y., Chen, Y., Wang, Y., Li, S. Y., Wang, Y. F., et al. (2021). Mechanisms underlying antidepressant effect of transcutaneous auricular vagus nerve stimulation on CUMS model rats based on hippocampal α7nAchR/NF-κB signal pathway. *J. Neuroinflammation* 18:291. doi: 10.1186/s12974-021-02341-6

Wu, Y. H., Yu, J., Hong, L. R., and Luo, B. Y. (2021). Neuromodulatory therapies for patients with prolonged disorders of consciousness. *Chin. Med. J.* 134, 765–776. doi: 10.1097/cm9.0000000000001377

Yakunina, N., Kim, S. S., and Nam, E. C. (2017). Optimization of transcutaneous vagus nerve stimulation using functional MRI. *Neuromodulation* 20, 290–300. doi: 10.1111/ner.12541

Yang, Y., Yang, L. Y., Orban, L., Cuylear, D., Thompson, J., Simon, B., et al. (2018). Non-invasive vagus nerve stimulation reduces blood-brain barrier disruption in a rat model of ischemic stroke. *Brain Stimul.* 11, 689–698. doi: 10.1016/j.brs.2018.01.034

Yifei, W., Yi, Y., Yu, W., Jinling, Z., Weihang, Z., Shaoyuan, L. I., et al. (2022). Transcutaneous auricular vague nerve stimulation improved brain connection activity on patients of disorders of consciousness: a pilot study. *J. Tradit. Chin. Med.* 42, 463–471. doi: 10.19852/j.cnki.jtcm.2022.03.012

Yu, Y., Yang, Y., Gan, S., Guo, S., Fang, J., Wang, S., et al. (2021). Cerebral hemodynamic correlates of transcutaneous auricular vagal nerve stimulation in consciousness restoration: an open-label pilot study. *Front. Neurol.* 12:684791. doi: 10.3389/fneur.2021.684791

Yu, Y. T., Yang, Y., Wang, L. B., Fang, J. L., Chen, Y. Y., He, J. H., et al. (2017). Transcutaneous auricular vagus nerve stimulation in disorders of consciousness monitored by fMRI: the first case report. *Brain Stimul.* 10, 328–330. doi: 10.1016/j.brs.2016.12.004

Yuan, Y., Hassel, J. L., Doytchinova, A., Adams, D., Wright, K. C., Meshberger, C., et al. (2017). Left cervical vagal nerve stimulation reduces skin sympathetic nerve activity in patients with drug resistant epilepsy. *Heart Rhythm.* 14, 1771–1778. doi: 10.1016/j.hrthm.2017.07.035

Yuan, H., and Silberstein, S. D. (2016). Vagus nerve and vagus nerve stimulation, a comprehensive review: part I. *Headache* 56, 71–78. doi: 10.1111/head.12647

Zachs, D. P., Offutt, S. J., Graham, R. S., Kim, Y., Mueller, J., Auger, J. L., et al. (2019). Noninvasive ultrasound stimulation of the spleen to treat inflammatory arthritis. *Nat. Commun.* 10:951. doi: 10.1038/s41467-019-08721-0

Zhai, W., Jiao, H., Zhuang, Y., Yang, Y., Zhang, J., Wang, Y., et al. (2023). Optimizing the modulation paradigm of transcutaneous auricular vagus nerve stimulation in patients with disorders of consciousness: a prospective exploratory pilot study protocol. *Front. Neurosci.* 17:1145699. doi: 10.3389/fnins.2023.1145699

Zhang, Y., Huang, Y., Li, H., Yan, Z., Zhang, Y., Liu, X., et al. (2021). Transcutaneous auricular vagus nerve stimulation (taVNS) for migraine: an fMRI study. *Reg. Anesth. Pain Med.* 46, 145–150. doi: 10.1136/rapm-2020-102088

Zhang, Y., Liu, J., Li, H., Yan, Z., Liu, X., Cao, J., et al. (2019). Transcutaneous auricular vagus nerve stimulation at 1 Hz modulates locus coeruleus activity and resting state functional connectivity in patients with migraine: An fMRI study. *Neuroimage Clin.* 24:101971. doi: 10.1016/j.nicl.2019.101971

Zhang, J., Ma, L., Chang, L., Pu, Y., Qu, Y., and Hashimoto, K. (2020). A key role of the subdiaphragmatic vagus nerve in the depression-like phenotype and abnormal

composition of gut microbiota in mice after lipopolysaccharide administration. *Transl. Psychiatry* 10:186. doi: 10.1038/s41398-020-00878-3

Zhang, Y., Yang, Y., Si, J., Xia, X., He, J., and Jiang, T. (2018). Influence of inter-stimulus interval of spinal cord stimulation in patients with disorders of consciousness: a preliminary functional near-infrared spectroscopy study. *Neuroimage Clin.* 17, 1–9. doi: 10.1016/j.nicl.2017.09.017

Zhao, C., Yang, X., Su, E. M., Huang, Y., Li, L., Matthay, M. A., et al. (2017). Signals of vagal circuits engaging with AKT1 in α7 nAChR(+)CD11b(+) cells lessen E. Coli and LPS-induced acute inflammatory injury. *Cell Discov.* 3:17009. doi: 10.1038/celldisc.2017.9

Zhao, X. P., Zhao, Y., Qin, X. Y., Wan, L. Y., and Fan, X. X. (2019). Non-invasive Vagus nerve stimulation protects against cerebral ischemia/reperfusion injury and promotes microglial M2 polarization via interleukin-17A inhibition. *J. Mol. Neurosci.* 67, 217–226. doi: 10.1007/s12031-018-1227-7

Zheng, Y., Yu, Z., Zhang, W., and Sun, T. (2021). *Lactobacillus rhamnosus* probio-M9 improves the quality of life in stressed adults by gut microbiota. *Foods* 10:2384. doi: 10.3390/foods10102384

Zhou, Y. F., Kang, J. W., Xiong, Q., Feng, Z., and Dong, X. Y. (2023). Transauricular vagus nerve stimulation for patients with disorders of consciousness: a randomized controlled clinical trial. *Front. Neurol.* 14:1133893. doi: 10.3389/fneur.2023.1133893

Zhou, S., Zou, G., Xu, J., Su, Z., Zhu, H., Zou, Q., et al. (2019). Dynamic functional connectivity states characterize NREM sleep and wakefulness. *Hum. Brain Mapp.* 40, 5256–5268. doi: 10.1002/hbm.24770

frontiers | Frontiers in Neuroscience

TYPE Review
PUBLISHED 19 October 2023
DOI 10.3389/fnins.2023.1280180

OPEN ACCESS

EDITED BY
Gahangir Hossain,
University of North Texas, United States

REVIEWED BY
Mario Versaci,
Mediterranea University of Reggio Calabria, Italy
Nem Kumar Jain,
ITM University, India

*CORRESPONDENCE
Qiang Gao
✉ gaoqiang_hxkf@163.com

†These authors have contributed equally to this work and share first authorship

RECEIVED 19 August 2023
ACCEPTED 05 October 2023
PUBLISHED 19 October 2023

CITATION
Wei Y-X, Tu L-D, He L, Qiu Y-t, Su W, Zhang L, Ma R-t and Gao Q (2023) Research hotspots and trends of transcranial magnetic stimulation in Parkinson's disease: a bibliometric analysis. *Front. Neurosci.* 17:1280180. doi: 10.3389/fnins.2023.1280180

Research hotspots and trends of transcranial magnetic stimulation in Parkinson's disease: a bibliometric analysis

Yi-xin Wei[1,2†], Liang-dan Tu[3†], Lin He[1,2], Yi-tong Qiu[1,2], Wei Su[1,2], Li Zhang[1,2], Run-ting Ma[1,2] and Qiang Gao[1,2*]

[1]Department of Rehabilitation Medicine, West China Hospital, Sichuan University, Chengdu, China, [2]Key Laboratory of Rehabilitation Medicine in Sichuan Province, West China Hospital, Sichuan University, Chengdu, China, [3]Neurology Department, West China Hospital, Sichuan University, Chengdu, China

Background: Transcranial magnetic stimulation (TMS), as a non-invasive neuromodulation technique, has been widely used in the treatment of Parkinson's disease (PD). The increasing application of TMS has promoted an increasing number of clinical studies. In this paper, a bibliometric analysis of existing studies was conducted to reveal current research hotspots and guide future research directions.

Method: Relevant articles and reviews were obtained from the Science Citation Index Expanded of Web of Science Core Collection database. Data related to publications, countries, institutions, authors, journals, citations, and keywords in the studies included in the review were systematically analyzed using VOSviewer 1.6.18 and Citespace 6.2.4 software.

Result: A total of 1,894 papers on the topic of TMS in PD between 1991 and 2022 were analyzed and visualized to identify research hotspots and trends in the field. The number of annual publications in this field of study has increased gradually over the past 30 years, with the number of annual publications peaking in 2022 ($n = 150$). In terms of publications and total citations, countries, institutions, and authors from North America and Western Europe were found to make significant contributions to the field. The current hotspot focuses on the effectiveness of TMS for PD in different stimulation modes or different stimulated brain regions. The keyword analysis indicates that the latest research is oriented to the mechanism study of TMS for motor symptoms in PD, and the non-motor symptoms are also receiving more attention.

Conclusion: Our study offers insights into the current hotspots and emerging trends of TMS in the rehabilitation of PD. These findings may serve as a guide for future research and the application of TMS for PD.

KEYWORDS

bibliometric analysis, transcranial magnetic stimulation, Parkinson's diseases, hotspots, research trends

1. Introduction

Parkinson's Disease (PD) is the second most frequent neurodegenerative disorder (Thomas and Beal, 2007). Studies have been conservatively estimating that the number of people with PD will increase from 6.9 million in 2015 to 14.2 million in 2040 (Pringsheim et al., 2014; Dorsey et al., 2018). Clinical symptoms of PD are mainly resting tremor, physical dyskinesia, postural instability, gait difficulty and rigidity (Jankovic, 2008; Salmon et al., 2023; Scully et al., 2023). However, the pathogenesis of PD is still unclear, and the mainstream view is that PD is caused by a combination of genetic, environmental and aging factors that may lead to degeneration and apoptosis of dopaminergic neurons in the substantia nigra (Puschmann, 2017; Zhang et al., 2018; Marras et al., 2019). Pharmacological treatment significantly improves quality of life and functional capacity in patients with PD and L-3,4-dihydroxyphenylalanine (L-DOPA) is the most potent drug (Fahn, 2008; Jenner, 2008). However, long-term use L-DOPA leads to adverse effects including levodopa-induced dyskinesia (LID) in most patients (Cenci and Konradi, 2010; Cerasa et al., 2015).

Based on such clinical complications of PD, non-pharmacological treatments are used as attempted treatments. Transcranial Magnetic Stimulation (TMS) has received close attention as a possible treatment for PD over the past two decades (Fregni et al., 2005; Elahi et al., 2009). In 1985, Baker and colleagues conducted the first experiments of TMS in humans (Barker et al., 1985), which has been developed in the following 30 years (Hallett, 2007; Pitcher et al., 2021). TMS is defined as a magnetic stimulation technique that utilizes a pulsed magnetic field that acts on the central nervous system of the brain to alter the membrane potential of cerebral cortical nerve cells, causing them to generate induced currents that affect metabolic and neuroelectric activity in the brain, thereby inducing a series of physiological and biochemical responses (Hallett, 2000). TMS has been found to be useful as a research tool for evaluating cortical function in a variety of neuropathological states (Gilio et al., 2002; Caipa et al., 2018), and it also has a place in the treatment of a variety of neurological disorders, such as depression, chronic pain, post-stroke deficits, and PD (Shukla et al., 2016; Zhang et al., 2017; De Risio et al., 2020; Zhu et al., 2022).

As a non-invasive treatment, TMS for PD neuromodulation therapy has attracted many studies on the therapeutic management of PD. Several randomized controlled trials have explored the therapeutic effects and mechanisms of TMS for PD (Taib et al., 2019; Chung et al., 2020). Common examples of TMS on PD neuromodulation are as follows: (1) rTMS improves upper limb function in the short-term, walking performance and UPDRS III in the short-and long-terms in PD individuals and primary motor cortex (M1) is considered a more prominent stimulus point (Chung and Mak, 2016). (2) For the non-motor symptoms of PD, some studies suggest that using high frequency of rTMS on the dorsolateral prefrontal cortex (DLPFC) may be a potentially effective way to alleviate depressive symptoms (Zhang et al., 2022). (3) In addition, repetitive magnetic pulses change the excitability of the stimulation site and affect the cortical connectivity of PD individuals (Gonzalez-Garcia et al., 2011; Chung et al., 2020; Mi et al., 2020). However further studies are required to investigate optimal rTMS therapeutic protocols for PD (Chen and Chen, 2019).

Bibliometric analysis is carried out using visualization tools to analyze large volumes of published academic literature, which can be used to explore qualitatively and quantitatively the contributions of authors, countries/regions, institutions, and their partnerships. More importantly, bibliometric analysis can identify hotspots and frontiers, and predict trends in a given field, which can be an important indicator for future follow-up research. Citespace and VOSviewer are two commonly software for visualization and analysis. CiteSpace, one of the most suitable software for bibliometric analysis is developed by Prof. Chaomei Chen (Drexel University, United States) (Chen, 2004; Chen, 2006; Pan et al., 2018). Citespace is based on co-citation analysis theory and pathfinding network algorithm, which makes it easier to analyze and explore the trends and research hotspots of related disciplines (Chen and Song, 2019). VOSviewer developed by Leiden University's Centre for Science and Technology Studies is also a software tool for visualizing bibliometric networks (You et al., 2021). In recent years, several researchers have conducted visualization analyses in the field of TMS or PD. Li et al. conducted a 20-year visualization analysis of PD acupuncture treatment, which revealed the future research potential of PD acupuncture treatment (Li X. et al., 2022). Zhang et al. conducted a 20-year bibliometric analysis of non-motor symptoms of depression and anxiety in PD, concluding that non-motor symptoms have increasingly become a hotspot for future research (Zhang et al., 2023). Liu et al. conducted a visual analysis of postural deformities in PD and summarized the current peripheral and central etiology of postural deformities in PD and rehabilitation treatment options (Zhang et al., 2023). Similarly, a study that assessed the breadth of the TMS literature base using a bibliometric approach evaluated the development over the last 30 years, helping to understand the historical progress of TMS over the last few decades (McLean, 2019).

Over the past decade, a considerable number of scholars and academic journals have focused on publishing TMS in PD. Moreover, no studies performed an innovative overview of TMS in PD neurorehabilitation through bibliometric analysis to this point. This study conducted a bibliometric analysis of TMS for PD based on records published from the inception (1900) to 2022. We used the VOSviewer 1.6.18 and Citespace 6.2.4 to identify publication patterns and emerging trends based on the Web of Science Core Collection (WoSCC) database. This article aimed to help clinicians and researchers to comprehend the issues and research hotspots related to TMS for PD and gain new insights that can guide future research and applications.

2. Materials and methods

2.1. Data collection

We use the Web of Science (WOS) database, a renowned scientific data services platform developed by Clarivate (version © 2021 Clarivate). We can retrieve the Clarivate Journal Impact Factor (IF) for the last 5 years from the WOS. Publications with related themes from the inception (1900) to 2022 were searched from the Science Citation Index Expanded (SCIE) of the WoSCC database. SCIE is a subdatabase of WoSCC, which consists of global journals of basic science research, covering neuroscience and medical research related to the theme of this study, "TMS in PD."

The data were obtained on 15th June 2023 from SCIE. To obtain documents explicitly employing the concerning terms we performed

a topical search with the query TS = ("Parkinson Disease" OR Parkinson* OR "Idiopathic Parkinson's Disease" OR "Lewy Body Parkinson's Disease" OR "Parkinson's Disease, Idiopathic" OR "Parkinson's Disease, Lewy Body" OR "Parkinson Disease, Idiopathic" OR "Idiopathic Parkinson Disease" OR "Lewy Body Parkinson Disease" OR "Primary Parkinsonism" OR "Parkinsonism, Primary" OR "Paralysis Agitans") and TS = ("Transcranial Magnetic Stimulation" OR magnetic field therap* OR "Magnetic Stimulation, Transcranial" OR "Magnetic Stimulations, Transcranial" OR "Stimulation, Transcranial Magnetic" OR "Stimulations, Transcranial Magnetic" OR "Transcranial Magnetic Stimulations" OR "Transcranial Magnetic Stimulation, Single Pulse" OR "Transcranial Magnetic Stimulation, Paired Pulse" OR "Transcranial Magnetic Stimulation, Repetitive" OR "noninvasive brain stimulation" OR TMS OR TBS). We only selected articles or reviews in English, other document types, such as letters, commentaries, and meeting abstracts, were excluded. Finally, a total of 3,174 literature records were included.

2.2. Data import and deduplication

All included documents were required to undergo peer review. All bibliometric data were imported into Endnote 20 to deduplicate, and then we screened the titles, abstracts, and full texts of the included papers to identify the available studies independently based on the exclusion criteria. Exclusion criteria were as follows: (1) The intervention modality is not TMS; (2) Targeted conditions are unrelated to PD; (3) The theme of the paper is uncorrelated to the implementation of TMS in PD neuromodulation. Finally, we included a total of 1,894 articles (1,392 articles, 502 reviews) that met the requirements. The bibliometric search and analysis flowchart is presented in Figure 1.

2.3. Data merging

After screening and verifying through Endnote, relevant literature was handpicked from the WOS database. The plain text containing information about these documents was downloaded from the WOS database. After data download, the items of the field need to be manually merging. We identify three common scenarios that require data merging and propose solutions for each of them. These scenarios are: (1) different spellings or formats of the same country name, e.g., USA and United States of America will be merged into USA; (2) different abbreviations or variations of the same author name, which we resolve by using ORCID information and author affiliation; and (3) different terms or expressions that refer to the same concept, e.g., TMS and transcranial magnetic stimulation will be merged into transcranial magnetic stimulation.

2.4. Data analysis and visualization

After data deduplication and merging, the plain text will import into VOSviewer 1.6.18 and Citespace 6.2.4 for further analysis and visualization. Citespace proposes the concepts of burst detection, correlation, centrality, and heterogeneous networks, which can help to find the central point, turning point, hotspot and trend of research in related fields. VOSviewer provides text mining capabilities that can be used to build the clustering map of countries, journal, and institutions.

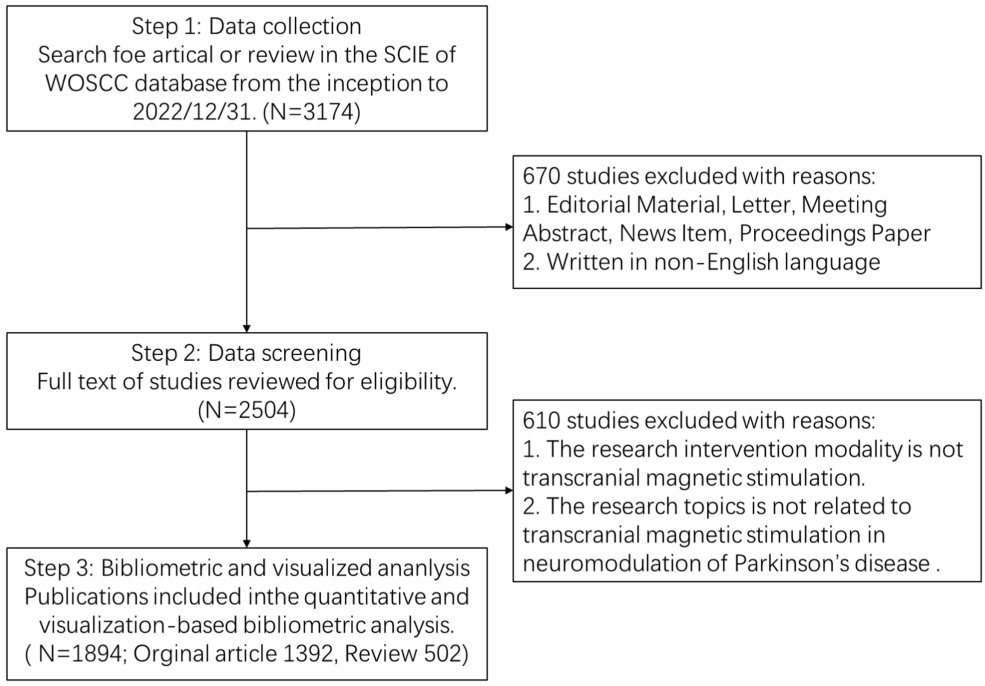

FIGURE 1
Flow chart of TMS for PD studies inclusion.

3. Results

3.1. Publication outputs and time trend

The initial search of the WoSCC database identified 31,74 publications. After excluding other literature types, limited English language, and irrelevant research topics, 1,894 papers were ultimately included in the analysis. These papers consisted of 1,392 articles and 502 reviews and were published between 1991 and 2022. The distribution and time trend of annual publication outputs and total annual publication outputs from the inception to 2022 are shown in Figure 2. The timing of publications can be divided into three phases: the infancy phase (1991–1995), the slow-growth phase (1996–2015), and the high-growth phase (2016–2022). In the infancy stage, the number of annual publications has been below 10 except in 1994. In the slow-growth stage, there is a slow but steady year-by-year upward trend from 19 papers in 1996 to 96 papers in 2015. In the high-growth stage, it maintains a high growth rate of more than 100 publications per year, and the number of annual publications increases year by year. Meanwhile, linear regression analysis showed a positive correlation ($y = 2.0669 \times 2 - 9.0232\times$, $R2 = 0.9978$) between the total annual number of articles. It is expected that research in this area will continue to grow in the future.

3.2. Distribution of countries

The top 10 countries/regions in terms of number of publications are displayed in Table 1. Figure 3 presents a network map of countries involved in TMS research for PD. The United States has the most publications (293), followed by Italy (184), China (151), England (119), and Canada (100) have more than 100 publications. The year each country began research is represented by the different shades of the circles. The United States represents the early start of western countries in the use of TMS for PD research, and China has seen a rapid increase in the number of publications in this field in the last decade. Centrality indicates the strength of the number of connections between a node and other nodes in the entire network; high centrality means that key nodes have a strong influence on the relationships in the network. The pink outer circle in Figure 3 indicates that the centrality is greater than 0.1, indicating high centrality, and in Table 1 suggests that China (0.02) has a low central influence in this field and Germany (0.27) has the highest central influence.

3.3. Analysis of institutions

According to author addresses, 1,888 institutions contributed to these 1,894 papers. The 10 institutions that published the most papers are listed in Table 2. The institution with the most publications is the University of Toronto (Canada, 95 papers). It was followed by Harvard University (USA, 74 papers) and the Sapienza University of Rome (Italy, 63 papers). The Sapienza University of Rome had the highest number of citations (3888) and citations per paper (61.71). Figure 4 displays the collaborative network between top institutions that apply TMS to PD neuromodulation research. The top-ranked institutions have extensive collaborative relationships with other institutions, and the yellow blocks represent the density of collaboration between institutions. We found that the collaboration between the University of Toronto, Harvard University and the Sapienza University of Rome is very close among all institutions.

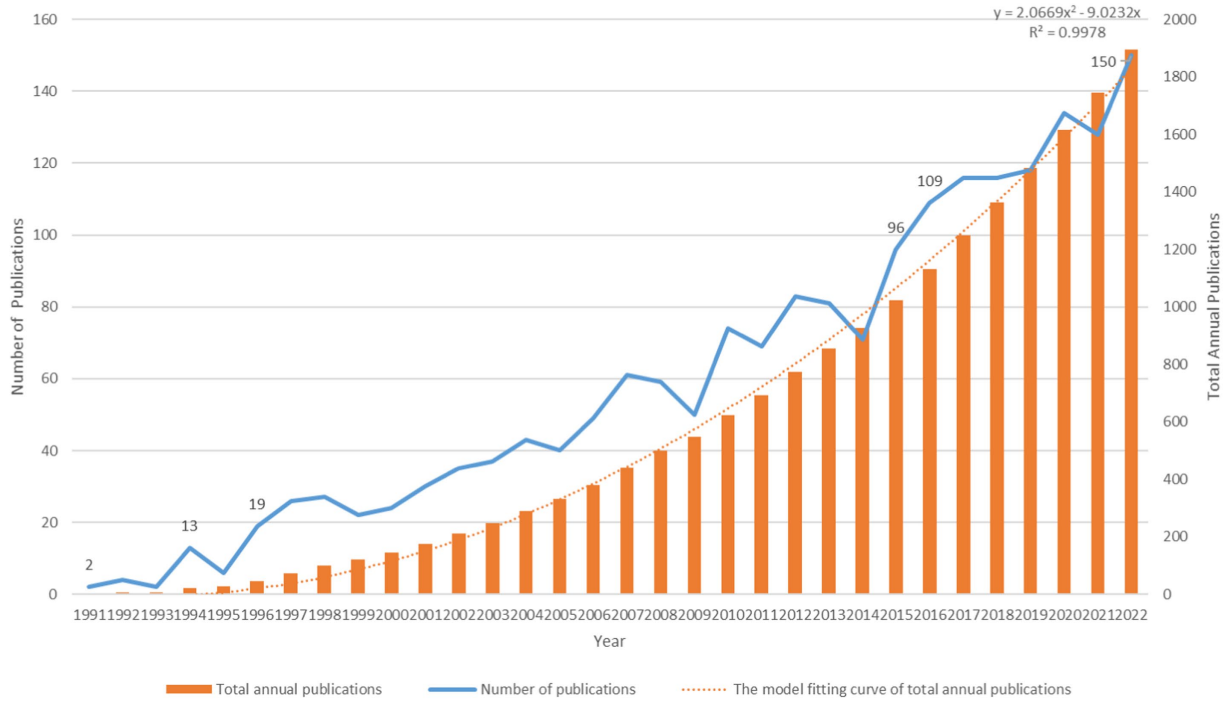

FIGURE 2
Annual publications, total annual publications, and the model fitting curve of total annual publications.

3.4. Analysis of journal co-citation

The 1,894 papers included in this analysis were published in 557 academic journals. According to Bradford's law, core journals are those that publish papers more than one-third of all journals in the relevant field (Goffman and Morris, 1970; Weinstock, 1971; Venable et al., 2016). In this research field, there were 9 core journals, 54 related journals and 494 journals were non-related journals. Table 3 shows that the top 10 journals with the highest number of publications accounted for 37.06% (702) of all studies. Movement disorder had the highest number of publications (234), followed by Clinical neurophysiology (105), Neurology (59), and Experimental brain research (59 articles). The top 10 journals with the highest IF in the last 5 years were Brain (16.173). Five journals had an IF>5.000, four journals held an IF from 3.000 to 5.000, and one journal had an IF < 3.000. The impact of scholarly publications on a research area is determined by the number of co-citations they receive. The co-citation analysis was operated by the VOSviewer and displayed in Figure 5. The size of the nodes indicates the number of co-citations, and the lines between the nodes indicate co-citation relationships. In terms of color for the cluster analysis, the red cluster represents journals specializing in neurology, such as Movement disorder and Neurology. The green cluster represents academic journals in the field of Parkinson's research, with Parkinsonism and Related Disorders being representative journal. Brain science neuromodulation journals, represented by Brain, are classified as blue cluster.

TABLE 1 The top 10 countries of TMS for PD research.

Rank	Country	Count	Centrality
1	USA	293	0.22
2	Italy	184	0.13
3	China	151	0.02
4	England	119	0.21
5	Canada	100	0.08
6	Germany	99	0.27
7	Spain	57	0.15
8	Australia	56	0.09
9	Japan	56	0.01
10	France	53	0.14

3.5. Analysis of authors

A total of 7,659 authors were involved in the literature on neuromodulation of TMS against PD. Table 4 shows the top 10 most active authors and their relevant information. Chen Robert published 65 publications, ranking first among all authors, followed by Berardelli Alfredo (60 publications) and Hallett Mark (54 publications). The top 10 authors are scattered in different research institutions. As shown in Table 4, Hallett Mark from the National Institute of Neurological Disorders and Stroke ranked first in terms

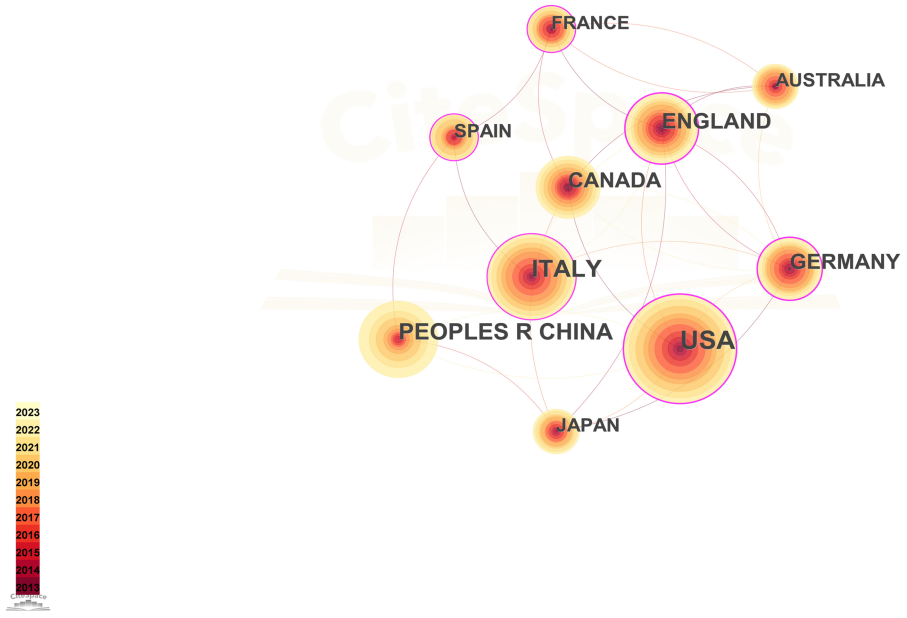

FIGURE 3
Network map of countries engaged in TMS for PD research.

TABLE 2 The top 5 productive institutions regarding the research on TMS for PD.

Rank	Institution	Country	Count	Citations	Citations per paper
1	University of Toronto	Canada	95	5,454	57.41
2	Harvard University	USA	74	5,929	80.12
3	Sapienza University of Rome	Italy	63	3,888	61.71
4	University College London	England	62	3,781	60.98
5	National Institute of Neurological Disorders and Stroke	USA	49	3,833	78.22
6	University of Tokyo	Japan	33	1,922	58.24
7	Istituto di Ricovero e Cura a Carattere Scientifico	Italy	31	1,820	58.71
8	University of Sao Paulo	Brazil	29	1,702	58.69
9	University of Sydney	Australia	28	1,507	53.82
10	University Health Network	Canada	27	705	26.11

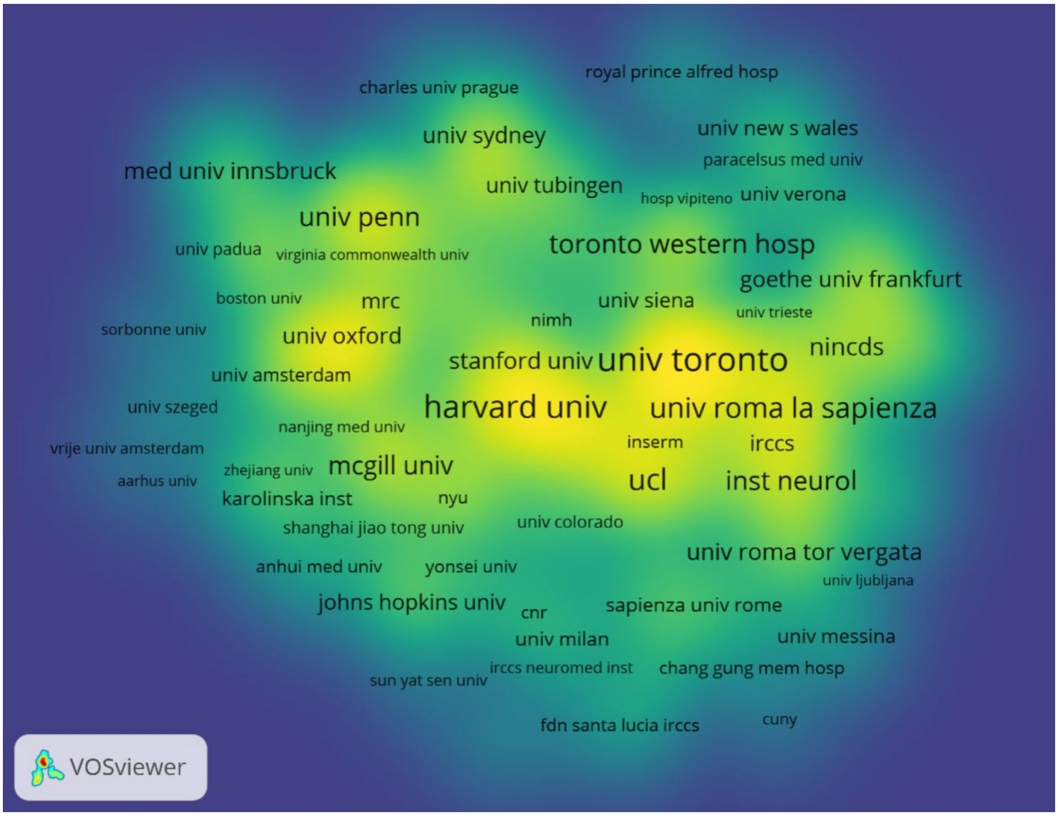

FIGURE 4
The VOSviewer network map of institutions in the field of TMS for PD.

of total citations (2,243 citations). In terms of the average number of citations per paper, Pascual-leone Alvaro from Harvard Medical School ranked first. In addition, the H-index can also accurately reflect the academic achievements of authors. Rothwell John Christine is ranked first (163) in H-index and has the largest impact in the field. Figure 6 is an overlay visualization of the author co-occurrence analysis generated by VOSviewer. The graph forms major clusters centered on the top 10 authors. The collaboration between them is very close and stronger between authors in the same cluster.

3.6. Analysis of keywords

Keywords are words that have substantial meaning in the center of a paper. These high-frequency or emergent keywords

TABLE 3 The top 10 journals that published articles regarding the research on TMS for PD.

Rank	Journal title	Country	Count	Citations	Citations per journal	JCR	IF 5 year
1	Movement Disorders	USA	234	8,040	34.36	Q1	9.956
2	Clinical Neurophysiology	Ireland	105	5,475	52.14	Q1	4.720
3	Neurology	USA	59	4,578	77.59	Q1	11.786
4	Experimental Brain Research	Germany	59	2,454	41.59	Q4	2.193
5	Parkinsonism and Related Disorders	England	50	855	17.10	Q2	4.515
6	Frontiers in Neurology	Switzerland	47	543	11.55	Q2	3.403
7	Brain Stimulation	USA	46	1,497	32.54	Q1	9.611
8	Brain	England	35	5,371	153.46	Q1	16.173
9	Journal of the Neurologic Science	USA	35	1,089	31.11	Q2	3.580
10	Journal of Neurology	Germany	32	631	19.72	Q1	5.138

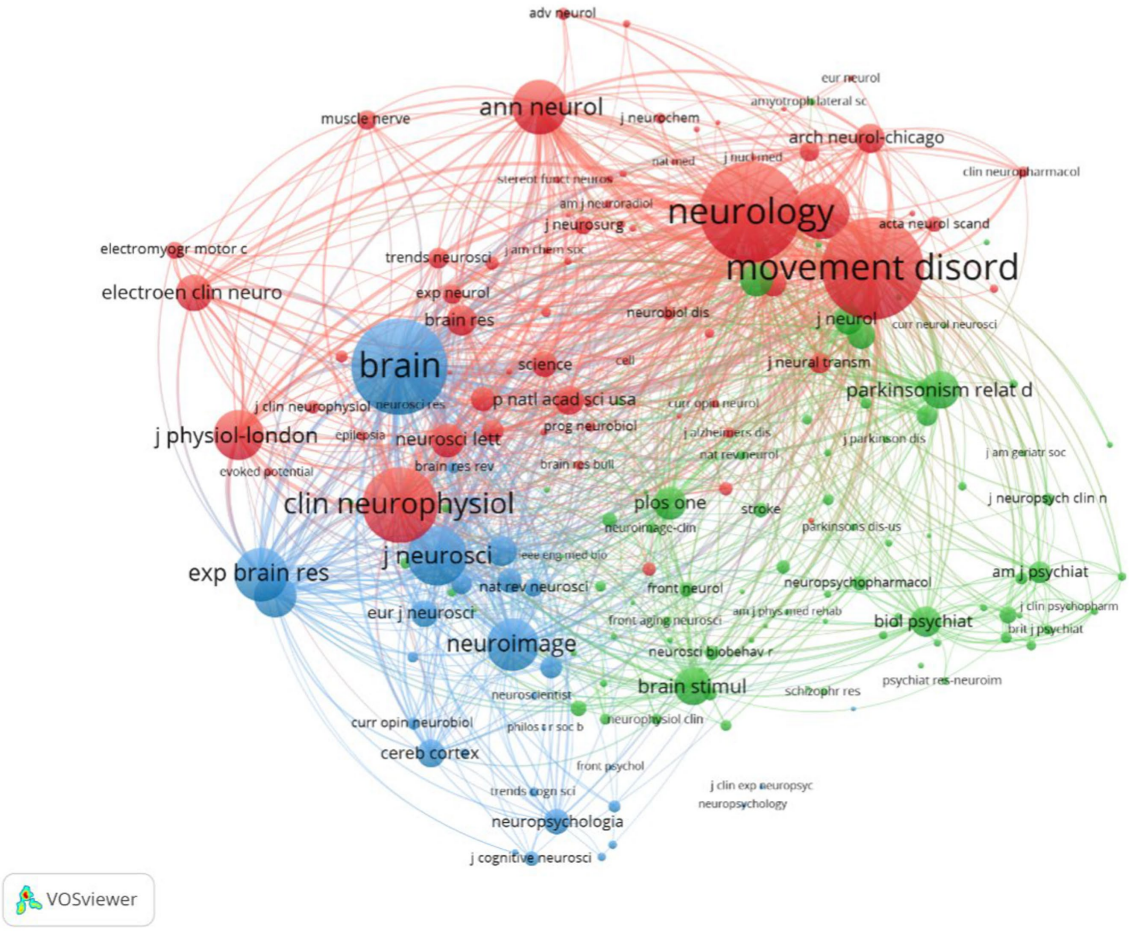

FIGURE 5
VOSviewer co-citation analysis clustering map of journal in the field of TMS for PD.

can reflect current topics and predict future research frontiers. As shown in Figure 7A, the top three most frequent keywords are Parkinson's disease, transcranial magnetic stimulation and human motor cortex. Other highly frequent keywords mainly include different stimulation modes and stimulation of cortical areas in the treatment of TMS for PD. According to the different types of keywords, the keywords can be categorized into 7 clusters shown in Figure 7B. The #0 and #2 clusters mainly describe the cortical physiological changes after TMS stimulation for Parkinson's. The #0 and #2 clusters mainly describe the cortical

TABLE 4 The top 10 authors and co-cited authors in TMS for PD research.

cRank	Author	Institution	Country	Publications	Citations	Citations per paper	H-index
1	Chen, Robert	University of Toronto	Canada	65	3,957	60.88	83
2	Berardelli, Alfredo	Sapienza University of Rome	Italy	60	4,054	67.57	21
3	Hallett, Mark	National Institute of Neurological Disorders and Stroke	USA	54	5,547	102.72	116
4	Rothwell, John Christine	University College London	England	42	1,622	38.62	159
5	Ugawa, yoshikazu	Fukushima Medical University	Japan	32	1,349	42.16	61
6	Pascual-leone, Alvaro	Harvard Medical School	USA	31	4,544	146.58	150
7	Rektorova, Irena	Masaryk University	Czech	31	578	18.65	31
8	Koch, Giacomo	Istituto di Ricovero e Cura a Carattere Scientifico	Italy	30	1,354	45.13	60
9	Fregni, Felipe	University of Sao Paulo	Brazil	25	2,496	99.84	30
10	Ziemann Ulf	University of Tubingen	Germany	24	3,374	140.58	93

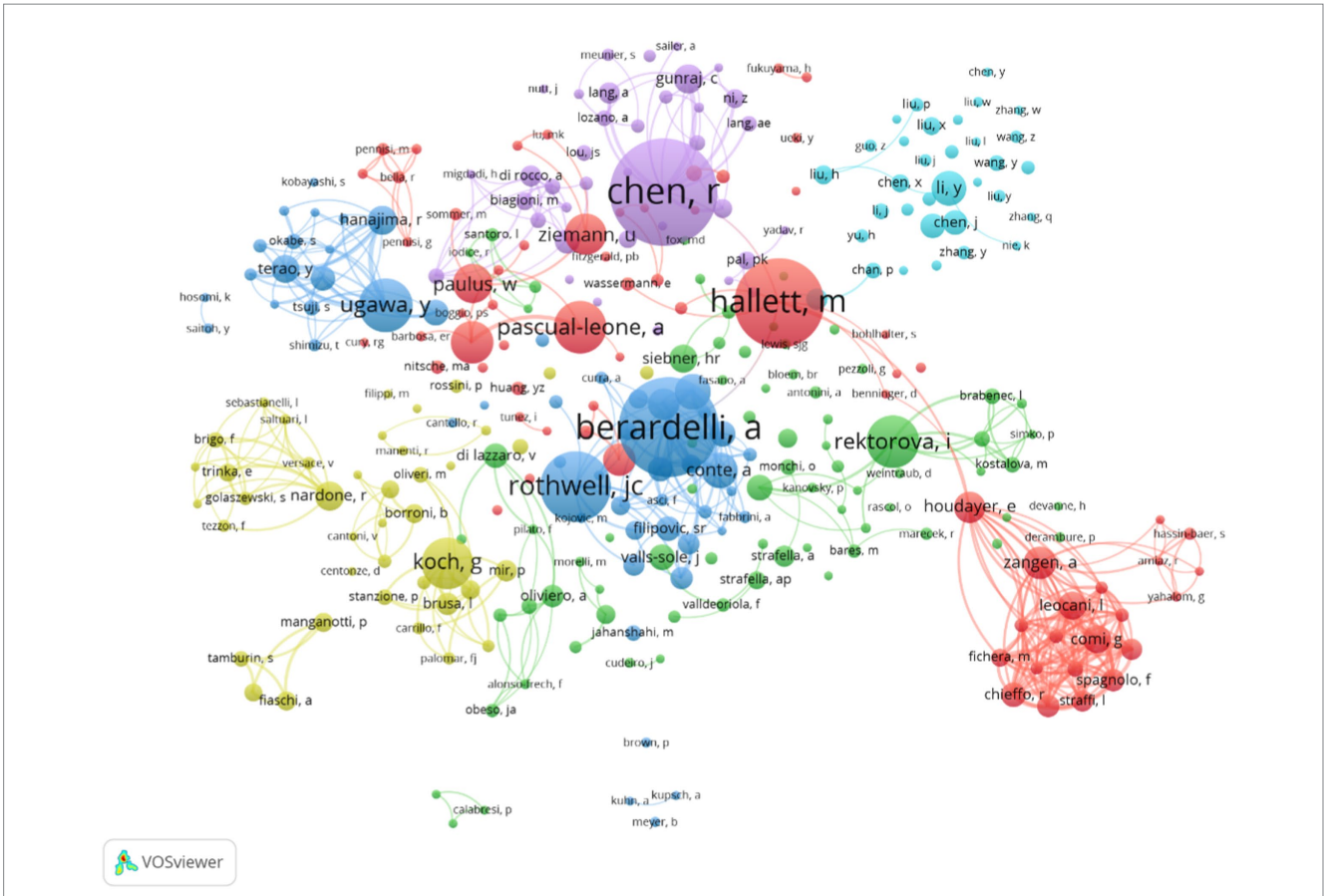

FIGURE 6
Co-author network in the field of TMS for PD.

physiological changes after TMS over PD cortex. The #1 and #4 clusters mainly show the various directions of dysfunction research of TMS over PD. The other clusters represent the stimulation modalities of TMS, stimulation of brain regions and the treatment modes of other sensorimotor integration.

Citation burst analysis is a good atlas that provides a good analysis of specific areas of research for specific year hotspots and trends (Chen et al., 2014). We used Citespace to generate the top 25 keywords with the strongest bursts and the results are shown in Figure 8. The keywords were categorized into three periods based on the time of the burst: 1993

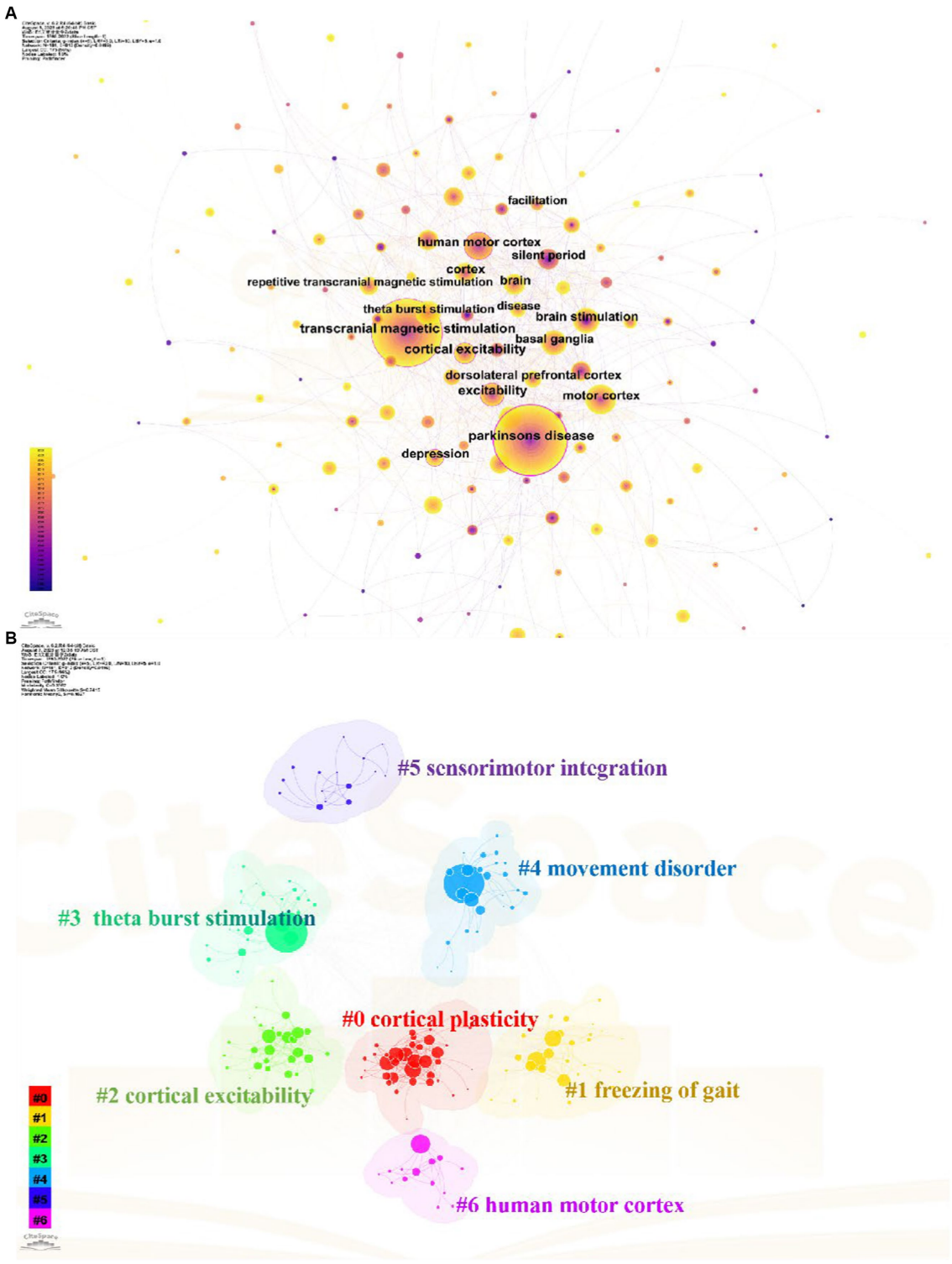

FIGURE 7
Analysis of keywords related to TMS for PD field. **(A)** The keywords co-occurrence network map. **(B)** The keywords cluster map.

to 2000, 2001 to 2015, and 2016 to 2022. Among these keywords silent period has the highest burst intensity. Connectivity mild cognitive impairment quality of life and motor and double blind are the most recent emergent keywords which indicates the recent research direction.

4. Discussion

4.1. General information

In the past decades, TMS has received a lot of attention and research from scholars, and the number of related studies is increasing year by year. In this bibliometric study, a total of 1,894 papers on the topic of TMS in PD were analyzed and visualized using VOSviewer and Citespace to identify research hotspots and trends in the field. The changes in research activity and productivity were evident in the publications on related topics, which can be divided into three phases. Prior to 1995, the number of papers remained relatively constant. In 1985, Baker successfully developed the first transcranial magnetic stimulator (Barker et al., 1985). However, due to the immaturity of the technology and its untapped potential for application, TMS was not widely used in PD therapy. After 1996, with the application and promotion of TMS and high-quality studies confirming its feasibility for neuromodulation, the number of papers steadily increased, attracting increasing attention from medical professionals and researchers. Since 2016, the number of annual publications has maintained a high growth rate of over 100, reaching 150 by 2022. This trend indicates that the tremendous research potential of TMS as a non-invasive and safe neuromodulation technique for the management of motor and non-motor symptoms in PD has attracted increasing attention from scholars (Dinkelbach et al., 2017; Li R. et al., 2022). So, we can anticipate that this research area will continue to be popular in the future.

Of the 10 countries with the highest number of publications in this research area, nine are developed countries and only one developing country, China, is represented. The USA, Italy, Canada, England, and Germany took the dominant places in this field. Although China is a late starter in this field of research, it has developed rapidly. Especially in the last decades, the number of publications has increased rapidly. However, the low centrality (0.02) of China indicates that there are fewer links between developing countries such as China and developed countries in this field of research and a lack of international cooperation. This is also evident from the network of institutional collaborations in Figure 4 and Table 2, which shows that the field of neuromodulation research in TMS for PD is still dominated by national institutions in Europe, the United States, and Canada, such as: the University of Toronto in Canada, Harvard University in the United States, University College London in England, and Sapienza University of Rome in Italy.

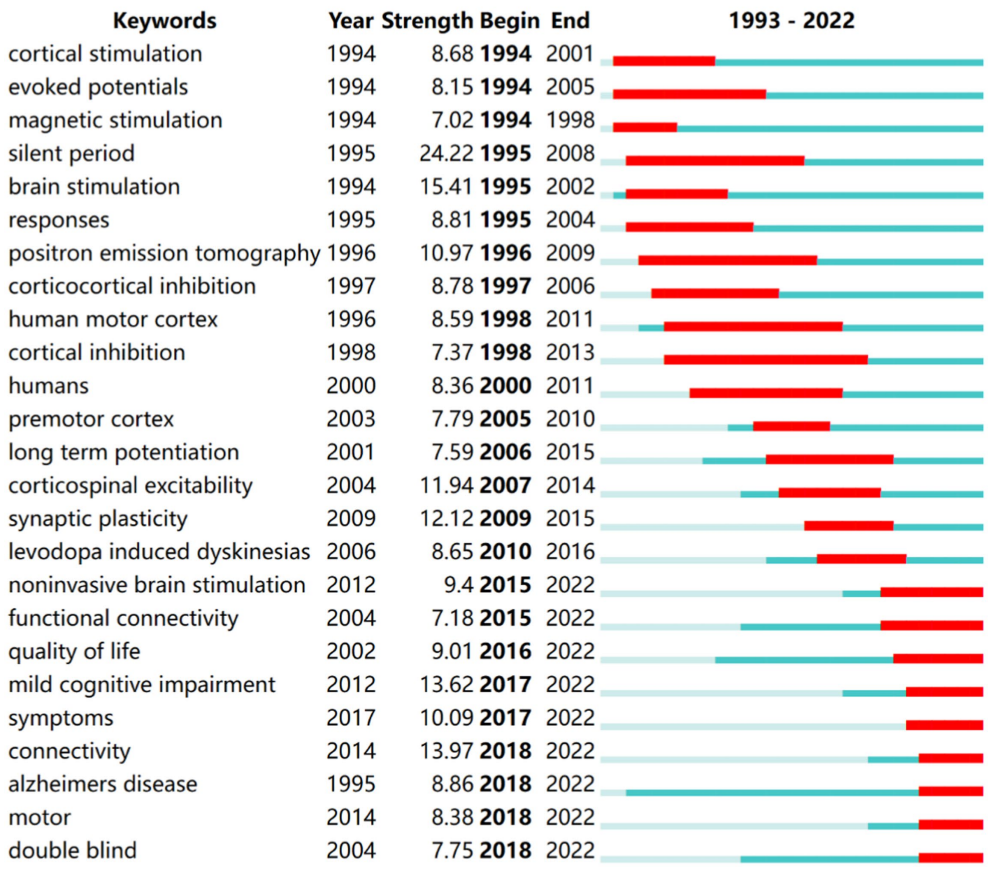

FIGURE 8
Top 25 keywords with the strongest citation bursts of the 1,894 included studies from 1993 to 2022.

Therefore, the visual analysis of countries and institutions shows that the most active and highlighted institutions were nearly from the well-established universities from developed countries with rich academic resources, so there is a certain imbalance in the exchange of academic resources between developing countries and developed countries. This phenomenon can perhaps be explained in several ways. Firstly, the developed countries started their research in the field of TMS neuromodulation earlier in 2002 or even earlier, while the developing countries, represented by China, have published more articles, and established some connections with related countries only in the last decade. Secondly, the financial constraint and inadequate attention of developing countries hinder their sustained investment in the application of TMS technologies to healthcare management. This may lead developing countries lack high-quality research results.

The distribution of author clusters is characterized by similarities with that of the country and institution clusters. The top 10 ranked authors in Table 4 are basically from research institutions in developed countries. From the network diagram of author clusters in Figure 6, it is found that Chen Robert, Berardelli Alfredo, Hallett Mark, and Rothwell John Christine constitute three clusters in the field with more extensive collaborations. Chen and Berardelli reviewed the clinical neurophysiology of movement disorders in PD, which help to advance knowledge of detecting cortical excitability with single and paired TMS (Chen R. et al., 2022). Rothwell and Berardelli assessed M1 and pre-SMA excitability in PD using TMS, which provides an innovative way to investigate motor cortical network changes of PD (Leodori et al., 2022). Mark et al. indicated 1 and 25 Hz rTMS can promotes gait training in PD by rebalancing cortical excitability (Chung et al., 2020).

The data collected from publication outputs and citations indicate that Movement Disorders is the most influential journal in this area. The journal is an official journal of the International Parkinson and Movement Disorder Society (MDS) with a 2022 impact factor of 9.698. The journal includes articles on movement disorders due to lesions of the basal ganglia, the cerebellum, and its connectivity network, including PD, chorea, and others. This has greatly contributed to our understanding of the disorders commonly seen in movement disorders and the associated brain mechanisms. For instance, the 2019 revision of evidence-based medical guidelines for managing non-motor symptoms of PD propose the short-term efficacy of TMS in ameliorating Parkinson's depressive symptoms alongside pharmacotherapy. Nevertheless, the effectiveness of TMS still requires further evidence-based support (Seppi et al., 2019). In addition to Movement Disorders, several neuroscience journals, such as Brain, Journal of Neuroscience and Brain Stimulation, and Neurology, have also contributed high-quality research to the field. The number of papers published in the top 10 journals was more than one-third of the overall papers. Meanwhile, these active journals have a high IF, with only one journal lower than 3. Therefore, the top 10 journals of TMS for PD show high research standards with excellent clinical trials, providing reliable evidence for researchers.

4.2. Research hotspots and trends

The keyword is intended to help understand emerging trends and future research directions (Chen, 2006). Therefore, the following views on the future research direction hotspots of TMS for neuromodulation in patients with PD are based on the analysis of keywords.

4.2.1. About TMS stimulation of cortical areas in patients with PD

An essential factor to optimize TMS treatment of PD is the chosen target site since various brain areas are implicated in PD (Eidelberg, 2009). So far, most studies have focused on the primary motor cortex (M1) or the prefrontal cortex (Fregni et al., 2005). Chou et al. suggested that high-frequency rTMS targeting M1 or low-frequency rTMS applied to other frontal regions showed significant improvement in motor symptoms in PD (Chou et al., 2015). Several studies have also proposed that stimulation of SMA can significantly improve motor symptoms such as tremor and freezing of gait in PD patients, but high-quality RCT evidence is still needed (Shirota et al., 2013; Mi et al., 2019). For the non-motor symptoms, Xie et al. (2015) point out HF-rTMS over left DLPFC in PD patients may provide possible antidepressant efficacy. However, recent studies suggest that the DLPFC may not be an ideal target site for rTMS (Chen et al., 2006). Therefore, it is essential to determine in future trials whether DLPFC is the optimal region to be involved in depression.

4.2.2. About the efficacy of TMS on motor function in patients with PD

Based on the results of keyword burst and cluster analysis motor function in people with PD has received increasing attention from researchers in the past decades. This reason can be the freezing of gait is one of the common motor symptoms in patients with PD and is a major risk factor for falls, which greatly reduces mobility and quality of life (Giladi and Nieuwboer, 2008; Nutt et al., 2011; Rocha et al., 2023). Recent studies suggested that TMS has a certain improvement effect on some indicators of gait in people with PD, and this effect is not maintained in the long term, but only in the short term (Xie et al., 2020). However, Chung et al. proposed that 1 Hz and 25 Hz rTMS stimulation of the M1 could improve walking performance in people with PD in the short and long term compared to the sham rTMS group (Chung et al., 2020). Mi et al. (2018) used 10 Hz rTMS to stimulate SMA and found that the improvement in turn to sit duration lasted for at least 4 weeks, but the improvement in stride length and stride velocity was not significant. Shirota et al. (2013) also found that high-frequency rTMS had only transient beneficial effects, while low-frequency rTMS had long-term beneficial effects. Therefore, TMS has a complex impact on gait parameters in individuals with PD (Gilat et al., 2021). The patient's equilibrium and capacity to execute intricate motor tasks are also taken into consideration, and it is strongly connected to the patient's cognitive ability, with walking in a straight line usually necessitating less cognitive ability, while turning necessitates more cognitive capacity to modify the gait pattern (Gilat et al., 2021). Based on keyword and literature co-citation analysis it can be concluded that TMS parameters, stimulation of the cerebral cortex and maintenance effects need further investigation.

4.2.3. About the mechanism of neuromodulation effect of TMS on PD

From the visual analysis of keywords in the last decade, researchers' attention is not limited to the effect of different parameters and stimulation of different brain regions, but more and more attention is paid to the study of the mechanism of action of TMS for Parkinson's patients.

TMS has the ability to modulate connectivity within the stimulated network and can be used to assess the excitability of motor

cortex in bilateral hemispheres (Lefaucheur et al., 2004; Chen J. et al., 2022), for example, motor threshold (MT) is used to assess the excitability of cortical glutamatergic (Glu)-ergic motor neurons (Ziemann et al., 1996), motor evoked potential (MEP) size reflects the overall excitability of corticospinal pathways (Welch et al., 2020), and ipsilateral silent period (ISP) reflects the functional integrity of corpus callosum connections (Werhahn et al., 1995). Meanwhile, the combination of magnetic resonance imaging (fMRI) can also better reflect the connectivity and excitability of the brain of PD patients (Hallett et al., 2020). In combination with fMRI there is a study showing increased connectivity of the internal globus pallidus with the cerebello-thalamocortical circuit in PD tremor patients with compared to non-tremor and healthy populations (Helmich et al., 2011). Other fMRI studies have also suggested enhanced cerebellar-SMA functional connectivity in PD patients (Mueller et al., 2017). Mi et al. used rTMS over SMA in combination with fMRI to demonstrate that the alleviation of freezing of gait in PD patients was associated with normalization of brain connectivity patterns (Mi et al., 2018).

5. Conclusion

According to a comprehensive analysis, the use of TMS in the treatment of PD is increasing. Although North America and Europe have a significant academic influence, several institutions in developing nations, particularly China, have demonstrated limitless promise in this area. Most high-impact institutions and authors are in developed countries, indicating an imbalance in academic development. Additionally, most journals in the field have high IF, making them valuable sources of scholarly reference. There are still questions about the best modulation strategy for TMS in PD (e.g., the best choice of cerebral cortex stimulation for various motor and non-motor symptoms, the choice of stimulation intensity and stimulation duration), and the justification for the neuromodulation mechanisms used by TMS for people with PD. These clinical difficulties have not only received a lot of attention lately but will also be the subject of further study.

Author contributions

Y-xW: Conceptualization, Data curation, Formal analysis, Methodology, Project administration, Resources, Software, Validation, Visualization, Writing – original draft, Writing – review & editing, Supervision. L-dT: Data curation, Formal analysis, Methodology, Validation, Writing – review & editing, Visualization. LH: Software, Supervision, Validation, Writing – review & editing. Y-tQ: Supervision, Validation, Visualization, Writing – review & editing. WS: Supervision, Validation, Visualization, Writing – review & editing. LZ: Supervision, Validation, Visualization, Writing – review & editing. R-tM: Supervision, Validation, Visualization, Writing – review & editing. QG: Conceptualization, Funding acquisition, Project administration, Supervision, Validation, Writing – original draft, Writing – review & editing.

Funding

The author(s) declare financial support was received for the research, authorship, and/or publication of this article. This study was funded by the NSFC 82172540 from the National Natural Science Foundation of China.

Acknowledgments

The authors would like to thank the researchers involved who work at the Department of Rehabilitation Medicine of West China Hospital at Sichuan University.

Conflict of interest

The authors declare that the research was conducted in the absence of any commercial or financial relationships that could be construed as a potential conflict of interest.

Publisher's note

All claims expressed in this article are solely those of the authors and do not necessarily represent those of their affiliated organizations, or those of the publisher, the editors and the reviewers. Any product that may be evaluated in this article, or claim that may be made by its manufacturer, is not guaranteed or endorsed by the publisher.

References

Barker, A. T., Jalinous, R., and Freeston, I. L. (1985). Non-invasive magnetic stimulation of human motor cortex. *Lancet* 325, 1106–1107. doi: 10.1016/s0140-6736(85)92413-4

Caipa, A., Alomar, M., and Bashir, S. (2018). TMS as tool to investigate the effect of pharmacological medications on cortical plasticity. *Eur. Rev. Med. Pharmacol. Sci.* 22, 844–852. doi: 10.26355/eurrev_201802_14321

Cenci, M. A., and Konradi, C. (2010). "Maladaptive striatal plasticity in L-DOPA-induced dyskinesia" in *Recent advances in Parkinsons disease: Basic research*. eds. A. Bjorklund and M. A. Cenci (Amsterdam: Elsevier Science Bv), 209–233.

Cerasa, A., Koch, G., Donzuso, G., Mangone, G., Morelli, M., Brusa, L., et al. (2015). A network centred on the inferior frontal cortex is critically involved in levodopa-induced dyskinesias. *Brain* 138, 414–427. doi: 10.1093/brain/awu329

Chen, C. (2004). Searching for intellectual turning points: progressive knowledge domain visualization. *Proc. Natl. Acad. Sci. U. S. A.* 101, 5303–5310. doi: 10.1073/pans.0307513100

Chen, C. (2006). CiteSpace II: detecting and visualizing emerging trends and transient patterns in scientific literature. *J. Am. Soc. Inf. Sci. Technol.* 57, 359–377. doi: 10.1002/asi.20317

Chen, R., Berardelli, A., Bhattacharya, A., Bologna, M., Chen, K. S., Fasano, A., et al. (2022). Clinical neurophysiology of Parkinson's disease and parkinsonism. *Clin. Neurophysiol. Pract.* 7, 201–227. doi: 10.1016/j.cnp.2022.06.002

Chen, K. S., and Chen, R. (2019). Invasive and noninvasive brain stimulation in Parkinson's disease: clinical effects and future perspectives. *Clin. Pharmacol. Ther.* 106, 763–775. doi: 10.1002/cpt.1542

Chen, C., Dubin, R., and Kim, M. C. (2014). Orphan drugs and rare diseases: a scientometric review (2000 – 2014). *Expert Opin. Orphan Drugs* 2, 709–724. doi: 10.1517/21678707.2014.920251

Chen, J., Fan, Y. Z., Wei, W., Wang, L. Y., Wang, X. Y., Fan, F. M., et al. (2022). Repetitive transcranial magnetic stimulation modulates cortical-subcortical connectivity in sensorimotor network. *Eur. J. Neurosci.* 55, 227–243. doi: 10.1111/ejn.15571

Chen, Y., Guo, J. J., Zhan, S., and Patel, N. C. (2006). Treatment effects of antidepressants in patients with post-stroke depression: a meta-analysis. *Ann. Pharmacother.* 40, 2115–2122. doi: 10.1345/aph.1H389

Chen, C., and Song, M. (2019). Visualizing a field of research: a methodology of systematic scientometric reviews. *PloS One* 14:e0223994. doi: 10.1371/journal.pone.0223994

Chou, Y. H., Hickey, P. T., Sundman, M., Song, A. W., and Chen, N. K. (2015). Effects of repetitive transcranial magnetic stimulation on motor symptoms in Parkinson disease a systematic review and Meta-analysis. *JAMA Neurol.* 72, 432–440. doi: 10.1001/jamaneurol.2014.4380

Chung, C. L., and Mak, M. K. (2016). Effect of repetitive transcranial magnetic stimulation on physical function and motor signs in Parkinson's disease: a systematic review and Meta-analysis. *Brain Stimul.* 9, 475–487. doi: 10.1016/j.brs.2016.03.017

Chung, C. L. H., Mak, M. K. Y., and Hallett, M. (2020). Transcranial magnetic stimulation promotes gait training in Parkinson disease. *Ann. Neurol.* 88, 933–945. doi: 10.1002/ana.25881

De Risio, L., Borgi, M., Pettorruso, M., Miuli, A., Ottomana, A. M., Sociali, A., et al. (2020). Recovering from depression with repetitive transcranial magnetic stimulation (rTMS): a systematic review and meta-analysis of preclinical studies. *Transl. Psychiatry* 10:393. doi: 10.1038/s41398-020-01055-2

Dinkelbach, L., Brambilla, M., Manenti, R., and Brem, A. K. (2017). Non-invasive brain stimulation in Parkinson's disease: exploiting crossroads of cognition and mood. *Neurosci. Biobehav. Rev.* 75, 407–418. doi: 10.1016/j.neubiorev.2017.01.021

Dorsey, E. R., Sherer, T., Okun, M. S., and Bloem, B. R. (2018). The emerging evidence of the Parkinson pandemic. *J. Parkinsons Dis.* 8, S3–s8. doi: 10.3233/jpd-181474

Eidelberg, D. (2009). Metabolic brain networks in neurodegenerative disorders: a functional imaging approach. *Trends Neurosci.* 32, 548–557. doi: 10.1016/j.tins.2009.06.003

Elahi, B., Elahi, B., and Chen, R. (2009). Effect of transcranial magnetic stimulation on Parkinson motor function--systematic review of controlled clinical trials. *Mov. Disord.* 24, 357–363. doi: 10.1002/mds.22364

Fahn, S. (2008). The history of dopamine and levodopa in the treatment of Parkinson's disease. *Mov. Disord.* 23, S497–S508. doi: 10.1002/mds.22028

Fregni, F., Simon, D. K., Wu, A., and Pascual-Leone, A. (2005). Non-invasive brain stimulation for Parkinson's disease: a systematic review and meta-analysis of the literature. *J. Neurol. Neurosurg. Psychiatry* 76, 1614–1623. doi: 10.1136/jnnp.2005.069849

Giladi, N., and Nieuwboer, A. (2008). Understanding and treating freezing of gait in parkinsonism, proposed working definition, and setting the stage. *Mov. Disord.* 23, S423–S425. doi: 10.1002/mds.21927

Gilat, M., Ginis, P., Zoetewei, D., De Vleeschhauwer, J., Hulzinga, F., D'Cruz, N., et al. (2021). A systematic review on exercise and training-based interventions for freezing of gait in Parkinson's disease. *NPJ Parkinsons Dis* 7:81. doi: 10.1038/s41531-021-00224-4

Gilio, F., Curra, A., Inghilleri, M., Lorenzano, C., Manfredi, M., and Berardelli, A. (2002). Repetitive magnetic stimulation of cortical motor areas in Parkinson's disease: implications for the pathophysiology of cortical function. *Mov. Disord.* 17, 467–473. doi: 10.1002/mds.1255

Goffman, W., and Morris, T. G. (1970). Bradford's law and library acquisitions. *Nature* 226, 922–923. doi: 10.1038/226922a0

Gonzalez-Garcia, N., Armony, J. L., Soto, J., Trejo, D., Alegria, M. A., and Drucker-Colin, R. (2011). Effects of rTMS on Parkinson's disease: a longitudinal fMRI study. *J. Neurol.* 258, 1268–1280. doi: 10.1007/s00415-011-5923-2

Hallett, M. (2000). Transcranial magnetic stimulation and the human brain. *Nature* 406, 147–150. doi: 10.1038/35018000

Hallett, M. (2007). Transcranial magnetic stimulation: A primer. *Neuron* 55, 187–199. doi: 10.1016/j.neuron.2007.06.026

Hallett, M., de Haan, W., Deco, G., Dengler, R., Di Iorio, R., Gallea, C., et al. (2020). Human brain connectivity: clinical applications for clinical neurophysiology. *Clin. Neurophysiol.* 131, 1621–1651. doi: 10.1016/j.clinph.2020.03.031

Helmich, R. C., Janssen, M. J., Oyen, W. J., Bloem, B. R., and Toni, I. (2011). Pallidal dysfunction drives a cerebellothalamic circuit into Parkinson tremor. *Ann. Neurol.* 69, 269–281. doi: 10.1002/ana.22361

Jankovic, J. (2008). Parkinson's disease: clinical features and diagnosis. *J. Neurol. Neurosurg. Psychiatry* 79, 368–376. doi: 10.1136/jnnp.2007.131045

Jenner, P. (2008). Molecular mechanisms of L-DOPA-induced dyskinesia. *Nat. Rev. Neurosci.* 9, 665–677. doi: 10.1038/nrn2471

Lefaucheur, J. P., Drouot, X., Von Raison, F., Ménard-Lefaucheur, I., Cesaro, P., and Nguyen, J. P. (2004). Improvement of motor performance and modulation of cortical excitability by repetitive transcranial magnetic stimulation of the motor cortex in Parkinson's disease. *Clin. Neurophysiol.* 115, 2530–2541. doi: 10.1016/j.clinph.2004.05.025

Leodori, G., De Bartolo, M. I., Guerra, A., Fabbrini, A., Rocchi, L., Latorre, A., et al. (2022). Motor cortical network excitability in Parkinson's disease. *Mov. Disord.* 37, 734–744. doi: 10.1002/mds.28914

Li, R., He, Y., Qin, W., Zhang, Z., Su, J., Guan, Q., et al. (2022). Effects of repetitive transcranial magnetic stimulation on motor symptoms in Parkinson's disease: a Meta-analysis. *Neurorehabil. Neural Repair* 36, 395–404. doi: 10.1177/15459683221095034

Li, X., Wei, W., Wang, Y., Wang, Q., and Liu, Z. (2022). Global trend in the Research and Development of acupuncture treatment on Parkinson's disease from 2000 to 2021: a bibliometric analysis. *Front. Neurol.* 13:906317. doi: 10.3389/fneur.2022.906317

Marras, C., Canning, C. G., and Goldman, S. M. (2019). Environment, lifestyle, and Parkinson's disease: implications for prevention in the next decade. *Mov. Disord.* 34, 801–811. doi: 10.1002/mds.27720

McLean, A. L. (2019). Publication trends in transcranial magnetic stimulation: a 30-year panorama. *Brain Stimul.* 12, 619–627. doi: 10.1016/j.brs.2019.01.002

Mi, T. M., Garg, S., Ba, F., Liu, A. P., Liang, P. P., Gao, L. L., et al. (2020). Repetitive transcranial magnetic stimulation improves Parkinson's freezing of gait via normalizing brain connectivity. *NPJ Parkinsons Dis* 6:16. doi: 10.1038/s41531-020-0118-0

Mi, T. M., Garg, S., Ba, F., Liu, A. P., Wu, T., Gao, L. L., et al. (2019). High-frequency rTMS over the supplementary motor area improves freezing of gait in Parkinson's disease: a randomized controlled trial. *Parkinsonism Relat. Disord.* 68, 85–90. doi: 10.1016/j.parkreldis.2019.10.009

Mi, T. M., Garg, S., Ba, F., Wu, T., Liang, P. P., Gao, L. L., et al. (2018). Alleviation of freezing of gait in patients with Parkinson's disease by high-frequency rTMS over SMA is associated with normalization of brain connectivity patterns. *Mov. Disord.* 33, S16–S17.

Mueller, K., Jech, R., Hoskovcová, M., Ulmanová, O., Urgošík, D., Vymazal, J., et al. (2017). General and selective brain connectivity alterations in essential tremor: a resting state fMRI study. *Neuroimage Clin* 16, 468–476. doi: 10.1016/j.nicl.2017.06.004

Nutt, J. G., Bloem, B. R., Giladi, N., Hallett, M., Horak, F. B., and Nieuwboer, A. (2011). Freezing of gait: moving forward on a mysterious clinical phenomenon. *Lancet Neurol.* 10, 734–744. doi: 10.1016/s1474-4422(11)70143-0

Pan, X., Yan, E., Cui, M., and Hua, W. (2018). Examining the usage, citation, and diffusion patterns of bibliometric mapping software: a comparative study of three tools. *J. Informet.* 12, 481–493. doi: 10.1016/j.joi.2018.03.005

Pitcher, D., Parkin, B., and Walsh, V. (2021). Transcranial magnetic stimulation and the understanding of behavior. *Annu. Rev. Psychol.* 72, 97–121. doi: 10.1146/annurev-psych-081120-013144

Pringsheim, T., Jette, N., Frolkis, A., and Steeves, T. D. (2014). The prevalence of Parkinson's disease: a systematic review and meta-analysis. *Mov. Disord.* 29, 1583–1590. doi: 10.1002/mds.25945

Puschmann, A. (2017). New genes causing hereditary Parkinson's disease or parkinsonism. *Curr. Neurol. Neurosci. Rep.* 17:66. doi: 10.1007/s11910-017-0780-8

Rocha, P. S., de Sousa, B. B. L., D'Amelio, M., Pompeu, J. E., Garcia, P. A., Leal, J. C., et al. (2023). Exergaming in the treatment of gait, balance, and quality of life in Parkinson's disease: overview of systematic reviews. *Physiother. Res. Int.* 28. doi: 10.1002/pri.2002

Salmon, R., Preston, E., Mahendran, N., Ada, L., and Flynn, A. (2023). People with mild Parkinson's disease have impaired force production in upper limb muscles: a cross-sectional study. *Physiother. Res. Int.* 28:e1976. doi: 10.1002/pri.1976

Scully, A. E., Tan, D., Oliveira, B. I. R., Hill, K. D., Clark, R., and Pua, Y. H. (2023). Scoring festination and gait freezing in people with Parkinson's: the freezing of gait severity tool-revised. *Physiother. Res. Int.* e2016:e2016. doi: 10.1002/pri.2016

Seppi, K., Ray Chaudhuri, K., Coelho, M., Fox, S. H., Katzenschlager, R., Perez Lloret, S., et al. (2019). Update on treatments for nonmotor symptoms of Parkinson's disease-an evidence-based medicine review. *Mov. Disord.* 34, 180–198. doi: 10.1002/mds.27602

Shirota, Y., Ohtsu, H., Hamada, M., Enomoto, H., Ugawa, Y., and Res Comm, R. T. P. (2013). Supplementary motor area stimulation for Parkinson disease a randomized controlled study. *Neurology* 80, 1400–1405. doi: 10.1212/WNL.0b013e31828c2f66

Shukla, A. W., Shuster, J. J., Chung, J. W., Vaillancourt, D. E., Patten, C., Ostrem, J., et al. (2016). Repetitive transcranial magnetic stimulation (rTMS) therapy in Parkinson disease: a Meta-analysis. *PM R* 8, 356–366. doi: 10.1016/j.pmrj.2015.08.009

Taib, S., Ory-Magne, F., Brefel-Courbon, C., Moreau, Y., Thalamas, C., Arbus, C., et al. (2019). Repetitive transcranial magnetic stimulation for functional tremor: a randomized, double-blind, controlled study. *Mov. Disord.* 34, 1210–1219. doi: 10.1002/mds.27727

Thomas, B., and Beal, M. F. (2007). Parkinson's disease. *Hum. Mol. Genet.* 16, R183–R194. doi: 10.1093/hmg/ddm159

Venable, G. T., Shepherd, B. A., Loftis, C. M., McClatchy, S. G., Roberts, M. L., Fillinger, M. E., et al. (2016). Bradford's law: identification of the core journals for neurosurgery and its subspecialties. *J. Neurosurg.* 124, 569–579. doi: 10.3171/2015.3.Jns15149

Weinstock, M. (1971). Bradford's law. *Nature* 233:434. doi: 10.1038/233434a0

Welch, J. F., Argento, P. J., Mitchell, G. S., and Fox, E. J. (2020). Reliability of diaphragmatic motor-evoked potentials induced by transcranial magnetic stimulation. *J. Appl. Physiol.* 129, 1393–1404. doi: 10.1152/japplphysiol.00486.2020

Werhahn, K. J., Classen, J., and Benecke, R. (1995). The silent period induced by transcranial magnetic stimulation in muscles supplied by cranial nerves: normal data and changes in patients. *J. Neurol. Neurosurg. Psychiatry* 59, 586–596. doi: 10.1136/jnnp.59.6.586

Xie, C. L., Chen, J., Wang, X. D., Pan, J. L., Zhou, Y., Lin, S. Y., et al. (2015). Repetitive transcranial magnetic stimulation (rTMS) for the treatment of depression in Parkinson disease: a meta-analysis of randomized controlled clinical trials. *Neurol. Sci.* 36, 1751–1761. doi: 10.1007/s10072-015-2345-4

Xie, Y. J., Gao, Q., He, C. Q., and Bian, R. (2020). Effect of repetitive transcranial magnetic stimulation on gait and freezing of gait in Parkinson disease: a systematic review and Meta-analysis. *Arch. Phys. Med. Rehabil.* 101, 130–140. doi: 10.1016/j.apmr.2019.07.013

You, Y., Li, W., Liu, J., Li, X., Fu, Y., and Ma, X. (2021). Bibliometric review to explore emerging high-intensity interval training in health promotion: a new century picture. *Front. Public Health* 9:697633. doi: 10.3389/fpubh.2021.697633

Zhang, P. L., Chen, Y., Zhang, C. H., Wang, Y. X., and Fernandez-Funez, P. (2018). Genetics of Parkinson's disease and related disorders. *J. Med. Genet.* 55, 73–80. doi: 10.1136/jmedgenet-2017-105047

Zhang, W., Deng, B., Xie, F., Zhou, H., Guo, J. F., Jiang, H., et al. (2022). Efficacy of repetitive transcranial magnetic stimulation in Parkinson's disease: a systematic review and meta-analysis of randomised controlled trials. *EClinicalMed* 52:101589. doi: 10.1016/j.eclinm.2022.101589

Zhang, L., Xing, G., Shuai, S., Guo, Z., Chen, H., McClure, M. A., et al. (2017). Low-frequency repetitive transcranial magnetic stimulation for stroke-induced upper limb motor deficit: a Meta-analysis. *Neural Plast.* 2017, 2758097–2758012. doi: 10.1155/2017/2758097

Zhang, T., Yang, R., Pan, J., and Huang, S. (2023). Parkinson's disease related depression and anxiety: a 22-year bibliometric analysis (2000-2022). *Neuropsychiatr. Dis. Treat.* 19, 1477–1489. doi: 10.2147/ndt.S403002

Zhu, Y., Li, D., Zhou, Y., Hu, Y., Xu, Z., Lei, L., et al. (2022). Systematic review and Meta-analysis of high-frequency rTMS over the dorsolateral prefrontal cortex. On chronic pain and chronic-pain-accompanied depression. *ACS Chem. Nerosci.* 13, 2547–2556. doi: 10.1021/acschemneuro.2c00395

Ziemann, U., Rothwell, J. C., and Ridding, M. C. (1996). Interaction between intracortical inhibition and facilitation in human motor cortex. *J. Physiol.* 496, 873–881. doi: 10.1113/jphysiol.1996.sp021734

frontiers | Frontiers in Neuroscience

TYPE Review
PUBLISHED 19 October 2023
DOI 10.3389/fnins.2023.1288765

OPEN ACCESS

EDITED BY
Mark H. Myers,
University of Tennessee Health Science Center (UTHSC), United States

REVIEWED BY
Benito de Celis Alonso,
Meritorious Autonomous University of Puebla, Mexico
Quanguang Zhang,
Augusta University, United States
LSU Health Sciences Center - Shreveport, United States

*CORRESPONDENCE
Jian Liang
✉ 19961087@m.scnu.edu.cn
Zhong-Wei Yang
✉ 19981080@m.scnu.edu.cn

RECEIVED 04 September 2023
ACCEPTED 05 October 2023
PUBLISHED 19 October 2023

CITATION
Zhang J-H, Liang J and Yang Z-W (2023) Non-invasive brain stimulation for fibromyalgia: current trends and future perspectives. *Front. Neurosci.* 17:1288765. doi: 10.3389/fnins.2023.1288765

Non-invasive brain stimulation for fibromyalgia: current trends and future perspectives

Jia-Hao Zhang[1], Jian Liang[2]* and Zhong-Wei Yang[2]*

[1]Laboratory of Laser Sports Medicine, School of Physical Education and Sports Science, South China Normal University, Guangzhou, China, [2]Laboratory of Sports Rehabilitation, School of Physical Education and Sports Science, South China Normal University, Guangzhou, China

Fibromyalgia, a common and enduring pain disorder, ranks as the second most prevalent rheumatic disease after osteoarthritis. Recent years have witnessed successful treatment using non-invasive brain stimulation. Transcranial magnetic stimulation, transcranial direct current stimulation, and electroconvulsion therapy have shown promise in treating chronic pain. This article reviews the literature concerning non-invasive stimulation for fibromyalgia treatment, its mechanisms, and establishes a scientific basis for rehabilitation, and discusses the future directions for research and development prospects of these techniques are discussed.

KEYWORDS

non-invasive brain stimulation (NIBS), fibromyalgia (FM), repetitive transcranial magnetic stimulation (rTMS), transcranial direct current stimulation (tDCS), electroconvulsive therapy (ECT), transcranial alternating current stimulation (tACS), reduced impedance non-invasive cortical electrostimulation (RINCE), transcranial focused ultrasound (tFUS)

1. Introduction

Fibromyalgia (FM) stands as a common chronic pain disorder (Giorgi et al., 2023), ranking second among rheumatic diseases after osteoarthritis (Clauw, 2014). Its prevalence remains consistent across races, approximately ranging from 2% to 4% (Sarzi-Puttini et al., 2020), with a female-to-male ratio of 7:1 (Neumann and Dan, 2003; Weir et al., 2006). FM is associated with various comorbidities (Robinson et al., 2004) and impacts global quality of life (Clauw, 2014; Chinn et al., 2016), though its pathogenesis remains partially understood (Sarzi-Puttini et al., 2020), implicating central sensitization, neurotransmitter imbalances, neurofunctional irregularities, and endocrine metabolic disturbances.

Pharmacological treatment remains predominant for FM; however, evidence suggests inadequacies in symptom alleviation and adverse reactions in some patients (Mease et al., 2013; Arnold et al., 2015; Gilron et al., 2016). Traditional analgesics, such as acetaminophen, yield inefficacy and severe side effects, leading some to consider antipsychotics for sleep improvement (Moldofsky et al., 1996). While quetiapine shows advantages in pain and sleep issues, its recommendation the level of evidence remains limited, suitable primarily for short-term FM treatment (Calandre et al., 2014; Walitt et al., 2016). A meta-analysis indicates partial symptom relief from drugs like amitriptyline, growth hormone, and sodium oxybate (Perrot and Russell, 2014). In summary, pharmacological treatments inadequately address FM symptoms, necessitating improved approaches (Rathore and Afridi, 2020). With the recognition of central pain system abnormalities in FM's occurrence, non-invasive brain stimulation (NIBS) techniques

emerge as potential non-pharmacological treatments (Fregni et al., 2006; Sampson et al., 2006; O'brien et al., 2018).

Non-invasive brain stimulation (NIBS), widely employed in treating depression, exhibits significant therapeutic effects. The co-occurrence of chronic pain and depression, likely stemming from functional impairment due to persistent pain (Thompson et al., 2016; Michaelides and Zis, 2019), underscores the potential of NIBS as a valuable intervention. Shared neuroanatomical structures and neurochemical phenomena further establish the link between depression and pain (Banks Sara and Kerns Robert, 1996), rendering NIBS not only applicable to depression but also to fibromyalgia (FM).

Among the commonly used and extensively studied NIBS techniques are repetitive transcranial magnetic stimulation (rTMS), transcranial direct current stimulation (tDCS), and electroconvulsive therapy (ECT). These techniques have shown efficacy in addressing FM symptoms, notably improving pain, fatigue, and sleep issues. However, there are other emerging branches of NIBS technology, such as Transcranial Alternating Current Stimulation (tACS), Reduced Impedance Non-Invasive Cortical Electrostimulation (RINCE), Transcranial Focused Ultrasound (tFUS), and Transcranial Random Noise Stimulation (tRNS). These methods possess their own unique characteristics and advantages. While they have fewer related studies compared to transcranial magnetic stimulation, tDCS, and electroconvulsive therapy, they hold significant promise for the future of FM relief and warrant further exploration. In this review, we focus on rTMS, tDCS, and ECT, delving into their mechanisms, clinical effects, and distinctions. This comprehensive examination establishes a solid scientific foundation for the rehabilitation of FM (Figure 1).

2. The role of repetitive transcranial magnetic stimulation in fibromyalgia

2.1. Introduction to repetitive transcranial magnetic stimulation (rTMS)

Repetitive Transcranial Magnetic Stimulation (rTMS) employs an inductor and a capacitor to generate changing magnetic fields. These fields induce a reverse current in specific brain regions, affecting neuronal functions and electrical activities. The therapeutic impacts of rTMS rely on stimulation parameters, intervention duration, and targeted brain areas. Stimulation intensity typically ranges from 80 to 120% of the participant's resting motor threshold. rTMS encompasses both excitatory (high-frequency rTMS, HF-rTMS, $\geq$5 Hz) and inhibitory (low-frequency rTMS, LF-rTMS, $\leq$1 Hz) modes, provoking neuronal excitation or reduction, respectively (Rosen et al., 2009; Ansari et al., 2021). The multipulse properties of this technique induce physiological neurological changes, which can have lasting effects for up to 15 min or more, even after the stimulation ends (Chen et al., 1997). In the case of fibromyalgia patients, they continued to experience significant pain relief following 10 or more consecutive sessions of transcranial magnetic stimulation, in contrast to the sham stimulation and placebo groups (Boyer et al., 2014; Altas et al., 2019). Notably, analgesic outcomes can extend for weeks (Moisset and Lefaucheur, 2019). In contrast to conventional pharmacological methods, rTMS offers a safer, lower side-effect approach for fibromyalgia treatment. Moreover, rTMS addresses concurrent symptoms in fibromyalgia patients, such as sleep disruptions, fatigue, and functional impairments (Su et al., 2021).

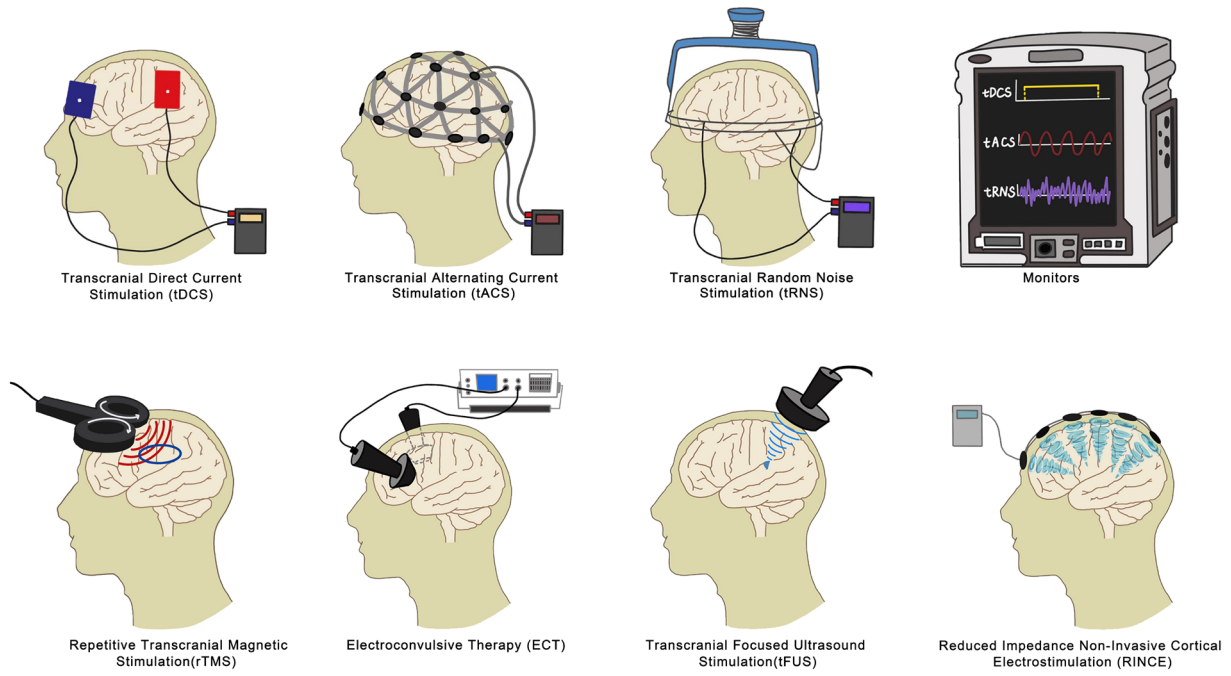

FIGURE 1
A brief schematic of different non-invasive brain stimulation methods of action.

2.2. Application and mechanism of rTMS in fibromyalgia treatment

2.2.1. Analgesic effects of rTMS via primary motor cortex and dorsolateral prefrontal cortex

Studies by Tamura et al. (2004) and Sampson et al. (2006) reveal that applying LF-rTMS (1 Hz) to the primary motor cortex (M1) and dorsolateral prefrontal cortex (DLPFC) respectively, alleviates acute pain and offers potential pain regulatory effects in fibromyalgia treatment. Intriguingly, HF-rTMS also contributes to pain relief. Altas' research demonstrates HF-rTMS (10 Hz) applied to M1 and DLPFC enhances physical function and emotional well-being in fibromyalgia patients (Altas et al., 2019). Furthermore, both high-frequency HF-rTMS and low-frequency LF-rTMS on the right DLPFC manifest analgesic and antidepressant outcomes (Ansari et al., 2021). Collectively, both HF-rTMS and LF-rTMS alleviate fibromyalgia pain through M1 and DLPFC modulation.

2.2.2. Analgesic effects of rTMS via neurotransmitter modulation

rTMS engages cortical neurons, affecting cortical excitability and brain activity to modulate pain processing. Disrupted neurotransmitter concentrations, notably glutamate N-methyl-D-aspartate (NMDA) receptor, contribute to central sensitization and fibromyalgia pain development. rTMS potentially mitigates pain by top-down neurotransmitter modulation (Dall'agnol et al., 2014).

Numerous investigations affirm rTMS's engagement with the endogenous opioid system, generating analgesic effects. Dysregulation of the endogenous opioid peptide system and diminished opioid receptors characterize fibromyalgia patients (Ansari et al., 2021). Neuroimaging exposes pain-processing regions like the cingulate gyrus, orbitofrontal and prefrontal cortex, thalamus, and periaqueductal gray matter (Peyron et al., 2000; Apkarian et al., 2005). rTMS regulates dopamine, serotonin, and opioid peptide receptors, restoring homeostasis. Further, rTMS on rats' cerebellar cortex reduces metabolic glutamate receptors and Protein kinase C synthesis, influencing neuronal activity and calcium levels, thus providing analgesic effects (Lee et al., 2014). HF-rTMS might alleviate pain via nitric oxide synthase (nNOS) down-regulation.

FM pain associates with gamma-aminobutyric acid (GABA) and glutamate (Glu) mechanism dysregulation (Mhalla et al., 2010). rTMS of the ipsilateral motor cortex significantly elevates inhibitory neurotransmitter GABA, with the contralateral side experiencing a decrease (Clauw, 2014). Consequently, impaired GABAergic neurotransmission correlates with FM pain. Motor cortex-targeted rTMS reinstates GABAergic and glutamatergic system balance, curbing excitatory and bolstering inhibitory neurotransmitter activity for fibromyalgia pain relief. To summarize, rTMS stands as a secure, non-invasive cortical stimulation technique.

3. The role and mechanism of transcranial direct current stimulation treatment in fibromyalgia

3.1. Introduction to transcranial direct current stimulation (tDCS)

tDCS employs small, constant currents (1–2 mA) externally to modulate brain neuronal activity. It has gained diverse applications in brain injury rehabilitation, cognitive and emotional regulation, and chronic pain management. Renowned for its affordability and tolerance, tDCS stands as a widely used non-invasive brain stimulation method (Saavedra et al., 2015). The stimulation modes categorize as anodal (a-tDCS), cathodal (c-tDCS), or sham (s-tDCS), each differing in action (Liu et al., 2021). Notably, while transcranial electrical stimulation adjusts neural network activity, transcranial magnetic stimulation triggers neuronal firing via suprathreshold stimulation. At the neuronal level, tDCS achieves effects by polarizing the resting membrane potential through different polarities, thus modulating cortical excitability. Notably, membrane polarization is the primary mechanism for transcranial electrical stimulation, with a-tDCS heightening cortical excitability and c-tDCS inhibiting it. The evidence-based recommendation for the application of tDCS in fibromyalgia is categorized as level B, according to the Standards of the European Federation of Neurological Societies (Lefaucheur et al., 2017).

3.2. Application and mechanism of tDCS in fibromyalgia treatment

3.2.1. tDCS and analgesic effects via targeting brain regions

Distinct tDCS types can be employed to mitigate fibromyalgia (FM) pain by focusing on diverse brain regions. Application of c-tDCS on S1, M1, or DLPFC reduces brain hyperexcitability, increasing pain thresholds and reducing sensitivity. However, targeting DLPFC for pain relief in FM patients is somewhat debated (Fregni et al., 2006). Nevertheless, research suggests c-tDCS applied to DLPFC could alleviate pain (Mariano et al., 2015). Valle's study indicates a-tDCS on left M1 is more effective than left DLPFC in producing analgesic effects (Valle et al., 2009). Additionally, Fregni et al. (2006) find that a-tDCS targeting M1 substantially improves FM pain, sustaining analgesic effects for over 3 weeks. This suggests that M1 targeting is more effective. Still, the analgesic effects of c-tDCS on M1 remain debated (Steffen et al., 2018). Conversely, Roizenblatt et al. (2007) propose tDCS on M1 improves sleep in FM patients. Other studies suggest M1 stimulation could influence thalamus and basal ganglia function, thereby alleviating FM pain (Khedr et al., 2017). In summary, targeting M1 with tDCS seems more effective in alleviating FM pain symptoms.

3.2.2. tDCS and analgesic effects via neurotransmitter modulation

The analgesic effects of tDCS relate to neurotransmitter alterations. Studies underscore NMDA receptor activation's role in pain generation and maintenance, a potential mechanism in fibromyalgia (FM). NMDA receptor non-competitive antagonist MK-801 reduces capsaicin-induced heat hyperalgesia and mechanical hypersensitivity. During tDCS, changes in membrane potential influence NMDA receptor expression and enhance γ-aminobutyric acid (GABA) release, thus easing pain (Foerster et al., 2015). N-acetylaspartate (NAA), an abundant brain metabolite, serves as a neuroprotective neurotransmitter, significant in pain management. Bradley R. Foerster et al. find tDCS decreases clinical pain scores, reduces glutamate and glutamine levels, and increases γ-GABA, hinting at enhanced neurotransmitter modulation to ease pain.

Furthermore, tDCS elevates N-acetylaspartate levels, overall impacting neurotransmitters for pain relief. In addition, Kadetoff et al. (2012) observed elevated interleukin-8 (IL-8) in the cerebrospinal fluid of fibromyalgia (FM) patients, which is likely pivotal in the central sensitization process.

4. The role of electroconvulsive therapy in fibromyalgia treatment

4.1. Introduction to electroconvulsive therapy (ECT)

ECT involves applying electrical potential to the brain via stimulation electrodes affixed to the scalp, creating diverse electric fields based on electrode positioning. This induces synchronized neural cell oscillations and simultaneous autonomic nervous system excitation across extensive brain areas (Couvreur et al., 1989; Peterchev et al., 2010). Since Cerletti and Bini's initial use of ECT for schizophrenia treatment in 1938(Kalinowsky, 1986), physicians have applied it to various conditions. Rasmussen et al. reviewed ECT's pain treatment literature, concluding its efficacy in chronic pain management based on synthesized case reports spanning decades (Rasmussen and Rummans, 2002). Moreover, reports indicate ECT's analgesic effects across different pain syndromes (Canavero and Bonicalzi, 2001; Wasan et al., 2004).

4.2. Application and mechanism of ECT in fibromyalgia treatment

4.2.1. ECT and analgesic effects via enhanced cerebral blood flow

Usui et al.'s study tracked regional cerebral blood flow (rCBF) changes pre and post ECT, revealing thalamic rCBF increase in fibromyalgia (FM) patients. This correlated with reduced tender points and pain scores (visual analog scale, VAS), indicating significant pain relief possibly tied to augmented rCBF (Usui et al., 2006). Neuroimaging verifies the prefrontal cortex, anterior cingulate cortex, insula, and amygdala's roles in pain and emotion regulation (Rainville, 2002). Severe depression and chronic pain patients exhibit abnormal blood flow in these regions (Marsh et al., 1996), which ECT can normalize in severe depression (Elizagarate et al., 2001) and chronic pain (Fukui et al., 2002b). While some studies suggest ECT's efficacy in low thalamic blood flow neuropathic pain (Fukui et al., 2002a, 2002b), other studies report mixed results (Salmon et al., 1988, McCance et al., 1996). Notably, ECT could raise brain-derived neurotrophic factor (BDNF) (Okamoto et al., 2008; Piccinni et al., 2009), pivotal in antidepressant actions through neural plasticity and linked to pain improvement.

4.2.2. ECT and analgesic effects via neurotransmitter modulation

ECT heightens responsiveness of serotonin, norepinephrine, and dopamine systems pivotal in central pain processing (King and Liston, 1990). ECT can stimulate inhibitory pathways by activating these neurotransmitter systems (Newman et al., 1998). Post-ECT treatment, neurotransmitter release increases, bolstering serotonin, norepinephrine, dopamine, and others. This enhances peripheral stimulus signal processing through central nervous system descending pathways, reinforcing brain inhibitory pain pathways (Canavero et al., 1994; Wasan et al., 2004).

ECT fosters central neurotransmitter systems' new equilibrium through electrical stimulation. Past studies indicate repeated ECT boosts plasma beta-endorphin levels (Abrams, 2002). Insufficient beta-endorphin levels correlate with pain hypersensitivity. ECT might relieve fibromyalgia pain by promoting endorphin production, reducing pain sensitivity, and achieving analgesic effects. Okabe et al. note ECT's potential to increase neuropeptide Y (NPY) expression (Okabe et al., 2010). NPY, a hormone with central and peripheral presence, plays diverse roles, including pain modulation. The mechanism by which ECT treats pain in patients with FM may involve promoting elevated NPY expression, thereby reducing pain sensitivity in patients and achieving analgesic effects.

5. Profiles of several non-invasive brain neurostimulation techniques

5.1. Transcranial alternating current stimulation (tACS)

tACS, a non-invasive brain stimulation technique, modulates neural activity by applying sinusoidal alternating current to the scalp, thus generating an electric field within the brain (Wischnewski et al., 2023). Much like direct current stimulation (tDCS), tACS effectively modulates cortical excitability (Sabel et al., 2020). However, when compared to tDCS, tACS demonstrates superior efficacy in precisely directing endogenous brain oscillations. It has the unique capability to mimic the natural alternation of brain oscillations and induce long-term synaptic plasticity, thereby effectively regulating brain function.

Despite being a more widely adopted non-invasive brain stimulation method, tACS is still relatively nascent in its development, particularly in the context of fibromyalgia. In recent years, researchers have successfully addressed the traditional limitations of tACS, which struggled with the precise localization of specific brain regions. They have accomplished this through innovative techniques, including high-definition tACS, phase-shifting tACS, amplitude-modulated tACS, temporal interference (TI) techniques, and intersecting short pulses (ISPs) (Wu et al., 2021). These advancements have propelled tACS into a more advanced stage of development and have expanded its potential in the treatment and alleviation of fibromyalgia symptoms.

5.2. Reduced impedance non-invasive cortical electrostimulation (RINCE)

RINCE is among the less explored methods of electrical stimulation within the realm of non-invasive brain stimulation. In RINCE, electrodes attached to the patient's scalp generate a

specific current frequency, allowing the current to penetrate deeper into the cortex by reducing the impedance of the skin and skull (O'Connell et al., 2018), potentially leading to improved stimulation effects. There are limited reports on RINCE therapy, and its adverse effects include transient mild head discomfort and localized cutaneous reactions (Szymoniuk et al., 2023). In an RCT investigating RINCE therapy for fibromyalgia control, it was found that mean pressure points and pressure pain thresholds improved in the active treatment group compared to the sham treatment group (Hargrove et al., 2012). Patients with fibromyalgia reported decreased pain VAS scores following RINCE treatment. Although there is limited current research on RINCE, these results are statistically and clinically significant, suggesting that RINCE offers advantages and potential for development in fibromyalgia treatment.

5.3. Transcranial focused ultrasound (tFUS)

tFUS emerges as a significant non-invasive brain stimulation technique (Aubry and Tanter, 2016). While it may not have received the same level of research attention as rTMS, tDCS, or other established methods, it boasts remarkable spatial precision, capable of targeting and stimulating deep brain regions with millimeter accuracy. This technique employs piezoelectric-element transducers that emit ultrasound pulses, effectively reaching and stimulating deep brain areas.

5.4. Transcranial random noise stimulation (tRNS)

tRNS, a non-invasive brain stimulation method, is renowned for its reduced discomfort levels in comparison to other tES techniques. In an analgesic study, tRNS demonstrated the capability to induce both immediate and sustained analgesia when applied to area m1 of the cerebral cortex. This analgesic effect was attributed to a reduction in pain anticipation (Yao et al., 2021). Furthermore, it exhibits potential for enhancing behaviors through long-term neuroplasticity effects (van der Groen et al., 2022). Nonetheless, the precise physiological mechanisms responsible for tRNS's impact on nerves remain elusive.

6. Discussion

Limited studies have investigated the effects of tRNS, RINCE, and tFUS on fibromyalgia compared to tACS. In a double-blind randomized crossover study conducted by Bernardi et al., participants were randomly assigned to receive either transcranial alternating current stimulation (tACS) or random noise stimulation (RNS) treatment 5 days a week for 2 weeks. The intervention group received tACS, while the control group received RNS. The study defined three measurement time points: T0 (baseline), T1 (post-stimulation), and T2 (1 month or 4 weeks after stimulation) (Bernardi et al., 2021).

The results showed that, in comparison to RNS, tACS led to an increase in EEG alpha1 activity [(8–10) Hz] at T1, a reduction in pain symptoms assessed through visual analog scales at T1, and enhancements in self-reported cognitive skills and neuropsychological scores at both T1 and T2. Notably, improvements were observed in both the tACS and RNS groups after receiving treatment. However, it's important to note that this study had a small sample size and potential bias due to variations in participants' medication regimens. To address this limitation, future studies should aim to validate this treatment approach using larger samples. Additionally, maintaining consistent medication regimens among study participants throughout the research is essential to mitigate potential bias from concurrent medication use.

7. Conclusion and future perspectives

The emergence of non-invasive brain stimulation techniques has revolutionized chronic pain treatment. Methods like rTMS, tDCS, and ECT have proven effective in addressing conditions such as fibromyalgia, showcasing considerable potential. Lesser-known techniques like rINCE, tFUS, tACS, and RNS, while having fewer studies behind them, exhibit promising traits and are poised for development. This paper delves into the intricacies of non-invasive brain stimulation mechanisms, identifies technical challenges, and outlines future research directions.

However, research on the application of non-invasive brain stimulation for fibromyalgia and analogous chronic pain conditions is still in its infancy. Several crucial considerations should guide our future endeavors:

1. The current clinical sample size for non-invasive brain stimulation in fibromyalgia remains relatively small. It is imperative to conduct comprehensive, large-scale, and standardized randomized controlled trials to determine optimal stimulation parameters and models for various non-invasive brain stimulation techniques (Hou et al., 2016).
2. Enhancing the credibility of experimental data necessitates supplementing subjective rating scales with objective measures. Furthermore, maintaining the integrity of participant blinding is of paramount importance.
3. An in-depth exploration is vital to pinpoint precise stimulation sites and understand how distinct parameters and target locations influence treatment outcomes. Utilizing neuroimaging and high-resolution electroencephalography can enhance localization, while integrating neurophysiological markers and diverse imaging modalities can refine the determination of stimulation intensity and duration.
4. Recognizing the synergy between non-invasive brain stimulation and pharmacology in fibromyalgia treatment is essential, given the frequent combination of these approaches. This synergy holds the promise of heightened therapeutic efficacy and adherence to rigorous technical standards, optimizing pain relief for fibromyalgia patients.
5. Currently, RINCE, tACS, tFUS, and tRNS, as branches of NIBS technology, have a relatively small number of studies compared with rTMS, tDCS, and ECT, and subsequent researchers have paid more attention to their development and deeper mechanistic studies. These developments are not only conducive to the overall development of non-invasive brain

stimulation but will also play a greater potential role in the treatment of fibromyalgia disorders.

6. In light of the unique analgesic mechanisms of various non-invasive stimulation techniques, future research should explore their integration. This approach can overcome individual limitations, paving the way for personalized non-invasive stimulation methods and precision medicine. Such advancements will significantly contribute to the treatment of fibromyalgia and chronic pain, ultimately enhancing patient well-being and quality of life.

Author contributions

J-HZ: Writing – original draft, Writing – review & editing, Conceptualization, Data curation, Formal Analysis, Validation. JL: Conceptualization, Supervision, Validation, Writing – review & editing. Z-WY: Conceptualization, Supervision, Validation, Writing – review & editing.

Funding

The author(s) declare that no financial support was received for the research, authorship, and/or publication of this article.

Conflict of interest

The authors declare that the research was conducted in the absence of any commercial or financial relationships that could be construed as a potential conflict of interest.

Publisher's note

References

Abrams, R. (2002). *Electroconvulsive therapy* (*4th ed.*). Oxford: Oxford University Press

Altas, E. U., Askin, A., Besiroglu, L., and Tosun, A. (2019). Is high-frequency repetitive transcranial magnetic stimulation of the left primary motor cortex superior to the stimulation of the left dorsolateral prefrontal cortex in fibromyalgia syndrome? *Somatosens. Mot. Res.* 36, 56–62. doi: 10.1080/08990220.2019.1587400

Ansari, A. H., Pal, A., Ramamurthy, A., Kabat, M., Jain, S., and Kumar, S. (2021). Fibromyalgia pain and depression: an update on the role of repetitive transcranial magnetic stimulation. *ACS Chem. Neurosci.* 12, 256–270. doi: 10.1021/acschemneuro.0c00785

Apkarian, A. V., Bushnell, M. C., Treede, R. D., and Zubieta, J. K. (2005). Human brain mechanisms of pain perception and regulation in health and disease. *Eur. J. Pain* 9, 463–484. doi: 10.1016/j.ejpain.2004.11.001

Arnold, L. M., Sarzi-Puttini, P., Arsenault, P., Khan, T., Bhadra Brown, P., Clair, A., et al. (2015). Efficacy and safety of pregabalin in patients with fibromyalgia and comorbid depression taking concurrent antidepressant medication: a randomized, placebo-controlled study. *J. Rheumatol.* 42, 1237–1244. doi: 10.3899/jrheum.141196

Aubry, J. F., and Tanter, M. (2016). MR-guided transcranial focused ultrasound. *Adv. Exp. Med. Biol.* 880, 97–111. doi: 10.1007/978-3-319-22536-4_6

Banks Sara, M., and Kerns Robert, D. (1996). Explaining high rates of depression in chronic pain: a diathesis-stress framework. *Psychol. Bull.* 119, 95–110. doi: 10.1037/0033-2909.119.1.95

Bernardi, L., Bertuccelli, M., Formaggio, E., Rubega, M., Bosco, G., Tenconi, E., et al. (2021). Beyond physiotherapy and pharmacological treatment for fibromyalgia syndrome: tailored tACS as a new therapeutic tool. *Eur. Arch. Psychiatry Clin. Neurosci.* 271, 199–210. doi: 10.1007/s00406-020-01214-y

Boyer, L., Dousset, A., Roussel, P., Dossetto, N., Cammilleri, S., Piano, V., et al. (2014). rTMS in fibromyalgia: a randomized trial evaluating QoL and its brain metabolic substrate. *Neurology* 82, 1231–1238. doi: 10.1212/WNL.0000000000000280

Calandre, E. P., Rico-Villademoros, F., Galán, J., Molina-Barea, R., and Morillas-Arques, P. (2014). Quetiapine extended-release (Seroquel-Xr) versus amitriptyline monotherapy for treating patients with fibromyalgia: a 16-week, randomized, flexible-dose, open-label trial. *Psychopharmacology* 231, 2525–2531. doi: 10.1007/s00213-013-3422-0

Canavero, S., and Bonicalzi, V. (2001). Electroconvulsive therapy and pain. *Pain* 89, 301–302. doi: 10.1016/S0304-3959(00)00377-8

Canavero, S., Bonicalzi, V., and Pagni, C. A. (1994). Chronic pain, electroconvulsive therapy and reverberation. *Pain* 59:423. doi: 10.1016/0304-3959(94)90029-9

Chen, R., Classen, J., Gerloff, C., Celnik, P., Wassermann, E. M., Hallett, M., et al. (1997). Depression of motor cortex excitability by low-frequency transcranial magnetic stimulation. *Neurology* 5, 1398–1403.

Chinn, S., Caldwell, W., and Gritsenko, K. (2016). Fibromyalgia pathogenesis and treatment options update. *Curr. Pain Headache Rep.* 20:25. doi: 10.1007/s11916-016-0556-x

Clauw, D. J. (2014). Fibromyalgia: a clinical review. *JAMA* 311, 1547–1555. doi: 10.1001/jama.2014.3266

Couvreur, V., Ansseau, M., and Franck, G. (1989). Electroconvulsive therapy and its mechanism of action. *Acta Psychiatr. Belg.* 89, 96–109.

Dall'agnol, L., Medeiros, L. F., Torres, I. L., Deitos, A., Brietzke, A., Laste, G., et al. (2014). Repetitive transcranial magnetic stimulation increases the corticospinal inhibition and the brain-derived neurotrophic factor in chronic myofascial pain syndrome: an explanatory double-blinded, randomized, sham-controlled trial. *J. Pain* 15, 845–855. doi: 10.1016/j.jpain.2014.05.001

Elizagarate, E., Cortes, J., Gonzalez Pinto, A., Gutierrez, M., Alonso, I., Alcorta, P., et al. (2001). Study of the influence of electroconvulsive therapy on the regional cerebral blood flow by HMPAO-SPECT. *J. Affect. Disord.* 65, 55–59. doi: 10.1016/S0165-0327(00)00200-7

Foerster, B. R., Nascimento, T. D., Deboer, M., Bender, M. A., Rice, I. C., Truong, D. Q., et al. (2015). Brief report: excitatory and inhibitory brain metabolites as targets of motor cortex transcranial direct current stimulation therapy and predictors of its efficacy in fibromyalgia. *Arthritis Rheumatol.* 67, 576–581. doi: 10.1002/art.38945

Fregni, F., Gimenes, R., Valle, A. C., Ferreira, M. J., Rocha, R. R., Natalle, L., et al. (2006). A randomized, sham-controlled, proof of principle study of transcranial direct current stimulation for the treatment of pain in fibromyalgia. *Arthritis Rheum.* 54, 3988–3998. doi: 10.1002/art.22195

Fukui, S., Shigemori, S., and Nosaka, S. (2002a). Central pain associated with low thalamic blood flow treated by electroconvulsive therapy. *J. Anesth.* 16, 255–257. doi: 10.1007/s005400200036

Fukui, S., Shigemori, S., Yoshimura, A., and Nosaka, S. (2002b). Chronic pain with beneficial response to electroconvulsive therapy and regional cerebral blood flow changes assessed by single photon emission computed tomography. *Reg. Anesth. Pain Med.* 27, 211–213. doi: 10.1053/rapm.2002.31205

Gilron, I., Chaparro, L. E., Tu, D., Holden, R. R., Milev, R., Towheed, T., et al. (2016). Combination of pregabalin with duloxetine for fibromyalgia: a randomized controlled trial. *Pain* 157, 1532–1540. doi: 10.1097/j.pain.0000000000000558

Giorgi, V., Bazzichi, L., Batticciotto, A., Pellegrino, G., Di Franco, M., Sirotti, S., et al. (2023). Fibromyalgia: one year in review 2023. *Clin. Exp. Rheumatol.* 41, 1205–1213. doi: 10.55563/clinexprheumatol/257e99

Hargrove, J. B., Bennett, R. M., Simons, D. G., Smith, S. J., Nagpal, S., and Deering, D. E. (2012). A randomized placebo-controlled study of noninvasive cortical electrostimulation in the treatment of fibromyalgia patients. *Pain Med.* 13, 115–124. doi: 10.1111/j.1526-4637.2011.01292.x

Hou, W. H., Wang, T. Y., and Kang, J. H. (2016). The effects of add-on non-invasive brain stimulation in fibromyalgia: a meta-analysis and meta-regression of randomized controlled trials. *Rheumatology (Oxford)* 55, 1507–1517. doi: 10.1093/rheumatology/kew205

Kadetoff, D., Lampa, J., Westman, M., Andersson, M., and Kosek, E. (2012). Evidence of central inflammation in fibromyalgia-increased cerebrospinal fluid interleukin-8 levels. *J. Neuroimmunol.* 242, 33–38. doi: 10.1016/j.jneuroim.2011.10.013

Kalinowsky, L. B. (1986). History of convulsive therapy. *Ann. N. Y. Acad. Sci.* 462, 1–4. doi: 10.1111/j.1749-6632.1986.tb51233.x

Khedr, E. M., Omran, E., Ismail, N. M., El-Hammady, D. H., Goma, S. H., Kotb, H., et al. (2017). Effects of transcranial direct current stimulation on pain, mood and serum endorphin level in the treatment of fibromyalgia: a double blinded, randomized clinical trial. *Brain Stimul.* 10, 893–901. doi: 10.1016/j.brs.2017.06.006

King, B. H., and Liston, E. H. (1990). Proposals for the mechanism of action of convulsive therapy: a synthesis. *Biol. Psychiatry* 27, 76–94. doi: 10.1016/0006-3223(90)90022-T

Lee, S. A., Oh, B. M., Kim, S. J., and Paik, N. J. (2014). The molecular evidence of neural plasticity induced by cerebellar repetitive transcranial magnetic stimulation in the rat brain: a preliminary report. *Neurosci. Lett.* 575, 47–52. doi: 10.1016/j.neulet.2014.05.029

Lefaucheur, J. P., Antal, A., Ayache, S. S., Benninger, D. H., Brunelin, J., Cogiamanian, F., et al. (2017). Evidence-based guidelines on the therapeutic use of transcranial direct current stimulation (tDCS). *Clin. Neurophysiol.* 128, 56–92. doi: 10.1016/j.clinph.2016.10.087

Liu, X., Qiu, F., Hou, L., and Wang, X. (2021). Review of noninvasive or minimally invasive deep brain stimulation. *Front. Behav. Neurosci.* 15:820017. doi: 10.3389/fnbeh.2021.820017

Mariano, T. Y., Mascha, V. T. W., Garnaat, S. L., Rasmussen, S. A., and Greenberg, B. D. (2015). Transcranial direct current stimulation (tDCS) targeting left dorsolateral prefrontal cortex modulates task-induced acute pain in healthy volunteers. *Pain Med.* 17, 737–745. doi: 10.1093/pm/pnv042

Marsh, L., Lauriello, J., Sullivan, E. V., and Pfefferbaum, A. (1996). Neuroimaging in psychiatric disorders. In: *Neuroimaging II*, Ed. ED Bigler. New York: Plenum Press. 73–125. doi: 10.1007/978-1-4899-1769-0_4

Mccance, S., Hawton, K., Brighouse, D., and Glynn, C. (1996). Does electroconvulsive therapy (ECT) have any role in the management of intractable thalamic pain? *Pain* 68, 129–131. doi: 10.1016/S0304-3959(96)03169-7

Mease, P. J., Farmer, M. V., Palmer, R. H., Gendreau, R. M., Trugman, J. M., and Wang, Y. (2013). Milnacipran combined with pregabalin in fibromyalgia: a randomized, open-label study evaluating the safety and efficacy of adding milnacipran in patients with incomplete response to pregabalin. *Ther. Adv. Musculoskelet Dis.* 5, 113–126. doi: 10.1177/1759720X13483894

Mhalla, A., De Andrade, D. C., Baudic, S., Perrot, S., and Bouhassira, D. (2010). Alteration of cortical excitability in patients with fibromyalgia. *Pain* 149, 495–500. doi: 10.1016/j.pain.2010.03.009

Michaelides, A., and Zis, P. (2019). Depression, anxiety and acute pain: links and management challenges. *Postgrad. Med.* 131, 438–444. doi: 10.1080/00325481.2019.1663705

Moisset, X., and Lefaucheur, J. P. (2019). Non pharmacological treatment for neuropathic pain: invasive and non-invasive cortical stimulation. *Rev. Neurol. (Paris)* 175, 51–58. doi: 10.1016/j.neurol.2018.09.014

Moldofsky, H., Lue, F. A., Mously, C., Roth-Schechter, B., and Reynolds, W. J. (1996). The effect of zolpidem in patients with fibromyalgia: a dose ranging, double blind, placebo controlled, modified crossover study. *J. Rheumatol.* 23, 529–533.

Neumann, L., and Dan, B. (2003). Epidemiology of fibromyalgia. *Curr. Pain Headache Rep.* 7, 362–368. doi: 10.1007/s11916-003-0035-z

Newman, M. E., Gur, E., Shapira, B., and Lerer, B. (1998). Neurochemical mechanisms of action of ECS: evidence from in vivo studies. *J. ECT* 14, 153–171. doi: 10.1097/00124509-199809000-00002

O'brien, T. A., Bertolucci, F., Torrealba-Acosta, G., Huerta, R., Fregni, F., and Thibaut, A. (2018). Non-invasive brain stimulation for fine motor improvement after stroke: a meta-analysis. *Eur. J. Neurol.* 25, 1017–1026. doi: 10.1111/ene.13643

O'connell, N. E., Marston, L., Spencer, S., Desouza, L. H., and Wand, B. M. (2018). Non-invasive brain stimulation techniques for chronic pain. *Cochrane Database Syst. Rev.* 4:Cd008208. doi: 10.1002/14651858.CD008208.pub4

Okabe, T., Sato, C., Matsumoto, K., Ozawa, H., and Sakamoto, A. (2010). Electroconvulsive stimulation (ECS) increases the expression of neuropeptide Y (NPY) in rat brains in a model of neuropathic pain: a quantitative real-time polymerase chain reaction (RT-PCR) study. *Pain Med.* 10, 1460–1467. doi: 10.1111/j.1526-4637.2009.00678.x

Okamoto, T., Yoshimura, R., Ikenouchi-Sugita, A., Hori, H., Umene-Nakano, W., Inoue, Y., et al. (2008). Efficacy of electroconvulsive therapy is associated with changing blood levels of homovanillic acid and brain-derived neurotrophic factor (BDNF) in refractory depressed patients: a pilot study. *Prog. Neuro-Psychopharmacol. Biol. Psychiatry* 32, 1185–1190. doi: 10.1016/j.pnpbp.2008.02.009

Perrot, S., and Russell, I. J. (2014). More ubiquitous effects from non-pharmacologic than from pharmacologic treatments for fibromyalgia syndrome: a meta-analysis examining six core symptoms. *Eur. J Pain* 18, 1067–1080. doi: 10.1002/ejp.564

Peterchev, A. V., Rosa, M. A., Deng, Z. D., Prudic, J., and Lisanby, S. H. (2010). Electroconvulsive therapy stimulus parameters: rethinking dosage. *J. ECT* 26, 159–174. doi: 10.1097/YCT.0b013e3181e48165

Peyron, R., Laurent, B., and García-Larrea, L. (2000). Functional imaging of brain responses to pain. A review and meta-analysis. *Neurophysiol. Clin.* 30, 263–288. doi: 10.1016/S0987-7053(00)00227-6

Piccinni, A., Debbio, A. D., Medda, P., Bianchi, C., Roncaglia, I., Veltri, A., et al. (2009). Plasma brain-derived neurotrophic factor in treatment-resistant depressed patients receiving electroconvulsive therapy. *Eur. Neuropsychopharmacol.* 19, 349–355. doi: 10.1016/j.euroneuro.2009.01.002

Rainville, P. (2002). Brain mechanisms of pain affect and pain modulation. *Curr. Opin. Neurobiol.* 12, 195–204. doi: 10.1016/S0959-4388(02)00313-6

Rasmussen, K. G., and Rummans, T. A. (2002). Electroconvulsive therapy in the management of chronic pain. *Curr. Pain Headache Rep.* 6, 17–22. doi: 10.1007/s11916-002-0019-4

Rathore, F. A., and Afridi, A. (2020). Is combination pharmacotherapy effective for management of fibromyalgia in adults? A Cochrane review summary with commentary. *J. Musculoskelet. Neuronal Interact.* 20, 297–300.

Robinson, R. L., Birnbaum, H. G., Morley, M. A., Sisitsky, T., Greenberg, P. E., and Wolfe, F. (2004). Depression and fibromyalgia: treatment and cost when diagnosed separately or concurrently. *J. Rheumatol.* 31, 1621–1629.

Roizenblatt, S., Fregni, F., Gimenez, R., Wetzel, T., Rigonatti, S. P., Tufik, S., et al. (2007). Site-specific effects of transcranial direct current stimulation on sleep and pain in fibromyalgia: a randomized, sham-controlled study. *Pain Pract.* 7, 297–306. doi: 10.1111/j.1533-2500.2007.00152.x

Rosen, A. C., Ramkumar, M., Nguyen, T., and Hoeft, F. (2009). Noninvasive transcranial brain stimulation and pain. *Curr. Pain Headache Rep.* 13, 12–17. doi: 10.1007/s11916-009-0004-2

Saavedra, L. C., Gebodh, N., Bikson, M., Diaz-Cruz, C., and Fregni, F. (2015). Clinically effective treatment of fibromyalgia pain with high-definition transcranial direct current stimulation: phase ii open-label dose optimization. *J Pain* 17:14. doi: 10.1016/j.jpain.2015.09.009

Sabel, B. A., Thut, G., Haueisen, J., Henrich-Noack, P., Herrmann, C. S., Hunold, A., et al. (2020). Vision modulation, plasticity and restoration using non-invasive brain stimulation – an IFCN-sponsored review. *Clin. Neurophysiol.* 131, 887–911. doi: 10.1016/j.clinph.2020.01.008

Salmon, J. B., Hanna, M. H., Williams, M., Toone, B., and Wheeler, M. (1988). Thalamic pain--the effect of electroconvulsive therapy (ECT). *Pain* 33, 67–71. doi: 10.1016/0304-3959(88)90205-9

Sampson, S. M., Rome, J. D., and Rummans, T. A. (2006). Slow-frequency RTMS reduces fibromyalgia pain. *Pain Med.* 7, 115–118. doi: 10.1111/j.1526-4637.2006.00106.x

Sarzi-Puttini, P., Giorgi, V., Marotto, D., and Atzeni, F. (2020). Fibromyalgia: an update on clinical characteristics, aetiopathogenesis and treatment. *Nat. Rev. Rheumatol.* 16, 645–660. doi: 10.1038/s41584-020-00506-w

Steffen, N., Josephine, B., Nina, T., Christoph, K., and Diener, H.-C. (2018). Polarity-specific modulation of pain processing by transcranial direct current stimulation – a blinded longitudinal FMRI study. *J. Headache Pain* 19:99. doi: 10.1186/s10194-018-0924-5

Su, Y.-C., Guo, Y.-H., Hsieh, P.-C., and Lin, Y.-C. (2021). Efficacy of repetitive transcranial magnetic stimulation in fibromyalgia: a systematic review and meta-analysis of randomized controlled trials. *J. Clin. Med.* 10:4669. doi: 10.3390/jcm10204669

Szymoniuk, M., Chin, J. H., Domagalski, Ł., Biszewski, M., JóŹwik, K., and Kamieniak, P. (2023). Brain stimulation for chronic pain management: a narrative review of analgesic mechanisms and clinical evidence. *Neurosurg. Rev.* 46:127. doi: 10.1007/s10143-023-02032-1

Tamura, Y., Okabe, S., Ohnishi, T., D, N. S., Arai, N., Mochio, S., et al. (2004). Effects of 1-Hz repetitive transcranial magnetic stimulation on acute pain induced by capsaicin. *Pain* 107, 107–115. doi: 10.1016/j.pain.2003.10.011

Thompson, T., Correll, C. U., Gallop, K., Vancampfort, D., and Stubbs, B. (2016). Is pain perception altered in people with depression? A systematic review and Meta-analysis of experimental pain research. *J. Pain* 17, 1257–1272. doi: 10.1016/j.jpain.2016.08.007

Usui, C., Doi, N., Nishioka, M., Komatsu, H., Yamamoto, R., Ohkubo, T., et al. (2006). Electroconvulsive therapy improves severe pain associated with fibromyalgia. *Pain* 121, 276–280. doi: 10.1016/j.pain.2005.12.025

Valle, A., Roizenblatt, S., Botte, S., Zaghi, S., Riberto, M., Tufik, S., et al. (2009). Efficacy of anodal transcranial direct current stimulation (TDCS) for the treatment of fibromyalgia: results of a randomized, sham-controlled longitudinal clinical trial. *J Pain Manag* 2, 353–361.

Van Der Groen, O., Potok, W., Wenderoth, N., Edwards, G., Mattingley, J. B., and Edwards, D. (2022). Using noise for the better: the effects of transcranial random noise stimulation on the brain and behavior. *Neurosci. Biobehav. Rev.* 138:104702. doi: 10.1016/j.neubiorev.2022.104702

Walitt, B., Klose, P., Üçeyler, N., Phillips, T., and Häuser, W. (2016). Antipsychotics for fibromyalgia in adults. *Cochrane Database Syst. Rev.* 6:Cd011804. doi: 10.1002/14651858.CD011804.pub2

Wasan, A. D., Artin, K., and Clark, M. R. (2004). A case-matching study of the analgesic properties of electroconvulsive therapy. *Pain Med.* 5, 50–58. doi: 10.1111/j.1526-4637.2004.04006.x

Weir, P. T., Harlan, G. A., Nkoy, F. L., Jones, S. S., Hegmann, K. T., Gren, L. H., et al. (2006). The incidence of fibromyalgia and its associated comorbidities: a population-based retrospective cohort study based on international classification of diseases, 9th revision codes. *J. Clin. Rheumatol.* 12, 124–128. doi: 10.1097/01.rhu.0000221817.46231.18

Wischnewski, M., Alekseichuk, I., and Opitz, A. (2023). Neurocognitive, physiological, and biophysical effects of transcranial alternating current stimulation. *Trends Cogn. Sci.* 27, 189–205. doi: 10.1016/j.tics.2022.11.013

Wu, L., Liu, T., and Wang, J. (2021). Improving the effect of transcranial alternating current stimulation (TACS): a systematic review. *Front. Hum. Neurosci.* 15:652393. doi: 10.3389/fnhum.2021.652393

Yao, J., Li, X., Zhang, W., Lin, X., Lyu, X., Lou, W., et al. (2021). Analgesia induced by anodal TDCS and high-frequency TRNS over the motor cortex: immediate and sustained effects on pain perception. *Brain Stimul.* 14, 1174–1183. doi: 10.1016/j.brs.2021.07.011

frontiers | Frontiers in Neuroscience

TYPE Original Research
PUBLISHED 10 November 2023
DOI 10.3389/fnins.2023.1282322

OPEN ACCESS

EDITED BY
Mark H. Myers,
University of Tennessee Health Science Center (UTHSC), United States

REVIEWED BY
Detlef H. Heck,
University of Minnesota Duluth, United States
Anders Rasmussen,
Lund University, Sweden

*CORRESPONDENCE
Mesut Sahin
✉ sahin@njit.edu

RECEIVED 24 August 2023
ACCEPTED 30 October 2023
PUBLISHED 10 November 2023

CITATION
Kang Q, Lang EJ and Sahin M (2023) Transsynaptic entrainment of cerebellar nuclear cells by alternating currents in a frequency dependent manner.
Front. Neurosci. 17:1282322.
doi: 10.3389/fnins.2023.1282322

Transsynaptic entrainment of cerebellar nuclear cells by alternating currents in a frequency dependent manner

Qi Kang[1], Eric J. Lang[2] and Mesut Sahin[1]*

[1]Biomedical Engineering Department, New Jersey Institute of Technology, Newark, NJ, United States, [2]Department of Neuroscience and Physiology, Neuroscience Institute, New York University Grossman School of Medicine, New York City, NY, United States

Transcranial alternating current stimulation (tACS) is a non-invasive neuromodulation technique that is being tested clinically for treatment of a variety of neural disorders. Animal studies investigating the underlying mechanisms of tACS are scarce, and nearly absent in the cerebellum. In the present study, we applied 10–400 Hz alternating currents (AC) to the cerebellar cortex in ketamine/xylazine anesthetized rats. The spiking activity of cerebellar nuclear (CN) cells was transsynaptically entrained to the frequency of AC stimulation in an intensity and frequency-dependent manner. Interestingly, there was a tuning curve for modulation where the frequencies in the midrange (100 and 150 Hz) were more effective, although the stimulation frequency for maximum modulation differed for each CN cell with slight dependence on the stimulation amplitude. CN spikes were entrained with latencies of a few milliseconds with respect to the AC stimulation cycle. These short latencies and that the transsynaptic modulation of the CN cells can occur at such high frequencies strongly suggests that PC simple spike synchrony at millisecond time scales is the underlying mechanism for CN cell entrainment. These results show that subthreshold AC stimulation can induce such PC spike synchrony without resorting to supra-threshold pulse stimulation for precise timing. Transsynaptic entrainment of deep CN cells via cortical stimulation could help keep stimulation currents within safety limits in tACS applications, allowing development of tACS as an alternative treatment to deep cerebellar stimulation. Our results also provide a possible explanation for human trials of cerebellar stimulation where the functional impacts of tACS were frequency dependent.

KEYWORDS

transcranial AC stimulation (tACS), tDCS, tES, cerebellum, Purkinje cell synchrony, neuromodulation

1. Introduction

In transcranial electric stimulation (tES), electric fields that are induced in the cortex are several times higher than those in deep structures of the brain, as shown with direct measurements in humans (Guidetti et al., 2022) and animals (Asan et al., 2018). This loss of field strength with depth stands as an impediment for directly targeting deep brain structures in all types of transcranial electric stimulation paradigms, regardless of their temporal pattern (continuous, pulsed, sinusoidal or interleaved). Thus, cortical areas near the skull surface will

always be advantageous to target for tES in order to keep the current levels low and thereby minimize spreading of the stimulus to adjacent areas that may confound the functional benefits. Cerebellar neuroanatomy presents a unique case where the output of the lateral cerebellar cortex projects to the CN, which then project to areas throughout much of the cerebral cortex via the thalamus. Thus, modulation of cerebellar output should be able to affect areas throughout the forebrain. A technique that can modulate the CN indirectly by entrainment of the cells in the cerebellar cortex would provide a powerful tool that can be utilized to treat a plethora of neurological disorders in which the cerebellum is involved. Indeed, it has been suggested that activation of cerebellar efferent pathways may be a more effective method for inducing plasticity in the forebrain regions than direct stimulation of them (Brunoni et al., 2011; Ferrucci et al., 2012; Bostan and Strick, 2018; Milardi et al., 2019).

The cerebellum has traditionally been thought of as critical for motor coordination. The anatomical, clinical and imaging evidence now indicate that the cerebellum also has central roles in cognition and emotion (Middleton and Strick, 2000; Stoodley and Schmahmann, 2009; Strick et al., 2009; Grimaldi and Manto, 2012), and that cerebellar dysfunction impacts these functions. For example, patients with cerebellar damage often suffer from comorbid cognitive impairments, including impaired timing, attention, memory, and language (Schmahmann, 1998; Gottwald et al., 2004). These symptoms are sometimes termed 'dysmetria of thought' (Schmahmann, 1998; Schmahmann, 2004), in contrast to the 'dysmetria of movement' classically associated with cerebellar dysfunction, and are clinically referred to as cerebellar cognitive affective syndrome (CCAS) (Pope, 2015). Consistent with these findings of cerebellar involvement in both motor and non-motor functions, projections from the CN target, via the thalamus, both motor and non-motor areas in the basal ganglia (Bostan et al., 2010, 2018; Bostan and Strick, 2010, 2018) and cortex (Bostan et al., 2018; Milardi et al., 2019). Concurrent with increased recognition of the cerebellum's clinical importance, use of cerebellar transcranial electrical stimulation (ctES) has surged, mostly using direct currents (Ferrucci et al., 2008, 2012; Brunoni et al., 2011; Galea et al., 2011; Grimaldi et al., 2014, 2016; Hardwick & Celnik, 2014; Herzfeld et al., 2014; Priori et al., 2014). These studies show that ctES can improve motor learning, and cognitive (Ferrucci et al., 2008) and emotional processes (Ferrucci et al., 2012) in normal (Galea et al., 2011; Ferrucci et al., 2012; Hardwick and Celnik, 2014; Herzfeld et al., 2014) and brain injured individuals (for review, see Grimaldi et al., 2014, 2016; Priori et al., 2014).

Although tACS has been used in other brain areas for some time, the majority of transcranial stimulation studies in cerebellum thus far have used direct currents (DC) to perturb cerebellar networks. However, cerebellar transcranial alternating current stimulation (ctACS) has lately been garnering interest. The earliest ctACS application was an attempt less than a decade ago to demonstrate that tremor frequencies could be entrained in healthy subjects (Mehta et al., 2014). More recently, the effects of different AC frequencies (10, 50, and 300 Hz) was investigated on the excitability of the contralateral motor cortex using cerebellum-brain inhibition (CBI) (Naro et al., 2016, 2017). CBI is mediated by Purkinje cell (PC) projections from the cerebellar cortex that are inhibitory to the CN cells, many of which, in turn, provide excitatory projections to the motor cortex via the thalamus. Five minutes of 50 Hz ctACS as a conditioning stimulus caused weakening of CBI, quantified by short-lasting elevations in the excitability of the contralateral M1. Interestingly, the 300 Hz stimulation had the opposite effect on CBI and the 10 Hz ctACS was ineffective, suggesting a frequency dependency of ctACS.

Animal studies investigating the underlying mechanisms of ctACS, and ctES in general, are scarce. Electric fields required to modulate Purkinje cell spiking activity was studied in an *in vitro* turtle cerebellum preparation (Chan and Nicholson, 1986). In 2020, Asan et al. reported the first *in vivo* study that demonstrated entrainment of the PC simple spikes (SS) in the rat cerebellar cortex by AC stimulation in an amplitude, frequency, and direction dependent manner (Asan et al., 2020). Phase-locking of SS to AC cycle became stronger as the frequency was increased from 2 Hz to 40 Hz. Further increasing the stimulation frequency to 100 Hz, beyond the spontaneous frequency of the cells, led to spikes skipping the AC cycles while maintaining the phase locking.

The principle mechanism that we aim to leverage here is PC-SS synchrony. Several dozens of PCs converge on each CN cell with inhibitory (GABAergic) connections (Wu and Raman, 2017). Transient synchrony among the SS of those projecting PCs have been shown as a potential mechanism for modulation of the CN cells (Person and Raman, 2011, 2012). Thus, entrainment of a group of PC-SSs around the stimulation electrode by the same AC waveform should lead to synchrony and thereby modulation of the CN cell spikes at the stimulation frequency. The results suggest that CN cell modulation via stimulation of the cerebellar cortex is feasible in an intensity and frequency dependent manner, and that the most effective range of AC frequencies varies between CN cells.

2. Methods

2.1. Animal surgery

Experiments were performed in accordance with the National Institute of Health *Guide for the Care and Use of Laboratory Animals*. All procedures were approved and performed in accordance to the guidelines of the Institutional Animal Care and Use Committee, Rutgers University, Newark, NJ. Eleven Sprague Dawley rats (200–350 g, male, Charles River) were used in this study. Animals were first anesthetized with 5% isoflurane in an induction chamber, and then moved to a stereotaxic frame. The animal was switched to ketamine/xylazine mixture (80 mg/kg and 8 mg/kg, IP) during the course of surgery and data collection. Additional doses of ketamine (15 mg/kg, IP) were injected as needed such that the pedal reflexes were absent. Body temperature was measured with a rectal probe and regulated with a heating pad under the animal (ATC 1000, WPI, Sarasota, FL). Blood oxygen level was monitored with a pulse oximeter attached to the hind paw. The hair over the head was shaved and a midline skin incision was made to expose the skull over the cerebellum. A craniotomy hole was opened for insertion of the CN recording electrode at AP = −11.5 mm on the midline and extended laterally to the right side for 2 mm. For stimulation of the cerebellar cortex, the skull over the right side of the posterior cerebellum and the vermis was opened with rongeurs and the dura was kept intact and moist with normal saline.

2.2. Stimulation of cerebellar cortex with AC

Stimulus waveforms were generated in Matlab (Mathworks, MA), sent out through a data acquisition card (PCI-6071, National Instruments, Austin, TX), and passed through a V/I converter (Linear Current Isolator, Caputron, Hillsborough, NJ) before being applied to the cerebellar surface via a stimulus electrode (Figure 1). The stimulus electrode consisted of a silver wire (0.5 mm diameter) whose tip was sanded (220 grit paper), to obtain a flat circular footprint, and coated with AgCl, by immersing it in 1.84% sodium hypochlorite solution overnight. The circular tip was pressed against the dura to deliver the AC stimulation at different points across the cerebellar cortex. A disposable electromyogram electrode was attached to the tail as the return electrode for the stimulus current. The 1 kHz AC impedance between the two electrodes was typically around 12 kΩ. Any fluids accumulating around the stimulus electrode were removed as needed using Q-tip cotton applicators to minimize the spread of current laterally over the dura.

2.3. Electrophysiological data collection

A glass micropipette (3–4 MΩ) filled with normal saline was inserted through the cranial hole on top at a lateral angle of 20° with the vertical axis and a rostrocaudal position of −2.5 mm from the interaural line to target the interpositus nucleus (IPN). The estimated mediolateral positions and the depths of the recorded cell positions are shown in Figure 2, based on the stereotaxic coordinates. Signals were filtered at 300 Hz–5 kHz and amplified (Model 2200, A-M Systems, Carlsborg, WA) by a gain of 1,000 or 10,000, sampled at 100 kHz onto the computer via a data acquisition board (PCI-6071), and analyzed during the experiment. Neural signals were monitored simultaneously on an oscilloscope and an audio speaker. Each trial consisted of a 10 s long baseline recording followed by a 20 s long stimulation at frequencies ranging from 10 Hz to 400 Hz to investigate entrainment of the CN activity through cortex stimulation. The stimulus current amplitudes were varied from 10 μA to 60 μA in steps of 10 μA. All current amplitudes are given as the peak of the sinusoidal waveform. Before collecting AC data, an anodic- or cathodic-first biphasic and charge-balanced current pulse (20 Hz, 200–300 μA, duration 200 μs, 2 ms gap between phases to minimize the hyperpolarizing effect of the first pulse) was applied through the stimulation electrode on the cerebellar cortex with respect to another similar electrode at ~1 mm lateral distance (bipolar stimulation) to ensure that the PCs underneath the stimulation electrode were projecting to the CN cell that was recorded. The paravermal area in crus II (~2 mm from the paravermal vein, Figure 1) was found to produce the strongest CN inhibition with current pulses and the lowest thresholds for CN modulation with AC. The connectivity was confirmed for each of the 20 cells from 10 animals (1 cell in each of 3 rats, 2 cells in each of 7 rats, and 3 cells in 1 rat) with a spike-triggered histogram that showed a period of silence or significantly decreased activity following the stimulus pulse (Figure 3). In 13 out of 20 cells, the AC stimulation was also superimposed on a positive or negative DC current with different amplitudes to observe the combined effect (AC + DC) on the CN spike entrainment as well as the mean firing rates.

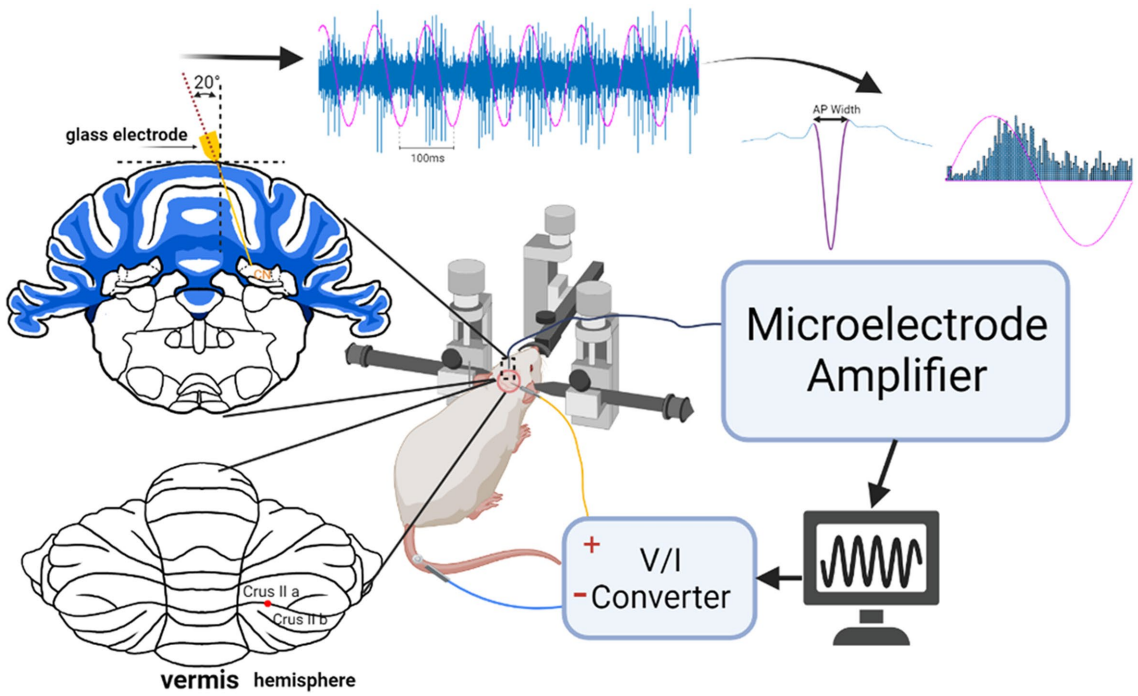

FIGURE 1
Experimental setup for stimulation of the cerebellar cortex and recording CN activity. The coronal section on top left shows the penetration angle of the recording microelectrode through a craniotomy on the dorsal side. The posterior view of the cerebellum depicts where the cortex was stimulated at the border of crus IIa and IIb about 2 mm from the paravermal vein with a circular Ag/AgCl electrode (flat end of a wire). The raw signal is an example of CN spike entrainment and the associated histogram. AC waveform (magenta) is superimposed to show the stimulation phase.

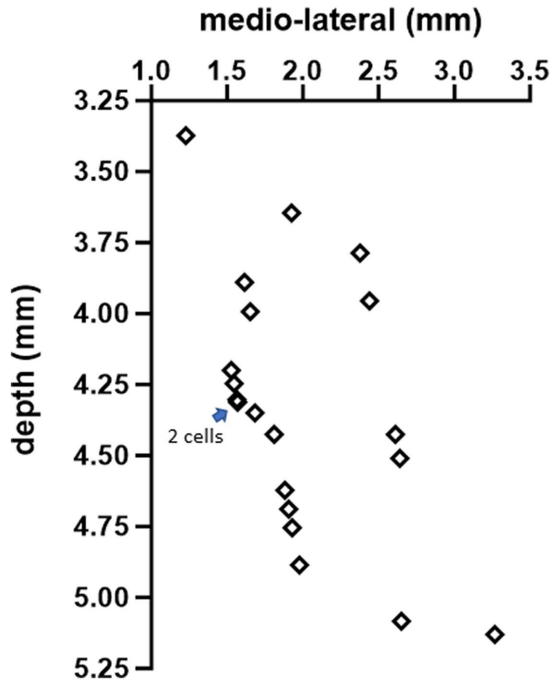

FIGURE 2
The estimated positions of all 20 cells, based on stereotaxic coordinates, in the coronal plane at AP = −2.5 mm from the interaural line.

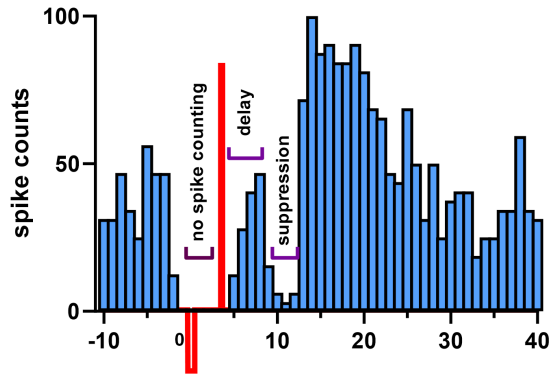

FIGURE 3
Demonstration of synaptic connectivity from the stimulated cortical area to a CN cell. Stimulus triggered histogram of CN spikes shows inhibition. One hundred biphasic current pulses (200μs anodic pulse, preceded by a 2ms gap and a 800μs cathodic phase for charge balancing) were applied through the same cortical electrode used for AC modulation. The CN spikes are suppressed for a few ms after a delay that can account for the propagation time from the cortex to CN. In most cases, the anodic simulation was more effective than the cathodic one to produce such inhibition. Notice that the spike count increases above the baseline after the inhibition period. Spikes were not counted during the biphasic stimulus waveform due to artifact.

2.4. Spike analysis

All data processing was performed in Matlab. Raw signals were band-pass filtered (300–5,000 Hz or 500–5,000 Hz depending on the stimulus frequency) and the negative spikes were detected by thresholding. Then, scatter plots were produced using the first two principal components of the detected action potential waveforms within a 1.5 ms window around its negative peak. The user, then, manually selected a cluster of spikes that putatively belonged to a single cell. Time points of the selected spikes were plotted with respect to the AC stimulus phase as a histogram. The phase lock value (PLV) was defined (Krause et al., 2019) as PLV = abs(mean($e^{i\theta}$)), where the θ are the phase angles of individual spikes with respect to the AC cycle, and used as an index of CN modulation or entrainment. The time lag of the spike entrainment was found from the angle of the PLV vector. The modulation levels that are detectable by PLV depend on the duration of the signal (Mc Laughlin et al., 2022). In order to determine the smallest PLV level that can detect modulation above the chance level for the length of the episodes we have, the PLVs were computed from all the baseline recordings available in a cell (~120 10-s epochs were combined in pairs to make ~60 20-s epochs matched in duration to the stimulation episodes). Then, the PLV threshold corresponding to the probability of 5% error of false positive was calculated from the distribution for each cell. The average of all threshold PLVs from 20 cells was 0.057 (min = 0.042 and max = 0.088). Based on this analysis, we considered any PLV above 0.088 as detectable modulation and used 0.15 in some cases as a more conservative value.

The interspike intervals (ISIs) were computed for the baseline and stimulation periods and they were compared using Kolmogorov–Smirnov (KS) tests for the probability distributions, and two-tailed paired-*t* tests for the means. After-effects of the stimulus were not analyzed in this study because the short stimulus durations that were used were not expected to produce any plastic effects.

3. Results

3.1. Measurement of cerebellar volume conductance

Electrical stimulation applied to the cerebellar cortex can have both direct effects on the CN cells and transsynaptic effects through PC modulation. In order to show that the electric fields (e-fields) directly induced on the CN cells are relatively much smaller than the e-fields induced on the PCs of the cortex, we employed both direct measurements of the e-fields in the cerebellum and the analytical method of estimation. The conductivity of the cerebellum as a volume conductor needs to be known to solve the analytical equations of the e-field. To this end, a train of current pulses was applied to the stimulating electrode while the electrode back voltage was recorded. The impedance of the electrode-tissue interface was excluded from the measurements by identifying the capacitive charging component of the waveform and taking only the initial sharp edge of the voltage transition into account. Then, using the voltage equation at the surface ($V=I/4\sigma a$, where I is current and $a = 0.5$ mm is the electrode radius) derived for a disk electrode on the surface of a semi-infinite medium (Wiley and Webster, 1982), the lumpsum equivalent conductivity (σ) for the cerebellum as a volume conductor was found to be 0.42 S/m.

3.2. Predicted and measured electric fields in the cerebellum

The voltage distribution inside a semi-infinite volume conductor for a disk electrode was analytically solved by Wiley and Webster

(1982). One can find the electric field by differentiating their voltage equation given in polar coordinates. The vertical e-field ($E = I / [2\pi\sigma(a^2 + z^2)]$), found by differentiating the Wiley's equation in the z direction, was estimated to be around 150 mV/mm at the PC layer (depth of ~$z = 300$ µm including dura) for a 60 µA current, electrode diameter of a = 0.5 mm, and our measured conductivity of 0.42 S/m. This equation predicts that the e-field strength is reduced to 1.12 mV/mm (by a factor of ~123 from the PC layer) at a depth corresponding to about the middle of CN ($z = 4.5$ mm) assuming a homogenous and isotropic medium.

We also measured the e-fields experimentally in the CN using 10 Hz, 100 Hz, and 1 kHz sinusoidal currents as well as rectangular pulses (Asan et al., 2018). A recording electrode (1.5 MΩ glass micropipette) was advanced in steps of 200 µm into the CN from an insertion point next to the simulating electrode that was located ~2–3 mm lateral from the midline and near the crus IIa - crus IIb border, which we found as the most effective region on the cortex for CN modulation. The measured e-field at a depth of 4.5 mm was 1.74 mV/mm, 1.5 mV/mm, and 1.44 mV/mm with the three sinusoidal currents respectively, and 1.5 mV/mm with the rectangular pulses for the largest (60 µA) stimulation current used. These e-fields in the CN were in the same ballpark with the value predicted by the theoretical calculations (1.12 mV/mm) above. It should be mentioned, however, that the decline in the e-field by depth may not be so steep depending on where in the cerebellum the measurements are made with respect to the walls of folia (Avlar et al., 2023), in part because of higher conductivities along the axon tracts (anisotropy).

3.3. Verifying PC-CN connectivity by cortical stimulation

In order to verify that we stimulated a cortical area that projected to the CN cell being recorded, we applied brief shocks with a bipolar electrode to that area and looked for responses whose sign and latency indicated a direct synaptic connection. In Figure 3, the mean delay from the stimulus pulse to the start of inhibition was 2.31 ± 0.92 ms (13 cells). In the remaining 7 cells, the start of the inhibition was not possible to determine due to stimulus artifact, however, the end of inhibition period was clearly visible. The average duration of inhibition was 2.56 ± 2.03 ms (range 0.4 ms to 9.0 ms, 13 cells). IPSC decay times vary dramatically from ~2 ms for the large CN cells to ~25 ms for some of the small nucleo-olivary CN cells in mice (Najac and Raman, 2015). Thus, the brevity of the inhibition we observed strongly suggests that CN cells of this study mostly belong to the class of large non-GABAergic CN cells, which include the cells that project to the thalamus.

3.4. Spike histograms were mostly monomodal

The responses of CN neurons to AC stimulation were visualized by plotting histograms triggered off of the start of the AC cycle. Most of the histograms had a mono-modal distribution as in Figure 4A, but in very few cases the distribution was bimodal (Figure 4B, right panel). The PLV statistic was used to quantify the modulation apparent in the histograms. A PLV value of zero indicates that spikes distributed uniformly across the stimulus cycle, and PLV produces a maximum value of 1 when the entrainment is perfect, i.e., all spikes occur with the same exact phase lag in the cycle. It produced a maximum value of π/4 in our simulations if the spike histogram had the appearance of the positive half cycle of a sinusoidal, similar to the one in Figure 4A. However, PLV yields a small value for symmetrical distributions even if the modulation is substantial, such as the one that resembles a rectified sinusoidal waveform as in Figure 4B, because of spikes canceling each other's contributions to the mean that are 180° apart around the unit circle. The bimodal cases were fewer in number and did not affect the overall conclusions (13% of all trials). The elevated spike probability in negative AC cycle of these bimodal histograms were possibly produced by the projecting PCs that were located on the periphery of the stimulated cortical area and their

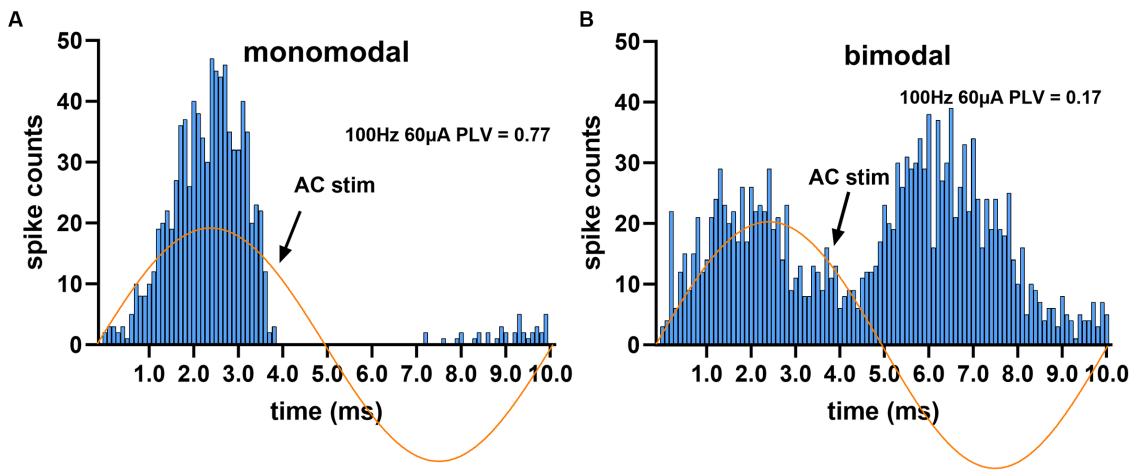

FIGURE 4
Spike timing histograms from two different cells, triggered off of the AC cycle. AC stimulus amplitude was set to the highest (60 µA at 100 Hz) to maximize entrainment. **(A)** Monomodal distribution with a single peak and a complete suppression during most of the negative cycle. **(B)** The second peak during the negative cycle gives the appearance of a bimodal distribution.

somatodendritic axis was oriented in the electrical field in the opposite direction.

3.5. CN spike activity modulates with a short latency with respect to AC peak

Histograms triggered off the start of the AC cycle showed entrainment of the CN activity at the AC frequency (Figure 5). At 50 Hz, the histogram shows a peak that lags the peak of the sine wave by approximately 1/8 of a cycle (2–3 ms) and that is followed by a suppression of activity during the negative half of the AC cycle. As the stimulus frequency is increased from 100 Hz to 250 Hz, CN activity shows an increasing phase lag, until at 250 Hz the lag is so great that the CN activity appears to lead the AC cycle and at 300 Hz has an essentially in-phase relationship albeit with a much weaker modulation amplitude. At the other end of the frequency range (10 Hz), the histograms had such wider distributions that made it difficult to find a clear peak for delay measurements.

Considering this frequency dependence, time lags were measured using the data at 100 Hz stimulation where entrainment was strongest and the cycle length was long enough to find the histogram peak in the same AC cycle. The average and median time lags were 4.3 ± 2.7 ms and 5.4 ms (31 trials, 14 cells), respectively. Overall, the modulation lags measured from the histograms suggest that the CN cells generated a spike with short latencies following the AC waveform peak. Furthermore, the short delays in CN inhibition following pulse stimulation of the cortex (see "PC-CN Connectivity" above) are in agreement with having such short lags in the modulation histograms.

3.6. No change in mean firing frequency

In most cases, the envelope of the ISI distribution of a cell did not change substantially but assumed a multi-peak appearance during stimulation (Figure 6). Particularly in cases with strong modulation, the ISI histograms had a clear peak corresponding to the AC stimulus cycle, but also at multiples of it, showing entrainment of the spikes at subharmonic frequencies (Figure 6B). This multi-peak histogram pattern is an indication that the consecutive spikes are skipping one or more AC cycles when the stimulation frequency is higher than the spontaneous firing frequency of the cell. This raises the question of whether the average firing frequency of the cell is modified by the stimulation relative to its baseline rate.

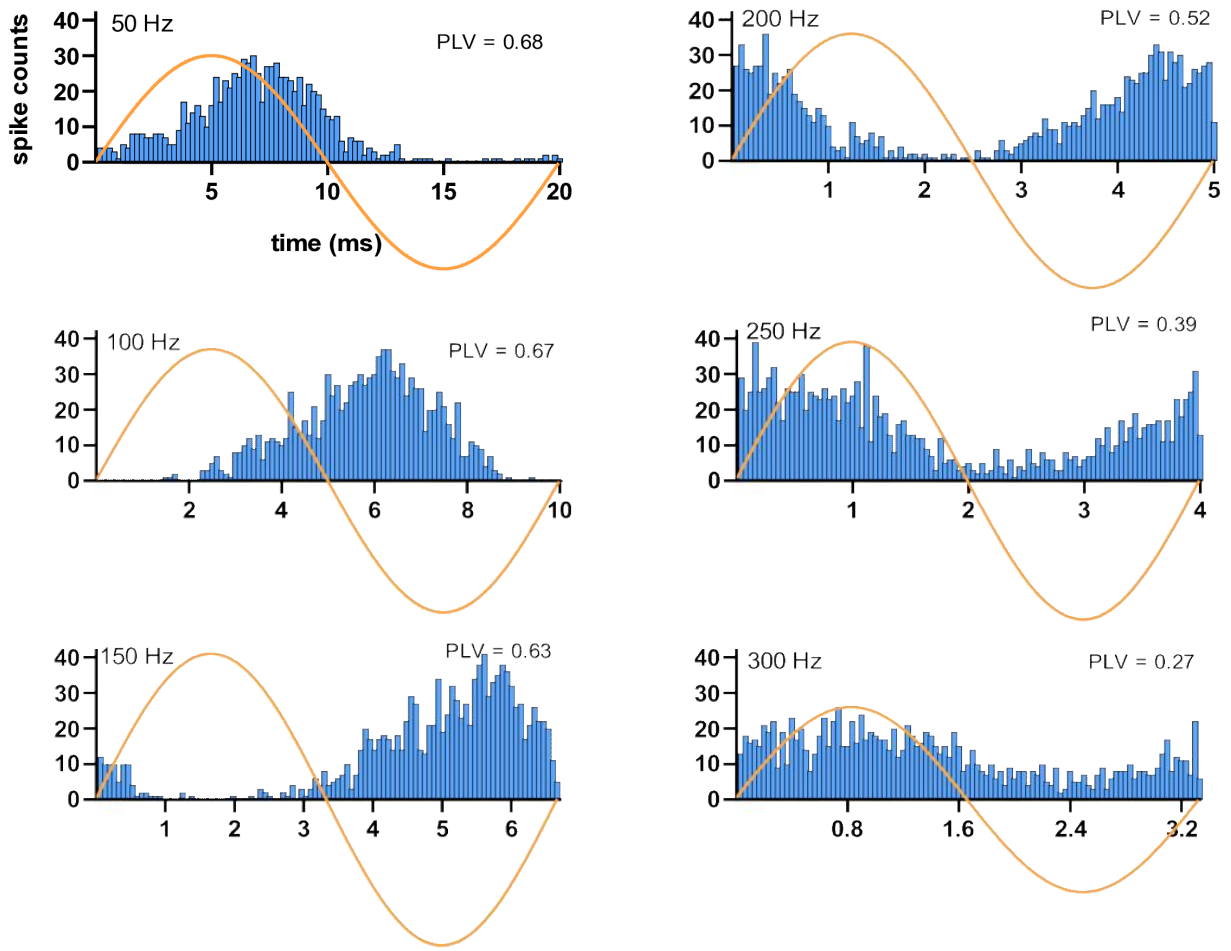

FIGURE 5
Spiking timing histograms for a CN cell at stimulation frequencies ranging from 50 Hz to 300 Hz. Note the change in the latency of the modulation with respect to the AC cycle. Stimulus amplitude is 40 μA. PLVs are also indicated in each case.

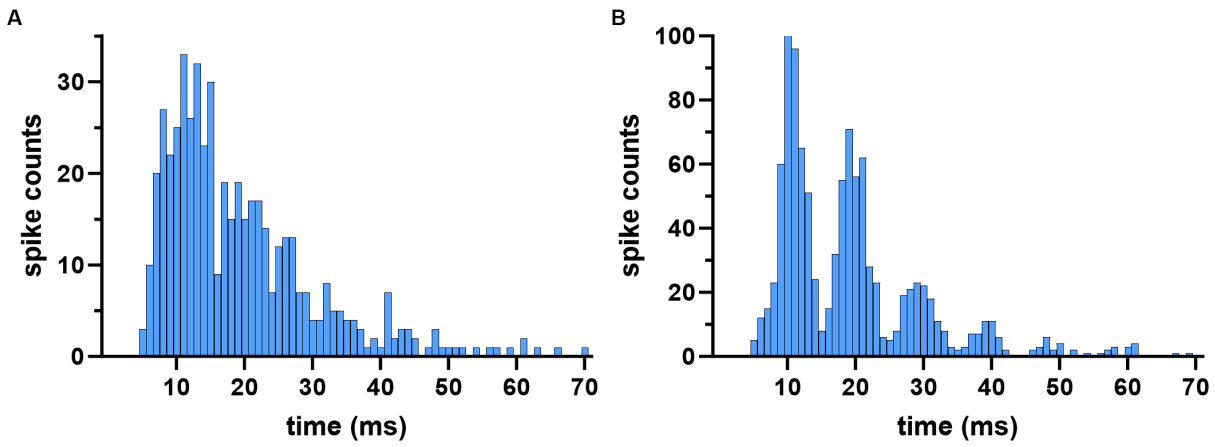

FIGURE 6
Inter-spike-interval histograms during the baseline **(A)** and stimulation **(B)** periods in a cell modulated at 100 Hz. Histogram peaks occur at multiples of the AC cycle (10 ms) during stimulation indicating modulation at subharmonic frequencies. Subharmonic peaks emerge when the spikes start skipping one or more AC cycles, which tended to occur when the stimulus frequency is larger than the cell's spontaneous firing frequency.

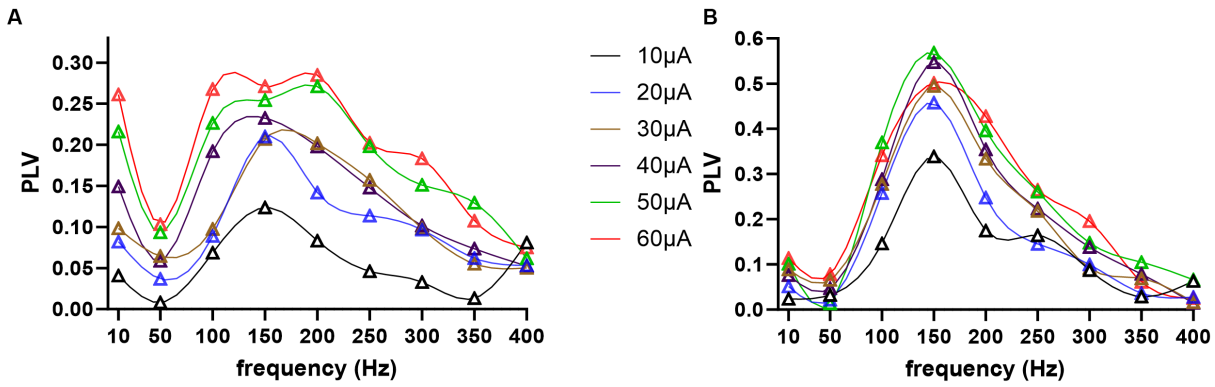

FIGURE 7
Modulation index, phase lock value (PLV), as a function of frequency and stimulus amplitude, coded in different colors, for two sample cells in **(A,B)**.

In 427 out of 492 trials (of all stimulation amplitudes and frequencies in 20 cells) where the modulation was clearly above the noise level (PLV > 0.15) and the stimulation frequency was higher than the spontaneous firing rate of the cell, no significant change was found in the mean firing frequency of the cells from the baseline ($p = 0.2$, two-tailed Student's t). However, the K-S test indicated that the ISI distributions were altered ($p < 0.05$) in the same trials. In 236 (55%) trials out of these 427, the spiking frequency was decreased (from 46.8 ± 18.6 spikes/s to 37.6 ± 20 spikes/s) and in the remaining 191 (45%) trials increased (from 44.4 ± 20 spikes/s to 51.8 ± 19.4 spikes/s), although the stimulation frequency was higher than the spontaneous firing rate in all these cases. Person et al. also observed an increase in the firing of some CN cells and a decrease in others under synchronized PC inhibition (Person and Raman, 2011). The changes in the firing rates must be due to spontaneous variations, rather than a result of stimulation, although the baseline recordings for comparison were immediately preceding the stimulation interval. Thus, it seems that spontaneous variations of the cells were strong enough to obscure any alterations induced on the mean firing rates by the AC stimulation in these 20-s stimulation episodes.

3.7. Frequency tuning of modulation

All cells were entrained by the AC stimulation in an amplitude and frequency dependent manner, as shown in two sample cells in Figure 7. The modulation index as a function of frequency revealed a tuning curve where a range of mid-frequencies were most effective. In the first cell (Figure 7A), maximum entrainment occurred at 150 Hz for 10–40 μA stimulation, and moved to 200 Hz for 50 μA. In this particular cell, there was an increase in modulation at 10 Hz for larger stimulation amplitudes. However, this was a rare case, rather than the norm, and it was perhaps due to direct modulation of the CN cell through volume conduction of the stimulation current, and not due to transsynaptic modulation. In the second cell (Figure 7B), the PLV plots were more consistent for different stimulation amplitudes,

perhaps because the entrainment was stronger and clearly above the noise level.

In general, the peak modulation levels increased as a function of stimulus amplitude as expected, but also varied between the cells for the same current. However, this may be a matter of finding the best spot for stimulation on the cortex that is well connected to the recorded CN cell, rather than a reflection of some electrophysiological characteristics of the cell related to how effectively the cell can be modulated transsynaptically. The peak modulation frequency also varied between cells, ranging from 50 to 250 Hz. For instance, with 30 μA AC stimuli, 5 cells had their maximal PLV at 50 Hz, 7 cells at 100 Hz, 6 cells at 150 Hz, 2 cells at 200 Hz, and 1 cell at 250 Hz.

The frequency dependence of the modulation amplitude for the entire population of recorded CN cells is shown in Figure 8, where the PLV of each cell is plotted for each tested frequency. In order to minimize the risk of direct modulation of the CN by the AC stimulus, PLVs plotted in Figure 8 were in response to 30 μA AC stimulation, which was large enough to produce significant transsynaptic modulation (e.g., Figure 7, brown curve) and further increases of stimulus intensity produced only minimal increases in PLV. In general, 10 Hz was very inefficient for modulation. The PLV decreased toward higher frequencies after its peak, except in one cell that maintained a PLV of 0.5 up to 400 Hz (filled circles).

3.8. Correlating the modulation type to cellular electrophysiology

A positive correlation was found between the action potential durations from all cells and their peak PLV frequencies ($r = 0.35$, $p = 0.0002$). The true correlation, however, may be higher, as the band-pass filter (fc = 300 Hz or 500 Hz to 5 kHz) that we had to use to eliminate the stimulation artifacts from the data may have also filtered out some of the cell-to-cell differences in spike durations. The average spike durations during baseline recordings was 0.62 ± 0.18 ms, which is closer to that of the large cells than the nucleo-olivary cells in mice (half-width is 0.3 ms vs. 1.05 ms, respectively, in Najac and Raman, 2015), particularly as we used the full amplitude of action potentials to measure the spike widths (inset in Figure 1). Uusisaari and Knöpfel set the 0.6 ms half-width duration as the upper threshold to differentiate the large non-GABAergic cells from the small ones and the GABAergic cells also, which had an average half-width of 0.99 ms (Uusisaari et al., 2007; Uusisaari and Knopfel, 2011). Thus, the CN cells of this study were estimated to include mostly the large non-GABAergic cells, and imply that they show significant heterogeneity in their modulation characteristics, such as the PLV peak frequency.

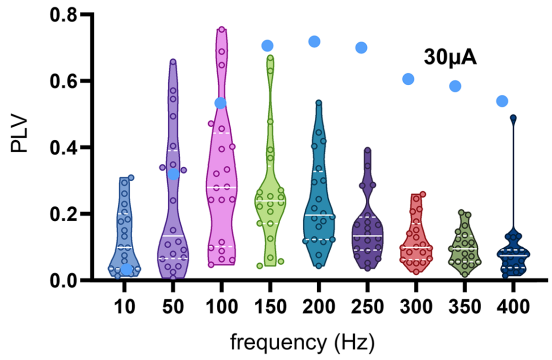

FIGURE 8
PLV as a function of frequency from all cells at 30 μA stimulation. Small circles are actual data points from 19 cells, the horizontal dash lines are the medians, and the dotted lines are the quartiles. The blue filled circles belong to the 20th cell, which had a different trend than the rest with substantial modulation even at the higher end of the frequency range.

The highly sporadic nature of the CN spike train patterns (coefficient of variation-CV of ISI is 0.62 ± 0.5) made it difficult to classify the cells based on their mean firing frequencies. For instance, the average spontaneous firing frequency was 51.7 ± 19.6 Hz ($N = 1{,}754$ trials from 20 cells). The mode of firing frequency (i.e., the reciprocal of the modal interspike interval in the baseline period preceding each trial), however, was much higher (107 ± 47 Hz), suggesting short episodes of high frequency bursts in the baseline. It should be mentioned, however, that imperfections in isolating the spikes from a single cell using the principal components method can lead to contributions from nearby cells and thereby cause miscalculations on spike firing rates and durations.

3.9. AC+DC stimulation

Finally, we were interested to know if altering the PC baseline firing rates with a DC component would influence the level of CN modulation by the AC stimulation. Thus, entrainment of CN spikes was tested with a DC offset superimposed on the AC stimulus waveform in 160 trials in 13 cells from 8 animals. The DC offset was set to ±50, ±70, and ± 90 μA to which a 100 Hz, 50 μA peak amp AC signal was added. Interestingly, the PLV was observed to change only as a function of the AC stimulus frequency and amplitude (data not shown) as in other trials, but it was independent of DC amplitude and/or polarity (Figure 9), i.e., no significant difference in PLV was found in all cases due to DC (ANOVA, $F = 0.01$, $p = 0.98$). These results lead us to two significant conclusions. One, the DC stimulation of the cerebellar cortex, which was shown to alter the PC spike frequencies almost immediately (Asan et al., 2020), does not affect the modulation of the CN cells induced by the AC component of the stimulus. This suggests that altering the PC baseline firing rate may not necessarily predispose the PCs for stronger or weaker synchronization of the simple spikes, at least not at the current levels that were tested here. Two, the direct effects of the cerebellar cortex stimulation on the CN cells through volume conduction was not significant enough to alter the results of transsynaptic modulation from the AC stimulation of the cortex.

4. Discussion

Our goal in this study was to investigate if the CN cells could be entrained transsynaptically by alternating currents applied to the cerebellar cortex. We employed electric stimulation of the cortex with rectangular pulses (to show inhibition of CN cells by PC activation) to ensure that the cortical area being stimulated projected to the CN cell that is recorded. Moreover, the cortical location with the lowest threshold for modulation was searched for, and the AC amplitudes

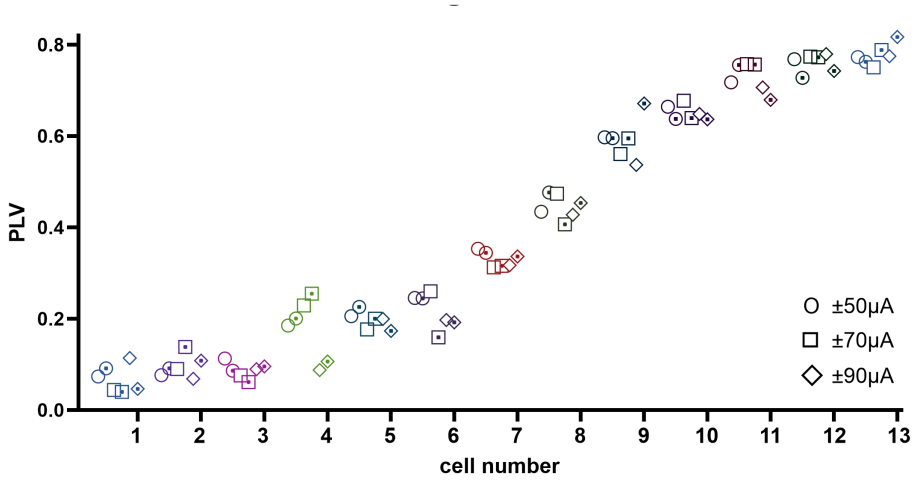

FIGURE 9
PLV measures from 13 cells (coded in different shapes with dot (negative DC) and without dot (positive DC) inside) at ±50, ±70, and ± 90 μA DC (from left to right respectively) superimposed on 100 Hz 50 μA AC stimulation. The cells are ordered with increasing PLV values left to right for appearance only. Overall, DC component has no significant effect on the PLV within each cell.

were kept low in order to minimize the direct effects on the CN cells through volume conduction of the current.

In our data, all 20 cells estimated to be in the CN by stereotaxic coordinates and confirmed to be projected by the cortical cells showed modulation by an AC stimulus in an amplitude and frequency dependent manner. In contrast, in the pre- and postcentral gyri of awake nonhuman primates, only 10–20% of cells were responsive to 10 Hz tACS (Johnson et al., 2020). Responsiveness of neurons to tACS or the lack of it was ascribed to differences in their morphology, orientation in the electric field, and dynamic biophysical properties. In our recent study, lower frequencies (0.5–20 Hz) and larger currents were tested to directly modulate the cortical and nuclear cells in the rat cerebellum (Avlar et al., 2023); where essentially all cells were responsive to the stimulus, though to different levels and with phase delays that varied with their locations with respect to the stimulus electrode. An advantage of transsynaptic modulation of CN cells is that the electric field direction only matters at the cortical level for the cells that are under the direct effect of the current. In the cerebellar cortex, especially atop the folia, the PCs, the cortical cells that project to the CN, have a well-known orientation and position with respect to the induced electric fields. Nevertheless, the variations in the electrophysiological properties of the PCs across the cortex in different zebrin bands (Xiao et al., 2014; Zhou et al., 2014; Tang et al., 2017) and lobes, as well as the PC to CN cell projection maps (Sugihara and Shinoda, 2007; Chung et al., 2009; Sugihara, 2011), may need to be considered for more targeted functional results.

4.1. Frequency tuning

The decline in the PLV curve below the peak frequency reflects an interesting phenomenon (Figures 7, 8). The reason behind this decline could not be at the PC level, since the PCs were entrained at frequencies even as low as 2 Hz (Asan et al., 2020), or even 0.5 Hz (Avlar et al., 2023) with cortical stimulation. A more likely mechanism is that SS synchrony among the PCs that are under the influence of the stimulation current would become much weaker at the lower frequencies since the spikes are now distributed over a much longer time period. If we consider one half the AC cycle as the duration within which the PC spike timings are rearranged to synchronize, this time interval is 10 ms to 2 ms for frequencies from 50 Hz to 250 Hz, where the entrainment is the strongest. This interval agrees with most reports on PC SS synchrony that found spikes occurring within ~4 ms of each another (Shin and De Schutter, 2006; Heck et al., 2007; de Solages et al., 2008; Wise et al., 2010). The half cycle for 10 Hz (50 ms), however, is relatively much longer to have a useful level of spike coincidence between the PCs being modulated. Additional support for the SS synchrony being the mechanism for CN entrainment is provided by the AC + DC data where the DC offset in the waveform did not alter the CN modulation levels induced by the AC component alone, despite the fact that DC offset is expected to affect the PC spike rates (Asan et al., 2020). This suggests that using electric currents with alternating waveforms is an efficient way of transiently increasing PC spike synchrony for CN entrainment, and the average PC firing rate does not predispose the PC synchrony to strengthen or weaken the CN entrainment, not at least when the AC and DC stimulation components are in the same amplitude range.

The negative slopes at the higher frequencies of the PLV curves also need an explanation. An excellent study by Lee et al. demonstrated, with intracellular recordings of the transmembrane voltage in cortical cells, that the passive membrane parameters do not filter the extracellular AC fields at subthreshold membrane voltages (Lee et al., 2023). Thus, the decline in the PLV plots above 100 Hz (Figure 8) should not be because of passive filtering of high frequencies by the cell membrane at the PC level. Moreover, the PCs continued to be entrained at stimulation frequencies higher than their spontaneous firing rates by skipping one or multiple cycles of the AC (Asan et al., 2020). On the other hand, the time to the first spike following a synchronized PC inhibition in the large CN cells is about ~4 ms (see Figure 7 in Wu and Raman, 2017). For stimulation frequencies above 100 Hz, the jittering in the timing of the first spike following PC inhibition can be significant compared to the AC cycle length. Thus,

the same level of jittering that does not have a significant effect on modulation at mid-frequencies can deteriorate the spike histograms and lower the PLV at higher frequencies. This limit at higher frequencies may simply be a reflection of the temporal precision at which the CN cells are capable of processing the information in PC spike synchrony patterns. The interesting finding is that the modulation can still be quite large at stimulation frequencies several times the cell's spontaneous firing frequency by the mechanism of subharmonic modulation. In fact, it seems that the shortening of AC cycle length at higher frequencies increases the precision of PC synchrony until it is no longer useful in the face of biological jittering.

Finally, our results are in agreement with human trials where low frequency stimulation (10 Hz) of the cerebellum was ineffective and higher frequencies produced higher levels of modulation (Naro et al., 2016, 2017). Our entrainment plots show in general that the optimum range of frequencies for transsynaptic modulation is different in each CN cell but mostly above 50 Hz. However, it should be acknowledged that anesthesia can affect synaptic efficiencies and the preferred frequencies we show here for CN cells may shift in awake animals.

4.2. Electric field strengths

Transsynaptic, as opposed to direct (Tai and Tseng, 2022; Baker et al., 2023; Cajigas et al., 2023), modulation of deep cerebellar nuclei has the advantage that the injected current amplitudes can be much lower, and thus keep the electric fields within safe limits. In this study, for the largest stimulation current used (60 μA), the estimated electric field (150 mV/mm) at the cortical level was quite high compared to the e-fields intended (<1 mV/mm) at the targeted brain regions for clinical applications of transcranial stimulation (Guidetti et al., 2022). Modulation was detectable even at 10–20 μA in most cases, but our goal was to demonstrate a clear modulation of the cells above the noise floor to be able to look at the frequency tuning properties. Thus, we extended the upper range of the stimulus amplitude 2–3 times above the threshold levels. However, we believe that useful levels of CN modulation that can lead to functional benefits are possible at much lower electric fields when applied for longer periods of time.

Regarding the safety of the stimulation, as the AC frequency increases, the charge injected per half cycle decreases proportionally. In transcranial applications, the half-cell potential built-up on the surface electrodes will be reversed in the following half-cycle before it leads to chemical reactions with toxic byproducts. Similar arguments could be made in favor of AC stimulation regarding the maximum electric fields that can safely be induced on the excitable cells. Because of the transient nature of the AC currents, maximum allowable stimulation intensities may be much higher than DC stimulation, especially at high frequencies of AC, before harmful cellular effects can occur. Therefore, the safety limits on the currents injected and the electric fields induced at the cortical level should be evaluated on different grounds for transcranial DC and AC applications.

Although the direct effects on the CN cells through volume conduction were much smaller (~1.5 mV/mm at 60 μA) than those on the cortical cells, we cannot completely rule out the possibility of direct e-field effects on CN cells. But we conclude that the transsynaptic effect is the dominant mode of modulation in our data because of the following reasons: (1) The peak of the spike histograms are delayed with respect to the AC stimulus peaks by time intervals that agree with PC-CN propagation delay. (2) CN modulation levels are much lower at 10 Hz than higher frequencies and virtually absent at 1 Hz, 60 μA (data not shown). This strongly argues that the observed entrainment was transsynaptic because the e-fields have much longer time windows at lower frequencies to perturb the transmembrane potential if the effect was direct. (3) The SS synchrony mechanism for transsynaptic entrainment of CN cells predicts that low frequencies will be less effective as discussed above.

4.3. Cerebellar conductivity

Finally, the measured conductivity of the cerebellum (0.42 S/m) was slightly lower than 0.57 S/m that was predicted for the rat brain over the sensorimotor cortex (Asan et al., 2018), but still higher than some of the reported conductivities measured in the molecular and granular layers in the cat (0.17–0.3 S/m) (Yedlin et al., 1974) and turtle (0.15–0.25 S/m) cerebellar cortices (Okada et al., 1994). The higher cerebellar conductivity measured in our case may be explained by the contribution made by the underlying white matter that is highly anisotropic.

5. Conclusion

The cerebellar nuclear cells can be entrained through modulation of the cortical cells transsynaptically using AC stimulation. The CN cells have different ranges of stimulation frequencies for optimum entrainment and with peaks ranging between 50 Hz and 250 Hz. The 10 Hz AC stimulation, recently tested in human trials, is ineffective for transsynaptic modulation in the cerebellum. The overall interpretation of the data lead us to the conclusion that PC-SS synchrony is the most likely mechanism for the transsynaptic entrainment of the CN cells with AC stimulation of the cerebellar cortex. Indirect modulation of the CN by transcranial stimulation of the cerebellar cortex may be developed as an alternative method in clinical disorders where deep cerebellar stimulation is implicated as a treatment.

Data availability statement

The original contributions presented in the study are included in the article/supplementary material, further inquiries can be directed to the corresponding author.

Ethics statement

The animal study was approved by Institutional Animal Care and Use Committee, Rutgers University. The study was conducted in accordance with the local legislation and institutional requirements.

Author contributions

QK: Writing – original draft, Formal analysis. EL: Writing – review & editing. MS: Writing – original draft, Writing – review & editing.

Funding

This work was supported by grants from the National Institute of Neurological Disorders to MS (R21NS101386), and to EL and MS (1RF1NS122741).

Conflict of interest

The authors declare that the research was conducted in the absence of any commercial or financial relationships that could be construed as a potential conflict of interest.

The author(s) declared that they were an editorial board member of Frontiers, at the time of submission. This had no impact on the peer review process and the final decision.

Publisher's note

All claims expressed in this article are solely those of the authors and do not necessarily represent those of their affiliated organizations, or those of the publisher, the editors and the reviewers. Any product that may be evaluated in this article, or claim that may be made by its manufacturer, is not guaranteed or endorsed by the publisher.

References

Asan, A. S., Gok, S., and Sahin, M. (2018). Electric fields induced by transcutaneous and intracranial current injections in the rat brain. *Annu. Int. Conf. IEEE Eng. Med. Biol. Soc.* 2018, 2252–2255. doi: 10.1109/EMBC.2018.8512770

Asan, A. S., Lang, E. J., and Sahin, M. (2020). Entrainment of cerebellar purkinje cells with directional AC electric fields in anesthetized rats. *Brain Stimul.* 13, 1548–1558. doi: 10.1016/j.brs.2020.08.017

Avlar, B., Rahman, R., Vendidandi, S., Cetinkaya, E., Asan, A. S., Sahin, M., et al. (2023). Modulation of cerebellar cortical, cerebellar nuclear and vestibular nuclear activity using alternating electric currents. *Front. Syst. Neurosci.* 17:1173738. doi: 10.3389/fnsys.2023.1173738

Baker, K. B., Plow, E. B., Nagel, S., Rosenfeldt, A. B., Gopalakrishnan, R., Clark, C., et al. (2023). Cerebellar deep brain stimulation for chronic post-stroke motor rehabilitation: a phase I trial. *Nat. Med.* 29, 2366–2374. doi: 10.1038/s41591-023-02507-0

Bostan, A. C., Dum, R. P., and Strick, P. L. (2010). The basal ganglia communicate with the cerebellum. *Proc. Natl. Acad. Sci. U. S. A.* 107, 8452–8456. doi: 10.1073/pnas.1000496107

Bostan, A. C., Dum, R. P., and Strick, P. L. (2018). Functional anatomy of basal ganglia circuits with the cerebral cortex and the cerebellum. *Prog. Neurol. Surg.* 33, 50–61. doi: 10.1159/000480748

Bostan, A. C., and Strick, P. L. (2010). The cerebellum and basal ganglia are interconnected. *Neuropsychol. Rev.* 20, 261–270. doi: 10.1007/s11065-010-9143-9

Bostan, A. C., and Strick, P. L. (2018). The basal ganglia and the cerebellum: nodes in an integrated network. *Nat. Rev. Neurosci.* 19, 338–350. doi: 10.1038/s41583-018-0002-7

Brunoni, A. R., Ferrucci, R., Bortolomasi, M., Vergari, M., Tadini, L., Boggio, P. S., et al. (2011). Transcranial direct current stimulation (tDCS) in unipolar vs. bipolar depressive disorder. *Prog. Neuro-Psychopharmacol. Biol. Psychiatry* 35, 96–101. doi: 10.1016/j.pnpbp.2010.09.010

Cajigas, I., Morrison, M. A., San Luciano, M., and Starr, P. (2023). Cerebellar deep brain stimulation in cerebral palsy: promising early results and a look forward to a larger clinical trial. *World Neurosurg.* 174, 223–224. doi: 10.1016/j.wneu.2023.03.069

Chan, C. Y., and Nicholson, C. (1986). Modulation by applied electric fields of Purkinje and stellate cell activity in the isolated turtle cerebellum. *J. Physiol.* 371, 89–114. doi: 10.1113/jphysiol.1986.sp015963

Chung, S. H., Marzban, H., and Hawkes, R. (2009). Compartmentation of the cerebellar nuclei of the mouse. *Neuroscience* 161, 123–138. doi: 10.1016/j.neuroscience.2009.03.037

de Solages, C., Szapiro, G., Brunel, N., Hakim, V., Isope, P., Buisseret, P., et al. (2008). High-frequency organization and synchrony of activity in the purkinje cell layer of the cerebellum. *Neuron* 58, 775–788. doi: 10.1016/j.neuron.2008.05.008

Ferrucci, R., Giannicola, G., Rosa, M., Fumagalli, M., Boggio, P. S., Hallett, M., et al. (2012). Cerebellum and processing of negative facial emotions: cerebellar transcranial DC stimulation specifically enhances the emotional recognition of facial anger and sadness. *Cognit. Emot.* 26, 786–799. doi: 10.1080/02699931.2011.619520

Ferrucci, R., Marceglia, S., Vergari, M., Cogiamanian, F., Mrakic-Sposta, S., Mameli, F., et al. (2008). Cerebellar transcranial direct current stimulation impairs the practice-dependent proficiency increase in working memory. *J. Cogn. Neurosci.* 20, 1687–1697. doi: 10.1162/jocn.2008.20112

Galea, J. M., Vazquez, A., Pasricha, N., de Xivry, J. J., and Celnik, P. (2011). Dissociating the roles of the cerebellum and motor cortex during adaptive learning: the motor cortex retains what the cerebellum learns. *Cereb. Cortex* 21, 1761–1770. doi: 10.1093/cercor/bhq246

Gottwald, B., Wilde, B., Mihajlovic, Z., and Mehdorn, H. M. (2004). Evidence for distinct cognitive deficits after focal cerebellar lesions. *J. Neurol. Neurosurg. Psychiatry* 75, 1524–1531. doi: 10.1136/jnnp.2003.018093

Grimaldi, G., Argyropoulos, G. P., Bastian, A., Cortes, M., Davis, N. J., Edwards, D. J., et al. (2016). Cerebellar transcranial direct current stimulation (ctDCS): a novel approach to understanding cerebellar function in health and disease. *Neuroscientist* 22, 83–97. doi: 10.1177/1073858414559409

Grimaldi, G., Argyropoulos, G. P., Boehringer, A., Celnik, P., Edwards, M. J., Ferrucci, R., et al. (2014). Non-invasive cerebellar stimulation—a consensus paper. *Cerebellum* 13, 121–138. doi: 10.1007/s12311-013-0514-7

Grimaldi, G., and Manto, M. (2012). Topography of cerebellar deficits in humans. *Cerebellum* 11, 336–351. doi: 10.1007/s12311-011-0247-4

Guidetti, M., Arlotti, M., Bocci, T., Bianchi, A. M., Parazzini, M., Ferrucci, R., et al. (2022). Electric fields induced in the brain by transcranial electric stimulation: a review of *in vivo* recordings. *Biomedicine* 10:2333. doi: 10.3390/biomedicines10102333

Hardwick, R. M., and Celnik, P. A. (2014). Cerebellar direct current stimulation enhances motor learning in older adults. *Neurobiol. Aging* 35, 2217–2221. doi: 10.1016/j.neurobiolaging.2014.03.030

Heck, D. H., Thach, W. T., and Keating, J. G. (2007). On-beam synchrony in the cerebellum as the mechanism for the timing and coordination of movement. *Proc. Natl. Acad. Sci. U. S. A.* 104, 7658–7663. doi: 10.1073/pnas.0609966104

Herzfeld, D. J., Pastor, D., Haith, A. M., Rossetti, Y., Shadmehr, R., and O'Shea, J. (2014). Contributions of the cerebellum and the motor cortex to acquisition and retention of motor memories. *NeuroImage* 98, 147–158. doi: 10.1016/j.neuroimage.2014.04.076

Johnson, L., Alekseichuk, I., Krieg, J., Doyle, A., Yu, Y., Vitek, J., et al. (2020). Dose-dependent effects of transcranial alternating current stimulation on spike timing in awake nonhuman primates. *Sci. Adv.* 6:eaaz2747. doi: 10.1126/sciadv.aaz2747

Krause, M. R., Vieira, P. G., Csorba, B. A., Pilly, P. K., and Pack, C. C. (2019). Transcranial alternating current stimulation entrains single-neuron activity in the primate brain. *Proc. Natl. Acad. Sci. U. S. A.* 116, 5747–5755. doi: 10.1073/pnas.1815958116

Lee, S. Y., Baftizadeh, F., Campagnola, L., Jarsky, T., Koch, C., and Anastassiou, C. A. (2023). Cell class-specific electric field entrainment of neural activity. *bioRxiv*. doi: 10.1101/2023.02.14.528526

Mc Laughlin, M., Khatoun, A., and Asamoah, B. (2022). Detection of tACS entrainment critically depends on epoch length. *Front. Cell. Neurosci.* 16:806556. doi: 10.3389/fncel.2022.806556

Mehta, A. R., Brittain, J. S., and Brown, P. (2014). The selective influence of rhythmic cortical versus cerebellar transcranial stimulation on human physiological tremor. *J. Neurosci.* 34, 7501–7508. doi: 10.1523/JNEUROSCI.0510-14.2014

Middleton, F. A., and Strick, P. L. (2000). Basal ganglia and cerebellar loops: motor and cognitive circuits. *Brain Res. Brain Res. Rev.* 31, 236–250. doi: 10.1016/S0165-0173(99)00040-5

Milardi, D., Quartarone, A., Bramanti, A., Anastasi, G., Bertino, S., Basile, G. A., et al. (2019). The cortico-basal ganglia-cerebellar network: past, present and future perspectives. *Front. Syst. Neurosci.* 13:61. doi: 10.3389/fnsys.2019.00061

Najac, M., and Raman, I. M. (2015). Integration of Purkinje cell inhibition by cerebellar nucleo-olivary neurons. *J. Neurosci.* 35, 544–549. doi: 10.1523/JNEUROSCI.3583-14.2015

Naro, A., Bramanti, A., Leo, A., Manuli, A., Sciarrone, F., Russo, M., et al. (2017). Effects of cerebellar transcranial alternating current stimulation on motor cortex excitability and motor function. *Brain Struct. Funct.* 222, 2891–2906. doi: 10.1007/s00429-016-1355-1

Naro, A., Leo, A., Russo, M., Cannavo, A., Milardi, D., Bramanti, P., et al. (2016). Does transcranial alternating current stimulation induce cerebellum plasticity? Feasibility, safety and efficacy of a novel electrophysiological approach. *Brain Stimul.* 9, 388–395. doi: 10.1016/j.brs.2016.02.005

Okada, Y. C., Huang, J. C., Rice, M. E., Tranchina, D., and Nicholson, C. (1994). Origin of the apparent tissue conductivity in the molecular and granular layers of the *in vitro* turtle cerebellum and the interpretation of current source-density analysis. *J. Neurophysiol.* 72, 742–753. doi: 10.1152/jn.1994.72.2.742

Person, A. L., and Raman, I. M. (2011). Purkinje neuron synchrony elicits time-locked spiking in the cerebellar nuclei. *Nature* 481, 502–505. doi: 10.1038/nature10732

Person, A. L., and Raman, I. M. (2012). Synchrony and neural coding in cerebellar circuits. *Front. Neural Circuits* 6:97. doi: 10.3389/fncir.2012.00097

Pope, P. A. (2015). Modulating cognition using transcranial direct current stimulation of the cerebellum. *J. Vis. Exp.* e52302. doi: 10.3791/52302

Priori, A., Ciocca, M., Parazzini, M., Vergari, M., and Ferrucci, R. (2014). Transcranial cerebellar direct current stimulation and transcutaneous spinal cord direct current stimulation as innovative tools for neuroscientists. *J. Physiol.* 592, 3345–3369. doi: 10.1113/jphysiol.2013.270280

Schmahmann, J. D. (1998). Dysmetria of thought: clinical consequences of cerebellar dysfunction on cognition and affect. *Trends Cogn. Sci.* 2, 362–371. doi: 10.1016/S1364-6613(98)01218-2

Schmahmann, J. D. (2004). Disorders of the cerebellum: ataxia, dysmetria of thought, and the cerebellar cognitive affective syndrome. *J. Neuropsychiatry Clin. Neurosci.* 16, 367–378. doi: 10.1176/jnp.16.3.367

Shin, S. L., and De Schutter, E. (2006). Dynamic synchronization of Purkinje cell simple spikes. *J. Neurophysiol.* 96, 3485–3491. doi: 10.1152/jn.00570.2006

Stoodley, C. J., and Schmahmann, J. D. (2009). Functional topography in the human cerebellum: a meta-analysis of neuroimaging studies. *NeuroImage* 44, 489–501. doi: 10.1016/j.neuroimage.2008.08.039

Strick, P. L., Dum, R. P., and Fiez, J. A. (2009). Cerebellum and nonmotor function. *Annu. Rev. Neurosci.* 32, 413–434. doi: 10.1146/annurev.neuro.31.060407.125606

Sugihara, I. (2011). Compartmentalization of the deep cerebellar nuclei based on afferent projections and aldolase C expression. *Cerebellum* 10, 449–463. doi: 10.1007/s12311-010-0226-1

Sugihara, I., and Shinoda, Y. (2007). Molecular, topographic, and functional organization of the cerebellar nuclei: analysis by three-dimensional mapping of the olivonuclear projection and aldolase C labeling. *J. Neurosci.* 27, 9696–9710. doi: 10.1523/JNEUROSCI.1579-07.2007

Tai, C. H., and Tseng, S. H. (2022). Cerebellar deep brain stimulation for movement disorders. *Neurobiol. Dis.* 175:105899. doi: 10.1016/j.nbd.2022.105899

Tang, T., Xiao, J., Suh, C. Y., Burroughs, A., Cerminara, N. L., Jia, L., et al. (2017). Heterogeneity of Purkinje cell simple spike-complex spike interactions: zebrin- and non-zebrin-related variations. *J. Physiol.* 595, 5341–5357. doi: 10.1113/JP274252

Uusisaari, M., and Knopfel, T. (2011). Functional classification of neurons in the mouse lateral cerebellar nuclei. *Cerebellum* 10, 637–646. doi: 10.1007/s12311-010-0240-3

Uusisaari, M., Obata, K., and Knopfel, T. (2007). Morphological and electrophysiological properties of GABAergic and non-GABAergic cells in the deep cerebellar nuclei. *J. Neurophysiol.* 97, 901–911. doi: 10.1152/jn.00974.2006

Wiley, J. D., and Webster, J. G. (1982). Analysis and control of the current distribution under circular dispersive electrodes. *I.E.E.E. Trans. Biomed. Eng.* 29, 381–385.

Wise, A. K., Cerminara, N. L., Marple-Horvat, D. E., and Apps, R. (2010). Mechanisms of synchronous activity in cerebellar Purkinje cells. *J. Physiol.* 588, 2373–2390. doi: 10.1113/jphysiol.2010.189704

Wu, Y., and Raman, I. M. (2017). Facilitation of mossy fibre-driven spiking in the cerebellar nuclei by the synchrony of inhibition. *J. Physiol.* 595, 5245–5264. doi: 10.1113/JP274321

Xiao, J., Cerminara, N. L., Kotsurovskyy, Y., Aoki, H., Burroughs, A., Wise, A. K., et al. (2014). Systematic regional variations in Purkinje cell spiking patterns. *PLoS One* 9:e105633. doi: 10.1371/journal.pone.0105633

Yedlin, M., Kwan, H., Murphy, J. T., Nguyen-Huu, H., and Wong, Y. C. (1974). Electrical conductivity in cat cerebellar cortex. *Exp. Neurol.* 43, 555–569. doi: 10.1016/0014-4886(74)90195-2

Zhou, H., Lin, Z., Voges, K., Ju, C., Gao, Z., Bosman, L. W., et al. (2014). Cerebellar modules operate at different frequencies. *elife* 3:e02536. doi: 10.7554/eLife.02536

frontiers | Frontiers in Neuroscience

TYPE Original Research
PUBLISHED 20 November 2023
DOI 10.3389/fnins.2023.1269267

OPEN ACCESS

EDITED BY
Gahangir Hossain,
University of North Texas, United States

REVIEWED BY
Noboru Sasaki,
Hokkaido University, Japan
Silvia Palombella,
IRCCS Ospedale Galeazzi Sant'Ambrogio, Italy

*CORRESPONDENCE
Yanbo Zhang
✉ yanbo9@ualberta.ca
Jie Chen
✉ jc65@ualberta.ca

†These authors have contributed equally to this work

RECEIVED 29 July 2023
ACCEPTED 30 October 2023
PUBLISHED 20 November 2023

CITATION
Ye X, Wang Z, van Bruggen R, Li X-M, Zhang Y and Chen J (2023) Low-intensity pulsed ultrasound enhances neurite growth in serum-starved human neuroblastoma cells. *Front. Neurosci.* 17:1269267. doi: 10.3389/fnins.2023.1269267

Low-intensity pulsed ultrasound enhances neurite growth in serum-starved human neuroblastoma cells

Xuanjie Ye[1†], Zitong Wang[2†], Rebekah van Bruggen[2], Xin-Min Li[2], Yanbo Zhang[2*] and Jie Chen[1*]

[1]Department of Electrical and Computer Engineering, University of Alberta, Edmonton, AB, Canada, [2]Department of Psychiatry, Faculty of Medicine and Dentistry, University of Alberta, Edmonton, AB, Canada

Introduction: Low-intensity pulsed ultrasound (LIPUS) is a recognized tool for promoting nerve regeneration and repair; however, the intracellular mechanisms of LIPUS stimulation remain underexplored.

Method: The present study delves into the effects of varying LIPUS parameters, namely duty cycle, spatial average-temporal average (SATA) intensity, and ultrasound amplitude, on the therapeutic efficacy using SK-N-SH cells cultured in serum-starved conditions. Four distinct LIPUS settings were employed: (A) 50 mW/cm^2, 40%, (B) 25 mW/cm^2, 10%, (C) 50 mW/cm^2, 20%, and (D) 25 mW/cm^2, 10%.

Results: Immunochemistry analysis exhibited neurite outgrowth promotion in all LIPUS-treated groups except for Group D. Further, LIPUS treatment was found to successfully promote brain-derived neurotrophic factor (BDNF) expression and enhance the phosphorylation of extracellular signal-regulated kinase (ERK)1/2, protein kinase B (Akt), and mammalian target of rapamycin (mTOR) signaling pathways, as evidenced by western blot analysis.

Discussion: The study suggests that the parameter combination of LIPUS determines the therapeutic efficacy of LIPUS. Future investigations should aim to optimize these parameters for different cell types and settings and delve deeper into the cellular response mechanism to LIPUS treatment. Such advancements may aid in tailoring LIPUS treatment strategies to specific therapeutic needs.

KEYWORDS

low-intensity pulsed ultrasound, ultrasound parameters, neurite outgrowth, serum-starved cell model, SK-N-SH cells

Highlights

- Our study reveals the capacity of LIPUS to promote nerve regeneration and repair.
- By systematically exploring the effects of varying LIPUS parameters on SK-NSH neuroblastoma cells, our research uncovers crucial mechanisms that underscore the therapeutic efficacy of LIPUS.
- These findings are profoundly important for neurological treatment, particularly considering the pervasive challenge of nerve regeneration in various neurodegenerative conditions.

- The capacity of LIPUS to stimulate neuroblastoma cells and facilitate neurite outgrowth could be harnessed for therapies targeting neurodegenerative diseases such as Alzheimer's, Parkinson's, and others.
- This approach could also be applicable in recovery after neurotrauma.

1 Introduction

Neurological disorders are often associated with severe consequences, impacting the affected individuals and exerting a substantial burden on the healthcare system and society (D'Andrea et al., 2003; Winkler et al., 2011; Wen and Huse, 2017; Lizarraga-Valderrama, 2021). Prevalent conditions such as traumatic brain and spinal cord injuries, cerebrovascular incidents, Alzheimer's disease, and peripheral nerve injuries significantly reduce a patient's quality of life (Seddon, 1942, 1943; McKhann et al., 1984; Bramlett and Dietrich, 2007; Bains and Hall, 2012; Smajlović, 2015; Scheltens et al., 2016). Numerous studies have highlighted the importance of promoting nerve regeneration and repair as a solution to recover impaired nerve functionality (Schwob, 2002; Steward et al., 2013). Consequently, considerable interest has converged toward investigating effective therapeutic strategies to enhance neural repair and regeneration.

A range of potential interventions is emerging with advances in neurobiology and related technologies. These encompass but are not limited to, stem cell therapy (Lavorato et al., 2021), gene therapy (Müller et al., 2006), utilization of biomaterials (Subramanian et al., 2009; Joung et al., 2020), and electrical stimulation (Gordon and English, 2016; Zhang et al., 2021). Supported by experimental evidence, these innovative therapeutic approaches show promise for managing neurological disorders. A further step is understanding the molecular and cellular mechanisms associated with these therapeutic approaches that control nerve repair and regeneration, which is critical to developing treatment protocols (Scheib and Höke, 2013).

Low-intensity pulsed ultrasound (LIPUS) has recently become a safe and effective method in non-invasive physical therapy, significantly advancing in various treatment areas (Khanna et al., 2009; Zhao et al., 2012; Shaheen et al., 2013). It is postulated that the therapeutic efficacy of LIPUS is based on the mechanical and non-thermal influences of ultrasound waves, leading to biologically beneficial effects within the intra- and extracellular environment (Khanna et al., 2009). Evidence shows that LIPUS can help improve bone healing and bone density recovery in cases of fractures. Similarly, LIPUS has demonstrated commendable therapeutic outcomes on soft tissue injuries (Lai et al., 2021), wound healing (Iwanabe et al., 2016), inflammation (Nakao et al., 2014), tooth-root healing (Ang et al., 2010), and others (Zhao et al., 2014; Jiang et al., 2019; Huang et al., 2020).

In addition to the aforementioned applications, accumulated evidence has revealed the vital role of LIPUS in promoting nerve regeneration and repair. For instance, a study conducted by Zhao et al. (2016) demonstrated the efficacy of combining LIPUS and nerve growth factor (NGF) in promoting neurite outgrowth via mechanotransduction-mediated extracellular signal-regulated kinase (ERK)1/2-CREB-Trx-1 signaling pathways. In addition, Han et al. (2020) reported that LIPUS can enhance the regeneration of injured dorsal root ganglion neurons through mTOR upregulation. Interestingly, mTOR has been recognized as a vital regulator in neuronal development and plasticity by participating in multiple signaling pathways, whereby disturbed mTOR signaling correlates with abnormal neuronal function and failure of many cellular processes (Licausi et al., 2010; Archer et al., 2018). Therefore, these findings underscore the considerable promise of LIPUS as a potential therapeutic strategy for neural regeneration and repair.

Despite the numerous advancements made by LIPUS in treating neurological disorders, several key issues must be addressed before clinical translation. One of these challenges is the determination of specific LIPUS parameters, including the ultrasound fundamental frequency (UFF), pulse repetition frequency (PRF), spatial average-temporal average (SATA) intensity, and duty cycle (DC). Optimal parameter settings may differ according to specific neurological conditions. Moreover, the molecular and cellular mechanisms underlying the therapeutic effects of LIPUS in neurological disorders remain inadequately explored, and conclusive assertions have yet to be established (Miller et al., 2012). Therefore, future research endeavors should focus on identifying the optimal ultrasound parameters for various neurological disorders and exploring the therapeutic mechanisms of LIPUS.

To explore the effects of LIPUS on the nervous system, we conducted an *in vitro* study utilizing SK-N-SH cells in a serum-starved environment as the experimental model. The SK-N-SH cells are derived from a human neuroblastoma cell line. Extensively employed in neurobiological research, they serve as an archetypal model for the nervous system (Green et al., 1996; Wang et al., 2007; Zhou et al., 2021; Journal of Healthcare Engineering, 2023). Our study aimed to evaluate the influence of LIPUS on neural cell growth and its interaction with protein signaling pathways. The serum-deprivation model is frequently employed as an *in vitro* injury model due to its ability to generate oxidative stress and disrupt protein expression (White et al., 2020). It has become a standard approach in numerous prior studies focusing on therapeutic development and investigating the mechanisms of recovery (Zhao et al., 2016). Building upon existing research, we utilized the serum-starved model to examine the positive influences of LIPUS on neuronal growth and uncover the related biochemical mechanisms. Specifically, we focused on proteins related to the growth and proliferation of neurons, encompassing the mammalian target of rapamycin (mTOR), ERK1/2, Protein kinase B (also known as Akt), and brain-derived neurotrophic factor (BDNF). mTOR is a serine/threonine protein kinase, functioning as a core regulator of cell growth, metabolism, and protein synthesis, and playing an essential role in neural development, synaptic plasticity, and memory formation (Saxton and Sabatini, 2017). ERK, a subset of mitogen-activated protein kinases (MAPKs), governs a range of cellular processes such as cell survival, proliferation, and differentiation, and is integral to neuronal plasticity and long-term memory formation (Roskoski, 2012). Akt is a serine/threonine kinase implicated in regulating cell survival, growth, and metabolism, and its dysregulation is linked to various neurological disorders (Manning et al., 1995).

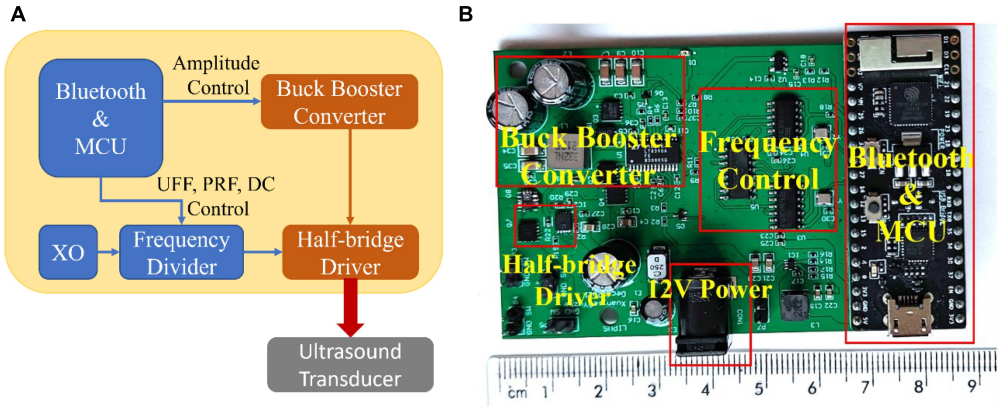

FIGURE 1
The customized miniature LIPUS driver system. **(A)** The circuit block diagram of the customized miniaturized LIPUS driver system and **(B)** the prototype.

BDNF, a neurotrophin, promotes the survival of existing neurons and stimulates the growth, differentiation, and synaptic plasticity of new neurons (Bramham and Messaoudi, 2005). In addition to investigating these signaling pathways, we also examined different ultrasound parameters to identify optimal conditions for LIPUS treatment. Overall, this research sought to explore the therapeutic mechanisms of LIPUS and its effective parameters.

2 Materials and methods

2.1 Customized miniaturized LIPUS driver system

In this study, we engineered a customized miniaturized LIPUS driver system. Figure 1A depicts the overall circuit block diagram, while Figure 1B displays the prototype. The solution for the Bluetooth communication and microcontroller unit (MCU) control module was implemented using the ESP32-PICO-KIT V4 development board [Espressif Systems (Shanghai) Co., Ltd., China]. The MCU output signal controls the output amplitude of the buck-boost converter (5-40V), UFF, PRF, and DC. The buck-boost converter is based on the synchronous 4-switch buck-boost DC/DC controller IC chip LT8390A. The system employs a half-bridge driver to drive the transducers, composed of a half-bridge gate driver IC chip DGD05463FN-7 and a dual N-channel MOSFET IC chip NTTFD4D0N04HLTWG. This device facilitates precise adjustment of ultrasound amplitude, UFF, PRF, and DC, thus allowing for quick and simple configuration and delivery of a wide array of LIPUS parameters.

2.2 LIPUS exposure system

The well-on-transducer method was employed for the *in vitro* ultrasound therapy, where each well was coupled with a planar transducer via a gel medium. This setup is prevalent in cell and tissue sample ultrasound studies due to its simplicity (Hensel et al., 2011). The coupling layer, composed of gel or water, facilitates acoustic matching, ensuring optimal energy transfer from the transducer to the sample. Customized ultrasound transducers for this experiment have a single resonant frequency of 1.5 MHz and a 25 mm diameter. Before each use, the SATA intensity of the ultrasound transducer was quantified utilizing the ultrasound power meter UPM-DT-1000PA (OHMIC Instruments, MO, USA). The ultrasound coupling agent and the base of the cell culture well were attached to the ultrasound transducer so that the penetrating loss of ultrasound energy would be included in the measurement.

A 12-well cell culture plate, arranged in a 3 × 4 matrix, was used for the cell culture. Each well had a diameter of 22 mm, smaller than the ultrasound transducer, which exposed all cells within the well to the LIPUS. The cells were seeded in the wells located at the four corners. This enabled simultaneous LIPUS treatment across four wells, enhancing experimental efficiency. The unoccupied central wells minimized ultrasound crosstalk between neighboring wells. To assure efficient ultrasound transmission, an ultrasound gel (Wavelength® MP Blue Multi-Purpose Ultrasound Gel, ON, Canada) was used as the coupling medium between the ultrasound transducer and the cell culture plate, as depicted in Figure 2A.

To measure the ultrasonic field intensity distribution at the well bottom, a customized 3D-printed jig was developed for accurate hydrophone (HNR-1000, Onda Corporation, CA, USA) placement. The sampling procedure commenced from the center of the well, systematically moving outward at 30° intervals and sampling every 1 mm in the radial direction. Each sampled point represented the local pressure distribution, which was subsequently converted into power intensity using the equation $I = \frac{p_0^2}{2z}$, where I, p_0, z stands for the power intensity, ultrasonic pressure, and acoustic impedance, respectively. During testing, the ultrasound system was adjusted to output a constant sound field SATA intensity of 125 mW/cm^2 at a duty cycle of 100%, as measured by an ultrasound power meter UPM-DT-1000PA. This resulted in a SATA intensity of 25 mW/cm^2 by adjusting the duty cycle to 20%. The outcome of our measurements is presented in Figure 2B, where the red dot signifies the location of the test point. Although some variations in the sound field distribution were observed, leading to

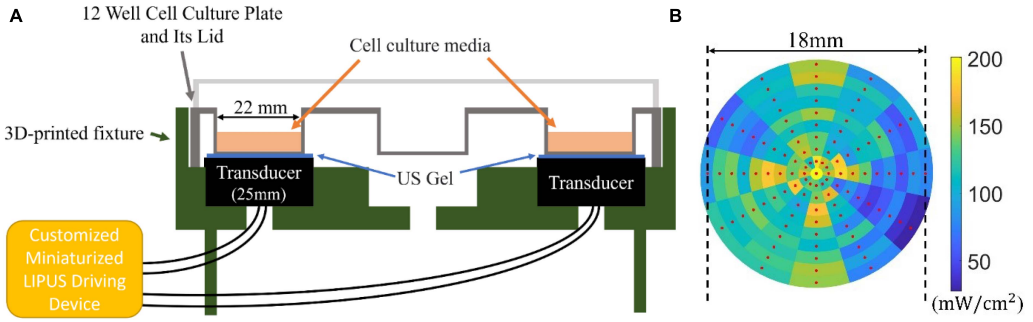

FIGURE 2
(A) Sketch of the LIPUS exposure setup. A 12-well culture plate (well diameter of 22 mm) was placed on a 3D-printed base. Four 25 mm transducers placed in the four corners of the plate contacted the well through ultrasound (US) gel medium. The transducers were connected to the customized miniaturized LIPUS driving device. **(B)** The ultrasonic sound field distribution measured from the bottom of the well (SATA intensity 125 mW/cm^2 with a duty cycle of 100%).

higher (200 mW/cm^2) and lower (50 mW/cm^2) intensity areas, the majority of the tested regions remained from 100 to 150 mW/cm^2.

2.3 Cell culture and LIPUS treatment

The overall LIPUS stimulation protocol is shown in Figure 3. The SK-N-SH cell line was kindly provided by Dr. Tom Hobman, Department of Cell Biology, Faculty of Medicine and Dentistry, University of Alberta, Edmonton, Canada. SK-N-SH cells were cultured in Dulbecco's Modified Eagle Medium (DMEM; 319-005-CL, WISENT INC.) with 10% fetal bovine serum (FBS; 090150, WISENT INC.) within a humidified 37°C incubator. This culture medium is referred to as complete media. For seeding, SK-N-SH cell suspension was adjusted to a concentration of 10,000 cells/mL, and each well was loaded with 1 mL of the suspension, resulting in an initial seeding density of 10,000 cells per well. Approximately 6 h later, following adherence of the majority of cells to the well surface, the culture medium was aspirated and the wells were washed 3 times with DMEM without FBS. The culture medium was then replaced with a low-serum media, composed of DMEM supplemented with 1% FBS, creating a serum-starved cell model.

Two control groups were included: (1) SK-N-SH cells cultured in complete media (10% FBS) without LIPUS stimulation were used as a healthy control group, and (2) SK-N-SH cells grown in low-serum media without LIPUS stimulation were used as the control for serum starvation. Four LIPUS treatment groups grown in low-serum media (1% FBS) were tested. To investigate the effect of various SATA intensities (mW/cm^2) and DC (%) on cellular responses, four distinct LIPUS treatment parameter configurations were tested: (A) 50 mW/cm^2, 40%, (B) 25 mW/cm^2, 20%, (C) 50 mW/cm^2, 20%, and (D) 25 mW/cm^2, 10%. Groups A and C shared the same ultrasound intensity but varied in duty cycles. This pattern was mirrored in groups B and D. Notably, the ultrasound amplitude in groups B and D was approximately 0.707 times that of groups A and C. UFF was set at 1.5 MHz and the PRF was set to 1 kHz in the four groups and remained constant. LIPUS treatment began 18 h post-transition to the low-serum media (on day 2) for 10 min. To ensure a uniform ultrasound distribution, the transducer was rotated 180° following the initial 5-min treatment period, then continued for 5 min. The 10-min LIPUS treatment was repeated every 24 h. Ten minutes after the fourth LIPUS treatment (on day 5), the supernatants were collected for cell viability assessments, and the cells were either collected for protein extraction or imaged using immunocytochemistry (ICC).

2.4 Cell cytotoxicity quantification

The LDH-Cytotoxicity Assay Kit II (ab65393) was utilized to quantify lactate dehydrogenase (LDH) release to indicate cytotoxicity. Cell supernatants were collected and cleared of debris via centrifugation (600×g). Following the manufacturer's instructions, a water-soluble tetrazolium (WST) substrate mix was added to the cleared supernatant and mixed thoroughly in a 96-well plate. Following a 30-min incubation at room temperature, the absorbance was measured at 450 nm, with a reference wavelength of 650 nm using a colorimetric microplate reader (FLUOstar Omega Microplate Reader, BMG). A low LDH control, composed of cell-free media, and a high LDH control, composed of the supernatant of the SK-N-SH cells cultured in the complete media for 5 days, were used to calculate cell cytotoxicity. Cytotoxicity (%) was calculated using the following calculation: Cytotoxicity = (Test Sample – Low Control)/(High Control – Low Control) × 100%. Results were normalized to the cytotoxicity of the healthy control group.

2.5 Cell visualization

ICC was employed to visualize cellular structures to observe cell morphology. For ICC experiments, glass coverslips were washed, sterilized, and placed in the 12-well cell culture plate before SK-N-SH seeding. Cells were treated as outlined above. On the fifth day of the experiment (after the fourth LIPUS treatment), cells were rinsed once with phosphate-buffered saline (PBS; 311-010-CL, WISENT INC.) and then fixed in a solution of 4% paraformaldehyde (PFA; 441244, Sigma-Aldrich) diluted in 1 × PBS. This fixation process was carried out at room temperature for 10 min. Subsequently, cells were rinsed twice with 1 × PBS. Cell membranes were permeabilized using 0.2% Triton X-100 (A16046, Thermo Fisher

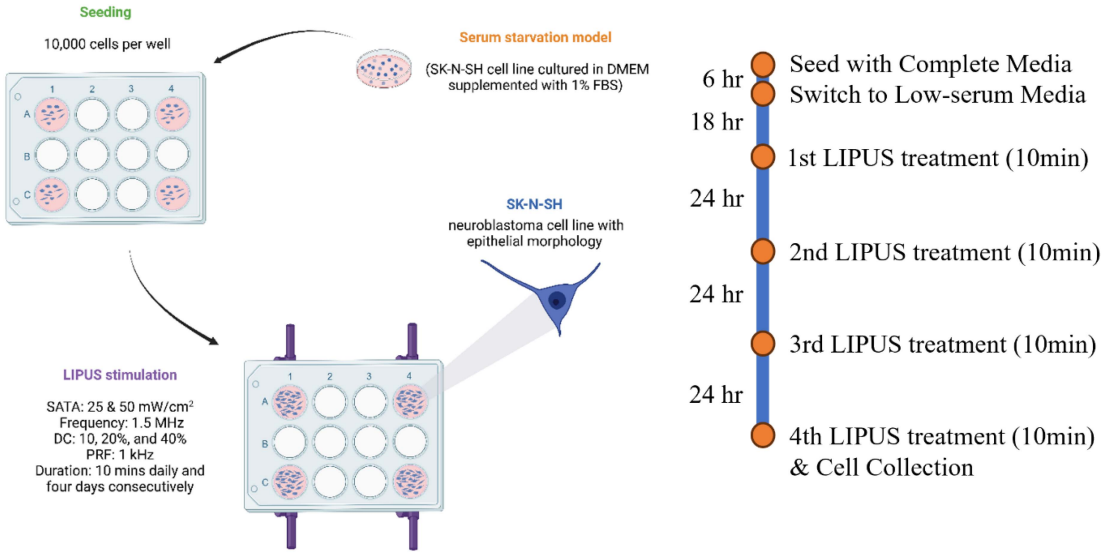

FIGURE 3
LIPUS stimulation protocol. Serum-starved SK-N-SH cells were treated with 10 min of LIPUS stimulation daily for four consecutive days (UFF: 1.5 MHz; PRF: 1 kHz; SATA intensity: either 25 or 50 mW/cm^2; DC: either 10, 20, or 40%).

Scientific) diluted in 1 × PBS, for 5 min at room temperature, followed by three washes with 1 × PBS. The coverslips were then transferred onto a strip of parafilm in a humidifying chamber and incubated with blocking buffer (0.5% bovine serum albumin (BSA; A2134, Biomatik) and 6% normal goat serum (ab7481, Abcam) diluted in 1× PBS) for 1 h at room temperature. Following this, primary antibodies (Tubulin, 1:500, MAB1637, Sigma-Aldrich) diluted in a 1:1 mixture of blocking buffer and 1 × PBS were added to the samples and incubated either for 2 h at room temperature or overnight at 4°C. The coverslips were then washed three times for 5 min in 1 × PBS and incubated with the secondary antibody solution [goat anti-mouse (1:1000, Alexa Fluor 594, A-11032, Invitrogen)] diluted in 1 × PBS for 1 h at room temperature. Subsequently, the secondary antibody solution was aspirated, and the coverslips were rinsed three times with 1 × PBS. The coverslips were then mounted using ProLong Gold antifade reagent with DAPI (P36935; Invitrogen) and were allowed to dry overnight at room temperature, protected from light. Finally, the ICC imaging was conducted using the EVOS M5000 Imaging system (Thermo Fisher Scientific Inc., MA, USA).

2.6 Western blot

Western blot analysis was utilized to quantify BDNF, ERK1/2, Akt, and mTOR expression levels. Cells for Western blot analysis were removed from the plate wells using Trypsin-EDTA (0.05% with phenol red, 325-043-EL, Wisent) and resuspended in DMEM with 10% FBS. Cells were collected via centrifugation (1000 rpm, 10 min) and then lysed using RIPA buffer (150 mM NaCl, 25 mM Tris-HCl pH 7.6, 5 mM EDTA, 1% Triton X-100, 0.1% SDS, 1% sodium deoxycholate) mixed with phosphate inhibitor (A32957, Thermo Scientific) and protease inhibitor (A32963, Thermo Scientific). Protein lysates were quantified using the Bradford protein assay kit (Bio-Rad). The resultant absorbance was measured with the FLUOstar Omega Microplate Reader (BMG). Subsequently, 5 µg of each protein sample was loaded onto a hand-cast 10% Sodium Dodecyl Sulfate Polyacrylamide Gel Electrophoresis (SDS-PAGE) gel. Proteins were transferred onto a 0.2 µm nitrocellulose membrane (1620112, Bio-Rad). The membranes were blocked using 5% BSA in 1 × Tris-Buffered Saline (TBS) and incubated in the desired primary antibody solution overnight at 4°C. Then, membranes were washed and probed with secondary antibodies at room temperature for 1 h. Protein bands were visualized using the imaging system, with the images captured and quantified using Image Studio Lite software (LI-COR Biosciences, Lincoln, NE, Ver 5.2). Glyceraldehyde 3-phosphate dehydrogenase (GAPDH) was utilized as a loading control to ensure equal sample loading. The band intensities were quantified using ImageJ. The relative band intensities were normalized as follows: BDNF normalized to GAPDH, phosphorylated Akt (p-Akt) to total Akt, phosphorylated ERK1/2 (p-ERK1/2) to total ERK1/2, and phosphorylated mTOR (p-mTOR) to total mTOR.

The primary antibodies used in the study were diluted 1:1000 with 5% BSA in 1 × TBS: rabbit anti-BDNF (ab108319, Abcam), rabbit anti-ERK1/2 (9102S, Cell Signaling), rabbit anti-p-ERK1/2 (4376S, Cell Signaling), mouse anti-Akt (1:1000; 2920S, Cell Signaling), rabbit anti-p-Akt (4060S, Cell Signaling), rabbit anti-mTOR (2983S, Cell Signaling), rabbit anti-p-mTOR (5536S, Cell Signaling), and mouse anti-GAPDH (1:1000; 97166S, Cell Signaling). The secondary antibodies were diluted 1:10000 with 5% BSA in 1 × TBS: goat anti-rabbit-IR800 (926-32211, LI-COR Biosciences) and goat anti-mouse-IR680 (926-68070, LI-COR Biosciences).

2.7 Statistical analysis

Statistical analysis was conducted on data for LDH quantification results, neurite length, soma size, and western

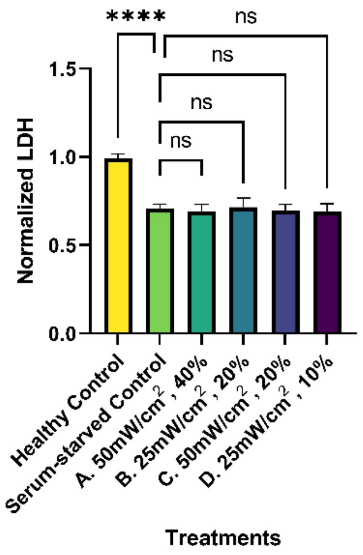

FIGURE 4
Normalized percent cytotoxicity from SK-N-SH cells treated with LIPUS. LDH levels from the supernatant of untreated (healthy control and serum-starved control) and LIPUS-treated SK-N-SH cells were quantified using a commercially available LDH assay. All results were normalized to the healthy control group. N = 5/group. ns: no statistical significance; ****$p < 0.0001$.

blot quantification outcomes using GraphPad Prism software (GraphPad Software, MA, USA, version 9.4). The comparison among the healthy control, serum-starved control, and LIPUS-treatment groups was based on the one-way analysis of variance (ANOVA) followed by a *post hoc* multiple comparison test. The observed power for each analysis was calculated to ascertain that the sample size was sufficient to substantiate the findings. Statistical significance was designated at a p-value threshold of less than 0.05.

3 Results

3.1 Cytotoxicity results

To determine if the LIPUS treatment altered cell viability, LDH levels from all treatment groups were evaluated as a measure of cytotoxicity. Dying cells release LDH, which can be measured using a commercially available kit. Analysis of the cytotoxicity assay revealed that LDH levels in all serum-starved groups (serum-starved control and LIPUS treatment groups A, B, C, D), were significantly lower than the healthy (complete media) control with a value of roughly 0.7 ($p < 0.0001$), as presented in Figure 4. However, no statistical significance was observed among the serum-starved control group and the LIPUS-treatment groups A, B, C, and D, suggesting that the LIPUS treatments did not alter cell survival in serum-deprived conditions.

3.2 ICC results

An in-depth analysis of neurite lengths in the serum-starved control and LIPUS-treatment groups was performed to understand how different LIPUS settings can influence nerve cell growth. Representative ICC images of each group are shown in Figure 5. The lengths of the neurites were measured using NeuronJ, an ImageJ plugin tailored for neurite tracing and analysis. In the analysis, we exclusively focused on the longest neurite of each cell, typically considered the axon. The length of the axon is crucial for nerve signal transmission and the overall function of the nerve cell (Debanne et al., 2011). Additionally, we measured the width of the cell body at its widest point. Any neurite lengths less than the diameter of the cell body were excluded as they were considered inadequately developed neurites. As the healthy control group exhibited a high cell density with most of the neurites densely interwoven, neurite length was not quantified. To facilitate statistical analysis, neurite length was quantified from the edge of the cell nucleus (DAPI) to the distal end of the cell skeleton (Tubulin) using the NeuronJ. The measurements were conducted following the guidelines provided by NeuronJ, and default parameters were employed for the neurite length measurements.

No significant differences were observed among the cell body/soma diameters between SK-N-SH cells in control or LIPUS treatment groups under low-serum conditions, as presented in Figure 6A. However, LIPUS-treatment groups A, B, and C, exhibited a significant enhancement in neurite growth compared to the serum-starved control group ($p < 0.005$), whereby the mean ± standard error length for each group was as follows: serum-starved control group 117.1 ± 57.0 μm, Group A 138.9 ± 63.5 μm, Group B 137.7 ± 64.1 μm, and Group C 138.7 ± 70.5 μm, as shown in Figure 6B. The LIPUS-treatment group D (25 mW/cm^2, 10%) did not show a significant difference in neurite length (mean ± standard error neurite length: 118.6 ± 60.8 μm) compared to the serum-starved control group.

3.3 Western blot results

Western blot analyses were conducted to evaluate BDNF levels and the activation of the BDNF signaling pathway, namely by assessing the phosphorylation status of ERK, Akt, and mTOR, in response to the LIPUS treatments. Serum starvation significantly decreased BDNF levels compared to cells grown in complete media. However, this decrease was ameliorated by three of the four LIPUS treatment parameters ($p < 0.01$, Figure 7). SK-N-SH cells treated with a SATA of 50 mW/cm^2 (Groups A and C) or with a SATA of 25 mW/cm^2 group and the higher duty cycle of 20% (Group B) exhibited increased BDNF levels. Notably, while the Group D treatment parameters (SATA 25 mW/cm^2, 10% DC) significantly upregulated BDNF levels, these parameters failed to elicit significant elevation in downstream signaling events. Increased BDNF levels were associated with an increase in phosphorylation levels of Akt, ERK1/2, and mTOR for LIPUS-treatment groups A, B, and C, though not group D (Figure 6), suggesting that these pathways were activated in the SK-N-SH cells upon treatment.

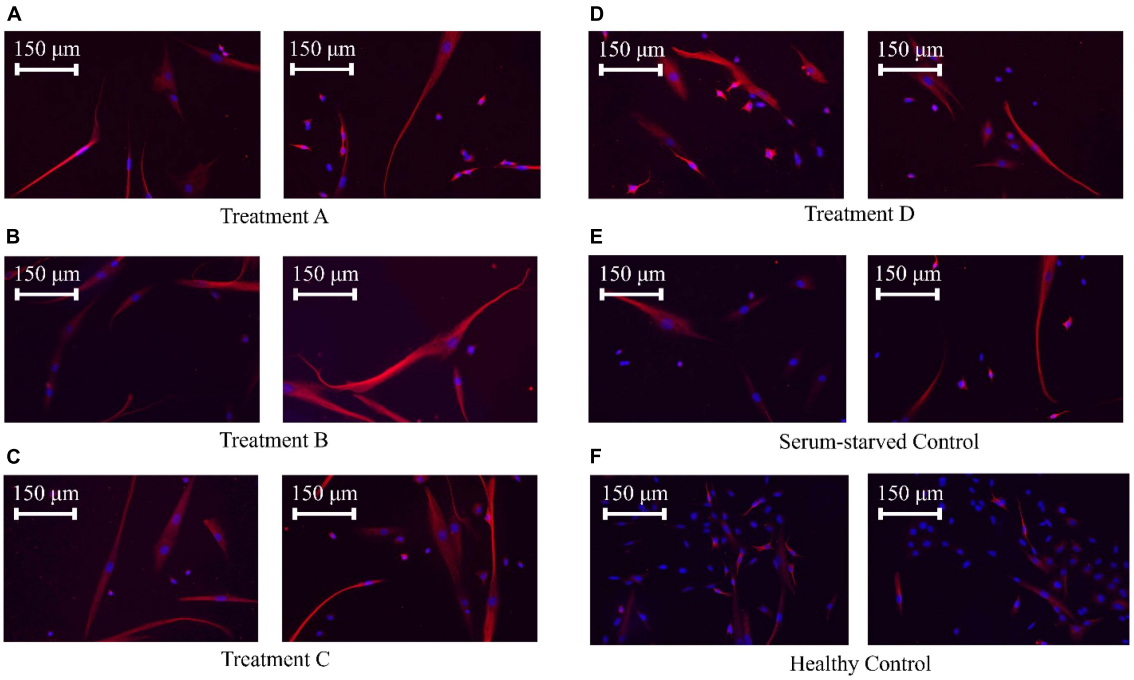

FIGURE 5
SK-N-SK cell ICC staining. Nuclei were stained with DAPI (blue), and microtubules, which represent the cytoskeleton, were stained with an anti-tubulin antibody (red). **(A)** SK-N-SH cells treated with LIPUS (50 mW/cm^2, 40%). **(B)** SK-N-SH cells treated with LIPUS (25 mW/cm^2, 20%). **(C)** SK-N-SH cells treated with LIPUS (50 mW/cm^2, 20%). **(D)** SK-N-SH cells treated with LIPUS (25 mW/cm^2, 10%). **(E)** Serum-starved control. **(F)** Healthy control.

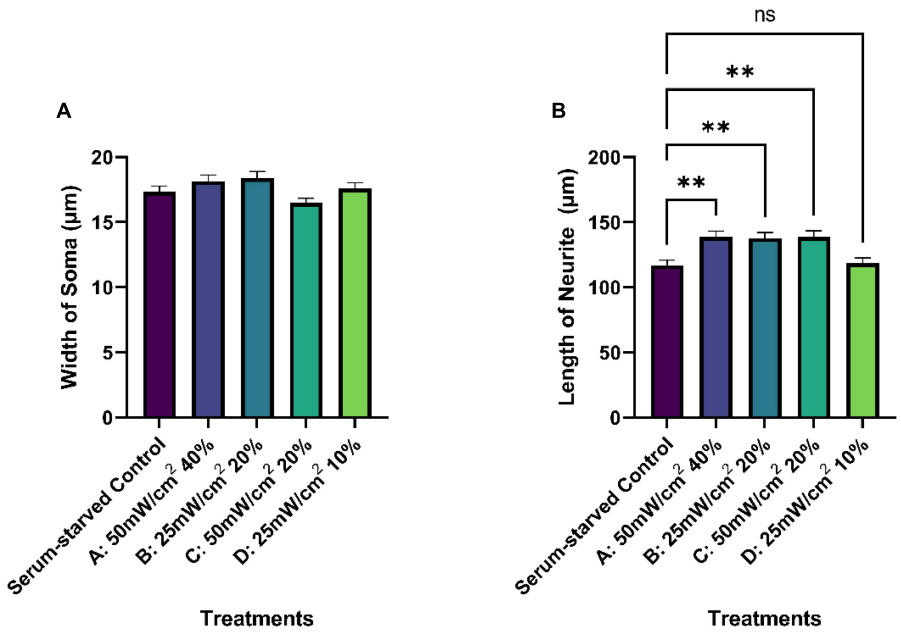

FIGURE 6
Quantification of average soma width **(A)** and neurite length (μm) **(B)** of serum-starved SK-N-SH cells under different treatment conditions (control and LIPUS treatment, Groups A-D). N = 250. Ns, no statistica significance; $^{**}p < 0.005$.

4 Discussion

Previous research has demonstrated that LIPUS can stimulate nerve regeneration and neurite outgrowth through the ERK1/2 and mTOR signaling pathways (Miller et al., 2012; Lv et al., 2015; Jiang et al., 2016; Sato et al., 2016; Zhao et al., 2016, 2017; Han et al., 2020). This study sought to determine the optimal intensity and duty cycle of ultrasound stimulation on serum-deprived SK-N-SH cells

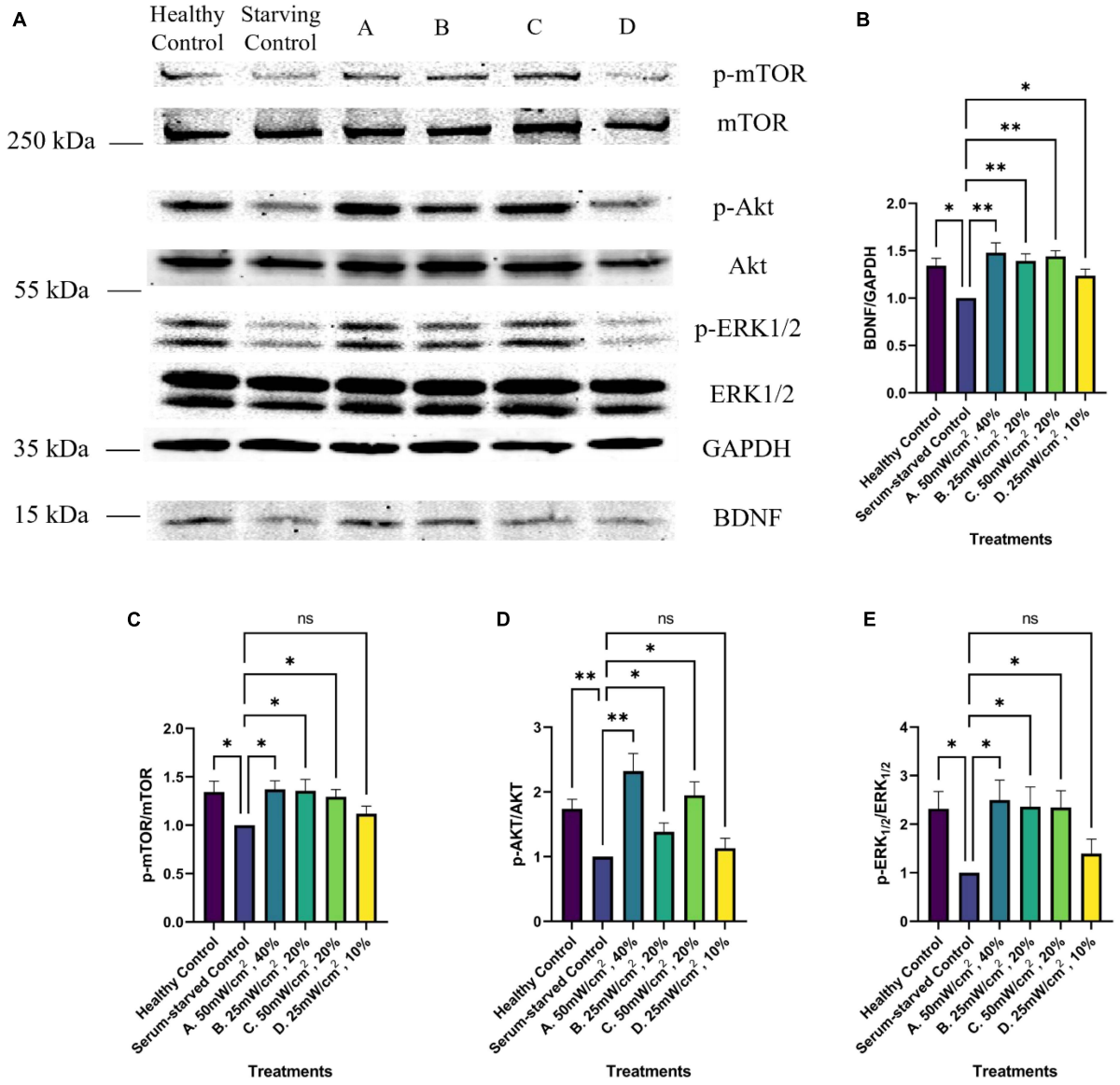

FIGURE 7
Western blot analysis of BDNF growth factor signaling pathway activation upon LIPUS stimulation. **(A)** Representative Western Blot imaging results of GAPDH, BDNF, p-mTOR, mTOR, p-ERK1/2, ERK1/2, p-Akt, and Akt from untreated (healthy control, Serum-starved Control) and LIPUS-treated (A, B, C, D) SK-N-SH cells. *N* = 5 replicates per group. Comparative analysis of normalized Western blot protein band intensity of panel **(B)** BDNF, **(C)** mTOR, **(D)** Akt, and **(E)** ERK1/2 across various treatment groups (*N* = 5). $*p < 0.05$, $**p < 0.01$, ns, no statistical significance.

and explore the underlying molecular mechanisms under LIPUS stimulation.

In cell culture, serum is an important source of nutrients and growth hormones. Decreasing the serum level in media can induce a starvation state, which can alter cell signaling and growth. In this study, SK-N-SH cells were cultured in serum-starved conditions for 4 days, leading to limited nutrient availability. This resulted in a reduced metabolic state and slower cell division due to nutrient deprivation. Compared to cells in complete media (healthy control), those in serum-starvation conditions exhibited slower growth, as evident from the ICC analysis and cytotoxicity levels. In addition, lower cell growth rates were observed alongside reduced BDNF levels and decreased activation of the Akt, ERK1/2, and mTOR pathways compared to healthy controls. These findings confirm the successful establishment of the experimental starvation model. Interestingly, LIPUS stimulation under the tested conditions had no significant impact on cell proliferation or cytotoxicity when compared to the serum-starved control group. Furthermore, LIPUS treatment did not affect the soma size of SK-N-SH cells. Altogether, these results suggest that the LIPUS treatment does not impact neuronal proliferation – either negatively or positively.

While the LIPUS treatment appeared to have no impact on cell proliferation, enhanced neurite growth was found in three out of the four tested LIPUS treatments. In addition, the three LIPUS conditions (A, B, C) leading to increased neurite length were associated with higher BDNF expression and increased phosphorylation of ERK1/2, Akt, and mTOR, compared to the

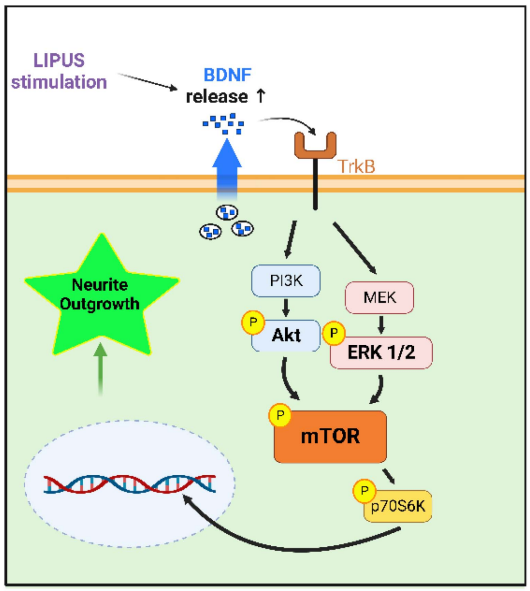

FIGURE 8
Hypothesized mechanism by which LIPUS stimulates neurite outgrowth. LIPUS stimulation increases the release of the growth factor BDNF, activating the mTOR pathway downstream of Akt and ERK1/2, leading to neurite outgrowth.

serum-starved control. Previous studies have highlighted the pivotal roles of the ERK1/2 and Akt signaling pathways in mediating the effects of growth factors such as nerve growth factor and BDNF on neuronal growth under LIPUS treatment (Zhao et al., 2016; Guo et al., 2021). Additionally, evidence supports the role of LIPUS in promoting the regeneration of injured dorsal root ganglion neurons through activation of the mTOR pathway (Han et al., 2020). This study replicates these findings, demonstrating the upregulation of these proliferation-related proteins in nerve cells stimulated by LIPUS, and proposes a comprehensive mechanistic pathway, as depicted in Figure 8. The discrepancy in p-Akt levels among conditions A, B, and C can be attributed to variable responses induced by different LIPUS parameters. While condition B showed lower p-Akt levels compared to A and C, it still elevated p-Akt levels compared to the serum-starved control. Moreover, the consistent expression of p-mTOR across conditions suggests that ERK1/2 may play a predominant role in mTOR regulation within LIPUS therapy.

This study investigated the effects of four distinct ultrasound parameter settings on SK-N-SH cells cultured in a low-serum environment. It is widely believed that the therapeutic effects of LIPUS arise mainly from non-thermal effects, including cavitation and mechanical effects (Snehota et al., 2020). Our experimental results corroborated this perspective, underscoring that the therapeutic efficacy of LIPUS is not primarily attributable to its thermal effects. Within the LIPUS treatment groups, groups B and D shared identical SATA intensities, indicating a similar thermal influence. Nonetheless, while group B exhibited enhanced neurite growth associated with increased BDNF signaling, group D displayed no significant deviation from the serum-starved control group. Notably, although group B had only half the thermal effect of groups A and C, they showed a similar promoting effect on neurite outgrowth. Overall, these findings suggest that the non-thermal effects of LIPUS, rather than the thermal effects, play a more significant role in promoting neurite growth and altering protein signaling pathway expression. Moreover, from a safety perspective in the context of LIPUS treatment, group B, possessing only half the SATA power of groups A and C, consistently demonstrated a comparable enhancement in neurite growth. This observation underscores the potential of parameter B (25 mW/cm^2, 20%) as a safer choice for both future research endeavors and clinical applications.

Future studies are required to systematically investigate the effects of different LIPUS parameters, encompassing duty cycle, SATA intensity, and ultrasound amplitude, on therapeutic efficacy. The comparison between group D and other groups reveals that slight adjustments in these parameters can significantly alter the therapeutic effect of LIPUS. Understanding the contribution of these parameters to the overall treatment effect is crucial for developing more effective LIPUS treatment strategies. In addition, in-depth studies of the molecular and cellular processes that control the observed therapeutic effects are also needed. Expanding knowledge of the underlying mechanisms and interactions among LIPUS parameters would enable researchers and clinicians to tailor LIPUS therapies to specific therapeutic needs.

5 Conclusion

This study investigated the effects of various LIPUS parameters on SK-N-SH cells cultured in serum-starved conditions. Four parameter settings were studied, altering either the SATA (mW/cm^2) or the duty cycle (%): A (50 mW/cm^2, 40%), B (25 mW/cm^2, 10%), C (50 mW/cm^2, 20%), and D (25 mW/cm^2, 10%). ICC results revealed that parameter groups A, B, and C stimulated neurite outgrowth, associated with increased BDNF expression and enhanced the phosphorylation of ERK1/2, Akt, and mTOR signaling pathways. The investigation also revealed that the combination of SATA intensity, duty cycle, and ultrasound amplitude critically determined the therapeutic efficacy of LIPUS, which appears unrelated to any thermal effects of ultrasound. Future research is required to optimize different parameters for various cell types and experimental settings, and explore the in-depth mechanism of cellular response to LIPUS treatment. These advancements will help researchers and clinicians tailor LIPUS treatment strategies to specific treatment needs.

Data availability statement

The original contributions presented in this study are included in this article/supplementary material, further inquiries can be directed to the corresponding authors.

Ethics statement

Ethical approval was not required for the studies on humans in accordance with the local legislation and institutional

requirements because only commercially available established cell lines were used.

Author contributions

XY: Conceptualization, Data curation, Formal analysis, Investigation, Methodology, Software, Validation, Visualization, Writing – original draft, Writing – review and editing. ZW: Conceptualization, Investigation, Methodology, Software, Validation, Visualization, Writing – review and editing. RB: Formal analysis, Investigation, Methodology, Writing – review and editing. X-ML: Funding acquisition, Resources, Supervision, Writing – review and editing. YZ: Funding acquisition, Project administration, Supervision, Writing – review and editing. JC: Conceptualization, Funding acquisition, Project administration, Resources, Supervision, Writing – review and editing.

Funding

The author(s) declare financial support was received for the research, authorship, and/or publication of this article. This study was supported by the Start-up Fund (RES0052505) from the University of Alberta to YZ. The scholarship support from China Scholarship Council for XY is gratefully acknowledged (No. 201806320348). **Figures 3**, **8** were created with Biorender.com.

Conflict of interest

The authors declare that the research was conducted in the absence of any commercial or financial relationships that could be construed as a potential conflict of interest.

Publisher's note

All claims expressed in this article are solely those of the authors and do not necessarily represent those of their affiliated organizations, or those of the publisher, the editors and the reviewers. Any product that may be evaluated in this article, or claim that may be made by its manufacturer, is not guaranteed or endorsed by the publisher.

References

Ang, W. T., Scurtescu, C., Hoy, W., El-Bialy, T., Tsui, Y. Y., and Chen, J. (2010). Design and implementation of therapeutic ultrasound generating circuit for dental tissue formation and tooth-root healing. *IEEE Trans. Biomed. Circuits Syst.* 4, 49–61. doi: 10.1109/TBCAS.2009.2034635

Archer, T., Ehrenberger, T., Mundt, F., Gold, M., Krug, K., Mah, C., et al. (2018). Proteomics, post-translational modifications, and integrative analyses reveal molecular heterogeneity within medulloblastoma subgroups. *Cancer Cell.* 34, 396–410.e1.

Bains, M., and Hall, E. D. (2012). Antioxidant therapies in traumatic brain and spinal cord injury. *Biochim. Biophysica Acta* 1822, 675–684.

Bramham, C. R., and Messaoudi, E. (2005). BDNF function in adult synaptic plasticity: the synaptic consolidation hypothesis. *Prog. Neurobiol.* 76, 99–125.

Bramlett, H. M., and Dietrich, W. D. (2007). Progressive damage after brain and spinal cord injury: pathomechanisms and treatment strategies. *Prog. Brain Res.* 161, 125–141.

D'Andrea, J. A., Chou, C., Johnston, S. A., and Adair, E. R. (2003). Microwave effects on the nervous system. *Bioelectromagnetics* 24, S107–S147.

Debanne, D., Campanac, E., Bialowas, A., Carlier, E., and Alcaraz, G. (2011). Axon physiology. *Physiol. Rev.* 91, 555–602. doi: 10.1152/physrev.00048.2009

Gordon, T., and English, A. W. (2016). Strategies to promote peripheral nerve regeneration: electrical stimulation and/or exercise. *Eur. J. Neurosci.* 43, 336–350.

Green, P. S., Gridley, K. E., and Simpkins, J. W. (1996). Estradiol protects against β-amyloid (25–35)-induced toxicity in SK-N-SH human neuroblastoma cells. *Neurosci. Lett.* 218, 165–168.

Guo, H., Baker, G., Hartle, K., Fujiwara, E., Wang, J., Zhang, Y., et al. (2021). Exploratory study on neurochemical effects of low-intensity pulsed ultrasound in brains of mice. *Med. Biol. Eng. Comput.* 59, 1099–1110. doi: 10.1007/s11517-021-02351-9

Han, S., Park, J., Choi, W. S., and Youn, I. (2020). Ultrasound stimulation increases neurite regeneration in injured dorsal root ganglion neurons through mammalian target of rapamycin activation. *Brain Sci.* 10:409.

Hensel, K., Mienkina, M., and Schmitz, G. (2011). Analysis of ultrasound fields in cell culture wells for in vitro ultrasound therapy experiments. *Ultrasound Med. Biol.* 37, 2105–2115. doi: 10.1016/j.ultrasmedbio.2011.09.007

Huang, D., Gao, Y., Wang, S., Zhang, W., Cao, H., Zheng, L., et al. (2020). Impact of low-intensity pulsed ultrasound on transcription and metabolite compositions in proliferation and functionalization of human adipose-derived mesenchymal stromal cells. *Sci. Rep.* 10:13690. doi: 10.1038/s41598-020-69430-z

Iwanabe, Y., Masaki, C., Tamura, A., Tsuka, S., Mukaibo, T., Kondo, Y., et al. (2016). The effect of low-intensity pulsed ultrasound on wound healing using scratch assay in epithelial cells. *J. Prosthodont. Res.* 60, 308–314. doi: 10.1016/j.jpor.2016.03.002

Jiang, W., Wang, Y., Tang, J., Peng, J., Wang, Y., Guo, Q., et al. (2016). Low-intensity pulsed ultrasound treatment improved the rate of autograft peripheral nerve regeneration in rat. *Sci. Rep.* 6:22773. doi: 10.1038/srep22773

Jiang, X., Savchenko, O., Li, Y., Qi, S., Yang, T., Zhang, W., et al. (2019). A review of low-intensity pulsed ultrasound for therapeutic applications. *IEEE Trans. Biomed. Eng.* 66, 2704–2718. doi: 10.1109/TBME.2018.2889669

Joung, D., Lavoie, N., Guo, S., Park, S., Parr, A., and McAlpine, M. (2020). 3D printed neural regeneration devices. *Adv. Funct. Mater.* 30:201906237. doi: 10.1002/adfm.201906237

Journal of Healthcare Engineering (2023). Retracted: Inhibiting autophagy pathway of PI3K/AKT/mTOR promotes apoptosis in SK-N-SH cell model of Alzheimer's disease. *J. Healthc Eng.* 2023:9780432. doi: 10.1155/2023/9780432

Khanna, A., Nelmes, R., Gougoulias, N., Maffulli, N., and Gray, J. (2009). The effects of LIPUS on soft-tissue healing: a review of literature. *Br. Med. Bull.* 89, 169–182. doi: 10.1093/bmb/ldn040

Lai, W., Iglesias, B., Mark, B., and Wang, D. (2021). Low-intensity pulsed ultrasound augments tendon, ligament, and bone-soft tissue healing in preclinical animal models: A systematic review. *Arthroscopy* 37, 2318–2333.e1. doi: 10.1016/j.arthro.2021.02.019

Lavorato, A., Raimondo, S., Boido, M., Muratori, L., Durante, G., Cofano, F., et al. (2021). Mesenchymal Stem Cell Treatment Perspectives in Peripheral Nerve Regeneration: Systematic Review. *Int. J. Mol. Sci.* 22:572. doi: 10.3390/ijms22020572

Licausi, F., van Dongen, J., Giuntoli, B., Novi, G., Santaniello, A., Geigenberger, P., et al. (2010). HRE1 and HRE2, two hypoxia-inducible ethylene response factors, affect anaerobic responses in Arabidopsis thaliana. *Plant J.* 62, 302–315. doi: 10.1111/j.1365-313X.2010.04149.x

Lizarraga-Valderrama, L. (2021). Effects of essential oils on central nervous system: Focus on mental health. *Phytother. Res.* 35, 657–679. doi: 10.1002/ptr.6854

Lv, Y., Nan, P., Chen, G., Sha, Y., Xia, B., and Yang, L. (2015). In vivo repair of rat transected sciatic nerve by low-intensity pulsed ultrasound and induced pluripotent stem cells-derived neural crest stem cells. *Biotechnol. Lett.* 37, 2497–2506. doi: 10.1007/s10529-015-1939-5

Manning, L., Chamberlain, N., Leahy, M., and Cordingley, F. (1995). Assessment of the therapeutic potential of cytokines, cytotoxic drugs and effector cell populations for the treatment of multiple myeloma using the 5T33 murine myeloma model. *Immunol. Cell Biol.* 73, 326–332. doi: 10.1038/icb.1995.50

McKhann, G., Drachman, D., Folstein, M., Katzman, R., Price, D., and Stadlan, E. (1984). Clinical diagnosis of Alzheimer's disease: Report of the NINCDS-ADRDA work group under the auspices of department of health and human services task force on Alzheimer's disease. *Neurology* 34, 939–944. doi: 10.1212/wnl.34.7.939

Miller, D., Smith, N., Bailey, M., Czarnota, G., Hynynen, K., Makin, I., et al. (2012). Overview of therapeutic ultrasound applications and safety considerations. *J. Ultrasound Med.* 31, 623–634. doi: 10.7863/jum.2012.31.4.623

Müller, F.-J., Snyder, E. Y., and Loring, J. F. (2006). Gene therapy: can neural stem cells deliver? *Nat. Rev. Neurosci.* 7, 75–84.

Nakao, J., Fujii, Y., Kusuyama, J., Bandow, K., Kakimoto, K., Ohnishi, T., et al. (2014). Low-intensity pulsed ultrasound (LIPUS) inhibits LPS-induced inflammatory responses of osteoblasts through TLR4-MyD88 dissociation. *Bone* 58, 17–25. doi: 10.1016/j.bone.2013.09.018

Roskoski, R. (2012). ERK1/2 MAP kinases: structure, function, and regulation. *Pharmacol. Res.* 66, 105–143. doi: 10.1016/j.phrs.2012.04.005

Sato, M., Motoyoshi, M., Shinoda, M., Iwata, K., and Shimizu, N. (2016). Low-intensity pulsed ultrasound accelerates nerve regeneration following inferior alveolar nerve transection in rats. *Eur. J. Oral Sci.* 124, 246–250. doi: 10.1111/eos.12271

Saxton, R. A., and Sabatini, D. M. (2017). mTOR signaling in growth, metabolism, and disease. *Cell* 168, 960–976.

Scheib, J., and Höke, A. (2013). Advances in peripheral nerve regeneration. *Nat. Rev. Neurol.* 9, 668–676.

Scheltens, P., Blennow, K., Breteler, M., de Strooper, B., Frisoni, G., Salloway, S., et al. (2016). Alzheimer's disease. *Lancet* 388, 505–517. doi: 10.1016/S0140-6736(15)01124-1

Schwob, J. (2002). Neural regeneration and the peripheral olfactory system. *Anat. Rec.* 269, 33–49. doi: 10.1002/ar.10047

Seddon, H. (1942). A classification of nerve injuries. *Br. Med. J.* 2, 237–239. doi: 10.1136/bmj.2.4260.237

Seddon, H. (1943). Peripheral nerve injuries. *Glasgow Med. J.* 139, 61–75.

Shaheen, M., Choi, M., Ang, W., Zhao, Y., Xing, J., Yang, R., et al. (2013). Application of low-intensity pulsed ultrasound to increase bio-ethanol production. *Renew. Ener.* 57, 462–468.

Smajlović, D. (2015). Strokes in young adults: epidemiology and prevention. *Vasc. Health Risk Manag.* 11, 157–164. doi: 10.2147/VHRM.S53203

Snehota, M., Vachutka, J., Ter Haar, G., Dolezal, L., and Kolarova, H. (2020). Therapeutic ultrasound experiments in vitro: Review of factors influencing outcomes and reproducibility. *Ultrasonics* 107:106167. doi: 10.1016/j.ultras.2020.106167

Steward, M. M., Sridhar, A., and Meyer, J. S. (2013). Neural regeneration. *N. Perspect. Regener.* 2013, 163–191.

Subramanian, A., Krishnan, U. M., and Sethuraman, S. (2009). Development of biomaterial scaffold for nerve tissue engineering: Biomaterial mediated neural regeneration. *J. Biomed. Sci.* 16, 1–11.

Wang, X., Perez, E., Liu, R., Yan, L., Mallet, R., and Yang, S. (2007). Pyruvate protects mitochondria from oxidative stress in human neuroblastoma SK-N-SH cells. *Brain Res.* 1132, 1–9. doi: 10.1016/j.brainres.2006.11.032

Wen, P. Y., and Huse, J. T. (2017). 2016 World Health Organization classification of central nervous system tumors. *Continuum* 23, 1531–1547.

White, E., Pennant, N., Carter, J., Hawsawi, O., Odero-Marah, V., and Hinton, C. (2020). Serum deprivation initiates adaptation and survival to oxidative stress in prostate cancer cells. *Sci. Rep.* 10:12505. doi: 10.1038/s41598-020-68668-x

Winkler, E. A., Bell, R. D., and Zlokovic, B. V. (2011). Central nervous system pericytes in health and disease. *Nat. Neurosci.* 14, 1398–1405.

Zhang, J., Zhang, X., Wang, C., Li, F., Qiao, Z., Zeng, L., et al. (2021). Conductive composite fiber with optimized alignment guides neural regeneration under electrical stimulation. *Adv. Healthc. Mater.* 10, e2000604. doi: 10.1002/adhm.202000604

Zhao, L., Feng, Y., Hu, H., Shi, A., Zhang, L., and Wan, M. (2016). Low-intensity pulsed ultrasound enhances nerve growth factor-induced neurite outgrowth through mechanotransduction-mediated ERK1/2-CREB-Trx-1 signaling. *Ultrasound Med. Biol.* 42, 2914–2925. doi: 10.1016/j.ultrasmedbio.2016.07.017

Zhao, L., Feng, Y., Shi, A., Zhang, L., Guo, S., and Wan, M. (2017). Neuroprotective Effect of Low-Intensity Pulsed Ultrasound Against MPP+-Induced Neurotoxicity in PC12 Cells: Involvement of K2P Channels and Stretch-Activated Ion Channels. *Ultrasound Med. Biol.* 43, 1986–1999. doi: 10.1016/j.ultrasmedbio.2017.04.020

Zhao, Y., Ang, W. T., Xing, J., Zhang, J., and Chen, J. (2012). Applications of ultrasound to enhance mycophenolic acid production. *Ultrasound Med. Biol.* 38, 1582–1588.

Zhao, Y., Xing, J., Xing, J. Z., Ang, W. T., and Chen, J. (2014). Applications of low-intensity pulsed ultrasound to increase monoclonal antibody production in CHO cells using shake flasks or wavebags. *Ultrasonics* 54, 1439–1447.

Zhou, S., Zhang, D., Guo, J., Chen, Z., Chen, Y., and Zhang, J. (2021). Deficiency of NEAT1 prevented MPP+-induced inflammatory response, oxidative stress and apoptosis in dopaminergic SK-N-SH neuroblastoma cells via miR-1277-5p/ARHGAP26 axis. *Brain Res.* 1750:147156. doi: 10.1016/j.brainres.2020.147156

frontiers | Frontiers in Human Neuroscience

TYPE Systematic Review
PUBLISHED 30 November 2023
DOI 10.3389/fnhum.2023.1297894

OPEN ACCESS

EDITED BY
Gahangir Hossain,
University of North Texas, United States

REVIEWED BY
Gonzalo Javier Revuelta,
The Medical University of South Carolina, United States
Keng Siang Lee,
King's College Hospital NHS Foundation Trust, United Kingdom

*CORRESPONDENCE
Oliver Flouty
✉ oliverflouty@usf.edu

RECEIVED 20 September 2023
ACCEPTED 30 October 2023
PUBLISHED 30 November 2023

CITATION
Shaheen N, Shaheen A, Elgendy A, Bezchlibnyk YB, Zesiewicz T, Dalm B, Jain J, Green AL, Aziz TZ and Flouty O (2023) Deep brain stimulation for chronic pain: a systematic review and meta-analysis. *Front. Hum. Neurosci.* 17:1297894. doi: 10.3389/fnhum.2023.1297894

Deep brain stimulation for chronic pain: a systematic review and meta-analysis

Nour Shaheen[1], Ahmed Shaheen[1], Abdelrahman Elgendy[2], Yarema B. Bezchlibnyk[3], Theresa Zesiewicz[4], Brian Dalm[5], Jennifer Jain[4], Alexander L. Green[6], Tipu Z. Aziz[6] and Oliver Flouty[3]*

[1]Alexandria Faculty of Medicine, Alexandria, Egypt, [2]Faculty of Medicine, Mansoura University, Mansoura, Egypt, [3]Department of Neurosurgery and Brain Repair, University of South Florida, Tampa, FL, United States, [4]Department of Neurology, University of South Florida, Tampa, FL, United States, [5]Department of Neurosurgery, The Ohio State University, Columbus, OH, United States, [6]Oxford Functional Neurosurgery, Department of Neurosurgery, John Radcliffe Hospital, University of Oxford, Oxford, United Kingdom

Background: Deep brain stimulation (DBS) has shown promise in effectively treating chronic pain. This study aimed to assess the efficacy of DBS in this context.

Methods: We conducted a systematic literature search using PubMed, Scopus, and Web of Science, following the PRISMA guidelines. A well-constructed search strategy was utilized. Our literature search identified two groups of subjects: one group underwent DBS specifically for chronic pain treatment (DBS-P), while the second group received DBS for other indications (DBS-O), such as Parkinson's disease or dystonia, with pain perception investigated as a secondary outcome in this population. Meta-analysis was performed using R version 4.2.3 software. Heterogeneity was assessed using the tau^2 and I^2 indices, and Cochran's *Q*-test was conducted.

Results: The analysis included 966 patients in 43 original research studies with chronic pain who underwent DBS (340 for DBS-P and 625 for DBS-O). Subgroup analysis revealed that DBS-P exhibited a significant effect on chronic pain relief, with a standardized mean difference (SMD) of 1.65 and a 95% confidence interval (CI) of [1.31; 2.00]. Significant heterogeneity was observed among the studies, with an I^2 value of 85.8%. However, no significant difference was found between DBS-P and DBS-O subgroups. Subgroup analyses based on study design, age, pain diseases, and brain targets demonstrated varying levels of evidence for the effectiveness of DBS across different subgroups. Additionally, meta-regression analyses showed no significant relationship between age or pain duration and DBS effectiveness for chronic pain.

Conclusion: These findings significantly contribute to the expanding body of knowledge regarding the utility of DBS in the management of chronic pain. The study underscores the importance of conducting further research to enhance treatment outcomes and elucidate patient-specific factors that are associated with treatment response.

Systematic review registration: https://www.crd.york.ac.uk/prospero/display_record.php?RecordID=428442, identifier CRD42023428442.

KEYWORDS

chronic pain, pain, deep brain stimulation, DBS, neuromodulation, neurostimulation

1 Introduction

Chronic pain refers to a persistent type of pain that extends beyond the expected duration for healing, commonly lasting for a period exceeding 3 months. This condition gives rise to a wide range of adverse effects, encompassing medical, social, and economic consequences. Individuals experiencing chronic pain may encounter challenges in their interpersonal relationships, witness a decline in productivity, and face escalated healthcare expenditures (Chou et al., 2015). According to the Institute of Medicine, pain constitutes a significant public health concern with profound financial implications for the United States. It has been estimated that the economic burden associated with pain, encompassing healthcare expenditures and diminished productivity, ranges from $560 to $635 billion annually (Institute of Medicine (US) Committee on Advancing Pain Research, Care, and Education, 2011). In recent years, studies have shown that in modern industrialized nations, prevalence studies indicate that approximately 20–30% of the population experience chronic pain across various conditions (Leadley et al., 2012; Karra et al., 2021). Given the prevalent occurrence and long-lasting nature of chronic pain, along with the undesirable consequences linked to dependence on pain medication, there has been an increasing emphasis on treatment approaches that integrate adjunctive therapies or non-pharmacological alternatives (Chiesa and Serretti, 2011).

Neurosurgeons commonly employ DBS as a therapeutic technique involving the implantation of electrodes in specific subcortical regions of the brain to administer electrical currents. The primary objective of this procedure is to address various movement disorders, notably Parkinson's disease (PD), dystonia, and essential tremor (ET). However, scientists and medical professionals are actively investigating additional potential applications of DBS in the treatment of conditions such as obsessive-compulsive disorder, Tourette's syndrome, depression, cluster headache (CH), and epilepsy. It is worth noting that the utilization of DBS for managing chronic pain dates back to the early 1970's (Bittar et al., 2005a; Hamani et al., 2006).

Deep brain stimulation presents itself as an appealing option in the field of neurosurgery due to its minimally invasive nature, setting it apart from other surgical techniques. Additionally, DBS is generally well-tolerated by patients. In comparison to alternative neurosurgical methods, DBS carries a significantly lower risk. Notably, it falls under the category of neuromodulation, allowing for adjustments and reversibility, unlike previous procedures that involved the creation of brain lesions (Tan et al., 2023).

Two multicenter studies were conducted to assess the efficacy of DBS for pain relief and obtain approval from the FDA. However, both trials failed to meet the predetermined efficacy criteria, which required that a minimum of 50% pain relief be reported by at least half of the patients 1 year after the surgery. The pursuit of FDA approval was discontinued, and the utilization of DBS for pain management has been considered "off-label. Consequently, medical insurance reimbursement for this procedure is lacking. As a result, only a limited number of surgeons currently perform DBS for pain outside of Europe, where it has been approved by the European Federation of Neurological Societies (EFNS) and the United Kingdom National Institute for Health and Clinical Excellence (NICE) (Cruccu et al., 2007; National Institute for Health and Clinical Excellence, 2010).

Deep brain stimulation has shown efficacy in treating various pain syndromes, including post-stroke pain, phantom limb pain, brachial plexus injury, failed back surgery syndrome and the pain accompanying the PD (Bittar et al., 2005a; Falowski, 2015; Frizon et al., 2020; Flouty et al., 2022). Nevertheless, despite the available information, there continues to be a persistent drive to investigate and enhance the utility of DBS in the management of chronic pain. Our study aims to assess the impact of DBS on pain relief in two distinct contexts. We will first examine the effects of DBS specifically targeting chronic pain as the primary indication (DBS-P). Secondly, we will investigate the efficacy of DBS in alleviating pain when it is implanted for indications other than pain (DBS-O). By evaluating these different scenarios, we aim to gain a comprehensive understanding of the role of DBS in pain management across various conditions, contributing to the advancement of therapeutic interventions in the field.

2 Materials and methods

This study's methodology adhered to the Cochrane Handbook for Systematic Reviews of Interventions (Higgins et al., 2023), incorporating guidelines for comprehensive literature searches, rigorous study selection criteria, and robust data synthesis techniques. Moreover, it followed the Preferred Reporting Items for Systematic Reviews and Meta-Analyses (PRISMA) guidelines (Page et al., 2021), ensuring transparent reporting of study selection, data extraction, and meta-analysis procedures according to Lee et al. (2022). The study protocol was prospectively registered in PROSPERO (CRD42023428442), ensuring transparency and adherence to established research guidelines.

In this meta-analysis, we adhered to the PICO framework for formulating our research question as outlined below:

Population (P): We focused on two distinct patient populations, categorized as follows:

- DBS-P: Patients with chronic pain as the primary indication for deep brain stimulation (DBS).
- DBS-O: Patients with indications other than chronic pain, such as Parkinson's disease or dystonia, who underwent DBS.

Intervention (I): The primary intervention under examination was Deep Brain Stimulation (DBS).

Comparison (C): Our analysis encompassed several key comparative aspects:

- Evaluation of pain scores before DBS stimulation compared to pain scores after DBS stimulation (or 'DBS off').
- Assessment of the effectiveness of DBS in relation to movement disorders (e.g., Parkinson's disease, dystonia).
- Investigation of the impact of stimulation targets (brain regions) on pain alleviation.
- Examination of the relationship between DBS and pain duration.

Outcome (O): Our primary outcome of interest was the quantification of pain reduction following DBS stimulation.

2.1 Search strategy

We searched the electronic databases (PubMed, Scopus, Web of science) using the following keywords: ("Chronic Pain" OR "Pain"[Mesh]) AND ("Deep Brain Stimulation" OR "DBS" OR "neuromodulation" OR "Neurostimulation"[Mesh]). The search was limited to articles published in English and published in peer-reviewed journals.

2.2 Eligibility criteria

The inclusion criteria for articles were that they were written in English, published in a peer-reviewed academic journal, and pertained to interventions or treatments, rehabilitation, or epidemiological examinations of pain. We excluded studies involving animals, reviews, descriptive articles, case reports that do not include the available outcomes, book chapters, and technical notes from the meta-analysis, evaluating them on an individual basis.

2.3 Data synthesis

We independently conducted the selection of articles, data extraction, and assessment of methodological quality. Outcome measures were extracted from diverse studies based on predefined inclusion criteria, following the quality assessment criteria outlined by the Oxford Centre for Evidence-Based Medicine levels of evidence (levels I-V) (Marx et al., 2015). Study characteristics were summarized, encompassing details such as DBS location, pain type, primary and secondary outcomes, DBS nucleus target subgroup, pain duration, duration subgrouping, pain questionnaire tools, pain scale utilized, pain relief achieved, effect size, standard deviation of the effect size, percentage of pain reduction, and follow-up duration in years. Treatment effect sizes were computed from reported means and variances of pre- and post-DBS data. Pain levels were assessed using standardized scales, including CH-QoL Pain scale, EUROQOL EQ-5D VAS, Kansas City Pain Disability Scale (KPDPS), McGill Pain Questionnaire (MPQ), among others (see **Supplementary Table 1**).

2.4 Statistical analysis

Statistical analysis was conducted in R using the meta package for a meta-analysis. Data, imported with readxl, underwent meta-analysis using the metacont function, specifying patient numbers, pre- and post-treatment means, standard deviations, and effect size (SMD). Forest plots were generated for visualization. Summary statistics, funnel plots, and sensitivity analyses were performed using various functions. The interpretation referred to Egger et al. (1997) BMJ study (Egger et al., 1997). To address pain measure heterogeneity, effect sizes were computed for each outcome, aggregated through averaging. Metacont function was reapplied for subgroup analysis based on study design, DBS brain target, or meta-regression on age and pain duration. Sensitivity analysis assessed the pooled estimate's robustness by exploring individual studies or methodological choices.

3 Results

3.1 Literature search

A total of 1,106 records were obtained across all databases. After eliminating duplicated articles, 439 journal articles were selected based on their relevance to DBS as a treatment for addiction. Subsequently, these 439 articles underwent screening using our pre-assigned inclusion criteria, leading to the identification of 43 (21 for DBS-P and 16 for DBS-O) original research studies that met the potential eligibility requirements for inclusion in the study **Supplementary Figure 1**: PRISMA flow diagram.

3.2 Study characteristics

The analysis encompassed 966 patients with chronic pain who underwent DBS (340 for DBS-P and 625 for DBS-O), with an average age of 52.8 ± 11.2 years and a mean pain duration of 11.6 ± 10.3 years. The sample consisted of 40% females. The average follow-up period was 2.2 ± 2 years. The findings from the meta-analysis revealed that DBS exhibited a significant reduction in chronic pain, with an average pain reduction of 47.67 ± 20.01% for the DBS-P group and 59.59 ± 23.81% [51.01 ± 21.4% for both groups] (**Table 1**).

3.3 DBS indication

The results of the subgroup analysis for DBS specifically targeting chronic pain (DBS-P) are as follows: In the random effects model, the standardized mean difference (SMD) for DBS-P is 1.65, with a 95% confidence interval (CI) of [1.31; 2.00]. The z-value is 9.45, and the corresponding p-value is less than 0.0001, indicating a significant effect of DBS-P on chronic pain.

Quantifying heterogeneity, the estimated tau^2 is 0.92, with a 95% CI of [0.61; 2.39]. The corresponding tau value is 0.9620, with a 95% CI of [0.78; 1.54]. The I^2 value, representing the percentage of total variation across studies due to heterogeneity, is 85.8%, with a 95% CI of [81.6%; 89.1%]. The estimated H value, which represents the ratio of total variation to sampling variation, is 2.66, with a 95% CI of [2.33; 3.03]. The test of heterogeneity shows a Q-value of 275.02 with 39 degrees of freedom and a p-value less than 0.0001, indicating significant heterogeneity among the studies.

Analyzing the subgroups within the random effects model, the DBS-P subgroup includes 22 studies. The SMD for DBS-P is 1.91, with a 95% CI of [1.32; 2.49]. The estimated tau^2 for this subgroup is 1.46, and the corresponding tau value is 1.2105. The Q-value for this subgroup is 134.93, with an I^2 value of 84.4%.

The DBS-O subgroup, which represents a different indication for DBS, includes 18 studies. The SMD for DBS-O is 1.4689, with

TABLE 1 Study design, countries, number of patients, patient demographics (age and sex), DBS location, the type of pain being treated, the reason for using DBS, pain duration, pain scale used, pain reduction percentage, the follow-up duration in years and quality assessment.

References	Study design	Country	Number of patients	Age (mean ± SD)	Sex-female (No)	DBS location	Pain	DBS-indication	DBS nucleus target subgroup	Pain duration	The pain scale used	Pain score improvement		Pain Reduction (%)	Follow-up duration (years)	Quality assessment
												Effect size	SD (effect size)			
For pain																
Saway et al., 2023	Case report	United States	1	59	0	VPM, MCS	Facial neuropathic pain	DBS-P		5	VAS	6	1	66.67	1	4
Abreu et al., 2022	Prospective	Portugal	16	53 ± 69.1	2	VPL	Post-traumatic neuropathic limb pain	DBS-P	VPL	20.2 ± 12.8	VAS	6.620847109	0.7551903733	76.9	5	1b
Krüger et al., 2021	RCT	Canada	1	63	1	CM, VPM, anterior pulvinar.	Neuropathic dental pain (NDP)	DBS-P			VAS	1.272792206	3.535533906	70	1	1b
Cappon et al., 2021	Clinical trial	United Kingdom	10	45.4 ± 11.9	2	VTA	Headache	DBS-P	VTA	16.0 ± 7.1	CH-QoL Pain	0.7175929249	1.254192968	11.8	1	3b
Kashanian et al., 2020	Case series	United States	9	57 ± 15.5	4	VPM, PVG	Facial Pain	DBS-P		6.8 ± 6	VAS	1.965795847	1.780449381	33	3.36 ± 4.4	4
Polanski et al., 2019	RCT	Germany	3	59.7 ± 3.9	1	PLIC, VPL, PVG	Chronic pain after brachial plexus injury	DBS-P		29 ± 9.9	NRS	4.880361175	0.6147086031	59.1	1	1b
Levi et al., 2019	Clinical trial	Italy	5	55.8 ± 8.96	1	Dorsal ACC	Thalamic pain syndrome (TPS)	DBS-P	ACC	5 ± 1.58	NRS	3.409584548	0.9385307667	35	1.5	3b
Cappon et al., 2019	Case series	United Kingdom	18	46.73	3	VTA	Chronic cluster headache	DBS-P	VTA	2	MPQ	−0.3593330256	11.74398037	−9.16	1.17 ± 0.38	4
Ben-Haim et al., 2018	Clinical trial	United States	7	55.1 ± 9.25	3	VPM, PAG	Neuropathic facial pain	DBS-P		14.4 ± 9.75	VAS	5.734172473	1.116115713	70	1	3b
Holland et al., 2018	Case report	United States	1	60	1	VC/VS, GPi	Entral post-stroke pain	DBS-P		7	MPQ	0.7	0	70.59	1	4
Abreu et al., 2017, 2022	Prospective	Portugal	16	53 ± 9.1	2	VPN thalamus	Neuropathic pain due to traumas	DBS-P		20.2 ± 2.8	VAS	3.106610192	1.36805062	53.1	3	1b
Lempka et al., 2017	RCT	United States	10	51.3 ± 4.75	4	VS/ALIC	Post-stroke pain	DBS-P		4.7 ± 2	VAS	−1.400619157	4.540848931	3.4	2	1b
Boccard et al., 2017	Clinical trial	United Kingdom	24	49.1 ± 11.2	5	ACC	Neuropathic Pain	DBS-P	ACC	NA	NRS	8.285651982	0.4706931945	47.56	3.2	3b
Kim et al., 2016	Clinical trial	United States	5	56 ± 14.8	3	VPN, VPL, PAG	Medically refractory pain	DBS-P		9.4 ± 9.5	NRS	16.90308509	0.2958039892	66.7	2.4 ± 0.96	3b
Rezaei Haddad et al., 2015	Case report	United States	1	50	0	VPL, VPM	body pain syndrome	DBS-P		7	OS	0.6	0	40	3.2	4

(Continued)

10.3389/fnhum.2023.1297894

TABLE 1 (Continued)

References	Study design	Country	Number of patients	Age (mean ± SD)	Sex-female (No)	DBS location	Pain	DBS-indication	DBS nucleus target subgroup	Pain duration	The pain scale used	Pain score improvement		Pain Reduction (%)	Follow-up duration (years)	Quality assessment
												Effect size	SD (effect size)			
For pain																
Son et al., 2014	Clinical trial	Republic of Korea	9	49.3 ± 10.75	3	contralateral VC thalamus	Chronic intractable neuropathic pain	DBS-P		8.1 ± 12.2	NRS	3.237075006	0.926762585	37.5	3.2 ± 1.9	3b
Gray et al., 2014	Prospective	United Kingdom	18	50.42 ± 10.37	4	PVG/PAG, ST	Neuropathic pain	DBS-P	PVG and PAG	7.25 ± 4.16	MPQ	1.296240837	10.41473129	42.267	0.5	1b
Pereira et al., 2013	Clinical trial	Portugal	12	53 ± 10	2	VPL	Neuropathic pain	DBS-P	VPL	20 ± 13	VAS	2.087614349	2.299275248	52.7	1	3b
Boccard et al., 2013	prospective cohort	United States	85	52.1 ± 13.3	25	PVG, VPL/VPM	Neuropathic pain	DBS-P		2	VAS	2.418052643	1.488801334	45.8	1.6	1b
Pereira et al., 2010	Clinical trial	United Kingdom	16	51 ± 14.3	3	PAG	Chronic neuropathic pain	DBS-P	PAG	9.44 ± 6.68	VAS	3.077891804	1.033174719	84	NA	3b
Owen et al., 2008	Clinical trial	United Kingdom	4	NA	NA	PVG and PAG	Chronic pain	DBS-P	PVG and PAG	NA	MPQ PRI	0.8809297784	18.67345208	53.5	NA	3b
Owen et al., 2007	Clinical trial	United Kingdom	34	50.4 ± 13	10	PVG, VPL/VPM	Neuropathic pain	DBS-P		NA	VAS	3.034738077	1.519076732	53.29	1.54 ± 0.9	3b
Pereira et al., 2007	Clinical trial	United Kingdom	3	52.7 ± 8.14	1	PVG and VPL	Chronic neuropathic pain	DBS-P	PVG and VPL	4.8	VAS	14.07232143	2.544001015	39.65	1	3b
Spooner et al., 2007	Case report	United States	1	40	0	PVG, cingulum	Neuropathic pain	DBS-P		12	VAS	19.79898987	0.1767766953	43.75	1	4
Owen et al., 2006	Clinical trial	United Kingdom	12	57.4 ± 10.8	3	PVG and VPL	Post-stroke pain	DBS-P	PVG and VPL	5.2	VAS	2.47042262	1.619156159	48.8	2.25	3b
Green et al., 2006	Prospective	United Kingdom	16	52	3	PAG	Chronic neuropathic pain	DBS-P	PAG	NA	MPQ	3.070536746	7.099735911	64.1	1	1b
Bittar et al., 2005b	Comparative Study	United Kingdom	3	55.67 ± 19.1	0	PVG, TS	Chronic neuropathic pain	DBS-P		NA	EUROQOL EQ-5D VAS	1.984143634	11.79350104	61.7	1.12 ± 0.25	2a
For other conditions																
Wang et al., 2020	Retrospective	China	23	41.13 ± 13.49	10	GPi	Cervical DYT	DBS-O	GPi	3.6 ± 4.5	TWSTRS pain	2.203138278	2.555445592	71.7	1.59 ± 1.4	2b
Perides et al., 2020; Krüger et al., 2021	Retrospective	United Kingdom	138	11.5 ± 4	69	GPi	Dystonic pain	DBS-O	GPi	11.5 ± 4	NPRS	2.821223801	1.772280525	68.5	1	2b

(Continued)

10.3389/fnhum.2023.1297894

TABLE 1 (Continued)

References	Study design	Country	Number of patients	Age (mean ± SD)	Sex-female (No)	DBS location	Pain	DBS-indication	DBS nucleus target subgroup	Pain duration	The pain scale used	Pain score improvement		Pain Reduction (%)	Follow-up duration (years)	Quality assessment
												Effect size	SD (effect size)			
For pain																
Perides et al., 2020; Krüger et al., 2021	Retrospective	United Kingdom	2	11.5 ± 5	69	STN	Dystonic pain	DBS-O	STN	11.5 ± 5	NPRS	2.431801915	2.056088519	68.5	1	2b
Gong et al., 2020	Retrospective	China	36	62.3 ± 10.4	9	STN	PD-Related Pain	DBS-O	STN	3.3 ± 3.4	NRS	4.465178791	0.7054588735	79 ± 27	8	2b
Gong et al., 2020	Retrospective	China	28	63.2 ± 9.1	15	GPi	PD-Related Pain	DBS-O	GPi	2.1 ± 1.7	NRS	4.435433621	0.7890998488	75 ± 27		2b
Kaelin-Lang et al., 2020	Prospective	Switzerland	5	39 ± 6.75	3	GPi	Cervical DYT	DBS-O	GPi	5 ± 1.25	TWSTRS pain score	0.2931841924	4.43407262	16.5	11.5 ± 0.7	1b
DiMarzio et al., 2018	Prospective	United States	18	63.8 ± 8.5	4	STN, GPi	PD pain	DBS-O		11.6 ± 1.02	KPDPS	5.330780047	2.645016278	54.7	0.5	1b
Fabbri et al., 2017	Cross-sectional study	Portugal	32	62.5 ± 13.3	13	STN	PD-related pain	DBS-O	STN	18.7 ± 5.1	VAS-p	0.3338166355	1.797393947	35.3	4.6 ± 1.3	3b
Cury et al., 2016	Clinical Trial	Brazil	37	59 ± 10.8	12	STN	PD-related pain	DBS-O	STN	15 ± 7.2	VAS	2.419615423	17.85820986	72.5	1	3b
Jung et al., 2015	Clinical Trial	Republic of Korea	24	59.1 ± 7.6	9	STN	PD-related pain	DBS-O	STN	18.0 ± 3.8	Ordinal scale from 0 to 1	0.899854933	1.555806329	22.58	8	3b
Sürücü et al., 2013	Retrospective	Switzerland	14	62.8 ± 5.69	6	STN	PD-related pain	DBS-O	STN	12.3 ± 3.82	Ordinal scale	2.304728268	2.451482059	65.9	1.3 ± 1	2b
Dellapina et al., 2012	RCT	France	8	65.1 ± 5.0	8	STN	PD-related pain	DBS-O	STN	12.4 ± 2.6	VAS	1.317009216	1.594521872	28	0.25	1b
Kim et al., 2012	Clinical Trial	Republic of Korea	21	58.3 ± 7.9	13	STN	PD-related pain	DBS-O	STN	10.6 ± 4.0	OS	1.424182765	1.123451315	23.53	2	3b
Oshima et al., 2012	Prospective	Japan	69	63.0 ± 7.8		STN	PD-related pain	DBS-O	STN	63.0 ± 7.8	VAS	3.90472786	1.075619134	80.77	1	1b
Cury et al., 2014	Clinical Trial	Brazil	44	60 ± 10.4	14	STN	PD-related pain	DBS-O	STN	6.52 ± 6.50	VAS	2.077258568	1.396070785	44.6		3b
Pellaprat et al., 2014	Prospective	France	58	60.3 ± 7.8	21	STN	PD-related pain	DBS-O	STN	12.3 ± 3.8	MPQ-QDSA	1.242343385	4.990568691	45	1	1b
Kim et al., 2008	Retrospective	Republic of Korea	29	59 ± 7.7	15	STN	PD-related pain	DBS-O	STN	9.9 ± 4.6	NPRS	1.021763182	1.174440439	19	0.25–0.5	2b
Witjas et al., 2007	Prospective	France	40	59 ± 8	10	STN	PD-related pain	DBS-O	STN	12.4 ± 4.5	NMF	3.866208623	0.3621118612	84.2	1	1b

10.3389/fnhum.2023.1297894

a 95% CI of [1.07; 1.86]. The estimated tau^2 for this subgroup is 0.5747, and the corresponding tau value is 0.7581. The *Q*-value for this subgroup is 137.18, with an I^2 value of 87.6%.

The test for subgroup differences within the random effects model yields a *Q*-value of 1.50 with 1 degree of freedom and a *p*-value of 0.2213, indicating no significant difference between the DBS-P and DBS-O subgroups. Overall, these results suggest a significant positive effect of DBS specifically targeting chronic pain (DBS-P) based on the random effects model. However, there is significant heterogeneity among the studies, and no significant difference is observed between the DBS-P and DBS-O subgroups **Figure 1**.

3.4 Risk of bias

These results indicate that the linear regression test did not find significant asymmetry in the funnel plot. The test result shows a *t*-value of 0.82 with 38 degrees of freedom, resulting in a *p*-value of 0.41, which is greater than the conventional threshold for statistical significance (usually 0.05). The sample estimates provide additional information. The estimated bias is 0.71, with a standard error of 0.87. The intercept is estimated to be 1.33, with a standard error of 0.30.

Furthermore, the details of the analysis reveal the multiplicative residual heterogeneity variance, tau^2, which is calculated to be 7.11. Overall, these results suggest that there is no significant funnel plot asymmetry, indicating that publication bias or other forms of bias may not be influencing the results of the study (**Supplementary Figure 2**).

3.5 Sensitivity analysis

The sensitivity analysis explored the influence of omitting individual studies on the results. Here are the key findings: When omitting Saway et al. (2023), the SMD remained significant and had a similar effect size as the pooled estimate. The *p*-value remained <0.0001, indicating a significant effect of DBS on chronic pain relief. The heterogeneity measures (tau^2, tau, I^2) also remained similar. Similarly, omitting Holland et al. (2018), Cappon et al. (2021), Krüger et al. (2021), and Abreu et al. (2022) did not substantially affect the overall results. The *p*-value remained <0.0001, and the effect sizes and heterogeneity measures remained consistent. Omitting other studies also showed similar patterns. The *p*-value remained <0.0001, and the effect sizes (SMD) and heterogeneity measures (tau^2, tau, I^2) were relatively stable. The pooled estimate, representing the overall effect of DBS on chronic pain relief, remained statistically significant with a *p*-value <0.0001. The SMD, 95% CI, and heterogeneity measures (tau^2, tau, I^2) were consistent with the original analysis. Overall, the sensitivity analysis suggests that the findings of the study are robust. Omitting individual studies did not significantly alter the overall results or conclusions regarding the effectiveness of DBS for chronic pain relief (**Supplementary Figure 3**).

4 Subgroup analysis

4.1 Study designs

The subgroup analysis of DBS specifically targeting chronic pain (DBS-P) revealed different subgroups based on study design. Among the subgroups, the observational studies-P subgroup (2 studies) showed an SMD of 0.71 with a 95% CI of [−1.24; 2.67], indicating a moderate effect size. The cohort-P subgroup (6 studies) demonstrated a higher SMD of 1.9087 with a narrower CI of [1.18; 2.63]. The RCT-P subgroup (2 studies) displayed a lower SMD of 0.92 with a wide CI of [−3.45; 5.29], suggesting substantial heterogeneity. The non-RCT-P subgroup (12 studies) had the largest effect size of 2.3298 and a relatively narrow CI of [1.63; 3.02]. The cohort-O subgroup (12 studies) had an SMD of 1.74 and a CI of [1.24; 2.24]. The remaining subgroups, observational studies-O, non-RCT-O, RCT-O, and non-RCT, each had only one study, and their effect sizes ranged from 0.23 to 1.20. The tests for subgroup differences indicated significant heterogeneity among the subgroups ($Q = 33.41$, df = 8, $p < 0.0001$), suggesting that the effectiveness of DBS for chronic pain varied across different study designs (**Supplementary Figure 4**).

4.2 Pain diseases

The results suggest varying levels of evidence for the effectiveness of DBS across different pain subgroups. The subgroup of facial neuropathic pain (P) and traumatic pain (P) showed strong evidence for a significant effect, with SMDs of 2.85 (95% CI: 0.43 to 5.27) with a moderate tau^2 value of 2.35 and substantial heterogeneity (I2 = 75.8%), and 2.77 (95% CI: 1.05 to 4.48) with tau^2 = 1.55 and I^2 = 79.3%, respectively. The subgroup of chronic cluster headache (P) presented weak evidence, with an SMD of 0.0809 (95% CI: −0.64 to 0.80) with low heterogeneity (tau^2 = 0.1246, I^2 = 43.8%). The subgroups of post-stroke pain (P), dystonic pain (O), and PD-related pain (O) exhibited moderate evidence, with SMDs of 0.37 (95% CI: −2.31 to 3.07) with higher heterogeneity (tau^2 = 3.5450, I^2 = 93.7%), 1.33 (95% CI: 0.40 to 2.26) with tau^2 = 0.58 and I^2 = 79.9%, and 1.50 (95% CI: 1.05 to 1.94) with tau^2 = 0.62 and I^2 = 88.2%, respectively. The test for subgroup differences was statistically significant ($Q = 16.18$, df = 5, $p = 0.0063$), indicating that the effectiveness of DBS varies among different pain subgroups (**Supplementary Figure 5**).

4.3 Brain targets

Deep brain stimulation primary for treating chronic pain (DBS-P) analysis: The subgroup analysis revealed variations in the effect sizes of DBS targeting different brain nuclei for the treatment of chronic pain. The subgroup with the largest effect size was the ventral posterior lateral (VPL) thalamus, with an SMD of 2.74 (95% CI [0.70; 4.78]) with high heterogeneity (tau^2 = 1.86, I^2 = 85.7%), indicating a large treatment effect. The subgroups of anterior cingulate cortex (ACC) and PAG also showed significant effects, with SMDs of 2.98 (95% CI [1.90; 4.06]) with low heterogeneity (tau^2 = 0.2265, I^2 = 31.7%), and 2.08 (95% CI [1.46;

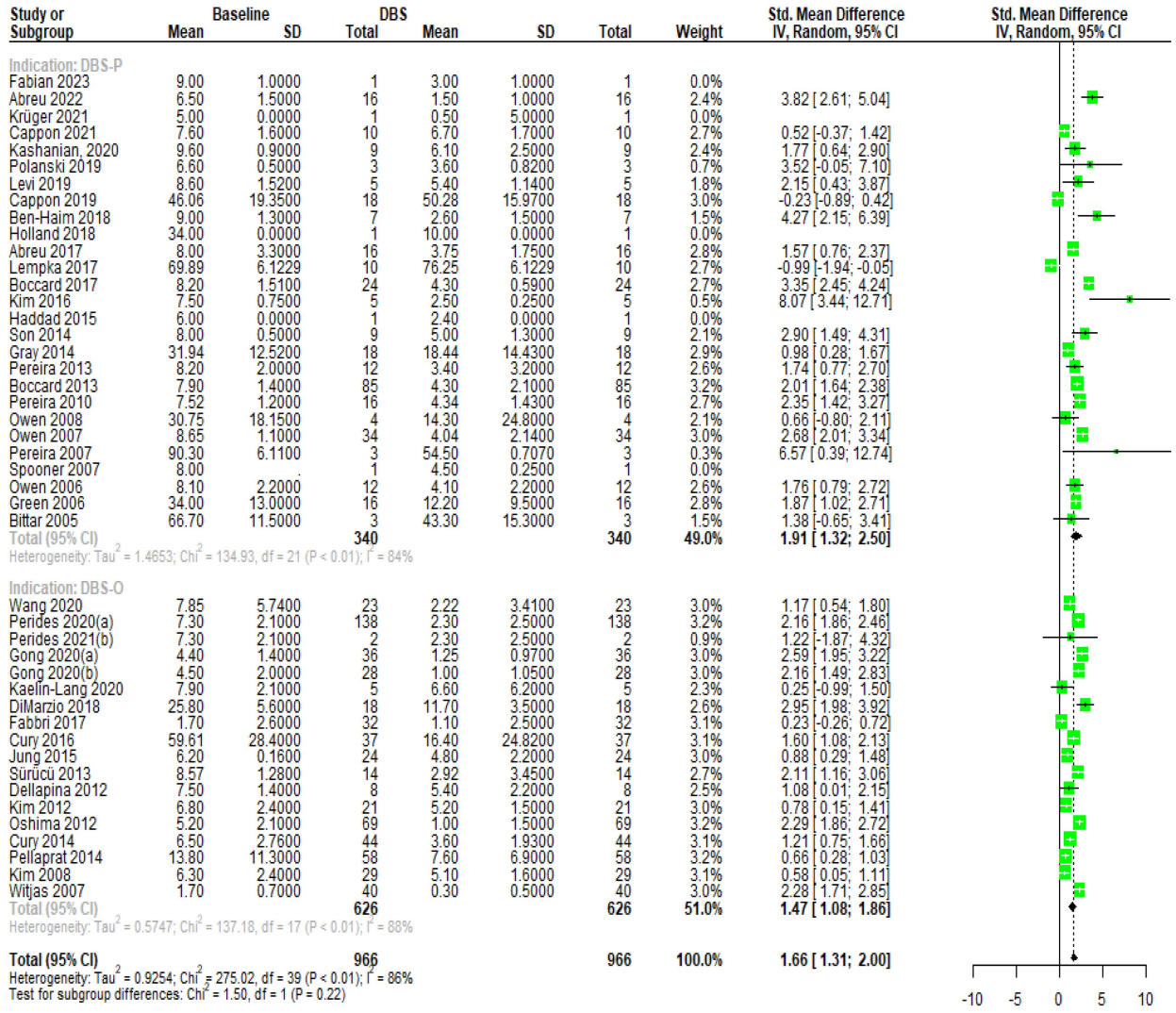

FIGURE 1
Forest plot, illustrating the significant effect of DBS on chronic pain and the substantial heterogeneity observed among the included studies.

2.71]) with no observed heterogeneity, respectively, suggesting moderate to large treatment effects. On the other hand, the ventral tegmental area (VTA) and periaqueductal/periventricular gray matter region (PVG and PAG) subgroups demonstrated small and non-significant effects, with SMDs of 0.0809 (95% CI [−0.64; 0.80]) with low heterogeneity (tau^2 = 0.12, I^2 = 43.8%) and 0.9176 (95% CI [0.29; 1.54]) with no observed heterogeneity, respectively. The subgroup of PVG and VPL had a wide confidence interval and substantial heterogeneity (tau^2 = 6.49, I^2 = 56.1%), making the treatment effect uncertain.

Deep brain stimulation for other indications (DBS-O) analysis: The globus pallidus internus (GPi) subgroup exhibited a moderate effect size (SMD = 1.56, 95% CI [0.77; 2.35]) with high heterogeneity (tau^2 = 0.51, I^2 = 80.3%). The largest subgroup, subthalamic nucleus (STN), demonstrated a moderate effect size (SMD = 1.3425, 95% CI [0.89; 1.78]) with high heterogeneity (tau^2 = 0.53, I^2 = 87.1%). The test for subgroup differences indicated significant heterogeneity between the subgroups (Q = 30.27, df = 7, p < 0.0001), suggesting that the treatment effects varied significantly among the different DBS nucleus target subgroups **Figure 2**.

4.4 Meta-regression analysis

4.4.1 Age meta-regression

The meta-regression analysis examined the relationship between age and the effectiveness of DBS for treating chronic pain. The analysis included three subgroups: overall (k = 42), DBS primary for treating chronic pain (DBS-P) (k = 24), and DBS for other indications (DBS-O) (k = 18), F (df1 = 1, df2 = 40) = 0.13, p-val = 0.71.

4.4.1.1 Overall analysis of age meta-regression

The test of moderators for age as a predictor was not significant (p = 0.71), suggesting that age did not significantly moderate the effectiveness of DBS for chronic pain. The estimated amount of residual heterogeneity (tau^2) was 23.45, indicating significant

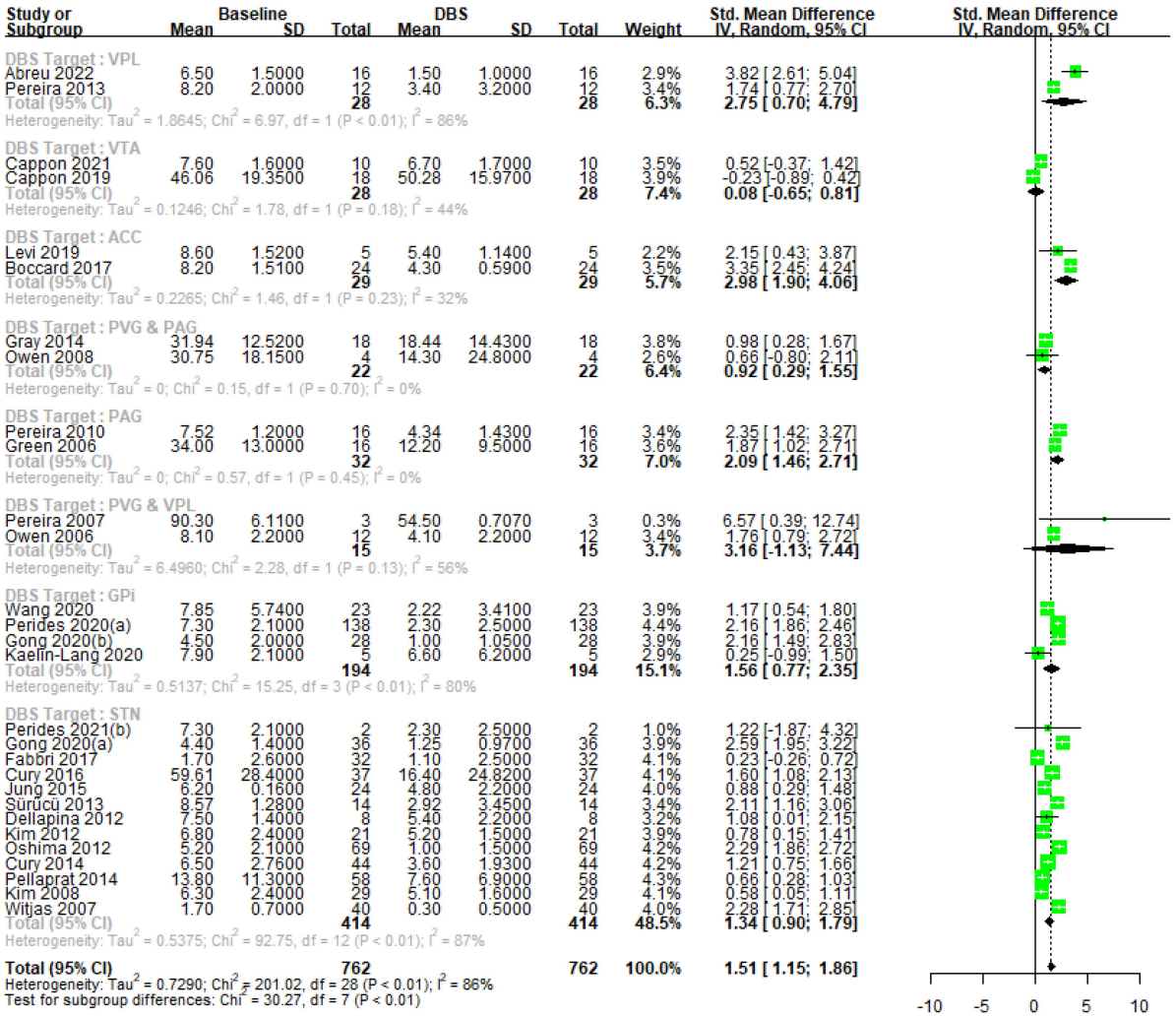

FIGURE 2
Deep brain stimulation (DBS) brain target nuclei subgroup analysis.

heterogeneity among the studies. The I^2 value was 99.78%, indicating that most of the variability in the effect sizes was due to heterogeneity. The test for residual heterogeneity was highly significant ($p < 0.0001$).

4.4.1.2 DBS primary for treating chronic pain (DBS-P) analysis

The test of moderators for age as a predictor was not significant F(df1 = 1, df2 = 22) = 1.1608, ($p = 0.29$), indicating that age did not significantly moderate the effectiveness of DBS-P for chronic pain The estimated amount of residual heterogeneity (tau^2) was 43.86, indicating considerable heterogeneity among the studies. The I^2 value was 99.81%, indicating a high proportion of variability in effect sizes due to heterogeneity. The test for residual heterogeneity was significant ($p < 0.0001$).

4.4.1.3 DBS for other indications (DBS-O) analysis

The test of moderators for age as a predictor was not significant F(df1 = 1, df2 = 16) = 0.04, ($p = 0.83$), indicating that age The estimated amount of residual heterogeneity (tau^2) was 1.46, indicating some residual heterogeneity among the studies. The I^2 value was 97.33%, suggesting a substantial proportion of variability in effect sizes due to heterogeneity. The test for residual heterogeneity was highly significant ($p < 0.0001$). did not significantly moderate the effectiveness of DBS-O for chronic pain **Figure 3**.

4.4.2 Pain duration meta-regression

The results of the meta-regression analyzing the effect of pain duration on DBS for treating chronic pain indicate limited evidence of a significant association. The overall analysis, including 37 studies, showed no significant relationship between pain duration and DBS effectiveness F (df1 = 1, df2 = 35) = 0.0028 ($p = 0.95$). The DBS primary subgroup analysis, comprising 19 studies, also found no significant association F(df1 = 1, df2 = 17) = 0.07 ($p = 0.79$), The DBS-O subgroup, consisting of 18 studies, demonstrated a weak but significant positive association between pain duration and DBS effectiveness ($p = 0.74$), F(df1 = 1, df2 = 16) = 0.10. However, it should be noted that the amount of heterogeneity accounted for was minimal across all analyses, indicating that pain duration explains only a small proportion of the variability in DBS outcomes for chronic pain **Figure 4**.

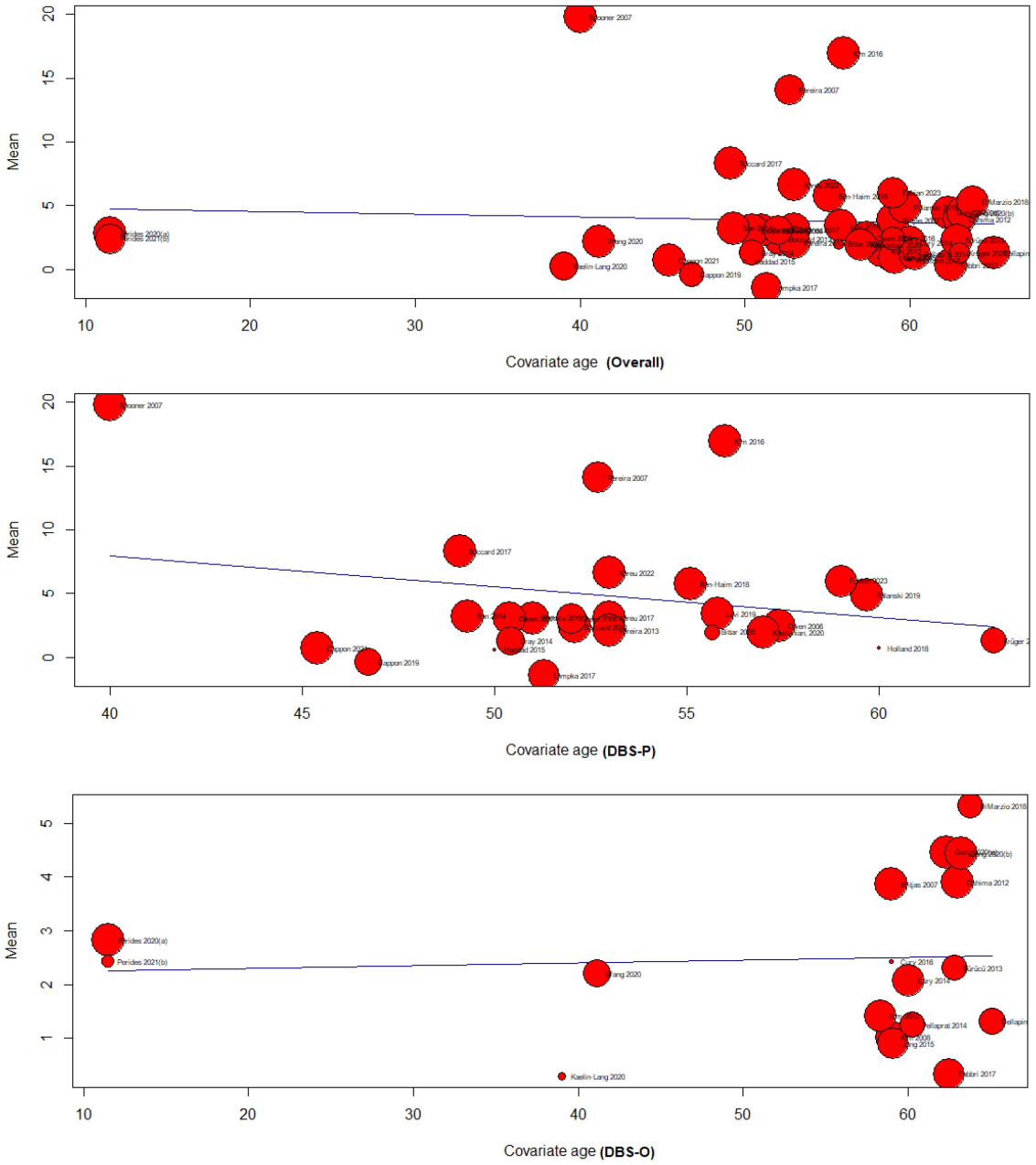

FIGURE 3
Age meta-regression analysis.

5 Discussion

5.1 Summary of findings

The current literature does not provide a clear consensus on the optimal use and effectiveness of DBS for chronic pain. This meta-analysis represents the first comprehensive investigation into the effects of DBS on chronic pain. To the best of our knowledge, no prior meta-analyses have examined the impact of DBS on chronic pain, whether it was utilized as a primary treatment modality or in conjunction with DBS for other medical conditions. The results revealed a significant effect of DBS-P on chronic pain, with SMD of 1.65 and a 95% CI of [1.31; 2.00]. However, notable heterogeneity among the studies was observed, as reflected by high I^2 values and significant *Q*-values. This heterogeneity can be attributed to the diverse brain targets selected for DBS application, as evident from the subgroup analysis based on brain target grouping.

Subgroup analyses based on study designs exhibited different effect sizes for DBS-P. Observational studies-P demonstrated a moderate effect size, while cohort-P and non-randomized controlled trials (non-RCT)-P subgroups showed larger effect sizes. The randomized controlled trials (RCT)-P subgroup exhibited substantial heterogeneity. The observed differences in effect sizes between RCTs and observational or cohort studies highlight the importance of study design in accurately capturing the effectiveness

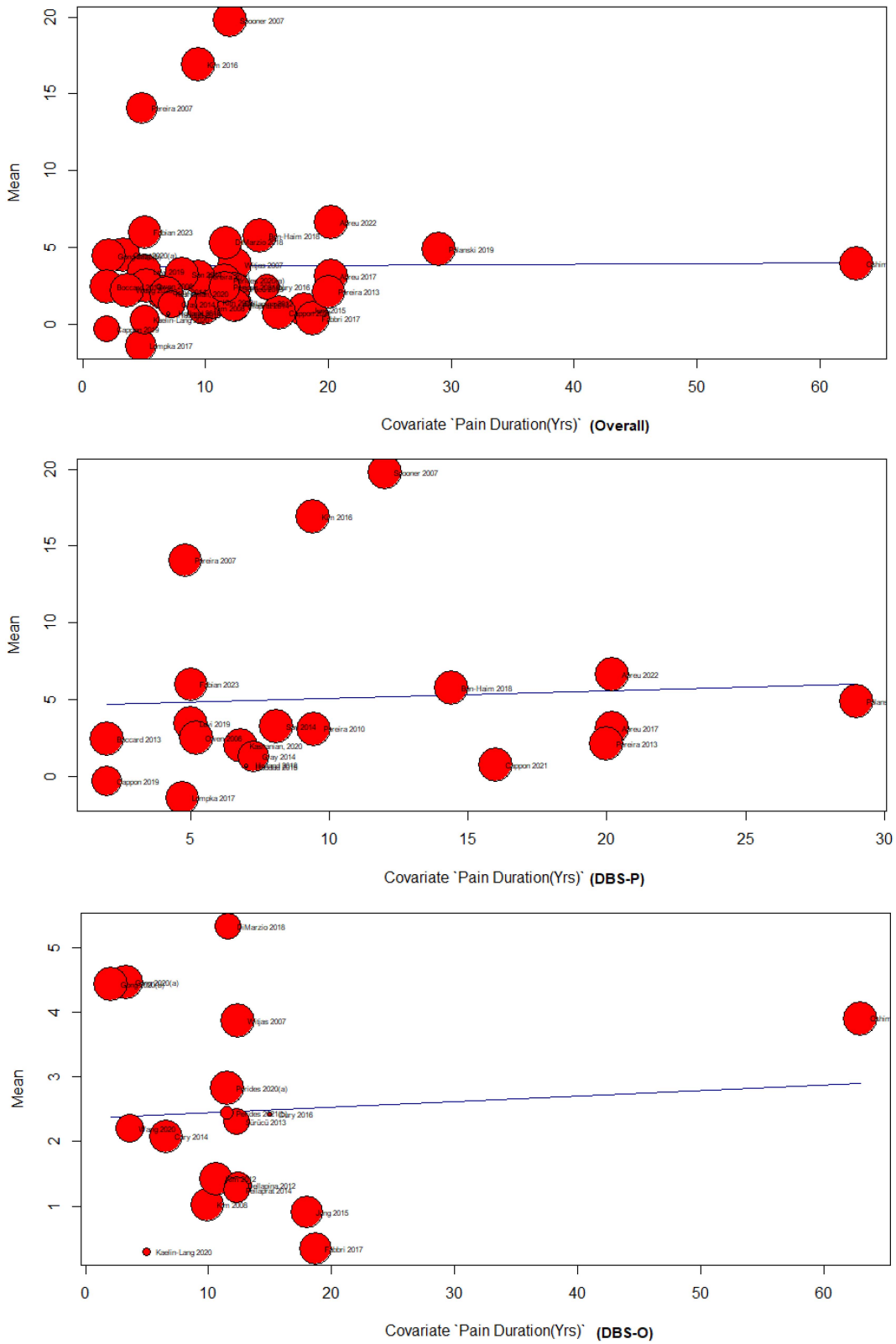

FIGURE 4
Pain duration meta-regression analysis.

of DBS for chronic pain. This suggests that the more rigorous design of RCTs may provide a more accurate representation of DBS effectiveness. The marked difference in effect sizes between RCTs and non-RCTs underscores the potential limitations of non-randomized studies in truly representing the effect. It is imperative for readers and clinicians to approach the findings of non-RCTs

with caution, bearing in mind the potential biases and confounders that might inflate or diminish the observed effects.

In the meta-regression analysis, the relationship between age and the effectiveness of DBS for chronic pain was explored. The results suggest that age is not a significant factor in determining the effectiveness of DBS for treating chronic pain in both DBS-P and DBS-O analyses. Also, the results show that DBS can be an effective treatment for some types of chronic pain that are resistant to other therapies. The meta-analysis also assessed the effectiveness of DBS across different pain subgroups. Facial neuropathic pain and traumatic pain showed strong evidence of a significant effect, while chronic cluster headache presented weak evidence. Post-stroke pain, dystonic pain, and PD-related pain demonstrated moderate evidence.

Regarding the meta-regression analyzing the effect of pain duration on DBS for chronic pain, limited evidence of a significant association was found. The overall analysis and the DBS-P subgroup analysis did not find a significant relationship, while the DBS-O subgroup showed a weak but significant positive association. Our study adds to the current literature complexity by revealing that pain duration may not reliably predict DBS outcomes. In our meta-regression analysis, we investigated the impact of pain duration on the effectiveness of DBS in treating chronic pain. However, the results indicate a scarcity of substantial evidence supporting a significant association between these variables. Both the overall analysis and the primary subgroup analysis focusing on DBS revealed no significant relationship between pain duration and DBS effectiveness ($p = 0.95$ and $p = 0.79$, respectively). Nonetheless, in the DBS-O subgroup analysis, we observed a weak but significant positive association between pain duration and DBS effectiveness ($p = 0.74$); however, this association only accounted for a small proportion of the variability in DBS outcomes.

The findings demonstrate that DBS applied to various brain nuclei has differing effects on chronic pain. Notably, the VPL, ACC, and PVG and PAG emerged as the most effective targets, exhibiting substantial or moderate treatment effects with significant SMD between the DBS and control groups. These targets are implicated in both the sensory-discriminative and affective components of pain perception (Frizon et al., 2020; Li et al., 2020). Conversely, the VTA and the combination of PVG and PAG displayed limited effectiveness, with small or non-significant effects. The VTA, being part of the reward system, may not directly contribute to pain modulation (Li et al., 2020). Furthermore, the combined stimulation of PVG and PAG may not be optimal due to the distinct roles these regions play in pain processing, potentially necessitating different stimulation parameters (Frizon et al., 2020). Regarding other targets, such as GPi, STN, and PVG and VPL combination, moderate effects were observed; however, high heterogeneity and wide confidence intervals indicate variability and uncertainty in treatment outcomes. These targets primarily participate in motor control and may exert indirect influences on pain by modulating movement disorders like dystonia (Rodrigues et al., 2019; Frizon et al., 2020; Fan et al., 2021).

DBS has been used for the treatment of chronic pain since the early 1970s, but it remains off-label in the United States and its indications are contested (Falowski, 2015). This technique has the capacity to modulate the activity of neural circuits associated with pain processing and perception (Falowski, 2015; Prosky et al., 2021; Alamri and Pereira, 2022). Although the precise mechanism underlying the pain-relieving effects of DBS remains incompletely understood, it is believed to involve various factors. These include the alteration of the balance between inhibitory and excitatory neurotransmitters within pain pathways, the reduction of activity in nociceptive signal-transmitting neurons, the enhancement of endogenous opioid systems responsible for mediating analgesia (Prosky et al., 2021; Alamri and Pereira, 2022), and the modification of emotional and cognitive aspects of pain such as anxiety, depression, and catastrophizing (Falowski, 2015; Prosky et al., 2021; Alamri and Pereira, 2022). The effects of DBS on chronic pain relief may vary depending on the specific brain target utilized. Some common targets include the sensory thalamus (ST), (ventral posterior lateral and ventral posterior medial), which is primarily associated with sensory-discriminative pain aspects such as location, intensity, and quality (Falowski, 2015; Prosky et al., 2021; Alamri and Pereira, 2022). the periaqueductal gray and periventricular gray matter, involved in descending pain modulation and endogenous opioid release; and the ACC, implicated in affective-motivational pain aspects such as unpleasantness, suffering, and coping (Falowski, 2015; Prosky et al., 2021; Alamri and Pereira, 2022).

5.2 Meta-analysis limitations

This meta-analysis represents the first comprehensive examination of deep brain stimulation (DBS) effectiveness in treating chronic pain. It encompasses various indications for DBS use, brain targets for stimulation, and potentially influential factors such as patient age and pain duration.

However, it is important to acknowledge the limitations of this study. Firstly, significant heterogeneity was observed among the included studies, as indicated by high I^2 values. This heterogeneity may arise from variations in patient characteristics, study designs, DBS techniques, and outcome measures employed across different studies. The presence of heterogeneity may restrict the generalizability of the findings and limit the ability to draw definitive conclusions. Secondly, due to ethical considerations, there was a lack of control group standardization. Implementing a sham or controlled procedure in patients who are already experiencing illness presents ethical challenges. As a result, it was not feasible to establish a standardized control group for comparison. This limitation needs to be taken into account when interpreting the study's results. Hence, the study emphasizes the need for additional research especially RCTs to improve treatment results and better understand the patient-specific factors linked to treatment response.

6 Conclusion

The meta-analysis reveals a significant positive effect of DBS in reducing chronic pain. Subgroup analysis indicates a larger effect size in the DBS-P group compared to DBS-O, with varying effects based on study design, showing the most substantial effect in the non-RCT-P subgroup. Age did not significantly moderate the effectiveness of DBS. Strong evidence supports DBS effectiveness

in facial neuropathic pain and traumatic pain subgroups, while weak evidence is found for chronic cluster headache. Pain duration did not significantly impact DBS effectiveness. VPL demonstrated the largest effect among different brain targets, with significant heterogeneity observed. These findings contribute valuable insights into DBS's utility for chronic pain, emphasizing the need for further research to optimize outcomes and identify patient-specific factors influencing treatment response.

Data availability statement

The original contributions presented in the study are included in the article/**Supplementary material**, further inquiries can be directed to the corresponding author.

Author contributions

NS: Conceptualization, Data curation, Formal analysis, Methodology, Writing – original draft, Writing – review and editing. AS: Writing – review and editing, AE: Data curation, Writing – review and editing. YB: Writing – review and editing. TZ: Writing – review and editing. BD: Writing – review and editing. JJ: Writing – review and editing. AG: Writing – review and editing. TA: Writing – review and editing. OF: Conceptualization, Funding acquisition, Investigation, Methodology, Supervision, Writing – original draft, Writing – review and editing.

Funding

The author(s) declare financial support was received for the research, authorship, and/or publication of this article. This study was funded by the Department of Neurosurgery and Brain Repair at the University of South Florida.

Conflict of interest

The authors declare that the research was conducted in the absence of any commercial or financial relationships that could be construed as a potential conflict of interest.

Publisher's note

Supplementary material

The Supplementary Material for this article can be found online at: https://www.frontiersin.org/articles/10.3389/fnhum.2023.1297894/full#supplementary-material

References

Abreu, V., Vaz, R., Chamadoira, C., Rebelo, V., Reis, C., Costa, F., et al. (2022). Thalamic deep brain stimulation for post-traumatic neuropathic limb pain: Efficacy at five years' follow-up and effective volume of activated brain tissue. *Neurochirurgie* 68, 52–60. doi: 10.1016/j.neuchi.2021.06.006

Abreu, V., Vaz, R., Rebelo, V., Rosas, M. J., Chamadoira, C., Gillies, M. J., et al. (2017). Thalamic deep brain stimulation for neuropathic pain: Efficacy at three years' follow-up. *Neuromodulation* 20, 504–513. doi: 10.1111/ner.12620

Alamri, A., and Pereira, E. (2022). Deep brain stimulation for chronic pain. *Neurosurg. Clin. N. Am.* 33, 311–321. doi: 10.1016/j.nec.2022.02.013

Ben-Haim, S., Mirzadeh, Z., and Rosenberg, W. (2018). Deep brain stimulation for intractable neuropathic facial pain. *Neurosurg. Focus* 45, E15. doi: 10.3171/2018.5.FOCUS18160

Bittar, R., Kar-Purkayastha, I., Owen, S., Bear, R., Green, A., Wang, S., et al. (2005a). Deep brain stimulation for pain relief: a meta-analysis. *J. Clin. Neurosci.* 12, 515–519. doi: 10.1016/j.jocn.2004.10.005

Bittar, R., Otero, S., Carter, H., and Aziz, T. (2005b). Deep brain stimulation for phantom limb pain. *J. Clin. Neurosci.* 12, 399–404. doi: 10.1016/j.jocn.2004.07.013

Boccard, S., Pereira, E., Moir, L., Aziz, T., and Green, A. (2013). Long-term outcomes of deep brain stimulation for neuropathic pain. *Neurosurgery* 72, 221–230. doi: 10.1227/NEU.0b013e31827b97d6

Boccard, S., Prangnell, S., Pycroft, L., Cheeran, B., Moir, L., Pereira, E., et al. (2017). Long-term results of deep brain stimulation of the anterior cingulate cortex for neuropathic pain. *World Neurosurg.* 106, 625–637. doi: 10.1016/j.wneu.2017.06.173

Cappon, D., Ryterska, A., Lagrata, S., Miller, S., Akram, H., Hyam, J., et al. (2019). Ventral tegmental area deep brain stimulation for chronic cluster headache: Effects on cognition, mood, pain report behaviour and quality of life. *Cephalalgia* 39, 1099–1110. doi: 10.1177/0333102419839957

Cappon, D., Ryterska, A., Akram, H., Lagrata, S., Cheema, S., Hyam, J., et al. (2021). The sensitivity to change of the cluster headache quality of life scale assessed before and after deep brain stimulation of the ventral tegmental area. *J. Headache Pain* 22:52. doi: 10.1186/s10194-021-01251-5

Chiesa, A., and Serretti, A. (2011). Mindfulness-Based Interventions for Chronic Pain: A Systematic Review of the Evidence. *J. Altern. Complement. Med.* 17, 83–93. doi: 10.1089/acm.2009.0546

Chou, R., Turner, J., Devine, E., Hansen, R., Sullivan, S., Blazina, I., et al. (2015). The Effectiveness and Risks of Long-Term Opioid Therapy for Chronic Pain: A Systematic Review for a National Institutes of Health Pathways to Prevention Workshop. *Ann. Intern. Med.* 162, 276–286. doi: 10.7326/M14-2559

Cruccu, G., Aziz, T., Garcia-Larrea, L., Hansson, P., Jensen, T., Lefaucheur, J., et al. (2007). EFNS guidelines on neurostimulation therapy for neuropathic pain. *Eur. J. Neurol.* 14, 952–970. doi: 10.1111/j.1468-1331.2007.01916.x

Cury, R., Galhardoni, R., Fonoff, E., Dos Santos Ghilardi, M., Fonoff, F., and Arnaut, D. (2014). Effects of deep brain stimulation on pain and other nonmotor symptoms in Parkinson disease. *Neurology* 83, 1403–1409. doi: 10.1212/WNL.0000000000000887

Cury, R., Galhardoni, R., Teixeira, M., Dos Santos Ghilardi, M., Silva, V., and Myczkowski, M. (2016). Subthalamic deep brain stimulation modulates conscious perception of sensory function in Parkinson's disease. *Pain* 157, 2758–2765. doi: 10.1097/j.pain.0000000000000697

Dellapina, E., Ory-Magne, F., Regragui, W., Thalamas, C., Lazorthes, Y., Rascol, O., et al. (2012). Effect of subthalamic deep brain stimulation on pain in Parkinson's disease. *Pain* 153, 2267–2273. doi: 10.1016/j.pain.2012.07.026

DiMarzio, M., Pilitsis, J. G., Gee, L., Peng, S., Prusik, J., Durphy, J., et al. (2018). King's Parkinson's disease pain scale for assessment of pain relief following deep brain stimulation for Parkinson's disease. *Neuromodulation* 21, 617–622. doi: 10.1111/ner.12778

Egger, M., Smith, G., Schneider, M., and Minder, C. (1997). Bias in meta-analysis detected by a simple, graphical test. *BMJ* 315, 629–634. doi: 10.1136/bmj.315.7109.629

Fabbri, M., Coelho, M., Guedes, L., Rosa, M., Abreu, D., Gonçalves, N., et al. (2017). Acute response of non-motor symptoms to subthalamic deep brain stimulation in Parkinson's disease. *Parkinsonism Relat. Disord.* 41, 113–117. doi: 10.1016/j.parkreldis.2017.05.003

Falowski, S. (2015). Deep brain stimulation for chronic pain. *Curr. Pain Headache Rep.* 19:27. doi: 10.1007/s11916-015-0504-1

Fan, H., Zheng, Z., Yin, Z., Zhang, J., and Lu, G. (2021). Deep Brain Stimulation Treating Dystonia: A Systematic Review of Targets, Body Distributions and Etiology Classifications. *Front. Hum. Neurosci.* 15:757579. doi: 10.3389/fnhum.2021.757579

Flouty, O., Yamamoto, K., Germann, J., Harmsen, I., Jung, H., Cheyuo, C., et al. (2022). Idiopathic Parkinson's disease and chronic pain in the era of deep brain stimulation: a systematic review and meta-analysis. *J. Neurosurg.* 137, 1821–1830. doi: 10.3171/2022.2.JNS212561

Frizon, L., Yamamoto, E., Nagel, S., Simonson, M., Hogue, O., and Machado, A. (2020). Deep brain stimulation for pain in the modern era: A systematic review. *Neurosurgery* 86, 191–202. doi: 10.1093/neuros/nyy552

Gong, S., Xu, M., Tao, Y., Jin, H., Liu, Y., Sun, X., et al. (2020). Comparison of subthalamic nucleus and Globus *Pallidus internus* deep brain stimulation surgery on Parkinson disease-related pain. *World Neurosurg.* 135, e94–e99. doi: 10.1016/j.wneu.2019.11.026

Gray, A., Pounds-Cornish, E., Eccles, F., Aziz, T., Green, A., and Scott, R. (2014). Deep brain stimulation as a treatment for neuropathic pain: a longitudinal study addressing neuropsychological outcomes. *J. Pain* 15, 283–292. doi: 10.1016/j.jpain.2013.11.003

Green, A., Wang, S., Owen, S., Xie, K., Bittar, R., Stein, J., et al. (2006). Stimulating the human midbrain to reveal the link between pain and blood pressure. *Pain* 124, 349–359. doi: 10.1016/j.pain.2006.05.005

Hamani, C., Schwalb, J., Rezai, A., Dostrovsky, J., Davis, K., and Lozano, A. (2006). Deep brain stimulation for chronic neuropathic pain: long-term outcome and the incidence of insertional effect. *Pain* 125, 188–196. doi: 10.1016/j.pain.2006.05.019

Higgins, J., Thomas, J., Chandler, J., Cumpston, M., Li, T., Page, M., et al. (2023). *Cochrane Handbook for Systematic Reviews of Interventions version 6.4*. Hoboken, NJ: Cochrane.

Holland, M., Zanaty, M., Li, L., Thomsen, T., Beeghly, J., Greenlee, J., et al. (2018). Successful deep brain stimulation for central post-stroke pain and dystonia in a single operation. *J. Clin. Neurosci.* 50, 190–193. doi: 10.1016/j.jocn.2018.01.036

Institute of Medicine (US) Committee on Advancing Pain Research, Care, and Education (2011). *Relieving Pain in America: A Blueprint for Transforming Prevention, Care, Education, and Research*. Washington (DC): National Academies Press (US).

Jung, Y., Kim, H., Jeon, B., Park, H., Lee, W., and Paek, S. (2015). An 8-year follow-up on the effect of subthalamic nucleus deep brain stimulation on pain in Parkinson Disease. *JAMA Neurol.* 72, 504–510. doi: 10.1001/jamaneurol.2015.8

Kaelin-Lang, A., You, H., Burgunder, J., Lönnfors-Weitze, T., Loher, T., Taub, E., et al. (2020). Bilateral pallidal stimulation improves cervical dystonia for more than a decade. *Parkinsonism Relat. Disord.* 81, 78–81. doi: 10.1016/j.parkreldis.2020.10.028

Karra, R., Holten-Rossing, S., Mohammed, D., Parmeggiani, L., Heine, M., and Namnun, O. (2021). Unmet needs in the management of functional impairment in patients with chronic pain: A multinational survey. *Pain Manag.* 11, 303–314. doi: 10.2217/pmt-2020-0098

Kashanian, A., DiCesare, J., Rohatgi, P., Albano, L., Krahl, S., Bari, A., et al. (2020). Case series: Deep brain stimulation for facial pain. *Oper. Neurosurg.* 19, 510–517. doi: 10.1093/ons/opaa170

Kim, H., Jeon, B., Lee, J., Paek, S., and Kim, D. (2012). The benefit of subthalamic deep brain stimulation for pain in Parkinson disease: a 2-year follow-up study. *Neurosurgery* 70, 18–23. doi: 10.1227/NEU.0b013e3182266664

Kim, H., Paek, S., Kim, J., Lee, J., Lim, Y., Kim, M., et al. (2008). Chronic subthalamic deep brain stimulation improves pain in Parkinson disease. *J. Neurol.* 255, 1889–1894. doi: 10.1007/s00415-009-0908-0

Kim, W., Chivukula, S., Hauptman, J., and Pouratian, N. (2016). Diffusion tensor imaging-based thalamic segmentation in deep brain stimulation for chronic pain conditions. *Stereotact. Funct. Neurosurg.* 94, 225–234. doi: 10.1159/000448079

Krüger, M., Avecillas-Chasin, J., Heran, M., Naseri, Y., Sandhu, M., Polyhronopoulos, N., et al. (2021). Directional Deep Brain Stimulation Can Target the Thalamic "Sweet Spot" for Improving Neuropathic Dental Pain. *Oper. Neurosurg.* 21, 81–86. doi: 10.1093/ons/opab136

Leadley, R., Armstrong, N., Lee, Y., Allen, A., and Kleijnen, J. (2012). Chronic diseases in the European Union: The prevalence and health cost implications of chronic pain. *J. Pain Palliat. Care Pharmacother.* 26, 310–325. doi: 10.3109/15360288.2012.736933

Lee, K., Zhang, J., Nga, V., Ng, C., Tai, B., Higgins, J., et al. (2022). Tenets for the proper conduct and use of meta-analyses: A practical guide for neurosurgeons. *World Neurosurg.* 161, 291–302.e1. doi: 10.1016/j.wneu.2021.09.034

Lempka, S., Malone, D., Hu, B., Baker, K., Wyant, A., Ozinga, J., et al. (2017). Randomized clinical trial of deep brain stimulation for poststroke pain. *Ann. Neurol.* 81, 653–663. doi: 10.1002/ana.24927

Levi, V., Cordella, R., D'Ammando, A., Tringali, G., Dones, I., Messina, G., et al. (2019). Dorsal anterior cingulate cortex (ACC) deep brain stimulation (DBS): a promising surgical option for the treatment of refractory thalamic pain syndrome (TPS). *Acta Neurochir.* 161, 1579–1588. doi: 10.1007/s00701-019-03975-5

Li, N., Baldermann, J., Kibleur, A., Treu, S., Akram, H., Elias, G., et al. (2020). A unified connectomic target for deep brain stimulation in obsessive-compulsive disorder. *Nat. Commun.*11, 1–12. doi: 10.1038/s41467-020-16734-3

Marx, R., Wilson, S., and Swiontkowski, M. (2015). Updating the assignment of levels of evidence. *J. Bone Joint Surg. Am.* 97, 1–3. doi: 10.2106/JBJS.N.01112

National Institute for Health and Clinical Excellence (2010). *Reducing the Risk of Venous Thromboembolism (Deep Vein Thrombosis and Pulmonary Embolism) in Patients Admitted to Hospital (CG 92)*. London: National Institute for Health and Clinical Excellence.

Oshima, H., Katayama, Y., Morishita, T., Sumi, K., Otaka, T., Kobayashi, K., et al. (2012). Subthalamic nucleus stimulation for attenuation of pain related to Parkinson disease. *J. Neurosurg.* 116, 99–106. doi: 10.3171/2011.7.JNS11158

Owen, S., Green, A., Nandi, D., Bittar, R., Wang, S., and Aziz, T. (2007). Deep brain stimulation for neuropathic pain. *Acta Neurochir. Suppl.* 97, 111–116. doi: 10.1007/978-3-211-33081-4_13

Owen, S. L., Green, A. L., Stein, J. F., and Aziz, T. Z. (2006). Deep brain stimulation for the alleviation of post-stroke neuropathic pain. *Pain* 120, 202–206. doi: 10.1016/j.pain.2005.09.035

Owen, S., Heath, J., Kringelbach, M., Green, A., Pereira, E., Jenkinson, N., et al. (2008). Pre-operative DTI and probabilisitic tractography in four patients with deep brain stimulation for chronic pain. *J. Clin. Neurosci.* 15, 801–805. doi: 10.1016/j.jocn.2007.06.010

Page, M., McKenzie, J., Bossuyt, P., Boutron, I., Hoffmann, T., Mulrow, C., et al. (2021). The PRISMA 2020 statement: an updated guideline for reporting systematic reviews. *BMJ* 372, n71. doi: 10.1136/bmj.n71

Pellaprat, J., Ory-Magne, F., Canivet, C., Simonetta-Moreau, M., Lotterie, J., Radji, F., et al. (2014). Deep brain stimulation of the subthalamic nucleus improves pain in Parkinson's disease. *Parkinsonism Relat. Disord.* 20, 662–664. doi: 10.1016/j.parkreldis.2014.03.011

Pereira, E., Boccard, S., Linhares, P., Chamadoira, C., Rosas, M., Abreu, P., et al. (2013). Thalamic deep brain stimulation for neuropathic pain after amputation or brachial plexus avulsion. *Neurosurg. Focus* 35, E7. doi: 10.3171/2013.7.FOCUS1346

Pereira, E., Green, A., Bradley, K., Soper, N., Moir, L., Stein, J., et al. (2007). Regional cerebral perfusion differences between periventricular grey, thalamic and dual target deep brain stimulation for chronic neuropathic pain. *Stereotact. Funct. Neurosurg.* 85, 175–183. doi: 10.1159/000101296

Pereira, E., Lu, G., Wang, S., Schweder, P., Hyam, J., Stein, J., et al. (2010). Ventral periaqueductal grey stimulation alters heart rate variability in humans with chronic pain. *Exp. Neurol.* 223, 574–581. doi: 10.1016/j.expneurol.2010.02.004

Perides, S., Lin, J. P., Lee, G., Gimeno, H., Lumsden, D., Ashkan, K., et al. (2020). Deep brain stimulation reduces pain in children with dystonia, including in dyskinetic cerebral palsy. *Dev. Med. Child. Neurol.* 62, 917–925. doi: 10.1111/dmcn.14555

Polanski, W., Zolal, A., Klein, J., Kitzler, H., Schackert, G., Eisner, W., et al. (2019). Somatosensory functional MRI tractography for individualized targeting of deep brain stimulation in patients with chronic pain after brachial plexus injury. *Acta Neurochir.* 161, 2485–2490. doi: 10.1007/s00701-019-04065-2

Prosky, J., Cagle, J., Sellers, K., Gilron, R., de Hemptinne, C., Schmitgen, A., et al. (2021). Practical closed-loop strategies for deep brain stimulation: Lessons from chronic pain. *Front. Neurosci.* 15:762097. doi: 10.3389/fnins.2021.762097

Rezaei Haddad, A., Ughratdar, I., and Ashkan, K. (2015). A single thalamic target for deep brain stimulation to treat hemi-body pain syndrome. *Acta Neurochir.* 157, 1519–1523. doi: 10.1007/s00701-015-2504-7

Rodrigues, F., Duarte, G., Prescott, D., Ferreira, J., and Costa, J. (2019). Deep brain stimulation for dystonia. *Cochrane Database Syst. Rev.* 2019:CD012405. doi: 10.1002/14651858.CD012405.pub2

Saway, B. F., Webb, T., Weber, A., Triano, M., Barley, J., Spampinato, M., et al. (2023). Functional MRI'guided motor cortex and deep brain stimulation for intractable facial pain: A novel, personalized approach in 1 patient. *Oper. Neurosurg.* 24, 103–110. doi: 10.1227/ons.0000000000000440

Son, B., Kim, D., Kim, H., and Lee, S. (2014). Simultaneous trial of deep brain and motor cortex stimulation in chronic intractable neuropathic pain. *Stereotact. Funct. Neurosurg.* 92, 218–226. doi: 10.1159/000362933

Spooner, J., Yu, H., Kao, C., Sillay, K., and Konrad, P. (2007). Neuromodulation of the cingulum for neuropathic pain after spinal cord injury. *Case report. J. Neurosurg.* 107, 169–172. doi: 10.3171/JNS-07/07/0169

Sürücü, O., Baumann-Vogel, H., Uhl, M., Imbach, L., and Baumann, C. (2013). Subthalamic deep brain stimulation versus best medical therapy for L-dopa responsive pain in Parkinson's disease. *Pain* 154, 1477–1479. doi: 10.1016/j.pain.2013.03.008

Tan, H., Yamamoto, E., Elkholy, M., and Raslan, A. (2023). Treating chronic pain with deep brain stimulation. *Curr. Pain Headache Rep.* 27, 11–17. doi: 10.1007/s11916-022-01099-7

Wang, X., Mao, Z., Ling, Z., and Yu, X. (2020). Predictive factors for outcome of pallidal deep brain stimulation in cervical dystonia. *Clin. Neurol. Neurosurg.* 192:105720. doi: 10.1016/j.clineuro.2020.105720

Witjas, T., Kaphan, E., Régis, J., Jouve, E., Chérif, A., Péragut, J., et al. (2007). Effects of chronic subthalamic stimulation on nonmotor fluctuations in Parkinson's disease. *Mov. Disord.* 22, 1729–1734. doi: 10.1002/mds.21602

frontiers | Frontiers in Neuroscience

TYPE Original Research
PUBLISHED 11 December 2023
DOI 10.3389/fnins.2023.1303014

OPEN ACCESS

EDITED BY
Mark H. Myers,
University of Tennessee Health Science Center (UTHSC), United States

REVIEWED BY
Wenxuan Jiang,
University of Southern California, United States
Huijing Xu,
University of Southern California, United States

*CORRESPONDENCE
Tsung-Hsun Hsieh
✉ hsiehth@mail.cgu.edu.tw

RECEIVED 27 September 2023
ACCEPTED 24 November 2023
PUBLISHED 11 December 2023

CITATION
Nguyen TXD, Kuo C-W, Peng C-W, Liu H-L, Chang M-Y and Hsieh T-H (2023) Transcranial burst electrical stimulation contributes to neuromodulatory effects in the rat motor cortex.
Front. Neurosci. 17:1303014.
doi: 10.3389/fnins.2023.1303014

Transcranial burst electrical stimulation contributes to neuromodulatory effects in the rat motor cortex

Thi Xuan Dieu Nguyen[1], Chi-Wei Kuo[1], Chih-Wei Peng[2], Hao-Li Liu[3], Ming-Yuan Chang[4] and Tsung-Hsun Hsieh[1,5,6]*

[1]School of Physical Therapy and Graduate Institute of Rehabilitation Science, Chang Gung University, Taoyuan, Taiwan, [2]School of Biomedical Engineering, College of Biomedical Engineering, Taipei Medical University, Taipei, Taiwan, [3]Department of Electrical Engineering, National Taiwan University, Taipei, Taiwan, [4]Division of Neurosurgery, Department of Surgery, Min-Sheng General Hospital, Taoyuan, Taiwan, [5]Healthy Aging Research Center, Chang Gung University, Taoyuan, Taiwan, [6]Neuroscience Research Center, Chang Gung Memorial Hospital, Taoyuan, Taiwan

Background and objective: Transcranial Burst Electrical Stimulation (tBES) is an innovative non-invasive brain stimulation technique that combines direct current (DC) and theta burst stimulation (TBS) for brain neuromodulation. It has been suggested that the tBES protocol may efficiently induce neuroplasticity. However, few studies have systematically tested neuromodulatory effects and underlying neurophysiological mechanisms by manipulating the polarity of DC and TBS patterns. This study aimed to develop the platform and assess neuromodulatory effects and neuronal activity changes following tBES.

Methods: Five groups of rats were exposed to anodal DC combined with intermittent TBS (tBES+), cathodal DC combined with continuous TBS (tBES–), anodal and cathodal transcranial direct current stimulation (tDCS+ and tDCS–), and sham groups. The neuromodulatory effects of each stimulation on motor cortical excitability were analyzed by motor-evoked potentials (MEPs) changes. We also investigated the effects of tBES on both excitatory and inhibitory neural biomarkers. We specifically examined c-Fos and glutamic acid decarboxylase (GAD-65) using immunohistochemistry staining techniques. Additionally, we evaluated the safety of tBES by analyzing glial fibrillary acidic protein (GFAP) expression.

Results: Our findings demonstrated significant impacts of tBES on motor cortical excitability up to 30 min post-stimulation. Specifically, MEPs significantly increased after tBES (+) compared to pre-stimulation ($p = 0.026$) and sham condition ($p = 0.025$). Conversely, tBES (–) led to a notable decrease in MEPs relative to baseline ($p = 0.04$) and sham condition ($p = 0.048$). Although tBES showed a more favorable neuromodulatory effect than tDCS, statistical analysis revealed no significant differences between these two groups ($p > 0.05$). Additionally, tBES (+) exhibited a significant activation of excitatory neurons, indicated by increased c-Fos expression ($p < 0.05$), and a reduction in GAD-65 density ($p < 0.05$). tBES (–) promoted GAD-65 expression ($p < 0.05$) while inhibiting c-Fos activation ($p < 0.05$), suggesting the involvement of cortical inhibition with tBES (–). The expression of GFAP showed no significant difference between tBES and sham conditions ($p > 0.05$), indicating that tBES did not induce neural injury in the stimulated regions.

Conclusion: Our study indicates that tBES effectively modulates motor cortical excitability. This research significantly contributes to a better understanding of

the neuromodulatory effects of tBES, and could provide valuable evidence for its potential clinical applications in treating neurological disorders.

KEYWORDS

transcranial burst electrical stimulation, neuromodulation, motor evoked potential, neuroplasticity, rats

1 Introduction

In recent decades, there has been a growing interest in non-invasive brain stimulation (NIBS) techniques that have demonstrated the ability to modify brain activity and modulate cortical plasticity. These techniques can be employed individually or in conjunction with other rehabilitative therapies to enhance training effectiveness (Schulz et al., 2013; Cirillo et al., 2017; Polanía et al., 2018; Sanches et al., 2020; Grippe et al., 2022). Currently, available NIBS methods include repetitive transcranial magnetic stimulation (rTMS), transcranial direct current stimulation (tDCS), transcranial alternating current stimulation (tACS), random noise stimulation (tRNS), and transcranial ultrasound stimulation (TUS; Terranova et al., 2018; Bhattacharya et al., 2022). Nevertheless, among these techniques, rTMS and tDCS remain the most frequently used in clinical settings for the treatment of neurological diseases and disorders. These NIBS have received substantial research support and have yielded positive results, such as reducing sleep disturbances in neurological and neuropsychiatric conditions, enhancing cognitive functions in Alzheimer's disease, aiding in the recovery of upper and lower limb functions in stroke patients, and improving both motor and non-motor symptoms in patients with Parkinson's disease, among others (Fregni and Pascual-Leone, 2007; Cirillo et al., 2017; Santos Ferreira et al., 2019; Begemann et al., 2020; Sanches et al., 2020; Chu et al., 2021; Herrero Babiloni et al., 2021; Madrid and Benninger, 2021; Parikh et al., 2021; Semmler et al., 2021; Veldema and Gharabaghi, 2022).

Regarding tDCS, a weak direct electric current (usually less than 2 mA) is applied to the brain using two or more electrodes positioned on the scalp. tDCS generates currents between the anode and cathode electrodes, resulting in polarity-specific changes in the resting membrane potential of neuronal cells, producing the desired effect (Morya et al., 2019; Santos Ferreira et al., 2019; Lefaucheur et al., 2020; Chan et al., 2021). tDCS offers several practical advantages over rTMS, as it is safer (not associated with seizures; Bikson et al., 2016), more cost-effective, easier to administer, may even be used as a home-based medical device (Charvet et al., 2015). In contrast, repetitive transcranial magnetic stimulation (rTMS) stimulates the target brain area using a magnetic coil to induce a magnetic field. rTMS can be applied at different frequencies, including low (≤1 Hz) and high (>1 Hz) frequencies (Lefaucheur et al., 2020). Among various rTMS protocols, theta burst stimulation (TBS) induced by either TMS or electrical stimulation is a recent pattern designed to mimic hippocampal theta rhythms. These rhythms have been demonstrated to induce long-term potentiation/depression-like effects (Nguyen and Kandel, 1997; Paulus, 2005; Kouvaros and Papatheodoropoulos, 2016; Cacace et al., 2017). TBS generates more powerful and longer-lasting effects compared to previous protocols. It consists of bursts of three pulses delivered at 50 Hz, repeated every 200 ms, and lasting for 2 s. TBS is administered in two forms: intermittent TBS (iTBS), involving a 2-s train of bursts repeated every 10 s, and continuous TBS (cTBS), where a continuous train of bursts is delivered. iTBS generates an excitatory effect, while cTBS induces an inhibitory effect (Huang et al., 2005; Rounis and Huang, 2020).

By integrating the advantages of tDCS with the effective patterns of TBS, a novel NIBS protocol known as transcranial burst electrical stimulation (tBES) has attracted considerable attention. The innovative tBES protocol, which combines direct current (DC) with TBS-like waveforms, was proposed and has shown preliminary findings indicating that the combination of anodal DC with an intermittent theta burst stimulation (iTBS) waveform may enhance the effectiveness of brain neuroplasticity (Li et al., 2019). More recent studies suggest that applying tBES via conventional or high-definition (HD) electrodes targeting the affected hemisphere has yielded positive neurorehabilitation outcomes in upper limb function among stroke patients (Chen et al., 2021; Huang Y. J. et al., 2022). The potential of tBES waveforms could be a promising neuromodulatory approach for further neurological treatment. However, the complete tBES protocols, including facilitative and inhibitive waveforms for inducing neuromodulation effects and the related underlying neurophysiological mechanisms, remain to be fully elucidated.

This study, conducted at the bench stage of translational research, aimed to investigate the neuromodulatory effects of tBES on cortical motor activation by analyzing the variability of motor-evoked potentials (MEPs). To investigate the underlying neurophysiological mechanisms, particularly the NIBS-induced changes in neuronal activity, previous studies utilized immediate-early genes such as c-Fos or GAD-65 as markers of excitatory and inhibitory neuronal activity in the brains of rodents that had undergone rTMS (Trippe et al., 2009; Moretti et al., 2022). Therefore, we also examined the impact of tBES on excitatory and inhibitory neural biomarkers, specifically assessing c-Fos (an immediate-early gene) and glutamic acid decarboxylase (GAD-65) through immunohistochemistry staining. Finally, we assessed the safety of tBES by analyzing glial fibrillary acidic protein (GFAP) expression in astrocytes. We hypothesized that tBES can significantly modulate cortical excitability within the stimulated region compared to sham stimulation and enhance the corresponding neural biomarkers, and show no differences in GFAP expression compared to the sham group.

2 Materials and methods

2.1 Animal preparation and experimental design

All animal experiments were conducted in accordance with the guidelines and were approved by the Institutional Animal Care and

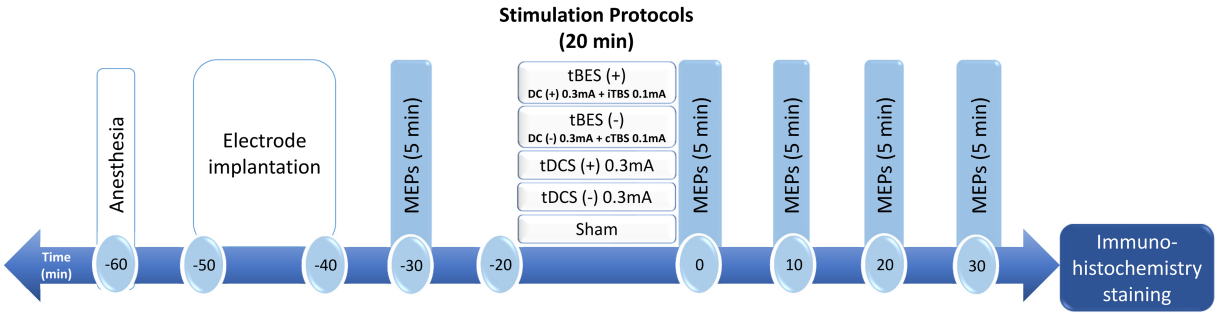

FIGURE 1
Schematic diagram of the experimental design for testing changes in cortical excitability after transcranial burst electrical stimulation (tBES), transcranial direct current stimulation (tDCS) or sham stimulation in anesthetized rats. In this representative experiment, anesthetized rats received intervention protocols for a duration of 20 min. Motor-evoked potentials (MEPs) were measured at baseline and at 0, 10, 20, and 30 min following the intervention. Subsequently, the rat brains were removed and subjected to immunohistochemistry for further investigation. DC, direct current; iTBS, intermittent theta burst stimulation; cTBS, continuous theta burst stimulation.

Use Committee of Chang Gung University (IACUC No. CGU108-202). Forty male adult Sprague–Dawley rats (280–320 g; BioLASCO, Taipei, Taiwan) were utilized for the experiments. These rats were individually housed in standard cages with unrestricted access to food and water, and they were maintained in a temperature-controlled environment with a 12-h light/dark cycle prior to the commencement of the experiment. Every effort was made to minimize the use of rats in this study. The rats were randomly assigned to one of five groups (tBES+, tBES−, tDCS+, tDCS−, and sham), each consisting of eight rats. These rats received electrical stimulation protocols and underwent electrophysiological recordings under anesthesia. The experimental design is illustrated in Figure 1.

2.2 Experimental setup

On the day of the experiment, the rat was deeply anesthetized for approximately 2.5 h with an intraperitoneal injection (i.p.) of tiletamine-zolazepam (50 mg/kg; Zoletil, Vibac, France) and xylazine (10 mg/kg; Rompun, Bayer, Germany). Once the rat lost its toe-pinch reflex, it was securely positioned on a stereotaxic frame. Subsequently, the scalp and tissue were carefully removed and cleaned, exposing the bregma line to identify the electrode's location. To administer the intervention protocols and deliver the stimuli to the motor cortex, a circular plastic socket with an inner diameter of 3 mm was affixed to the skull, precisely above the left primary motor cortex, corresponding to the right forelimb. This attachment was achieved using cyanoacrylate glue and dental cement. The center of this socket was positioned at coordinates 2.5 mm laterally and 1.5 mm anteriorly from the bregma point, focusing on the motor cortex of the unilateral forelimb in rats, as determined by stereotactic measurements (Fonoff et al., 2009). Immediately before stimulation, the socket was filled with conductive gel, and a 0.2 mm diameter silver wire, serving as the active electrode, was connected to an electrical stimulator (STG4002, Multichannel Systems, Reutlingen, Germany). The reference electrode consisted of a saline-soaked sponge placed within the abdomen (7 cm × 5 cm, EASYpadTM, Soterix Medical Inc., NY, United States; Figure 2).

2.3 Stimulation protocols

The stimulation protocols were programmed using Multichannel Stimulus II software, compatible with a two-channel electrical stimulator (STG4002, Multichannel Systems, Reutlingen, Germany). Figure 3 presents the details of all the stimulation protocols. Traditional tDCS and Theta Burst Stimulation (TBS) protocols are widely used neuromodulation approaches for various neurological disorders (Bologna et al., 2015; Bornheim et al., 2022; Huang W. et al., 2022; Zhang et al., 2022). For example, anodal tDCS increases neuronal excitability, producing long-term potentiation (LTP)-like effects, while cathodal tDCS induces long-term depression (LTD)-like effects (Rroji et al., 2015; Kronberg et al., 2017). Additionally, continuous TBS (cTBS) induces LTD-like cortical plasticity, whereas intermittent TBS (iTBS) produces LTP-like effects (Kirkovski et al., 2023). In this study, the tBES pattern combines both facilitation and inhibition waveforms from direct current and TBS. The tBES (+) and tBES (−) waveforms were selected to investigate whether the tBES protocols may yield synergistic and higher neuromodulatory effects. Therefore, five stimulus protocols, including tBES (+), tBES (−), tDCS (+), tDCS (−), or the sham protocol, were designed. For the tBES (+) and tBES (−) groups, the intensity was set at 0.3 mA of direct current combined with 0.1 mA of theta burst. For tDCS, a constant anodal or cathodal direct current of 0.3 mA, with a charge density of 5.1 C/cm^2 and a current density of 4.2 mA/cm^2, was delivered to healthy rats for 20 min. The current density of these tDCS protocols was reported to induce no damage to brain tissues (Bikson et al., 2016; Chhatbar et al., 2017). The sham group received a fixed current amplitude of 0 mA. Each stimulation session was performed for 20 min.

2.4 Assessments of cortical excitability

The electrophysiological recording was conducted after 30 min anesthesia to ensure that the anesthesia had reached a stable condition (Hsieh et al., 2015; Liu et al., 2019). Furthermore, to confirm no confounding effects of anesthesia, MEPs were recorded at multiple time points in the sham-stimulation group. For measuring MEPs, the electromyography (EMG) data was recorded using 27G stainless steel needle electrodes (Axon Systems Inc., Hauppauge, NY, United States)

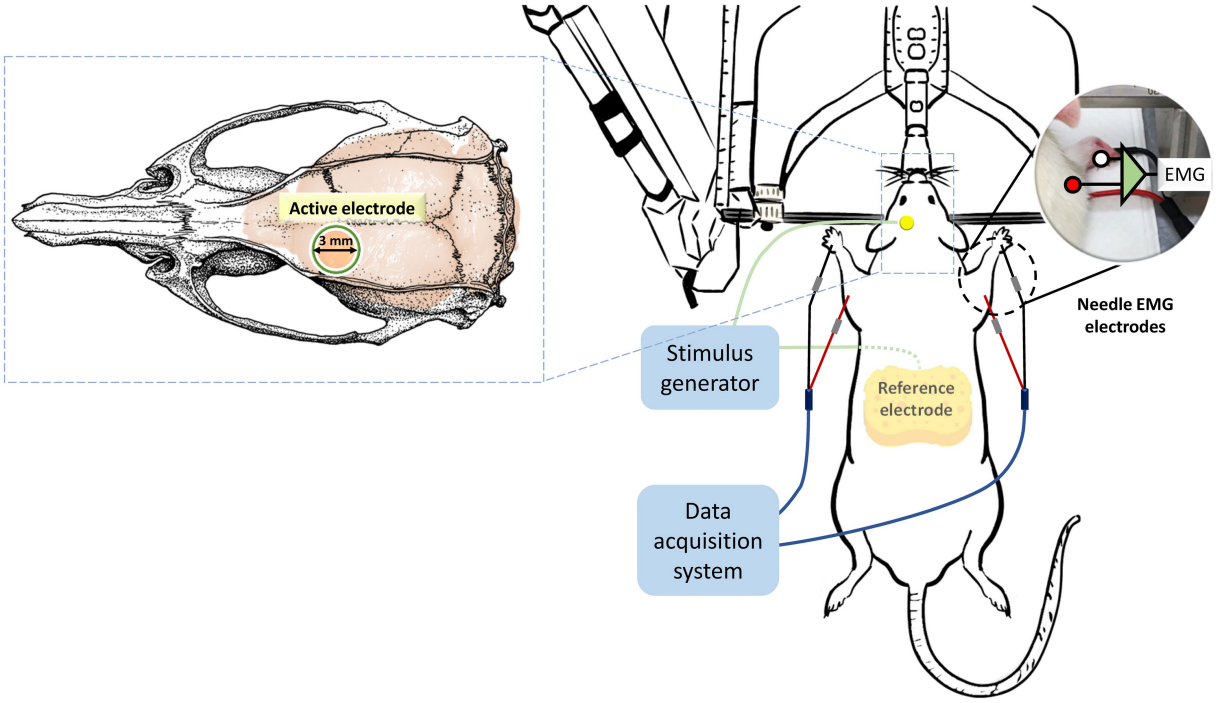

FIGURE 2
Placement and assembly of stimulation and recording electrodes. Throughout the entire experimental period, the rats were securely mounted on a stereotactic apparatus. Stimulation protocols were administered using an active electrode positioned 2.5 mm laterally and 1.5 mm anterior to the bregma, while a reference electrode was placed in the abdominal region. The same electrode configurations were employed to elicit motor-evoked potentials (MEPs). MEP data, recorded from the brachioradialis muscles, were subsequently analyzed to assess alterations in cortical excitability resulting from the intervention protocols.

inserted into the left and right brachioradialis muscles, with the reference electrode positioned distally in the paw. The ground electrode was inserted at the base of the rat's tail. The EMG data were subsequently amplified (gain ×1,000) and filtered (notch 60 Hz and bandpass 10–1,000 Hz) before digitization at a sampling rate of 10 kHz using a data acquisition system (MP36, BIOPAC system, California, United States). The recorded data were saved for offline analyses. The same epicranial stimulation electrode montages were used to deliver single stimuli for measuring cortical excitability through MEPs. Stimulation was applied to the unilateral motor cortex, and the magnitude of the evoked muscle contractions in both contralateral and ipsilateral limbs was assessed. Regarding MEP recording, single biphasic pulses with a pulse duration of 1 ms and 10-s intervals were initially delivered to determine the Resting Motor Threshold (RMT). RMT was defined as the minimum intensity of electrical stimulation required to elicit peak-to-peak MEPs greater than 20 μV in five out of 10 trials. Subsequently, MEPs were collected continuously every 10 s at an intensity of 120% of RMT for 5 min. MEP recordings were conducted at specific time points, including before the intervention stimulation (baseline), immediately after the intervention, and at 10-min intervals up to 30 min after the intervention stimulation ended (post 0, 10, 20, and 30 min, respectively; Figure 1).

2.5 Immunohistochemistry staining

After conducting electrophysiological assessments, we transcardially perfused rats with saline, followed by ice-cold 4% paraformaldehyde (PFA) in 0.1 M phosphate-buffered saline (PBS). The rat brains were then post-fixed in a 4% PFA solution for 2 days and cryoprotected in a 30% sucrose solution at 4°C overnight until they sank. Subsequently, the brains were coronally sectioned into serial sections with a thickness of 30 μm using a cryostat after being frozen at −81°C (Leica CM3050S Cryostat, FL, United States). Selected sections were incubated in a blocking solution (PBS with 10% goat serum) at room temperature for 1 h, following the inhibition of endogenous antigen activity with 0.3% H2O2 in PBS for 10 min. Afterward, these sections were exposed to primary rabbit antibodies against GFAP (1:1,000, AB7260, Millipore, United States), c-Fos (1:1,000, AB11959, Millipore, United States), and GAD-65 (1:100, AB239372, Millipore, United States) for 1 h at room temperature, followed by secondary anti-rabbit antibodies (1:200, MP-7401, Vector Labs, United States) for 1 h at room temperature. The sections were washed three times before adding a solution of 3.3-diaminobenzidine (DAB, SK-4105, Vector Labs, United States) for 10 min, and then all markers were visualized under specific colors.

Finally, using a digital pathology slide scanner (Aperio CS2, Leica Biosystems Inc., Buffalo Grove, IL, United States), images of regions of interest (ROI) on slide-mounted sections were captured at 40X optical zoom (0.25 M/pixel). Quantitative analysis of GFAP, c-fos, and GAD-65 was carried out manually and automatically to determine the level of expressed cells. Cell counting was performed on images obtained from the Aperio ImageScope viewer program at high magnification. A defined threshold for specific cells in the ROI, consistent across all images, was applied, and the resulting images were converted to black and white (BW). Next, cell density in specific

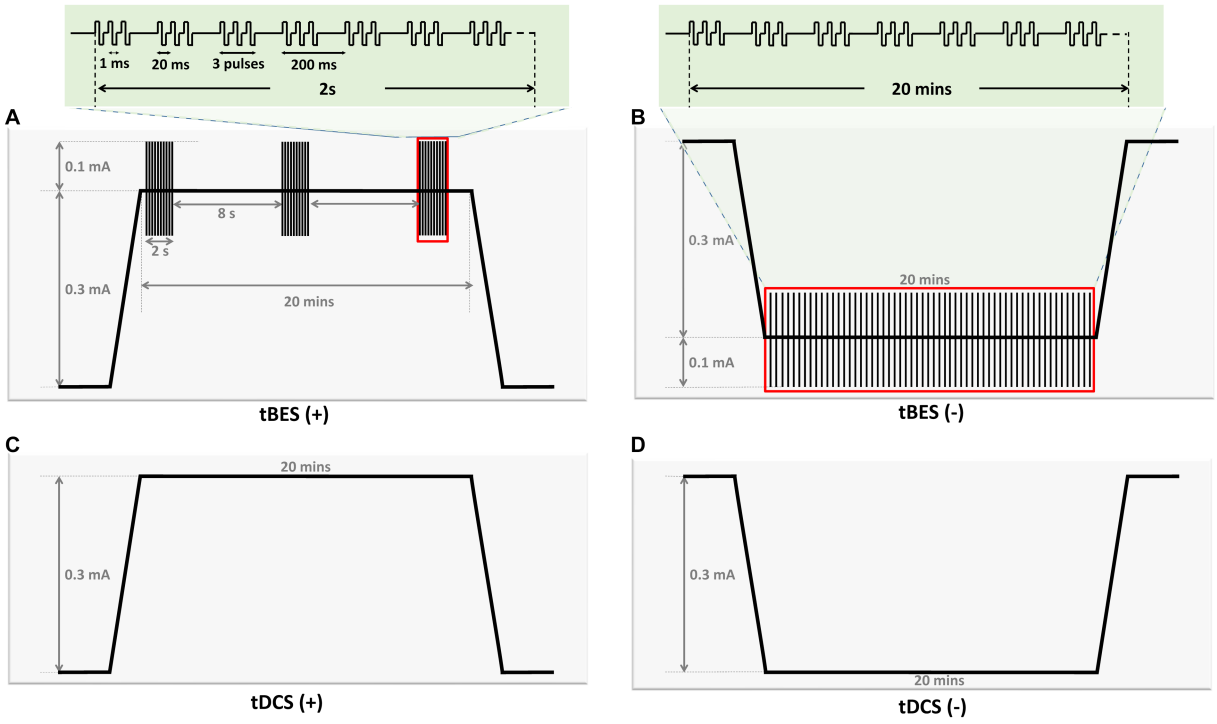

FIGURE 3
Graph illustrating parameters of four stimulation protocols in the current study. The graph provides an overview of the parameters for the four stimulation protocols utilized in this study. tBES (+): This protocol combines tDCS (+) with intermittent theta burst (iTBS) mode. iTBS comprises 10 bursts of three pulses delivered at a frequency of 50 Hz, with each burst lasting 200 ms and repeated for 2 s, followed by an 8-s rest **(A)**. tBES (–): In this protocol, tDCS (–) is paired with continuous theta burst (cTBS) mode, consisting of bursts of three pulses delivered at a frequency of 50 Hz, with each burst lasting 200 ms **(B)**. tDCS (+): Anodal direct current stimulation is applied at an intensity of 0.3 mA **(C)**. tDCS (–): Cathodal direct current stimulation is applied at an intensity of 0.3 mA **(D)**. All stimulation protocols were administered for 20 min.

regions was measured using computer-based image analysis software (Image-Pro, Media Cybernetics, Bethesda, MD, USA). Two researchers then thoroughly examined the results to ensure the correct identification of immunoreactivity patterns. Finally, the density of expressing cells was calculated within each ROI and expressed as the mean number of cells per mm^2 (cells/mm^2).

2.6 Data and statistical analysis

The peak-to-peak amplitudes of the MEPs were processed using MATLAB R2021a version (The MathWorks Inc., United States), and the average amplitudes of 30 consecutive MEPs were manually determined. Before performing statistical analysis, we normalized the averaged MEP amplitudes at each post-intervention time point to the averaged baseline MEP amplitude. Next, we proceeded to compare MEP amplitudes between groups utilizing a two-way repeated measures analysis of variance (ANOVA) conducted in SPSS version 22.0 for Windows (SPSS Inc., United States). The within-subject factor was TIME, with five levels: pre-intervention, 0, 10, 20, and 30 min after interventions, across five intervention protocols. If significant main effects and interactions were found, we performed independent *t*-tests to compare the groups at each time point. We also assessed the time course of changes in each protocol on the absolute amplitude values of MEPs using a separate one-way ANOVA, followed by post-hoc Fisher's LSD tests to determine differences between time points. Additionally, comparing immuno-histochemical data between and within groups required independent and paired *t*-tests. All data were presented using the mean and standard error of the mean (SEM), and we established a value of p cutoff of 0.05 for statistical significance.

3 Results

3.1 Neuromodulatory effects

When comparing the MEP responses in the contralateral limb (right limb) among the intervention protocols, the two-way repeated ANOVA did not reveal a significant main effect of time [$F(2.776; 97.152) = 1.531$, $p = 0.214$]. However, there were substantial differences between groups [$F(4;35) = 8.570$, $p < 0.001$] and a significant interaction [TIME × GROUP: $F(11.103; 97.152) = 3.986$, $p < 0.001$], indicating significant differences in MEP amplitudes between groups and over time within each group. Subsequently, we conducted a one-way ANOVA to evaluate differences within each group at each time point and an independent t-test to compare across groups at each time point.

Figure 4 illustrates the time course changes in raw MEPs produced under each intervention protocol. Both tBES (+) and tDCS (+) resulted in MEP amplitude facilitation at all time points, with tBES (+) generally having a more robust effect than tDCS (+), although there

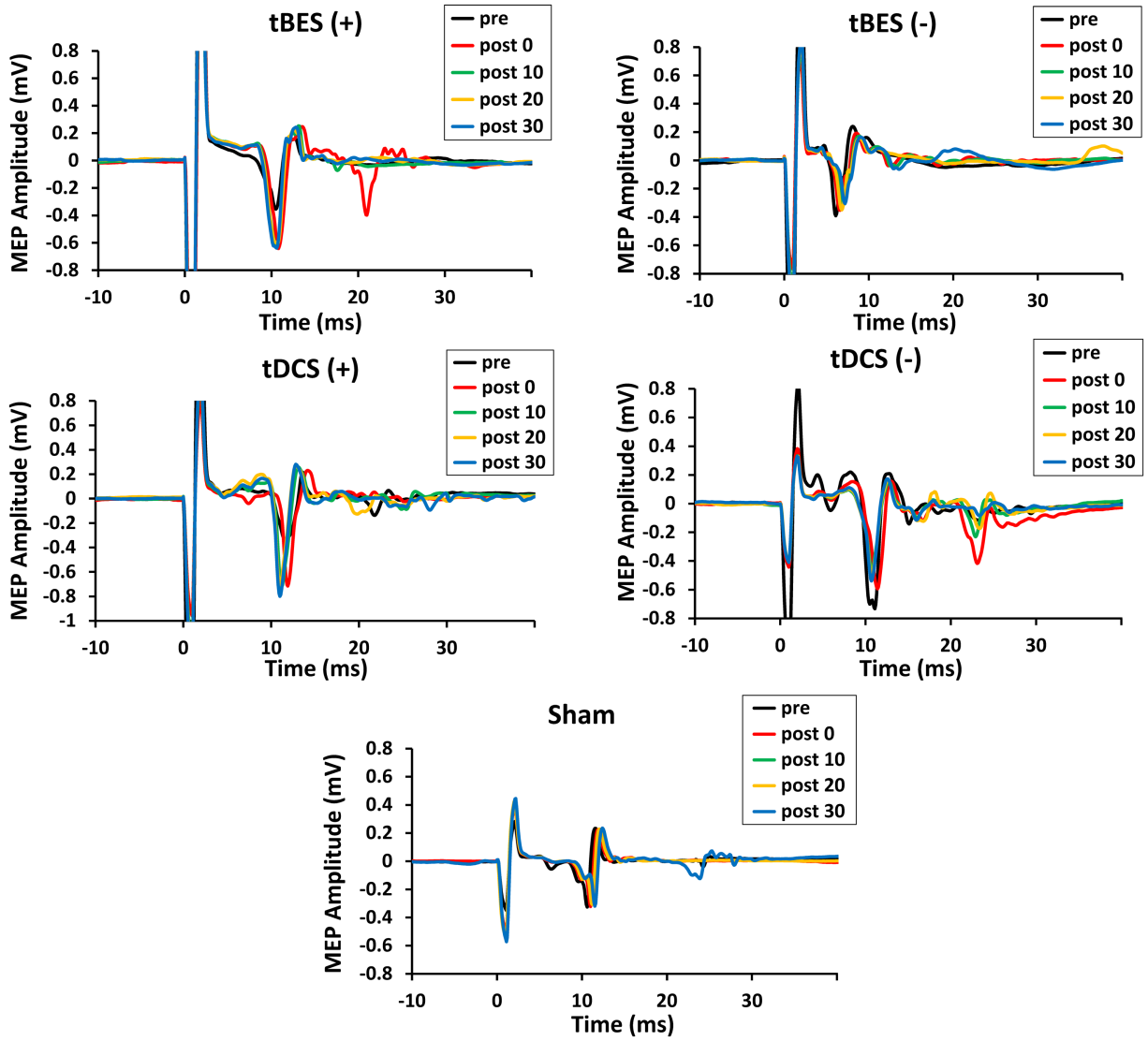

FIGURE 4
The time course changes in raw motor-evoked potential (MEP) signals for tBES (+), tDCS (+), tBES (−), tDCS (−), and the sham condition. MEP amplitudes increased after tBES (+) and tDCS (+), while they decreased following tBES (−) and tDCS (−) over the 30-min post-intervention period compared to baseline. No significant changes in MEP signals were observed under the sham condition.

was no statistically significant difference in averaged MEP amplitudes between these two treatments ($p > 0.05$).

Notably, MEP amplitudes significantly increased after tBES (+) compared to baseline, although this increase slightly decreased at 10-, 20-, and 30-min post-stimulation; significant differences were identified for all time periods compared to the sham group at the same time points ($p < 0.05$). Similarly, tDCS (+) had an apparent influence on MEPs, with a statistical difference observed at post-0 ($p = 0.048$) and 10-min ($p = 0.043$) time points compared to the sham stimulation group (Figure 5A). In terms of MEP suppression, both tBES (−) and tDCS (−) resulted in reduced MEP amplitudes compared to the sham stimulation group and pre-intervention baseline. However, at specific time points (post 10- and post 30-min for tBES−; post 0- and post 30-min for tDCS−), statistical analyses did not reveal significant variations in mean MEP amplitudes. Additionally, there were no discernible differences in MEPs between the two intervention protocols ($p > 0.05$).

Additionally, MEPs showed varied in the ipsilateral limb (left limb) after stimulation (Figure 5B). Statistical analyses on the MEP data did not reveal any significant main effects [TIME: $F(2.528; 88.470) = 0.679$, $p = 0.543$; GROUP: $F(4; 35) = 0.929$, $p = 0.458$], nor did they show a significant interaction between time and group [TIME × GROUP: $F(10.111; 88.470) = 0.722$, $p = 0.703$]. It indicates that MEPs obtained from the ipsilateral limb were not markedly affected by contralateral stimulation.

To compare the neuromodulatory effects among the different stimulation groups, we averaged the longitudinal MEP responses over 30 min. Figure 5C displays averaged level of MEPs at pre- and across 30 min post-tBES (+), tDCS (+), tBES (−), tDCS (−), and sham stimulation. The average MEP responses to tBES (+), tBES (−), tDCS (+), and tDCS (−) were significantly larger than those to the sham

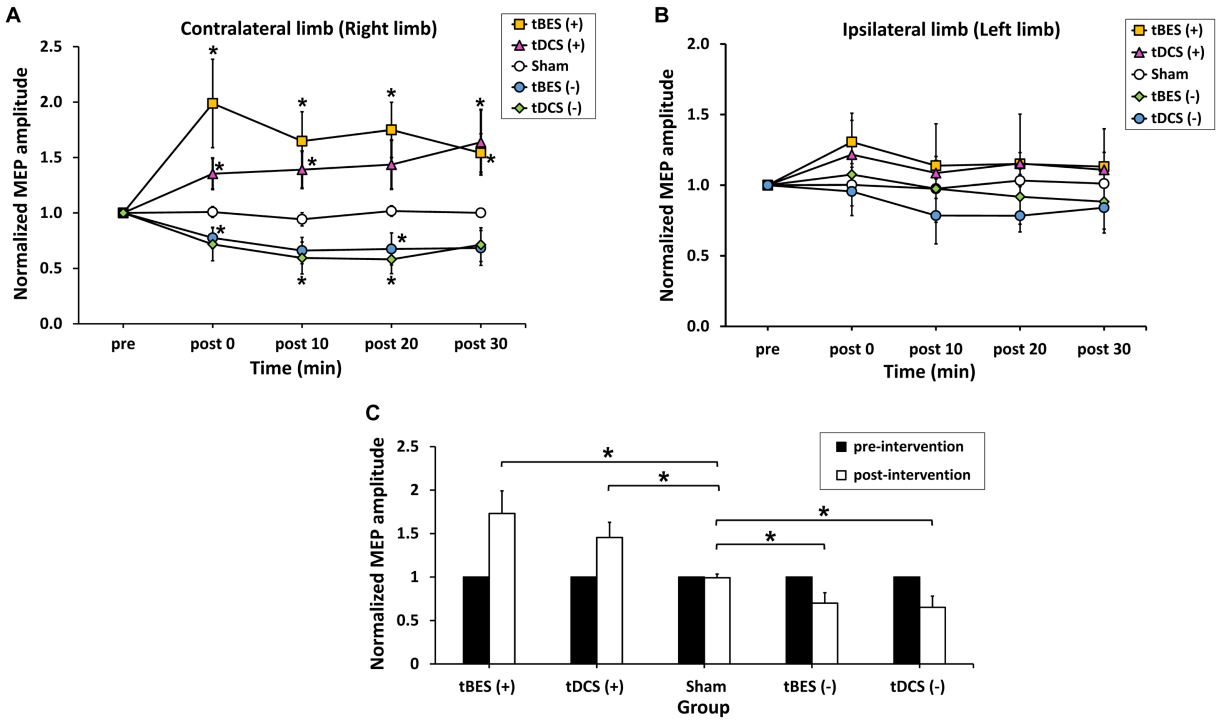

FIGURE 5
The average normalized motor-evoked potential (MEP) amplitudes for the contralateral limb **(A)** and ipsilateral limb **(B)** across the five intervention protocols (tBES+, tDCS+, tBES−, tDCS−, and sham). The averaged responses of cortical excitability were calculated for each intervention group within 30 min following different stimulations on the contralateral limb **(C)**. Asterisks (*) indicate statistically significant differences when comparing tBES (+), tBES (−), tDCS (+), and tDCS (−) with the sham group at the same time point. The data are presented as means, with error bars representing the standard error of the mean (SEM); $*p \leq 0.05$.

stimulation, confirming that four intervention regimens had substantial impacts on the overall changes in mean MEPs.

3.2 Histological assays

To confirm whether tBES indeed activates neurons and GABAergic synaptic terminals, as indicated by the increase in immediate early genes c-Fos and GAD-65, respectively, we conducted experiments on 12 rats divided into three groups: tBES (+), tBES (−), and sham, with four rats in each group. These rats received the stimulation protocols and were subsequently transcardially perfused after 20 min of stimulation, and their brains were subjected to immunohistochemistry (IHC) analysis.

Our findings revealed that tBES (+) significantly increased the number of c-Fos positive cells in the stimulated region, specifically the left side of the motor cortex, at 20 min post-stimulation (Figure 6A). This increase was statistically significant when compared to both the contralateral motor cortex in the tBES (+) group ($p = 0.012$) and the sham group ($p = 0.015$). In contrast, following tBES (−) stimulation, we observed a decrease in c-Fos expression compared to sham stimulation and tBES (+) on the same side and compared to the right side of the motor cortex. However, a statistically significant difference was only found within the tBES (−) group ($p = 0.05$), not between the tBES (−) and sham groups. Significantly, sham stimulation did not affect the expression of c-Fos on either side of the motor cortex (Figure 6).

Regarding the inhibitory neurobiological marker, after tBES (−) stimulation, we observed an elevation in GAD-65 expression in the stimulated region but not in the contralateral region ($p = 0.004$). Furthermore, the quantity of GAD-65+ cells in the tBES (−) group was greater than that in the sham group when compared to the sham group in the same hemisphere ($p = 0.047$; Figure 7). Our results confirm that tBES (+) and tBES (−), but not sham stimulation, clearly activate excitatory and inhibitory neurons, respectively.

We then further assessed the safety of tBES by examining the expression of GFAP-immunoreactive astrocytes, which are known to become activated in response to brain damage (Luoto et al., 2017). Immunohistochemistry (IHC) staining was performed to detect GFAP-positive cells 24 h after stimulation. Our IHC analyses revealed a slight increase in the density of GFAP-positive cells in rats subjected to either tBES (+) or tBES (−) compared to the non-stimulation region in both the tBES and sham groups. However, these changes were not statistically significant (all $p > 0.05$; Figure 8).

4 Discussion

The field of neuromodulation is continuously evolving, with a focus on enhancing treatment efficacy. Innovative techniques based on NIBS methods that are already in use are being developed (Terranova et al., 2018; Antal et al., 2022). The recent introduction of tBES may help bridge existing gaps and provide therapists with an alternative for treating neurological disorders. Since tBES

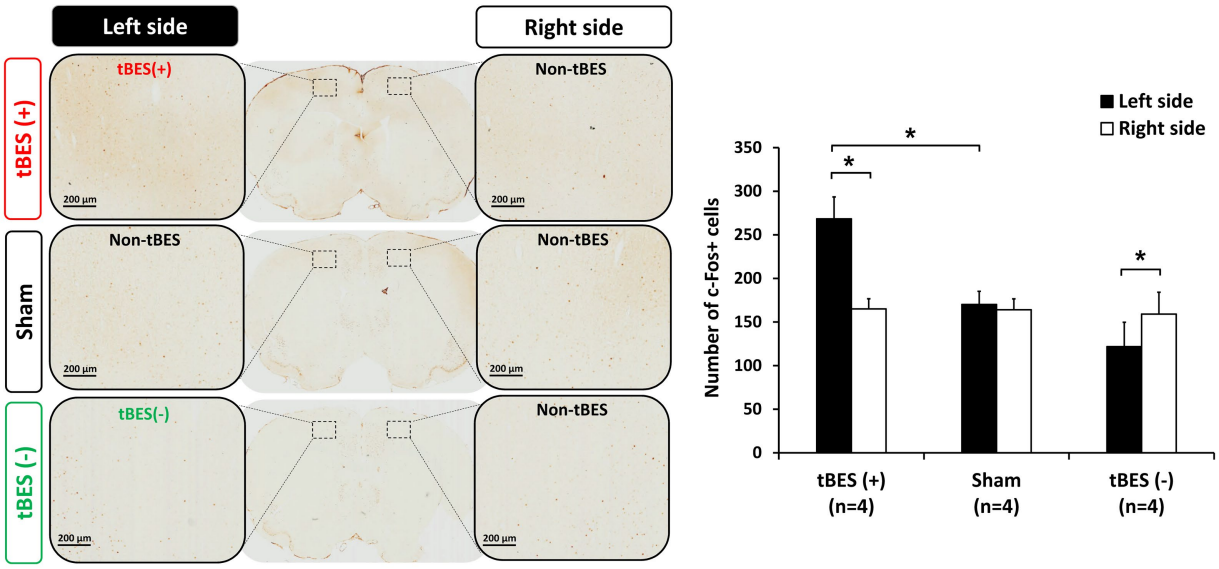

FIGURE 6
Representative immunohistochemically stained slices with regions of interest (ROI) **(A)**. Data for c-Fos are presented as the number of labeled cells within the ROI. The changes in cortical expression of c-Fos following tBES (+), tBES (–), and sham stimulation **(B)**. Asterisks (*) indicate statistically significant differences, either between the right and left sides of the brain within a group or when compared to the sham group on the same side of the brain. The data are presented as means, with error bars representing the standard error of the mean (SEM); $*p \leq 0.05$.

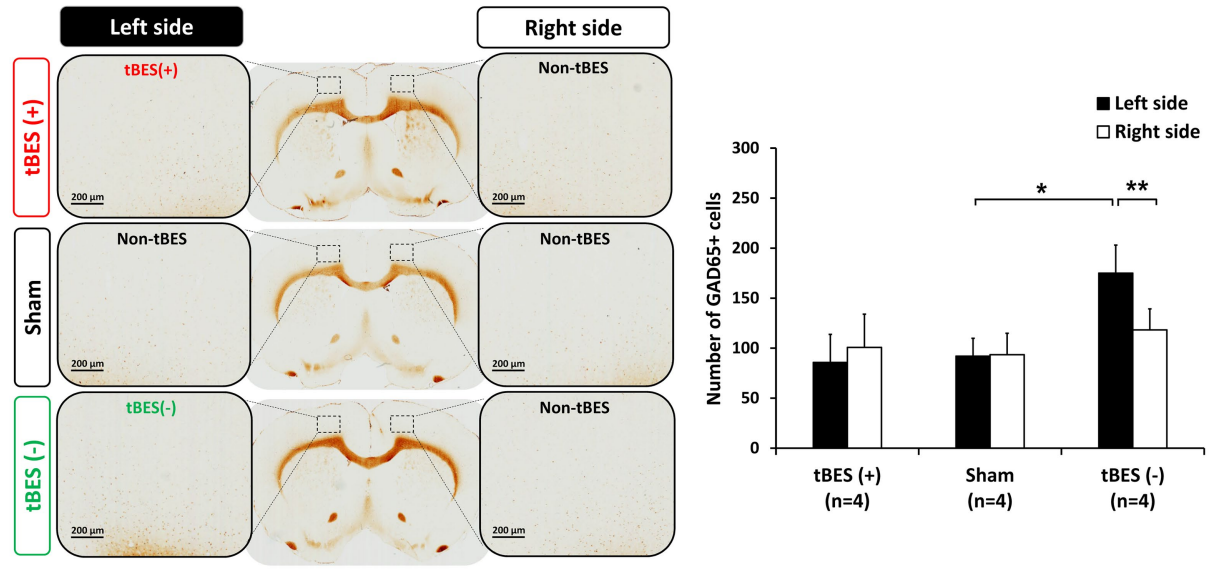

FIGURE 7
Representative images of GAD-65 immunostaining **(A)** and the average changes in GAD-65 expression following tBES (+), tBES (–), and sham stimulation **(B)**. Asterisks (*) indicate statistically significant differences between the right and left sides of the brain within a group or when compared to the sham group on the same side of the brain. The data are presented as means, with error bars representing the standard error of the mean (SEM); $**p \leq 0.05$, $*p \leq 0.01$.

combines direct current and theta burst waveforms, it is expected to have a superior impact on neural plasticity and offer therapeutic benefits for neurological diseases such as stroke, Alzheimer's, and Parkinson's disease.

In the current study, we aimed to identify and compare the effects of tBES and pure tDCS on cortical excitability using a rodent model. We performed unilateral cortical motor stimulation using a plastic socket filled with electrolyte and an electrode, similar to a human experiment setup. To validate the neuromodulatory effects of tBES, we assessed MEPs, which reflect long-term potentiation (LTP)-like and long-term depression (LTD)-like plasticity in the motor cortex (Delvendahl et al., 2012). Based on the analysis of contralateral MEP data, our findings support the hypothesis that tBES (+) significantly increases motor cortex excitability. This increase was greater than that produced by sham stimulation and pure tDCS (+). On the other hand, the tBES (–) group exhibited a more significant reduction in cortical excitability than the sham (–) group but did not differ significantly from the pure tDCS (–) group. Additionally, our results indicate that

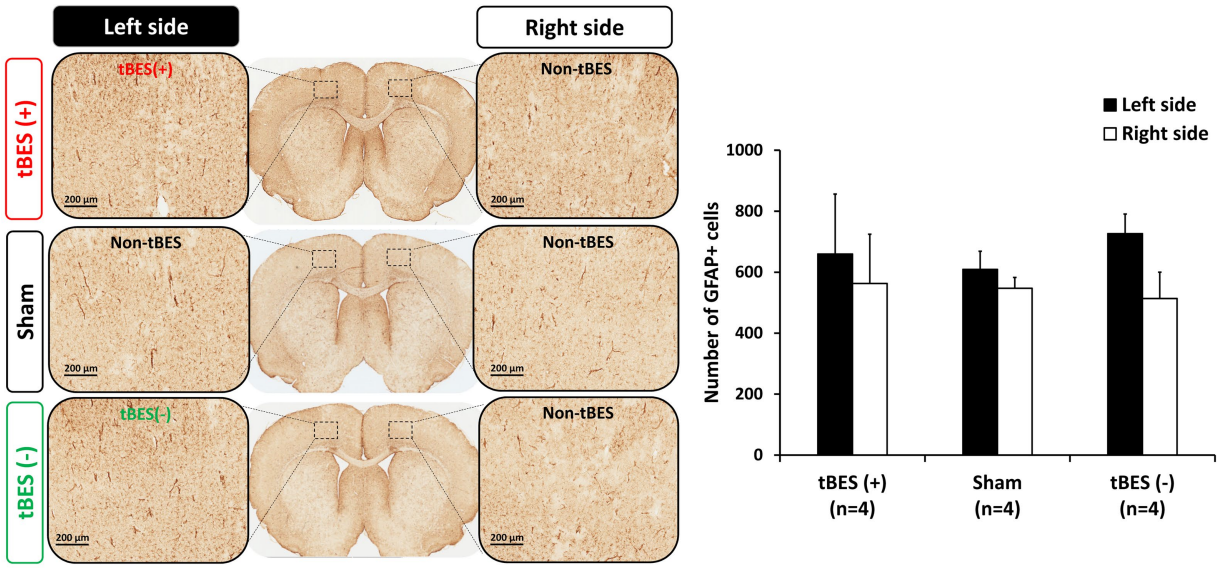

FIGURE 8
Representative images of glial fibrillary acidic protein (GFAP) immunostaining **(A)** and the average changes in GFAP expression following tBES (+), tBES (–), and sham stimulation **(B)**. Asterisks (*) indicate statistically significant differences either between the right and left sides of the brain within a group or when compared to the sham group on the same side of the brain. Data are presented as means, with error bars representing the standard error of the mean (SEM).

tBES-induced MEPs in the contralateral limb were larger than those in the ipsilateral limb, suggesting that tBES may have a targeted effect on the desired cortical region. While our study did not include behavioral tests following stimulation protocols, it is worth noting that MEPs are often interpreted in the context of motor function execution, suggesting a potential correlation between tBES-induced MEPs and changes in motor function (Bestmann and Krakauer, 2015).

In addition to investigating the mechanisms underlying tBES's promotion of LTP- or LTD-like plasticity through NMDA or GABA receptor activation, we examined the density of neural cells, specifically c-Fos, and GAD-65, within motor cortical areas. The NMDA receptor, an essential glutamate receptor, plays a crucial role in LTP and synaptic plasticity by involving key molecules like calcium ions, PSD-95, CaMK II, PKA, MAPK, CREB, and immediate early genes (IEGs) in the NMDA signaling pathway (Brigman et al., 2010; Wang and Peng, 2016). Among these, c-Fos is an IEG whose expression is positively correlated with the induction of LTP (Abraham et al., 1991; Lüscher and Malenka, 2012; Wang and Peng, 2016). c-Fos is also a valuable marker for identifying excited neurons following stimulation, providing insight into the neuronal mechanisms of treatment effects (Doi et al., 2001; Zhang et al., 2002; Hoppenrath and Funke, 2013; Li et al., 2015). Previous research has shown that anodal tDCS increases c-Fos expression in both the primary motor cortex and substantia nigra (SN) in Parkinson's disease monkeys (Li et al., 2015). On the other hand, GABA is the primary inhibitory neurotransmitter, responsible for reducing neuronal excitability (Wong et al., 2003). The activity and expression of GAD are closely linked to GABA levels and subsequent inhibitory neurotransmission at synapses (Lee et al., 2019). GAD-65 expression in cortical inhibitory interneurons is often assessed after NIBS (Trippe et al., 2009; Hoppenrath and Funke, 2013). GABA is synthesized by GAD-65 in an activity-dependent manner, contributing to the balance between excitatory and inhibitory mechanisms (Müller et al., 2015; Lee et al., 2019; Kajita and Mushiake, 2021). Earlier studies have indicated that GAD-65 expression decreases following anodal tDCS (Heimrath et al., 2020; Zhao et al., 2020; Yamada and Sumiyoshi, 2021). Consistent with previous NIBS research on excitatory and inhibitory mechanisms, our findings demonstrate that tBES (+) enhances the synthesis of NMDA receptors, as indicated by upregulated c-Fos and downregulated GAD-65 expression. In contrast, tBES (−) increases the number of GAD-65 cells and decreases the number of c-Fos cells, suggesting that GABA receptors may be abundantly activated under tBES (−). These results align with those of MEPs at the same time points.

GFAP, responsible for providing structural stability to astrocyte processes, plays a crucial role in modulating astrocyte mobility and morphology. When brain damage occurs, astrocytes become reactive, rapidly synthesize GFAP, and respond (Eng et al., 2000). Numerous *in vivo* and *in vitro* studies have shown that regulating GFAP in astrocytes is not only beneficial for understanding the physiology of healthy brains but also serves as a biomarker for neurological diseases like Alzheimer's and Parkinson's disease (Gomes et al., 1999; Pekny and Pekna, 2004; Middeldorp and Hol, 2011). We evaluated GFAP expression to assess whether the motor cortex was damaged following tBES. Our results show that tBES upregulates GFAP expression 24 h after tBES, but not significantly. This increase may be explained by our choice of investigating GFAP expression 24 h after stimulation, as GFAP has been shown to peak at this time and then rapidly decline afterward (Fujiki and Steward, 1997).

We acknowledge several limitations in our study. First, we assessed MEP alterations in short-term after-effects, which may fluctuate over a longer-term observation with additional time points beyond the 30-min post-stimulation protocols. Thus, future research could explore the longer-term after-effects of tBES, potentially extending the measurement period to an hour or beyond. Second, we examined the

safety of tBES in rats that underwent intervention protocols and MEP recordings. Although we investigated GFAP expression on both sides of the brain and used a sham group, it is possible that single pulses used to generate MEPs might impact the significant increase in the number of GFAP expressions within the stimulated area. Furthermore, we did not measure other neural activity indicators or additional parameters to definitively determine the neurophysiological mechanisms of tBES efficacy. To address this limitation, further studies should consider investigating changes in synaptic plasticity, neurotransmitter levels, or other relevant outcome measures to provide a more comprehensive understanding of the neuromodulatory effects of tBES. In conclusion, our study highlights the potential of tBES as a safe neuromodulation technique capable of inducing neural plasticity and activating neural cells. The relevance of our findings to human and disease models should be validated in future studies.

Data availability statement

The original contributions presented in the study are included in the article/Supplementary material, further inquiries can be directed to the corresponding author.

Ethics statement

The animal study was approved by Institutional Animal Care and Use Committee of Chang Gung University (IACUC No. CGU108-202). The study was conducted in accordance with the local legislation and institutional requirements.

Author contributions

TXDN: Conceptualization, Data curation, Formal analysis, Investigation, Methodology, Writing – original draft, Writing – review & editing. C-WK: Data curation, Formal analysis, Investigation, Methodology, Writing – original draft, Writing – review & editing. C-WP: Resources, Writing – original draft, Writing – review & editing. H-LL: Resources, Writing – original draft, Writing – review & editing. M-YC: Resources, Writing – original draft, Writing – review & editing. T-HH: Conceptualization, Data curation, Formal analysis, Funding acquisition, Investigation, Methodology, Project administration, Resources, Software, Supervision, Validation, Visualization, Writing – original draft, Writing – review & editing.

Funding

The author(s) declare financial support was received for the research, authorship, and/or publication of this article. This work was supported by the National Science and Technology Council (grant NSTC112-2314-B182-022, NSTC112-2321-B002-021, MOST109-2314-B182-029-MY3, and MOST111-2622-B182-002) and Chang Gung Medical Foundation, Taiwan (CMRPD1M0252 and CMRPD1M0701).

Conflict of interest

The authors declare that the research was conducted in the absence of any commercial or financial relationships that could be construed as a potential conflict of interest.

Publisher's note

All claims expressed in this article are solely those of the authors and do not necessarily represent those of their affiliated organizations, or those of the publisher, the editors and the reviewers. Any product that may be evaluated in this article, or claim that may be made by its manufacturer, is not guaranteed or endorsed by the publisher.

Supplementary material

The Supplementary material for this article can be found online at: https://www.frontiersin.org/articles/10.3389/fnins.2023.1303014/full#supplementary-material

References

Abraham, W. C., Dragunow, M., and Tate, W. P. (1991). The role of immediate early genes in the stabilization of long-term potentiation. *Mol. Neurobiol.* 5, 297–314. doi: 10.1007/BF02935553

Antal, A., Luber, B., Brem, A. K., Bikson, M., Brunoni, A. R., Cohen Kadosh, R., et al. (2022). Non-invasive brain stimulation and neuroenhancement. *Clin. Neurophysiol. Pract.* 7, 146–165. doi: 10.1016/j.cnp.2022.05.002

Begemann, M. J., Brand, B. A., Ćurčić-Blake, B., Aleman, A., and Sommer, I. E. (2020). Efficacy of non-invasive brain stimulation on cognitive functioning in brain disorders: a meta-analysis. *Psychol. Med.* 50, 2465–2486. doi: 10.1017/S0033291720003670

Bestmann, S., and Krakauer, J. W. (2015). The uses and interpretations of the motor-evoked potential for understanding behaviour. *Exp. Brain Res.* 233, 679–689. doi: 10.1007/s00221-014-4183-7

Bhattacharya, A., Mrudula, K., Sreepada, S. S., Sathyaprabha, T. N., Pal, P. K., Chen, R., et al. (2022). An overview of noninvasive brain stimulation: basic principles and clinical applications. *Can. J. Neurol. Sci.* 49, 479–492. doi: 10.1017/cjn.2021.158

Bikson, M., Grossman, P., Thomas, C., Zannou, A. L., Jiang, J., Adnan, T., et al. (2016). Safety of transcranial direct current stimulation: evidence based update 2016. *Brain Stimul.* 9, 641–661. doi: 10.1016/j.brs.2016.06.004

Bologna, M., Di Biasio, F., Conte, A., Iezzi, E., Modugno, N., and Berardelli, A. (2015). Effects of cerebellar continuous theta burst stimulation on resting tremor in Parkinson's disease. *Parkinsonism Relat. Disord.* 21, 1061–1066. doi: 10.1016/j.parkreldis.2015.06.015

Bornheim, S., Thibaut, A., Beaudart, C., Maquet, P., Croisier, J. L., and Kaux, J. F. (2022). Evaluating the effects of tDCS in stroke patients using functional outcomes: a systematic review. *Disabil. Rehabil.* 44, 13–23. doi: 10.1080/09638288.2020.1759703

Brigman, J. L., Wright, T., Talani, G., Prasad-Mulcare, S., Jinde, S., Seabold, G. K., et al. (2010). Loss of GluN2B-containing NMDA receptors in CA1 hippocampus and cortex impairs long-term depression, reduces dendritic spine density, and disrupts learning. *J. Neurosci.* 30, 4590–4600. doi: 10.1523/JNEUROSCI.0640-10.2010

Cacace, F., Mineo, D., Viscomi, M. T., Latagliata, E. C., Mancini, M., Sasso, V., et al. (2017). Intermittent theta-burst stimulation rescues dopamine-dependent corticostriatal synaptic plasticity and motor behavior in experimental parkinsonism: possible role of glial activity. *Mov. Disord.* 32, 1035–1046. doi: 10.1002/mds.26982

Chan, M. M. Y., Yau, S. S. Y., and Han, Y. M. Y. (2021). The neurobiology of prefrontal transcranial direct current stimulation (tDCS) in promoting brain plasticity: a systematic review and meta-analyses of human and rodent studies. *Neurosci. Biobehav. Rev.* 125, 392–416. doi: 10.1016/j.neubiorev.2021.02.035

Charvet, L. E., Kasschau, M., Datta, A., Knotkova, H., Stevens, M. C., Alonzo, A., et al. (2015). Remotely-supervised transcranial direct current stimulation (tDCS) for clinical trials: guidelines for technology and protocols. *Front. Syst. Neurosci.* 9:26. doi: 10.3389/fnsys.2015.00026

Chen, S. C., Yang, L. Y., Adeel, M., Lai, C. H., and Peng, C. W. (2021). Transcranial electrostimulation with special waveforms enhances upper-limb motor function in patients with chronic stroke: a pilot randomized controlled trial. *J. Neuroeng. Rehabil.* 18:106. doi: 10.1186/s12984-021-00901-8

Chhatbar, P. Y., George, M. S., Kautz, S. A., and Feng, W. (2017). Quantitative reassessment of safety limits of tDCS for two animal studies. *Brain Stimul.* 10, 1011–1012. doi: 10.1016/j.brs.2017.07.008

Chu, C. S., Li, C. T., Brunoni, A. R., Yang, F. C., Tseng, P. T., Tu, Y. K., et al. (2021). Cognitive effects and acceptability of non-invasive brain stimulation on Alzheimer's disease and mild cognitive impairment: a component network meta-analysis. *J. Neurol. Neurosurg. Psychiatry* 92, 195–203. doi: 10.1136/jnnp-2020-323870

Cirillo, G., Di Pino, G., Capone, F., Ranieri, F., Florio, L., Todisco, V., et al. (2017). Neurobiological after-effects of non-invasive brain stimulation. *Brain Stimul.* 10, 1–18. doi: 10.1016/j.brs.2016.11.009

Delvendahl, I., Jung, N. H., Kuhnke, N. G., Ziemann, U., and Mall, V. (2012). Plasticity of motor threshold and motor-evoked potential amplitude--a model of intrinsic and synaptic plasticity in human motor cortex? *Brain Stimul.* 5, 586–593. doi: 10.1016/j.brs.2011.11.005

Doi, W., Sato, D., Fukuzako, H., and Takigawa, M. (2001). C-Fos expression in rat brain after repetitive transcranial magnetic stimulation. *Neuroreport* 12, 1307–1310. doi: 10.1097/00001756-200105080-00050

Eng, L. F., Ghirnikar, R. S., and Lee, Y. L. (2000). Glial fibrillary acidic protein: GFAP-thirty-one years (1969-2000). *Neurochem. Res.* 25, 1439–1451. doi: 10.1023/A:1007677003387

Fonoff, E. T., Pereira, J. F., Camargo, L. V., Dale, C. S., Pagano, R. L., Ballester, G., et al. (2009). Functional mapping of the motor cortex of the rat using transdural electrical stimulation. *Behav. Brain Res.* 202, 138–141. doi: 10.1016/j.bbr.2009.03.018

Fregni, F., and Pascual-Leone, A. (2007). Technology insight: noninvasive brain stimulation in neurology—perspectives on the therapeutic potential of rTMS and tDCS. *Nat. Clin. Pract. Neurol.* 3, 383–393. doi: 10.1038/ncpneuro0530

Fujiki, M., and Steward, O. (1997). High frequency transcranial magnetic stimulation mimics the effects of ECS in upregulating astroglial gene expression in the murine CNS. *Brain Res. Mol. Brain Res.* 44, 301–308. doi: 10.1016/S0169-328X(96)00232-X

Gomes, F. C., Paulin, D., and Moura Neto, V. (1999). Glial fibrillary acidic protein (GFAP): modulation by growth factors and its implication in astrocyte differentiation. *Braz. J. Med. Biol. Res.* 32, 619–631. doi: 10.1590/S0100-879X1999000500016

Grippe, T., Desai, N., Arora, T., and Chen, R. (2022). Use of non-invasive neurostimulation for rehabilitation in functional movement disorders. *Front Rehabil Sci* 3:1031272. doi: 10.3389/fresc.2022.1031272

Heimrath, K., Brechmann, A., Blobel-Lüer, R., Stadler, J., Budinger, E., and Zaehle, T. (2020). Transcranial direct current stimulation (tDCS) over the auditory cortex modulates GABA and glutamate: a 7 T MR-spectroscopy study. *Sci. Rep.* 10:20111. doi: 10.1038/s41598-020-77111-0

Herrero Babiloni, A., Bellemare, A., Beetz, G., Vinet, S. A., Martel, M. O., Lavigne, G. J., et al. (2021). The effects of non-invasive brain stimulation on sleep disturbances among different neurological and neuropsychiatric conditions: a systematic review. *Sleep Med. Rev.* 55:101381. doi: 10.1016/j.smrv.2020.101381

Hoppenrath, K., and Funke, K. (2013). Time-course of changes in neuronal activity markers following iTBS-TMS of the rat neocortex. *Neurosci. Lett.* 536, 19–23. doi: 10.1016/j.neulet.2013.01.003

Hsieh, T. H., Huang, Y. Z., Rotenberg, A., Pascual-Leone, A., Chiang, Y. H., Wang, J. Y., et al. (2015). Functional dopaminergic neurons in substantia Nigra are required for transcranial magnetic stimulation-induced motor plasticity. *Cereb. Cortex* 25, 1806–1814. doi: 10.1093/cercor/bht421

Huang, W., Chen, J., Zheng, Y., Zhang, J., Li, X., Su, L., et al. (2022). The effectiveness of intermittent Theta burst stimulation for stroke patients with upper limb impairments: a systematic review and Meta-analysis. *Front. Neurol.* 13:896651. doi: 10.3389/fneur.2022.896651

Huang, Y. Z., Edwards, M. J., Rounis, E., Bhatia, K. P., and Rothwell, J. C. (2005). Theta burst stimulation of the human motor cortex. *Neuron* 45, 201–206. doi: 10.1016/j.neuron.2004.12.033

Huang, Y. J., Wang, S. M., Chen, C., Chen, C. A., Wu, C. W., Chen, J. J., et al. (2022). High-definition transcranial direct current with electrical Theta burst on post-stroke motor rehabilitation: a pilot randomized controlled trial. *Neurorehabil. Neural Repair* 36, 645–654. doi: 10.1177/15459683221121751

Kajita, Y., and Mushiake, H. (2021). Heterogeneous GAD65 expression in subtypes of GABAergic neurons across layers of the cerebral cortex and Hippocampus. *Front. Behav. Neurosci.* 15:869. doi: 10.3389/fnbeh.2021.750869

Kirkovski, M., Donaldson, P. H., Do, M., Speranza, B. E., Albein-Urios, N., Oberman, L. M., et al. (2023). A systematic review of the neurobiological effects of theta-burst stimulation (TBS) as measured using functional magnetic resonance imaging (fMRI). *Brain Struct. Funct.* 228, 717–749. doi: 10.1007/s00429-023-02634-x

Kouvaros, S., and Papatheodoropoulos, C. (2016). Theta burst stimulation-induced LTP: differences and similarities between the dorsal and ventral CA1 hippocampal synapses. *Hippocampus* 26, 1542–1559. doi: 10.1002/hipo.22655

Kronberg, G., Bridi, M., Abel, T., Bikson, M., and Parra, L. C. (2017). Direct current stimulation modulates LTP and LTD: activity dependence and dendritic effects. *Brain Stimul.* 10, 51–58. doi: 10.1016/j.brs.2016.10.001

Lee, S. E., Lee, Y., and Lee, G. H. (2019). The regulation of glutamic acid decarboxylases in GABA neurotransmission in the brain. *Arch. Pharm. Res.* 42, 1031–1039. doi: 10.1007/s12272-019-01196-z

Lefaucheur, J. P., Aleman, A., Baeken, C., Benninger, D. H., Brunelin, J., Di Lazzaro, V., et al. (2020). Evidence-based guidelines on the therapeutic use of repetitive transcranial magnetic stimulation (rTMS): an update (2014-2018). *Clin. Neurophysiol.* 131, 474–528. doi: 10.1016/j.clinph.2019.11.002

Li, Y. T., Chen, S. C., Yang, L. Y., Hsieh, T. H., and Peng, C. W. (2019). Designing and implementing a novel transcranial electrostimulation system for Neuroplastic applications: a preliminary study. *IEEE Trans. Neural Syst. Rehabil. Eng.* 27, 805–813. doi: 10.1109/TNSRE.2019.2908674

Li, H., Lei, X., Yan, T., Li, H., Huang, B., Li, L., et al. (2015). The temporary and accumulated effects of transcranial direct current stimulation for the treatment of advanced Parkinson's disease monkeys. *Sci. Rep.* 5:12178. doi: 10.1038/srep12178

Liu, H. H., He, X. K., Chen, H. Y., Peng, C. W., Rotenberg, A., Juan, C. H., et al. (2019). Neuromodulatory effects of transcranial direct current stimulation on motor excitability in rats. *Neural Plast.* 2019, 1–9. doi: 10.1155/2019/4252943

Luoto, T. M., Raj, R., Posti, J. P., Gardner, A. J., Panenka, W. J., and Iverson, G. L. (2017). A systematic review of the usefulness of glial fibrillary acidic protein for predicting acute intracranial lesions following head trauma. *Front. Neurol.* 8:652. doi: 10.3389/fneur.2017.00652

Lüscher, C., and Malenka, R. C. (2012). NMDA receptor-dependent long-term potentiation and long-term depression (LTP/LTD). *Cold Spring Harb. Perspect. Biol.* 4:a005710. doi: 10.1101/cshperspect.a005710

Madrid, J., and Benninger, D. H. (2021). Non-invasive brain stimulation for Parkinson's disease: clinical evidence, latest concepts and future goals: a systematic review. *J. Neurosci. Methods* 347:108957. doi: 10.1016/j.jneumeth.2020.108957

Middeldorp, J., and Hol, E. M. (2011). GFAP in health and disease. *Prog. Neurobiol.* 93, 421–443. doi: 10.1016/j.pneurobio.2011.01.005

Moretti, J., Terstege, D. J., Poh, E. Z., Epp, J. R., and Rodger, J. (2022). Low intensity repetitive transcranial magnetic stimulation modulates brain-wide functional connectivity to promote anti-correlated c-Fos expression. *Sci. Rep.* 12:20571. doi: 10.1038/s41598-022-24934-8

Morya, E., Monte-Silva, K., Bikson, M., Esmaeilpour, Z., Biazoli, C. E. Jr., Fonseca, A., et al. (2019). Beyond the target area: an integrative view of tDCS-induced motor cortex modulation in patients and athletes. *J. Neuroeng. Rehabil.* 16:141. doi: 10.1186/s12984-019-0581-1

Müller, I., Alışkan, G., and Stork, O. (2015). The GAD65 knock out mouse—a model for GABAergic processes in fear- and stress-induced psychopathology. *Genes Brain Behav.* 14, 37–45. doi: 10.1111/gbb.12188

Nguyen, P. V., and Kandel, E. R. (1997). Brief theta-burst stimulation induces a transcription-dependent late phase of LTP requiring cAMP in area CA1 of the mouse hippocampus. *Learn. Mem.* 4, 230–243. doi: 10.1101/lm.4.2.230

Parikh, V., Medley, A., Chung, Y. C., and Goh, H. T. (2021). Optimal timing and neural loci: a scoping review on the effect of non-invasive brain stimulation on post-stroke gait and balance recovery. *Top. Stroke Rehabil.* 30, 1–17. doi: 10.1080/10749357.2021.1990467

Paulus, W. (2005). Toward establishing a therapeutic window for rTMS by Theta burst stimulation. *Neuron* 45, 181–183. doi: 10.1016/j.neuron.2005.01.008

Pekny, M., and Pekna, M. (2004). Astrocyte intermediate filaments in CNS pathologies and regeneration. *J. Pathol.* 204, 428–437. doi: 10.1002/path.1645

Polanía, R., Nitsche, M. A., and Ruff, C. C. (2018). Studying and modifying brain function with non-invasive brain stimulation. *Nat. Neurosci.* 21, 174–187. doi: 10.1038/s41593-017-0054-4

Rounis, E., and Huang, Y. Z. (2020). Theta burst stimulation in humans: a need for better understanding effects of brain stimulation in health and disease. *Exp. Brain Res.* 238, 1707–1714. doi: 10.1007/s00221-020-05880-1

Rroji, O., Van Kuyck, K., Nuttin, B., and Wenderoth, N. (2015). Anodal tDCS over the primary motor cortex facilitates long-term memory formation reflecting use-dependent plasticity. *PloS One* 10:e0127270. doi: 10.1371/journal.pone.0127270

Sanches, C., Stengel, C., Godard, J., Mertz, J., Teichmann, M., Migliaccio, R., et al. (2020). Past, present, and future of non-invasive brain stimulation approaches to treat cognitive impairment in neurodegenerative diseases: time for a comprehensive critical review. *Front. Aging Neurosci.* 12:578339. doi: 10.3389/fnagi.2020.578339

Santos Ferreira, I., Teixeira Costa, B., Lima Ramos, C., Lucena, P., Thibaut, A., and Fregni, F. (2019). Searching for the optimal tDCS target for motor rehabilitation. *J. Neuroeng. Rehabil.* 16:90. doi: 10.1186/s12984-019-0561-5

Schulz, R., Gerloff, C., and Hummel, F. C. (2013). Non-invasive brain stimulation in neurological diseases. *Neuropharmacology* 64, 579–587. doi: 10.1016/j.neuropharm.2012.05.016

Semmler, J. G., Hand, B. J., Sasaki, R., Merkin, A., and Opie, G. M. (2021). Age-related changes in motor cortex plasticity assessed with non-invasive brain stimulation: an update and new perspectives. *Exp. Brain Res.* 239, 2661–2678. doi: 10.1007/s00221-021-06163-z

Terranova, C., Rizzo, V., Cacciola, A., Chillemi, G., Calamuneri, A., Milardi, D., et al. (2018). Is there a future for non-invasive brain stimulation as a therapeutic tool? *Front. Neurol.* 9:1146. doi: 10.3389/fneur.2018.01146

Trippe, J., Mix, A., Aydin-Abidin, S., Funke, K., and Benali, A. (2009). theta burst and conventional low-frequency rTMS differentially affect GABAergic neurotransmission in the rat cortex. *Exp. Brain Res.* 199, 411–421. doi: 10.1007/s00221-009-1961-8

Veldema, J., and Gharabaghi, A. (2022). Non-invasive brain stimulation for improving gait, balance, and lower limbs motor function in stroke. *J. Neuroeng. Rehabil.* 19:84. doi: 10.1186/s12984-022-01062-y

Wang, H., and Peng, R. Y. (2016). Basic roles of key molecules connected with NMDAR signaling pathway on regulating learning and memory and synaptic plasticity. *Mil. Med. Res.* 3:26. doi: 10.1186/s40779-016-0095-0

Wong, C. G., Bottiglieri, T., and Snead, O. C. (2003). GABA, gamma-hydroxybutyric acid, and neurological disease. *Ann. Neurol.* 54, S3–S12. doi: 10.1002/ana.10696

Yamada, Y., and Sumiyoshi, T. (2021). Neurobiological mechanisms of transcranial direct current stimulation for psychiatric disorders; neurophysiological, chemical, and anatomical considerations. *Front. Hum. Neurosci.* 15:838. doi: 10.3389/fnhum.2021.631838

Zhang, J. J., Bai, Z., and Fong, K. N. K. (2022). Priming intermittent Theta burst stimulation for Hemiparetic upper limb after stroke: a randomized controlled trial. *Stroke* 53, 2171–2181. doi: 10.1161/STROKEAHA.121.037870

Zhang, J., Zhang, D., Mcquade, J. S., Behbehani, M., Tsien, J. Z., and Xu, M. (2002). C-fos regulates neuronal excitability and survival. *Nat. Genet.* 30, 416–420. doi: 10.1038/ng859

Zhao, X., Ding, J., Pan, H., Zhang, S., Pan, D., Yu, H., et al. (2020). Anodal and cathodal tDCS modulate neural activity and selectively affect GABA and glutamate syntheses in the visual cortex of cats. *J. Physiol.* 598, 3727–3745. doi: 10.1113/JP279340

frontiers | Frontiers in Neuroscience

TYPE Opinion
PUBLISHED 08 January 2024
DOI 10.3389/fnins.2023.1336134

OPEN ACCESS

EDITED BY
Mark H. Myers,
University of Tennessee Health Science Center (UTHSC), United States

REVIEWED BY
Tsung-Hsun Hsieh,
Chang Gung University, Taiwan

*CORRESPONDENCE
Jack Jiaqi Zhang
jack-jq.zhang@connect.polyu.hk

RECEIVED 10 November 2023
ACCEPTED 20 December 2023
PUBLISHED 08 January 2024

CITATION
Zhang JJ (2024) Cortico-cortical paired associative stimulation: a novel neurostimulation solution for modulating brain connectivity and networks.
Front. Neurosci. 17:1336134.
doi: 10.3389/fnins.2023.1336134

Cortico-cortical paired associative stimulation: a novel neurostimulation solution for modulating brain connectivity and networks

Jack Jiaqi Zhang *

Department of Rehabilitation Sciences, The Hong Kong Polytechnic University, Kowloon, Hong Kong SAR, China

KEYWORDS

paired associative stimulation (PAS), transcranial magnetic stimulation (TMS), connectivity, neural network, neuromodulation

Introduction

Transcranial magnetic stimulation (TMS) noninvasively modulates brain excitability. Despite its advancement in research and clinical utility, current interventional TMS protocols can only target a single brain region. When applying two sequential TMS sessions to different regions, the overall after-effect is found to be uncontrollable. For instance, Do et al. (2018) have used sequentially applied theta burst stimulation (TBS, a patterned form of repetitive TMS) in two brain regions in healthy adults, including dorsolateral prefrontal cortex-primary motor cortex (M1), ventral premotor cortex (PMv)-M1, and M1-M1; however, the after-effects seem largely unpredictable due to response variability and complex metaplastic interactions between two brain regions. Therefore, there is indeed a lack of a reliable and robust neurostimulation protocol for modulating interregional connectivity and networks.

Paired associative stimulation (PAS) is a form of neuromodulation using TMS and peripheral nerve stimulation (Stefan et al., 2000). Its cellular mechanism is based on spike-timing dependent plasticity (STDP), i.e., if an input spike to a neuron tends to occur immediately before that neuron's output spike, then the connection is strengthened. If an input spike tends to occur immediately after an output spike, then the connection is weakened (Dan and Poo, 2004). PAS combines single pulses of electrical stimulation to a peripheral nerve (for stimulating the primary somatosensory cortex, S1) and single pulses of TMS over the contralateral M1. If the interval between the peripheral nerve stimulation and the TMS is 25ms (or individual N20[1] latency), the S1 is activated immediately before the M1 activation, and the connection between S1 and M1 is strengthened (Stefan et al., 2000; Ziemann et al., 2004). When the interval is 10 ms (or individual N20 latency-5 ms), the activation of the S1 is always after the M1 activation, so their connection is weakened (Stefan et al., 2000; Ziemann et al., 2004). Research using PAS has demonstrated that a STDP-like effect can be induced in human M1-S1 connections.

Cortico-cortical paired associative stimulation (ccPAS) differs from the 'classical' PAS, which uses a dual-coil TMS approach to apply repetitive paired-pulse stimulations over two cortical regions (Guidali et al., 2021) (Figure 1A). ccPAS is believed to induce STDP-like plasticity over a cortico-cortical connection. Previous research has applied ccPAS paradigms in several cortico-cortical connections, such as M1-M1, PMv-M1,

1 N20 component of the somatosensory evoked potential.

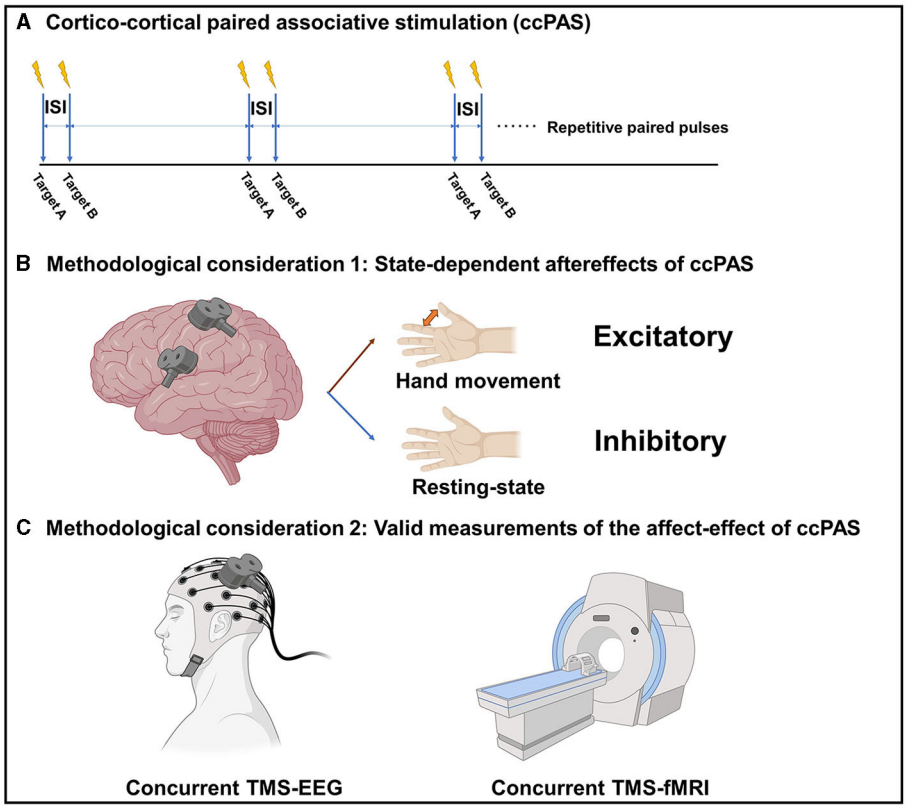

FIGURE 1
(A) The paradigm of cortico-cortical paired associative stimulation (ccPAS). **(B)** State-dependent after-effects of ccPAS. **(C)** Valid measurements of the after-effects of ccPAS. ISI, Inter-stimulus interval; TMS, Transcranial magnetic stimulation; EEG, electroencephalography; fMRI, functional magnetic resonance imaging. The figure was created with BioRender.com.

supplementary motor area (SMA)-M1, and posterior parietal cortex (PPC)-M1 (Guidali et al., 2021). The inter-stimulus interval is determined based on the estimated projection time between the two brain regions, in order to produce a bidirectional modulatory effect according to the rule of STDP.

Discussion: methodological considerations of ccPAS

State-dependence

The effect of ccPAS appears to be state-dependent. For example, it has been shown that the modulatory effect of PMv-M1 ccPAS is dependent on the current motor state. At resting state, ccPAS over the PMv and M1 could decrease the motor-evoked potential (MEP) in healthy adults, while ccPAS over the PMv and M1 tapped into motor tasks could increase the MEP in healthy adults (Davare et al., 2008; Buch et al., 2011). The reason behind this is that, during the resting state, the overall effect is inhibitory because the PMv-M1 glutamatergic projection activates the local inhibitory circuits more than the excitatory circuits within the M1. However, during movement status, the local inhibitory circuits are transiently blocked, so the projection activates the local excitatory circuits within the M1 therefore increasing the corticospinal excitability (Figure 1B). Therefore, the modulatory effect of ccPAS is likely to be bidirectional and depends on the current brain state.

Valid measurements of the affect-effect of ccPAS

While it is assumed that ccPAS can modulate brain connectivity and networks, its modulatory effect has not been thoroughly examined using reliable techniques and biomarkers. Paired-pulse TMS-electromyography (EMG) measurements over a brain connection is the most commonly used outcome measure; however, they can only be applied to ccPAS that involves M1, and their output, in the form of a MEP, is not a pure cortical response. Indeed, we still need a valid measurement to assess the effect of ccPAS on modulating corticocortical connectivity and brain networks. Concurrent TMS-functional magnetic resonance imaging (fMRI) and TMS-electroencephalography (EEG) techniques are emerging cross-modal neuroscience measurement tools that may be used to study the modulatory effect of ccPAS on brain connectivity or networks. Upon perturbing a single brain region using TMS, the combined fMRI and/or EEG can capture the immediate and subsequent effects on the connected brain regions and the dynamics of neural networks, therefore making them unique solutions for evaluating brain connectivity and networks. There

are also some pioneer works using concurrent recordings to study brain connectivity and networks. A concurrent TMS-fMRI study conducted by Bestmann et al. (2008) contributed a measurement of the connectivity between the dorsal premotor cortex (dPMC) and contralateral M1. Furthermore, the authors found that the facilitatory projection from the contralesional dorsal premotor cortex to the ipsilesional M1 was increased in patients after stroke with severe motor impairment in a compensatory manner (Bestmann et al., 2010). Additionally, a concurrent TMS-EEG study conducted by Bai et al. (2023) revealed a decrease in global efficacy when TMS stimulation was applied over the ipsilesional M1 compared to the contralesional M1 in stroke patients. This suggests an impairment of the brain network related to the ipsilesional M1 in chronic stroke. Thus, co-registration techniques enable the probing of brain connectivity and networks, potentially yielding a range of neural biomarkers for a comprehensive evaluation of the ccPAS effect (Figure 1C). It is of importance to note that a major limitation of concurrent TMS-fMRI and TMS-EEG is the contamination from non-neural sources in association with TMS. Therefore, a realistic sham condition is always required, which inevitably extends the measurement time (Gordon et al., 2018).

Conclusion

ccPAS holds the promise to become a revolutionary neurostimulation paradigm for directionally modulating interregional brain connectivity and networks. It can serve a neuroscience research tool for studying the causal relationship between interregional connectivity and human behaviors. On the other, it could possibly become a novel therapeutic solution for repairing neural circuits, as various neurological and psychiatric conditions like stroke, Parkinson's disease, and major depressive disorders have been linked to impairments of brain connectivity and networks. Further study is encouraged to investigate the state-dependence of ccPAS to order to yield a robust modulatory effect and to establish a valid measurement for its affect-effect on brain connectivity and networks.

Author contributions

JZ: Resources, Writing – original draft, Writing – review & editing.

Funding

The author(s) declare that no financial support was received for the research, authorship, and/or publication of this article.

Conflict of interest

The author declares that the research was conducted in the absence of any commercial or financial relationships that could be construed as a potential conflict of interest.

Publisher's note

References

Bai, Z., Zhang, J. J., and Fong, K. N. K. (2023). Intracortical and intercortical networks in patients after stroke: a concurrent TMS-EEG study. *J. Neuroeng. Rehabil.* 20, 100. doi: 10.1186/s12984-023-01223-7

Bestmann, S., Swayne, O., Blankenburg, F., Ruff, C. C., Haggard, P., Weiskopf, N., et al. (2008). Dorsal premotor cortex exerts state-dependent causal influences on activity in contralateral primary motor and dorsal premotor cortex. *Cereb. Cortex.* 18, 1281–1291. doi: 10.1093/cercor/bhm159

Bestmann, S., Swayne, O., Blankenburg, F., Ruff, C. C., Teo, J., Weiskopf, N., et al. (2010). The role of contralesional dorsal premotor cortex after stroke as studied with concurrent TMS-fMRI. *J. Neurosci.* 30, 11926–11937. doi: 10.1523/JNEUROSCI.5642-09.2010

Buch, E. R., Johnen, V. M., Nelissen, N., O'Shea, J., and Rushworth, M. F. (2011). Noninvasive associative plasticity induction in a corticocortical pathway of the human brain. *J. Neurosci.* 31, 17669–17679. doi: 10.1523/JNEUROSCI.1513-11.2011

Dan, Y., and Poo, M. M. (2004). Spike timing-dependent plasticity of neural circuits. *Neuron.* 44, 23–30. doi: 10.1016/j.neuron.2004.09.007

Davare, M., Lemon, R., and Olivier, E. (2008). Selective modulation of interactions between ventral premotor cortex and primary motor cortex during precision grasping in humans. *J. Physiol.* 586, 2735–2742. doi: 10.1113/jphysiol.2008.152603

Do, M., Kirkovski, M., Davies, C. B., Bekkali, S., Byrne, L. K., Enticott, P. G., et al. (2018). Intra- and inter-regional priming of ipsilateral human primary motor cortex with continuous theta burst stimulation does not induce consistent neuroplastic effects. *Front. Hum. Neurosci.* 12, 123. doi: 10.3389/fnhum.2018.00123

Gordon, P. C., Desideri, D., Belardinelli, P., Zrenner, C., and Ziemann, U. (2018). Comparison of cortical EEG responses to realistic sham versus real TMS of human motor cortex. *Brain Stimul.* 11, 1322–1330. doi: 10.1016/j.brs.2018.08.003

Guidali, G., Roncoroni, C., and Bolognini, N. (2021). Paired associative stimulations: Novel tools for interacting with sensory and motor cortical plasticity. *Behav. Brain. Res.* 414, 113484. doi: 10.1016/j.bbr.2021.113484

Stefan, K., Kunesch, E., Cohen, L. G., Benecke, R., and Classen, J. (2000). Induction of plasticity in the human motor cortex by paired associative stimulation. *Brain.* 123, 572–584. doi: 10.1093/brain/123.3.572

Ziemann, U., Ili,ć, T. V., Pauli, C., Meintzschel, F., and Ruge, D. (2004). Learning modifies subsequent induction of long-term potentiation-like and long-term depression-like plasticity in human motor cortex. *J. Neurosci.* 24, 1666–1672. doi: 10.1523/JNEUROSCI.5016-03.2004

frontiers | Frontiers in Neuroscience

TYPE Original Research
PUBLISHED 07 February 2024
DOI 10.3389/fnins.2024.1313639

OPEN ACCESS

EDITED BY
Mark H. Myers,
University of Tennessee Health Science Center (UTHSC), United States

REVIEWED BY
Alessandro Martorana,
University of Rome Tor Vergata, Italy
Francesco Di Lorenzo,
Santa Lucia Foundation (IRCCS), Italy

*CORRESPONDENCE
Shuai Zhang
✉ zs@hebut.edu.cn

RECEIVED 10 October 2023
ACCEPTED 22 January 2024
PUBLISHED 07 February 2024

CITATION
Zhang S, Guo Z, Xu Y, Mi J, Liu J, Li Z, Xie X and Xu G (2024) Transcranial magneto-acoustic stimulation improves spatial memory and modulates hippocampal neural oscillations in a mouse model of Alzheimer's disease. *Front. Neurosci.* 18:1313639. doi: 10.3389/fnins.2024.1313639

Transcranial magneto-acoustic stimulation improves spatial memory and modulates hippocampal neural oscillations in a mouse model of Alzheimer's disease

Shuai Zhang[1,2,3]*, Zhongsheng Guo[1,2,3], Yihao Xu[2,3], Jinrui Mi[2,3], Jun Liu[2,3], Zichun Li[2,3], Xiaofeng Xie[2,3] and Guizhi Xu[1,2,3]

[1]State Key Laboratory of Reliability and Intelligence of Electrical Equipment, Hebei University of Technology, Tianjin, China, [2]Hebei key Laboratory of Bioelectromagnetism and Neural Engineering, Hebei University of Technology, Tianjin, China, [3]Tianjin Key Laboratory of Bioelectromagnetic Technology and Intelligent Health, Tianjin, China

Introduction: In our study, we applied transcranial magneto-acoustic stimulation (TMAS), a technique based on focused ultrasound stimulation within a static magnetic field, in the APP/PS1 mouse model of Alzheimer's disease (AD) to explore the feasibility of TMAS on improving AD related spatial memory deficits and abnormal neural oscillations.

Methods: The mice treated with TMAS once daily for 21 days. We recorded local field potential signals in the hippocampal CA1 region of the mice after TMAS treatment with *in-vivo* electrophysiology and evaluated the neural rehabilitative effect of TMAS with sharp-wave ripple (SWR), gamma oscillations during SWRs, and phase-amplitude coupling (PAC). The spatial memory function of the mice was examined by the Morris water maze (MWM) task.

Results: We found that TMAS improved the performance of MWM related spatial cognitive functions compared with AD group. Furthermore, our results implied that TMAS alleviated abnormalities in hippocampal SWRs, increased slow gamma power during SWRs, and promoted theta-slow gamma phase-amplitude coupling. These findings suggest that TMAS could have a positive influence on spatial memory through the modulation of neural oscillations.

Discussion: This work emphasizes the potential of TMAS to serve as a non-invasive method for Alzheimer's disease rehabilitation and promote the application of TMAS for the treatment of more neurological and brain aging diseases in the future.

KEYWORDS

transcranial magneto-acoustic stimulation, neuromodulation, Alzheimer's disease, neural oscillations, local field potentials

1 Introduction

As global life expectancy continues to increase, the world's aging population is growing. Concurrently, the prevalence of neurodegenerative disorders, including dementia, is also increasing (Livingston et al., 2020). Among these conditions, Alzheimer's disease (AD) emerges as the most common form of dementia, primarily affecting the elderly (Dolgin, 2016). AD is a neurodegenerative disorder that leads to cognitive impairments and memory dysfunction (Wu et al., 2022). The deposition of amyloid beta and the formation

of neurofibrillary tangles are the pathological processes associated with AD (Yokoyama et al., 2022). These pathological features have the potential to disrupt synaptic and neuronal activity, causing network abnormalities in various brain regions (Casula et al., 2022; Luo et al., 2023; Pless et al., 2023). In the brains of AD patients, various neurophysiological features have been detected, including hyperexcitability in the precuneus cortex (Casula et al., 2023) and impairment of cerebellar-cortical plasticity mechanisms (Di Lorenzo et al., 2020). These abnormal neural activities may lead to neuronal network dysfunction in AD, thereby contributing to cognitive impairment. The hippocampus, a critical brain region for memory encoding, storage, and retrieval, is among the earliest regions affected by AD pathology (Gillespie et al., 2016; Caccavano et al., 2020). Researchers have detected anomalies in neural oscillations that are linked to with cognitive processes involved in memory by using electroencephalogram or local field potential (LFP) recordings in the hippocampal region of both AD patients and animal models (Roux and Uhlhaas, 2014; Miller et al., 2018; Jafari and Kolb, 2020; Zhou et al., 2022). Further exploration of their role within the context of AD pathology has revealed potential opportunities for interventions in the treatment of AD (Chan et al., 2021; Traikapi and Konstantinou, 2021).

The hippocampus contains a significant population of interneurons that play a crucial role in driving neuronal synchronization (da Cruz et al., 2020; He et al., 2021). Gamma oscillations within the hippocampus have been associated with memory and cognition in both animals and humans, and it is possible that functional distinctions exist across various frequency ranges (Mably and Colgin, 2018). Specifically, slow gamma oscillations (25 Hz−50 Hz) are thought to enhance memory retrieval processes within the hippocampus (Zheng et al., 2016), with increased slow gamma activity being observed during tasks involving higher memory demands (Rangel et al., 2016). Hippocampal sharp-wave ripple (SWR) plays an important role in supporting memory consolidation and replay (Buzsaki, 2015; Katsuki et al., 2022). Disruption of SWR can impair memory performance (Aleman-Zapata et al., 2022), while prolonging the duration of SWR through optogenetic stimulation improves memory performance in rats during maze tasks (Fernández-Ruiz et al., 2019). Research has revealed defects in hippocampal gamma oscillations and SWR in AD (Hollnagel et al., 2016; Klein et al., 2016; Witton et al., 2016; Benthem et al., 2020).

Neural stimulation is a method of neuroregulation that involve delivering stimulations, such as electrical, magnetic, optical, and ultrasound, to selected brain areas in order to modulate local and network-wide neuronal activity (Yuan et al., 2020). Transcranial magneto-acoustic stimulation (TMAS) is an innovative form of a non-invasive tool that allows for the stimulation of specific brain regions within a static magnetic field using low-intensity focused ultrasound (Yuan and Chen, 2016; Wang et al., 2019). In 2003, Norton proposed the idea of using ultrasounds for stimulation in a static magnetic field (Norton, 2003). The motion of ionic particles induced by ultrasounds inside brain tissue will form Lorentz force under a static magnetic field, and TMAS allows the combined action of a magneto-acoustic electric field and an ultrasound wave (Wang et al., 2016; Yuan et al., 2016). Notably, even in deep brain regions, TMAS can provide a high spatial resolution stimulating electric field at the target site due to the utilization of focused ultrasound (Liu et al., 2019; Yu et al., 2021). TMAS possesses distinct advantages that address the demands of depth and improved localization, holding significant research value and promising potential applications in the development of intervention techniques for brain functional disorders (Chu et al., 2023).

Research indicates that TMAS, as a non-invasive neurostimulation approach, can modulate neuronal activity to enhance brain function (Liu et al., 2019; Wang et al., 2019; Zhang et al., 2022). In this study, we applied TMAS to treat AD model mice model and examined its impact on neuronal activity in the hippocampus. To assess the impact of TMAS on spatial memory in AD mice, we conducted Morris water maze (MWM) tests. Additionally, we recorded *in vivo* electrophysiological signals of the mouse hippocampus to explore potential underlying mechanisms. Our findings demonstrate that TMAS can improve spatial memory in AD mice and regulate hippocampal oscillations, providing a promising intervention approach for AD treatment.

2 Materials and methods

2.1 Animals

The animal model for Alzheimer's Disease (AD) in this study comprised 14 male APP/PS1 mice, aged 4 months, along with 7 age-matched male C57/BL6 mice (all purchased from Beijing HFK-Bio-Technology Co. Ltd., China). The animals were housed in the animal laboratory of Hebei University of Technology throughout the experimental period, with each mouse kept in a standard cage. The light cycle was maintained at 12 h (lights on at 7 am, off at 7 pm), and the housing environment was maintained at a temperature of 24°C and 50% humidity. Food and water were provided *ad libitum*. The 14 AD model mice were randomly divided into two groups of 7 mice each: the no-stimulation group and the TMAS group. Additionally, 7 C57 mice were included in the WT group. All experimental procedures were approved by Biomedical Ethics Committee of the Hebei University of Technology.

2.2 Operation

After sedating the mice with 2% isoflurane in the induction box, they were fixed onto a stereotactic frame (51670, Stoelting, USA). The mice's head was immobilized using ear bars and positioned horizontally, while 1%-2% isoflurane was administered via an anesthesia mask to maintain anesthetic state. Fur was removed from the scalp, the skin was cleaned with physiological 0.9% sodium chloride solution and sterilized with 70% ethanol. The scalp was incised along the midline of the skull to expose the bone, and the tissue was cleaned with 2% hydrogen peroxide. According to the stereotaxic map, a 1 mm square window was drilled through the skull for placing the recording electrode in the hippocampal CA1 region (AP: −1.82 mm, ML: 1.20 mm, DV: −1.30 mm). The electrode was then secured using dental cement in layers. After the surgery, mice were given a recovery period of at least 1 week.

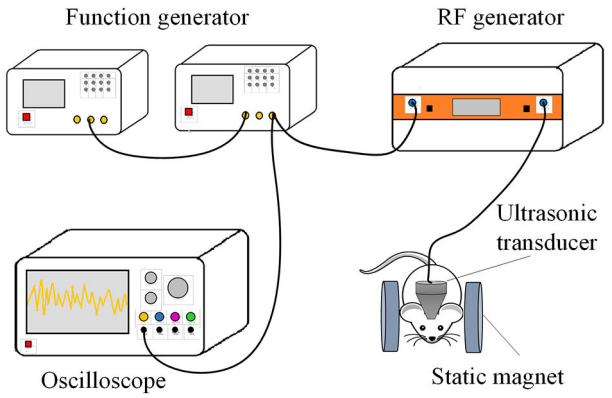

FIGURE 1
Diagram of transcranial magneto-acoustic stimulation system.

2.3 TMAS treatment of AD model mice

After surgical recovery, the TMAS group received 21 days of stimulation. The TMAS system, as depicted in Figure 1, consists of 2 function generators (33500B Series, KEYSIGHT, USA), a radiofrequency power amplifier (Model 150A100C, AR, USA), an ultrasonic transducer (P20FG, Shantou Electronics, China), an oscilloscope (TDS3014, Tektronix, USA), and 2 cylindrical neodymium iron boron permanent magnets. Two cylindrical neodymium iron boron permanent magnets with a diameter of 40 mm and thickness of 10 mm were employed to provide a horizontal static magnetic field of 0.3 T. The pulsed signals generated by two function generators were fed to the radiofrequency power amplifier and then sent to drive the ultrasonic transducer. The ultrasonic fundamental frequency was 0.5 MHz, the pulse repetition frequency was 1 kHz, the tone-burst duration was 0.5 ms, the sonication duration was 400 ms, the ultrasonic pressure was 0.3 MPa, the spatial-peak pulse-average intensity was 2.839 W/cm^2, and the stimulation duration was 2 min. During stimulation, the mouse was anesthetized by 1% isoflurane, and TMAS was applied by connecting an ultrasound transducer through a conical collimator filled with bubble-free ultrasound coupling gel onto the mouse skull, targeting the hippocampal region. Mice of AD-TMAS group received TMAS once daily for a consecutive period of 21 days. Mice of AD groups received sham stimulation by keeping the turned-off ultrasound probe on the mouse head located within the same static magnetic field for the same amount of time as AD-TMAS groups.

2.4 Morris water maze test

The mice underwent 8 days of behavioral testing in the MWM. The round tank was divided into four equal quadrants by creating two invisible perpendicular lines. Each mouse was trained 4 times a day with an interval of at least 10 min between each session, during both the visible platform training and the hidden platform training. In the visible platform training, the platform was positioned at the center of one quadrant, elevated 0.5 cm to 1 cm above the water's surface. Mice were placed into water from the opposite quadrant, and their time to reach the platform and swimming speed were recorded using the Morris Water Maze video analysis system (SA201, SANS, China) to assess visual acuity and motor ability. If the mice did not find the platform after 60 s, they were guided to the platform and allowed to stay for 30 s—60 s. During the hidden platform training, the platform was kept in a constant position at the center of one quadrant and submerged 1 cm below the water's surface. The escape latency of mice was recorded, and if a mouse did not reach the platform within 60 s, it was guided to the platform, and the latency was recorded as 60 s. The probe trial was conducted 24 h after the completion of the hidden platform training. In this trial, the platform was removed, and each mouse underwent a 60-s test, during which the number of crossings through the target quadrant and the time spent in the target quadrant were recorded.

2.5 Electrophysiological recording

The electrophysiological signals of the mice were recorded for the subsequent 5 days after the completion of the entire stimulation period. Hippocampal electrophysiological activity was recorded using a 126-channel Plexon neural data acquisition system (Omniplex, Plexon Inc) while mice were in their home cages. Neurophysiological signals were collected at a frequency of 40 kHz through a headstage cable connected to the DigiAmp digital amplifier. LFP signals were stored on a PC and down-sampled to 1 kHz for offline analysis.

2.6 Data analysis

To detect SWR events, the local field potential (LFP) was bandpass filtered between 150 Hz—250 Hz, and the Hilbert transform was applied to obtain the SWR envelope amplitude. SWRs were identified as times when the envelope of the ripple-filtered trace exceeded 5 SDs of the signal for at least 15 ms (Cheng and Frank, 2008). The entire SWR was defined as the periods, containing times immediately before and after that prolonged threshold crossing event during which the envelope exceeded the baseline value. Analysis of SWRs was confined to periods of extended immobility. Spectrogram analysis was conducted using the multitaper method (Chronux toolbox) (Bokil et al., 2010). Spectrograms of SWRs were computed for a window extending 400 ms before and after the onset of each SWR. For evaluating cross-frequency coupling strength, the mean and standard deviation of the computed spectrograms were used to calculate z-score power for each frequency band. The quantification of slow gamma power during SWRs was calculated as the averaged the z-score power over a 30 Hz—50 Hz frequency band at 1 ms—100 ms after the initiation of SWR.

For the assessment of cross-frequency coupling strength, phase-amplitude coupling (PAC) was computed using the instantaneous phase and amplitude of the filtered LFP signal (Belluscio et al., 2012). Phase and amplitude in specific frequency bands were obtained through Hilbert transforms. The modulation index (MI)

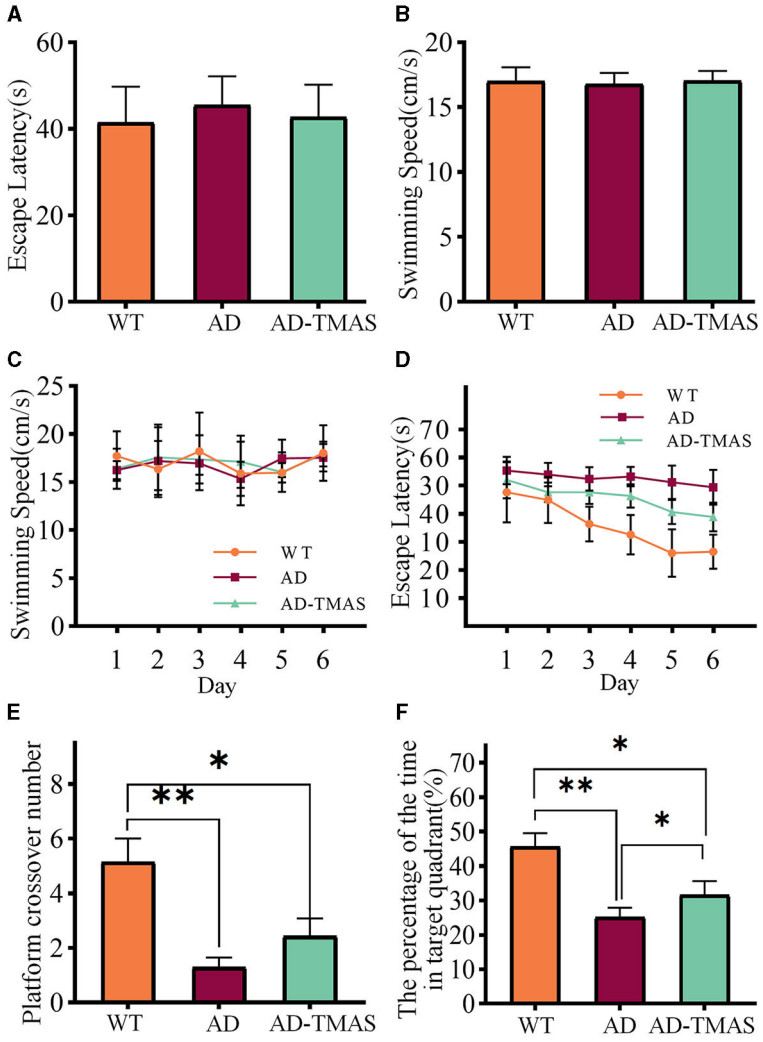

FIGURE 2
MWM training and test results. **(A)** Escape latencies during visible platform day. **(B)** Swimming speeds during visible platform day. **(C)** Swimming speeds during hidden platform days. **(D)** Escape latencies during hidden platform days. **(E)** Platform crossover number during probe day. **(F)** Percentage of duration spent in the target quadrant. *$p < 0.05$; **$p < 0.01$.

was calculated to quantify PAC between the theta band (4 Hz−12 Hz) and the slow gamma band (30 Hz−50 Hz).

2.7 Statistics

The results are presented as mean ± standard error of the mean (SEM). Data analysis was performed using the statistical software SPSS (IBM SPSS Statistics, IBM Corp., Armonk, NY, USA), and graph generation was carried out using GraphPad Prism software (GraphPad Software Inc., La Jolla, CA, USA). Levene's test was used to assess homogeneity of variances. For normally distributed data, one-way ANOVA was employed for comparison among multiple groups, followed by *post-hoc* evaluation using the Scheffe multiple range test. For non-normally distributed data, the Kruskal–Wallis test was used to assess differences in medians, and the Bonferroni method was applied for correcting multiple comparisons. $P < 0.05$ were considered statistically significant. *$P < 0.05$; **$P < 0.01$.

3 Results

3.1 Behavioral improvement after TMAS

The results of spatial memory assessment in various groups of mice using the Morris water maze (MWM) test as shown in Figure 2. During the visible platform training, there were no significant differences in the time taken by mice from different groups to reach the platform [$F_{(2,18)} = 0.53$, $P > 0.05$] and in the swimming speed of mice in different groups [$F_{(2,18)} = 0.14$, $P > 0.05$] (Figures 2A, B). At this stage, the AD mice showed no motor impairment, and their visual acuity was normal. Subsequently, a 6 day hidden platform training was conducted, and the swimming speed (Figure 2C) and time to reach the platform (Figure 2D) of mice from different groups were recorded. The swimming speed of mice in different groups showed no significant changes as the experiment days progressed [$F_{(5,17)} = 2.40$, $P > 0.05$], indicating that the escape latency during the hidden platform phase was

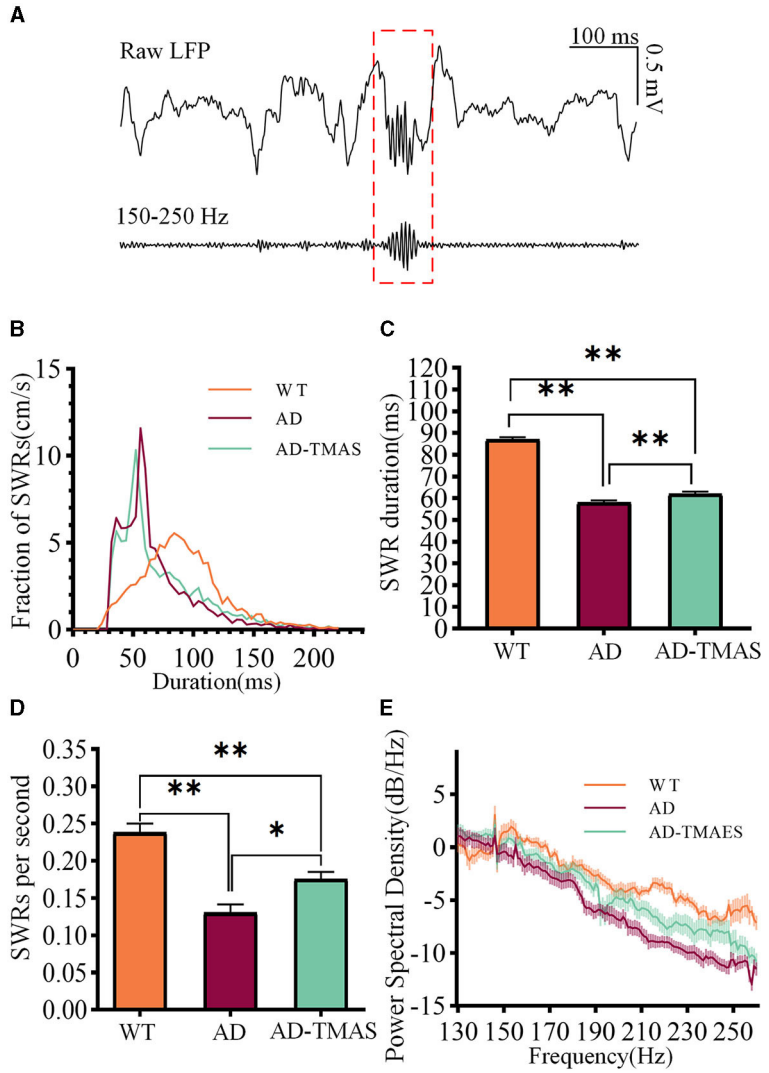

FIGURE 3
Characteristics of SWRs. **(A)** Representative traces of band-pass filtered SWRs (150 Hz–250 Hz). **(B)** Frequency distribution of SWR durations. **(C)** SWR durations (median with 95% confidence interval). **(D)** Average incidence rate of SWRs. **(E)** Power spectral density of LFPs. The values are presented as mean ± SEM unless otherwise specified; *$p < 0.05$; **$p < 0.01$.

negligible influenced by swimming speed. In fact, it was primarily affected by spatial memory capability of the mice. The escape latency of the control group mice was notably lower than that of the AD group mice from the second day. While the escape latency of the control group mice decreased as the experiment days progressed, the AD group mice showed no significant decrease in escape latency. The stimulation group demonstrated a reduced escape latency when compared to the AD group. Finally, a one-day probe trial was conducted to assess the number of crossings through the original platform location (Figure 2E) and the proportion of time spent in the quadrant of the original platform (Figure 2F). During the probe trial, there was a significant difference in the number of crossings between groups [$F_{(2,18)} = 9.16$, $P < 0.01$], with the AD-TMAS group exhibiting a higher mean value compared to the AD group (AD-TMAS: mean ± SEM = 2.43 ± 1.72, AD: mean ± SEM = 1.29 ± 0.95, $p = 0.48$). The proportion of time spent in the target quadrant also showed significant inter-group variation [$F_{(2,18)} = 14.50$, $P < 0.01$], with the AD-TMAS group displaying significant differences compared to the AD group ($P < 0.05$). The WT group mice exhibited higher numbers of platform crossings and a greater proportion of time spent in the target quadrant compared to the other two groups. The spatial learning and memory ability of AD mice was impaired, whereas TMAS demonstrated a certain degree of improvement in the spatial learning and memory deficits of the AD model mice.

3.2 Changes in hippocampal SWR after TMAS

SWRs reflect synchronized population activity patterns in the mammalian brain which are crucial for certain aspects of memory functions in the hippocampus. After detecting and recording SWRs (Figure 3A), we examined the characteristics of SWRs. Deficiencies in SWR duration were observed in the AD model mice (Figures 3B, C), with fewer longer duration of SWR compared to the WT

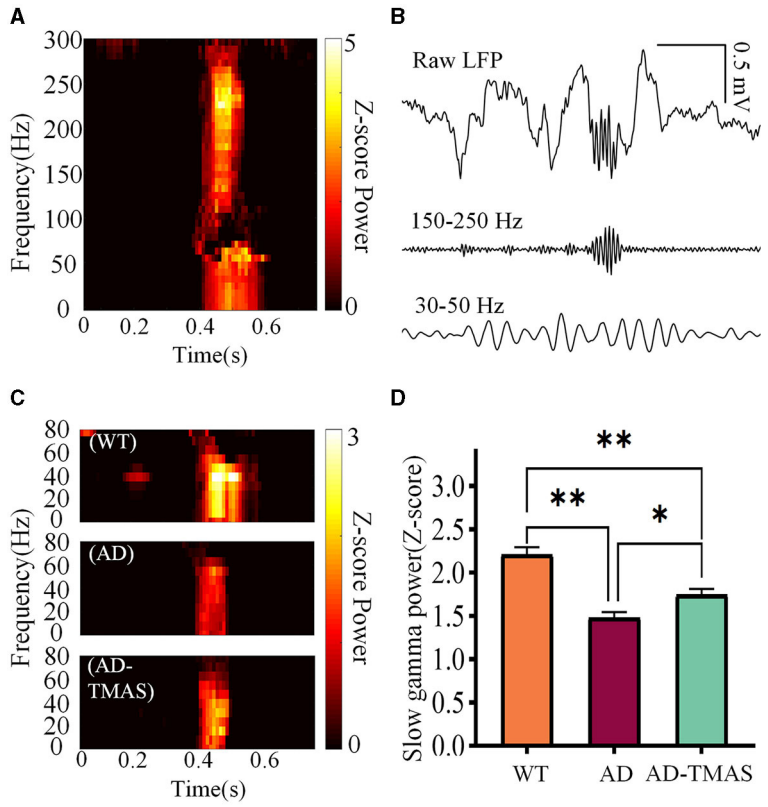

FIGURE 4
Slow gamma rhythm during SWRs. **(A)** Representative SWR-triggered spectrogram. **(B)** Illustrative trace of slow gamma bandpass filtered signals (30 Hz−50 Hz) during SWRs. **(C)** Representative triggered spectrograms during SWRs for different groups of mice. **(D)** Average SG Z-scores power during SWRs. The values are presented as mean ± SEM; *$p < 0.05$; **$p < 0.01$.

group (Kruskal–Wallis test, Bonferroni correction, $P < 0.01$). In comparison to the AD group, TMAS increased the duration of SWRs in the AD-TMAS group (Kruskal–Wallis test, Bonferroni correction, $P < 0.01$). There were significant differences in the incidence rate of SWRs [$F_{(2,18)} = 23.40, P < 0.01$] (Figure 3D). *Post-hoc* Scheffe tests indicated that the SWR incidence rate was lower in the AD group compared to the WT and AD-TMAS groups (WT vs. AD, $P < 0.01$; AD vs. AD-TMAS, $P < 0.05$). The AD group exhibited lower power spectral density traces in the LFP frequency range of 150 Hz to 250 Hz compared to the WT and AD-TMAS groups (Figure 3E).

3.3 TMAS can modulates slow gamma oscillations during SWRs

The time-frequency diagram revealed an increase in power within the ripple frequency range during SWRs, accompanied by a transient augmentation in slow gamma power (Figure 4A). Then we applied a 30 Hz to 50 Hz band-pass filter to the raw LFP signals (Figure 4B) and computed SWR triggered spectrograms for the 400 ms preceding and following SWRs (Figure 4C). To quantify SG power during SWRs, we calculated the Z-scored power of the SG frequency band (30 Hz−50 Hz) within the first 100 ms after SWR initiation (Figure 4D). Notably, SG power exhibited significant differences during SWRs [$F_{(2,102)} = 24.56$, $P < 0.01$], with AD mice displaying lower SG power compared to WT mice ($P < 0.01$). In comparison to the AD group, the AD-TMAS group demonstrated higher SG power during SWRs ($P < 0.05$).

3.4 TMAS enhances phase amplitude coupling in AD mice

In order to assess the synchronization and coordination of neural oscillatory networks, we calculated the phase-amplitude coupling (PAC) between theta oscillations and slow gamma oscillations, where the amplitude of slow gamma oscillations was modulated by the phase of theta oscillations. Subsequently, we computed the modulation index (MI) of PAC. In the WT group, strong theta-gamma cross-frequency coupling was observed (Figures 5A, B). A one-way analysis of variance of the average MI of theta-low gamma PAC revealed significant differences among the groups [Figure 5C; $F_{(2,102)} = 32.48$, $P < 0.01$]. *Post-hoc* tests indicated that the average MI of theta-low gamma PAC in the AD group was statistically lower than in the WT group ($P < 0.01$). Comparatively, TMAS increased the MI of theta-low gamma PAC

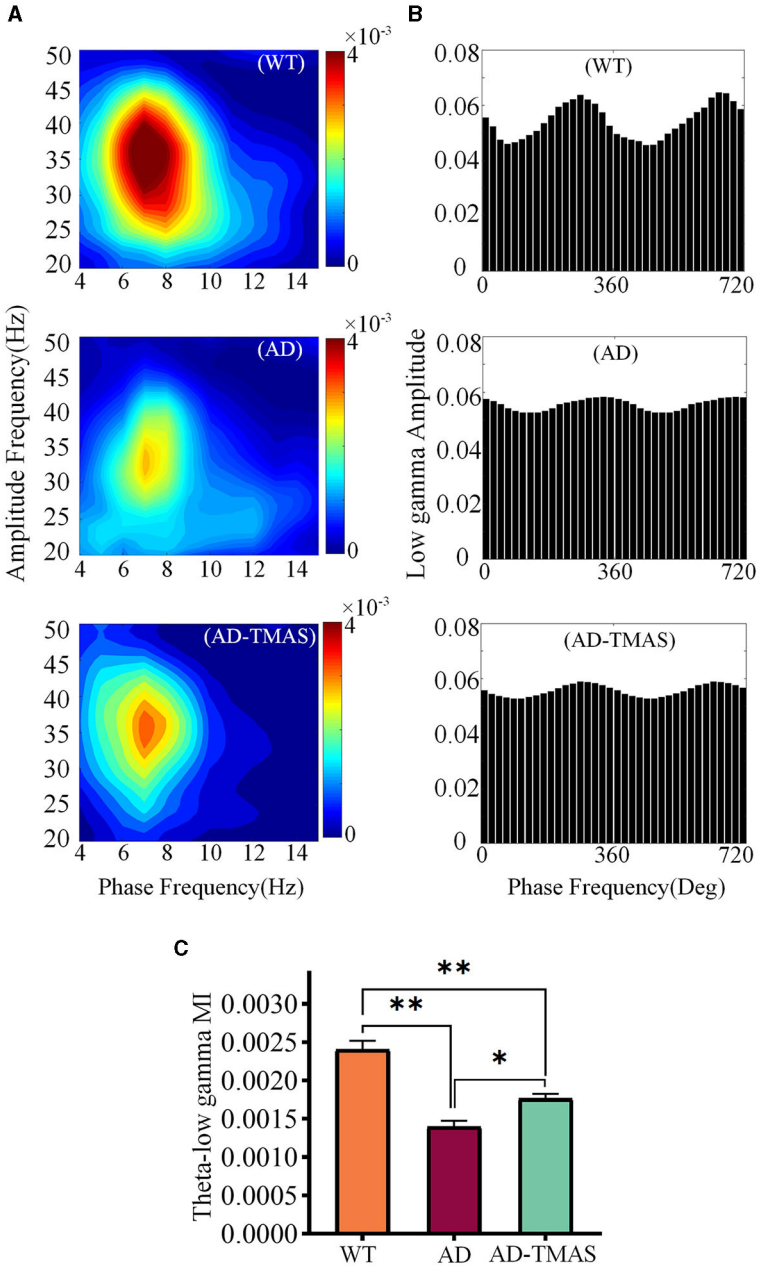

FIGURE 5
Phase amplitude coupling of hippocampal neural oscillations. **(A)** Example of Phase amplitude coupling of the theta and gamma bands. **(B)** Example of distribution of theta phase and slow gamma amplitude. **(C)** Average modulation index of theta-slow gamma PAC. The values are presented as mean ± SEM; *$p < 0.05$; **$p < 0.01$.

in the AD-TMAS group when compared to the AD group ($P < 0.05$).

4 Discussion

Here, we intervened with a magneto-acoustic couple stimulation that combines static magnetic field and ultrasound in APP/PS1 AD model mice. We found that AD model mice exhibited deficits in the MWM test, and that TMAS improved the results of the MWM test. To investigate the underlying mechanisms, we monitored LFPs in the mouse hippocampus, which reflect neuronal electrophysiological activity. Furthermore, we measured and compared neural oscillations in the hippocampus, an important feature of memory function in the hippocampus. It was found that SWRs features, slow gamma power during SWRs, and theta-gamma PAC were improved by TMAS treatment in the hippocampus of AD model mice.

TMAS is a non-invasive focused neuromodulation technique with the advantages of precision and depth of focused ultrasound stimulation (Zhang et al., 2018; Ning et al., 2022; Xie et al., 2022). TMAS combines the ultrasonic field with the electric field

generated by the magneto-acoustic coupling, and the stimulation intensity can be regulated by the ultrasonic parameters. Previous studies have shown that the effect of TMAS is superior to that of transcranial ultrasound stimulation (Zhou et al., 2019; Zhang et al., 2022). We have shown that TMAS can modulate neural oscillatory activity and affect the cross-frequency coupling of LFPs in rats (Dang et al., 2022). The treatment of TMAS on Parkinson's disease model rats also showed beneficial effects of TMAS on learning and memory (Wang et al., 2019). Hence, TMAS has important research value and application prospects for the treatment of neurodegenerative diseases.

The MWM test is a widely employed behavioral paradigm for assessing spatial learning and memory abilities in rodents, demonstrating heightened sensitivity to hippocampal memory impairments (Possin et al., 2016). In our MWM task, the performance of AD group exhibited a pronounced deficit relative to WT group, aligning consistently with prior research outcomes (Luo et al., 2023). During the hidden platform training, AD mice exhibited prolonged latency in locating the platform, indicative of compromised spatial learning abilities in this cohort. Furthermore, impaired memory retention was observed in AD mice, as evidenced by reduced time spent within the target quadrant during the probe test and a diminished preference for the target platform area. In this study, the application of TMAS demonstrated improvements in the performance of AD model mice in the MWM test, suggesting facilitation of spatial learning and memory consolidation.

The hippocampus is a crucial brain region for memory formation and consolidation, coordinating the encoding of episodic memory, spatial navigation, and contextual learning through its normal functioning (Jeffery, 2018). Alzheimer's disease often leads to disruptions in hippocampal function, affecting memory acquisition and recall deficits, thus impacting overall cognitive performance (Dautricourt et al., 2021). In non-invasive neural modulation for AD patients, regions interconnected with the hippocampus are common stimulation targets. The combined approach of transcranial magnetic stimulation and electroencephalography allows for the measurement of cortical hyperexcitability in the Precuneus region of AD patients (Casula et al., 2023), serving as a potentially valuable biomarker. Research on cerebellar-cortical plasticity implies that modulating cerebellar neural activity could be a potential therapeutic strategy for AD patients (Di Lorenzo et al., 2020). Future applications targeting effective stimulation points in humans still require further investigation. Neural oscillations involve rhythmic and coordinated neuronal firing, playing a vital role in memory consolidation and retrieval processes within the hippocampus (Mehak et al., 2022). With its dense population of neurons and distinct interneurons, the hippocampus facilitates long-range synchronization across regions, making it an ideal model system for studying brain rhythms (Ellender and Paulsen, 2010).

Hippocampal SWR, an eruption of hippocampal activity, represents an essential neuronal oscillatory phenomenon that is closely associated with the encoding of memories and the transfer of recently acquired memory traces to the neocortex for long-term storage (Xie et al., 2023). It is suggested that SWRs emerge as a result of synchronized activation of the CA1 region, driven by inputs from hippocampal CA3 pyramidal neurons (Buzsaki, 2015). Place cells within the hippocampus exhibit specific firing patterns when animals occupy distinct locations in their environment (He et al., 2023). These precise firing sequences of place cells can be reactivated ("replayed") during subsequent SWRs that occur during periods of sleep or wakeful immobility (Zhou and Norimoto, 2023).This implies that SWRs may play a crucial role in recalling and consolidating spatial memories. Hippocampal SWRs facilitate the regulation of synchronized neuronal firing and encourage coordinated activity across brain regions, and impaired coordination may conceivably impair memory processes. Studies have demonstrated that ripple disruption and sleep deprivation after one-session learning in rats affected their performance in maze-based spatial memory tasks, leading to the elimination of long-term memory expression (Aleman-Zapata et al., 2022). Furthermore, research suggests that rats exhibit extended SWR durations under conditions of heightened memory demand, and artificially prolonging SWR duration through optogenetic techniques has been demonstrated to enhance maze learning performance (Fernández-Ruiz et al., 2019).

Neural activity critical for memory can be disrupted thereby leading to neural network dysfunction due to the effects of AD pathology on the hippocampus (Prince et al., 2021; Wu et al., 2023). Anomalies in hippocampal SWRs have been observed in various AD mouse models, potentially offering insights into the mechanisms underlying memory deficits in AD (Sanchez-Aguilera and Quintanilla, 2021; He et al., 2023). *In vivo* studies have indicated a reduced incidence of SWRs in 5xFAD mice (overexpressing amyloid-like proteins) (Iaccarino et al., 2018), rTg4510 mice (overexpressing human Tau protein) (Witton et al., 2016), apoE4-KI mice (knocking in Apolipoprotein E4 gene) (Gillespie et al., 2016), and APP/PS1 mice (overexpressing human genes for amyloid precursor protein and presenilin 1) (Jura et al., 2019). Decreased SWR durations have also been reported in 5xFAD mice (Prince et al., 2021), APP-KI mice (knocking in Amyloid Precursor Protein gene) (Funane et al., 2022), and TgF344 rats (bearing the human APP gene with Swedish mutation and the human PS1 gene with the deltaE9 mutation) (van den Berg et al., 2023). These findings may be attributed to AD pathology inducing disruptions in synaptic plasticity and interneuronal function, thereby interfering with precise spike-timing during SWRs and resulting in shortened SWR durations. In fact, in this study, abnormalities in both the incidence and duration of SWRs were identified, and these aberrations were improved with the application of TMAS.

Gamma oscillations (25 Hz−100 Hz) prominently feature in multiple brain regions, including the hippocampus, exhibiting distinct relevance to cognition and memory processes, and slow gamma (25 Hz−50 Hz) is postulated to enhance memory retrieval by facilitating CA1 input to CA3 (Mably and Colgin, 2018). Slow gamma modulates the timing of neuronal spiking, orchestrates inter-regional communication, and likely serves as a mediator for neural integration and information processing linked to sensory and cognitive functions (Hudson and Jones, 2022). Slow gamma activity in the hippocampus increases during SWRs, and higher coherence and phase locking of slow gamma between CA3 and CA1 correlate with memory replay quality (Jones et al., 2019). Similarly, we found the increase in slow gamma power during

SWR in the hippocampus. However, memory-related deficits have been associated with reduced slow gamma during SWRs in several AD mouse models (Stoiljkovic et al., 2019). This decrease in slow gamma during SWRs is thought to be linked to the intricate disruption of synaptic and neuronal function due to the accumulation of Aβ and hyperphosphorylated tau. The deposition of Aβ in the cerebrospinal fluid of AD patients is one of the earliest signs in the progression of Alzheimer's disease. This accompanies neurodegenerative processes and may strongly modulate synaptic efficiency in pathological aging (Martorana et al., 2015). Acetylcholine plays a crucial role in the encoding, consolidation, and retrieval of memory, and disruptions in cholinergic neurotransmission at higher levels may be associated with Aβ levels (Martorana et al., 2014). Cholinergic activity is correlated with human memory tasks and may be modulated through neurophysiological means (Bonni et al., 2017). Our findings indicate a reduced slow gamma activity in the AD group of mice compared to the WT group during SWRs. The AD-TMAS group exhibited an elevation in slow gamma activity during SWRs, potentially linked to the enhancement of neural plasticity through TMAS treatment (Wang et al., 2019).

A reduction in theta-gamma PAC can be observed in both AD patients and AD mouse models, similar to the observations in the current study (van den Berg et al., 2023). An increase in theta-slow gamma PAC was observed in AD model mice after TMAS treatment. The coordination of neuronal activity has been observed not only within neuronal networks and brain regions but also across various frequency bands of neural oscillations (Marzetti et al., 2019). This cross frequency coupling, involving different frequency bands, is considered a fundamental aspect of cognitive function (Yakubov et al., 2022). Such relationships of coupling can unveil interactions among different frequency components of signals, thereby aiding in the comprehension of dynamic properties and information transmission mechanisms of the nervous system. PAC refers to the modulation of the amplitude of high-frequency components of electrophysiological signals by the phase of low-frequency components (Özkurt, 2012). During animal engagement in spatial learning and navigation, research has shown a notable enhancement in theta-gamma PAC power (Kitchigina, 2018). Consequently, the strength of theta-gamma coupling within the hippocampus is typically associated with accurate performance in cognitive tasks.

5 Conclusion

In conclusion, our study demonstrates the beneficial effects of TMAS treatment on spatial memory deficits and abnormal neural oscillations in the APP/PS1 transgenic AD mouse model. The memory impairments in AD model mice are possibly associated with defects in hippocampal oscillations, which can be alleviated through TMAS intervention. These findings suggest the potential of rescuing cognitive impairments caused by neurodegenerative diseases through the modulation of brain oscillations via neurostimulation. This study demonstrates that TMAS presents a hopeful opportunity for non-intrusive therapeutic interventions in AD.

Data availability statement

The original contributions presented in the study are included in the article/supplementary material, further inquiries can be directed to the corresponding author.

Ethics statement

The animal study was approved by the Biomedical Ethics Committee of the Hebei University of Technology. The study was conducted in accordance with the local legislation and institutional requirements.

Author contributions

SZ: Data curation, Formal analysis, Investigation, Methodology, Validation, Visualization, Writing—original draft, Writing—review & editing. ZG: Data curation, Formal analysis, Investigation, Methodology, Validation, Visualization, Writing—original draft, Writing—review & editing. YX: Methodology, Writing—review & editing. JM: Methodology, Writing—review & editing, Investigation. JL: Writing—review & editing, Investigation, Methodology. ZL: Investigation, Writing—review & editing, Methodology. XX: Investigation, Methodology, Writing—review & editing. GX: Writing—review & editing, Investigation, Methodology.

Funding

The author(s) declare financial support was received for the research, authorship, and/or publication of this article. The paper was supported by the National Natural Science Foundation under Grant No. 52377224 and the Central Guidance for Local Scientific and Technological Development Foundation under Grant No. 236Z7711G.

Conflict of interest

The authors declare that the research was conducted in the absence of any commercial or financial relationships that could be construed as a potential conflict of interest.

Publisher's note

References

Aleman-Zapata, A., Morris, R. G. M., and Genzel, L. (2022). Sleep deprivation and hippocampal ripple disruption after one-session learning eliminate memory expression the next day. *Proc. Natl. Acad. Sci.* 119, e2123424119. doi: 10.1073/pnas.2123424119

Belluscio, M. A., Mizuseki, K., Schmidt, R., Kempter, R., and Buzsáki, G. (2012). Cross-frequency phase-phase coupling between theta and gamma oscillations in the hippocampus. *J. Neurosci.* 32, 423–435. doi: 10.1523/JNEUROSCI.4122-11.2012

Benthem, S. D., Skelin, I., Moseley, S. C., Stimmell, A. C., Dixon, J. R., Melilli, A. S., et al. (2020). Impaired hippocampal-cortical interactions during sleep in a mouse model of Alzheimer's diseas. *Curr. Biol.* 30, 2588–2601. doi: 10.1016/j.cub.2020.04.087

Bokil, H., Andrews, P., Kulkarni, J. E., Mehta, S., and Mitra, P. P. (2010). Chronux: a platform for analyzing neural signals. *Neurosci. Methods*. 192, 146–151. doi: 10.1016/j.jneumeth.2010.06.020

Bonni, S., Ponzo, V., Lorenzo, D., Caltagirone, F. C., and Koch, G. (2017). Real-time activation of central cholinergic circuits during recognition memory. *Eur. J. Neurosci.* 45, 1485–1489. doi: 10.1111/ejn.13588

Buzsaki, G. (2015). Hippocampal sharp wave-ripple: a cognitive biomarker for episodic memory and planning. *Hippocampus* 25, 1073–1188. doi: 10.1002/hipo.22488

Caccavano, A., Bozzelli, P. L., Forcelli, P. A., Pak, D. T. S., Wu, J., Conant, K., et al. (2020). Inhibitory parvalbumin basket cell activity is selectively reduced during hippocampal sharp wave ripples in a mouse model of familial Alzheimer's disease. *J. Neurosci*., 40, 5116–5136. doi: 10.1523/JNEUROSCI.0425-20.2020

Casula, E. P., Borghi, I., and Maiella, M., Pellicciari, M. C., Bonni, S., Mencarelli, L., et al. (2023). Regional precuneus cortical hyperexcitability in Alzheimer's disease patients. *Ann. Neurol.* 93, 371–383. doi: 10.1002/ana.26514

Casula, E. P., Pellicciari, M. C., Bonn,ì, S., Borghi, I., Maiella, M., Assogna, M., et al. (2022). Decreased frontal gamma activity in Alzheimer disease patients. *Ann. Neurol.* 92, 464–475. doi: 10.1002/ana.26444

Chan, D., Suk, H. J., Jackson, B., Milman, N. P., Stark, D., Beach, S. D., et al. (2021). Induction of specific brain oscillations may restore neural circuits and be used for the treatment of Alzheimer's disease. *J. Intern. Med.* 290, 993–1009. doi: 10.1111/joim.13329

Cheng, S., and Frank, L. M. (2008). New experiences enhance coordinated neural activity in the hippocampus. *Neuron* 57, 303–313. doi: 10.1016/j.neuron.2007.11.035

Chu, F., Tan, R. X., Wang, X., Zhou, X., Ma, R., Ma, X., et al. (2023). Transcranial magneto-acoustic stimulation attenuates synaptic plasticity impairment through the activation of Piezo1 in Alzheimer's disease mouse model. *Research* 6:0130. doi: 10.34133/research.0130

da Cruz, J. F. O., Busquets-Garcia, A., Zhao, Z., Varilh, M., Lavanco, G., Bellocchio, L., et al. (2020). Specific hippocampal interneurons shape consolidation of recognition memory. *Cell Rep.* 32, 108046. doi: 10.1016/j.celrep.2020.108046

Dang, J., Zhang, S., You, S., Du, W., and Xu, G. (2022). Phase amplitude coupling analysis of local field potentials in working memory of rats affected by transcranial magneto-acoustic-electrical stimulation. *J. Biomed. Eng* 39, 267–275. doi: 10.7507/1001-5515.202108036

Dautricourt, S., de Flores, R., Landeau, B., Poisnel, G., Vanhoutte, M., Delcroix, N., et al. (2021). Longitudinal changes in hippocampal network connectivity in Alzheimer's disease. *Ann. Neurol.* 90, 391–406. doi: 10.1002/ana.26168

Di Lorenzo, D., Bonni, F., Picazio, S., Motta, S., Caltagirone, C., Martorana, C., et al. (2020). Effects of cerebellar theta burst stimulation on contralateral motor cortex excitability in patients with Alzheimer's disease. *Brain Topogr.* 33, 613–617. doi: 10.1007/s10548-020-00781-6

Dolgin, E. (2016). How to defeat dementia. *Nature* 539, 156–158. doi: 10.1038/539156a

Ellender, T., and Paulsen, O. (2010). The many tunes of perisomatic targeting interneurons in the hippocampal network. *Front. Cell. Neurosci.* 4, 00026. doi: 10.3389/fncel.2010.00026

Fernández-Ruiz, A., Oliva, A., de Oliveira Rocha-Almeida, E. F., Tingley, F. D., and Buzsáki, G. (2019). Long-duration hippocampal sharp wave ripples improve memory. *Science* 364, 1082–1086. doi: 10.1126/science.aax0758

Funane, T., Jun, H. C., Sutoko, S., Saido, T. C., Kandori, A., Igarashi, K. M., et al. (2022). Impaired sharp-wave ripple coordination between the medial entorhinal cortex and hippocampal CA1 of knock-in model of Alzheimer's disease. *Front. Syst. Neurosci.* 16: 955178. doi: 10.3389/fnsys.2022.955178

Gillespie, A. K., Jones, E. A., Lin, Y., Karlsson, M. P., Kay, K., Yoon, S. Y., et al. (2016). Apolipoprotein E4 causes age-dependent disruption of slow gamma oscillations during hippocampal sharp-wave ripples. *Neuron* 90, 740–751. doi: 10.1016/j.neuron.2016.04.009

He, H., Guan, H., and McHugh, T. J. (2023). The expanded circuitry of hippocampal ripples and replay. *Neurosci. Res.* 189, 13–19. doi: 10.1016/j.neures.2022.12.010

He, X., Li, J., Zhou, G., Yang, J., McKenzie, S., Li, Y., et al. (2021). Gating of hippocampal rhythms and memory by synaptic plasticity in inhibitory interneurons. *Neuron* 109, 1013–1028. doi: 10.1016/j.neuron.2021.01.014

Hollnagel, J. O., Elzoheiry, S., Gorgas, K., Kins, S., Beretta, C. A., Kirsch, J., et al. (2016). Early alterations in hippocampal perisomatic GABAergic synapses and network oscillations in a mouse model of Alzheimer's disease amyloidosis. *PLoS ONE* 14, e0209228. doi: 10.1371/journal.pone.0209228

Hudson, M. R., and Jones, N. C. (2022). Deciphering the code: Identifying true gamma neural oscillations. *Exp. Neurol.* 357: 114205. doi: 10.1016/j.expneurol.2022.114205

Iaccarino, H. F., Singer, A. C., Martorell, A. J., Rudenko, A., Gao, F., Gillingham, T. Z., et al. (2018). Gamma frequency entrainment attenuates amyloid load and modifies microglia. *Nature* 562: E1. doi: 10.1038/s41586-018-0351-4

Jafari, Z., and Kolb, B. E. (2020). Neural oscillations and brain stimulation in Alzheimer's disease. *Prog. Neurobiol.* 194, 101878. doi: 10.1016/j.pneurobio.2020.101878

Jeffery, K. J. (2018). The hippocampus: from memory, to map, to memory map. *Trends Neurosci.* 41, 64–66. doi: 10.1016/j.tins.2017.12.004

Jones, E. A., Gillespie, A. K., Yoon, S. Y., Frank, L. M., and Huang, Y. D. (2019). Early hippocampal sharp-wave ripple deficits predict later learning and memory impairments in an Alzheimer's disease mouse model. *Cell Rep.* 29, 2123–2133. doi: 10.1016/j.celrep.2019.10.056

Jura, B., Macrez, N., Meyrand, P., and Bem, T. (2019). Deficit in hippocampal ripples does not preclude spatial memory formation in APP/PS1 mice. *Sci. Rep.* 9: 20129. doi: 10.1038/s41598-019-56582-w

Katsuki, F., Gerashchenko, D., and Brown, R. E. (2022). Alterations of sleep oscillations in Alzheimer's disease: a potential role for GABAergic neurons in the cortex, hippocampus, and thalamus. *Brain Res. Bull.* 187, 181–198. doi: 10.1016/j.brainresbull.2022.07.002

Kitchigina, V. F. (2018). Alterations of coherent theta and gamma network oscillations as an early biomarker of temporal lobe epilepsy and Alzheimer's disease. *Front. Integr. Neurosci.* 12: 36. doi: 10.3389/fnint.2018.00036

Klein, A. S., Donoso, J. R., Kempter, R., Schmitz, D., and Beed, P. (2016). Early cortical changes in gamma oscillations in Alzheimer's disease. *Front. Syst. Neurosci.* 10, 83. doi: 10.3389/fnsys.2016.00083

Liu, R., Ma, R., Liu, X., Zhou, X., Wang, X., Yin, T., and Liu, Z. (2019). A noninvasive deep brain stimulation method via temporal-spatial interference magneto-acoustic effect: simulation and experimental validation. *IEEE Trans. Ultrason. Ferroelectr. Freq. Control* 69, 2474–2483. doi: 10.1109/TUFFC.2022.3187748

Livingston, G., Huntley, J., Sommerlad, A., Ames, D., Ballard, C., Banerjee, S., et al. (2020). Dementia prevention, intervention, and care: 2020 report of the Lancet commission. *The Lancet* 396, 413–446. doi: 10.1016/S0140-6736(20)30367-6

Luo, Y., Sun, Y., Wen, H., Wang, X., Zheng, X., Ge, H., et al. (2023). Deep brain stimulation of the entorhinal cortex modulates CA1 theta-gamma oscillations in mouse models of preclinical Alzheimer's disease. Biocybern. Biomed. *Eng.* 43, 246–260. doi: 10.1016/j.bbe.2022.12.010

Mably, A. J., and Colgin, L. L. (2018). Gamma oscillations in cognitive disorders. *Curr. Opin. Neurobiol.* 52, 182–187. doi: 10.1016/j.conb.2018.07.009

Martorana, A., Di Lorenzo, F., Belli, F., Sancesario, L., Toniolo, G., Sallustio, S., et al. (2015). Cerebrospinal fluid Aβ42 levels: when physiological become pathological state. *CNS Neurosci. Ther.* 21, 921–925. doi: 10.1111/cns.12476

Martorana, A., Di Lorenzo, F., Manenti, G., Semprini, R., and Koch, G. (2014). Honnotaurine induces measurable changes of short latency afferent inhibition in a group of mild cognitive impairment individuals. *Front. Aging Neurosci.* 6: 254. doi: 10.3389/fnagi.2014.00254

Marzetti, L., Basti, A., Chella, F., D'Andrea, A., Syriala, J., Pizzella, V., et al. (2019). Brain functional connectivity through phase coupling of neuronal oscillations: a perspective from magnetoencephalog:aphy. *Front. Neurosci.* 13: 964. doi: 10.3389/fnins.2019.00964

Mehak, S. F., Shivakumar, A. B., Kumari, S., Muralidharan, B., and Gangadharan, G. (2022). Theta and gamma oscillatory dynamics in mouse models of Alzheimer's disease: a path to prospective therapeutic intervention. *Neurosci. Biobehav. Rev.* 136: 104628. doi: 10.1016/j.neubiorev.2022.104628

Miller, J., Watrous, A. J., Tsitsiklis, M., Lee, S. A., Sheth, S. A., Schevon, C. A., et al. (2018). Lateralized hippocampal oscillations underlie distinct aspects of human spatial memory and navigation. *Nat. Commun.* 9, 2423. doi: 10.1038/s41467-018-04847-9

Ning, S., Jorfi, M., Patel, S. R., Kim, D. Y., and Tanzi, R. E. (2022). Neurotechnological approaches to the diagnosis and treatment of Alzheimer's disease. *Front. Neurosci.* 16: 854992. doi: 10.3389/fnins.2022.854992

Norton, S. J. (2003). Can ultrasound be used to stimulate nerve tissue?. *BioMed. Eng.* 2:6. doi: 10.1186/1475-925X-2-6

Özkurt, T. E. (2012). Statistically reliable and fast direct estimation of phase-amplitude cross-frequency coupling. *IEEE Trans. Biomed. Eng.* 59, 1943–1950. doi: 10.1109/TBME.2012.2194783

Pless, A., Ware, D., Saggu, S., Rehman, H., Morgan, J., Wang, Q., et al. (2023). Understanding neuropsychiatric symptoms in Alzheimer's disease: challenges and advances in diagnosis and treatment. *Front. Neurosci.* 17, 1263771. doi: 10.3389/fnins.2023.1263771

Possin, K. L., Sanchez, P. E., Anderson-Bergman, C., Fernandez, R., Kerchner, G. A., Johnson, E. T., et al. (2016). Cross-species translation of the Morris maze for Alzheimer's disease. *J. Clin. Invest.* 126, 779–783. doi: 10.1172/JCI78464

Prince, S. M., Paulson, A. L., Jeong, N., Zhang, L., Amigues, S., Singer, A. C., et al. (2021). Alzheimer's pathology causes impaired inhibitory connections and reactivation of spatial codes during spatial navigation. *Cell Rep.* 35, 109008. doi: 10.1016/j.celrep.2021.109008

Rangel, L. M., Rueckemann, J. W., Riviere, P. D., Keefe, K. R., Porter, B. S., Heimbuch, I. S., et al. (2016). Rhythmic coordination of hippocampal neurons during associative memory processing. *eLife* 5, e09849. doi: 10.7554/eLife.09849

Roux, F., and Uhlhaas, P. J. (2014). Working memory and neural oscillations: alpha–gamma versus theta–gamma codes for distinct WM information?. *Trends Cogn. Sci.* 18, 16–25. doi: 10.1016/j.tics.2013.10.010

Sanchez-Aguilera, A., and Quintanilla, J. P. (2021). Sharp wave ripples in Alzheimer's disease: In search of mechanisms. *J. Neurosci.* 41, 1366–1370. doi: 10.1523/JNEUROSCI.2020-20.2020

Stoiljkovic, M., Kelley, C., Stutz, B., Horvath, T. L., and Hajós, M. (2019). Altered cortical and hippocampal excitability in TgF344-AD rats modeling Alzheimer's disease pathology. *Cereb. Cortex* 29, 2716–2727. doi: 10.1093/cercor/bhy140

Traikapi, A., and Konstantinou, N. (2021). Gamma oscillations in Alzheimer's disease and their potential therapeutic role. *Front. Syst. Neurosci.* 15, 782399. doi: 10.3389/fnsys.2021.782399

van den Berg, M., Toen, D., Verhoye, M., and Keliris, G. A. (2023). Alterations in theta-gamma coupling and sharp wave-ripple, signs of prodromal hippocampal network impairment in the TgF344-AD rat model. *Front. Aging Neurosci.* 15: 1081058. doi: 10.3389/fnagi.2023.1081058

Wang, H., Zhou, X., Cui, D., Liu, R., Tan, R., Wang, X., et al. (2016). Comparative study of transcranial magneto-acoustic stimulation and transcranial ultrasound stimulation of motor cortex. *Front. Behav. Neurosci.* 13, 241. doi: 10.3389/fnbeh.2019.00241

Wang, Y., Feng, L., Liu, S., Zhou, X., Yin, T., Liu, Z., et al. (2019). Transcranial magneto-acoustic stimulation improves neuroplasticity in hippocampus of Parkinson's disease model mice. *Neurotherapeutics* 16, 1210–1224. doi: 10.1007/s13311-019-00732-5

Witton, J., Staniaszek, L. E., Bartsch, U., Randall, A. D., Jones, M. W., Brown, J. T., et al. (2016). Disrupted hippocampal sharp-wave ripple-associated spike dynamics in a transgenic mouse model of dementia. *J. Physiol.* 594, , 4615–4630. doi: 10.1113/jphysiol.2014.282889

Wu, L., Cao, T., Li, S., Yuan, Y., Zhang, W., Huang, L., et al. (2022). Long-term gamma transcranial alternating current stimulation improves the memory function of mice with Alzheimer's disease. *Front. Aging Neurosci.* 14, 980636. doi: 10.3389/fnagi.2022.980636

Wu, L., Zhang, W., Li, S., Li, Y., Yuan, Y., Huang, L., et al. (2023). Transcranial alternating current stimulation improves memory function in Alzheimer's mice by ameliorating abnormal gamma oscillation. *IEEE Trans. Neural Syst. Rehabil. Eng.* 31, 2060–2068. doi: 10.1109/TNSRE.2023.3265378

Xie, B., Zhen, Z., Guo, O., Li, H., Guo, M., Zhen, J., et al. (2023). Progress on the hippocampal circuits and functions based on sharp wave ripples. *Brain Res. Bull.* 200: 110695. doi: 10.1016/j.brainresbull.2023.110695

Xie, Z., Yan, J., Dong, S., Ji, H., and Yuan, Y. (2022). Phase-locked closed-loop ultrasound stimulation modulates theta and gamma rhythms in the mouse hippocampus. *Front. Neurosci.* 16:994570. doi: 10.3389/fnins.2022.994570

Yakubov, B., Das, S., Zomorrodi, R., Blumberger, D. M., Enticott, P. G., Kirkovski, M., et al. (2022). Cross-frequency coupling in psychiatric disorders: a systematic review. *Neurosci. Biobehav. Rev.* 138: 104690. doi: 10.1016/j.neubiorev.2022.104690

Yokoyama, M., Kobayashi, H., Tatsumi, L., and Tomita, T. (2022). Mouse models of Alzheimer's disease. *Front. Mol. Neurosci.* 15, 912995. doi: 10.3389/fnmol.2022.912995

Yu, K., Liu, C., Niu, X., and He, B. (2021). Transcranial focused ultrasound neuromodulation of voluntary movement-related cortical activity in humans. *IEEE Trans. Biomed. Eng.* 68, 1923–1931. doi: 10.1109/TBME.2020.3030892

Yuan, T., Li, W., Zhang, C., Wei, H., Sun, S., Xu, N., et al. (2020). Targeting neuroplasticity in patients with neurodegenerative diseases using brain stimulation techniques. *Transl. Neurodegener.* 9, 44. doi: 10.1186/s40035-020-00224-z

Yuan, Y., and Chen, Y. (2016). A new brain stimulation method: Noninvasive transcranial magneto-acoustical stimulation. *Chin. Phys. B* 25:084301. doi: 10.1088/1674-1056/25/8/084301

Yuan, Y., Chen, Y., and Li, X. (2016). Theoretical analysis of transcranial magneto-acoustical stimulation with Hodgkin-Huxley neuron model. *Front. Comput. Neurosci.* 10:35. doi: 10.3389/fncom.2016.00035

Zhang, S., Cui, K., Zhang, X., Shi, X., Ge, M., Zhao, M., et al. (2018). Effect of transcranial ultrasonic–magnetic stimulation on two types of neural firing behaviors in modified Izhikevich model. *IEEE Trans. Magn.* 54, 1–4. doi: 10.1109/TMAG.2017.2773086

Zhang, S., Wu, J., Xu, J., Dang, J., Zhao, Y., Hou, W., et al. (2022). Effects of transcranial magneto-acoustic electrical stimulation on calcium signals in prefrontal nerve clusters. *J. Biomed. Eng.* 39, 19–27. doi: 10.7507/1001-5515.202107044

Zheng, C. G., Bieri, K. W., Hsiao, Y. T., and Colgin, L. L. (2016). Spatial sequence coding differs during slow and fast gamma rhythms in the hippocampus. *Neuron* 89, 398–408. doi: 10.1016/j.neuron.2015.12.005

Zhou, H., Li, H., Gowravaram, N., Quan, M., Kausar, N., Gomperts, S. N., et al. (2022). Disruption of hippocampal neuronal circuit function depends upon behavioral state in the APP/PS1 mouse model of Alzheimer's disease. *Sci. Rep.* 12, 21022. doi: 10.1038/s41598-022-25364-2

Zhou, X., Liu, S., Wang, Y., Yin, T., Yang, Z., Liu, Z., et al. (2019). High-resolution transcranial electrical stimulation for living mice based on magneto-acoustic effec. *Front. Neurosci.* 13: 1342. doi: 10.3389/fnins.2019.01342

Zhou, Z., and Norimoto, H. (2023). Sleep sharp wave ripple and its functions in memory and synaptic plasticity. *Neurosci. Res.* 189, 20–28. doi: 10.1016/j.neures.2023.01.011

frontiers | Frontiers in Neuroscience

TYPE Original Research
PUBLISHED 27 February 2024
DOI 10.3389/fnins.2024.1308370

OPEN ACCESS

EDITED BY
Gahangir Hossain,
University of North Texas, United States

REVIEWED BY
Zhijun Fan,
Shandong University, China
Aiden Payne,
Florida State University, United States

*CORRESPONDENCE
Yu Liu
✉ yuliu@sus.edu.cn

RECEIVED 06 October 2023
ACCEPTED 08 February 2024
PUBLISHED 27 February 2024

CITATION
Jiao F, Zhuang J, Nitsche MA, Lin Z, Ma Y and Liu Y (2024) Application of transcranial alternating current stimulation to improve eSports-related cognitive performance. *Front. Neurosci.* 18:1308370. doi: 10.3389/fnins.2024.1308370

Application of transcranial alternating current stimulation to improve eSports-related cognitive performance

Fujia Jiao[1,2], Jie Zhuang[3], Michael A. Nitsche[2,4,5], Zhenggen Lin[1], Yuanbo Ma[2,6] and Yu Liu[1]*

[1]Key Laboratory of Exercise and Health Sciences of Ministry of Education, Shanghai University of Sport, Shanghai, China, [2]Department Psychology and Neurosciences, Leibniz Research Centre for Working Environment and Human Factors, Dortmund, Germany, [3]School of Psychology, Shanghai University of Sport, Shanghai, China, [4]University Hospital OWL, Protestant Hospital of Bethel Foundation, University Clinic of Psychiatry and Psychotherapy and University Clinic of Child and Adolescent Psychiatry and Psychotherapy, Bielefeld University, Bielefeld, Germany, [5]German Center for Mental Health (DZPG), Bochum, Germany, [6]Department of Psychology, Ruhr University Bochum, Bochum, Germany

Introduction: Electronic Sports (eSports) is a popular and still emerging sport. Multiplayer Online Battle Arena (MOBA) and First/Third Person Shooting Games (FPS/TPS) require excellent visual attention abilities. Visual attention involves specific frontal and parietal areas, and is associated with alpha coherence. Transcranial alternating current stimulation (tACS) is a principally suitable tool to improve cognitive functions by modulation of regional oscillatory cortical networks that alters regional and larger network connectivity.

Methods: In this single-blinded crossover study, 27 healthy college students were recruited and exposed to 10 Hz tACS of the right frontoparietal network. Subjects conducted a Visual Spatial Attention Distraction task in three phases: T0 (pre-stimulation), T1 (during stimulation), T2 (after-stimulation), and an eSports performance task which contained three games ("Exact Aiming," "Flick Aiming," "Press Reaction") before and after stimulation.

Results: The results showed performance improvements in the "Exact Aiming" task and hint for a prevention of reaction time performance decline in the "Press Reaction" task in the real, as compared to the sham stimulation group. We also found a significant decrease of reaction time in the visual spatial attention distraction task at T1 compared to T0 in the real, but not sham intervention group. However, accuracy and inverse efficiency scores (IES) did not differ between intervention groups in this task.

Discussion: These results suggest that 10 Hz tACS over the right frontal and parietal cortex might improve eSports-related skill performance in specific tasks, and also improve visual attention in healthy students during stimulation. This tACS protocol is a potential tool to modulate neurocognitive performance involving tracking targets, and might be a foundation for the development of a new concept to enhance eSports performance. This will require however proof in real life scenarios, as well optimization.

KEYWORDS

eSports, visual attention, transcranial alternating current stimulation, visual spatial attention distraction task, eSports skill performance

1 Introduction

Electronic Sports (eSports) is an entertainment activity with increasing popularity in the 21st century, attractive for both, participants and spectators, and gains popularity mainly in young people (Chung et al., 2019; Nagorsky and Wiemeyer, 2020). eSports games require fast-paced, constant attention to movement, quick decision-making, good hand-eye coordination, and excellent combat and reaction time performance. eSports include especially Action Video Games (AVG), such as Multiplayer Online Battle Arena (MOBA), and First/Third Person Shooting Games (FPS/TPS) (Bediou et al., 2018). In contrast to traditional sports, where the success of athletes relies critically on the development and performance of complex motor skills, eSports athletes depend more on the development of cognitive functions, such as visual attention, decision-making skills, and reaction time (Himmelstein et al., 2017). Many studies show that AVG players have better visual attention than non-gamers, and that non-gamers can improve their cognitive abilities to some extent by game training (Green and Bavelier, 2003, 2006a, b).

Most of the studies conducted so far are cross-sectional studies to compare visual attention of AVG players and non-video game players. As early as 2003, it was reported that AVG players have better visual attention than non-players and that training of non-players improved visual attention (Green and Bavelier, 2003). In subsequent studies, it was reported that playing video games improved performance of various attentional and perceptual tasks, and similarly, performance of a functional visual field task was improved by video game experience (Green and Bavelier, 2010, 2015). Moreover, He et al. reported that AVG players had better attentional control in visual computer tasks, but speculated that transfer of performance gains to other tasks might be limited (He et al., 2022). Prolonged gaming is demanding with respect to attention control and related cognitive functions (Bavelier and Green, 2019). AVG games are considered to require cognitive skill training, including task switching, visuomotor coordination, processing speed, and attentional control in addition to enhancement of general physical fitness (Feng et al., 2007; Boot et al., 2008; Green and Bavelier, 2015; Billieux et al., 2017). However, regarding cognitive training, besides the daily gaming routine not much research focuses on improvement of cognitive functions of eSports athletes, including focused improvement of visual attention (Green and Bavelier, 2006a; Bediou et al., 2018).

Non-invasive Brain Stimulation (NIBS) is a potential tool for enhancing neurocognition in eSports athletes (Zhuang et al., 2020; Machado et al., 2021). NIBS includes a group of neuromodulation techniques that has been developed over the last three decades to modulate brain activity, as well as relevant cognitive and motor functions. Transcranial Magnetic Stimulation (TMS), based on electromagnetic principles, and Transcranial Electrical Stimulation (tES), based on the application of a weak, painless current to the scalp, are the most common methods used in NIBS (Polanía et al., 2018). In transcranial direct current stimulation (tDCS), a weak direct current is administered via electrodes placed on the head that depolarizes or hyperpolarizes the resting membrane potential of neurons, dependent on the direction of current flow, thereby altering cortical excitability (Nitsche and Paulus, 2000). Transcranial alternating current stimulation (tACS) uses oscillatory electrical stimulation to promote neuronal activity in specific frequency bands (Cabral-Calderin and Wilke, 2020; Riddle and Frohlich, 2021). Recent studies have moreover shown that tACS improves cognitive functions by enhancing brain oscillations that synchronize activity between distant brain regions (Herrmann et al., 2013; Johannes et al., 2018; Cabral-Calderin and Wilke, 2020). Indeed, studies have shown that stimulation of dual brain regions can improve synchronization of remote brain regions and thus improve cognitive function (Reinhart and Nguyen, 2019; Hosseinian et al., 2021).

Resting-state functional imaging data showed that blood oxygen level-dependent (BOLD) activity in the frontoparietal network correlates with alpha power (Sadaghiani et al., 2012). Zanto et al. (2010, 2011) observed increased alpha phase coherence between the right prefrontal and visual cortices during attention task performance. Visuospatial attention is associated with robust and sustained long-range synchronization of cortical oscillations exclusively in the high-alpha (10–14 Hz) frequency band. This synchronization between frontal, parietal and visual regions was observed concurrently with amplitude suppression of low-alpha (6–9 Hz) band oscillations in the visual cortex (Lobier et al., 2018). van Schouwenburg et al. (2016) found preliminary evidence that phase coherence enhancements via tACS of the right frontoparietal network may play a crucial role for top-down control of spatial attention, since enhanced alpha synchrony in the right frontal and parietal cortices was associated with improved performance in a visuospatial attention task. Therefore, alpha tACS might be suited to improve eSports performance related to visual attention involving the right frontoparietal network.

Although neuromodulation via non-invasive brain stimulation has been proposed as a performance-enhancing tool in eSports, still only few respective studies are available, and only one study reported an improving effect of tDCS on digital game performance (Zhuang et al., 2020; Friehs et al., 2021). In the current study, based on knowledge about the involvement of alpha activity and synchronization of the right hemispheric frontoparietal network, we hypothesized that strengthening of respective alpha activity via tACS will improve visual attention performance, and that for this improvement synchronization of frontal and parietal network components is required in eSports players. Hereby, we intended to probe whether tACS has potential as an effective tool to improve gaming performance via enhancement of visuospatial attention, and expected that main components of gaming performance, such as accuracy, quickness, and reflex-like reactions would improve by this intervention.

2 Materials and method

2.1 Participants

We recruited 27 healthy students (20 female, 7 male) from Shanghai Sport University, who had never played MOBA or FPS genre games (PC games or mobile games were included), and did not play AVG within 6 months before the experiments. Exclusion criteria were (1) Alcohol abuse and smoking, (2)

presence of personal or family neurological disease, metal implants or electronic devices in the head, or a history of head injury, (3) presence of cardiovascular disease (e.g., high blood pressure), (4) serious medical conditions, history of upper limb injury within the last 6 months, (5) history of brain surgery, and metal in the head, (6) cognitive impairment, psychiatric disease, and (7) long-term or recent use of CNS-active medication. All subjects gave written informed consent before participation, and the study was approved by the ethical committee of Shanghai University of Sport (approval number: 102772022RT047).

2.2 Procedure

This study was conducted in a crossover within-subject design. Before the experiment, participants were first conducting an eSports performance task, which was divided into three parts, each of which included a practice part. We chose a test of three games as the eSports performance task, and the duration of this task was about 10 min. Next, the participants were asked to conduct the visual spatial attention distraction task, which includes components of selective visuo-spatial, object-based and feature-based attention (for details refer to section "2.3 Visual spatial attention distraction task") (Maunsell and Treue, 2006; Cohen and Maunsell, 2011). The presentation order of 4 different blocks with different trial order in each experimental session was determined by two pseudorandomized orders A, and B (A: pre-12, middle-13, after-34; B: pre-12, middle- 24, after- 34). The association between order, and intervention condition was randomized between participants. Before the formal test, a practice session of about 24 trails was conducted to ensure an accuracy rate of above 70% in that test. Then the formal visual spatial attention distraction task which contained 2 blocks (one block including 152 trials) was performed. Task duration was about 20 min. Next, subjects were exposed to 20 min tACS (sham or real), and conducted the visual spatial attention distraction task again simultaneously. After tACS, the participants first performed the eSports task and then continued with the visual spatial attention distraction task. The total course of an experimental session is shown in **Figure 1**. Side effects and blinding success were tested at the end of the experiment via questionnaires (Zhang et al., 2022). The day before the experiment, participants were asked not to stay up late, not to drink coffee, alcohol or consume other central nervous system-affecting drinks or drugs within 24 h before the test, and not to perform strenuous physical activity within 24 h before the experiment. An interval of at least 1 week between sessions was obligatory.

2.3 Visual spatial attention distraction task

The experimental stimuli were displayed using E-Prime, version 3.0 (Psychology Software Tools Inc., USA). Each trial began with an attentional cue presented for 500 ms, followed by a target for 100 ms, and a blank screen for 2000∼3800 ms. Participants were instructed to respond as quickly as possible by pressing a button of the mouse when the target picture appeared. During the experiment, participants were asked to identify whether a blue butterfly was shown on the left or right side of the picture, by pressing the left or right mouse button with the index or middle finger of the right hand, respectively. Before the start of the main experiment, the participants performed a short practice session of 24 trials to get familiar with the experimental procedure. Participants performed two blocks before, 2 blocks during, and 2 blocks after intervention, each block was composed of 152 trials. The duration of 2 blocks was about 20 min (**Figure 2**).

The experimental design included two factors, namely distraction (with or without a distractor) and divided attention (valid or neutral cue) (**Figure 3**). An arrow symbol in the middle of each picture served as valid attentional cue, and directed attention to either the upper or lower panel of the picture, and the target (blue butterfly) always appeared in the panel indicated by the valid cue. In contrast, the "+" symbol, which served as alternative attentional cue, did not cue attention to either panel, here the target appeared with identical probability in either panel. The target pictures were divided into 4 categories: valid cue with distraction (52 experimental trials), valid cue without distraction (24 trials), neutral cue with distraction (52 trials), and neutral cue without distraction (24 trials) (**Figure 3**).

2.4 eSports performance task

The eSports performance task was performed on an ASUS desktop computer (CPU: Intel Core i7-10700k, GPU: NVIDIA Quadro P2200, RAM: Corsair DDR4 3600Mhz) connected to a standard full HD monitor, mouse and keyboard. The complete test procedure was explained to the participants before starting the test, and a practice test was conducted before the start of the specific test before intervention. The sensitivity of the mouse was adjusted to the comfort level of each participant.

We used the following three tests: "Exact Aiming," "Flick Aiming," and "Press Reaction" (Aimtastic video game).[1] In these three tests, the default difficulty level was used. In "Exact Aiming," bubbles of different size appeared on the screen for 100 s in total, which changed from small to large and then to small again, and had to be tapped before they disappeared. Targets appeared at higher frequency with increasing task duration. First, two bubbles appeared simultaneously in three trials (total duration of these trials 15 s), then the number of bubbles was increased by one up to eight, and each step was repeated 3 times with the exception of the 8 bubbles condition, which appeared only in two trials (total duration of these latter trials 10 s). The total number of trials was 124. Test scores were calculated based on the relation of hits and misses (100 points for hitting the target, minus 50 points for missing one). In the "Flick Aiming" test, first a red ball appears in the middle of the screen. Afterward, a white bubble randomly appears. The participants need to click on the white bubble, and then move the mouse over the red bubble to make it turn green. The duration of the "Flick Aiming" task was approximately 100 s. The test result was scored with 100 points added for a hit and 10 points subtracted for a miss, and 100 points added for a very accurate mouse path (in terms

1 https://aim400kg.com/

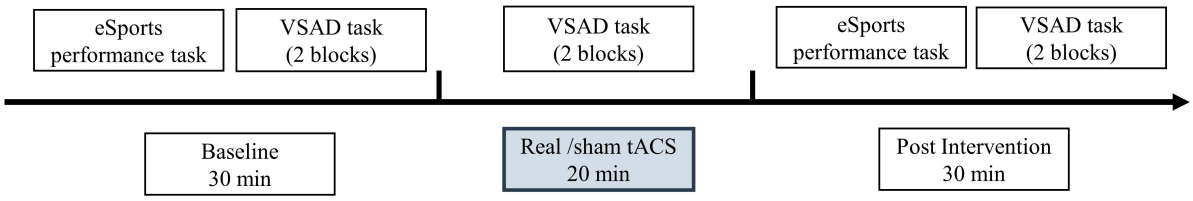

FIGURE 1
The course of the experimental sessions depicted in the top lines show the tasks the volunteers performed at respective time points, the bottom line indexes the duration of respective activities, and the middle line is spaced by black rectangles, subdividing baseline, intervention, and post-intervention time slots. The interval between the two sessions was 1 week minimum. VSAD task, visual spatial attention distraction task; tACS, transcranial alternating current stimulation; eSports performance task, this task contained three fixed eSports ability test games.

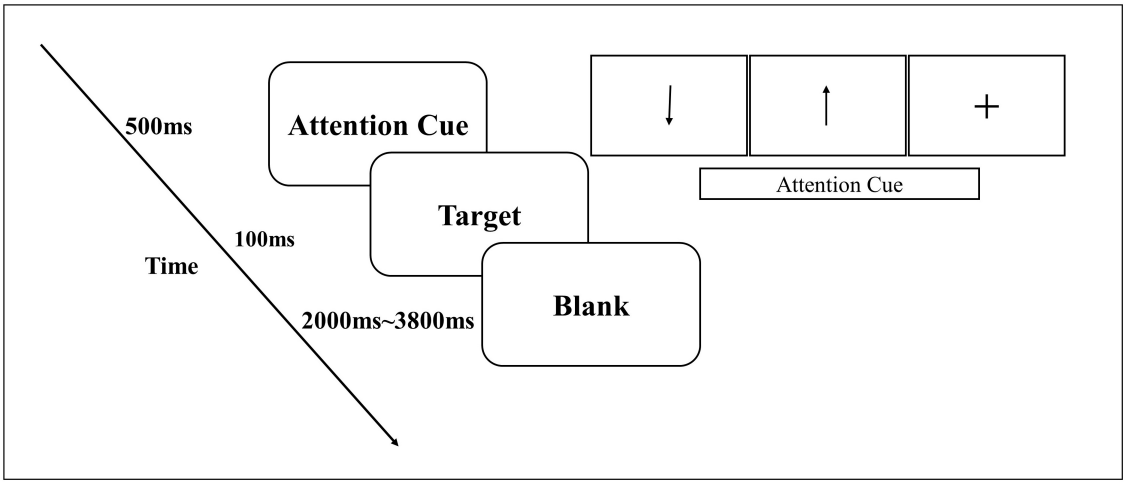

FIGURE 2
Schematic overview of the Visual Spatial Attention Distraction Task. The attention cue induced a bias (arrow), or no bias (+), the flow chart on the left shows the duration of stimulus presentation, and the time it took for completion of a trial. The duration of the task including two blocks was about 20 min.

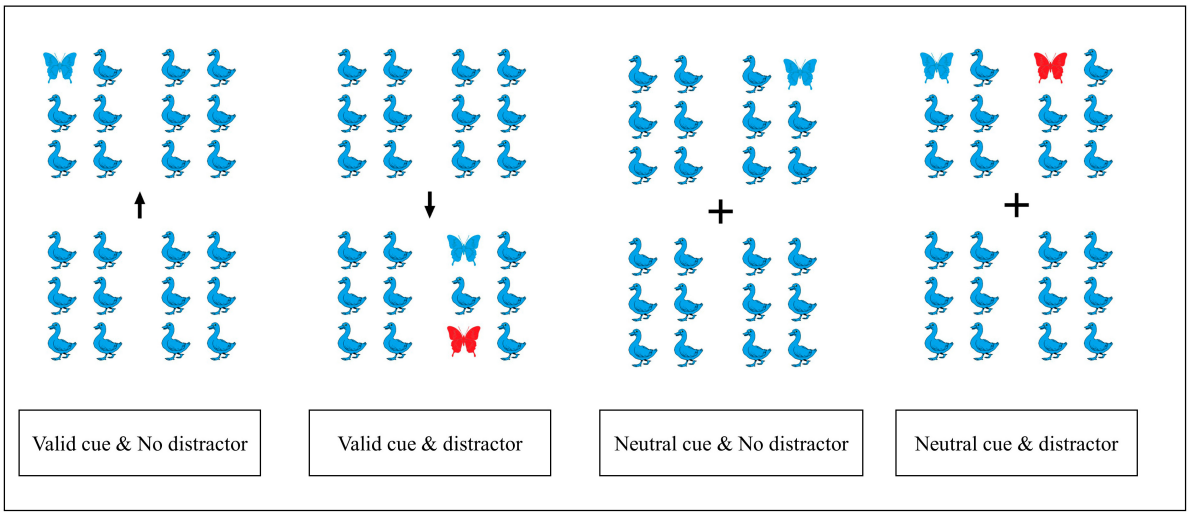

FIGURE 3
Shown are the four target categories. Participants were asked to identify if the blue butterfly was positioned on the **left** or **right** side. The red butterfly served as distractor. The arrow represents the valid cue, and its direction, "+" represents the neutral cue.

of the percentage value of a straight path of the mouse movement). In the "Press Reaction" test, only one target appears in the center of the screen at a random time point. The participants were instructed to point and click on the target as quickly as possible. The total trial number in the "Press Reaction" test was 10, outcome measures were reaction time for each trial, and an average reaction time was calculated over all trials. Conduction of all of these tasks took 10 min. For all performance tests, participants conducted a practice test before the start of the main experiment. and performed the tests before and after stimulation in the main experiment.

2.5 Transcranial alternating current stimulation

Stimulation was performed via a StarStim device (Neuroelectric, Barcelona, Spain) using round Ag/AgCl electrodes (Pistim) with a contact area of 3.14 cm^2. Electrode impedance was kept below 10 kΩ. Our stimulation protocol was designed to increase alpha coherence between the right frontal and parietal cortices.

In this experiment, based on previous research (van Schouwenburg et al., 2016), to stimulate the right frontoparietal network we placed the frontal stimulation electrode over F4. In addition, we placed the parietal stimulation electrode at P4, in the center of the posterior parietal cortex. The frontal and parietal cortices are integral parts of the fronto-parietal dorsal attention network, which is crucially involved in spatial attention (Harris et al., 2008; Martinaud et al., 2016), object-based attention (Hoba et al., 2022) and feature-based attention (Lanssens et al., 2020, 2022), which are all presumed to be relevant for gaming performance. Frequency was set to: α = 10 Hz, the stimulation lasted for 20 min, and in-phase stimulation with the electrodes over F4 and P4 with a sinusoidal alternating current with a peak to baseline intensity of 1000 μA was conducted. The return electrodes were placed at C2, C4, and C6 in order to disperse the heterophasic current over a larger area of disinterest. For stimulation blocks, in sham stimulation, current was immediately ramped up for 15 s and ramped down for 15 s, and again ramped up and down for 30 s at the end, and total stimulation duration was 20 min. The real stimulation was ramped up for 30 s at the beginning, then constant for 19 min, and then ramped down for 30 s. The electrical fields induced by tACS were calculated via the transcranial electrical stimulation simulation software SimNIBS (SimNIBS, University of Denmark, Denmark), and results are shown in **Figure 4**.

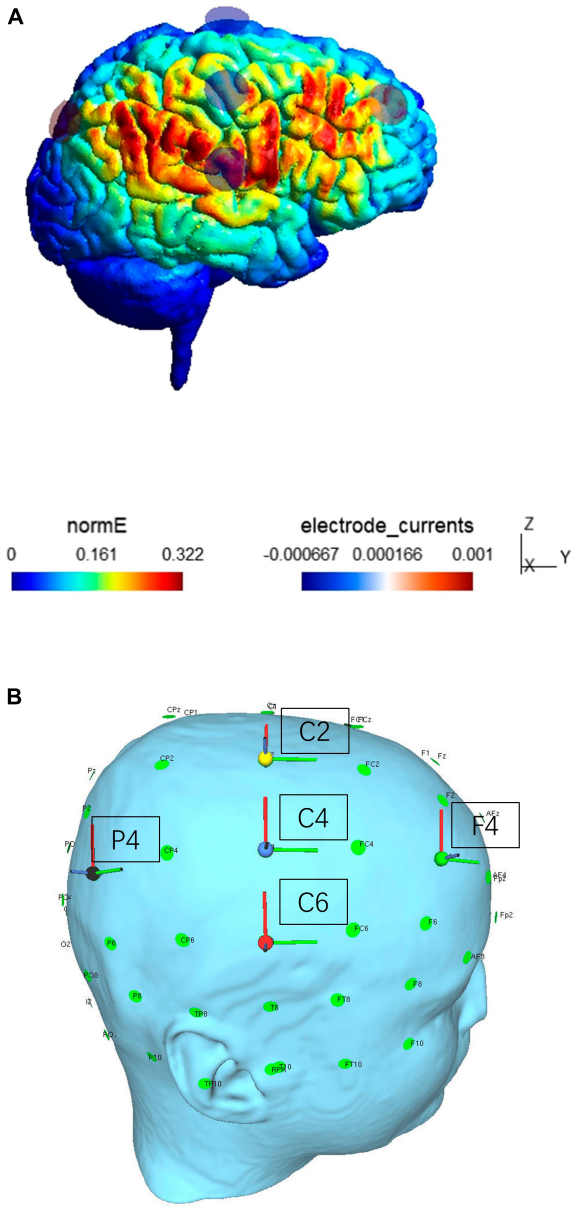

FIGURE 4
(A) Simulation of the electric field induced by tACS in this study. Colors indicate electrical field strength (nE, V/m), from low (blue) to large (red). **(B)** Shows the position of the stimulation electrodes, which were placed over F4 and P4, and the return electrodes, which were placed over C2, C4, and C6 positions.

2.6 Behavioral analysis

First, only for the VSAD task, we conducted three four-way ANOVAs with stimulation (real vs. sham), phase (pre vs. within vs. post-intervention), attention (valid vs. neutral cue) and conflict (distractor vs. no distractor) as within-subjects factors, and accuracy, reaction time (RT) and inverse efficiency scores (IES) (Liesefeld and Janczyk, 2019) as dependent variables. Accuracy (number of correct trials divided by the total number of trials), and the individual means of RT of the correct trials were calculated. Next, to account for a potential speed-accuracy trade-off, we calculated and analyzed the inverse efficiency score (IES) of each subject and condition, which was defined as mean reaction time of correct trials divided by accuracy. Two-way repeated measures ANOVAs were calculated for the eSports performance tasks. Stimulation (real vs. sham) and Time (pre vs. post) served as within-subject factors, and "Exact Aiming" scores, "Flick Aiming" scores and "Press Reaction" scores as dependent variables. Mauchly's tests were used to test the assumption of sphericity. In case of a violation of this assumption, the Greenhouse–Geisser correction was applied. In case of significant results of the ANOVAs, Bonferroni's-corrected *post-hoc* *t*-tests tests were conducted. The level of significance was set to $P \leq 0.05$ for all tests.

TABLE 1 Side effect ratings in two groups.

Stimulation	Real				Sham			
	None	Mild	Moderate	Severe	None	Mild	Moderate	Severe
Tingling	9	16	2	0	14	12	1	0
Itching	23	3	1	0	21	6	0	0
Burning	26	1	0	0	23	3	1	0
Pain	23	4	0	0	22	4	1	0
Skin redness	25	2	0	0	27	0	0	0
Fatigue	15	9	3	0	16	9	1	1
Phosphenes	24	3	0	0	23	3	1	0

To examine side effects (e.g., pain, itchiness, and burning) induced by stimulation, Mann-Whitney *U*-tests were used to compare ordinal-scaled variables described as numerical outcomes, based on information from the side-effect questionnaire. To verify blinding success, we included generalized estimating equations of the guessed stimulation conditions ("real tACS," "sham tACS," "I do not know"), and the actual stimulation condition (real tACS, sham) as factors. A Chi-square test was applied to evaluate blinding success.

3 Results

3.1 Side effects and blinding

The majority of subjects stated none or mild side effects. Mann-Whitney *U*-tests showed no significant difference in the ratings of side effects between the two groups (all $p = 0.21$–0.65). The majority of side effect ratings were "none," and "mild" (Table 1). The Chi-square test showed that blinding was successful ($p = 0.884$) (Table 2).

3.2 Visual spatial distraction task

We performed a four-way repeated measure ANOVA on reaction time (RT), including stimulation (real vs. sham), phase (T0, T1, T2), conflict (distractor vs. no distractor) and attention (valid and neutral cue) as factors. The results revealed significant main effects of time [$F_{(2,52)} = 27.973$, $p < 0.001$], conflict [$F_{(1,26)} = 12.618$, $p = 0.001$], and attention [$F_{(1,26)} = 111.536$, $p < 0.001$], but no main effect of stimulation [$F_{(1,26)} = 0.162$, $p = 0.691$]. However, a significant stimulation × phase interaction was found for RT [$F_{(2,54)} = 4.28$, $p = 0.021$]. All other interactions were not significant (Table 3). The *post-hoc* tests showed significant RT effects in the real stimulation group in all phases (T0 > T1, $p < 0.001$; T0 > T2, $p < 0.001$; T1 > T2, $p = 0.003$), but only in two phases in the sham group (T0 > T2, $p < 0.001$; T1 > T2, $p = 0.009$). However, there were no significant differences between real and sham stimulation. Only for T1 a trend wise difference was detected [$P = 0.098$, real (513.33 ± 13.04) < sham (530.201 ± 13.04)] (Figure 5). Additionally, we performed four-way repeated measure ANOVAs with accuracy and the inverse efficiency score as the dependent variables, including stimulation, phase, attention and conflict as within subject factors, which showed no significant main, or interaction effects.

TABLE 2 Blinding effect in two groups.

	Real stimulation	Sham stimulation
Correct guess	12	16
Wrong guess	15	11

3.3 eSports performance results

For the "Exact Aiming" scores, the main effect of stimulation [$F_{(1,26)} = 4.738$, $p = 0.039$, $\eta^2 = 0.154$], but not of time was significant. The interaction between time and stimulation was, however, significant [$F_{(1,26)} = 5.104$, $p = 0.032$, $\eta^2 = 0.164$] (Table 4). Follow-up *t*-tests showed that real and sham EA scores after, but not before intervention differed significantly ($p = 0.004$). The "Exact Aiming" scores after intervention were significantly larger in the real than in the sham stimulation group (11865 ± 395 vs. 10734 ± 345). For the "Flick Aiming" scores, the main effects of stimulation and time, as well as the respective interaction

TABLE 3 Results of the four-way ANOVA with stimulation, phase, conflict, and attention as within-subject factors for reaction time (RT) as dependent variable of the VSAD task.

Factor	df	F	*P*	η^2
Stimulation	1	0.162	0.691	0.006
Phase	2	27.973	<0.001*	0.535
Conflict	1	12.618	0.001*	0.327
Attention	1	111.536	<0.001*	0.811
Stimulation × Phase	2	3.867	0.027*	0.129
Stimulation × Conflict	1	0.051	0.823	0.002
Stimulation × Attention	1	3.160	0.087	0.108
Stimulation × Phase × Conflict	2	0.550	0.580	0.021
Stimulation × Phase × Attention	2	2.958	0.061	0.102
Stimulation × Conflict × Attention	1	3.139	0.088	0.129
Stimulation × Phase × Conflict × Attention	2	1.672	0.198	0.060

df, degrees of freedom; η2, indicates generalized eta-squared. Significant results are marked with asterisks.

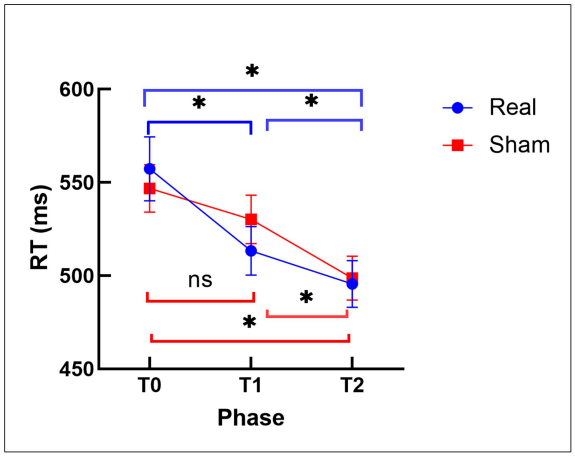

FIGURE 5
This figure shows VDST task reaction time in different phases (T0, T1, T2) in real and sham stimulation conditions. The figure shows that RT significantly differs between the three phases (T0 > T1, $p < 0.001$; T0 > T2, $p < 0.001$; T1 > T2, $p = 0.003$) in the real stimulation, but only in two phases in the sham stimulation group (T0 > T2, $p < 0.001$; T1 > T2, $p = 0.009$). Error bars show standard error of the mean. Significant results of the *post-hoc t*-tests are marked with asterisks. ns = not significant.

were not significant. With regard to "Press Reaction" reaction time, the ANOVA revealed a significant main effect of stimulation [$F_{(1,26)} = 6.731$, $p = 0.015$, $\eta^2 = 0.206$]. However, the interaction between stimulation and time was not significant. Follow-up *t*-tests revealed a significant difference of "Press Reaction" scores between real and sham conditions only after intervention (0.340 ± 0.008 s vs. 0.354 ± 0.008 s, $p = 0.036$) (Table 5 and Figure 6). For "Exact Aiming" and "Flick Aiming," larger scores are indicative for an improvement in gaming performance, suggesting enhanced gaming abilities. For "Press Reaction," lower scores indicate a larger skill level.

4 Discussion

In this study we aimed to test the effect of 10 Hz tACS over the right frontal-parietal cortex on eSports skill performance. As expected, 10 Hz tACS improved eSports skill performance in healthy non-gamers. Compared to sham, the results of the real stimulation group showed a significant better performance in "Exact Aiming" and preliminary hints for improved performance in the "Press Reaction" task. Moreover, in the visuo-spatial distraction task, RT in the real, but not the sham stimulation group was significantly reduced, and thus performance was significantly improved during stimulation as compared to baseline in that group. This is the first study which investigated frontoparietal network effects of tACS on eSports skill performance, and the results suggest that neuromodulation via tACS might be feasible to improve eSports performance.

With respect to mechanistic reasons for the visual spatial attention distraction task performance improvement accomplished by tACS, van Schouwenburg et al. (2016) reported that HD-alpha tACS over the frontoparietal network enhanced top–down control over visual regions. In that study, compared to sham stimulation, synchronous frontoparietal alpha band stimulation of the right hemisphere enhanced alpha coherence between the frontal and parietal-occipital cortex (van Schouwenburg et al., 2016). The frontoparietal network is crucial for the control of attention, based on network communication through coherence in the alpha band (Noudoost et al., 2010; Zanto et al., 2011; Gilbert and Li, 2013; Heinen et al., 2014; Doesburg et al., 2016; Paneri and Gregoriou, 2017). However, the same group did not replicate these results in 2018, where they found no spatially selective effects of stimulation on behavior or coherence in in-phase and anti-phase stimulation protocols, compared to sham (van Schouwenburg et al., 2018). Reasons for this unexpected result may be that current density over F4 and P4 was threefold higher in the first study, and different spatial attention tasks were used in both studies. Indeed, (after-) effects of stimulation seem to increase with increasing current density (Nitsche and Paulus, 2000). In the present experiment, we used the small electrodes (3.14 cm^2) applied in the study published in 2017, but stimulated for 20 min, and thus relevantly longer than that study (van Schouwenburg et al., 2016). The results of that study show that alpha frequency stimulation over the frontal and parietal cortices did improve performance, which was associated with a respective enhancement of fronto-parietal synchronization of alpha activity. This suggests that long-range alpha coherence is one mechanism by which the frontoparietal network controls spatial attention. The results of the present study suggest that

TABLE 4 The two-way ANOVA with stimulation and time as within-subject factor of eSports performance as dependent variable.

Task	Factor	df	F	*P*	η^2
Exact aiming	Stimulation	1	4.738	0.039*	0.154
	Time	1	4.006	0.056	0.133
	Stimulation × Time	1	5.104	0.032*	0.164
Flick aiming	Stimulation	1	0.025	0.876	0.001
	Time	1	1.817	0.189	0.065
	Stimulation × Time	1	0.003	0.958	<0.001
Press reaction	Stimulation	1	6.731	0.015*	0.206
	Time	1	0.325	0.573	0.012
	Stimulation × Time	1	0.209	0.652	0.008

df, indicates degrees of freedom; η^2, indicates eta-squared. Significant results are marked with asterisks.

TABLE 5 The scores of eSports task performance (mean ± SE) in real and sham stimulation conditions pre- and post-intervention.

Items	Times	Scores (Mean ± SE)	
		Real	Sham
Exact aiming	Pre	10972.4 ± 352.595	10774.963 ± 301.905
	Post	11865.4 ± 395.391	10734.92 ± 345.004
Flick aiming	Pre	2544.467 ± 79.754	2550.074 ± 80.024
	Post	2590.974 ± 64.985	2600.593 ± 70.617
Press reaction	Pre	0.3396 ± 0.006	0.3404 ± 0.006
	Post*	0.3494 ± 0.008	0.3545 ± 0.008

SE, standard error of means. Significant results between real and sham groups are marked with asterisks.

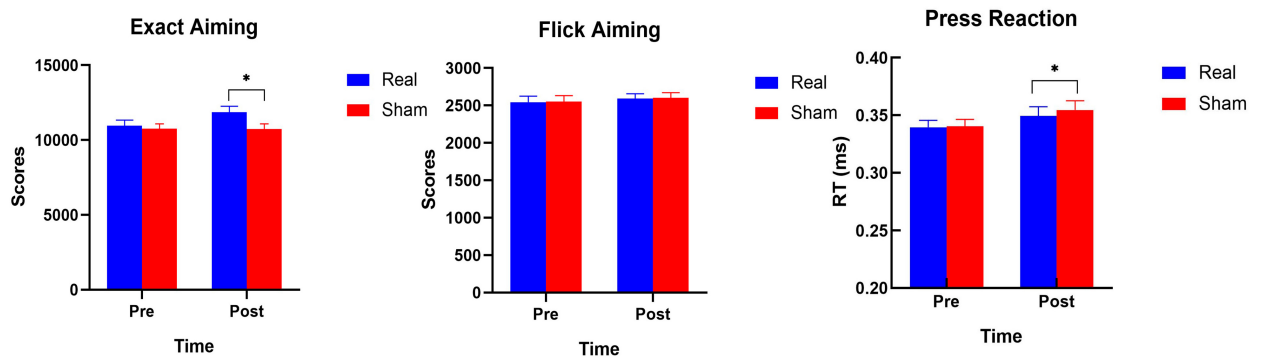

FIGURE 6
eSports skill performance before and after real, and sham stimulation. Significant results ($p \leq 0.05$) of the *post-hoc t*-tests are marked with asterisks. The error bars show the standard error of means.

this protocol improved visual attention ability with respect to RT during tACS, and this effect might be due to enhanced alpha band coherence between the frontal and parietal lobes. This is suggested by the significantly improved performance during stimulation in the real, but not the sham stimulation group relative to baseline. However, the respective between group difference at T1 was not significant, but showed only a trend, thus this study might have been underpowered to identify definite selective tACS effects in this task. At T2, and thus after stimulation, however, even this trendwise effect was absent, which might be in favor for a small, but specific effect of tACS during performance.

The visual spatial attention distraction task requires selective stimulus processing, including different variants of preparatory attention, such as spatial attention, feature-based attention, and object-based attention (Roelfsema et al., 1998; Treue and Martínez Trujillo, 1999; Buracas and Boynton, 2007; Snyder and Foxe, 2010; Noah et al., 2020), and thus mimics to a certain degree complex scene changes involved in action video games. Related studies have shown before that online alpha tACS improves attention, specifically it prevents attention decline (Clayton et al., 2019). This may be attributed to stronger attention alert in the visual field due to tACS of the right frontoparietal attention network (Posner and Petersen, 1990). Especially the alerting system has been associated with frontal and parietal regions of the right hemisphere, as has been shown for continuous performance and vigilance tasks (Fan et al., 2002; Petersen and Posner, 2012). Similar to the results of this study, a previous study reported that alpha tACS over the right dorsolateral prefrontal cortex improved performance of the arousal component of alertness and counteracted the typical vigilance decrement observed across time-on-task (Kemmerer et al., 2022). Therefore, tACS, as applied in the present study, might modulate visual attention via enhanced attention-related top-down control.

For eSports performance, the behavioral results showed that 10 Hz tACS over the right frontoparietal network improved performance significantly, as compared to the sham group, specifically in the "Exact Aiming" task. This task explores the ability to quickly capture many objects in a large game scene. A previous study demonstrated that alpha frequency tACS over the right frontal and parietal-occipital cortex increases long-range alpha coherence, which is one mechanism by which the frontoparietal network controls spatial attention (van Schouwenburg et al., 2016). The "Press Reaction" task requires conduction of a simple ballistic predefined movement. In the present study, press reaction time was less increased in the real as compared to the sham stimulation, and thus hints a performance improvement after real, as compared to sham stimulation. This result was, however, only evident for the *post-hoc* tests, but not the interaction of the respective ANOVA, is thus preliminary, and needs to be backed up by future studies. This result may be caused a stabilizing effect of tACS on visual attention (Clayton et al., 2019). For "Flick Aiming," which was not improved in the present study, in contrast to the other tasks, fine motor control of the mouse is critical. In this task, the volunteer has to move the mouse continuously to control movement of an arrow to dots displayed on the screen, and then back to a stable circle. Therefore, in this task performance depends more on the ability to control the mouse exactly, and the motor component of that task is relatively dominant, as compared to the other tasks. The absence of a significant effect may thus be due to the fact that motion control depends mainly on the primary motor cortex, and the motor network (Krause et al., 2016; Schilberg et al., 2018), while we conducted stimulation over frontal and parietal cortices to enhance visual attention. Moreover, for motor control, β and γ frequencies are critical (Pogosyan et al., 2009; Miyaguchi et al., 2019). In the present study we focused, however, mainly on the attention component of gaming performance, and thus applied tACS in the α frequency band, which is relevant for improving fronto-parietal network coherence to enhance visuo-spatial attention (Lobier et al., 2018). In future approaches, it might also make sense to focus on the motor component, which is also relevant for gaming performance, and where tACS with different frequencies over the motor network has been shown to improve performance. Taken together, the results of the present study suggest that 10 Hz tACS of the right frontoparietal network improves some components of tasks related to of eSports skills in naïve participants. The application of this intervention might thus potentially improve sports performance. This was, however, not shown nor aimed for directly in the present study, and would require studies with repeated stimulation over prolonged time courses, and other intervention-optimizing stimulation approaches in the respective target population for the targeted activities. The results of such studies might have ethical implications, dependent on their outcomes. The World Anti-Doping Agency (WADA) has

not classified electrical stimulation as a performance-enhancing substance at present and consequently this intervention does not face restrictions (Imperatori et al., 2018). However, neuro-doping is currently a vivid area under debate (Davis, 2013; Zhu et al., 2019), and while it is beyond the topic of this study to discuss this in detail, scientific information, such as delivered in the present study, is required as a foundation to come to scientifically informed regulatory decisions if this intervention should be rated as doping or not in future (Antal et al., 2022). Beyond application in sports, the positive cognitive effects of this intervention might make gaming combined with tACS a potentially attractive tool for rehabilitation in patients with cognitive deficits, which should be further explored. For potential application of this intervention in sports or clinical treatment, it should be taken, however, into account that this intervention has been most often been applied in a limited number of sessions, and with not optimized protocols, and respective studies would be required to explore its feasibility for application purposes in future.

Some limitations of this study should be taken into consideration. The design of this study was single blind, and principally double-blinding would have been advantageous. Since, however, the experimenter only communicated with the participants how to conduct the tasks before task performance, and the results of the blinding test show successful blinding, this limitation might have been minor in this specific case. Second, our sample consisted of a group of volunteers completely unfamiliar with eSports, and the eSports tasks were each conduced only once before and after intervention in each session. This might have resulted in suboptimal or floor effects. Enhanced effects might have been achieved with repetitive task performance after intervention via improved task learning caused by the intervention, and superior practice. Third, the transferability of these effects to skilled players cannot be taken for granted, but has to be explored in future studies, to explore the potential of the intervention for this group directly. Fourth, participants performed three consecutive visual attention task sessions, with less than 10 min between them, which might have led to cumulative effects independent from the intervention. In future studies, such practice effects should be avoided. Larger sample sizes in future studies would furthermore help to gain more clearly interpretable results of respective studies. The underlying physiology of the behavioral effects was not explored, thus mechanistic explanations remain speculative at present and future studies should add neuroimaging tools, such as EEG, and functional magnetic resonance tomography, to identify the physiological effects of this intervention. Furthermore, stimulation with the individual dominant alpha frequency has been suggested to be superior to stimulation with a standard frequency, and future studies should explore this option, and the return electrodes positioned between the target electrodes might have compromised efficacy of the stimulation to some degree because of antiphasic stimulation, thus alternative electrode positions should be probed.

5 Conclusion

The results of this study suggest that 10 Hz tACS over the right frontal and parietal cortex improves some aspects of eSports skill-related task performance in healthy students naïve to the tasks applied. HD-tACS improved visual spatial attention distraction task performance during stimulation, which might be due to enhanced alpha activity coherence between the frontal and parietal lobes. Since tACS also enhanced the ability to track multiple targets in a gaming task, we infer that this eSports performance improvement might have been caused by visual spatial attention enhancement. This is the first study which applied a tACS protocol to improve eSports performance, and the results supply preliminary hints that this intervention might be effective. However, this study was conducted in participants naïve to eSports gaming, and did not explore physiological mechanisms of these effects, which should be the topic of future studies. Moreover, the effects were relatively small, and likely short-lasting following this feasibility study. Therefore, we suggest that this tACS protocol might have principal potential as a neuromodulation tool to improve eSports athletes' performance, however, the approach needs to be optimized to make it potentially applicable for eSports performance, but also for other applications, including rehabilitation training in patients with cognitive deficits.

Data availability statement

The original contributions presented in the study are included in the article/**Supplementary material**, further inquiries can be directed to the corresponding author.

Ethics statement

The studies involving humans were approved by the Ethical committee of Shanghai University of Sport (approval number: 102772022RT047). The studies were conducted in accordance with the local legislation and institutional requirements. The participants provided their written informed consent to participate in this study.

Author contributions

FJ: Data curation, Formal Analysis, Writing – original draft. JZ: Data curation, Formal Analysis, Methodology, Writing – review and editing. MN: Supervision, Writing – review and editing. ZL: Data curation, Writing – original draft. YM: Formal Analysis, Writing – review and editing. YL: Funding acquisition, Supervision, Writing – review and editing.

Funding

The author(s) declare financial support was received for the research, authorship, and/or publication of this article. This study was supported by the grants from the National Natural Science Foundation of China (grant number: 11932013).

Conflict of interest

MN is member of the Scientific Advisory Boards of Neuroelectrics, and Precisis.

The authors declare that the research was conducted in the absence of any commercial or financial relationships that could be construed as a potential conflict of interest.

Publisher's note

All claims expressed in this article are solely those of the authors and do not necessarily represent those of their affiliated organizations, or those of the publisher, the editors and the reviewers. Any product that may be evaluated in this article, or claim that may be made by its manufacturer, is not guaranteed or endorsed by the publisher.

Supplementary material

The Supplementary Material for this article can be found online at: https://www.frontiersin.org/articles/10.3389/fnins.2024.1308370/full#supplementary-material

References

Antal, A., Luber, B., Brem, A. K., Bikson, M., Brunoni, A. R., Cohen Kadosh, R., et al. (2022). Non-invasive brain stimulation and neuroenhancement. *Clin. Neurophysiol. Pract.* 7, 146–165. doi: 10.1016/j.cnp.2022.05.002

Bavelier, D., and Green, C. S. (2019). Enhancing attentional control: Lessons from action video games. *Neuron* 104, 147–163. doi: 10.1016/j.neuron.2019.09.031

Bediou, B., Adams, D. M., Mayer, R. E., Tipton, E., Green, C. S., and Bavelier, D. (2018). Meta-analysis of action video game impact on perceptual, attentional, and cognitive skills. *Psychol. Bull.* 144, 77–110. doi: 10.1037/bul0000130

Billieux, J., Nuyens, F., Christiaens, M., and Deleuze, J. (2017). Shoot at first sight! First person shooter players display reduced reaction time and compromised inhibitory control in comparison to other video game players. *Comput. Hum. Behav.* 72, 570–576. doi: 10.1016/j.chb.2017.02.027

Boot, W. R., Kramer, A. F., Simons, D. J., Fabiani, M., and Gratton, G. (2008). The effects of video game playing on attention, memory, and executive control. *Acta Psychol.* 129, 387–398. doi: 10.1016/j.actpsy.2008.09.005

Buracas, G. T., and Boynton, G. M. (2007). The effect of spatial attention on contrast response functions in human visual cortex. *J. Neurosci.* 27, 93–97. doi: 10.1523/JNEUROSCI.3162-06.2007

Cabral-Calderin, Y., and Wilke, M. (2020). Probing the link between perception and oscillations: Lessons from transcranial alternating current stimulation. *Neuroscientist* 26, 57–73. doi: 10.1177/1073858419828646

Chung, T., Sum, S., Chan, M., Lai, E., and Cheng, N. (2019). Will esports result in a higher prevalence of problematic gaming? A review of the global situation. *J. Behav. Addict.* 8, 1–11. doi: 10.1556/2006.8.2019.46

Clayton, M. S., Yeung, N., and Cohen Kadosh, R. (2019). Electrical stimulation of alpha oscillations stabilizes performance on visual attention tasks. *J. Exp. Psychol. Gen.* 148, 203–220. doi: 10.1037/xge0000502

Cohen, M. R., and Maunsell, J. H. (2011). Using neuronal populations to study the mechanisms underlying spatial and feature attention. *Neuron* 70, 1192–1204. doi: 10.1016/j.neuron.2011.04.029

Davis, N. J. (2013). Neurodoping: Brain stimulation as a performance-enhancing measure. *Sports Med.* 43, 649–653. doi: 10.1007/s40279-013-0027-z

Doesburg, S. M., Bedo, N., and Ward, L. M. (2016). Top-down alpha oscillatory network interactions during visuospatial attention orienting. *Neuroimage* 132, 512–519. doi: 10.1016/j.neuroimage.2016.02.076

Fan, J., Mccandliss, B. D., Sommer, T., Raz, A., and Posner, M. I. (2002). Testing the efficiency and independence of attentional networks. *J. Cogn. Neurosci.* 14, 340–347. doi: 10.1162/089892902317361886

Feng, J., Spence, I., and Pratt, J. (2007). Playing an action video game reduces gender differences in spatial cognition. *Psychol. Sci.* 18, 850–855. doi: 10.1111/j.1467-9280.2007.01990.x

Friehs, M. A., Dechant, M., Vedress, S., Frings, C., and Mandryk, R. L. (2021). Shocking advantage! Improving digital game performance using non-invasive brain stimulation. *Int. J. Hum. Comput. Stud.* 148:102582. doi: 10.1016/j.ijhcs.2020.102582

Gilbert, C. D., and Li, W. (2013). Top-down influences on visual processing. *Nat. Rev. Neurosci.* 14, 350–363. doi: 10.1038/nrn3476

Green, C. S., and Bavelier, D. (2015). Action video game training for cognitive enhancement. *Curr. Opin. Behav. Sci.* 8, 103–108. doi: 10.1016/j.cobeha.2015.04.012

Green, C. S., and Bavelier, D. (2003). Action video game modifies visual selective attention. *Nature* 423, 534–537. doi: 10.1038/nature01647

Green, C. S., and Bavelier, D. (2006b). Enumeration versus multiple object tracking: The case of action video game players. *Cognition* 101, 217–245. doi: 10.1016/j.cognition.2005.10.004

Green, C. S., and Bavelier, D. (2006a). Effect of action video games on the spatial distribution of visuospatial attention. *J. Exp. Psychol. Hum. Percept. Perform.* 32, 1465–1478. doi: 10.1037/0096-1523.32.6.1465

Green, C. S., and Bavelier, D. (2010). Action-video-game experience alters the spatial resolution of vision. *Psychol. Sci.* 18, 88–94. doi: 10.1111/j.1467-9280.2007.01853.x

Harris, I. M., Benito, C. T., Ruzzoli, M., and Miniussi, C. (2008). Effects of right parietal transcranial magnetic stimulation on object identification and orientation judgments. *J. Cogn. Neurosci.* 20, 916–926. doi: 10.1162/jocn.2008.20513

He, M., Xu, L. X., Li, C. R., Liu, Z., Hu, J., Guo, X., et al. (2022). Do real-time strategy video gamers have better attentional control? *Hum. Factors* 66, 258–270. doi: 10.1177/00187208211064683

Heinen, K., Feredoes, E., Weiskopf, N., Ruff, C. C., and Driver, J. (2014). Direct evidence for attention-dependent influences of the frontal eye-fields on feature-responsive visual cortex. *Cereb. Cortex* 24, 2815–2821. doi: 10.1093/cercor/bht157

Herrmann, C. S., Rach, S., Neuling, T., and Strüber, D. (2013). Transcranial alternating current stimulation: A review of the underlying mechanisms and modulation of cognitive processes. *Front. Hum. Neurosci.* 7:279. doi: 10.3389/fnhum.2013.00279

Himmelstein, D., Liu, Y., and Shapiro, J. L. (2017). An exploration of mental skills among competitive league of legend players. *Int. J. Gaming Comput. Mediat. Simul.* 9, 1–21. doi: 10.4018/IJGCMS.2017040101

Hoba, S., Fink, G. R., Zeng, H., and Weidner, R. (2022). View normalization of object size in the right parietal cortex. *Vision (Basel)* 6:41. doi: 10.3390/vision6030041

Hosseinian, T., Yavari, F., Kuo, M. F., Nitsche, M. A., and Jamil, A. (2021). Phase synchronized 6 Hz transcranial electric and magnetic stimulation boosts frontal theta activity and enhances working memory. *Neuroimage* 245:118772. doi: 10.1016/j.neuroimage.2021.118772

Imperatori, L. S., Milbourn, L., and Garasic, M. D. (2018). Would the use of safe, cost-effective tDCS tackle rather than cause unfairness in sports? *J. Cogn. Enhance.* 2, 377–387. doi: 10.1007/s41465-018-0113-0

Johannes, V., Daniel, S., and Herrmann, C. S. (2018). Non-invasive brain stimulation: A paradigm shift in understanding brain oscillations. *Front. Hum. Neurosci.* 12:211. doi: 10.3389/fnhum.2018.00211

Kemmerer, S. K., De Graaf, T. A., Ten Oever, S., Erkens, M., De Weerd, P., and Sack, A. T. (2022). Parietal but not temporoparietal alpha-tACS modulates endogenous visuospatial attention. *Cortex* 154, 149–166. doi: 10.1016/j.cortex.2022.01.021

Krause, V., Meier, A., Dinkelbach, L., and Pollok, B. (2016). Beta Band Transcranial Alternating (tACS) and Direct Current Stimulation (tDCS) applied after initial learning facilitate retrieval of a motor sequence. *Front. Behav. Neurosci.* 10:4. doi: 10.3389/fnbeh.2016.00004

Lanssens, A., Mantini, D., de Beeck, H. O., and Gillebert, C. R. (2022). Activity in the fronto-parietal and visual cortex is modulated by feature-based attentional weighting. *Front. Neurosci.* 16:838683. doi: 10.3389/fnins.2022.838683

Lanssens, A., Pizzamiglio, G., Mantini, D., and Gillebert, C. R. (2020). Role of the dorsal attention network in distracter suppression based on features. *Cogn. Neurosci.* 11, 37–46. doi: 10.1080/17588928.2019.1683525

Liesefeld, H. R., and Janczyk, M. (2019). Combining speed and accuracy to control for speed-accuracy trade-offs(?). *Behav. Res. Methods* 51, 40–60. doi: 10.3758/s13428-018-1076-x

Lobier, M., Palva, J. M., and Palva, S. (2018). High-alpha band synchronization across frontal, parietal and visual cortex mediates behavioral and neuronal effects of visuospatial attention. *Neuroimage* 165, 222–237. doi: 10.1016/j.neuroimage.2017.10.044

Machado, S., Travassos, B., Teixeira, D. S., Rodrigues, F., Cid, L., and Monteiro, D. (2021). Could tDCS be a potential performance-enhancing tool for acute neurocognitive modulation in eSports? A perspective review. *Int. J. Environ. Res. Public Health* 18:3678. doi: 10.3390/ijerph18073678

Martinaud, O., Mirlink, N., Bioux, S., Bliaux, E., Champmartin, C., Pouliquen, D., et al. (2016). Mirrored and rotated stimuli are not the same: A neuropsychological and lesion mapping study. *Cortex* 78, 100–114. doi: 10.1016/j.cortex.2016.03.002

Maunsell, J. H., and Treue, S. (2006). Feature-based attention in visual cortex. *Trends Neurosci.* 29, 317–322. doi: 10.1016/j.tins.2006.04.001

Miyaguchi, S., Otsuru, N., Kojima, S., Yokota, H., Saito, K., Inukai, Y., et al. (2019). Gamma tACS over M1 and cerebellar hemisphere improves motor performance in a phase-specific manner. *Neurosci. Lett.* 694, 64–68. doi: 10.1016/j.neulet.2018.11.015

Nagorsky, E., and Wiemeyer, J. (2020). The structure of performance and training in esports. *PLoS One* 15:e0237584. doi: 10.1371/journal.pone.0237584

Nitsche, M. A., and Paulus, W. (2000). Excitability changes induced in the human motor cortex by weak transcranial direct current stimulation. *J. Physiol.* 527(Pt 3), 633–639. doi: 10.1111/j.1469-7793.2000.t01-1-00633.x

Noah, S., Powell, T., Khodayari, N., Olivan, D., Ding, M., and Mangun, G. R. (2020). Neural mechanisms of attentional control for objects: Decoding EEG alpha when anticipating faces, scenes, and tools. *J. Neurosci.* 40, 4913–4924. doi: 10.1523/JNEUROSCI.2685-19.2020

Noudoost, B., Chang, M. H., Steinmetz, N. A., and Moore, T. (2010). Top-down control of visual attention. *Curr. Opin. Neurobiol.* 20, 183–190. doi: 10.1016/j.conb.2010.02.003

Paneri, S., and Gregoriou, G. G. (2017). Top-down control of visual attention by the prefrontal cortex. functional specialization and long-range interactions. *Front. Neurosci.* 11:545. doi: 10.3389/fnins.2017.00545

Petersen, S. E., and Posner, M. I. (2012). The attention system of the human brain: 20 years after. *Annu. Rev. Neurosci.* 35, 73–89. doi: 10.1146/annurev-neuro-062111-150525

Pogosyan, A., Gaynor, L. D., Eusebio, A., and Brown, P. (2009). Boosting cortical activity at beta-band frequencies slows movement in humans. *Curr. Biol.* 19, 1637–1641. doi: 10.1016/j.cub.2009.07.074

Polanía, R., Nitsche, M. A., and Ruff, C. C. (2018). Studying and modifying brain function with non-invasive brain stimulation. *Nat. Neurosci.* 21, 174–187. doi: 10.1038/s41593-017-0054-4

Posner, M. I., and Petersen, S. E. (1990). The attention system of the human brain. *Annu. Rev. Neurosci.* 13, 25–42. doi: 10.1146/annurev.ne.13.030190.000325

Reinhart, R. M. G., and Nguyen, J. A. (2019). Working memory revived in older adults by synchronizing rhythmic brain circuits. *Nat. Neurosci.* 22, 820–827. doi: 10.1038/s41593-019-0371-x

Riddle, J., and Frohlich, F. (2021). Targeting neural oscillations with transcranial alternating current stimulation. *Brain Res.* 1765:147491. doi: 10.1016/j.brainres.2021.147491

Roelfsema, P. R., Lamme, V. A., and Spekreijse, H. (1998). Object-based attention in the primary visual cortex of the macaque monkey. *Nature* 395, 376–381. doi: 10.1038/26475

Sadaghiani, S., Scheeringa, R., Lehongre, K., Morillon, B., Giraud, A. L., D'Esposito, M., et al. (2012). α-band phase synchrony is related to activity in the fronto-parietal adaptive control network. *J. Neurosci.* 32, 14305–14310. doi: 10.1523/JNEUROSCI.1358-12.2012

Schilberg, L., Engelen, T., Ten Oever, S., Schuhmann, T., de Gelder, B., de Graaf, T. A., et al. (2018). Phase of beta-frequency tACS over primary motor cortex modulates corticospinal excitability. *Cortex* 103, 142–152. doi: 10.1016/j.cortex.2018.03.001

Snyder, A. C., and Foxe, J. J. (2010). Anticipatory attentional suppression of visual features indexed by oscillatory alpha-band power increases: A high-density electrical mapping study. *J. Neurosci.* 30, 4024–4032. doi: 10.1523/JNEUROSCI.5684-09.2010

Treue, S., and Martínez Trujillo, J. C. (1999). Feature-based attention influences motion processing gain in macaque visual cortex. *Nature* 399, 575–579. doi: 10.1038/21176

van Schouwenburg, M. R., Sörensen, L. K. A., De Klerk, R., Reteig, L. C., and Slagter, H. A. (2018). No differential effects of two different alpha-band electrical stimulation protocols over fronto-parietal regions on spatial attention. *Front. Neurosci.* 12:433. doi: 10.3389/fnins.2018.00433

van Schouwenburg, M., Zanto, T. P., and Gazzaley, A. (2016). Spatial attention and the effects of frontoparietal alpha band stimulation. *Front. Hum. Neurosci.* 10:658. doi: 10.3389/fnhum.2016.00658

Zanto, T. P., Rubens, M. T., Bollinger, J., and Gazzaley, A. (2010). Top-down modulation of visual feature processing: The role of the inferior frontal junction. *Neuroimage* 53, 736–745. doi: 10.1016/j.neuroimage.2010.06.012

Zanto, T. P., Rubens, M. T., Thangavel, A., and Gazzaley, A. (2011). Causal role of the prefrontal cortex in top-down modulation of visual processing and working memory. *Nat. Neurosci.* 14, 656–661. doi: 10.1038/nn.2773

Zhang, Y., Zhou, Z., Zhou, J., Qian, Z., Lü, J., Li, L., et al. (2022). Temporal interference stimulation targeting right frontoparietal areas enhances working memory in healthy individuals. *Front. Hum. Neurosci.* 16:918470. doi: 10.3389/fnhum.2022.918470

Zhu, Z., Zhou, J., Manor, B., Wang, X., Fu, W., and Liu, Y. (2019). Commentary: "Brain-Doping," is it a real threat? *Front. Physiol.* 10:1489. doi: 10.3389/fphys.2019.01489

Zhuang, W., Yin, K., Zi, Y., and Liu, Y. (2020). Non-invasive brain stimulation: Augmenting the training and performance potential in esports players. *Brain Sci.* 10:454. doi: 10.3390/brainsci10070454

frontiers | Frontiers in Neuroscience

TYPE Review
PUBLISHED 19 March 2024
DOI 10.3389/fnins.2024.1309736

OPEN ACCESS

EDITED BY
Mark H. Myers,
University of Tennessee Health Science Center (UTHSC), United States

REVIEWED BY
Weronika Dębowska,
Medical University of Warsaw, Poland
Xun Luo,
Kerry Rehabilitation Medicine Research Institute, China

*CORRESPONDENCE
Ling Zhao
✉ zhaoling@cdutcm.edu.cn

RECEIVED 08 October 2023
ACCEPTED 16 February 2024
PUBLISHED 19 March 2024

CITATION
Wang Y, Wang L, Ni X, Jiang M and Zhao L (2024) Efficacy of repetitive transcranial magnetic stimulation with different application parameters for post-stroke cognitive impairment: a systematic review.
Front. Neurosci. 18:1309736.
doi: 10.3389/fnins.2024.1309736

Efficacy of repetitive transcranial magnetic stimulation with different application parameters for post-stroke cognitive impairment: a systematic review

Yuhan Wang[1], Linjia Wang[1], Xixiu Ni[1], Minjiao Jiang[2] and Ling Zhao[1,3,4]*

[1]Acupuncture and Moxibustion College, Chengdu University of Traditional Chinese Medicine, Chengdu, Sichuan, China, [2]Acupuncture and Moxibustion College, Nanjing University of Traditional Chinese Medicine, Nanjing, China, [3]Acupuncture Clinical Research Center of Sichuan Province, Chengdu, China, [4]Key Laboratory of Acupuncture for Senile Disease (Chengdu University of TCM), Ministry of Education, Chengdu, China

Background: Cognitive impairment is a prevalent consequence of stroke, seriously affecting recovery and quality of life while imposing substantial burdens on both patients' families and society. Repetitive transcranial magnetic stimulation (rTMS) has emerged as an effective intervention for post-stroke cognitive impairment (PSCI). However, the a lack of standardized and explicit guidelines regarding rTMS application parameters. Therefore, this study systematically evaluated the efficacy of various parameters of rTMS in treating PSCI and explored its potential mechanism.

Methods: We conducted a comprehensive search across seven scientific databases, namely China National Knowledge Infrastructure (CNKI), Wanfang Data Knowledge Service Platform (Wanfang), China Science and Technology Journal Database (VIP), Web of Science, PubMed, Embase, and Cochrane Library, to identify randomized controlled trials (RCTs) investigating the efficacy of rTMS for PSCI. The search encompassed the period from database creation until July 28, 2023. To evaluate the risk of bias in included studies, we employed the Cochrane recommended risk of bias assessment tool. Furthermore, we extracted relevant clinical application parameters associated with rTMS and performed comparative analyses to assess their therapeutic effects under different parameter settings.

Results: The present study included 45 RCTs involving a total of 3,066 patients with PSCI. Both high-frequency repetitive transcranial magnetic stimulation (HF-rTMS) and low-frequency repetitive transcranial magnetic stimulation (LF-rTMS) demonstrated safety and efficacy, yet failed to exhibit significant differentiation in terms of cognitive improvement. Furthermore, intermittent theta burst stimulation (iTBS), although yielding positive results, did not surpass traditional rTMS in effectiveness. Combining HF-rTMS with LF-rTMS resulted in superior efficacy compared to single rTMS intervention. Moreover, the combination of rTMS with other cognitive therapies exhibited potential for enhanced benefits among patients.

Conclusion: rTMS can effectively and safely enhance cognitive function, improve quality of life, and enhance activities of daily living in patients with PSCI. Furthermore, the combination of rTMS with other conventional rehabilitation

methods can yield additional positive effects. However, due to insufficient evidence, an optimal parameter protocol for rTMS can not be currently recommended. Future research should prioritize orthogonal experimental design methods that incorporate multiple parameters and levels to determine the optimal parameter protocol for rTMS in PSCI.

KEYWORDS

stroke, cognitive impairment, repetitive transcranial magnetic stimulation, application parameters, randomized controlled trials

1 Introduction

The high morbidity, disability, and mortality rates associated with stroke have positioned it as the second leading cause of death globally and the primary cause of disability (Naghavi et al., 2017; Vos et al., 2020). Consequently, stroke has emerged as a critical public health concern worldwide (Tsao et al., 2023). Post-stroke cognitive impairment (PSCI), a common complication following stroke, is characterized by cognitive deficits that persist for 3 to 6 months after the event (Wang et al., 2021a). The prevalence of PSCI ranges from 24 to 53.4% among stroke patients (Douiri et al., 2013; Lo et al., 2019), with an increasing incidence trend observed (Huang et al., 2022). PSCI significantly impacts patients' quality of life, activities of daily living, and post-stroke survival rate (Rohde et al., 2019; Wang et al., 2021a).

For PSCI, the primary treatment modalities encompass pharmacotherapy and traditional non-pharmacological rehabilitation approaches, such as cognitive training. Pharmacotherapy options include cholinesterase inhibitors (e.g., donepezil) and N-methyl-D-aspartate receptor antagonists (e.g., carpalatin) (Gorelick et al., 2011; Kim et al., 2020). Although these drugs can enhance patients' cognitive function, they are associated with various adverse reactions, including diarrhea, nausea, insomnia, and even psychiatric symptoms like irritability and aggressive behavior (Farooq et al., 2017; Sun, 2018; Loetscher et al., 2019). However, the efficacy of traditional non-pharmacological cognitive rehabilitation training in PSCI remains limited due to prolonged intervention duration and suboptimal patient compliance, thus necessitating further exploration (Merriman et al., 2019).

Repetitive transcranial magnetic stimulation (rTMS) represents a highly promising non-invasive brain stimulation technique that can modulate cerebral cortex excitability in a non-invasive manner. By inducing enduring changes in neural plasticity through magnetic fields and reorganizing functional connectivity between specific regions, it holds the potential for enhancing brain network functionality and facilitating recovery of cognitive function among stroke patients (Hernandez-Pavon and Harvey, 2019).

Although numerous randomized controlled trials (RCTs) (Duan and Ding, 2016; Chen et al., 2017, 2019; Ding et al., 2019) have demonstrated the effective enhancement of cognitive function, daily living abilities, and quality of life in stroke patients through rTMS, there remains a lack of standardized and clear application parameters for rTMS, including intensity, frequency, and treatment duration. These parameters are crucial factors that influence the clinical outcomes. Therefore, this study aims to analyze recent RCTs investigating rTMS treatment for PSCI, evaluate the efficacy of various rTMS parameters on PSCI, and explore potential mechanisms of action. We hope that this study will offer valuable guidance and evidence-based medicine support for the clinical implementation of rTMS in the management of PSCI.

2 Methods

The protocol has been registered with PROSPERO (Registration number: CRD42023460450).

2.1 Inclusion criteria

The studies meeting the following criteria were included:

2.1.1 Types of studies

The scope of this study was confined to RCTs investigating the efficacy of rTMS in patients diagnosed with PSCI.

2.1.2 Population

The inclusion criteria were defined as follows: (1) all patients with ischemic or hemorrhagic stroke exhibited evident imaging pathological evidence on magnetic resonance imaging (MRI) or computed tomography (CT); (2) patients diagnosed with PSCI through clinical examination; (3) patients without any neurological disorders, including Parkinson's disease, Alzheimer's disease, or other causes of cognitive impairment.

2.1.3 Intervention and comparison

The intervention group was administered rTMS, while the control group received either standard rehabilitation or sham/placebo rTMS. Both groups were provided with the same standard care.

2.1.4 Outcome

Outcome measures included at least one of the following: The study considered one or more objective outcome indicators such as Montreal Cognitive Assessment Scale (MoCA), Mini-Mental State Examination (MMSE), Loewenstein Occupational Therapy Cognitive Assessment (LOTCA), the Tower of London Test (TOLT).

2.2 Exclusion criteria

We excluded literature from the search: (1) non-RCTs, such as case reports, reviews, and animal experiments; (2) baseline consistency

tests were not given; (3) data were incomplete or full text was unavailable; (4) duplicate articles were published.

2.3 Data sources and search strategy

We searched seven scientific databases: China National Knowledge Infrastructure(CNKI), Wanfang Data Knowledge Service Platform(Wanfang), China Science and Technology Journal Database(VIP), Web of Science, PubMed, Embase, and Cochrane Library. The search period was from the creation of the databases to July 28, 2023. There were no restrictions on publication source or language. The searched MeSH terms are listed as follows: ["Transcranial Magnetic Stimulation" [MeSH] OR "Theta Burst Stimulation" OR "rTMS"] AND ["Stroke" [MeSH] OR "Cerebral Infarction" [MeSH] OR "Cerebral Hemorrhage" [MeSH] OR "Cerebrovascular Accident"] AND ["Cognitive Impairment" [MeSH] OR "Cognitive Function"]. In addition, a complementary search was conducted for references included in the literature. The search formula is available in Supplementary File.

2.4 Data extraction and management

The retrieved literature was imported into the EndNote software for centralized management. Two researchers (YW and LX) independently screened the literature based on the proposed inclusion and exclusion criteria. After excluding duplicate literature using EndNote, both researchers independently reviewed the titles, keywords, and abstracts of the articles to preliminarily exclude those that did not meet the inclusion criteria. Subsequently, they downloaded and thoroughly read the full text to determine whether it met the inclusion criteria. In case of any necessary clarifications or missing information, we contacted the original authors via email or phone. Data extraction was performed by researchers independently using a pre-designed data extraction form for further analysis. The extracted data included: first author, publication year, patient characteristics (gender, age, time to stroke onset), study-specific parameters (study type, number of enrolled patients, duration of treatment, interventions, outcome indicators, follow-up, adverse events), as well as application parameters of rTMS (frequency, number of pulses, intensity, stimulation site, and duration of each treatment). If there is any disagreement, it will be referred to a third researcher (LZ) to determine the final results.

2.5 Assessment of risk of bias

The included studies were assessed for bias using the risk assessment tools recommended by Cochrane (Cumpston et al., 2019), which encompassed randomization, assignment concealment, blinding procedures, blinding of outcome evaluation, completeness of outcome data, selective reporting of results, and identification of other potential biases. In cases where evaluators (YW and LX) held differing opinions, a third investigator (LZ) was consulted for evaluation. The risk of bias plots were generated using RevMan 5.3 software.

2.6 Data analysis

We analyzed data obtained from RCTs. A narrative synthesis was employed as a preferred method, given its suitability for summarizing studies with heterogeneous results (Trung et al., 2019). The findings were presented in tabular format using a narrative synthesis approach.

3 Results

3.1 Literature search results

We searched 1,216 records and excluded 478 duplicates. After reading the title and abstract, 626 studies were excluded. After reading the complete text, we again excluded 67 studies. Eventually, 45 studies were considered for inclusion. The exclusion and screening process is detailed in Figure 1.

3.2 The characteristic of the included studies

45 RCTs were included, enrolling 3,066 patients with PSCI. Publication dates ranged from 2012 to 2023. RCTs included a minimum of 18 patients and a maximum of 200 patients. Adverse events were reported in 20 studies, as summarized in Table 1.

3.3 Results of bias risk assessment

We assessed the risk of bias in the included RCTs. 24 RCTs (Zuo and Zhang, 2013; Jiang et al., 2014; Li et al., 2015a,b; Park and Yoon, 2015; Tang et al., 2015; Duan and Ding, 2016; Hu et al., 2016; Chen et al., 2017; He and Zhou, 2017; Zhou et al., 2017; Ren et al., 2018; Chen et al., 2019; Yu and Zhang, 2019; Zhang and Zhou, 2019; Li et al., 2020a,b; Lv et al., 2020; Gao et al., 2021; Qi et al., 2021; Li et al., 2022; Wu et al., 2022; Xu et al., 2022; You et al., 2023) did not use sham rTMS in the control group, which may not have blinded patients and implementers, resulting in a high risk of bias. In addition, only seven studies (Park and Yoon, 2015; Yu and Zhang, 2019; Li et al., 2020c; Liu et al., 2020; Qi et al., 2021; Li et al., 2022) reported on allocation concealment, and 16 (Li et al., 2015a,b; Lu et al., 2015; Park and Yoon, 2015; Liao et al., 2017; Ren et al., 2018; Ding et al., 2019; Zhang and Zhou, 2019; Li et al., 2020c; Liu et al., 2020; Tsai et al., 2020; Zhang et al., 2020; Ma et al., 2021; Zhang et al., 2021; Li et al., 2022; Zhang et al., 2022) reported on assessor blindness. The specific results are presented in Figures 2–3.

3.4 rTMS application parameters

The application characteristics of rTMS were shown in Table 2.

3.4.1 Stimulation frequency

There was no standardized protocol for the application frequency of rTMS in the included studies. Based on frequency, rTMS could be categorized into high-frequency repetitive transcranial magnetic stimulation (HF-rTMS) and low-frequency repetitive transcranial

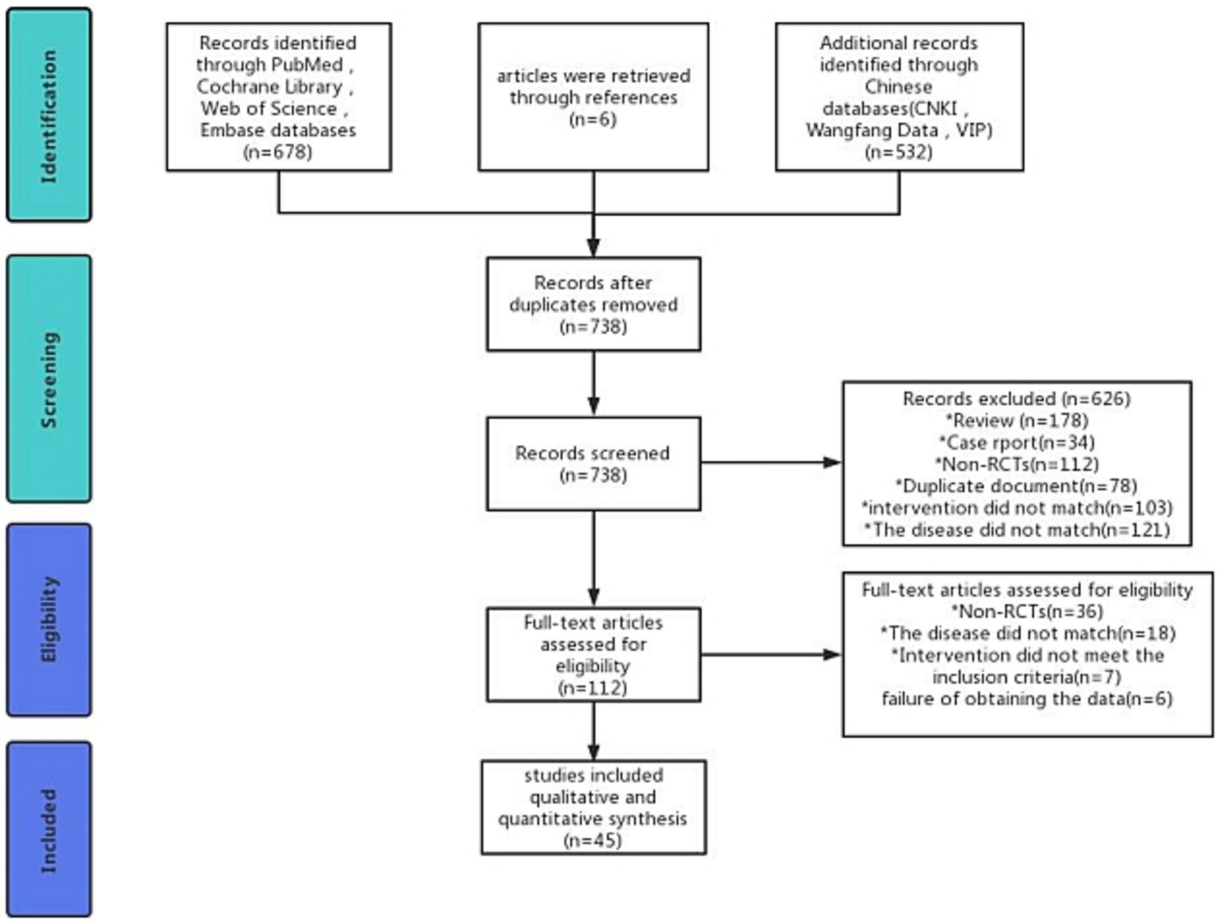

FIGURE 1
PRISMA flow diagram for study selection.

magnetic stimulation (LF-rTMS). Among low-frequency protocols, 1 Hz was the most commonly utilized, followed by 0.5 Hz. For high-frequency applications, 10 Hz was predominantly employed, although researchers had also explored rTMS frequencies of 3 Hz, 5 Hz, and 20 Hz. In all instances, rTMS consistently demonstrated significant improvements in cognitive function among patients. Based on the event-related potential (ERP) test results, Wu (Wu et al., 2022) applied stimulation to the bilateral dorsolateral prefrontal cortex (DLPFC), temporal lobe, precentral gyrus, and posterior 1/3 of inferior frontal gyrus. The selection of frequency was guided by the excitability of the target area: 1 Hz low-frequency rTMS was chosen for areas with higher excitability, while 5 Hz high-frequency rTMS was selected for areas with lower excitability.

However, it was noteworthy that seven studies (Kim et al., 2010; Liao et al., 2017; Ding et al., 2019; Zhang et al., 2020; Wang et al., 2021b; Mao et al., 2022; Li et al., 2023) had assessed the clinical effects of rTMS at various frequencies, and most of them had reported that both LF-rTMS and HF-rTMS could improve cognitive function (MoCA (Liao et al., 2017; Ding et al., 2019; Zhang et al., 2020; Wang et al., 2021b; Li et al., 2023), LOTCA (Wang et al., 2021b), MMSE (Zhang et al., 2020; Li et al., 2023), TOLT (Kim et al., 2010)), balance (Li et al., 2023), daily living ability (Kim et al., 2010; Liao et al., 2017; Li et al., 2023) and prolonged auditory event-related potential P3000 (AERP P3000) latency and promoted wave amplitude (Liao et al., 2017; Ding et al., 2019; Zhang et al., 2020). Interestingly, no significant difference in efficacy between these two frequencies had been observed. Only Mao (Mao et al., 2022), in a comparison of efficacy between 1 Hz and 10 Hz, found that at 10 Hz, rTMS was able to achieve more positive effects in the results of MMSE, Fuel-Meyer assessment (FMA), Modified Barthel Index (MBI), and MoCA. Conversely, the combination of high-frequency and low-frequency stimulation had been shown to yield superior clinical outcomes (Chen et al., 2017; Ding et al., 2019; Li et al., 2023). Ding (Ding et al., 2019) demonstrated that the 5 Hz group, 1 Hz group, and 5 Hz combined with the 1 Hz group (with high frequency applied to the affected side DLPFC and low frequency applied to the healthy side DLPFC, alternating stimulus) exhibited improvements in MOCA score, reduced AERP P300 latency and increased the amplitude. Notably, the combined group displayed the most significant effects. At the 8-week follow-up assessment, all rTMS treatment groups showed improvement compared to baseline measures as well as outperformed the control group. Furthermore, the combined group remained significantly superior to both the 5 Hz group and the 1 Hz group ($p < 0.05$).

3.4.2 Stimulus intensity

Regarding the application intensity, all studies were conducted based on the patient's resting motor potential threshold (RMT). The majority of studies utilized an intensity of 80% RMT, while some

TABLE 1 Characteristics of the included studies.

Study	Sample Size (gender)		Age (y)		intervention		Time after onset (d)		Adverse events
	T (male/ female)	C (male/ female)	T	C	T	C	T	C	
Chen (2017)	15(11/4)	15 (9/6)	58.0 ± 8.9	60.1 ± 7.7	rTMS+ST	ST	35.7 ± 20.3	37.8 ± 16.1	No
Chen (2019)	70 (37/33)	70 (39/31)	57.1 ± 5.0	56.8 ± 4.8	rTMS+ST	ST	87 ± 24	2.8 ± 0.8	No
Ding (2019)	Group 1:15 (10/5); Group 2:14 (10/4); Group 3:15 (8/7)	14 (9/5)	Group 1:53.67 ± 7.58; Group 2:54.40 ± 6.82; Group 3:54.33 ± 7.72	53.53 ± 7.65	rTMS+ST	Sham rTMS+ST	Group 1:53.20 ± 18.06; Group 2:50.89 ± 17.64; Group 3:55.51 ± 15.54	49.49 ± 14.84	No
Duan (2016)	59 (35/24)	59 (36/23)	65.8 ± 7.1	66.4 ± 7.2	rTMS+ST	ST	132 ± 57	126 ± 48	NA
Gao (2021)	24 (11/13)	24 (14/10)	48.79 ± 6.61	48.58 ± 6.59	rTMS+ST	ST	41.72 ± 10.22	42.00 ± 9.66	NA
Gu (2012)	16 (8/8)	20 (12/8)	66.8 ± 8.1	71.7 ± 7.0	rTMS+ST	Sham rTMS+ST	NA	NA	No
Li (2020)	44 (26/18)	44 (24/20)	54.2 ± 6.3	56.4 ± 7.0	rTMS+ST	ST	NA	NA	NA
He (2017)	16 (9/7)	14 (8/6)	48.00 ± 12.42	47.43 ± 13.67	rTMS+ST	ST	46.8 ± 21.9	54.0 ± 23.1	NA
Jiang (2014)	30 (NA)	30 (NA)	60.41 ± 8.03	59.52 ± 7.19	rTMS+ST	ST	NA	NA	3 patients experienced headaches in the intervention group
Li (2023)	Group 1:50 (21/29); Group 2:50 (26/24); Group 3:50 (25/25)	50 (22/28)	Group 1:57.63 ± 5.23; Group 2:57.42 ± 5.22; Group 3:56.37 ± 5.12	56.91 ± 5.17	rTMS+ST	Sham rTMS+ST	Group 1:75.11 ± 15.05; Group 2:78.05 ± 15.61; Group 3:79.59 ± 15.89	78.68 ± 15.75	NA
Li (2022)	41 (24/17)	41 (23/18)	59.97 ± 4.71	60.18 ± 3.74	rTMS+ST	ST	29.87 ± 4.51	30.05 ± 4.16	In the intervention group, 4 patients had headache and 1 patient had nausea, while 5 patients in the control group had headache.
Li (2020)	50 (29/21)	50 (31/19)	58.94 ± 3.76	59.61 ± 3.75	rTMS+ST	ST	27.41 ± 4.23	28.74 ± 5.13	In the intervention group, 4 patients had headache, 1 patient had nausea and vomiting, while in the control group, 3 patients had headache, 2 patients had nausea and vomiting， 1 patient had diarrhea, and 1 patient had epilepsy.

(Continued)

10.3389/fnins.2024.1309736

TABLE 1 (Continued)

Study	Sample Size (gender)		Age (y)		intervention		Time after onset (d)		Adverse events
	T (male/female)	C (male/female)	T	C	T	C	T	C	
Li (2015)	23 (11/12)	22 (12/10)	58.6 ± 4.2	57.9 ± 4.3	rTMS+ST	ST	120 ± 21	126 ± 24	2 patients in the intervention group complained of mild dizziness and headache discomfort
Ren (2018)	27 (14/13)	27 (13/14)	59.4 ± 7.1	58.6 ± 7.8	rTMS+ST	ST	50.0 ± 8.4	48.0 ± 10.7	NA
Li (2015)	32 (11/21)	30 (12/18)	58.2 ± 5.4	57.8 ± 6.1	rTMS+ST	ST	123 ± 24	129 ± 28	No
Liao (2017)	Group 1:30 (16/14); Group 2:30 (17/13)	30 (18/12)	Group 1:60.2 ± 6.5; Group 2:59.9 ± 6.7	60.5 ± 6.6	rTMS+ST	Sham rTMS+ST	Group 1:45.7 ± 5.3; Group 2:44.9 ± 5.7	45.8 ± 4.6	No
Lv (2020)	46 (28/18)	46 (29/17)	46.71 ± 10.98	46.35 ± 11.40	rTMS+ST	ST	123.0 ± 9.3	122.7 ± 8.7	Dizziness during rTMS treatment in 3 patients
Wu (2022)	Group 1:30 (17/13); Group 2:30 (18/12)	30 (16/14)	Group 1:55.4 ± 11.1; Group 2:54.2 ± 12.8	56.8 ± 11.7	Group 1:rTMS+AOT + ST; Group 2:rTms+ST	ST	Group 1:85.6 ± 31.3; Group 2:86.3 ± 29.7	88.7 ± 29.2	NA
Ma (2021)	37 (25/12)	38 (22/16)	60.95 ± 7.92	58.84 ± 10.89	rTMS+ST	Sham rTMS+ST	65.14 ± 26.62	63.63 ± 35.52	NA
Mao (2022)	Group 1:21 (16/5); Group 2:20 (14/6)	22 (16/6)	Group 1:58.48 ± 9.10; Group 2:60.00 ± 8.53	52.95 ± 14.62	rTMS+ST	Sham rTMS+ST	Group 1:62.10 ± 53.66; Group 2:46.86 ± 39.89	50.82 ± 30.90	NA
Pei (2022)	30 (18/13)	29 (22/7)	64.90 ± 5.46	66.93 ± 6.55	iTBS+ST	Sham iTBS+ST	90 ± 48	81 ± 48	NA
Tang (2015)	30 (17/13)	30 (18/12)	61.2 ± 10.8	60.9 ± 11.2	rTMS+ST	ST	NA	NA	No
Xu (2022)	65 (38/27)	65 (36/29)	64.09 ± 3.86	63.52 ± 4.27	rTMS+ST	ST	16.17 ± 3.54	15.64 ± 3.72	NA
Yin (2018)	12 (11/1)	13 (12/1)	58.58 ± 11.98	60.15 ± 10.29	rTMS+ST	Sham rTMS+ST	59.83 ± 30.59	56.15 ± 23.74	Transient headache during rTMS treatment in 3 patients
You (2023)	66 (39/27)	66 (35/31)	62.38 ± 4.44	62.13 ± 4.69	rTMS+ST	ST	NA	NA	NA
Yu (2019)	51 (29/22)	49 (25/24)	65.13 ± 10.32	62.15 ± 13.49	rTMS+ST	ST	397.5 ± 174.0	368.4 ± 193.5	NA
Zhang (2019)	30 (20/10)	30 (18/12)	58.44 ± 16.60	55.11 ± 18.03	rTMS+ST	ST	46.83 ± 28.13	49.00 ± 37.01	NA
Zhang (2022)	20 (11/9)	20 (8/12)	54 ± 7.0	57 ± 6	rTMS+ST	Sham rTMS+ST	180 ± 120	180 ± 120	NA
Zhang (2020)	Group 1:15 (8/7); Group 2:15 (7/8); Group 3:15 (9/6); Group 4:15 (8/7)	15 (10/5)	Group 1:59.87 ± 6.24; Group 2:59.47 ± 6.68; Group 3:55.20 ± 8.07; Group 4:58.00 ± 5.84	56.80 ± 9.69	rTMS+ST	Sham rTMS+ST	Group 1:147.0 ± 60.9; Group 2:143.1 ± 43.2; Group 3:153.9 ± 59.7; Group 4:150.9 ± 58.2	147.0 ± 61.8	2 patients developed dizziness after 10 Hz rTMS treatment
Zhang (2021)	21 (15/6)	22 (14/8)	60.67 ± 9.53	58.98 ± 7.88	rTMS+ST	Sham rTMS+ST	51.90 ± 21.90	49.59 ± 29.39	NA

(Continued)

10.3389/fnins.2024.1309736

TABLE 1 (Continued)

Study	Sample Size (gender)		Age (y)		intervention		Time after onset (d)		Adverse events
	T (male/female)	C (male/female)	T	C	T	C	T	C	
Zhou (2017)	15 (9/6)	15 (11/4)	55.14 ± 10.76	53.41 ± 11.29	rTMS+ST	ST	124.5 ± 68.4	128.1 ± 114.6	NA
Zheng (2020)	55 (36/19)	51 (33/18)	58.3 ± 7.9	59.7 ± 6.3	rTMS+ST	Sham rTMS+ST	48.7 ± 14.4	47.3 ± 11.8	One patient in the intervention group had poor concentration, one patient complained of sleep disturbance, and one patient in the control group had dizziness
Zuo (2013)	53 (30/23)	49 (27/22)	62.6 ± 7.3	64.3 ± 7.8	rTMS+ST	ST	NA	NA	NA
Bi (2022)	18 (13/5)	18 (12/6)	60.39 ± 10.87	59.50 ± 11.25	rTMS+ST	Sham rTMS+ST	58.11 ± 28.89	58.39 ± 24.70	No
Kim (2010)	Group 1:6 (2/4); Group 2:6 (4/2)	6 (4/2)	Group 1:68.3 ± 7.4; Group 2:53.5 ± 16.9	66.8 ± 17.2	rTMS+ST	Sham rTMS+ST	Group 1:404 ± 71.7; Group 2:241.2 ± 42.59	69.7 ± 39	NA
Li (2021)	33 (21/12)	32 (19/13)	61.79 ± 5.51	59.47 ± 6.75	rTMS+ST	Sham rTMS+ST	28.64 ± 12.60	27.78 ± 11.01	No
Li (2022)	28 (16/12)	30 (18/12)	69.14 ± 14.06	64.57 ± 17.12	iTBS+ST	Sham iTBS+ST	23.93 ± 10.16	24.29 ± 9.34	NA
Lu (2015)	19 (12/7)	21 (13/8)	42.5 ± 12.3	47.3 ± 11.8	rTMS+ST	Sham rTMS+ST	106.85 ± 90.75	86.99 ± 70.39	NA
Tsai (2020)	Group 1:15 (11/4); Group 2:11 (9/2)	15 (13/2)	Group 1:60.13 ± 14.1; Group 2:57.45 ± 12.3	56.23 ± 12	Group 1:rTMS+ST; Group 2:iTBS+ST	Sham rTMS+ST	Group 1:554.1 ± 606.3; Group 2:998.1 ± 792.0	1,140 ± 237	One patient in the intervention group developed transient headache and one patient developed dizziness, while one patient in the control group developed headache.
Li (2020)	15 (7/8)	15 (9/6)	65.47 ± 3.68	64.53 ± 4.72	rTMS+ST	Sham rTMS+ST	22.73 ± 8.05	19.13 ± 7.95	NA
Park (2015)	10 (4/6)	10 (5/5)	NA	NA	CACR+ST	rTMS+ST	NA	NA	NA
Liu (2020)	29 (10/19)	29 (16/13)	58.55 ± 6.24	57.69 ± 7.25	rTMS+ST	Sham rTMS+ST	263.7 ± 55.2	258.6 ± 55.2	NA
Wang (2021)	Group 1:15 (10/5); Group 2:15 (11/4)	15 (10/5)	Group 1:60.2 ± 11.6; Group 2:57.8 ± 13.0	58.8 ± 9.3	rTMS+ST	Sham rTMS+ST	Group 1:56.0 ± 25.4; Group 2:52.5 ± 21.6	57.3 ± 18.5	No
Qi (2021)	36 (NA)	36 (NA)	59.6 ± 8.0	58.7 ± 7.9	rTMS+ST	ST	1.45 ± 0.21	1.45 ± 0.20	NA
Hu (2016)	30 (14/16)	30 (15/15)	57.5 ± 13.3	56.2 ± 10.9	rTMS+ST	ST	NA	NA	2 patients in the intervention group developed headache and dizziness

T, treatment group; C, control group; y, year; m, month; d, day; rTMS, repetitive transcranial magnetic stimulation; ST, standard rehabilitation treatment; CACR, computer-assisted cognitive rehabilitation; iTBS, intermittent theta burst stimulation; AOT, action observation therapy; NA, not available.

10.3389/fnins.2024.1309736

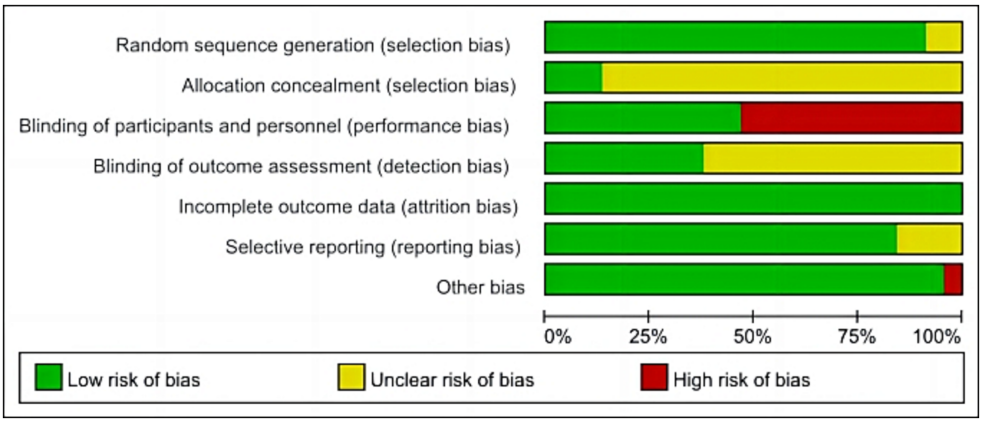

FIGURE 2
Risk of bias graph.

employed intensities of 70% RMT, 90% RMT, 100% RMT, 110% RMT, and 120% RMT. Notably, all stimulation intensities yielded positive outcomes. In terms of RMT detection methodology, most studies opted to measure the first interosseous dorsal muscle or abductor pollicis brevis. The minimum magnetic stimulation intensity capable of eliciting a muscle motor evoked potential (amplitude ≥50 μV) in at least five out of ten consecutive stimulations was considered as the RMT value.

3.4.3 Stimulus area

As for the site of rTMS, the dorsolateral prefrontal cortex (DLPFC) had been predominantly utilized in most studies, although some (Zuo and Zhang, 2013; Duan and Ding, 2016) had opted for bilateral frontal lobe, temporal lobe, and occipital lobe as stimulation sites. However, the selection of DLPFC location for rTMS also varied depending on the stroke site of patients. Certain studies (Park and Yoon, 2015; Hu et al., 2016; Chen et al., 2017; He and Zhou, 2017; Zhou et al., 2017; Ding et al., 2019; Li et al., 2020a; Gao et al., 2021; Li et al., 2021; Ma et al., 2021; Wang et al., 2021b; Zhang et al., 2021; Wu et al., 2022; Yingli et al., 2022; Li et al., 2023) had employed the affected side DLPFC as the high-frequency stimulation area while designating the healthy side DLPFC as the low-frequency stimulation area. Furthermore, certain studies (Kim et al., 2010; Gu et al., 2012; Jiang et al., 2014; Li et al., 2015a,b; Tang et al., 2015; Liao et al., 2017; Ren et al., 2018; Yin et al., 2018; Chen et al., 2019; Yu and Zhang, 2019; Zhang and Zhou, 2019; Li et al., 2020c; Liu et al., 2020; Lv et al., 2020; Tsai et al., 2020; Zhang et al., 2020; Zheng et al., 2020; Qi et al., 2021; Li et al., 2022; Mao et al., 2022; Pei et al., 2022; Zhang et al., 2022; You et al., 2023) solely targeted one side of DLPFC without considering patient-specific stroke locations.

3.4.4 Stimulation pulse count

The parameter of pulse count is crucial in rTMS research. Specifically, the range of pulse counts includes 450, 600, 700, 900, 1,000, 1,200, 1,500, 1,600, 2000, 3,000, and even up to a maximum of 6,000 pulses. Notably, Clinical trial evidence consistently demonstrates the efficacy of rTMS in enhancing cognitive function among patients with PSCI.

3.4.5 Duration of each treatment session

Each session lasted between 10 and 30 min, with the most prevalent treatment duration being 20 min. Kim et al. (2010) employed a 20-min treatment duration for low-frequency stimulation at 1 Hz and extended it to a 30-min duration for high-frequency stimulation at 10 Hz. In all instances, the outcomes exhibited significant positive effects.

3.4.6 Duration and frequency of treatment

The duration of treatment also exhibits variations, ranging from a minimum of 10 days to a maximum of 8 weeks. Most rTMS interventions typically span over 4 weeks. However, certain studies opt for intervention periods of either two or 3 weeks. Both high-frequency and low-frequency rTMS protocols commonly employ 2 weeks. Furthermore, the frequency of interventions varies between three times per week and up to six times per week, with the most prevalent being an intervention schedule consisting of five sessions per week.

3.5 iTBS application parameters

Three RCTs (Tsai et al., 2020; Li et al., 2022; Pei et al., 2022) were conducted to investigate the efficacy of intermittent theta burst stimulation (iTBS) in treating patients with PSCI. The left DLPFC was consistently chosen as the targeted stimulation site across all three studies. In two studies (Tsai et al., 2020; Pei et al., 2022), a stimulation intensity of 80% RMT was utilized, while Li et al. (2022) did not specify the exact stimulation intensity employed. The standardized stimulation pattern consisted of three consecutive pulses at 50 Hz, repeated at a frequency of 5 Hz (2 s on, 8 s off). Both Li et al. (2022) and Tsai et al. (2020) adopted a total pulse count of 600 over 192 s, whereas Pei et al. (2022) opted for a longer protocol with 1,200 pulses lasting for approximately 383.68 s. Regarding the frequency of intervention sessions, all three studies implemented once-daily sessions for 5 days per week. Li et al. (2022) and Tsai et al. (2020) conducted the treatment for 2 weeks, while Pei et al. (2022) administered a four-week course. Positive therapeutic effects were observed across all included studies.

FIGURE 3
Risk of bias summary.

3.6 rTMS combined with other treatments

Most studies had combined rTMS with various physical therapy techniques, encompassing neurodevelopmental therapy, motor relearning programs, activities of daily living training, guessing games, visual tracking, picture memory, recall picture sequence, short passage recitation, building blocks, chess playing, puzzles, number identification, looking for differences, maze games, making handicrafts. Additionally, interventions such as acupuncture, hyperbaric oxygen therapy, action observation therapy (AOT), Forbrain speech and auditory feedback training, computer-assisted cognitive rehabilitation (CACR), as well as conventional drug therapies including platelet inhibitors, lipid-lowering agents antihypertensive drugs hypoglycemic drugs, cholinesterase inhibitors, N-methyl-d-aspartic acid receptor antagonists, free radical scavengers, microcirculation promoters had been included in the studies. Positive effects were observed in both intervention groups and control groups with even better results achieved through combined use.

It was noteworthy that certain studies employed a combination of CACR and rTMS. CACR referred to a computer-based cognitive training program encompassing exercises and games, utilizing multimedia, informatics resources, as well as specific hardware and software systems to implement comprehensive cognitive training in memory, attention, problem-solving, job simulation, language proficiency, practice repetition, and processing speed. The combined treatment group exhibited significant improvements in patients' cognitive function (Lu et al., 2015; Park and Yoon, 2015; Yin et al., 2018; Zhang and Zhou, 2019; Zheng et al., 2020; Pei et al., 2022). Additionally, Park and Yoon (2015) observed that compared to 10 Hz rTMS treatment alone, CACR demonstrated more pronounced enhancements in Lowenstein Occupational Therapy Cognitive Assessment-Geriatric (LOTCA-G).

3.7 Safety

We conducted a safety analysis of the included RCTs. Adverse events were reported in 20 RCTs (Gu et al., 2012; Jiang et al., 2014; Li et al., 2015a,b; Tang et al., 2015; Hu et al., 2016; Chen et al., 2017; Liao et al., 2017; Yin et al., 2018; Chen et al., 2019; Ding et al., 2019; Li et al., 2020a; Lv et al., 2020; Tsai et al., 2020; Zhang et al., 2020; Zheng et al., 2020; Li et al., 2021; Wang et al., 2021b; Li et al., 2022; Yingli et al., 2022), while no adverse events were reported in 10 studies (Gu et al., 2012; Li et al., 2015b; Tang et al., 2015; Chen et al., 2017; Liao et al., 2017; Chen et al., 2019; Ding et al., 2019; Li et al., 2021; Wang et al., 2021b; Yingli et al., 2022). Conversely, adverse events following rTMS treatment encompassed headache (Jiang et al., 2014; Li et al., 2015a; Hu et al., 2016; Yin et al., 2018; Li et al., 2020a; Tsai et al., 2020; Li et al., 2022), dizziness (Li et al., 2015a; Hu et al., 2016; Lv et al., 2020; Tsai et al., 2020; Zhang et al., 2020), nausea and vomiting (Li et al., 2020a, 2022), sleep disturbances (Zheng et al., 2020), and poor concentration (Zheng et al., 2020). After rest, patients experienced relief from their symptoms. No studies had reported the occurrence of epilepsy, cerebral hemorrhage, or secondary cerebral infarction resulting from rTMS. Li et al. (2015a) observed no alterations in blood analysis results, urine analysis results, fecal analysis results, liver function, renal function, blood lipid spectrum, myocardial enzyme

TABLE 2 Repetitive transcranial magnetic stimulation intervention parameters.

Authors	Intensity	Frequency	Stimulus area	Total pulses	Time of each treatment	Number of sessions (Frequency)	Course of treatment
Chen (2017)	90%～120% RMT	0.5～1.0 Hz (Healthy side)/5～10 Hz (Diseased side)	DLPFC (Diseased/ Healthy side)	900-1200 (Healthy side)/600-800 (Diseased side)	NA	20 (5 days/weeks)	4 weeks
Chen (2019)	80% RMT	10 Hz	DLPFC (Left side)	NA	20 min	20 (5 days/weeks)	4 weeks
Ding (2019)	110% RMT	Group 1:5 Hz; Group 2:1 Hz; Group 3:5 Hz/1 Hz	Group 1:DLPFC (Diseased side); Group 2:DLPFC (Healthy side); Group 3:DLPFC (Diseased/Healthy side)	NA	20 min	12 (6 days/weeks)	2 weeks
Duan (2016)	80% RMT	3 Hz	Bilateral frontal, temporal and occipital lobes	600	NA	NA	2 weeks
Gao (2021)	120% RMT	10 Hz	DLPFC (Diseased side)	NA	20 min	24 (6 days/weeks)	4 weeks
Gu (2012)	110% RMT	5 Hz	DLPFC (Left side)	6,000	NA	10 consecutive days	10 days
Li (2020)	70% RMT	1 Hz	NA	600	20 min	20 (5 days/weeks)	4 weeks
He (2017)	80～120% RMT	10 Hz	DLPFC (Diseased side)	NA	20 min	20 (5 days/weeks)	4 weeks
Jiang (2014)	120% RMT	10 Hz	DLPFC (Left side)	3,000	NA	25 (5 days/weeks)	5 weeks
Li (2023)	80% RMT	Group 1:1 Hz; Group 2:10 Hz; Group 3:10 Hz/1 Hz	Group 1:DLPFC (Healthy side); Group 2:DLPFC (Diseased side); Group 3:DLPFC (Diseased/Healthy side)	NA	20 min	10 (5 days/weeks)	2 weeks
Li (2022)	80% RMT	10 Hz	NA	NA	20 min	20 (5 days/weeks)	4 weeks
Li (2020)	100% RMT	0.5 Hz	DLPFC (Diseased side)	NA	20 min	20 (5 days/weeks)	4 weeks
Li (2015)	80% RMT	5 Hz	DLPFC (Left side)	6,000	20 min	20 (5 days/weeks)	4 weeks
Ren (2018)	80% RMT	3 Hz	DLPFC (Left side)	6,000	20 min	20 (5 days/weeks)	4 weeks
Li (2015)	80% RMT	5 Hz	DLPFC (Left side)	NA	20 min	20 (5 days/weeks)	4 weeks
Liao (2017)	80% RMT	Group 1:0.5 Hz; Group 2:3 Hz	DLPFC (Left side)	NA	20 min	20 (5 days/weeks)	4 weeks
Lv (2020)	80% RMT	10 Hz	DLPFC (Left side)	NA	20 min	20 (5 days/weeks)	4 weeks
Wu (2022)	80% RMT	1 Hz/5 Hz	DLPFC (Healthy side)	NA	20 min (1 Hz)/10 min (5 Hz)	20 (5 days/weeks)	4 weeks
Ma (2021)	90% RMT	1 Hz	DLPFC (Healthy side)	1,000	20 min	20 (5 days/weeks)	4 weeks

(Continued)

10.3389/fnins.2024.1309736

TABLE 2 (Continued)

Authors	Intensity	Frequency	Stimulus area	Total pulses	Time of each treatment	Number of sessions (Frequency)	Course of treatment
Mao (2022)	80% RMT	Group 1:10 Hz; Group 2:1 Hz	Group 1:DLPFC (Left side); Group 2:DLPFC (Right side)	Group 1:2000;Group 2:1600	20 min	18 (6 days/weeks)	3 weeks
Pei (2022)	80% RMT	3 pulses of 50 Hz in 1 group, each group stimulated repeatedly at 5 Hz (2 s on, 8 s off)	DLPFC (Left side)	1,200	383.68 s	20 (5 days/weeks)	4 weeks
Tang (2015)	110% RMT	5 Hz	DLPFC (Left side)	600	NA	24 (5 days/weeks)	4 weeks
Xu (2022)	80% RMT	20 Hz	DLPFC (bilateral)	NA	30 min	40 (5 days/weeks)	8 weeks
Yin (2018)	80% RMT	10 Hz	DLPFC (Left side)	2000	20 min	20 (5 days/weeks)	4 weeks
You (2023)	NA	10 Hz	DLPFC (Left side)	NA	20 min	40 (5 days/weeks)	8 weeks
Yu (2019)	80% RMT	10 Hz	DLPFC (Left side)	NA	20 min	40 (5 days/weeks)	8 weeks
Zhang (2019)	80% RMT	5 Hz	DLPFC (Left side)	1,600	20 min	20 (5 days/weeks)	4 weeks
Zhang (2022)	80% RMT	5 Hz	DLPFC (Left side)	3,000	20 min	20 (5 days/weeks)	4 weeks
Zhang (2020)	Group 1/2:90% MT; Group 3/4:100% MT	Group 1:0.5 Hz; Group 2:1 Hz; Group 3:5 Hz; Group 4:10 Hz	Group 1/2:DLPFC (Right side); Group 3/4:DLPFC (Right side)	Group 1/2:600; Group 3/4:6000	20 min	20 (5 days/weeks)	4 weeks
Zhang (2021)	90% RMT	1 Hz	DLPFC (Healthy side)	1,000	20 min	20 (5 days/weeks)	4 weeks
Zhou (2017)	80% RMT	1 Hz	DLPFC (Healthy side)	NA	20 min	40 (5 days/weeks)	8 weeks
Zheng (2020)	80% RMT	10 Hz	DLPFC (Left side)	NA	20 min	20 (5 days/weeks)	4 weeks
Zuo (2013)	80% RMT	5 Hz	Bilateral frontal, temporal and occipital lobes	600	NA	20 (5 days/weeks)	4 weeks
Bi (2022)	80% RMT	1 Hz	DLPFC (Healthy side)	600	NA	40 (5 days/weeks)	8 weeks
Kim (2010)	80% RMT	Group 1:10 Hz; Group 2:1 Hz	DLPFC (Left side)	Group 1:450; Group 2:900	Group 1:30 min; Group 2:20 min	10 (5 days/weeks)	2 weeks
Li (2021)	90% RMT	1 Hz	DLPFC (Healthy side)	1,000	20 min	20 (5 days/weeks)	4 weeks
Li (2022)	NA	3 pulses of 50 Hz in 1 group, each group stimulated repeatedly at 5 Hz (2 s on, 8 s off)	DLPFC (Left side)	600	192 s	10 (5 days/weeks)	2 weeks
Lu (2015)	100% RMT	1 Hz	DLPFC (Right side)	600	NA	20 (5 days/weeks)	4 weeks

(Continued)

10.3389/fnins.2024.1309736

TABLE 2 (Continued)

Authors	Intensity	Frequency	Stimulus area	Total pulses	Time of each treatment	Number of sessions (Frequency)	Course of treatment
Tsai (2020)	80% RMT	Group 1:3 pulses of 50 Hz in 1 group, each group stimulated repeatedly at 5 Hz (2 s on, 8 s off); Group 2:5 Hz	DLPFC (Left side)	Group 1:600; Group 2:600	Group 1:190 s; Group 2:10 min	10 (5 days/weeks)	2 weeks
Li (2020)	100% RMT	5 Hz	DLPFC (Left side)	2000	NA	15 (5 days/weeks)	3 weeks
Park (2015)	100% RMT	10 Hz	DLPFC (Healthy side)	1,000	20 min	12 (3 days/weeks)	4 weeks
Liu (2020)	90% RMT	10 Hz	DLPFC (Left side)	700	NA	20 (5 days/weeks)	4 weeks
Wang (2021)	80% RMT	Group 1:10 Hz; Group 2:1 Hz	Group 1:DLPFC (Diseased side); Group 2:DLPFC (Healthy side)	NA	20 min	40 (5 days/weeks)	8 weeks
Qi (2021)	80% RMT	3 Hz	DLPFC (Left side)	6,000	20 min	12 (3 days/weeks)	4 weeks
Hu (2016)	100% RMT	10 Hz	DLPFC (Diseased side)	3,000	NA	20 (5 days/weeks)	4 weeks

RMT, resting motor potential threshold; DLPFC, dorsolateral prefrontal cortex; min, minute; s, second.

levels, electrocardiogram readings, or other tests before and after treatment.

3.8 Publication bias

We employed a funnel plot analysis to assess the presence of publication bias in MOCA, MMSE, AERP P3000 latency, and AERP P3000 amplitude. The findings revealed that the distribution of MOCA and AERP P3000 latency exhibited relative symmetry, suggesting a potential absence of publication bias. Conversely, the distribution of MMSE and AERP P3000 amplitude displayed noticeable asymmetry, indicating the presence of publication bias, as shown in Supplementary file.

4 Discussion

After conducting a comprehensive analysis of the included RCTs, we have observed that rTMS exhibits significant efficacy in enhancing cognitive function and improving the quality of life among patients with PSCI. The clinical effects of rTMS vary depending on different treatment parameters. Notably, combining rTMS with pharmacotherapy or cognitive rehabilitation training has demonstrated superior therapeutic effects.

There were variations in the selection of rTMS frequencies across different RCTs. In clinical practice, LF-rTMS commonly employs parameters of 0.5 Hz and 1 Hz, while HF-rTMS includes frequencies of 3 Hz, 5 Hz, 10 Hz, and 20 Hz. rTMS at different frequencies can modulate the excitability of the stimulated site or cerebral cortex by either inhibiting or facilitating neuronal activity. For instance, LF-rTMS (≤1 Hz) can suppress local neuronal activity and reduce cerebral cortex excitability. Conversely, HF-rTMS (>1 Hz) can enhance local neuronal function and increase cerebral cortex excitability (Lefaucheur et al., 2020). LF-rTMS can modulate the plasticity of hippocampal neuronal synapses through the BDNF–TrkB pathway, thereby enhancing learning and memory abilities (Ma et al., 2013). Additionally, it can reduce triiodothyronine levels to decrease oxygen consumption and metabolic rate in the body, facilitating the repair of injured sites (Alevizaki et al., 2007). Studies (Devanand et al., 2010) have revealed that cognitive dysfunction after stroke is primarily caused by decreased blood flow in the lesion itself and brain tissues such as the "ischemic penumbra." However, high-frequency rTMS has been shown to increase average blood flow in the middle cerebral artery (Ogiue-Ikeda et al., 2005; Duering et al., 2011), improve brain cell glucose metabolism, mitigate secondary cerebral ischemia damage, and enhance cognitive function (Kozel et al., 2011). Furthermore, high-frequency rTMS can improve tolerance of functional damage caused by ischemia in hippocampal and other nerve tissues. It promotes the survival of hippocampal neurons while inhibiting cell apoptosis. Moreover, it regulates excitability in both local and remote cerebral cortexes to achieve cortical functional area reconstruction. This process also facilitates the growth and repair of white matter in brain-injured areas (Kozel et al., 2011; Zhao et al., 2012). It is important to emphasize that in the comparison of the efficacy of HF-rTMS and LF-rTMS on cognitive function, most RCTs (Kim et al., 2010; Liao et al., 2017; Ding et al., 2019; Zhang et al., 2020; Wang et al., 2021b; Li et al., 2023) did not demonstrate significant

differences between the two interventions. This finding aligns with previous meta-analyses (Gong et al., 2023; Yin et al., 2023). Conversely, combining HF-rTMS and LF-rTMS has shown more favorable outcomes (Chen et al., 2017; Ding et al., 2019; Li et al., 2023). Furthermore, studies (Boggio et al., 2010; Kim et al., 2010) have indicated that HF-rTMS yields superior effects on psychological emotions compared to LF-rTMS.

The efficacy of rTMS is also influenced by the choice of stimulation site, with the DLPFC being commonly selected in most RCTs. Several studies (Sun et al., 2012; Van den Boom et al., 2018) have suggested that cognitive brain regions are predominantly situated within the bilateral DLPFC, which serves as a crucial hub in the brain network and exhibits close associations with cognitive functions such as memory, reasoning, and attention. Based on the dominant hemisphere theory (there is a structural and functional asymmetry between the right and left hemispheres of the brain, the left hemisphere of a right-handed person is mostly the dominant hemisphere, which is mainly responsible for speech, computation, writing, and logical reasoning.) and the human brain connectivity group theory (the brain is made up of multiple neurons, neuron clusters, or multiple brain regions that are connected to form a heterogeneous network structure, which accomplishes a wide range of brain functions through interactions) (Zheng et al., 2020). Since the RCTs chose to include right-handed patients for observation, the left DLPFC was mainly chosen as the stimulation site in the clinic. In addition, some studies have chosen the affected side of DLPEF as the HF-rTMS target area, while selecting the healthy side of DLPEF as the LF-rTMS target area. This selection may be attributed to the fact that under normal circumstances, there exists a balanced state of mutual inhibition between the left and right cerebral hemispheres in humans. However, brain damage disrupts this balance between hemispheres. Following a stroke, reduced inhibition from the damaged hemisphere on the unaffected hemisphere is likely to result in increased excitability of the unaffected hemisphere and heightened inhibition of the damaged hemisphere (Seniów et al., 2013). Consequently, clinical researchers aim to enhance cortical excitability by applying HF-rTMS to stimulate the affected side of DLPEF and reduce cortical excitability by employing LF-rTMS on the healthy side of DLPEF. This approach helps facilitate neural circuitry reorganization and normalize activation patterns across both hemispheres. It is plausible that this combined LF-rTMS and HF-rTMS strategy contributes to achieving superior outcomes.

Stimulus intensity exhibited variability, ranging from 70% RMT to 120% RMT, with the majority of RCTs opting for 80% RMT. Positive outcomes were observed across all stimulus intensities in rTMS. Furthermore, varying numbers of pulse stimulations also demonstrated improvements in cognitive function among patients, despite Kim et al. (2010) employing only 450 pulses. This observation may be attributed to both the stimulation intensity and number of pulse stimulations surpassing the threshold required for modulating cerebral cortex excitability and brain networks. It was found that patients with PSCI who underwent rTMS treatment at a frequency of 5 Hz and intensity set at 100% RMT exhibited significantly increased fractional amplitude of low-frequency fluctuation in specific brain regions, including the superior temporal gyrus, inferior frontal gyrus, and parahippocampal gyrus. Furthermore, there was an observed enhancement in functional connectivity between the LDPFC and precuneus, middle frontal gyrus, inferior frontal gyrus, inferior temporal gyrus, as well as limbic gyrus (Li et al., 2020c). Another study conducted rTMS treatment on 86 PSCI patients using a frequency of 5 Hz and intensity set at 80% RMT. Compared to pre-treatment values, significant decreases were found in the regional homogeneity values of the left superior frontal gyrus, right lobe, right superior marginal gyrus, left middle frontal gyrus, right inferior frontal gyrus, and other regions. Conversely, significant increases were observed in the regional homogeneity values of the left middle temporal gyrus, right inferior temporal gyrus, left superior temporal gyrus, right cerebellar hemisphere, and other regions. Additionally, a decrease in amplitude of low-frequency fluctuation (ALFF) was noted in the right anterior central gyrus while an increase was seen in ALFF within the right cerebellar Crus2 region and left inferior parietal angular gyri region (Li et al., 2023). The aforementioned findings demonstrate that rTMS can modulate neural excitability within specific cerebral regions while enhancing similarity and functional connectivity across distinct brain areas to facilitate recovery of cognitive function. However, it is important to note that high-intensity stimulation or excessive pulsed stimulation may elevate the risk for epilepsy development. Moreover, a higher incidence of dizziness and headache adverse events had been observed in RCTs encompassing a substantial number of pulses (Jiang et al., 2014; Li et al., 2015a; Hu et al., 2016; Yin et al., 2018; Zhang et al., 2020).

During each treatment session, the duration ranged from 20 to 30 min. However, it is important to note that longer treatment durations did not yield more satisfactory outcomes. In most cases of single-frequency rTMS interventions, a total intervention duration of 4 weeks was commonly employed, with a minimum duration of 10 days and a maximum duration of 8 weeks. Conversely, combination treatments involving HF-rTMS and LF-rTMS opted for either two or 4 weeks as the overall intervention period.

There were variations in the frequency of interventions, ranging from three to seven treatments per week (with only one treatment administered per day), with the majority of studies opting for five treatments per week. The rTMS stimulation has a cumulative effect, resulting in persistent biological effects even after the end of stimulation. Furthermore, each rTMS stimulus can be stored as a "memory" in the stimulated area, leading to new effects when subsequent stimuli are applied (Valero-Cabre et al., 2008). Repetitive stimulation activates subcortical neural network structures and modifies synaptic plasticity, thereby enhancing cognitive function (Rossi et al., 2009; Selimbeyoglu and Parvizi, 2010). However, there may exist an upper threshold for this cumulative effect. Prolonged and high-intensity application of high-frequency stimulation fails to yield superior outcomes and may even result in adverse consequences such as epilepsy, syncope, headache, cognitive or neuropsychological changes, and acute mental alterations (Rossi et al., 2009; Levkovitz et al., 2015).

iTBS represents an optimized form of rTMS, characterized by the advantages of employing low stimulus intensity, short stimulus cycles, and long-term benefits (Nowak et al., 2010). It exerts its effects on regulating neuroplasticity and excitability in the brain by reducing inhibitory control mechanisms and inducing neurotransmitter release (Hoy et al., 2016; Trung et al., 2019; Gebreegziabhere et al., 2022).

Although studies (Tsai et al., 2020; Li et al., 2022; Pei et al., 2022) have demonstrated the efficacy of iTBS in improving cognitive function and enhancing daily activities in patients with PSCI, further exploration is required to establish whether iTBS surpasses traditional rTMS, given the limited clinical evidence available from evidence-based medicine. Notably, Tsai et al. (2020) findings not only failed to identify any differences in efficacy between iTBS and 5 Hz rTMS but also indicated superior attention regulation effects within the 5 Hz rTMS group.

4.1 Strengths and limitations

It is worth emphasizing that this study included a total of 45 RCTs. We conducted an in-depth analysis of the variability in rTMS efficacy across different parameters and further explored its potential mechanisms of action. These findings provide evidence-based medical support for the clinical utilization of rTMS. Naturally, this study does have certain limitations. Firstly, the sample size of some included RCTs was relatively small, potentially impacting the reliability of the findings. Additionally, given that a majority of the studies originate from China, there may be a regional bias present. Secondly, as the clinical efficacy stems from multiple parameters working in conjunction with each other, it is worth noting that this study solely focuses on analyzing the impact of individual parameters within RCTs and lacks an assessment of their combined effects. This limitation also affects the applicability of the results. Thirdly, due to not aggregating data from RCTs, it becomes impossible to ascertain an overall effect size for relevant parameters or determine heterogeneity between studies, which, to a certain extent, may affect the reliability of the results. The assessment of bias risk in the included RCTs revealed deficiencies in the blinding procedure, potentially contributing to placebo effects and observer bias, thereby compromising the validity of conclusions.

4.2 Outlook

Currently, the majority of RCTs on rTMS parameters primarily focus on comparing single parameters at different levels, which lacks a comprehensive experimental design incorporating multiple parameters and levels. Consequently, there is limited research investigating the overall efficacy of multi-parameter rTMS. In future investigations, it is crucial to employ an orthogonal experimental design method encompassing multiple parameters and levels, which can identify treatment parameter combinations that align more closely with clinical practice and provide a scientific basis for guiding clinical interventions. Furthermore, we urge researchers to prioritize blinding methodologies in their RCTs as this will enhance the credibility of research conclusions and offer valuable evidence for clinical guidance.

5 Conclusion

rTMS demonstrates efficacy and safety in enhancing cognitive function, quality of life, and activities of daily living among patients with post-stroke cognitive dysfunction. Furthermore, the combination of rTMS with other conventional rehabilitation methods can provide a more positive impact. However, the majority of included rTMS studies focus on single-parameter comparative analyses at varying levels, limiting our ability to determine optimal therapeutic parameters protocol for rTMS. Future research should prioritize orthogonal experimental design methods encompassing multiple parameters and levels to provide more evidence-based medical evidence into the optimal parameter combination for the clinical application of rTMS.

Data availability statement

Original contributions from the study are included in the article and further inquiries can be directed to the corresponding author.

Author contributions

YW: Writing – original draft, Writing – review & editing. LW: Writing – original draft. XN: Writing – original draft. MJ: Writing – original draft. LZ: Writing – review & editing.

Funding

The author(s) declare financial support was received for the research, authorship, and/or publication of this article. This study was supported by the Young Qihuang Scholar of the "Tens of millions" talent project of the people republic of China, the Chengdu University of Traditional Chinese Medicine "Xinglin Scholars" Discipline Talent Research Promotion Plan - Postdoctoral Program (no. BSH2023018), the China Administration of Traditional Chinese Medicine TCM Innovation Team and Talent Support Program (ZYYCXTD-D-202003), the Key Project of Natural Science Foundation of Sichuan Province (24NSFSC0097) and the Open Project of National Clinical Research Center of Acupuncture and Moxibustion (NCRCOP2023001).

Conflict of interest

The authors declare that the research was conducted in the absence of any commercial or financial relationships that could be construed as a potential conflict of interest.

Publisher's note

Supplementary material

The Supplementary material for this article can be found online at: https://www.frontiersin.org/articles/10.3389/fnins.2024.1309736/full#supplementary-material

References

Alevizaki, M., Synetou, M., Xynos, K., Pappa, T., and Vemmos, K. N. (2007). Low triiodothyronine: a strong predictor of outcome in acute stroke patients. *Eur. J. Clin. Investig.* 37, 651–657. doi: 10.1111/j.1365-2362.2007.01839.x

Boggio, P. S., Rocha, M., Oliveira, M. O., Fecteau, S., Cohen, R. B., Campanhã, C., et al. (2010). Noninvasive brain stimulation with high-frequency and low-intensity repetitive transcranial magnetic stimulation treatment for posttraumatic stress disorder. *J. Clin. Psychiatry* 71, 992–999. doi: 10.4088/JCP.08m04638blu

Chen, H. J., Cong, S., Cheng, G. Q., Dong, B., and Tang, M. (2017). The efficacy of transcranial magnetic stimulation in treating patients with post-stroke cognitive dysfunction. *Chin. J. Phys. Med. Rehab.* 39, 677–679. doi: 10.3760/cma.j.issn.0254-1424.2017.09.010

Chen, Z. Y., Gong, J. Q., Wu, Y. F., Ping, R. X., Sun, Y. T., Ni, X. X., et al. (2019). The efficacy of repetitive transcranial magnetic stimulation combined with cognitive rehabilitation training in the treatment of post-stroke cognitive impairment. *Chin. J. Phys. Med. Rehab.* 41, 199–201. doi: 10.3760/cma.j.issn.0254-1424.2019.03.008

Cumpston, M., Li, T., Page, M. J., Chandler, J., Welch, V. A., Higgins, J. P. T., et al. (2019). Updated guidance for trusted systematic reviews: a new edition of the Cochrane handbook for systematic reviews of interventions. *Cochrane Libr* 10:142. doi: 10.1002/14651858.ed000142

Devanand, D. P., van Heertum, R., Kegeles, L. S., Liu, X., Jin, Z. H., Pradhaban, G., et al. (2010). (99m) Tc hexamethyl-propylene-aminoxime single-photon emission computed tomography prediction of conversion from mild cognitive impairment to Alzheimer disease. *Am. J. Geriatric Psychiatr.* 18, 959–972. doi: 10.1097/JGP.0b013e3181ec8696

Ding, Q. F., Li, Z., Guo, G. H., Guan, C. X., Le, L., Hao, D. J., et al. (2019). Effects of repetitive transcranial magnetic stimulation with different frequencies on cognitive impairment in stroke patients. *Chin. J. Rehab.* 34, 513–517. doi: 10.3870/zgkf.2019.010.002

Douiri, A., Rudd, A. G., and Wolfe, C. D. A. (2013). Prevalence of poststroke cognitive impairment: South London stroke register 1995–2010. *Stroke* 44, 138–145. doi: 10.1161/STROKEAHA.112.670844

Duan, L., and Ding, S. Y. (2016). Effect of TMS on plasma CRP and fib levels in patients with vascular cognitive dysfunction after cerebral infarction. *Chin. Pract. Med.* 11, 41–42. doi: 10.14163/j.cnki.11-5547/r.2016.11.025

Duering, M., Zieren, N., Hervé, D., Jouvent, E., Reyes, S., Peters, N., et al. (2011). Strategic role of frontal white matter tracts in vascular cognitive impairment: a voxel-based lesion-symptom mapping study in CADASIL. *Brain* 134, 2366–2375. doi: 10.1093/brain/awr169

Farooq, M. U., Min, J., Goshgarian, C., and Gorelick, P. B. (2017). Pharmacotherapy for vascular cognitive impairment. *CNS Drugs* 31, 759–776. doi: 10.1007/s40263-017-0459-3

Gao, Y. R., Guan, C. X., Li, Z., Guo, G. H., Le, L., and Hao, D. J. (2021). Effects of high-frequency repetitive transcranial magnetic stimulation on orientation, visual perception and ADL of stroke patients with cognitive impairment and aphasia. *Chin. J. Rehab.* 36, 520–523. doi: 10.3870/zgkf.2021.09.002

Gebreegziabhere, Y., Habatmu, K., Mihretu, A., Cella, M., and Alem, A. (2022). Cognitive impairment in people with schizophrenia: an umbrella review. *Eur. Arch. Psychiatry Clin. Neurosci.* 272, 1139–1155. doi: 10.1007/s00406-022-01416-6

Gong, C., Hu, H., Peng, X. M., Li, H., Xiao, L., Liu, Z., et al. (2023). Therapeutic effects of repetitive transcranial magnetic stimulation on cognitive impairment in stroke patients: a systematic review and meta-analysis. *Front. Hum. Neurosci.* 17:1177594. doi: 10.3389/fnhum.2023.1177594

Gorelick, P. B., Scuteri, A., Black, S. E., Decarli, C., Greenberg, S. M., Iadecola, C., et al. (2011). Vascular contributions to cognitive impairment and dementia: a statement for healthcare professionals from the American Heart Association/American Stroke Association. *Stroke* 42, 2672–2713. doi: 10.1161/STR.0b013e3182299496

Gu, Z. T., Lu, J. X., Zhang, S. C., Xu, R. Z., and Xu, S. S. (2012). Efficacy of repetitive transcranial magnetic stimulation in patients with mild cognitive dysfunction after cerebral infarction. *Chin. J. Rehab. Med.* 27, 964–966. doi: 10.3969/j.issn.1001-1242.2012.10.021

He, Y. G., and Zhou, Q. (2017). Effects of repetitive transcranial magnetic stimulation on non-dementia-type vascular cognitive dysfunction. *Chin. J. Phys. Med. Rehab.* 39, 464–466. doi: 10.3760/cma.j.issn.0254-1424.2017.06.018

Hernandez-Pavon, J. C., and Harvey, R. L. (2019). Noninvasive transcranial magnetic brain stimulation in stroke. *Phys. Med. Rehab. Clin.* 30, 319–335. doi: 10.1016/j.pmr.2018.12.010

Hoy, K. E., Bailey, N., Michael, M., Fitzgibbon, B., Rogasch, N. C., Saeki, T., et al. (2016). Enhancement of working memory and task-related oscillatory activity following intermittent theta burst stimulation in healthy controls. *Cereb. Cortex* 26, 4563–4573. doi: 10.1093/cercor/bhv193

Hu, L. M., Zhu, Q. X., Liu, Y. X., Lin, Y. M., Tang, N. S., Su, W. H., et al. (2016). The therapeutic effects of supplementing rehabilitation with repetitive transcranial magnetic stimulation in treating vascular cognitive impairment but no dementia. *Chin. J. Phys. Med. Rehab.* 38, 278–282. doi: 10.3760/cma.j.issn.0254-1424.2016.04.009

Huang, Y. Y., Chen, S. D., Leng, X. Y., Kuo, K., Wang, Z. T., Cui, M., et al. (2022). Post-stroke cognitive impairment: epidemiology, risk factors, and management. *J. Alzheimers Dis.* 86, 983–999. doi: 10.3233/JAD-215644

Jiang, W., Tang, X. Y., and Yuan, L. J. (2014). The clinical study of transcranial magnetic stimulation(TMS) treatment for cerebral infarction patients with mild cognitive impairment. *Anhui Med. J.* 35, 189–191,192. doi: 10.3969/j.issn.1000-0399.2014.02.017

Kim, B. R., Kim, D. Y., Ho Chun, M., Hwa Yi, J., and Sung Kwon, J. (2010). Effect of repetitive transcranial magnetic stimulation on cognition and mood in stroke patients: a double-blind, sham-controlled trial. *Am. J. Phys. Med. Rehabil.* 89, 362–368. doi: 10.1097/PHM.0b013e3181d8a5b1

Kim, J. O., Lee, S. J., and Pyo, J. S. (2020). Effect of acetylcholinesterase inhibitors on post-stroke cognitive impairment and vascular dementia: a meta-analysis. *PLoS One* 15:e0227820. doi: 10.1371/journal.pone.0227820

Kozel, F. A., Johnson, K. A., Nahas, Z., Nakonezny, P. A., Morgan, P. S., Anderson, B. S., et al. (2011). Fractional anisotropy changes after several weeks of daily left high-frequency repetitive transcranial magnetic stimulation of the prefrontal cortex to treat major depression. *J. ECT* 27, 5–10. doi: 10.1097/YCT.0b013e3181e6317d

Lefaucheur, J. P., Aleman, A., Baeken, C., Benninger, D. H., Brunelin, J., di Lazzaro, V., et al. (2020). Evidence-based guidelines on the therapeutic use of repetitive transcranial magnetic stimulation (rTMS): an update (2014–2018). *Clin. Neurophysiol.* 131, 474–528. doi: 10.1016/j.clinph.2019.11.002

Levkovitz, Y., Isserles, M., Padberg, F., Lisanby, S. H., Bystritsky, A., Xia, G., et al. (2015). Efficacy and safety of deep transcranial magnetic stimulation for major depression: a prospective multicenter randomized controlled trial. *World Psychiatry* 14, 64–73. doi: 10.1002/wps.20199

Li, H. N., Chen, Y. D., Huang, M., Zhong, J., Huang, S. F., Huang, M. L., et al. (2023). Effects of repetitive transcranial magnetic stimulation on cognitive function, central motor conduction time and balance ability in patients with post-stroke cognitive dysfunction. *Chin. J. Rehab.* 38, 140–143. doi: 10.3870/zgkf.2023.03.003

Li, J., Cui, L. H., and Ji, Y. T. (2020a). Effect of repetitive transcranial magnetic stimulation technique combined with donepezil in treating cognitive impairment after cerebral infarction. *J. Clin. Med. Pract.* 24, 39–42. doi: 10.7619/jcmp.202021012

Li, J., Cui, Y., and Jia, M. Y. (2022). Effect of repetitive transcranial magnetic stimulation in the treatment of cognitive dysfunction after ischemic stroke. *Chin. Med. Herald.* 19, 80–83. doi: 10.20047/j.issn1673-7210.2022.32.18

Li, J., Dong, J. H., and Zhang, K. (2023). Therapeutic effect of rTMS on post-stroke cognitive dysfunction: an analysis using functional MRI. *Chin. J. Med. Phys.* 40, 872–875.

Li, Q., Liu, L. S., Huo, J. J., and He, M. (2020b). The effect of transskull magnetic stimulation combined with speech auditory feedback training on cognitive function in patients with cerebral apoplexy. *Chin. J. Clini. Healthcare.* 23, 660–664. doi: 10.3969/J.issn.1672-6790.2020.05.020

Li, Y., Luo, H., Yu, Q., Yin, L., Li, K., Li, Y., et al. (2020c). Cerebral functional manipulation of repetitive transcranial magnetic stimulation in cognitive impairment patients after stroke: an fMRI study. *Front. Neurol.* 11:977. doi: 10.3389/fneur.2020.00977

Li, H., Ma, J., Zhang, J., Shi, W. Y., Mei, H. N., and Xing, Y. (2021). Repetitive transcranial magnetic stimulation (rTMS) modulates thyroid hormones level and cognition in the recovery stage of stroke patients with cognitive dysfunction. *Med. Sci. Monit.* 27, e931914–e931911. doi: 10.12659/MSM.931914

Li, W., Wen, Q., Xie, Y. H., Hu, A. L., Wu, Q., and Wang, Y. X. (2022). Improvement of poststroke cognitive impairment by intermittent theta bursts: A double-blind randomized controlled trial. *Brain Behav.* 12:e2569. doi: 10.1002/brb3.2569

Li, Y. M., Xu, L., Yang, Y., Tian, J. Y., and Yu, Q. (2015a). Effects of repetitive transcranial magnetic stimulation on cognitive ability in patients with mild cognitive impairment after ischemic stroke. *Chin. J. Rehab. Theory Pract.* 21, 1128–1132. doi: 10.3969/j.issn.1006-9771.2015.10.003

Li, Y. M., Xu, L., Yang, Y., Tian, J. Y., and Yu, Q. (2015b). The effects of repetitive transcranial magnetic stimulation on the cognitive ability in patients with mild cognitive impairment after ischemic stroke. *Chin. J. Phys. Med. Rehab.* 37, 739–742. doi: 10.3760/cma.j.issn.0254-1424.2015.010.004

Liao, L. H., Huang, D., Jiang, X. M., Deng, X. Q., and Zhou, B. F. (2017). Effects of high-frequency and low-frequency repetitive transcranial magnetic stimulation on cognitive function in patients with cerebral infarction. *Chin. J. Phys. Med. Rehab.* 39, 56–58. doi: 10.3760/cma.j.issn.0254-1424.2017.01.014

Liu, Y., Yin, M., Luo, J., Huang, L., Zhang, S., Pan, C., et al. (2020). Effects of transcranial magnetic stimulation on the performance of the activities of daily living and attention function after stroke: a randomized controlled trial. *Clin. Rehabil.* 34, 1465–1473. doi: 10.1177/0269215520946386

Lo, J. W., Crawford, J. D., Desmond, D. W., Godefroy, O., Jokinen, H., Mahinrad, S., et al. (2019). Profile of and risk factors for poststroke cognitive impairment in diverse ethnoregional groups. *Neurology* 93, e2257–e2271. doi: 10.1212/WNL.0000000000008612

Loetscher, T., Potter, K. J., Wong, D., and das Nair, R.Cochrane Stroke Group (2019). Cognitive rehabilitation for attention deficits following stroke. *Cochrane Database Syst. Rev.* 2019:11. doi: 10.1002/14651858.CD002842.pub3

Lu, H., Zhang, T., Wen, M., and Sun, L. (2015). Impact of repetitive transcranial magnetic stimulation on post-stroke dysmnesia and the role of BDNF Val66Met SNP. *Med. Sci. Monit.* 21, 761–768. doi: 10.12659/MSM.892337

Lv, M. X., Liu, S. J., Wang, Y. Q., Liang, J. J., and Li, T. T. (2020). Effects of 10 Hz high-frequency repetitive transcranial magnetic stimulation combined with hyperbaric oxygen on cognitive dysfunction and cerebral metabolism after stroke. *Chin. J. Microcircul.* 30, 26–31. doi: 10.3969/j.issn.1005-1740.2020.04.006

Ma, J., Li, H., Zhang, J., Zhao, Q. Q., and Shi, W. Y. (2021). Effects of low-frequency repetitive transcranial magnetic stimulation combined with cognitive training on thyroid hormone levels and cognitive function in patients with cognitive impairment after cerebral stroke. *Hebei Med. J.* 43, 2436–2441. doi: 10.3969/j.issn.1002-7386.2021.16.007

Ma, J., Zhang, Z., Su, Y., Kang, L., Geng, D., Wang, Y., et al. (2013). Magnetic stimulation modulates structural synaptic plasticity and regulates BDNF–TrkB signal pathway in cultured hippocampal neurons. *Neurochem. Int.* 62, 84–91. doi: 10.1016/j.neuint.2012.11.010

Mao, J., Hong, Y. F., Feng, X. J., Tang, X. X., Zhang, J. N., and Kan, X. L. (2022). Effect of repetitive transcranial magnetic stimulation of different frequencies on the cognition and movement of stroke patients. *Chin. J. Gen. Pract.* 20, 1036–1040. doi: 10.16766/j.cnki.issn.1674-4152.002518

Merriman, N. A., Sexton, E., McCabe, G., Walsh, M. E., Rohde, D., Gorman, A., et al. (2019). Addressing cognitive impairment following stroke: systematic review and meta-analysis of non-randomised controlled studies of psychological interventions. *BMJ Open* 9:e024429. doi: 10.1136/bmjopen-2018-024429

Naghavi, M., Abajobir, A. A., Abbafati, C., Abbas, K. M., Abd-Allah, F., Abera, S. F., et al. (2017). Global, regional, and national age-sex specific mortality for 264 causes of death, 1980–2016: a systematic analysis for the global burden of disease study 2016. *Lancet* 390, 1151–1210. doi: 10.1016/S0140-6736(17)32152-9

Nowak, D. A., Bösl, K., Podubeckà, J., and Carey, J. R. (2010). Noninvasive brain stimulation and motor recovery after stroke. *Restor. Neurol. Neurosci.* 28, 531–544. doi: 10.3233/RNN-2010-0552

Ogiue-Ikeda, M., Kawato, S., and Ueno, S. (2005). Acquisition of ischemic tolerance by repetitive transcranial magnetic stimulation in the rat hippocampus. *Brain Res.* 1037, 7–11. doi: 10.1016/j.brainres.2004.10.063

Park, I. S., and Yoon, J. G. (2015). The effect of computer-assisted cognitive rehabilitation and repetitive transcranial magnetic stimulation on cognitive function for stroke patients. *J. Phys. Ther. Sci.* 27, 773–776. doi: 10.1589/jpts.27.773

Pei, S., Wang, J., and Xia, J. Y. (2022). Effect of repetitive transcranial magnetic intermittent θ burst stimulation on post-stroke cognitive impairment. *Chongqing Med.* 51, 3120–3125. doi: 10.3969/j.issn.1671-8348.2022.18.012

Qi, F., Su, Y. L., and Zhang, H. (2021). Efficacy of hyperbaric oxygen combined with repetitive transcranial magnetic stimulation on patients with cognitive impairment after cerebral infarction and its effect on hemodynamics. *Chin. J. Naut. Med. Hyperbaric Med.* 28, 383–388. doi: 10.3760/cma.j.cn311847-20201117-00426

Ren, Y., Gu, X. D., Yao, Y. H., Fu, J. M., Yin, H. K., Li, L., et al. (2018). The effect of hyperbaric oxygen therapy combined with repetitive transcranial magnetic stimulation on patients with cognitive dysfunction after cerebral infarction. *Chin. J. Phys. Med. Rehab.* 40, 336–339. doi: 10.3760/cma.j.issn.0254-1424.2018.05.004

Rohde, D., Gaynor, E., Large, M., Mellon, L., Hall, P., Brewer, L., et al. (2019). The impact of cognitive impairment on poststroke outcomes: A 5-year follow-up. *J. Geriatr. Psychiatry Neurol.* 32, 275–281. doi: 10.1177/0891988719853044

Rossi, S., Hallett, M., Rossini, P. M., and Pascual-Leone, A.Safety of TMS Consensus Group (2009). Safety, ethical considerations, and application guidelines for the use of transcranial magnetic stimulation in clinical practice and research. *Clin. Neurophysiol.* 120, 2008–2039. doi: 10.1016/j.clinph.2009.08.016

Selimbeyoglu, A., and Parvizi, J. (2010). Electrical stimulation of the human brain: perceptual and behavioral phenomena reported in the old and new literature. *Front. Hum. Neurosci.* 4:46. doi: 10.3389/fnhum.2010.00046

Seniów, J., Waldowski, K., Leśniak, M., Iwański, S., Czepiel, W., and Członkowska, A. (2013). Transcranial magnetic stimulation combined with speech and language training in early aphasia rehabilitation: a randomized double-blind controlled pilot study. *Top. Stroke Rehabil.* 20, 250–261. doi: 10.1310/tsr2003-250

Sun, M.-K. (2018). Potential therapeutics for vascular cognitive impairment and dementia. *Curr. Neuropharmacol.* 16, 1036–1044. doi: 10.2174/1570159X15666171016164734

Sun, W., Mao, W., Meng, X., Wang, D., Qiao, L., Tao, W., et al. (2012). Low-frequency repetitive transcranial magnetic stimulation for the treatment of refractory partial epilepsy: a controlled clinical study. *Epilepsia* 53, 1782–1789. doi: 10.1111/j.1528-1167.2012.03626.x

Tang, X. Y., Yuan, L. J., Jiang, M. K., and Chen, Z. S. (2015). Effects of repetitive transcranial magnetic stimulation on cognitive function in post-cerebral infarction patients with mild cognitive impairment. *Stroke Nerv. Dis.* 22, 76–79. doi: 10.3969/j.issn.1007-0478.2015.02.003

Trung, J., Hanganu, A., Jobert, S., Degroot, C., Mejia-Constain, B., Kibreab, M., et al. (2019). Transcranial magnetic stimulation improves cognition over time in Parkinson's disease. *Parkinsonism Relat. Disord.* 66, 3–8. doi: 10.1016/j.parkreldis.2019.07.006

Tsai, P. Y., Lin, W. S., Tsai, K. T., Kuo, C. Y., and Lin, P. H. (2020). High-frequency versus theta burst transcranial magnetic stimulation for the treatment of poststroke cognitive impairment in humans. *J. Psychiatry Neurosci.* 45, 262–270. doi: 10.1503/jpn.190060

Tsao, C. W., Aday, A. W., Almarzooq, Z. I., Anderson, C. A. M., Arora, P., Avery, C. L., et al. (2023). Heart disease and stroke statistics—2023 update: a report from the American Heart Association. *Circulation* 147, e93–e621. doi: 10.1161/CIR.0000000000001123

Valero-Cabre, A., Pascual-Leone, A., and Rushmore, R. J. (2008). Cumulative sessions of repetitive transcranial magnetic stimulation (rTMS) build up facilitation to subsequent TMS-mediated behavioural disruptions. *Eur. J. Neurosci.* 27, 765–774. doi: 10.1111/j.1460-9568.2008.06045.x

Van den Boom, M. A., Jansma, J. M., and Ramsey, N. F. (2018). Rapid acquisition of dynamic control over DLPFC using real-time fMRI feedback. *Eur. Neuropsychopharmacol.* 28, 1194–1205. doi: 10.1016/j.euroneuro.2018.08.508

Vos, T., Lim, S. S., Abbafati, C., Abbas, K. M., Abbasi, M., Abbasifard, M., et al. (2020). Global burden of 369 diseases and injuries in 204 countries and territories, 1990–2019: a systematic analysis for the global burden of disease study 2019. *Lancet* 396, 1204–1222. doi: 10.1016/S0140-6736(20)30925-9

Wang, K., Dong, Q., Yu, J. T., and Hu, P. P. (2021a). Expert Consensus on post-stroke cognitive impairment management 2021. *Chin. J. Stroke.* 16, 376–389. doi: 10.3969/j.issn.1673-5765.2021.04.011

Wang, S. Y., Gu, Z. K., Chen, W., Wang, M., and Bi, Y. L. (2021b). Effects of repetitive transcranial magnetic stimulation at different frequencies on cognitive impairment after stroke. *Chin. J. Phys. Med. Rehab.* 43, 721–723. doi: 10.3760/cma.j.issn.0254-1424.2021.08.012

Wu, S. P., Ji, X., Qi, Y. W., Wang, H., and Ma, J. J. (2022). Combining transcranial magnetic stimulation with action observation therapy better improves the neurological functioning of stroke survivors. *Chin. J. Phys. Med. Rehab.* 44, 35–39. doi: 10.3760/cma.j.issn.0254-1424.2022.01.006

Xu, B. Y., Gu, Z. K., Wang, S. Y., Wang, X., and Ma, Z. Z. (2022). Effects of high-frequency repetitive transcranial magnetic stimulation combined with speech-auditory feedback training on event-related potential P300 and serum NSE and S100β proteins in patients with post-stroke cognitive impairment. *Prog. Mod. Biomed.* 22, 4541–4545. doi: 10.13241/j.cnki.pmb.2022.23.028

Yin, M. Y., Luo, J., Hu, X. Q., Xian, Q. L., Huang, L., Zhang, S. X., et al. (2018). Effects of high-frequency repetitive transcranial magnetic stimulation on post-stroke cognitive impairment. *Chin. J. Phys. Med. Rehab.* 33, 763–769. doi: 10.3969/j.issn.1001-1242.2018.07.003

Yin, Y. K., Wang, G. L., and Sun, J. Z. (2023). Therapeutic effect of different-frequency repetitive transcranial magnetic stimulations on post-stroke cognitive impairment: a Meta-analysis. *Chin. J. Tiss. Eng. Res.* 27, 3274–3280. doi: 10.12307/2023.150

Yingli, B., Zunke, G., Wei, C., and Shiyan, W. (2022). Cerebral activity manipulation of low-frequency repetitive transcranial magnetic stimulation in post-stroke patients with cognitive impairment. *Front. Neurol.* 13:951209. doi: 10.3389/fneur.2022.951209

You, F., Tian, M., Jiang, Z. W., Qian, J. Y., and Chen, B. (2023). Effects of enriched rehabilitation training combined with rTMS on cognitive function, plasma miR-146a-5p and TNF-α levels in patients with post-stroke cognitive impairment. *Chin. J. Pract. Nerv. Dis.* 26, 842–847. doi: 10.12083/SYSJ.221489

Yu, Z. Y., and Zhang, W. M. (2019). Effects of repetitive transcranial magnetic stimulation on patients with cognitive impairment. *Rehab. Med.* 29, 20–26. doi: 10.3724/SP.J.1329.2019.05020

Zhang, J., Ma, J., Li, H., Mei, H. N., and Tao, X. L. (2021). Effects of repetitive transcranial magnetic stimulation on post-stroke cognitive impairment and lipid metabolism. Chinese. *J. Rehabil.* 36, 584–588. doi: 10.3870/zgkf.2021.10.002

Zhang, J. J., Wu, L. L., Chen, D. D., Ren, J. X., Liu, L., and Li, Y. (2022). The effects of high-frequency repetitive transcranial magnetic stimulation on cognitive function after stroke observed based on electroencephalogram nonlinear analysis. *J. Chongqing Med. Univ.* 47, 762–767. doi: 10.13406/j.cnki.cyxb.003059

Zhang, F., and Zhou, S. Y. (2019). Effects of high frequency repetitive transcranial magnetic stimulation on cognitive function in stroke patients in convalescent stage. *Chin. J. Pract. Nerv. Dis.* 22, 2479–2485. doi: 10.12083/SYSJ.2019.22.404

Zhang, J. J., Zhu, M. L., Hu, D. X., Jiang, Y., Liu, B. L., Wang, Y. J., et al. (2020). The efficacy of different frequencies of repetitive transcranial magnetic stimulation in the treatment of mild cognitive impairment after cerebral infarction. *Shandong Med. J.* 60, 59–62. doi: 10.3969/j.issn.1002-266X.2020.10.015

Zhao, X. X., Han, X. H., Zhang, J. H., and Huang, X. L. (2012). Effects of high-frequency repetitive transcranial magnetic stimulation on learning and memory of rats with cerebral infarction. *Chin. J. Rehab. Med.* 27, 1087–1092. doi: 10.3969/j.issn.1001-1242.2012.12.001

Zheng, C. J., Xia, W. G., Duan, C., Li, Z. L., Wang, J., Cui, X. Y., et al. (2020). Repeated transcranial magnetic stimulation combined with donepezil can improve the cognition of cognitively impaired stroke survivors. *Chin. J. Phys. Med. Rehab.* 42, 32–36. doi: 10.3760/cma.j.issn.0254-1424.2020.01.008

Zhou, T., Gu, Z. K., Wang, S. Y., Wang, M., and Wang, Y. (2017). Effects of repetitive transcranial magnetic stimulation on post stroke cognitive impairment. *J. Xuzhou Med. Univ.* 37, 108–111. doi: 10.3969/j.issn.1000-2065.2017.02.012

Zuo, J. J., and Zhang, H. (2013). Effect of transcranial magnetic stimulation on cognitive impairment, C-reactive protein and fibrinogen in ischemic stroke patients. *Chin. J. Geriatric Heart Brain Vessel Dis.* 15, 614–616. doi: 10.3969/j.issn.1009-0126.2013.06.017

Frontiers in Neuroscience

Provides a holistic understanding of brain function from genes to behavior

Part of the most cited neuroscience journal series which explores the brain - from the new eras of causation and anatomical neurosciences to neuroeconomics and neuroenergetics.

Discover the latest Research Topics

See more →

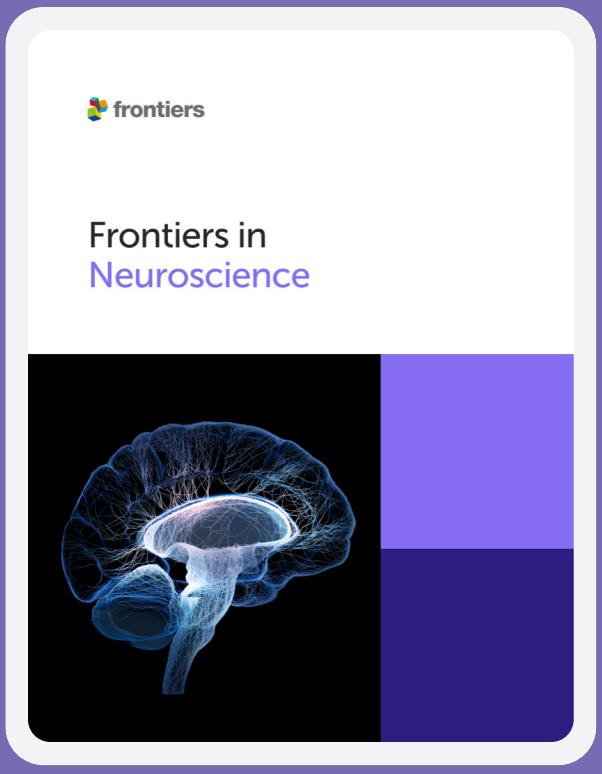

Frontiers

Avenue du Tribunal-Fédéral 34
1005 Lausanne, Switzerland
frontiersin.org

Contact us

+41 (0)21 510 17 00
frontiersin.org/about/contact